Oxidative Medicine and Cellular Longevity

Modulation of Oxidative Stress: Pharmaceutical and Pharmacological Aspects 2017

Lead Guest Editor: Luciano Saso
Guest Editors: Liudmila Korkina and Neven Zarkovic

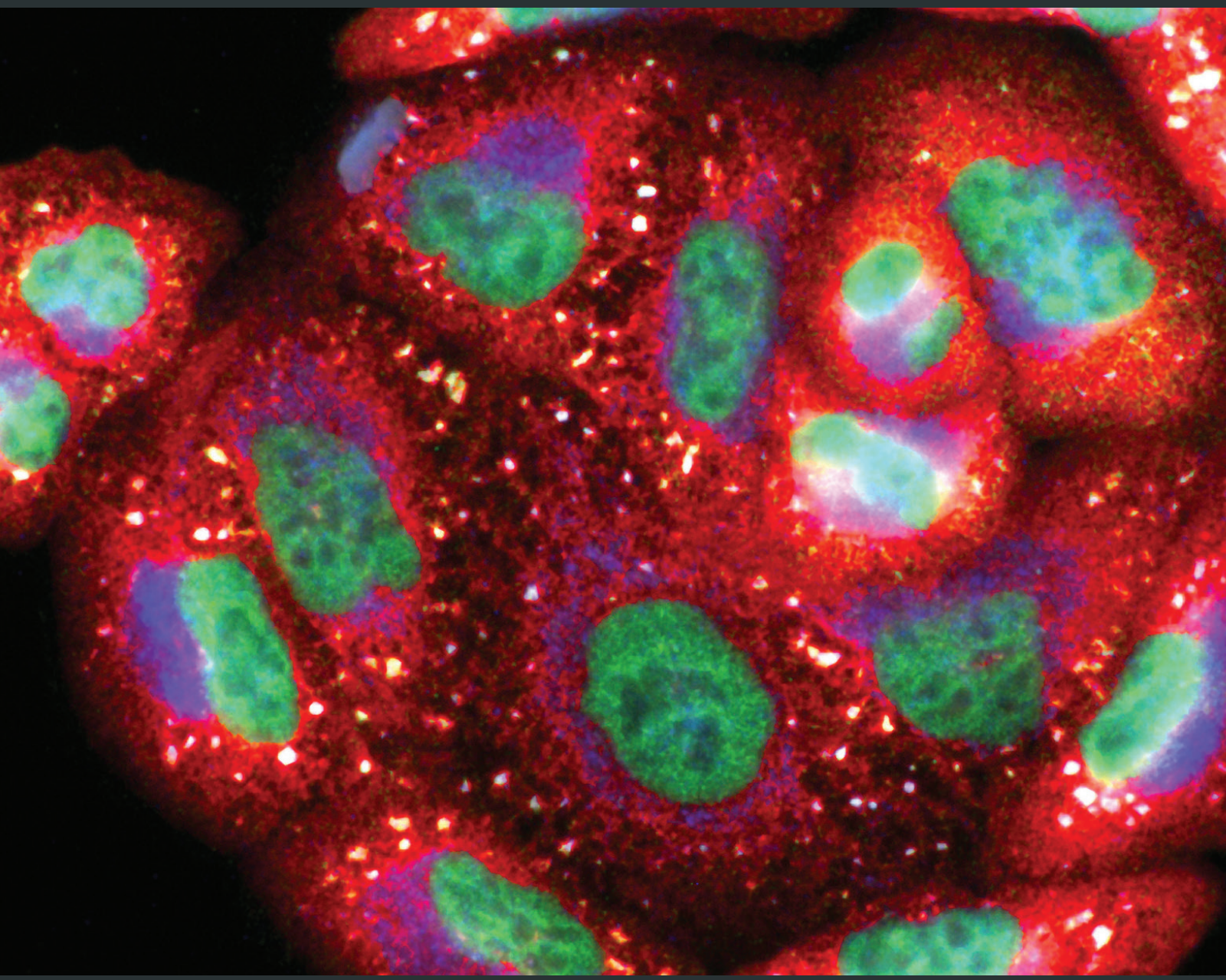

Modulation of Oxidative Stress: Pharmaceutical and Pharmacological Aspects 2017

Oxidative Medicine and Cellular Longevity

Modulation of Oxidative Stress: Pharmaceutical and Pharmacological Aspects 2017

Lead Guest Editor: Luciano Saso
Guest Editors: Liudmila Korkina and Neven Zarkovic

Editorial Board

Contents

Hindawi
Oxidative Medicine and Cellular Longevity
Volume 2017, Article ID 4802824, 2 pages
https://doi.org/10.1155/2017/4802824

Editorial

Modulation of Oxidative Stress: Pharmaceutical and Pharmacological Aspects 2017

Luciano Saso,[1] Liudmila Korkina,[2] and Neven Zarkovic[3]

[1]*Department of Physiology and Pharmacology "Vittorio Erspamer", Sapienza University of Rome, Rome, Italy*
[2]*Centre for Innovative Biotechnological Research, Moscow, Russia*
[3]*Rudjer Boskovic Institute, Zagreb, Croatia*

Correspondence should be addressed to Luciano Saso; luciano.saso@uniroma1.it

Received 28 November 2017; Accepted 29 November 2017; Published 17 December 2017

Reactive oxygen and nitrogen species are generated during normal cellular metabolic activities but can also play an etiopathogenetic role in a variety of conditions, including cardiovascular diseases, neurodegenerative diseases, and cancer.

Although the role of oxidative stress in human physiology and pathology has been intensely studied for several decades, it is still far from being understood. Certainly, the roles of free radicals and antioxidants have been significantly redefined. Some "negative" actions of free radicals in human biology and pathology are now known to be "positive," and the hypothesis that "classical antioxidants" (radical scavengers) could be always beneficial for the human health was not confirmed by several epidemiological and clinical studies. The possible reasons of the failures of the current antioxidant therapies, including methodological pitfalls in the drug development and delivery and the lack of good biological markers to select the patients, have been reviewed elsewhere [1, 2].

We currently believe that instead of "antioxidants," it is more appropriate to develop "modulators of oxidative stress" because, depending on the condition, it could be more beneficial to reduce or increase the oxidative stress.

In this special issue, several aspects of the modulation of oxidative stress were examined including the role of polyphenols ("Cytoprotective Mechanisms Mediated by Polyphenols from Chilean Native Berries against Free Radical-Induced Damage on AGS Cells" by Á. Felipe et al., "Curcumin Protects Skin against UVB-Induced Cytotoxicity via the Keap1-Nrf2 Pathway: The Use of a Microemulsion Delivery System" by M. B. Y. Greenwald et al., "Synthetic Isoliquiritigenin Inhibits Human Tongue Squamous Carcinoma Cells through Its Antioxidant Mechanism" by C. Hou et al., and "Oxidative Stress Triggered by Apigenin Induces Apoptosis in a Comprehensive Panel of Human Cervical Cancer-Derived Cell Lines" by R. P. Souza et al.) and other natural substances ("A Clinically Relevant Variant of the Human Hydrogen Sulfide-Synthesizing Enzyme Cystathionine β-Synthase: Increased CO Reactivity as a Novel Molecular Mechanism of Pathogenicity?" by J. B. Vicente et al., "Protective Mechanisms of the Mitochondrial-Derived Peptide Humanin in Oxidative and Endoplasmic Reticulum Stress in RPE Cells" by L. Minasyan et al., "Effect of Emodin on Preventing Postoperative Intra-Abdominal Adhesion Formation" by G. Wei et al., and "*Opuntia* spp.: Characterization and Benefits in Chronic Diseases" by M. del Socorro Santos Díaz et al.), some cardiovascular effects of modulators of oxidative stress ("Pentaerythritol Tetranitrate In Vivo Treatment Improves Oxidative Stress and Vascular Dysfunction by Suppression of Endothelin-1 Signaling in Monocrotaline-Induced Pulmonary Hypertension" by S. Steven et al., "4-Hydroxynonenal Contributes to Angiogenesis through a Redox-Dependent Sphingolipid Pathway: Prevention by Hydralazine Derivatives" by C. Camaré et al., "Cardiovascular Mitochondrial Dysfunction Induced by Cocaine: Biomarkers and Possible Beneficial Effects of Modulators of Oxidative Stress" by M. Graziani et al.), some neurological effects of modulators of oxidative stress ("Neuroprotective and Memory-Enhancing Effect of the Combined Extract of Purple Waxy Corn Cob and Pandan in Ovariectomized Rats" by W. Kirisattayakul et al. and "Alleviation of Oxidative Damage and Involvement of

Nrf2-ARE Pathway in Mesodopaminergic System and Hippocampus of Status Epilepticus Rats Pretreated by Intranasal Pentoxifylline" by Y. Kang), and some effects of modulators of oxidative stress related to cell growth and cancer development ("Dihydropyridine Derivatives as Cell Growth Modulators In Vitro" by I. Bruvere et al., "A Single Zidovudine (AZT) Administration Delays Hepatic Cell Proliferation by Altering Oxidative State in the Regenerating Rat Liver" by A. Butanda-Ochoa et al., "Preclinical Antileukemia Activity Of Tramesan: A Newly Identified Bioactive Fungal Metabolite" by M. R. Ricciardi et al., and "Markers of Oxidative Stress and Inflammation in Ascites and Plasma in Patients with Platinum-Sensitive, Platinum-Resistant, and Platinum-Refractory Epithelial Ovarian Cancer" by J. C. Cantón-Romero et al.).

In particular, this special issue contains two interesting contributions coming from INSERM Toulouse. The first one is an original research paper prepared in collaboration with CNRS and Palau Sabatier University in which C. Camare et al. investigated whether 4-hydroxynonenal (4-HNE), an aldehydic lipid oxidation product abundantly present in oxidized LDL, contributes to its proangiogenic properties. Using the immunofluorescence analysis of human atherosclerotic lesions, they found colocalization of HNE adducts with CD31 (marker of the endothelium), indicating a close relationship between 4-HNE and neovascularization. Moreover, they revealed that physiological concentrations of 4-HNE also enhance the formation of tubes by human microvascular endothelial cells (HMEC-1), through mechanisms involving reactive oxygen species (ROS) and activation of the neutral type 2 sphingomyelinase and sphingosine kinase-1 (nSMase2/SK-1) pathway. Eventually, they found that carbonyl scavengers hydralazine and bisvanillyl-hydralazone inhibited such proangiogenic effects of 4-HNE. In their second paper (in this time, a review paper) prepared jointly with partners from Mexico and from INRA in Toulouse, they described in detail features of the well-known plants of *Opuntia* spp. and their possible beneficial effects on chronic diseases. Thus, M. del Socorro Santos Díaz et al. point to the differences in the phytochemical composition between wild and domesticated (*O. ficus-indica*) *Opuntia* spp., stressing that all *Opuntia* components (pear, roots, cladodes, seeds, and juice) used as nutritional and pharmaceutical agents exhibit beneficial properties mainly resulting from their high content in antioxidants, while several other phytochemical components (biopeptides, soluble fibers), which have been characterized, also contribute to the medicinal properties of *Opuntia* spp. that might have a great economic potential because these plants grow in arid and desert regions.

In the original research paper prepared by partners from Riga and from Zagreb, we found novel information about growth-modulating effects of the dihydropyridine derivatives (DHPs) with potential antioxidant capacities. Thus, I. Bruvere et al. revealed that cell-type-specific differences in the growth-modifying effects of the DHPs in vitro can be attributed only to the novel types of the DHPs, which differentiate these substances from their well-known predecessor diludine. Since the growth-modifying effects of the novel DHPs indicate possible differential effects on cancer and on nonmalignant cells, which might be also different from their antioxidant effects, these substances deserve particular attention and further studies.

The original research paper prepared by three teams from Karlsruhe, Germany, reveals the possible beneficial effects of pentaerythritol tetranitrate (PETN), which were not described before. Namely, pulmonary arterial hypertension was induced by the ranging dosage of the i.v. applied monocrotaline, which induced endothelial dysfunction, pulmonary vascular wall thickening, and fibrosis, as well as protein tyrosine nitration, thus causing an increase in pulmonary arterial pressure, followed by the increase in heart/body and lung/body weight ratios. However, in this study, S. Steven et al. found also that PETN therapy could act beneficially upon these pathophysiological processes, most likely by upregulation of heme oxygenase-1 (HO-1).

Acknowledgments

The guest editorial team would like to thank all the authors of this special issue and the anonymous reviewers and the journal's team for its excellent assistance.

Luciano Saso
Liudmila Korkina
Neven Zarkovic

References

[1] L. Saso and O. Firuzi, "Pharmacological applications of antioxidants: lights and shadows," *Current Drug Targets*, vol. 15, no. 13, pp. 1177–1199, 2014.

[2] O. Firuzi, R. Miri, M. Tavakkoli, and L. Saso, "Antioxidant therapy: current status and future prospects," *Current Medicinal Chemistry*, vol. 18, no. 25, pp. 3871–3888, 2011.

Hindawi
Oxidative Medicine and Cellular Longevity
Volume 2017, Article ID 5061639, 8 pages
https://doi.org/10.1155/2017/5061639

Research Article

Preclinical Antileukemia Activity of Tramesan: A Newly Identified Bioactive Fungal Metabolite

M. R. Ricciardi,[1] R. Licchetta,[1] S. Mirabilii,[1] M. Scarpari,[2] A. Parroni,[2] A. A. Fabbri,[2] P. Cescutti,[3] M. Reverberi,[2] C. Fanelli,[2] and A. Tafuri[1]

[1]*Department of Clinical and Molecular Medicine, Sapienza University of Rome, Rome, Italy*
[2]*Department of Plant Biology, Sapienza University of Rome, Rome, Italy*
[3]*Department of Life Sciences, University of Trieste, Trieste, Italy*

Correspondence should be addressed to A. Tafuri; agostino.tafuri@uniroma1.it

Received 9 March 2017; Revised 4 August 2017; Accepted 12 September 2017; Published 15 November 2017

Academic Editor: Kum Kum Khanna

Despite improvements that occurred in the last decades in the acute myeloid leukemia (AML) treatment, clinical results are still unsatisfactory. More effective therapies are required, and innovative approaches are ongoing, including the discovery of novel antileukemia natural compounds. Several studies have described the activity of extracts from mushrooms which produce compounds that exhibited immunological and antitumor activities. The latter has been demonstrated to be promoted in vitro by mushroom polysaccharides via induction of apoptosis. However, the antileukemia activity of these compounds on primary cells is still not reported. In the present study, we examined the in vitro effects of Tramesan (TR), a bioactive compound extracted from *Trametes versicolor*, on leukemic cell lines and primary cells. Our results demonstrated that TR induced a marked growth inhibition of leukemic cell lines and primary cells from AML patients. The antiproliferative effects of TR were associated in primary AML cells with a significant increase of apoptosis. No significant cytotoxic effects were observed in normal peripheral blood mononuclear cells (MNC) from healthy donors. Our data demonstrated a cytotoxic activity of TR on leukemia cells prompting further translational applications. Ongoing studies are elucidating the molecular mechanisms underlying its antileukemic activity.

1. Introduction

Acute leukemia is a disorder of the hematopoietic system characterized by clonal proliferation of variably differentiated myeloid or lymphoid precursors [1]. These hematological disorders show a high level of genetic complexity, which is the major explanation of the high rate of chemotherapy failure and of the result stagnation over the last decades [1]. Therefore, efforts have been made to identify novel therapeutic approaches aimed at overcoming drug resistance and exploring novel approaches based on chemo-free strategies. The successful example of the acute promyelocytic leukemia, nowadays treated in the majority of the cases without chemotherapy by regimen based on the combined use of retinoic acid and arsenic trioxide [2], is worth mentioning. On this basis, many attempts are ongoing to identify other similar approaches. In fact, besides targeted therapies active on leukemia-specific aberrant molecular alterations [3], an increasing number of studies are directed toward the drug discovery attempt, including the evaluation of natural compounds on different pathologies [4–6].

Mushrooms are rich sources of natural compounds used as biological response modifiers for a long time in oriental medicine and nowadays also in Western countries [7–9]. Mushrooms have emerged as a rich font of antioxidant, immunomodulating, anti-inflammatory, antimicrobial, and anticancer [10] compounds. Among different extracts from mushrooms, polysaccharides are important bioactive molecules and known as potent inhibitors of proliferation and apoptosis inducers in *in vitro* experimental models. In particular, the antitumor activity of PSK, a protein-bound polysaccharide obtained from the fungus *Trametes versicolor* (*T. versicolor*), has been documented in *in vitro* and *in vivo* experimental models [11]. Efficacy of the adjuvant

immunotherapy with PSK was also demonstrated in human clinical trials [12–14]. Moreover, the combination of PSK with chemotherapy or radiotherapy has been shown to increase the efficacy of the latter in solid cancer treatments [7].

To date, few studies have reported the antineoplastic activity of PSK in hematologic models [11, 15–17]. In leukemia cell line, it was demonstrated that PSK exerted an antiproliferative and proapoptotic activity in HL-60 myeloid cell line, via activation of the mitochondrial and the p38 MAPK signaling cascades [16, 17].

Previous studies from our group have demonstrated that nonpurified extracts from the filtrates of *L. edodes* and *T. versicolor* inhibited mycotoxin synthesis in different fungi [18–20]. The mechanism of inhibition seems related to the promotion of fungal antioxidant activity on counteracting redox unbalance. It is now established that mycotoxigenic fungi are able to vehiculate the unscavenged ROS toward toxin synthesis.

Our group has patented a polysaccharidic fraction, *Tramesan* (TR), isolated from the liquid culture of the edible basidiomycete *T. versicolor* (Patent number RM2012A000573), able to significantly inhibit the synthesis of carcinogenic mycotoxins produced from different fungi (such as *Aspergillus flavus*, *A. parasiticus*, and Fusarium), by promoting an antioxidant activity [18, 20, 21].

The aim of this study was to investigate the activity of TR on leukemia cells by assessing proliferation inhibition and apoptosis induction on leukemia cell lines and on primary acute myeloid leukemia (AML) cells.

2. Materials and Methods

2.1. Fungal Strain and Growth Culture Conditions. The basidiomycete *Trametes versicolor* CF 117 was supplied from the mushroom collection of the laboratory of Mycology and Plant Pathology directed from Professor Corrado Fanelli (Sapienza University of Rome). The isolates were kept in potato dextrose agar (PDA) medium at 4°C, and the cultures have been renewed every 30 days.

2.2. Fungal Growth Substrate. T. versicolor was grown for 7 days in potato dextrose broth (PDB) and incubated at 25°C. The liquid culture was homogenized, in sterile condition in a Waring blender 8012. After homogenization, 5% (*v*/*v*) of the fungal culture was subsequently inoculated in 500 mL of PDB in 1 L Erlenmeyer flask and the *T. versicolor* cultures were incubated for 14 days at 25°C under shaken conditions (100 rpm). The mycelia were then separated from the culture filtrates by subsequent filtrations with different size filters (Whatman) to eliminate all the mycelia. The obtained culture filtrate was lyophilized and utilized for subsequent analyses.

2.3. Exopolysaccharide Extraction and Purification. The lyophilized *T. versicolor* culture filtrate (1 g) was dissolved in 30 mL of ultrapure H_2O and filtrated to separate the insoluble from the soluble part. The sample was then incubated at 4°C for 2 h, and at the same time, a solution of absolute ethanol was cooled at 4°C. The cooled culture filtrate was added slowly to cooled ethanol, mixing with a glass rod. The precipitate was recovered by centrifugation at 4000 rpm for 20 min at 4°C. The recovered pellet was resuspended in 4 mL of ultrapure H_2O and 4 mL of 20 mM phosphate buffer pH 7.5 to achieve the optimal conditions of ionic strength and pH for pronase E (Sigma-Aldrich) activity. The proteolysis was carried out at 37°C overnight. The elimination of salts and amino acids was performed through dialysis versus H_2O, utilizing membrane of 12000 Da cutoff. The dialyzed samples were lyophilized and subjected to total carbohydrate determination by Yemm and Willis [22].

To separate, on the basis of their molecular weight, the exopolysaccharides precipitated with EtOH and present in *T. versicolor* culture filtrates, a size exclusion chromatography was performed. The mobile phase was $NaNO_3$ 0.05 M degassed for about 30 min and filtered twice with Millipore 0.45 μm filters. The Sephacryl S-300 (1.6 id × 90 cm) column was equilibrated with the eluent for about 30 h, with a flux of about 6 mL/h. The gel performances of the column allow to discriminate polysaccharides with a molecular weight between 2 and 400 kDa. About 40 mg of the sample was dissolved in 1.9 mL of 50 mM $NaNO_3$, the solution was centrifuged for 10 min at 13000 rpm, and subsequently it was loaded in a column. The column was connected to a refractive index detector. Each fraction was collected every 20 min during 30 h.

The chromatographic fraction containing only polysaccharides (TR) was used for biological activity assays.

The polysaccharide TR, isolated and purified was patented from our group (Patent number RM2012A00057).

2.4. Cell Lines and Primary Samples. Human myeloid (OCI-AML3) and lymphoid (Jurkat) cell lines were maintained in RPMI 1640 medium containing 10% heat-inactivated fetal calf serum (FCS), 1 mM L-glutamine, and 50 μg/mL penicillin/streptomycin (Gibco, Milan), in a humidified atmosphere containing 5% CO_2 at 37°C. Cell lines were harvested in log-phase growth for all experiments, washed, and cultured to the appropriate concentration in RPMI 10% FCS ± TR at scalar concentrations (0.5–2 mg/mL).

Peripheral blood (PB) samples and bone marrow (BM) aspirate samples were obtained from normal donors and from 4 AML patients, respectively, all referred to our Hematology at Sapienza University of Rome, Italy. Written informed consent for *in vitro* studies was obtained from donors and patients in accordance with regulations and protocols sanctioned by the Human Subjects Committee of Helsinki and were approved by the Sapienza Institutional Review Board (protocol number 158/10 signed on February 18, 2010). MNC obtained from the PB of a normal volunteer donor and blast cells from the BM of AML patients were separated by layering on Ficoll-Hypaque density gradient (Lymphoprep; 1.007 g/mL). Cells used for *in vitro* studies were resuspended at a concentration of 1.0 × 106/mL, in RPMI 10% FCS ± TR at scalar concentrations (0.5–2 mg/mL). In particular, the circulating mononuclear cells obtained from healthy donors were placed in

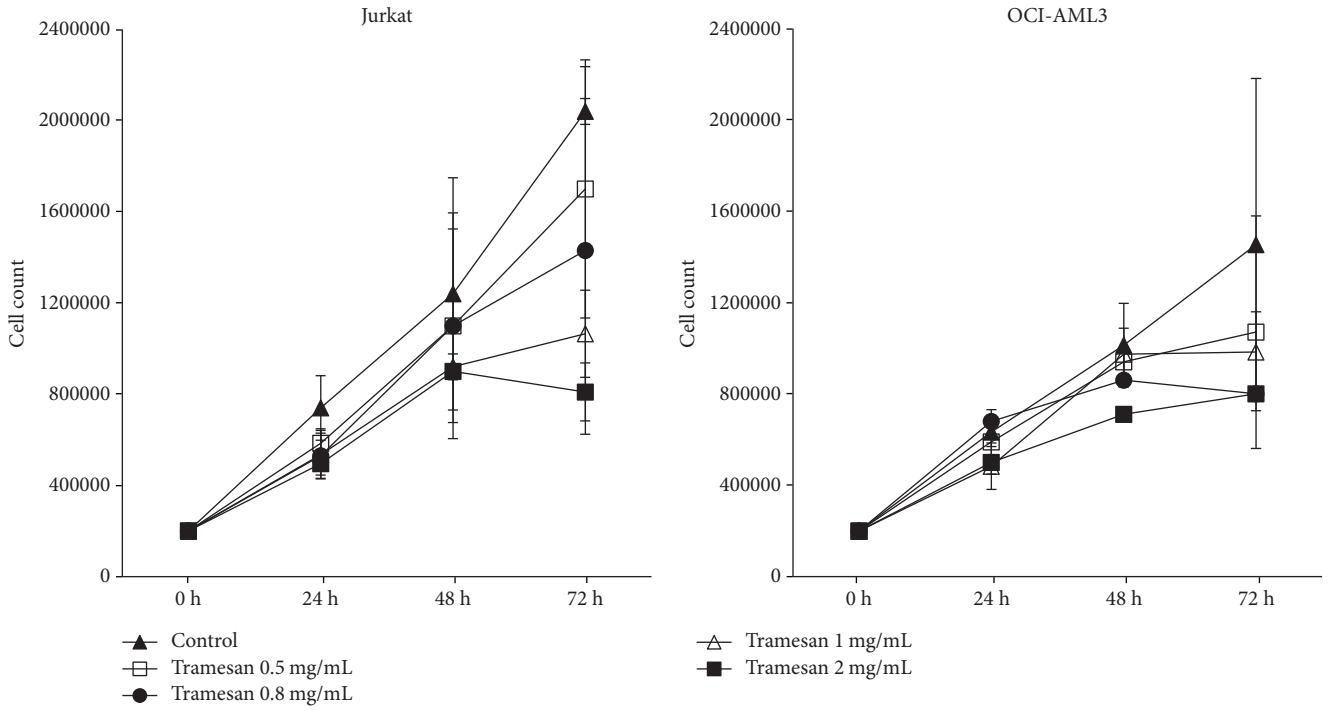

Figure 1: TR induces a dose-dependent reduction in cell count in hematopoietic cell lines. Jurkat and OCI-AML3 cells were exposed to increasing concentrations of TR for the indicated time points. Cell counts and viability were then assessed by trypan blue exclusion counting. Results are expressed as the average ± SD of seven independent experiments.

liquid culture ± scalar concentrations of TR in the absence and in the presence of a proliferative stimulus (PHA).

2.5. Cell Cycle and Apoptosis Analysis. Cell cycle distribution changes were evaluated using the Acridine Orange (AO) technique as previously described [23]. The percentage of cells in G0, G1, S, and G2 M was determined by measuring simultaneously the DNA and RNA total cellular content. The percentage of apoptotic cells was measured based on the decreased stainability of apoptotic elements in DNA green fluorescence (sub-G0/1 peak on DNA frequency histograms) coupled with a higher RNA red fluorescence (which is common to chromatin condensation); cell debris was excluded from the analysis on the basis of their forward light scatter properties. Cell cycle distribution was analyzed using the ModFit LT software (Verity Software House, Topsham, ME).

Induction of apoptosis was also assessed by measuring Annexin V binding to externalized phosphatidylserine, as previously described [24]. Briefly, cells were washed twice with PBS and resuspended in binding buffer (10 mM Hepes/NaOH pH 7.4, 140 mM NaCl, 2.5 mM $CaCl_2$, Sigma Chemical Co.). FITC-conjugated Annexin V (Roche Diagnostic Corp., Indianapolis, Indiana, USA) was added at a final concentration of 1 μg/mL. The mixture was incubated at room temperature for 15 min in the dark prior to flow cytometric analysis. Membrane integrity was simultaneously assessed by propidium iodide (PI, 0.25 μg/mL) exclusion.

2.6. Analysis of Intracellular ROS Levels. The generation of ROS was measured by using DCFH-DA, a ROS-sensitive fluorescent probe. Briefly, OCI-AML3 cells were cultured for 24 h with different concentrations of TR. After exposure, cells were incubated with 10 mM DCFH-DA for 30 min at 37°C, then washed, resuspended in PBS, and immediately analyzed by flow cytometry. Results were expressed as mean fluorescence intensity (MFI) relative to that of control.

2.7. Statistical Analysis. The two-sided Student t-test was used to evaluate the significance of differences between groups. Results were expressed as the mean ± standard deviation (SD). Values of $p < 0.05$ were considered significant from a statistical point of view.

3. Results

3.1. Effects of TR on Leukemia Cell Lines. We started to evaluate the effects of TR on human myeloid (OCI-AML3) and lymphoid (Jurkat) leukemia cell lines exposed to scalar concentrations of TR (0.5–2 mg/mL). Cell aliquots were harvested at 24, 48, and 72 hours and analyzed for cell counts (trypan blue), cell cycle (flow cytometric analysis by AO), and apoptosis (flow cytometry assessment with AO, Annexin V).

Exposure to TR induced a dose- and time-dependent reduction in cell count in all hematopoietic cell lines studied (Figure 1). In fact, the effects were markedly evident at a dose of 1 mg/mL after 48 hours of liquid culture. The prolonged exposure to TR and increasing scalar concentrations of the

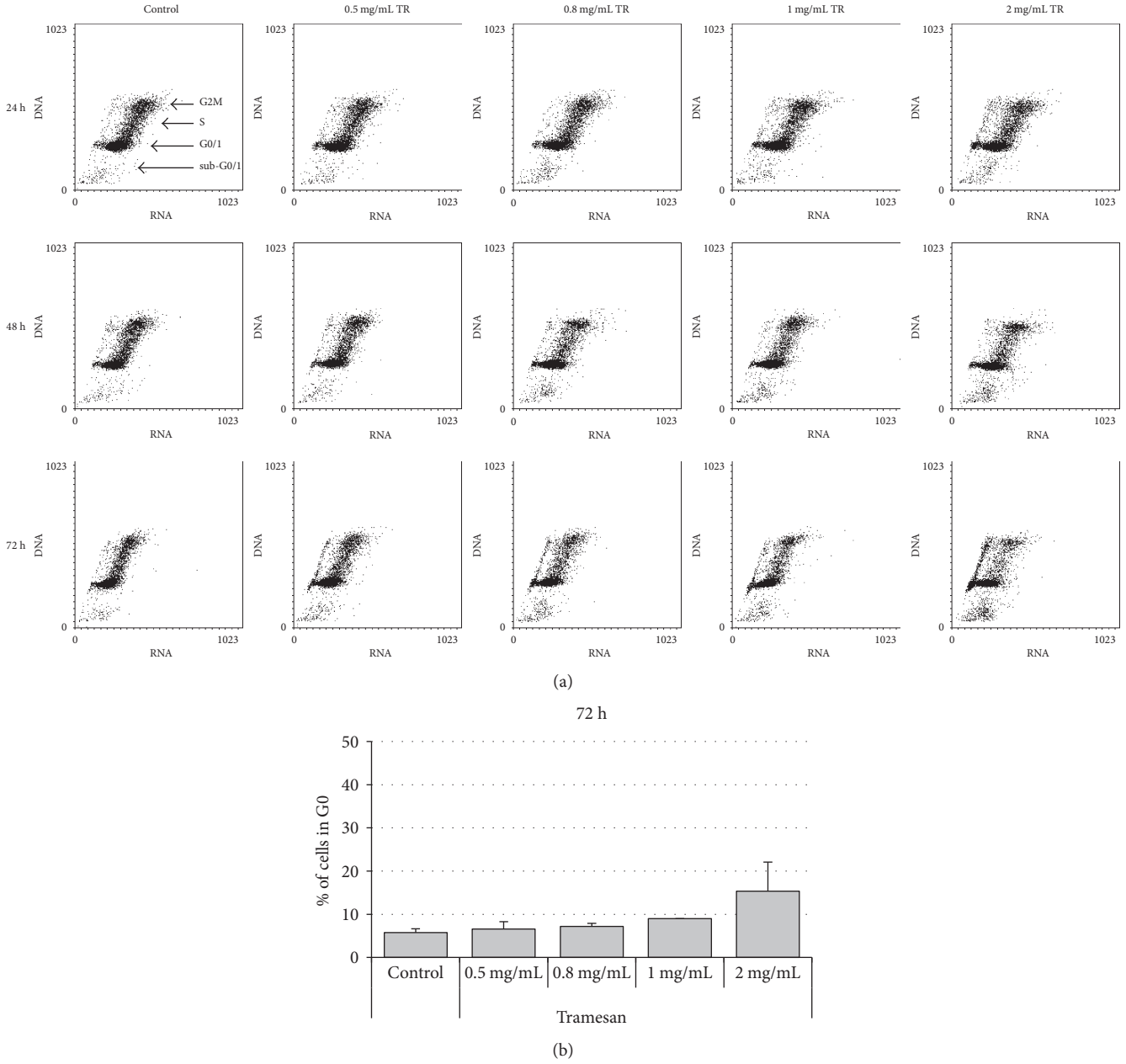

Figure 2: TR induces a dose-dependent increase of cells in G0 phase of cell cycle in hematopoietic cell lines. Jurkat cells were exposed to increasing concentrations of TR. Cell cycle changes were then evaluated by the AO technique. Results showed are representative of 7 independent experiments (a). Percentages of cells in G0 phase after 72 h of TR exposure are shown in (b).

molecule potentiated the effectiveness (Figure 1). Detection of cell cycle changes, measured at the same time points, however, showed that on leukemia cell lines TR was unable to affect cell cycle distribution and apoptosis. Only on Jurkat cell line it was observed, after 72 h of culture, a mild, not significant, dose-dependent increase of cells in G0 phase associated with a decrease of G1 and S compartment and with a nonsignificant increase of sub-G0/1 (Figure 2).

Analysis of intracellular ROS levels in cells stained with DCFH-DA depicts (Figure 3) that TR induced accumulation of ROS as demonstrated by an increase of DCFH-DA MFI in OCI-AML3 treated with TR as compared to control: from MFI of 0.46×10^6 (control) to MFI of 2.94×10^6, 2.61×10^6 and, 2.98×10^6 in the presence of 0.5, 1, and 2 mg/mL TR, respectively.

3.2. Effects of TR on Primary Cells from AML Patients. We then examined the biological effects induced in vitro by TR on primary cells from 4 patients with newly diagnosed AML. Our results indicate that TR induced reduction in cell count and significant cytotoxic effects in a dose- and time-dependent fashion in all (4/4) samples studied. After 72–120 hours of culture, TR was able to exert a significant reduction in cell counts from 1272500 ± 235425 cells/mL, in the control condition, to 885000 ± 392386 ($p = 0.06$), 787500 ± 493381 ($p = 0.04$), 675000 ± 470213 ($p = 0.02$), and

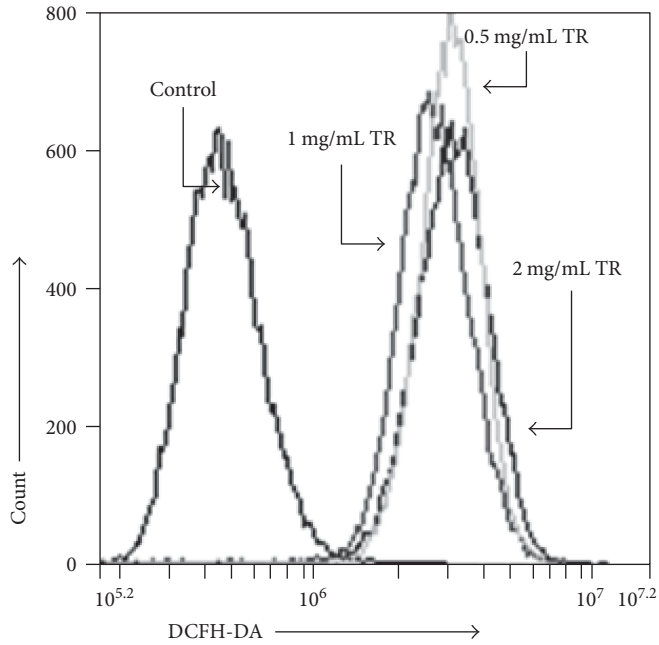

Figure 3: TR induced accumulation of ROS in hematopoietic cells line. Cells were exposed to increasing concentrations of TR. After 24 h, cells were stained with DCFH-DA for intracellular ROS level analysis.

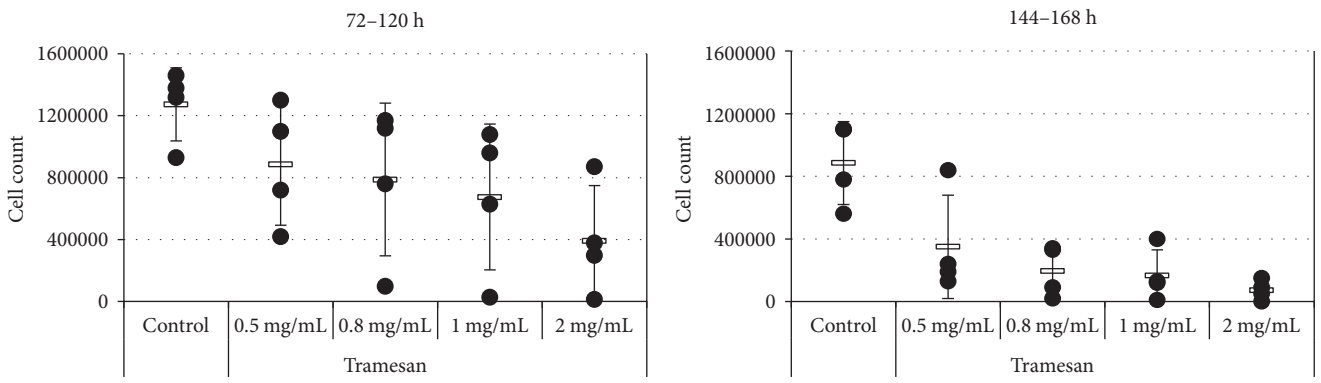

Figure 4: TR induces a dose- and time-dependent reduction in cell count in primary cells from AML patients. AML primary cells were exposed to the indicated concentrations of TR. Cell counts and viability were assessed for the individual sample after 72–120 h and 144–168 h by trypan blue exclusion.

391750 ± 356435 ($p = 0.01$) cells/mL in the presence of 0.5, 0.8, 1, and 2 mg/mL of TR, respectively (Figure 4).

Notably, in primary AML samples, TR significantly increased apoptosis levels (sub-G0/1) from 35.7 ± 13.8%, in the control conditions, to 48.9% ± 23.5, 67.9% ± 25.9, 65.9% ± 34.6, and 77.2% ± 28.3 ($p = 0.04$) in the presence of 0.5, 0.8, 1, and 2 mg/mL of TR, respectively (Figure 5(a)). This effect was, however, even more marked at a prolonged exposure to the molecule (144–168 hours), reaching the statistical significance already at the lowest dose: from 41.6% ± 23.5, in the control condition, to 77.5% ± 31.1 ($p = 0.04$), 88.6% ± 17.3 ($p = 0.01$), 86.5% ± 22.8 ($p = 0.01$), and 94.5% ± 8.4 ($p = 0.01$), with 0.5, 0.8, 1, and 2 mg/mL of TR, respectively (Figures 5(b) and 5(c)).

3.3. Effects of TR on Normal Cells. In order to analyze the activity of the compound on normal hematopoietic cells, we investigated the effects of TR on mononuclear cells obtained from PB of normal donors. The MNC were then exposed in liquid culture ± TR at scalar concentrations (0.5, 0.8, 1, and 2 mg/mL), in the absence and in the presence of a proliferative stimulus (PHA). The results obtained showed that TR was able to induce only a moderate, not statistically significant, proapoptotic activity, regardless of the dose: after 72 hours, apoptosis levels were 18.3% ± 15.6, in the control condition, and 25.65% ± 10.0, 29.5% ± 18.4, 35.5% ± 16.2, and 31.8% ± 15.8, with 0.5, 0.8, 1, and 2 mg/mL of TR, respectively (Figure 6(a)). These effects were not enhanced by the pretreatment with PHA: at 48 hours, apoptosis levels

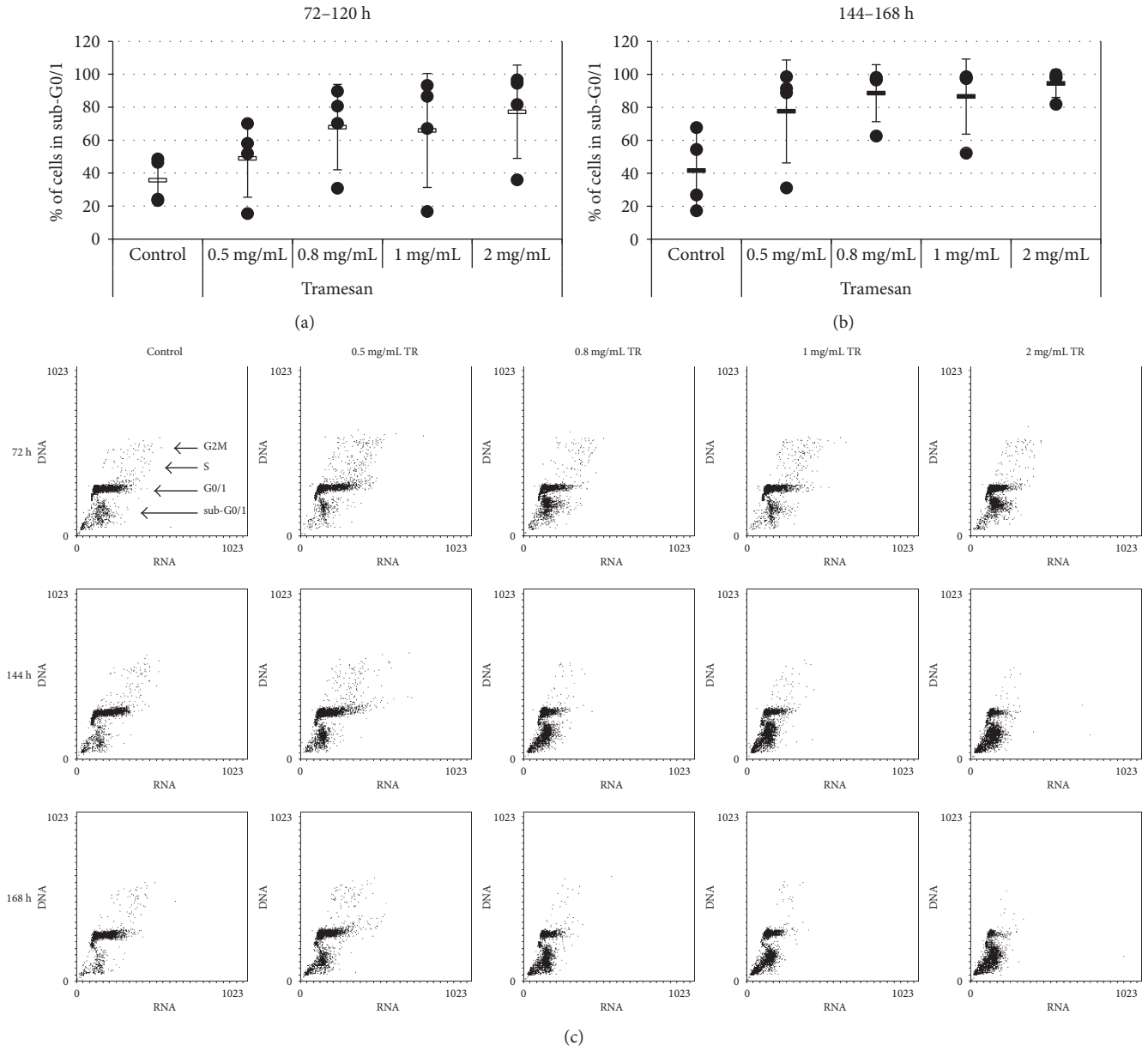

Figure 5: TR induces a dose- and time-dependent apoptosis in primary cells from AML. AML primary cells were exposed to the indicated concentrations of TR. Apoptosis induction was then evaluated by the AO technique. Percentages of sub-G0/1 cells are shown for the individual sample after 72–120 h (a) and 144–168 h (b) exposure to scalar concentrations of TR. A representative experiment is shown (c).

were 20.1% ± 5.0, in the control condition, and 18.9% ± 5.6, 14.1% ± 2.6, 23.4% ± 14.9, and 13.3% ± 1.0, with 0.5, 0.8, 1, and 2 mg/mL of TR, respectively (Figure 6(b)).

4. Discussion

The present study demonstrated that TR, a polysaccharide extract from *T. versicolor*, significantly suppresses cell growth of human leukemia cell lines from different ontogenesis and exerts a cytotoxic activity on primary cells from AML patients.

T. versicolor is one of the most commonly used medicinal mushrooms, and several extracts have already been investigated for their antineoplastic effects. The cytotoxic activity of PSP and PSK extract from *T. versicolor* has been reported in myeloid and lymphoid leukemia cell line [25, 26]. It was also demonstrated that an ethanol-water extract from wild *T. versicolor* exerted in vitro antiproliferative and cytotoxic effects against leukemia and lymphoma cell lines [26]. Moreover, the antioxidant effects of different molecular mass enzymatic hydrolysates from PSPs were described [27]. In addition, results from a phase 1 clinical trial proved that an orally administered preparation from the *T. versicolor* may improve immune response in women with breast cancer after standard chemotherapy and radiotherapy [14].

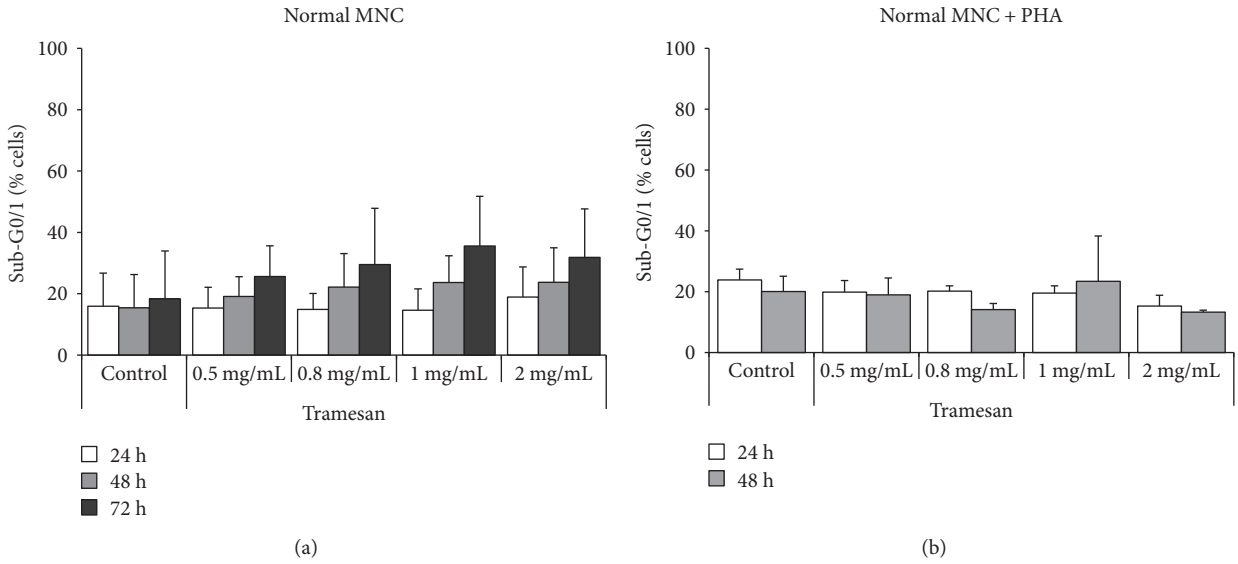

Figure 6: TR does not exert proapoptotic activity on normal MNC. Analysis of the levels of apoptosis (% sub-G0/1) in nonstimulated lympho-monocytes (a) and in those stimulated with PHA (b) and subsequently exposed to scalar concentrations of TR.

We demonstrated, for the first time at our knowledge, the *in vitro* cytotoxic activity of a polysaccharidic fraction purified from *T. versicolor* on primary AML cells, as shown by a time- and dose-dependent induction of apoptosis.

One of the fundamental hallmarks of cancer cells is their capacity to proliferate persistently, eluding cell cycle checkpoint controls and growth inhibitory signals [28, 29]. Moreover, the acquired resistance toward apoptosis represents another key hallmark of cancer. Hence, molecules capable to block the uncontrolled proliferation and/or to induce to cell death have been evermore considered very promising for therapeutic applications in cancers. Previous reports demonstrated that PSK induces *in vitro* cytotoxic activity in tumor cell lines, via arrest of cell cycle and induction of apoptosis [11, 15].

Data presented in our study demonstrated that TR causes in leukemia models a dose-dependent increase of cells in G0 phase and a decrease in both G1 and S phases. Nevertheless, lack of statistical significance argues in favor of a deceleration of cell cycle rather than a cell cycle arrest and apoptosis induction at these concentrations. The preclinical relevance of TR was showed on primary samples obtained from de novo AML patients. TR was indeed able to decrease the leukemic blast viability by significantly inducing apoptosis in all AML samples tested. By contrast, no significant cytotoxicity was observed on resting and activated normal MNC thus suggesting the existence of a therapeutic window in leukemia setting.

The direct antiproliferative effect of several fungal polysaccharides on cancer cells, caused by cell cycle arrest and apoptosis induction, has been also reported associated with oxidative stress [30, 31]. Here, in fact, we documented ROS accumulation in leukemia cell line. It was widely described that oxidants can contribute to cancer development by promoting cell mutation and growth [32]. Nevertheless, it was also reported that excessive oxidative stress can slow proliferation and induce cell death [32]. TR-induced cytotoxicity observed in primary AML samples could then be due to oxidative stress-induced cell death.

Although the literature seems to suggest the involvement of Toll-like receptors or of other cell surface receptors in the increased oxidative stress induced by fungal polysaccharides [33, 34], the exact mechanism remains to be clarified.

In conclusion, the cytotoxic preclinical activity of TR on primary leukemia cells, as compared to normal MNC obtained from healthy cells, makes TR an interesting bioactive compound among other antileukemic treatments and prompts further investigation aiming to elucidate its mechanism of action for a translational application.

Conflicts of Interest

The authors declare that they have no conflicts of interest.

Acknowledgments

The authors thank RomaAIL (Associazione Italiana contro le Leucemie-linfomi e Mieloma) for providing laboratory space. This work was supported by grants from Sapienza University of Rome (C26A10SW9X and C26A14CPRB) and Fondazione Frisiani-Santini.

References

[1] D. A. Arber, A. Orazi, R. Hasserjian et al., "The 2016 revision to the World Health Organization classification of myeloid neoplasms and acute leukemia," *Blood*, vol. 127, no. 20, pp. 2391–2405, 2016.

[2] L. Cicconi and F. Lo-Coco, "Current management of newly diagnosed acute promyelocytic leukemia," *Annals of Oncology*, vol. 27, no. 8, pp. 1474–1481, 2016.

[3] D. Shafer and S. Grant, "Update on rational targeted therapy in AML," *Blood Reviews*, vol. 30, no. 4, pp. 275–283, 2016.

[4] G. M. Cragg and D. J. Newman, "Plants as a source of anti-cancer agents," *Journal of Ethnopharmacology*, vol. 100, no. 1-2, pp. 72–79, 2005.

[5] S. Nobili, D. Lippi, E. Witort et al., "Natural compounds for cancer treatment and prevention," *Pharmacological Research*, vol. 59, no. 6, pp. 365–378, 2009.

[6] K. S. Siveen, S. Uddin, and R. M. Mohammad, "Targeting acute myeloid leukemia stem cell signalling by natural products," *Molecular Cancer*, vol. 16, no. 1, p. 13, 2017.

[7] A. G. Guggenheim, K. M. Wright, and H. L. Zwickey, "Immune modulation from five major mushrooms: application to integrative oncology," *Integrative Medicine*, vol. 13, no. 1, pp. 32–44, 2014.

[8] R. R. Paterson and N. Lima, "Biomedical effects of mushrooms with emphasis on pure compounds," *Biomedical Journal*, vol. 37, no. 6, pp. 357–368, 2014.

[9] P. S. Bisen, R. K. Baghel, B. S. Sanodiya, G. S. Thakur, and G. B. Prasad, "Lentinus edodes: a macrofungus with pharmacological activities," *Current Medicinal Chemistry*, vol. 17, no. 22, pp. 2419–2430, 2010.

[10] S. Patel and A. Goyal, "Recent developments in mushrooms as anti-cancer therapeutics: a review," *3 Biotech*, vol. 2, no. 1, pp. 1–15, 2012.

[11] E. Jiménez-Medina, E. Berruguilla, I. Romero et al., "The immunomodulator PSK induces in vitro cytotoxic activity in tumour cell lines via arrest of cell cycle and induction of apoptosis," *BMC Cancer*, vol. 8, no. 78, 2008.

[12] J. Sakamoto, S. Morita, K. Oba et al., "Efficacy of adjuvant immunochemotherapy with polysaccharide K for patients with curatively resected colorectal cancer: a meta-analysis of centrally randomized controlled clinical trials," *Cancer Immunology, Immunotherapy*, vol. 55, no. 4, pp. 404–411, 2006.

[13] Y. Ueda, T. Fujimura, S. Kinami et al., "A randomized phase III trial of postoperative adjuvant therapy with S-1 alone versus S-1 plus PSK for stage II/IIIA gastric cancer: Hokuriku-Kinki Immunochemo-Therapy Study Group-Gastric Cancer (HKIT-GC)," *Japanese Journal of Clinical Oncology*, vol. 36, no. 8, pp. 519–522, 2006.

[14] C. J. Torkelson, E. Sweet, M. R. Martzen et al., "Phase 1 clinical trial of *Trametes versicolor* in women with breast cancer," *ISRN Oncology*, vol. 2012, Article ID 251632, 7 pages, 2012.

[15] K. P. Hui, W. H. Sit, and J. M. Wan, "Induction of S phase cell arrest and caspase activation by polysaccharide peptide isolated from Coriolus versicolor enhanced the cell cycle dependent activity and apoptotic cell death of doxorubicin and etoposide, but not cytarabine in HL-60 cells," *Oncology Reports*, vol. 14, no. 1, pp. 145–155, 2005.

[16] N. Hirahara, M. Fujioka, T. Edamatsu et al., "Protein-bound polysaccharide-K (PSK) induces apoptosis and inhibits proliferation of promyelomonocytic leukemia HL-60 cells," *Anticancer Research*, vol. 31, no. 9, pp. 2733–2738, 2011.

[17] N. Hirahara, T. Edamatsu, A. Fujieda, M. Fujioka, T. Wada, and Y. Tajima, "Protein-bound polysaccharide-K induces apoptosis via mitochondria and p38 mitogen-activated protein kinase-dependent pathways in HL-60 promyelomonocytic leukemia cells," *Oncology Reports*, vol. 30, no. 1, pp. 99–104, 2013.

[18] M. Reverberi, A. A. Fabbri, S. Zjalic, A. Ricelli, F. Punelli, and C. Fanelli, "Antioxidant enzymes stimulation in *Aspergillus parasiticus* by *Lentinula edodes* inhibits aflatoxin production," *Applied Microbiology and Biotechnology*, vol. 69, no. 2, pp. 207–215, 2005.

[19] M. Reverberi, S. Zjalic, A. Ricelli et al., "Modulation of antioxidant defense in *Aspergillus parasiticus* is involved in aflatoxin biosynthesis: a role for the Ap*yapA* gene," *Eukaryotic Cell*, vol. 7, no. 6, pp. 988–1000, 2008.

[20] M. Scarpari, C. Bello, C. Pietricola et al., "Aflatoxin control in maize by *Trametes versicolor*," *Toxins*, vol. 6, no. 12, pp. 3426–3437, 2014.

[21] S. Zjalic, A. A. Fabbri, M. Reverberi, A. Ricelli, F. Punelli, and C. Fanelli, "Use of Trametes versicolor in control of aflatoxins produced by Aspergillus parasiticus," *International Journal of Medicinal Mushrooms*, vol. 9, no. 3&4, pp. 236-237, 2007.

[22] E. W. Yemm and A. J. Willis, "The estimation of carbohydrates in plant extracts by anthrone," *Biochemical Journal*, vol. 57, no. 3, pp. 508–514, 1954.

[23] A. Tafuri and M. Andreeff, "Kinetic rationale for cytokine induced recruitment of myeloblastic leukemia followed by cycle-specific chemotherapy in vitro," *Leukemia*, vol. 4, no. 12, pp. 826–834, 1990.

[24] M. R. Ricciardi, M. T. Petrucci, C. Gregorj et al., "Reduced susceptibility to apoptosis correlates with kinetic quiescence in disease progression of chronic lymphocytic leukaemia," *British Journal of Haematology*, vol. 113, no. 2, pp. 391–399, 2001.

[25] Y. Dong, M. M. Yang, and C. Y. Kwan, "In vitro inhibition of proliferation of HL-60 cells by tetrandrine and Coriolus versicolor peptide derived from Chinese medicinal herbs," *Life Sciences*, vol. 60, no. 8, pp. 135–140, 1997.

[26] C. B. Lau, C. Y. Ho, C. F. Kim et al., "Cytotoxic activities of *Coriolus versicolor* (Yunzhi) extract on human leukemia and lymphoma cells by induction of apoptosis," *Life Sciences*, vol. 75, no. 7, pp. 797–808, 2004.

[27] M. H. Jhan, C. H. Yeh, C. C. Tsai, C. T. Kao, C. K. Chang, and C. W. Hsieh, "Enhancing the antioxidant ability of *Trametes versicolor* polysaccharopeptides by an enzymatic hydrolysis process," *Molecules*, vol. 21, no. 9, p. 1215, 2016.

[28] D. Hanahan and R. A. Weinberg, "Hallmarks of cancer: the next generation," *Cell*, vol. 144, no. 5, pp. 646–674, 2011.

[29] T. Otto and P. Sicinski, "Cell cycle proteins as promising targets in cancer therapy," *Nature Reviews Cancer*, vol. 17, no. 2, pp. 93–115, 2017.

[30] T. C. Hsieh and J. M. Wu, "Suppression of proliferation and oxidative stress by extracts of Ganoderma lucidum in the ovarian cancer cell line OVCAR-3," *International Journal of Molecular Medicine*, vol. 28, no. 6, pp. 1065–1069, 2011.

[31] E. A. Queiroz, Z. B. Fortes, M. A. da Cunha, A. M. Barbosa, N. Khaper, and R. F. Dekker, "Antiproliferative and pro-apoptotic effects of three fungal exocellular β-glucans in MCF-7 breast cancer cells is mediated by oxidative stress, AMP-activated protein kinase (AMPK) and the Forkhead transcription factor, FOXO3a," *The International Journal of Biochemistry & Cell Biology*, vol. 67, pp. 14–24, 2015.

[32] M. Schieber and N. S. Chandel, "ROS function in redox signaling and oxidative stress," *Current Biology*, vol. 24, no. 10, pp. R453–R462, 2014.

[33] G. C. F. Chan, W. K. Chan, and D. M. Y. Sze, "The effects of β-glucan on human immune and cancer cells," *Journal of Hematology & Oncology*, vol. 2, p. 25, 2009.

[34] S. Batbayar, D. H. Lee, and H. W. Kim, "Immunomodulation of fungal β-glucan in host defense signaling by Dectin-1," *Biomolecules & Therapeutics*, vol. 20, no. 5, pp. 433–445, 2012.

Hindawi
Oxidative Medicine and Cellular Longevity
Volume 2017, Article ID 2873030, 8 pages
https://doi.org/10.1155/2017/2873030

Research Article

Markers of Oxidative Stress and Inflammation in Ascites and Plasma in Patients with Platinum-Sensitive, Platinum-Resistant, and Platinum-Refractory Epithelial Ovarian Cancer

Juan Carlos Cantón-Romero,[1] Alejandra Guillermina Miranda-Díaz,[2] Jose Luis Bañuelos-Ramírez,[1] Sandra Carrillo-Ibarra,[2] Sonia Sifuentes-Franco,[2] José Alberto Castellanos-González,[3] and Adolfo Daniel Rodríguez-Carrizalez[2]

[1]*Hospital of Gynecology and Obstetrics, Department of Oncology Gynecology, Sub-Specialty Medical Unit, National Occidental Medical Center, Mexican Social Security Institute, Guadalajara, JAL, Mexico*
[2]*Institute of Experimental and Clinical Therapeutics, Department of Physiology, University Health Sciences Centre, University of Guadalajara, Guadalajara, JAL, Mexico*
[3]*Specialties Hospital, National Occidental Medical Centre, Mexican Social Security Institute, Guadalajara, JAL, Mexico*

Correspondence should be addressed to Alejandra Guillermina Miranda-Díaz; kindalex1@outlook.com

Received 6 March 2017; Revised 1 June 2017; Accepted 27 June 2017; Published 7 August 2017

Academic Editor: Luciano Saso

Diverse proinflammatory biomarkers and oxidative stress are strongly associated with advanced epithelial ovarian cancer (EOC). *Objective*. To determine the behavior of markers of oxidative stress and inflammation in plasma and ascites fluid in patients with platinum-sensitive, platinum-resistant, and platinum-refractory EOC. *Methods*. A prospective cohort study. The colorimetric method was used to determine levels of the markers 8-isoprostanes (8-IP), lipid peroxidation products (LPO), and total antioxidant capacity (TAC) in plasma and ascites fluid; and with ELISA, the levels of interleukin-6 (IL-6) and tumor necrosis factor alpha (TNF-α) were determined in patients with EOC. *Results*. In ascites fluid, a significant increase in 8-IP versus baseline plasma levels was found ($p = 0.002$). There was an important leakage of the TAC levels in ascites fluid versus baseline plasma levels ($p < 0.001$). The IL-6 was elevated in ascites fluid versus baseline plasma levels ($p = 0.003$), and there were diminished levels of TNF-α in ascites fluid versus baseline plasma levels ($p = 0.001$). *Discussion*. We hypothesize that the ascites fluid influences the behavior and dissemination of the tumor. Deregulation between oxidants, antioxidants, and the proinflammatory cytokines was found to vary among platinum-sensitive, platinum-resistant, and platinum-refractory patients.

1. Introduction

The risk of developing epithelial ovarian cancer (EOC) in females > 65 years old fluctuates ~0.36% in developing countries and 0.64% in developed countries, which makes EOC very frequent in women [1]. In Europe, little more than one-third of women with EOC survive five years after diagnosis because the majority are diagnosed in advanced stages [2]. Globally, about 75% of cases are diagnosed at stages III and IV [3]. The hypothetical theory of incessant ovulation suggests that repeat ovulation is responsible for the epithelial transformation of the ovaries because the epithelial cells that surround the zone where the follicular rupture occurred are exposed to mutagenic mediators of inflammation during the preovulatory period, with the capacity to produce genomic damage conducive to apoptosis and the excessive production of inflammation and oxidative stress [4]. However, recent studies have shown that EOC does not always present the typical characteristics of the mesodermal epithelium, which brings forth the hypothesis that the EOC originates in the fallopian tubes in the form of inclusion cysts that may or may not be present in the cancerous state [5, 6].

The majority of women with EOC have a high grade of malignancy, and ~84% are found in stage IIIC. The EOC spreads across the peritoneal surface affecting the pelvic and abdominal cavity. Stage IV (12–21%) is characterized by distal metastasis (hepatic/splenic) and extra-abdominal metastasis [7]. Malignant ascites has gained recognition as a unique form of tumor environment responsible for the characteristics of EOC. Ascites is considered an important component for tumor progression [8]. The link between the presence of ascites and the progression of EOC was proposed by Rocconi et al., and since then, numerous studies have contributed to the categorization of the components of ascites, revealing the importance of its role in EOC [9]. The cellular components of ascites contain an ample and complex, heterogeneous mix of cell populations, including tumoral and stromal cells, each one with a defined role, including fibroblasts, endothelial or mesothelial cells, adipocytes, stromal cells derived from adipose tissue, stem cells derived from bone marrow, and immune cells [10]. Some of the cellular components of stroma cells are capable of activating the vascular endothelial growth factor (VEGF) [11]. Ascites is an inflammatory fluid that can be produced in large quantities in EOC. One recent study reported that the IL-6 is strongly associated with advanced EOC and that the IL-6 findings could be useful in combination with serum levels of CA-125 to differentiate between benign tumors and EOC [12]. A study published in 2013 reported significantly increased levels of the marker of oxidative DNA damage (8-hydroxy-2-deoxyguanosine) and the 8-isoprostanes (a marker of oxidative stress) in peritoneal fluid in women with severe endometriosis [13]. Thus, it is of interest to study the behavior of diverse proinflammatory biomarkers (IL-6 and TNF-α) and oxidative stress (products of lipid peroxidation, 8-isoprostanes, and the total antioxidant capacity) in plasma and in ascites fluid in patients with EOC.

In the standard treatment for locally advanced EOC in stages III and IV [14] with criteria of inoperability due to carcinomatosis, it is recommended to administer tricyclic neoadjuvant platinum-based chemotherapy and taxanes, followed by intervals of surgery and consolidation with platinum-based chemotherapy [15]. When cytoreduction is not feasible, neoadjuvant therapy is recommended in patients sensitive to the medications, and afterwards, they will undergo cytoreductive surgery [16]. The election of chemotherapy is actually based, in part, on the duration and type of response to initial therapy: for platinum-sensitive illness (an interval free of disease progression ≥ 6 months from the end of the taxane/platinum treatment) and for platinum-resistant illness (<6 months), nonplatinum regimens are used: liposomal pegylated doxorubicin, topotecan, gemcitabine, etoposide, and taxanes, which have been demonstrated to have similar efficacy and acceptable for use in these patients [17]. Another management alternative for platinum-resistant patients is the bevacizumab. The bevacizumab is a recombinant humanized monoclonal antibody with antiangiogenic effect that binds with all of the isoforms of the vascular endothelial growth factor (VEGF). It is approved by the European Medicines Agency as a treatment for the first recurrence of platinum-sensitive EOC and for the management of various solid tumors in combination with cytotoxic chemotherapy [18]. Women who present with progression despite the platinum are considered platinum-refractory and present with the worst prognosis [19].

The objective of the study was to determine the behavior of markers of oxidative stress and inflammation in plasma and ascites fluid in platinum-sensitive, platinum-resistant, and platinum-refractory EOC patients.

2. Materials and Methods

In a prospective cohort with 12 months of follow-up, all females who attended the Hospital of Gynecology and Obstetrics, Department of Oncology and Gynecology, at the National Occidental Medical Centre of the Mexican Social Security Institute in Guadalajara, Jalisco, Mexico, who had ascites fluid and a preoperative diagnosis of EOC, and who agreed to sign the informed consent form, were included. Not included were minors whose parents or guardians did not agree for them to participate in the study, those who had antecedents of cancer in another organ or system, those who had received chemotherapy previously, or adult patients who did not agree to sign the informed consent.

A 5 mL baseline blood sample and a 2 mL sample of ascites fluid were obtained before the onset of chemotherapy. After 12 months, another blood sample (5 mL) was obtained. We included the plasma of 6 healthy women who came for a regular visit with the gynecologist and the data served to establish the normal levels of the reagents.

2.1. Biochemical Analysis. The blood samples were collected with 0.1% of ethylenediaminetetraacetic (EDTA). The plasma and ascites fluid were separated by centrifugation at 2000 rpm for 10 min at room temperature and stored at −80°C until processing. All technical readings of optical density were made with the Synergy HT (BioTek®) microplate reader.

2.2. TNF-α and IL6. The IL-6 and TNF-α levels were determined by ELISA, following the instructions of the kit manufacturer (PeproTech®, Rocky Hill, NJ 08553, USA). Both cytokines had a detection limit of 32 pg/mL. First, 100 μL of diluted capture antibody was added, followed by incubation overnight at room temperature. Then, 300 μL of blocking buffer was added to the wells and it was incubated for 1 h at room temperature. Plasma or ascites fluid and standards were added, followed by incubation for 2 h at room temperature. After several washings, 100 μL of diluted detection antibody was added and incubated at room temperature for 2 h. Then, 100 μL diluted HRP-avidin conjugate was added, followed by incubation for 30 min at room temperature. Finally, 100 μL of substrate solution was added to each well. The plate was read at a wavelength of 405 nm with correction set at 650 nm and was reported in pg/mL. The TNF-α intra-assay coefficient of variation (CV) was 2.1%, and the intra-assay CV for IL-6 was 4.7%.

2.3. Products of Lipid Peroxidation. The levels of lipoperoxides (LPO) in plasma and ascites fluid were measured using the FR22 assay kit (Oxford Biomedical Research Inc., Oxford,

MI, USA) according to the manufacturer's instructions. The limit of detection for this test was 0.1 nmol/mL. In this assay, the chromogenic reagent reacts with malondialdehyde (MDA) and 4-hydroxy-alkenals to form a stable chromophore. First, 140 μL of plasma or ascites with 455 μL of N-methyl-2-phenylindole in acetonitrile (Reagent 1) was diluted with ferric iron in methanol. Samples were agitated; after which, 105 μL 37% HCl was added, followed by incubation at 45°C for 60 min and centrifugation at 12,791 rpm for 10 min. Next, 150 μL of the supernatant was added and absorbance was measured at 586 nm. The curve pattern with known concentrations of 1,1,3,3-tetramethoxypropane in Tris-HCl was used. The intra-assay CV was 8.5%.

2.4. 8-Isoprostane (8-IP). The immunoassay reagent kit from Cayman Chemical Company® (Michigan, USA) was used according to the manufacturer's instructions. The limit of detection was of 0.8 pg/mL. The 8-IP assay was based on the principle of competitive binding between sample 8-IP, 8-IP acetyl cholinesterase (AChE) conjugate, and 8-IP tracer. Then, 50 μL of samples or standard was added to each well and 50 μL of 8-IP AChE tracer was added to all wells except the total activity and blank wells; and 50 μL of 8-IP enzyme immunoassay antiserum was added to all wells except the total activity and blank wells. At once, 50 μL of 8-IP antiserum was added to all wells except total activity, nonspecific binding, and blank wells. The plate was covered and incubated at 4°C for 18 h and then washed 5 times with buffer. Absorbance was read at 420 nm. The intra-assay CV was 12.5%.

2.5. Total Antioxidant Capacity. The evaluations of total antioxidant capacity (TAC) were made following the instructions of the kit manufacturer (Total Antioxidant Power Kit, number TA02.090130, Oxford Biomedical Research®), to obtain the concentration in mM equivalents of uric acid. The detection limit was of 0.075 mM. The samples and standards were diluted 1 : 40, and 200 μL was placed in each well. The plate was read at 450 nm as a reference value, 50 μL of copper solution was added, and the plate was incubated at room temperature for 3 minutes. Afterwards, 50 μL of stop solution was added and the plate was read at 450 nm. The dilution factor was considered in the final result. The intra-assay CV was 7.8%.

2.6. CA-125. The evaluations of CA-125 were made following the instructions of the kit manufacturer (ELSA-CA 125 II Cusbio Bioassays®, France). The assay was performed on serum samples. 100 μL of calibrators, control, or samples was placed in the corresponding groups of tubes. And 300 μL of 125 I anti-CA-125 monoclonal antibody was added to each ELSA tube. The tubes were gently mixed with a vortex-type mixer. The tubes were incubated for 20 ± 2 h at room temperature (18–25°C). The tubes were washed, and afterwards, 3 mL of distilled water was added to each tube and then emptied again. The process was repeated twice more. Finally, the radioactivity bound to the ELSA with gamma scintillation counter was measured. The detection limit was 0.5 U/mL.

2.7. Statistical Analysis. Continuous variables are expressed as mean ± standard deviation (SD) or standard error of the mean (SEM) and were analyzed with nonparametric tests according to the results obtained by the Kolmogorov-Smirnov test. For the comparisons between groups, the Mann–Whitney U test was used, and Kruskall Wallis test for baseline–final results. The categorical variables are presented as frequencies and percentages and were analyzed with the chi^2 test. A value of $p \leq 0.05$ was considered statistically significant, and the confidence interval was 95%.

2.8. Ethical Considerations. The scientific research study abides by the regulations of the internationally established guidelines of the Declaration of Helsinki 1964, revised in October 2013 at the World Medical Assembly. All procedures were performed according to regulations stipulated in the General Health Legal Guidelines for Healthcare Research in Mexico, 2nd Title, in Ethical Aspects for Research in Human Beings, Chapter 1, Article 17, corresponding to a Category II study as research with a minimal risk, in prospective studies that involve data risks through common procedures in physical, psychological, or diagnostic examinations or routine treatments, with Registration number R-2014-1310-38. All patients gave and signed the informed consent form in the presence of signed witnesses. Patients had the right to withdraw from the study at any time without representing harm to the patient-doctor relationship and without affecting their treatment. At all times, total confidentiality was maintained, and the patients were informed of the results throughout the study.

3. Results

Twenty-two patients with ovarian tumor and ascites were recruited, and follow-up was 12 months. One patient was excluded due to presenting with germinal ovarian cancer, because its management requires a chemotherapy treatment scheme that differs from platinum. Then, 21 patients with OEC cancer were included. The average age of all patients included was 53.24 years, with a range of 34–73 years and a mode of 46 years. Table 1 shows the demographic and clinical data. Baseline levels of the CA-125 antigen were measured in all groups. The platinum-refractory patients had the highest levels of the CA-125 antigen with 963.80 ± 363.80 U/mL, and because they perished prior to the end of the first year, final evaluations were not obtained. At the end of the study, the platinum-resistant patients had CA-125 antigen levels of 4211.95 ± 2105.98 U/mL despite the paclitaxel- and carboplatin-based chemotherapy. The platinum-refractory patients were found in the most advanced clinical stages (IIIC and IV), followed by the platinum-resistant (IIIB, IIIC, and IV) patients. Of the platinum-sensitive patients, 2 were in stage IIB and 4 were in stage IIIC. Malignant ascites was found in 7 platinum-sensitive, in 4 platinum-resistant, and in 7 platinum-refractory patients. Optimal cytoreduction was possible in all of the borderline patients, all of the platinum-sensitive patients, and 1 platinum-resistant patient. Suboptimal cytoreduction was possible in 3 platinum-resistant patients and 7 platinum-

Table 1: Ovarian cancer clinical data. A predominance of ovarian serous cystadenocarcinoma with malignant ascites can be observed. Cytoreduction was optimal in 14 patients and suboptimal in 10 patients: only 10 patients were platinum-sensitive, 4 platinum-resistant, and 7 platinum-refractory (all 7 perished during the first year). The majority of patients were discovered in advanced stages.

	Platinum-sensitive	Platinum-resistant	Platinum-refractory
Weight (kg)	69 ± 19	75 ± 25	46 ± 21
Body mass index (BMI)	27 ± 7	30 ± 9	21 ± 4
Ag CA-125 baseline U/mL	607.37 ± 183.13	915.8 ± 373.87	963 ± 363.80
Ag CA-125 final U/mL	21.87 ± 6.59	4211.95 ± 2105.98	62.6 ± 25.56
Clinical stage			
IC	2		
IIB	2		
IIIB	2	1	
IIIC	4	2	5
IV		1	2
Histology	9 Cystadenocarcinoma 1 Undifferentiated	3 Cystadenocarcinoma 1 Endometrioid type	6 Cystadenocarcinoma 1 Endometrioid type
Ascites	3 Positive		
Malignant ascites	7 Positive	4 Positive	7 Positive
Cytoreduction	10 Optimal	3 Suboptimal 1 Optimal	7 Suboptimal
Cycle frequency days	21	21	5–1 cycle 1–6 cycles 1-2 cycles
Carboplatin (mg)	570 ± 109	471 ± 187	464 ± 124
Paclitaxel (mg)	300 ± 39	273 ± 106	254 ± 63
Deceased		2	7

refractory patients. All of the platinum-sensitive and platinum-resistant patients and 1 platinum-refractory patient received the 6 complete cycles of chemotherapy with intervals of 21 days. All of the 7 platinum-refractory patients perished, 5 of them during the first chemotherapy cycle; and 2 platinum-resistant patients died during the study period (Table 1).

The analysis of the results of the markers of oxidative stress and inflammation initially included all of the patients.

3.1. 8-Isoprostanes. The plasma levels of 8-IP for healthy controls had 12.35 ± 1.47 pg/mL. The baseline plasma levels of the 8-IP marker were 15.13 ± 1.50 pg/mL and final 16.90 ± 1.60 pg/mL, similar to those of the healthy controls. However, in ascites fluid, the 8-IP levels were significantly increased with 117.40 ± 62.70 ($p = 0.002$) versus healthy controls and versus baseline–final results. The 8-IP plasma levels, depending on the response to platinum, were similar in all groups: platinum-sensitive had 13.60 ± 2.14 pg/mL, platinum-resistant 10.40 ± 1.70 pg/mL, and platinum-refractory had 19.20 ± 2.80 pg/mL, without a significant difference versus healthy controls. Levels of the 8-IP marker in ascites fluid were significantly elevated among the different treatment groups ($p = 0.03$): 8-IP levels in platinum-sensitive patients were 86.62 ± 26.70 pg/mL, platinum-resistant patients had 36.70 ± 23.80 pg/mL, and platinum-refractory patients had 17.10 ± 1.50 pg/mL (Table 2).

3.2. LPO. Plasma levels of LPO in healthy controls were 2.68 ± 0.28 μM. The levels in all patients included were as follows: baseline 2.70 ± 0.30 μM and final 2.60 ± 0.30 μM. Findings showed elevated levels of LPO in ascites fluid with 12.60 ± 5.80 μM versus healthy controls, without a significant difference (Table 3). The plasma LPO levels between the different groups of EOC patients were similar: platinum-sensitive patients had 2.70 ± 0.29 μM, platinum-resistant patients had 1.78 ± 0.25 μM, and platinum-refractory patients had 3.20 ± 0.78 μM, without significant difference versus healthy controls (Table 4). The plasma LPO levels baseline–final did not demonstrate significant changes. The evaluation of LPO in ascites fluid among the groups treated with platinum produced significant differences ($p = 0.05$). The platinum-sensitive patients obtained 14.90 ± 9.30 μM, the platinum-resistant patients, 27.10 ± 23.90 μM, and the platinum-refractory patients had 3.40 ± 1.50 μMm (Table 2).

3.3. Total Antioxidant Capacity. The normal plasma levels of TAC in the healthy control group were 429.42 ± 61.50 mM versus the significant elevation found in the ascites fluid of all patients, 909.30 ± 78.60 mM ($p = 0.001$). In plasma, a significant decrease of TAC was found in the baseline evaluations with 294.40 ± 24.10 mM versus the amount found in ascites fluid ($p = 0.03$). The final evaluation was slightly increased with 337.80 ± 17.10 mM (Table 3). Table 4 shows the baseline plasma levels of platinum-sensitive

Table 2: Oxidative and inflammatory status in ascites due to ovarian cancer. The significant difference between study groups treated with platinum and the concentrations of LPO and 8-IP in ascites fluid is noteworthy.

	Platinum-sensitive	Platinum-resistant	Platinum-refractory	p^* (K-W)
Antioxidant				
TAC mM trolox	871.00 ± 137.90	899.90 ± 152.70	1008.80 ± 138.90	0.60
Oxidants				
LPO μM	14.90 ± 9.30	27.10 ± 23.90	3.40 ± 1.50	**0.05***
8-IP pg/mL	86.62 ± 26.70	36.70 ± 23.80	17.10 ± 1.50	**0.03***
Proinflammatory cytokines				
IL-6 pg/mL	1582.60 ± 346.10	969.60 ± 76.30	1382.30 ± 257.60	0.31
TNF-α pg/mL	146.10 ± 62.80	102.00 ± 27.50	75.10 ± 17.90	0.52

TAC: total antioxidant capacity; LPO: lipoperoxides; 8-IP: isoprostanes; IL-6: interleukin-6; TNF-α: tumor necrosis factor alpha; K-W: Kruskall-Walis test.
*Comparison between treatment response groups.

patients with 283.80 ± 33.30 mM, platinum-resistant with 179.10 ± 18.40 mM, and platinum-refractory with 393.40 ± 31.60 mM, with a significant difference between the different groups in response to platinum ($p = 0.015$). The final results did not produce significant changes compared to baseline. A significant difference was found between plasma levels of all groups versus healthy controls ($p = 0.007$). In evaluations of TAC in ascites fluid, an increase, without significant difference, was found between the different responses to platinum-based chemotherapy (Table 2): the platinum-sensitive patients had 871.00 ± 137.90 mM, platinum-resistant had 899.90 ± 152.70 mM, and platinum-refractory had 1008.80 ± 138.90.

3.4. IL-6. In ascites fluid, a significant increase in the levels of IL-6 was found, with 1342.30 ± 188.90 pg/mL ($p = 0.007$), versus plasma levels of healthy controls with 448.34 ± 279.00 pg/mL. IL-6 plasma baseline levels were 703.50 ± 162.40 pg/mL ($p = 0.03$ versus ascites fluid) and final 855.90 ± 327.90. (Table 3) There were no significant differences displayed among the different groups in plasma levels of IL-6: platinum-sensitive patients had 936.40 ± 284.60 pg/mL, platinum-resistant patients had 834.20 ± 31.00 pg/mL, and platinum-refractory patients had 363.60 ± 105.00 pg/mL, without a significant difference versus healthy controls. Despite the plasma levels of IL-6 in platinum-sensitive patients being elevated at 936.40 ± 284.60 pg/mL, there were no significant differences with all the other treatment groups including the control group (Table 4). The plasma levels in baseline–final results were similar in healthy controls and among the different groups subjected to platinum-based chemotherapy. Also, IL-6 levels in ascites fluid between the different groups included in the study were increased but not different (Table 2).

3.5. TNF-α. In the general evaluation of TNF-α, plasma levels in healthy controls were 160.30 ± 12.70 pg/mL, with a decrease of this cytokine in ascites fluid to 120.80 ± 30.90 pg/mL. However, the overall baseline plasma levels of TNF-α were significantly elevated with 190.40 ± 17.90 pg/mL versus levels in ascites fluid ($p = 0.001$) (Table 3). Plasma levels of TNF-α were similar in healthy controls and platinum-sensitive patients with 201.10 ± 30.00 pg/mL, in platinum-resistant patients with 249.80 ± 28.50 pg/mL and the platinum-refractory patients with 145.40 ± 22.30 pg/mL (Table 4). Also, plasma levels of TNF-α were similar in healthy controls and in the baseline–final results of all the different types of responses to chemotherapy. In addition, a significant difference was not found in levels of this cytokine in ascites fluid in the different groups treated with platinum (Table 2).

4. Discussion

Ovarian cancer is the primary cause of deaths by gynecological neoplasms. According to estimations by the American Cancer Society in 2014, 21,980 new cases of EOC were expected and 14,270 deaths due to EOC [20]. In Mexico, EOC represents 4% of neoplasms, occupies the third place in cases of cancer in females after cancer of the cervix and breast, and is considered the second cause of death due to cancer [21]. The States in the Republic of Mexico with the highest incidence of EOC are Monterrey, Mexico State, and the District Capital (Mexico City) [17]. The serous subtype of EOC was the most frequently found in the present study. It should be recognized that surgery in EOC is not only the cornerstone of treatment but it also plays an important role in the histological diagnosis and staging of the tumor [22]. The majority of patients in the study presented with advanced illness when they sought medical attention; therefore, relapses of the illness were expected even with the administration of standard, adjuvant, platinum-based chemotherapy and primary cytoreductive surgery. Survival free of progression in stage III is about ~17 months, and the global average survival can reach 45 months [23]. The patients who have short intervals without treatment (platinum-resistant) or who have never been in total remission (platinum-refractory) have response rates objective to second-line chemotherapy of about ~10–15% [24].

All of the platinum-refractory patients (100%) and 2 (50%) of the platinum-resistant patients perished soon after entering the study. Serum evaluation of the CA-125 antigen is considered fundamental in the diagnosis and in changes in levels after treatment, since it is a marker of response to treatment and forms part of the management criteria to follow [25]. In the current study, the CA-125 antigen

Table 3: Oxidative and inflammatory state in ovarian cancer. A significant increase of the 8-IP marker in ascites fluid versus baseline plasma levels can be observed. Also, an important leakage of antioxidants (TAC) in ascites fluid compared to plasma levels of healthy controls and the baseline TAC evaluations. A significant increase of IL-6 in ascites fluid versus baseline plasma levels was found. The TNF-α was significantly diminished in ascites and elevated in baseline evaluations.

	Healthy control plasma	Ascites	$^{₮}p$ = HC versus ascites	$^{¥}p$ = HC versus baseline	Plasma		$^{¤}p$ = baseline–final	$^{\$}p$ = plasma baseline versus ascites
					Basal	Final		
Oxidants								
8-IP pg/mL	12.35 ± 1.47	117.40 ± 62.70	**0.01**	0.48	15.13 ± 1.50	16.90 ± 1.60	0.14	**0.002**
LPO μM	2.68 ± 0.28	12.60 ± 5.80	0.50	0.56	2.70 ± 0.30	2.60 ± 0.30	0.26	0.11
Antioxidant								
TAC mM trolox	429.42 ± 61.50	909.30 ± 78.60	**0.001**	**0.03**	294.40 ± 24.10	337.80 ± 17.10	0.19	**<0.001**
Proinflammatory cytokines								
IL-6 pg/mL	448.34 ± 28.00	1342.30 ± 188.90	**0.007**	0.42	703.50 ± 162.40	855.90 ± 327.90	0.31	**0.003**
TNF-α pg/mL	160.30 ± 12.70	120.80 ± 30.90	0.06	0.36	190.40 ± 17.90	164.40 ± 34.22	0.18	**0.001**

TAC: total antioxidant capacity. $^{₮}$Healthy control (HC) versus ascites Mann–Whitney *U* test. $^{¥}$HC versus baseline plasma Mann–Whitney *U* test. $^{¤}$Baseline–final Wilcoxon test. $^{\$}$Baseline plasma versus ascites Mann–Whitney *U* test.

Table 4: Oxidative and inflammatory status in plasma due to ovarian cancer in all patients. Noteworthy are the levels in healthy controls versus the study groups and the significant difference depending on the response to platinum in relation to total antioxidant capacity.

	Healthy control	Platinum-sensitive	Platinum-resistant	Platinum-refractory	p^* (K-W)	p^{**} (K-W)
Antioxidant						
TAP mM trolox	429.42 ± 61.50	283.80 ± 33.30	179.10 ± 18.40	393.40 ± 31.60	**0.007**	**0.015**
Oxidants						
8-IP pg/mL	12.35 ± 1.47	13.60 ± 2.14	10.40 ± 1.70	19.20 ± 2.80	0.26	0.22
LPO μM	2.68 ± 0.28	2.70 ± 0.29	1.78 ± 0.25	3.20 ± 0.78	0.38	0.32
Proinflammatory cytokines						
IL-6 pg/mL	448.34 ± 28.00	936.40 ± 284.60	834.20 ± 31.00	369.60 ± 105.00	0.44	0.33
TNF-α pg/mL	160.30 ± 12.70	201.10 ± 30.00	249.80 ± 28.50	145.40 ± 22.30	0.27	0.21

*Comparison between the study groups with the healthy control. **Comparison between the study groups. TAC: total antioxidant capacity; LPO: lipoperoxides; 8-IP: isoprostanes; IL-6: interleukin-6; TNF-α: tumor necrosis factor alpha; K-W: Kruskall Wallis test.

was importantly incremented in the final evaluations of the platinum-resistant patients.

One of the characteristics of EOC is the production of ascites fluid. It should be considered that ascites forms an interesting tumor microenvironment, enriched with signals that favor proliferation of the tumor through invasion and antiapoptotic molecules, and so contributes to resistance to chemotherapy and tumor heterogeneity [8]. The profile of cytokines in ascites in EOC has demonstrated the presence of protumorigenic and antitumorigenic factors in the microenvironment, with elevated levels of protumorigenic cytokines that include IL-6, IL-8, IL-10, IL-15, IP-10, MCP-1, MIP-1β, and the VEGF, and the significant decrease in levels of the IL-2, IL-5, IL-7, and IL-17 and the platelet-derived growth factor [26]. These factors contribute in a cumulative way to the creation of the proinflammatory and immunosuppressor microenvironment that favors tumor proliferation [27] The IL-6 and the IL-10 have received major attention owing to their correlation to poor prognosis and inadequate response to treatment [12].

In 2012, the profile of cytokines in ascites was reported in 10 patients with EOC where the greatest expressions of various inflammation regulator factors were demonstrated, including IL-6, IL-6R, IL-8, IL-10, leptin, osteoprotegerin, and the urokinase-type plasminogen activator [28]. Also, the authors demonstrated that the increase in IL-6 in ascites fluid is an independent factor of poor prognosis for EOC [29]. The role of the IL-6 contributes to the progression of EOC by inhibiting apoptosis, stimulation of angiogenesis, increasing migration, and stimulation of cellular proliferation [28].

In the present study, we found an important increase in plasma levels of IL-6 baseline–final ($p = 0.003$) in all patients included, and levels of IL-6 in ascites fluid were elevated significantly versus healthy controls, as expected ($p = 0.007$). The implication of IL-6 in the pathogenesis of EOC is well-documented: it seems the primary source of IL-6 secreted in biological fluids is produced by the tumor tissue [30]. The ovarian tumor cells produce the stimulating factor of the macrophage colonies, and this factor is a potent chemical attractor for the monocytes that stimulates the monocytes and macrophages to produce TNF-α, IL-1α, or IL-1β; all with the capacity to stimulate the growth of the ovarian tumor cells [31]. In the present study, we found diminished levels of TNF-α in ascites fluid and significant increases in plasma in the baseline evaluations in all patients.

On the other hand, ascites is also very attractive as a resource for studies in discovering other biomarkers. Here, we found a significant increase in the 8-IP marker in ascites fluid ($p = 0.01$) and in the baseline plasma evaluations ($p = 0.02$) in all of the patients included. The plasma LPOs, in all evaluations, did not reveal any significant differences, although in ascites fluid in platinum-resistant patients there was a significant increase ($p = 0.05$) of LPO versus the platinum-refractory patients who had very low levels of LPO. Interestingly, we found a significant elevation of TAC in ascites ($p = 0.001$) and a decrease in this concentration in the baseline plasma results ($p = 0.031$), which suggests an important leakage of the antioxidants in the ascites fluid. Upon searching the literature, there were no available reports on the behavior of the markers 8-IP, LPO, and TAC in plasma and ascites fluid. Ascites is a proximal fluid with the capacity to reveal events in the early stages of EOC because the concentration of soluble factors associated with cancer tends to be much higher in ascites than in serum or plasma, which makes malignant ascites a promising source for investigation of diverse diagnostic, therapeutic, and prognostic markers [32].

In conclusion, EOC is a heterogeneous neoplasm with diverse responses to standard platinum-based treatment and cytoreductive surgery, which makes it a priority to develop new prognostic markers prior to treatment that identify patients who could have poor response to standard platinum-based chemotherapy.

The limitations of the study are based on the small number of patients included and the short length of follow-up.

Conflicts of Interest

The authors have no conflicts of interest to report.

References

[1] J. Ferlay, I. Soerjomataram, R. Dikshit et al., "Cancer incidence and mortality worldwide: sources, methods and major patternas," *International Journal of Cancer*, vol. 136, no. 5, pp. E359–E386, 2015.

[2] M. Sant, T. Aareleid, F. Berrino et al., "EUROCARE-3: survival of cancer patients diagnosed 1990-94-results and commentary," *Annals of Oncology*, vol. 14, Supplement 5, pp. v61–v118, 2003.

[3] K. A. Kujawa and K. M. Lisowska, "Ovarian cancer—from biology to clinic," *Postępy Higieny I Medycyny Doświadczalnej*, vol. 69, pp. 1275–1290, 2015.

[4] M. F. Fathalla, "Incessant ovulation—a factor in ovarian neoplasia?," *The Lancet*, vol. 298, no. 7716, p. 163, 1971.

[5] K. Levanon, C. Crum, and R. Drapkin, "New insights into the pathogenesis of serous ovarian cancer and its clinical impact," *Journal of Clinical Oncology*, vol. 26, no. 32, pp. 5284–5293, 2008.

[6] J. Li, O. Fadare, L. Xiang, B. Kong, and W. Zheng, "Ovarian serous carcinoma: recent concepts on its origin and carcinogénesis," *Journal of Hematology & Oncology*, vol. 5, p. 8, 2012.

[7] A. P. Heintz, F. Odicino, P. Maisonneuve et al., "Carcinoma of the ovary," *International Journal of Gynaecology and Obstetrics*, vol. 95, Supplement 1, pp. S161–S192, 2006.

[8] J. Ren, Y. J. Xiao, L. S. Singh et al., "Lysophosphatidic acid is constitutively produced by human peritoneal mesothelial cells and enhances adhesion, migration, and invasion of ovarian cancer cells," *Cancer Research*, vol. 66, no. 6, pp. 3006–3014, 2006.

[9] R. P. Rocconi, J. M. Straughn Jr., C. A. Leath 3rd et al., "Pegylated liposomal desorubicin consolidation therapy after platinum/paclitaxel-based chemotherapy for suboptimally debulked, advanced-stage epitelial ovarian cáncer patients," *The Oncologist*, vol. 11, no. 4, pp. 336–341, 2006.

[10] N. A. Bhowmick, E. G. Neilson, and H. L. Moses, "Stromal fibroblasts in cancer initiation and progression," *Nature*, vol. 432, pp. 332–337, 2004.

[11] M. Pasquet, M. Golzio, E. Mery et al., "Hospicells (ascites-derived stromal cells) promote tumorigenicity and angiogenesis," *International Journal of Cancer*, vol. 126, no. 9, pp. 2090–2101, 2010.

[12] D. Lane, I. Matte, P. Garde-Granger et al., "Inflammation-regulating factors in ascites as predictive biomarkers of drug resistance and progression-free survival in serous epithelial ovarian cancers," *BMC Cancer*, vol. 15, p. 492, 2015.

[13] G. Polak, I. Wertel, B. Barczyński, W. Kwaśniewski, W. Bednarek, and J. Kotarski, "Increased levels of oxidative stress markers in the peritoneal fluid of women with endometriosis," *European Journal of Obstetrics, Gynecology, and Reproductive Biology*, vol. 168, no. 2, pp. 187–190, 2013.

[14] J. Prat and FIGO Committee on Gynecologic Oncology, "FIGO's staging classification for cancer of the ovary, fallopian tube, and peritoneum: abridged republication," *Journal of Gynecologic Oncology*, vol. 26, no. 2, pp. 87–89, 2015.

[15] Y. Ansquer, E. Leblanc, K. Clough et al., "Neoadjuvant chemotherapy for unresectable ovarian carcinoma: a French multicenter study," *Cancer*, vol. 91, no. 12, pp. 2329–2334, 2001.

[16] I. Vergote, I. de Wever, W. Tjalma, M. V. Gramberen, J. Decloedt, and P. V. Dam, "Interval debulking surgery: an alternative for primary surgical debulking?," *Seminars in Surgical Oncology*, vol. 19, no. 1, pp. 49–53, 2000.

[17] Cancer Genome Atlas Research Network, "Integrated genomic analyses of ovarian carcinoma," *Nature*, vol. 474, no. 7353, pp. 609–615, 2011.

[18] S. Ramakrishnan, I. V. Subramanian, Y. Yokoyama, and M. Geller, "Angiogenesis in normal and neoplastic ovaries," *Angiogenesis*, vol. 8, no. 2, pp. 169–182, 2005.

[19] L. Stewart and Advanced Ovarian Cancer Trialists Group, "Chemotherapy for advanced ovarian cáncer. Advanced Ovarian Cancer Trialists Group," *Cochrane Database of Systematic Reviews*, vol. 2, article CD001418, 2000.

[20] American Cancer Society, *Cancer Facts & Figures*, 2014.

[21] Instituto Nacional de Estadística, Geografía e Informática de México, *II conteo de población y vivienda 2005*, 2005, Base de datos.

[22] J. S. Berek, M. Friedlander, and N. F. Hacker, "Epithelial ovarian, fallopian tube, and peritoneal cáncer," in *Berek & Hacker's Gynecologic Oncology*, J. S. Berek and N. F. Hacke, Eds., pp. 443–508, Lippincott Williams & Wilkins, Philadelphia, 2010.

[23] W. E. Winter 3rd, G. L. Maxwell, C. Tian et al., "Prognostic factors for stage III epithelial ovarian cancer: a gynecologic oncology group study," *Journal of Clinical Oncology*, vol. 25, pp. 3621–3627, 2007.

[24] T. Arimoto, S. Nakagawa, K. Oda, K. Kawana, T. Yasugi, and Y. Taketani, "Second-line chemotherapy with docetaxel and carboplatin in paclitaxel and platinum-pretreated ovarian, fallopian tube, and peritoneal cáncer," *Medical Oncology*, vol. 29, no. 2, pp. 1253-1254, 2012.

[25] K. K. Zorn, C. Tian, W. P. McGuire et al., "The prognostic value of pretreatment CA 125 in patients with advanced ovarian carcinoma: a gynecologic oncology group study," *Cancer*, vol. 115, no. 5, pp. 1028–1035, 2009.

[26] I. Matte, D. Lane, C. Laplante, C. Rancourt, and A. Piche, "Profiling of cytokines in human epithelial ovarian cancer ascites," *American Journal of Cancer Research*, vol. 2, no. 5, pp. 566–580, 2012.

[27] R. L. Giuntoli 2nd, T. J. Webb, A. Zoso et al., "Ovarian cancer-associated ascites demonstrates altered immune environment: implications for antitumor immunity," *Anticancer Research*, vol. 29, no. 8, pp. 2875–2884, 2009.

[28] S. Cohen, I. Bruuchim, D. Graiver et al., "Platinum-resistance in ovarian cancer cells is mediated by IL-6 secretion via the increased expression of its target cIAP-2," *Journal of Molecular Medicine*, vol. 91, pp. 357–368, 2013.

[29] D. Lane, I. Matte, and A. Piché, "Prognostic significance of IL-6 and IL-8 ascites levels in ovarian cancer patients," *BMC Cancer*, vol. 11, p. 210, 2011.

[30] S. Masoumi-Moghaddam, A. Amini, A. Q. Wei, G. Robertson, and D. L. Morris, "Intratumoral interleukin-6 predicts ascites formation in patients with epithelial ovarian cancer: a potential tool for close monitoring," *Journal of Ovarian Research*, vol. 8, p. 58, 2015.

[31] S. Wu, C. M. Boyer, R. S. Whitaker, A. Berchuck, J. R. Wiener, and J. B. Weinberg, "Tumor necrosis factor alpha as an autocrine and paracrine growth factor for ovarian cancer: monokine induction of tumor cell proliferation and tumor necrosis factor alpha expression," *Cancer Research*, vol. 53, no. 8, pp. 1939–1944, 1993.

[32] V. O. Shender, M. S. Pavlyukov, R. H. Ziganshin et al., "Proteome-metabolome profiling of ovarian cancer ascites reveals novel components involved in intercellular communication," *Molecular & Cellular Proteomics*, vol. 13, no. 12, pp. 3558–3571, 2014.

Hindawi
Oxidative Medicine and Cellular Longevity
Volume 2017, Article ID 1740317, 12 pages
https://doi.org/10.1155/2017/1740317

Research Article

Effect of Emodin on Preventing Postoperative Intra-Abdominal Adhesion Formation

Guangbing Wei,[1] Yunhua Wu,[1] Qi Gao,[1] Cancan Zhou,[2] Kai Wang,[1] Cong Shen,[3] Guanghui Wang,[1] Kang Wang,[1] Xuejun Sun,[1] and Xuqi Li[1]

[1]*Department of General Surgery, The First Affiliated Hospital of Xi'an Jiaotong University, Xi'an, Shaanxi 710061, China*
[2]*Department of Hepatobiliary Surgery, The First Affiliated Hospital of Xi'an Jiaotong University, Xi'an, Shaanxi 710061, China*
[3]*Department of Medical Imaging, The First Affiliated Hospital of Xi'an Jiaotong University, Xi'an, Shaanxi 710061, China*

Correspondence should be addressed to Xuejun Sun; sunxy@mail.xjtu.edu.cn and Xuqi Li; lixuqi@163.com

Received 12 February 2017; Revised 2 May 2017; Accepted 29 May 2017; Published 2 August 2017

Academic Editor: Luciano Saso

Background. Postoperative intra-abdominal adhesions are a major complication after abdominal surgery. Although various methods have been used to prevent and treat adhesions, the effects have not been satisfactory. Emodin, a naturally occurring anthraquinone derivative and an active ingredient in traditional Chinese herbs, exhibits a variety of pharmacological effects. In our study, we demonstrated the effect of emodin treatment on preventing postoperative adhesion formation. *Materials and Methods*. A total of 48 rats were divided into six groups. Abdominal adhesions were created by abrasion of the cecum and its opposite abdominal wall. In the experimental groups, the rats were administered daily oral doses of emodin. On the seventh day after operation, the rats were euthanized, and blood and pathological specimens were collected. Abdominal adhesion formation was evaluated by necropsy, pathology, immunohistochemistry, Western blot, and enzyme-linked immunosorbent assay analyses. *Results*. Abdominal adhesions were markedly reduced by emodin treatment. Compared with the control group, collagen deposition was reduced and the peritoneal mesothelial completeness rate was higher in the emodin-treated groups. Emodin had anti-inflammatory effects, reduced oxidative stress, and promoted the movement of the intestinal tract ($P < 0.05$). *Conclusion*. Emodin significantly reduced intra-abdominal adhesion formation in a rat model.

1. Introduction

Intra-abdominal adhesion formation is a major complication after abdominal surgery. Patients have a 90%–95% risk of developing intraperitoneal adhesions after laparotomy [1, 2], which is one of the most upsetting complications after gastrointestinal surgery. Peritoneal adhesions can cause various problems, such as small-bowel obstruction, female infertility, chronic abdominal pain, and increased difficulty during reoperation, all of which greatly influence quality of life and increase medical costs [3–5]. The strategies to treat and prevent adhesions can be divided into four categories: general principles, surgical techniques, chemical agents, and mechanical barriers [6, 7]. Although several methods have been applied to prevent adhesion formation, a "gold standard" for treatment has not been determined yet, and surgeons still need to seek more effective methods to prevent and treat postoperative abdominal adhesions [8].

The formation of abdominal adhesions is a complex process that involves inflammation, angiogenesis, fibrinolysis, peritoneal tissue repair, and other biochemical events [4, 9–11]. When injury or trauma occurs in the abdominal cavity, ischemia of the local area occurs and inflammatory and coagulation cascades are activated within a few minutes. Inflammatory cells, such as neutrophils and macrophages, and tissue repair cells will migrate to the injured area, and the coagulated blood will form a fibrin mesh [12, 13]. Then, after approximately 24 hours, the mesothelium will start to grow, followed by fibroblast proliferation on day 3 and angiogenesis on day 5. If the peritoneum repairs well and the fibrin mesh is absorbed, the adhesions are very minor; otherwise, abdominal adhesions will form [2, 4]. Fibroblasts

and the inflammatory system play major roles in the mechanism of abdominal adhesion formation [2, 14, 15]. Intestinal movements also play an important role in the formation of abdominal adhesion [16]. Early movement of the bowel disrupts the fibrin bridges and inhibits fibroblast invasion into the adhesive tissues. Additionally, mobilization encourages fibrinolysis through increased fluid movement and metabolite exchange in the peritoneum [16, 17].

Emodin (1,3,8-trihydroxy-6-methylanthraquinone) is a naturally occurring anthraquinone derivative and an active ingredient in traditional Chinese herbs, including *Rheum palmatum*, *Polygonum cuspidatum*, *Polygonum multiflorum*, *Aloe vera*, and *Cassia obtusifolia*. Emodin exhibits a variety of pharmacological benefits in pharmacological studies [18]. According to previous studies [18–21], emodin has been demonstrated to have various effects, including antiviral, antibacterial, antiallergenic, antiosteoporotic, antidiabetic, anti-inflammatory, and antitumor effects, and can reduce oxidative stress. Moreover, emodin can decrease collagen deposition in pancreatitis and pulmonary injuries and downregulate the TGF-β signaling pathway in many human cancers [20, 22]. As a laxative drug in traditional Chinese herbs [23], the primary effect of emodin is promoting intestinal movement. Since inflammation, collagen deposition, oxidative stress, and intestinal movement all play important roles in postoperative intra-abdominal adhesion formation, we speculated that emodin may reduce postoperative adhesion formation. In this study, we intended to demonstrate that emodin can prevent postoperative abdominal adhesion formation.

2. Materials and Methods

2.1. Animals and Chemicals. A total of 48 Sprague-Dawley rats weighing 200 to 250 g were purchased from the Experimental Animal Center of Xi'an Jiaotong University. The animals were treated in a humane manner in accordance with the Declaration of Helsinki. All animals were fed ad libitum with a commercial diet and had continuous access to fresh water. The animals were housed under standard laboratory conditions at $22 \pm 2^{\circ}$C. This experiment was accomplished in the Xi'an Jiaotong University Experimental Research Laboratory with the consent of the Experimental Animals Ethics Committee [24].

Emodin (PubChem CID: 10207) was purchased from Sigma-Aldrich Co. LLC® (St. Louis, MO) and was dissolved in 0.5% sodium carboxymethyl cellulose (0.5% CMC-Na®; Henan Qianzhi Company, Henan, China) at different concentrations [25].

2.2. Study Design and Surgical Procedure. All rats were fasted, and the hair on their abdomen was removed one day before surgery. The rats were equally divided into six groups. The animals were deeply anesthetized by an intraperitoneal injection of 50 mg/kg barbital sodium (Guidechem, Shanghai, China), and the abdominal skin was disinfected with povidone-iodine before the operation. As previously described [3, 26, 27], a vertical midline incision (2-3 cm long) was made, except in the animals with previous intra-abdominal adhesion formation. Excluding the sham operation group, the anterior surface of each cecum was scraped with a soft swab 40 times, which induced slight serosal hemorrhage resulting in the formation of surface lesions in an area of approximately 1.5 cm × 1.5 cm. The rat abdominal wall opposite to the scratched cecum was treated in the same manner. Prior to closing the abdominal cavity, the cecum was placed in its original position opposite to the wounded abdominal wall in full contact with each other. In the sham operation group, the rats did not undergo the abdominal adhesion formation procedure. In the sodium hyaluronate group, 2 mL of medical-grade hyaluronate gel (Qingdao Haitao Biochemical Co. Ltd., Qingdao, China) was daubed on the abraded area before closing the abdominal cavity. The abdomen was closed in two layers using interrupted 3-0 Vicryl® sutures. After the operation, the rats in the three experimental groups were orally administered 20 (low-dose group), 40 (middle-dose group), or 80 (high-dose group) mg/kg emodin daily. The sham operation group and the control group were orally administered the same amount of 0.5% CMC-Na once per day for one week.

2.3. Adhesion Grading and Assessment. One week after surgery, all animals were anesthetized as previously described, and a reverse U incision was performed to assess the adhesions. Adhesion formation was measured by two independent researchers who were blinded to the study protocol, according to the method described by Hoffmann et al. [28] and Lauder et al. [29]. The Hoffmann's scoring scheme considers the number, strength, and distribution of adhesions. Lauder's schemes were measured and expressed as a percent of the total deperitonealized surface area [7] (Supplementary Tables 1 and 2 available online at https://doi.org/10.1155/2017/1740317). After adhesion grading was performed, the tissues and blood serum were collected for the next experiments.

2.4. Histopathological Evaluation. Hematoxylin and eosin staining was used to evaluate the inflammation and fibrillation condition. After 24 hours of fixation, the adhesion tissues of the injured cecum wall and parietal peritoneum were embedded in paraffin and then cut into 4 μm thick serial paraffin sections. A portion of the paraffin sections was stained by hematoxylin and eosin to observe the morphology and adhesion conditions of the tissues. Histopathological evaluations of fibrosis and inflammation were made by light microscopy. The stained sections were evaluated by two pathologists from the Pathology Department of the First Affiliated Hospital of Xi'an Jiaotong University who were blinded to the experimental groups. At least five randomly selected high-power fields were reviewed for each section, and at least four sections per rat were evaluated and graded using the scoring system described in Supplementary Table 3 [30, 31].

2.5. Masson Staining for Collagen Deposition. A subset of the paraffin sections was used for Masson staining to observe the collagen content. The paraffin sections were stained using a Masson staining kit (Bogoo Biotechnology

Co. Ltd., Shanghai, China) following the manufacturer's instructions. The percentage of positive staining was assessed by the Image-Pro Plus 5.0 software (Leica Qwin Plus, Leica Microsystem Imaging Solutions Ltd., Cambridge, UK). Eight microscopic fields were randomly selected to measure the average collagen thickness in the adhesive tissues.

2.6. Immunohistochemical Staining. Immunohistochemical staining was used to assess collagen deposition (α-SMA, MMP-9), mesothelial cell healing (CK-18), and gastrointestinal dynamics (C-kit) and was performed using a streptavidin-biotin kit (Maxim, Fuzhou, China) following the manufacturer's instructions. The sections were deparaffinized and rehydrated, incubated with 30 g/L hydrogen peroxide solution at room temperature for 5 minutes, and blocked with goat serum. Subsequently, the sections were incubated with mouse anti-rat α-smooth muscle actin (α-SMA; 1 : 100 dilution, Santa Cruz Biotechnology, Dallas, TX, USA), tyrosine kinase receptor (C-kit; 1 : 100 dilution, Abcam, UK), cytokeratin-18 (CK-18; 1 : 50 dilution, Abcam, UK), and matrix metalloproteinase-9 antibodies (MMP-9; 1 : 100 dilution, Abcam) at 4°C overnight. The sections were then incubated with biotinylated rabbit anti-mouse IgG for 20 minutes. Incubation with streptavidin-biotin peroxidase complex at 37°C was performed for another 20 minutes. The sections were washed in phosphate-buffered saline four times for 5 minutes per wash. Diaminobenzidine tetrahydrochloride was used for visualization, and hematoxylin was used as the counterstain. The sections were dehydrated, mounted, and sealed. To evaluate the expression of these indicators, at least five random high-power fields of adhesion tissue were reviewed for each section as described in the histopathological evaluation. Then, the CK-18 stain was used to assess the completeness rate of the mesothelial cells. The rate was calculated by the stained mesothelial cell length in the adhesion tissue divided by the total mesothelial cell length in the selected fields. The α-SMA, C-kit, and MMP-9 scoring system is as follows: 0—no expression, 1—low expression, 2—moderate expression, 3—strong expression, and 4—very strong expression. The expression condition in the adhesive tissue was calculated as the average score of examined sections.

2.7. Western Blot. Western blot was performed according to previous studies [24, 32] to assess inflammation (COX-2) and collagen deposition (α-SMA, MMP-9) to further delineate the mechanism of emodin (SMAD3). Mammalian protein lysis buffer (Thermo Fisher Scientific, Waltham, MA, USA) was used to extract the total tissue protein. The same amounts of protein were subjected to sodium dodecyl sulfate-polyacrylamide gel electrophoresis and then transferred to polyvinylidene fluoride membranes (EMD Millipore, Billerica, MA, USA). The membranes were incubated in the diluted primary antibodies overnight and stored at 4°C. The primary antibodies were anti-COX-2 antibody (Santa Cruz, 1 : 200 dilution), anti-SMAD3 antibody (Santa Cruz, 1 : 500 dilution), anti-α-SMA antibody (Santa Cruz, 1 : 200 dilution), and anti-beta-actin (β-actin) antibody (Santa Cruz, 1 : 1000 dilution). The membranes were incubated with the secondary antibody followed by horseradish peroxidase (HRP; Santa Cruz). Then, an enhanced chemiluminescence system (EMD Millipore) was used to detect the bands. The intensity of the bands was calculated using Image-Pro Plus 5.0 software (Media Cybernetics Inc., Rockville, MD, USA).

2.8. Enzyme-Linked Immunosorbent Assay (ELISA). Interleukin-6 (IL-6) and transforming growth factor-β1 (TGF-β1) (indicators of inflammation) as well as gastrin and motilin (indicators of gastrointestinal dynamics) levels were measured in blood that was collected 7 days after surgery. Four commercial ELISA kits (all from Meilian Biology, Shanghai, China) for IL-6, TGF-β1, gastrin, and motilin were used according to the manufacturers' protocols. The concentrations of the samples were calculated using a standard curve. The levels of the assessed indicators are expressed as picograms per milligram of protein.

2.9. Chemiluminescence Test for Reactive Oxygen Species. As reported previously [33], reactive oxygen species (ROS) were measured in the peritoneal lavage fluid 7 days after the operation. The lavage fluids were collected before opening the abdominal cavity. A commercial ROS detection kit (Sinovac Biochemical Reagents, Shanghai, China) was used according to the manufacturer's protocol. The concentrations of the samples were calculated using a standard curve.

2.10. Gastrointestinal Dynamics Experiment. An ink-propelling test was performed to determine the condition of the gastrointestinal dynamics in the different groups. All rats were administered 2 mL of ink, consisting of 5% carbon powder and a 0.5% CMC-Na suspension, by oral gavage 30 minutes before the second laparotomy. After assessing the adhesion condition, the total small bowel was removed from the abdominal cavity. Then, the small intestine was cut along the antimesenteric side. Next, we measured the total length from the distal stomach to the ileocecal junction and the length from the pylorus to the furthest point that the carbon powder had reached. The intestinal propulsion rate was calculated using the following equation: intestinal propulsion rate (%) = length of carbon powder movement/total length of small intestine × 100%.

2.11. Statistical Analyses. All data were analyzed with the SPSS18.0 software (Chicago, IL, USA) and are presented as means ± standard errors of the mean (SEM). Analysis of variance (ANOVA) was performed to determine significant differences in normally distributed data, and the abnormally distributed data were analyzed by the Kruskal-Wallis test. Enumeration data were determined by Fisher's exact test. P values <0.05 were considered significant.

3. Results

3.1. Gross Observations Indicate That Emodin Treatment Reduced Abdominal Adhesions. No animals died during the operation or postoperative treatment; therefore, a total of 48 rats completed the study. No wound infections or disruptions occurred before the second laparotomy.

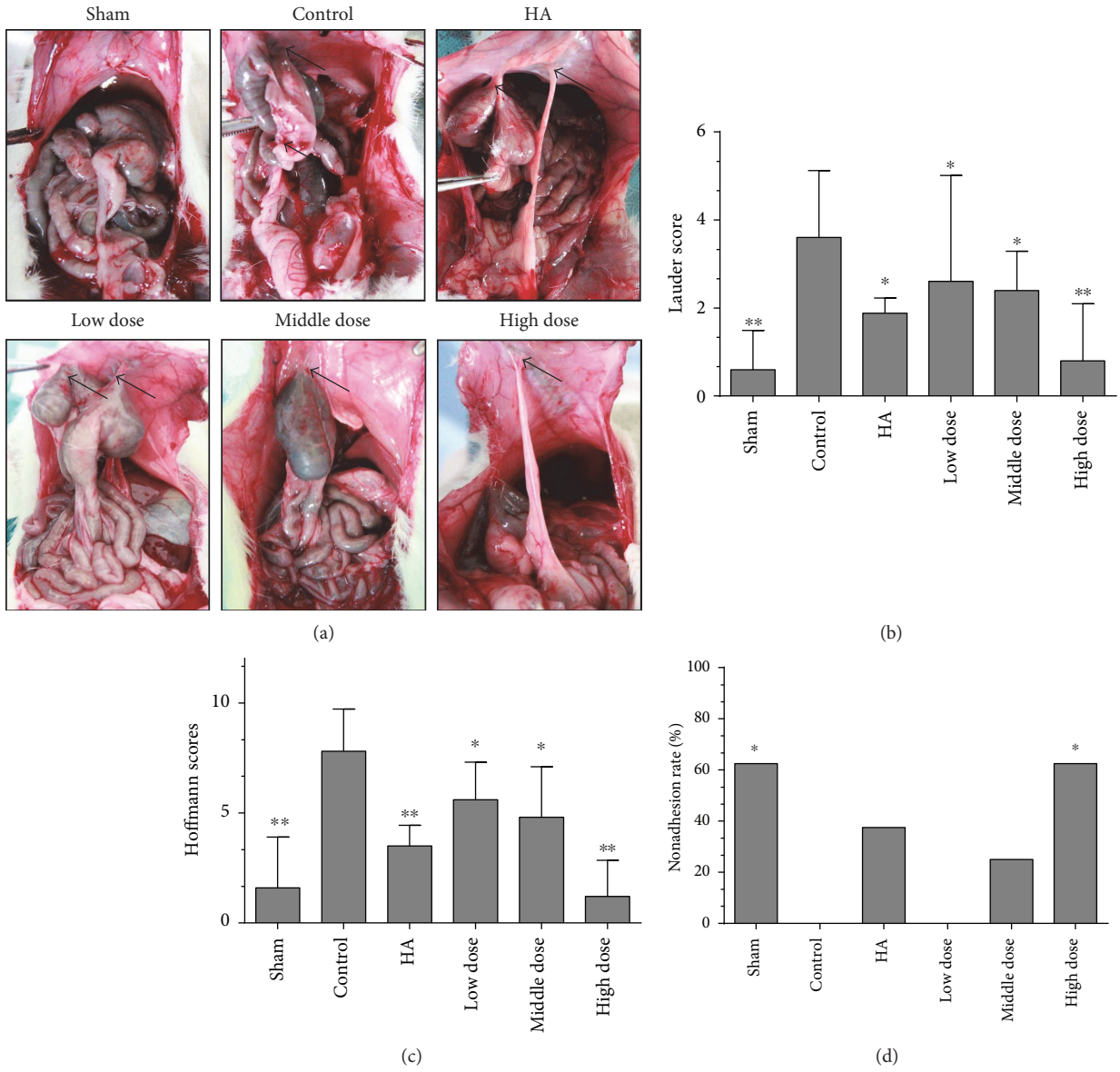

Figure 1: Emodin treatment prevents postoperative intra-abdominal adhesion formation in rats on the seventh day after the operation ($n = 8$). (a) The sham operation group (sham) rarely had intra-abdominal adhesions. Control group (control) animals developed a large number of extensive and thick adhesions that were difficult to separate. The sodium hyaluronate group (HA) had a few adhesion formations. The low-dose emodin group, middle-dose emodin group, and high-dose emodin group developed fewer adhesions than the control group. Black arrows indicate adhesions. (b) The Lauder scores of the different groups (total $P = 0.0022$ compared with the control group, $^{*}P < 0.05$ and $^{**}P < 0.01$, abnormally distributed, Kruskal-Wallis test). (c) The total Hoffmann scores of the different groups (total $P < 0.0001$ compared with the control group, $^{*}P < 0.05$ and $^{**}P < 0.01$, abnormally distributed, Kruskal-Wallis test). (d) The nonadhesion rates in the different groups (total $P = 0.004$ compared with the control group, $^{*}P < 0.05$, Fisher's exact test).

To investigate the effect of emodin on preventing adhesion formation after surgery, we first evaluated adhesion formation using the scoring system as described before when the abdominal cavity was opened 7 days after the operation (Figure 1(a)). There were significant differences between the groups, and the adhesions were remarkably relieved by emodin treatment, especially in the high-dose emodin group ($P < 0.05$) (Figures 1(b) and 1(c); $P = 0.0022$ and $P < 0.0001$, resp.). Additionally, the highest nonadhesion rates were found in the sham operation and high-dose emodin groups ($P = 0.011$) (Figure 1(d)). Therefore, our gross observations indicate that emodin effectively reduces intra-abdominal adhesion formation.

3.2. Emodin Inhibits Intra-Abdominal Collagen Deposition. Masson staining was used to assess collagen deposition in the adhesion tissues of different groups. The collagen layer

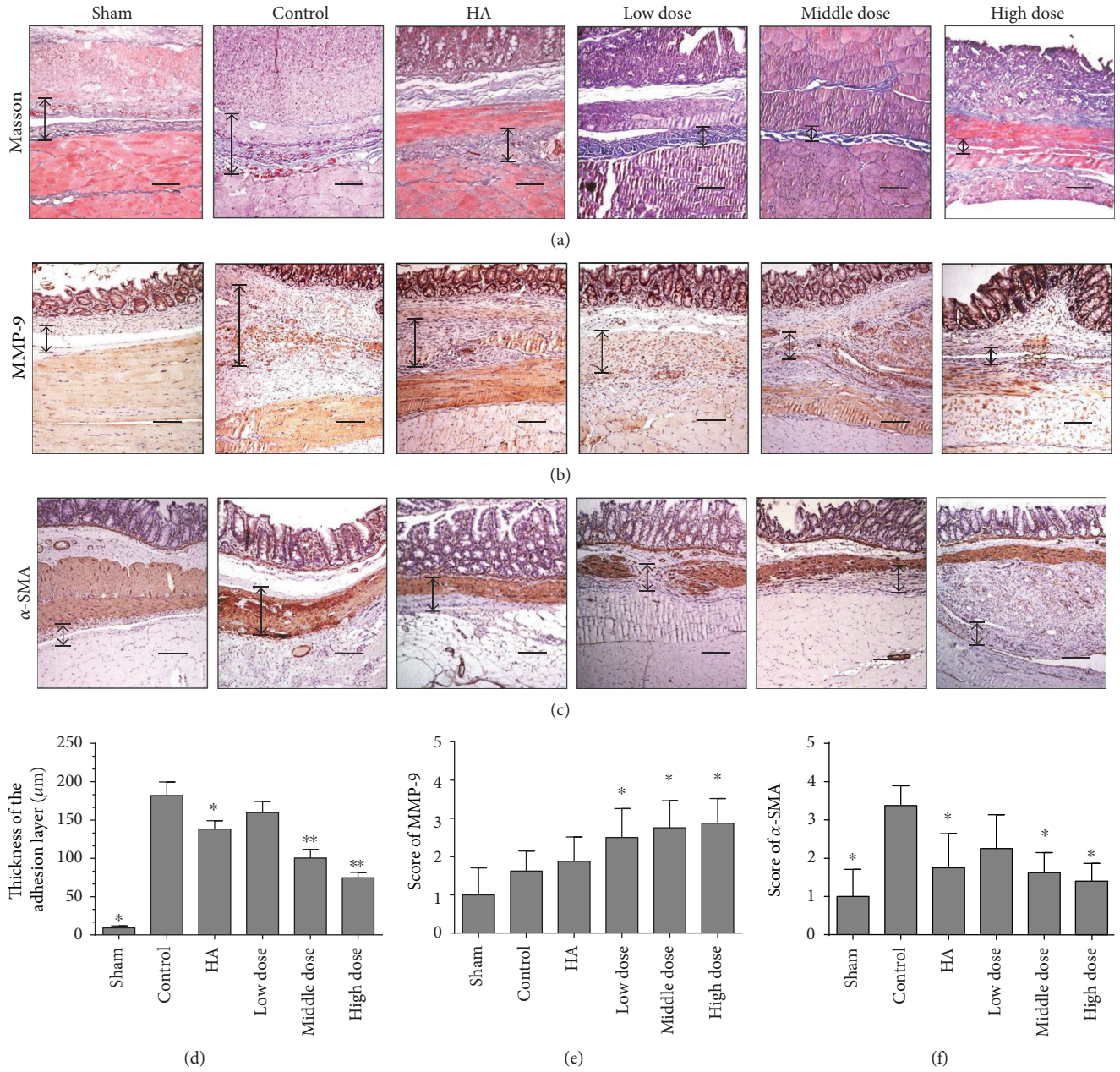

Figure 2: Emodin treatment reduced postoperative intra-abdominal collagen deposition seven days after operation. The magnification is 100× ($n = 8$; compared with the control group, $^{*}P < 0.05$ and $^{**}P < 0.01$). (a) Masson staining of the different groups (double-headed black arrows indicate adhesive tissues). (b) Immunohistochemical staining of MMP-9 among the different groups (double-headed black arrows indicate adhesive tissues). (c) Immunohistochemical staining of α-SMA (double-headed black arrows indicate adhesive tissue). (d) The score obtained from Masson staining shows that the thickness of the adhesion layer is thinner in the emodin-treated groups than in the other groups ($P < 0.0001$, abnormally distributed, Kruskal-Wallis test). (e) The score of MMP-9 staining among different groups (total $P = 0.0005$, abnormally distributed, Kruskal-Wallis test). (f) The score of α-SMA staining among different groups (total $P = 0.0005$, abnormally distributed, Kruskal-Wallis test).

was thinner in the emodin-treated groups ($P < 0.0001$) (Figures 2(a) and 2(d) and Supplementary Figure 1A).

To verify our results and to discover the possible mechanisms underlying the decrease in adhesive tissue collagen deposition after emodin treatment, we determined the MMP-9 and α-SMA expression levels using immunohistochemistry. Compared with the control group, MMP-9 levels were increased ($P = 0.0003$) (Figures 2(b) and 2(e) and Supplementary Figure 1B) and α-SMA levels were decreased ($P = 0.0002$) (Figures 2(c) and 2(f) and Supplementary Figure 1C) in the emodin-treated groups. These results suggest that emodin treatment inhibits collagen deposition.

3.3. Emodin Treatment Promotes Mesothelial Cell Healing. To evaluate healing of the peritoneal mesothelium, which plays an important role in abdominal adhesion formation,

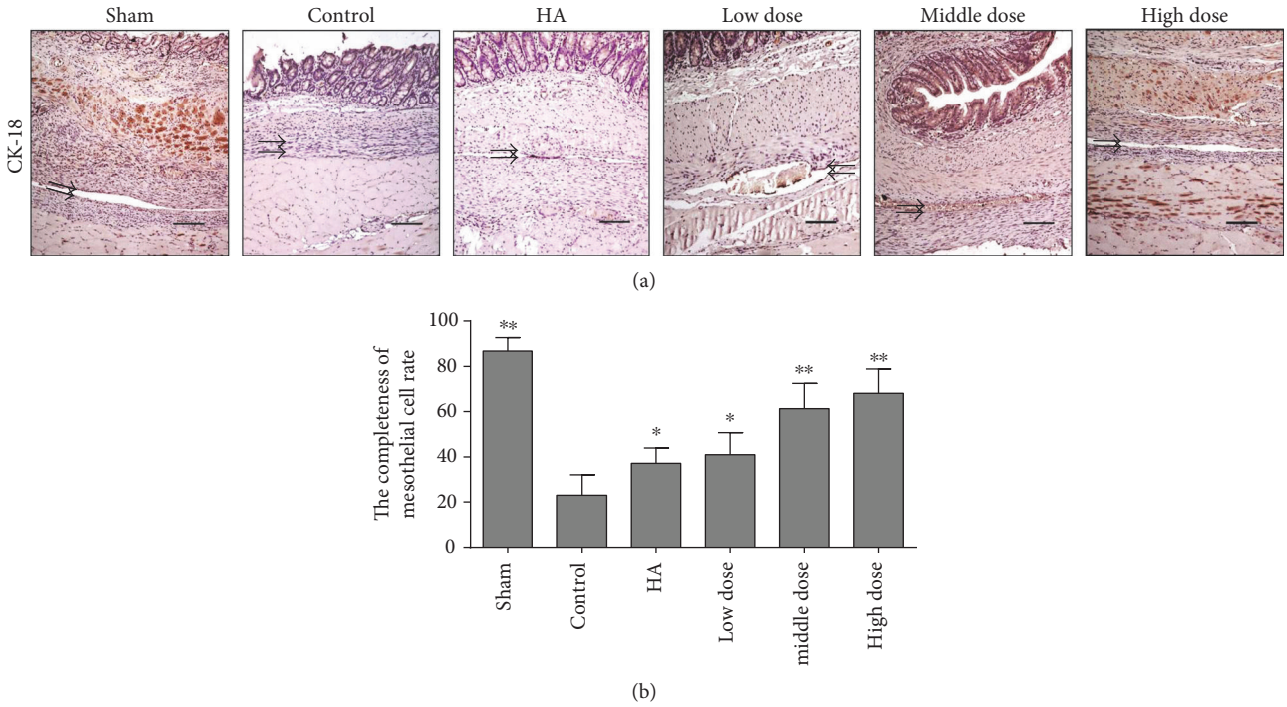

Figure 3: The completeness rate of normal mesothelial cells seven days after the operation ($n = 8$; compared with the control group, $^{*}P < 0.05$ and $^{**}P < 0.01$). (a) Immunohistochemical staining of CK-18 among the different groups. The magnification is 100× (black arrows indicate CK-18-positive mesothelial cells or injured mesothelial cell lines). (b) The emodin-treated groups had intact peritoneal mesothelial cell layers as detected by immunohistochemical staining for CK-18 (total $P < 0.0001$, abnormally distributed, Kruskal-Wallis test).

we used immunohistochemistry to determine the expression of cytokeratin in the peritoneal mesothelial cells of the different groups. In the groups treated with emodin, the peritoneal cells repaired the injured area more completely than those in the other groups ($P < 0.0001$) (Figures 3(a) and 3(b) and Supplementary Figure 1D). Emodin treatment promotes the process of mesothelial cell healing.

3.4. Emodin Treatment Alleviates Oxidative Stress. To determine additional mechanisms by which emodin treatment prevents abdominal adhesions, we determined the levels of ROS, indicators of oxidative stress reactions, in the peritoneal lavage fluids. The levels of ROS in the emodin-treated groups were lower than those in the control group ($P < 0.0001$) (Figure 4(a)). Therefore, a potential mechanism by which emodin prevents postoperative abdominal adhesions may be through alleviating oxidative stress reactions.

3.5. Emodin Treatment Inhibits Inflammation. To confirm our observations and determine a possible mechanism by which emodin prevents postoperative intra-abdominal adhesion formation, we performed a macroscopic evaluation of the inflammatory response. Fibrosis was remarkably reduced and the inflammation score was lower in the emodin-treated groups than in the control group ($P = 0.00177$) (Figures 4(b) and 4(c) and Supplementary Figure 1E). We assessed the levels of TGF-β and IL-6 in the blood on the seventh day after the operation and found that there was less of an inflammatory reaction in the emodin-treated groups than in the controls ($P < 0.0001$) (Figures 4(d) and 4(e)). In addition, COX2, an important indicator of inflammation, was decreased in the emodin-treated groups, as shown in Figures 5(a) and 5(c) ($P < 0.0001$). To determine the probable mechanisms by which emodin reduces inflammation, we assessed the expression of SMAD-3, an activator of the TGF-β signaling pathway, in the different groups. Emodin treatment successfully decreased the expression of SMAD-3 (Figures 5(a) and 5(d), $P < 0.0001$). Thus, these results suggest that emodin potentially inhibits inflammation through a mechanism associated with the TGF-β signaling pathway.

3.6. Emodin Treatment Promotes Gastrointestinal Dynamics. To further determine the condition of the gastrointestinal dynamics in the different groups, we performed an ink-propelling test. The ink moved further in the emodin-treated groups, which suggests that emodin treatment promotes bowel movements ($P < 0.0001$) (Figures 6(a) and 6(b)). In addition to these gastrointestinal dynamic evaluations, we assessed several objective indicators to confirm our findings. By testing the levels of gastrin and motilin in the blood seven days after the operation, the emodin-treated groups had higher levels of gastrointestinal hormones than the other groups ($P < 0.0001$) (Figures 6(c) and 6(d)). Based on the immunohistochemical staining of C-kit, a specific maker for intestinal movement [34, 35], we drew the same conclusion ($P < 0.0001$) (Figures 6(e) and 6(f) and Supplementary Figure 1F). Thus, emodin treatment can promote gastrointestinal movement.

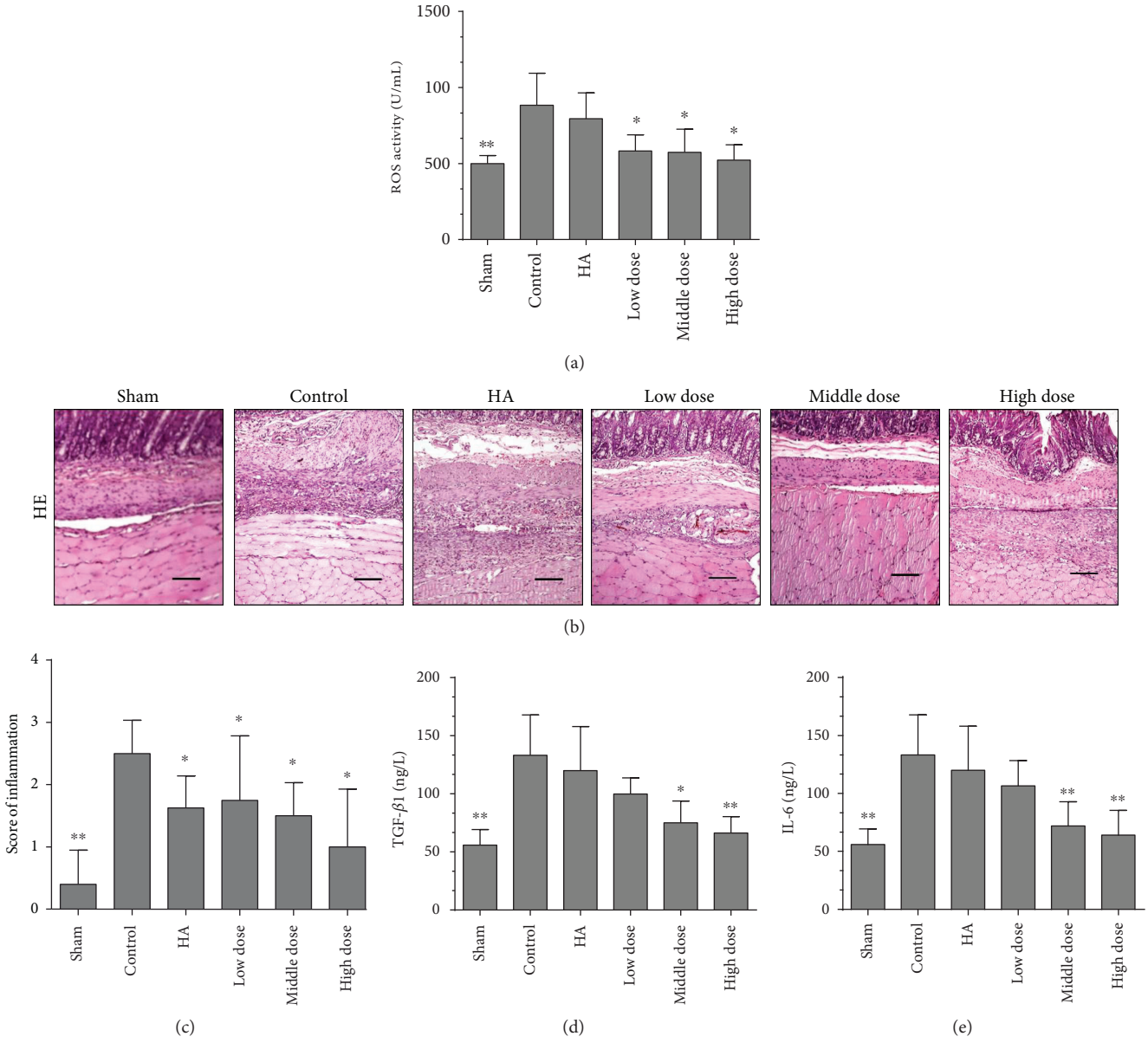

Figure 4: Emodin treatment alleviates oxidative stress and inhibits inflammation in rats seven days after the operation ($n = 8$; compared with the control group, $^{*}P < 0.05$ and $^{**}P < 0.01$). (a) Emodin-treated groups had lower expression levels of ROS (total $P < 0.0001$, abnormally distributed, Kruskal-Wallis test). (b) HE staining of the different groups. The magnification is 100×. (c) The scores of the inflammatory response determined by HE staining in the different groups (total $P = 0.00177$, abnormally distributed, Kruskal-Wallis test). (d) ELISA results showing the TGF-β1 levels in the blood on the seventh day after operation (total $P < 0.0001$, abnormally distributed, Kruskal-Wallis test). (e) ELISA results showing the IL-6 levels in the blood on the seventh day after operation (total $P < 0.0001$, abnormally distributed, Kruskal-Wallis test).

4. Discussion

Here, we demonstrated that emodin treatment could effectively reduce postoperative adhesion formation, reduce collagen formation, and accelerate healing of the peritoneal mesothelium. Emodin prevents adhesion formation in several ways, including the inhibition of inflammation, alleviation of oxidative stress, and promotion of intestinal tract movements. The results presented in this study strongly suggest that emodin can be an effective drug for the prevention of postoperative adhesion formation.

Emodin is a natural secondary plant product, originally isolated from the rhizomes of *Rheum palmatum*. In traditional Chinese medicine, emodin is used as an anti-inflammatory drug and to improve visceral stasis and promote movement of the gut [18, 36]. Emodin is a pleiotropic molecule capable of interacting with several major molecular targets, for example, TGF-β, NF-κB, AKT/mTOR, and STAT3 [18]. We chose emodin as an antiabdominal adhesion drug because of the following reasons. In a previous study, emodin inhibited inflammation through TGF-β [37]. Emodin also reduced liver and pulmonary fibrosis [22, 38]. In

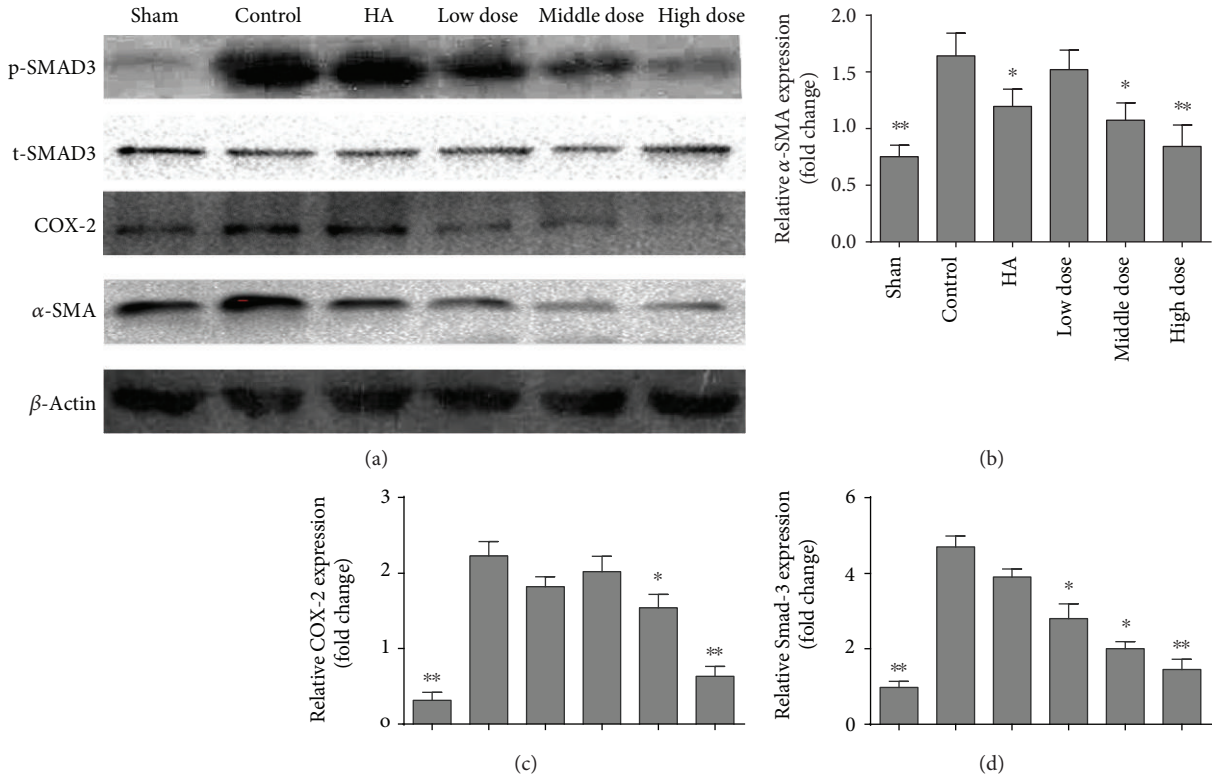

Figure 5: Western blot of SMAD-3, COX-2, and α-SMA in the different groups ($n = 8$; compared with the control group, $^{*}P < 0.05$ and $^{**}P < 0.01$, abnormally distributed, Kruskal-Wallis test). (a) Western blot of SMAD-3, COX-2, and α-SMA in the different groups. (b) The relative α-SMA expression of different groups (total $P < 0.0001$, abnormally distributed, Kruskal-Wallis test). (c) The relative COX-2 expression of different groups (total $P < 0.0001$, abnormally distributed, Kruskal-Wallis test). (d) The relative SMAD-3 expression of different groups (total $P < 0.0001$, abnormally distributed, Kruskal-Wallis test).

addition to its properties as a laxative drug, emodin can promote intestinal movement [23]. While the formation of intestinal adhesions involves inflammation, collagen deposition, and oxidative stress, the TGF-β pathway also plays important roles in abdominal formation [11, 39]. Thus, we speculated that emodin may inhibit abdominal adhesion formation. In our study, the main effect of emodin was to prevent abdominal adhesion formation via blockage of the TGF-beta signaling pathway.

The fibrinolytic system plays a central role in the formation of postoperative intra-abdominal adhesions [1]. If complete fibrinolysis does not occur within 5 to 7 days after peritoneal injury, the temporary fibrin matrix will persist and gradually will become more organized as fibroblasts secrete collagen, which can lead to the formation of postoperative adhesions. In our study, we used Masson staining to detect collagen and immunohistochemistry and Western blot analyses to detect α-SMA. Emodin treatment reduced the collagen content in adhesion tissues. MMP-9, which can degrade the extracellular matrix and reduce collagen levels, was increased in the emodin-treated groups compared with the controls.

The process of peritoneal healing plays an important role in postoperative abdominal adhesion formation. If the peritoneal cells can repair the locally injured peritoneal area in time, then, adhesion formation will be reduced [6]. Cytokeratin-18 is a specific marker for mesothelial cells [40]. We compared the positive cytokeratin expression rates of mesothelial cells among the different groups, and the emodin-treated groups had a higher rate of expression in normal mesothelial cells. We concluded that the peritoneal mesothelial cells healed faster in the emodin-treated groups.

Adhesion formation stems from trauma/injury that results in the initiation of an inflammatory response, which leads to the formation of a fibrin matrix [3, 41]. There are various molecular targets that emodin may modulate. Emodin may possess a great potential as a therapeutic agent for a variety of inflammatory conditions. Emodin exerts anti-inflammatory effects on CIA mice through inhibition of the NF-κB pathway [20, 42, 43]. In our study, through the evaluation of inflammatory scores in HE-stained sections and determination of TGF-β1 and IL-6 levels in blood and COX-2 expression in tissues, we concluded that emodin treatment decreased the inflammatory response. The potential mechanism of emodin in the reduction of inflammation may be through inhibition of the most important inflammatory pathway, the TGF-β signaling pathway. To investigate this possibility, we investigated the downstream molecule SMAD-3 [44]. Emodin treatment effectively decreased SMAD-3 expression. However, further study is required to fully elucidate the effects of emodin treatment on SMAD-3 expression.

Oxidative stress participates in the formation of postoperative abdominal adhesion formation, and inhibition of

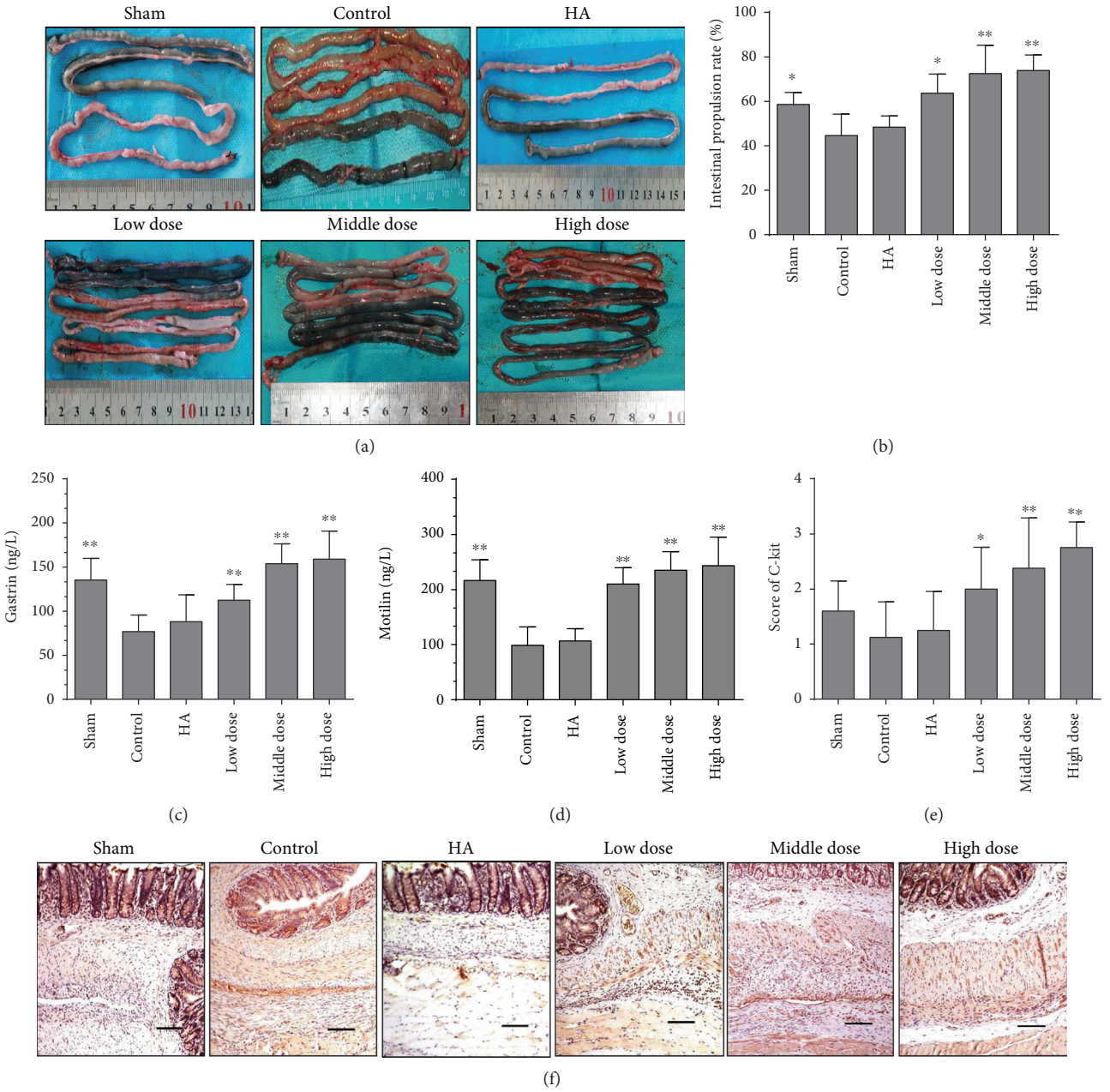

Figure 6: Gastrointestinal dynamics in the different groups (compared with the control group, $^{*}P < 0.05$ and $^{**}P < 0.01$). (a) Representative image of the ink-propelling test indicating intestinal movement conditions in different groups. (b) The intestinal propulsion rates determined by ink-propelling tests in the different groups (total $P < 0.0001$, abnormally distributed, Kruskal-Wallis test). (c) ELISA results showing gastrin levels in the blood on the seventh day after operation (total $P < 0.0001$, abnormally distributed, Kruskal-Wallis test). (d) ELISA results showing motilin levels in the blood on the seventh day after operation (total $P < 0.0001$, abnormally distributed, Kruskal-Wallis test). (e) The scores of C-kit expression in different groups (total $P < 0.0001$, abnormally distributed, Kruskal-Wallis test). (f) The immunohistochemical staining of C-kit expression in the different groups. The magnification is 100×.

the oxidative stress pathway can be beneficial for the prevention of adhesion formation [45]. ROS are an indicator of oxidative stress. In our study, the expression of ROS was decreased in the emodin-treated groups, suggesting that one possible mechanism of emodin in preventing postoperative adhesion formation is by reducing oxidative stress.

The other possible mechanism for the reduction of postoperative adhesion formation by emodin may be via the promotion of gastrointestinal movement. As a laxative, emodin is traditionally used to treat constipation and can increase the contractility of intestinal smooth muscle [46]. Researchers have shown that stasis is a key element in the development of postoperative adhesions, and intestinal mobilization can acutely lyse adhesions and prevent adhesions from forming [16, 17]. In our study, we tested the gastrointestinal dynamics of the different groups by objective

indicators and animal experiments. Emodin treatment markedly promoted the movement of the bowels. Intestinal movement could potentially reduce the probability of abdominal wall-to-bowel or bowel-to-bowel adhesion formation.

Importantly, increased intestinal motility may be associated with dehiscence following colonic anastomosis [47]. However, previous studies also proved that a moderate increase in intestinal movement does not increase the risk of anastomotic leakage [48]. In addition to this, according to the Enhanced Recovery After Surgery (ERAS®) guidelines for colonic surgery (colon resection and anastomosis) [49], patients are encouraged to take normal food as soon as possible after surgery and to drink immediately after recovery from anesthesia. Early food and fluid intake will inevitably promote intestinal motility [50]. Researchers have not observed an increase in anastomotic leakage among patients undergoing ERAS [51]. According to our study, increasing intestinal mobility has no significance on the development of anastomotic fistulas (Supplementary Figure 1C).

There were several limitations in this study. First, the mechanism of emodin with respect to adhesion reduction is still unclear. Second, we could not fully simulate the effects of emodin treatment on humans because we performed these experiments in animals. Thus, we could not ensure that the rat model accurately models the response in humans. Third, although emodin may be a new method for the treatment of postoperative abdominal adhesion formation, the side effects of this compound are unknown. In particular, toxicology and pharmacokinetic studies are warranted.

5. Conclusions

Emodin treatment exerts anti-inflammatory effects, alleviates oxidative stress, and promotes the movement of the intestinal tract. Therefore, emodin is a promising drug for the prevention of postoperative adhesion formation. However, the mechanisms of emodin treatment in preventing abdominal adhesions require further study.

Conflicts of Interest

The authors declare no conflicts of interest.

Authors' Contributions

Guangbing Wei and Yunhua Wu contributed equally to this work.

Acknowledgments

This study was supported by the National Natural Science Foundation of China (no. 81572734) and the Scientific and Technological Development Research Project Foundation of Shaanxi Province (2016SF-121 and 2016SF-157).

References

[1] B. Schnüriger, G. Barmparas, B. C. Branco, T. Lustenberger, K. Inaba, and D. Demetriades, "Prevention of postoperative peritoneal adhesions: a review of the literature," *American Journal of Surgery*, vol. 201, no. 1, pp. 111–121, 2011.

[2] G. M. Boland and R. J. Weigel, "Formation and prevention of postoperative abdominal adhesions," *The Journal of Surgical Research*, vol. 132, no. 1, pp. 3–12, 2006.

[3] E. Bianchi, K. Boekelheide, M. Sigman, D. J. Lamb, S. J. Hall, and K. Hwang, "Ghrelin inhibits post-operative adhesions via blockage of the TGF-β signaling pathway," *PLoS One*, vol. 11, no. 4, article e0153968, 2016.

[4] P. R. Koninckx, V. Gomel, A. Ussia, and L. Adamyan, "Role of the peritoneal cavity in the prevention of postoperative adhesions, pain, and fatigue," *Fertility and Sterility*, vol. 106, no. 5, pp. 998–1010, 2016.

[5] M. Ouaïssi, S. Gaujoux, N. Veyrie et al., "Post-operative adhesions after digestive surgery: their incidence and prevention: review of the literature," *Journal of Visceral Surgery*, vol. 149, no. 2, pp. e104–e114, 2012.

[6] D. Poehnert, M. Abbas, H. H. Kreipe, J. Klempnauer, and M. Winny, "Evaluation of 4DryField® PH as adhesion prevention barrier tested in an optimized adhesion model in rats," *European Surgical Research*, vol. 55, no. 4, pp. 341–351, 2015.

[7] R. M. Kamel, "Prevention of postoperative peritoneal adhesions," *European Journal of Obstetrics, Gynecology, and Reproductive Biology*, vol. 150, no. 2, pp. 111–118, 2010.

[8] E. Ersoy, V. Ozturk, A. Yazgan, M. Ozdogan, and H. Gundogdu, "Comparison of the two types of bioresorbable barriers to prevent intra-abdominal adhesions in rats," *Journal of Gastrointestinal Surgery*, vol. 13, no. 2, pp. 282–286, 2009.

[9] L. Holmdahl and M. L. Ivarsson, "The role of cytokines, coagulation, and fibrinolysis in peritoneal tissue repair," *The European Journal of Surgery*, vol. 165, no. 11, pp. 1012–1019, 1999.

[10] S. A. Buțureanu and T. A. Buțureanu, "Pathophysiology of adhesions," *Chirurgia (Bucur)*, vol. 109, no. 3, pp. 293–298, 2014.

[11] B. W. Hellebrekers and T. Kooistra, "Pathogenesis of postoperative adhesion formation," *The British Journal of Surgery*, vol. 98, no. 11, pp. 1503–1516, 2011.

[12] R. T. Beyene, S. L. Kavalukas, and A. Barbul, "Intra-abdominal adhesions: anatomy, physiology, pathophysiology, and treatment," *Current Problems in Surgery*, vol. 52, no. 7, pp. 271–319, 2015.

[13] V. Mais, "Peritoneal adhesions after laparoscopic gastrointestinal surgery," *World Journal of Gastroenterology*, vol. 20, no. 17, pp. 4917–4925, 2014.

[14] M. P. Diamond, E. El-Hammady, R. Wang, and G. Saed, "Regulation of matrix metalloproteinase-1 and tissue inhibitor of matrix metalloproteinase-1 by dichloroacetic acid in human fibroblasts from normal peritoneum and adhesions," *Fertility and Sterility*, vol. 81, no. 1, pp. 185–190, 2004.

[15] B. C. Ward and A. Panitch, "Abdominal adhesions: current and novel therapies," *The Journal of Surgical Research*, vol. 165, no. 1, pp. 91–111, 2011.

[16] G. M. Bove and S. L. Chapelle, "Visceral mobilization can lyse and prevent peritoneal adhesions in a rat model," *Journal of Bodywork and Movement Therapies*, vol. 16, no. 1, pp. 76–82, 2012.

[17] S. L. Chapelle and G. M. Bove, "Visceral massage reduces postoperative ileus in a rat model," *Journal of Bodywork and Movement Therapies*, vol. 17, no. 1, pp. 83–88, 2013.

[18] X. Dong, J. Fu, X. Yin et al., "Emodin: a review of its pharmacology, toxicity and pharmacokinetics," *Phytotherapy Research*, vol. 30, no. 8, pp. 1207–1218, 2016.

[19] J. W. Han, D. W. Shim, W. Y. Shin et al., "Anti-inflammatory effect of emodin via attenuation of NLRP3 inflammasome activation," *International Journal of Molecular Sciences*, vol. 16, no. 4, pp. 8102–8109, 2015.

[20] J. K. Hwang, E. M. Noh, S. J. Moon et al., "Emodin suppresses inflammatory responses and joint destruction in collagen-induced arthritic mice," *Rheumatology (Oxford)*, vol. 52, no. 9, pp. 1583–1591, 2013.

[21] A. Liu, L. Sha, Y. Shen, L. Huang, X. Tang, and S. Lin, "Experimental study on anti-metastasis effect of emodin on human pancreatic cancer," *Zhongguo Zhong Yao Za Zhi*, vol. 36, no. 22, pp. 3167–3171, 2011.

[22] M. X. Dong, Y. Jia, Y. B. Zhang et al., "Emodin protects rat liver from CCl_4-induced fibrogenesis via inhibition of hepatic stellate cells activation," *World Journal of Gastroenterology*, vol. 15, no. 38, pp. 4753–4762, 2009.

[23] Y. F. Zheng, C. F. Liu, W. F. Lai et al., "The laxative effect of emodin is attributable to increased aquaporin 3 expression in the colon of mice and HT-29 cells," *Fitoterapia*, vol. 96, pp. 25–32, 2014.

[24] G. Wei, C. Zhou, G. Wang, L. Fan, K. Wang, and X. Li, "Keratinocyte growth factor combined with a sodium hyaluronate gel inhibits postoperative intra-abdominal adhesions," *International Journal of Molecular Sciences*, vol. 17, no. 10, 2016.

[25] Z. Bayhan, S. Zeren, F. E. Kocak et al., "Antiadhesive and anti-inflammatory effects of pirfenidone in postoperative intra-abdominal adhesion in an experimental rat model," *The Journal of Surgical Research*, vol. 201, no. 2, pp. 348–355, 2016.

[26] G. Wei, X. Chen, G. Wang, L. Fan, K. Wang, and X. Li, "Effect of resveratrol on the prevention of intra-abdominal adhesion formation in a rat model," *Cellular Physiology and Biochemistry*, vol. 39, no. 1, pp. 33–46, 2016.

[27] G. Wei, X. Chen, G. Wang et al., "Inhibition of cyclooxygenase-2 prevents intra-abdominal adhesions by decreasing activity of peritoneal fibroblasts," *Drug Design, Development and Therapy*, vol. 9, pp. 3083–3098, 2015.

[28] N. E. Hoffmann, S. A. Siddiqui, S. Agarwal et al., "Choice of hemostatic agent influences adhesion formation in a rat cecal adhesion model," *The Journal of Surgical Research*, vol. 155, no. 1, pp. 77–81, 2009.

[29] C. I. Lauder, G. Garcea, A. Strickland, and G. J. Maddern, "Use of a modified chitosan-dextran gel to prevent peritoneal adhesions in a rat model," *The Journal of Surgical Research*, vol. 171, no. 2, pp. 877–882, 2011.

[30] M. H. Du, H. M. Luo, Y. J. Tian et al., "Electroacupuncture ST36 prevents postoperative intra-abdominal adhesions formation," *The Journal of Surgical Research*, vol. 195, no. 1, pp. 89–98, 2015.

[31] P. Parsaei, M. Karimi, S. Y. Asadi, and M. Rafieian-Kopaei, "Bioactive components and preventive effect of green tea (*Camellia sinensis*) extract on post-laparotomy intra-abdominal adhesion in rats," *International Journal of Surgery*, vol. 11, no. 9, pp. 811–815, 2013.

[32] Q. Xu, J. Ma, J. Lei et al., "α-Mangostin suppresses the viability and epithelial-mesenchymal transition of pancreatic cancer cells by downregulating the PI3K/Akt pathway," *BioMed Research International*, vol. 2014, Article ID 546353, 12 pages, 2014.

[33] M. Karimi, A. S. Yazdan, P. Parsaei, M. Rafieian-Kopaei, H. Ghaheri, and S. Ezzati, "The effect of ethanol extract of rose (Rosa damascena) on intra-abdominal adhesions after laparotomy in rats," *Wounds*, vol. 28, no. 5, pp. 167–174, 2016.

[34] E. Iwasaki, H. Suzuki, T. Masaoka et al., "Enhanced gastric ghrelin production and secretion in rats with gastric outlet obstruction," *Digestive Diseases and Sciences*, vol. 57, no. 4, pp. 858–864, 2012.

[35] D. Jain, K. Moussa, M. Tandon, J. Culpepper-Morgan, and D. D. Proctor, "Role of interstitial cells of Cajal in motility disorders of the bowel," *The American Journal of Gastroenterology*, vol. 98, no. 3, pp. 618–624, 2003.

[36] A. Kumar, S. Dhawan, and B. B. Aggarwal, "Emodin (3-methyl-1,6,8-trihydroxyanthraquinone) inhibits TNF-induced NF-kappaB activation, IkappaB degradation, and expression of cell surface adhesion proteins in human vascular endothelial cells," *Oncogene*, vol. 17, no. 7, pp. 913–918, 1998.

[37] J. Yang, Z. Zeng, T. Wu, Z. Yang, B. Liu, and T. Lan, "Emodin attenuates high glucose-induced TGF-β1 and fibronectin expression in mesangial cells through inhibition of NF-κB pathway," *Experimental Cell Research*, vol. 319, no. 20, pp. 3182–3189, 2013.

[38] L. Liu, H. Qian, H. Xiao et al., "Emodin alleviates pulmonary fibrosis through inactivation of TGF-β1/ADAMTS-1 signaling pathway in rats," *Xi Bao Yu fen Zi Mian Yi Xue Za Zhi*, vol. 32, no. 10, pp. 1342–1346, 2016.

[39] S. Yan, L. Yang, Y. Z. Yue et al., "Effect of ligustrazine nanoparticles nano spray on transforming growth factor-β/Smad signal pathway of rat peritoneal mesothelial cells induced by tumor necrosis factor-α," *Chinese Journal of Integrative Medicine*, vol. 22, no. 8, pp. 629–634, 2016.

[40] Q. Guo, Q. F. Li, H. J. Liu, R. Li, C. T. Wu, and L. S. Wang, "Sphingosine kinase 1 gene transfer reduces postoperative peritoneal adhesion in an experimental model," *The British Journal of Surgery*, vol. 95, no. 2, pp. 252–258, 2008.

[41] Y. C. Cheong, S. M. Laird, T. C. Li, J. B. Shelton, W. L. Ledger, and I. D. Cooke, "Peritoneal healing and adhesion formation/reformation," *Human Reproduction Update*, vol. 7, no. 6, pp. 556–566, 2001.

[42] D. Shrimali, M. K. Shanmugam, A. P. Kumar et al., "Targeted abrogation of diverse signal transduction cascades by emodin for the treatment of inflammatory disorders and cancer," *Cancer Letters*, vol. 341, no. 2, pp. 139–149, 2013.

[43] X. Zhu, K. Zeng, Y. Qiu, F. Yan, and C. Lin, "Therapeutic effect of emodin on collagen-induced arthritis in mice," *Inflammation*, vol. 36, no. 6, pp. 1253–1259, 2013.

[44] D. A. Gorvy, S. E. Herrick, M. Shah, and M. W. Ferguson, "Experimental manipulation of transforming growth factor-beta isoforms significantly affects adhesion formation in a murine surgical model," *The American Journal of Pathology*, vol. 167, no. 4, pp. 1005–1019, 2005.

[45] P. A. Swanson, A. Kumar, S. Samarin et al., "Enteric commensal bacteria potentiate epithelial restitution via reactive oxygen species-mediated inactivation of focal adhesion kinase phosphatases," *Proceedings of the National Academy of Sciences of the United States of America*, vol. 108, no. 21, pp. 8803–8808, 2011.

[46] D. Chen, Y. Xiong, L. Wang, B. Lv, and Y. Lin, "Characteristics of emodin on modulating the contractility of jejunal smooth muscle," *Canadian Journal of Physiology and Pharmacology*, vol. 90, no. 4, pp. 455–462, 2012.

[47] D. García-Olmo, J. Payá, F. J. Lucas, and D. C. García-Olmo, "The effects of the pharmacological manipulation of postoperative intestinal motility on colonic anastomoses. An experimental study in a rat model," *International Journal of Colorectal Disease*, vol. 12, no. 2, pp. 73–77, 1997.

[48] F. Fu, Y. Hou, W. Jiang, R. Wang, and K. Liu, "Escin: inhibiting inflammation and promoting gastrointestinal transit to attenuate formation of postoperative adhesions," *World Journal of Surgery*, vol. 29, no. 12, pp. 1614–1620, 2005, discussion 1621-1622.

[49] U. O. Gustafsson, M. J. Scott, W. Schwenk et al., "Guidelines for perioperative care in elective colonic surgery: Enhanced Recovery After Surgery (ERAS®) Society recommendations," *World Journal of Surgery*, vol. 37, no. 2, pp. 259–284, 2013.

[50] Y. Zhang, F. Gu, F. Wang, and Y. Zhang, "Effects of early enteral nutrition on the gastrointestinal motility and intestinal mucosal barrier of patients with burn-induced invasive fungal infection," *Pakistan Journal of Medical Sciences*, vol. 32, no. 3, pp. 599–603, 2016.

[51] U. O. Gustafsson, M. J. Scott, W. Schwenk et al., "Guidelines for perioperative care in elective colonic surgery: Enhanced Recovery After Surgery (ERAS®) Society recommendations," *Clinical Nutrition*, vol. 31, no. 6, pp. 783–800, 2012.

Hindawi
Oxidative Medicine and Cellular Longevity
Volume 2017, Article ID 1675230, 11 pages
https://doi.org/10.1155/2017/1675230

Review Article

Protective Mechanisms of the Mitochondrial-Derived Peptide Humanin in Oxidative and Endoplasmic Reticulum Stress in RPE Cells

Leonid Minasyan,[1] Parameswaran G. Sreekumar,[2] David R. Hinton,[1,3] and Ram Kannan[2]

[1]*Department of Pathology, Keck School of Medicine of the University of Southern California, Los Angeles, CA, USA*
[2]*Arnold and Mabel Beckman Macular Research Center, Doheny Eye Institute, Los Angeles, CA, USA*
[3]*Department Ophthalmology, USC Roski Eye Institute, Keck School of Medicine of the University of Southern California, Los Angeles, CA, USA*

Correspondence should be addressed to Ram Kannan; rkannan@doheny.org

Received 13 March 2017; Revised 13 June 2017; Accepted 28 June 2017; Published 26 July 2017

Academic Editor: Luciano Saso

Age-related macular degeneration (AMD) is the leading cause of severe and irreversible vision loss and is characterized by progressive degeneration of the retina resulting in loss of central vision. The retinal pigment epithelium (RPE) is a critical site of pathology of AMD. Mitochondria and the endoplasmic reticulum which lie in close anatomic proximity to each other are targets of oxidative stress and endoplasmic reticulum (ER) stress, respectively, and contribute to the progression of AMD. The two organelles exhibit close interactive function via various signaling mechanisms. Evidence for ER-mitochondrial crosstalk in RPE under ER stress and signaling pathways of apoptotic cell death is presented. The role of humanin (HN), a prominent member of a newly discovered family of mitochondrial-derived peptides (MDPs) expressed from an open reading frame of mitochondrial 16S rRNA, in modulation of ER and oxidative stress in RPE is discussed. HN protected RPE cells from oxidative and ER stress-induced cell death by upregulation of mitochondrial GSH, inhibition of ROS generation, and caspase 3 and 4 activation. The underlying mechanisms of ER-mitochondrial crosstalk and modulation by exogenous HN are discussed. The therapeutic use of HN and related MDPs could potentially prove to be a valuable approach for treatment of AMD.

1. Age-Related Macular Degeneration

Age-related macular degeneration (AMD) is a progressive degenerative retinal disease that impairs visual acuity and causes irreversible central vision loss. In the developed world, AMD is the leading cause of blindness of the geriatric population [1]. In the United States alone, approximately 11 million people suffer from AMD, and this number is expected to double to 22 million by the year 2050 [2]. To date, no viable treatments to cure AMD exist and the need for novel therapeutics is becoming increasingly vital to circumvent the economic burden of inflating health care costs resulting from an increasing patient population.

Clinically, AMD is classified into two phases, an early asymptomatic phase containing drusen deposits and areas of hyper- or hypopigmentation and an advanced/late phase marked by profound vision loss and retinal degeneration [3]. The early phase of the disease may progress into either of the two advanced AMD subtypes: geographic/atrophic AMD ("dry AMD" or GA) with loss of retinal pigment epithelium (RPE) cells and photoreceptors or exudative/neovascular AMD (or "wet AMD"), which is distinguished from the former by the presence of choroidal neovascularization (CNV) [4]. These subtypes are not mutually exclusive as patients may exhibit characteristics of both dry and wet AMD in one eye, dry in one eye and wet in the other, and even the evolution of dry to wet AMD and vice versa [5].

Though the etiology of AMD is enigmatic due to its multifactorial nature, the dynamic interplay of several pathological processes has been well documented in the macula and is associated with a plethora of risk factors including aging, genetic, metabolic, and environmental such as smoking and phototoxicity [4, 6]. Genome-wide association studies (GWAS) comparing AMD patients and controls identified 52 independently associated common and rare variants distributed across 34 loci [7].

The most notable pathogenic processes in AMD include (1) the accumulation of discrete drusen deposits (composed of partially degraded oxidized products) between the RPE and Bruch membrane (BM), (2) intracellular accumulation of lipofuscin granules in the RPE and its constituent bisretinoid N-retinylidene-N-retinylethanolamine (A2E), (3) chronic local inflammation, (4) innate immune activation of the complement system by the inflammasome nod-like receptor-P3 (NLRP3), (5) mtDNA damage, and (6) oxidative and endoplasmic reticulum stress. In addition, neovascular AMD is characterized by abnormal growth of immature and leaky choroidal vessels through BM which is associated with increased expression of vascular endothelial growth factor (VEGF) [1].

2. Critical Role of RPE in Retinal Function

The RPE cells are a postmitotic polarized cuboidal monolayer separating the photoreceptors of the neural retina and the vascular choroid. They are an essential component of the outer blood-retinal barrier and are critical for maintaining the eye as a site of relative immune privilege. Additional functions include mediating bidirectional fluid and ion transport, phagocytosis of shed photoreceptor outer segments (POS), synthesizing and regulating the subretinal extracellular matrix (ECM), secreting growth factors, and recycling rhodopsin as part of the visual cycle [8].

Prevailing knowledge implicates the exacerbation of oxidative stress (OS) coupled with the attenuation of adaptive defense responses with aging in the pathogenesis of macular lesions, and more recently, the crosstalk between oxidative stress (OS) and endoplasmic reticulum (ER) stress has attracted much attention [9–13].

Irrespective of what the primary pathogenic insult may be, RPE dysfunction is a hallmark of AMD with a growing body of evidence suggesting that mitochondrial dysfunction, particularly mitochondrial DNA (mtDNA) damage resulting from aging and the OS-ER stress interface, may be critical [1, 14]. A recent report by Terluk et al. [15] showed that mtDNA damage is limited to the RPE, and similar mtDNA damage is found in the macular and peripheral RPE. Further, the study revealed that mtDNA damage is limited to discrete regions of the mitochondrial genome, including the control region containing *cis*-elements responsible for mitochondrial transcription and replication [15]. Other damaged regions of the mitochondrial genome include genes for the 16S and 12S ribosomal RNAs and 8 of 22 tRNAs. The 16S rRNA region also produces mt-derived peptides (MDPs), including humanin, and small humanin-like peptides (SHLPs) [15, 16].

This review will discuss the emerging concept of MDPs and their homeostatic functions in RPE cells. It will predominantly focus on the MDP humanin (HN) and its modulation of retinal OS and ER stress, with emphasis to ER-mitochondrial crosstalk in RPE. Information on these MDPs may provide insight into developing novel AMD therapeutics in conjunction with other agents for combination-based therapies.

3. Evolution and Function of Mitochondria

Mitochondria are ancient organelles thought to have emerged from the phagocytosis of alpha-protobacteria by eukaryotic cells long ago. Mitochondria contain their own closed double-stranded circular DNA (mtDNA) that is distinct from nuclear DNA (nDNA) [17]. Through evolutionary processes, the mtDNA lost the majority of its genes through genomic transfer and incorporation of cytoplasmic mtDNA into the nuclear genome. mtDNA is 16,569-base-pair long, void of introns, and has only a few noncoding nucleotides [18, 19]. mtDNA contains a total of 37 genes of which it encodes 13 essential proteins (mRNAs) of the oxidative phosphorylation pathway, along with 22 tRNAs that are found between most mRNA regions, as well as 2 rRNAs known as the 16S and 12S regions [19]. The presence of these tRNAs and rRNAs enables mitochondria to synthesize proteins within the organelle independently of the ER. The remainder of the proteins found in mitochondria are encoded in the nucleus, translated in the cytoplasm, and subsequently transferred to the mitochondria [20].

Mitochondrial functions range from mass production of ATP by oxidative phosphorylation, mediation of calcium signaling and sequestration, and regulation of apoptosis as well as OS by producing the highest cellular concentration of reactive oxygen species (ROS) as a metabolic byproduct [21, 22]. As the "power house" of the cell and an essential mediator of cellular metabolic homeostasis, mitochondrial dysfunction is implicated in aging and numerous age-related diseases [22].

4. HN and Related MDPs within the Mitochondrial Genome

High-resolution sequencing identified the existence of short open reading frames (sORFs) within the 16S and 12S rRNA regions of the mtDNA that were previously undetected [23, 24]. These sORFs lead to the discovery of MDPs that are encoded and transcribed within the mitochondria. To date, the known MDPs in order of their discovery include humanin (HN), mitochondrial open reading frame of the 12S rRNA-c (MOTS-c), and small humanin-like peptides (SHLPs) of which 6 variants have been identified [16, 25–28]. A pictorial representation of the mitochondrial genome depicting the MDPs in the 16S and 12S rRNA along with other encoded mitochondrial proteins is presented in Figure 1. The amino acid sequences of the MDPs are listed in Table 1.

HN is a highly conserved 75 base pair transcript encoded within the sORF of mitochondrial 16S rRNA [25, 29]. Interestingly, mitochondrial translational machinery yield a distinct

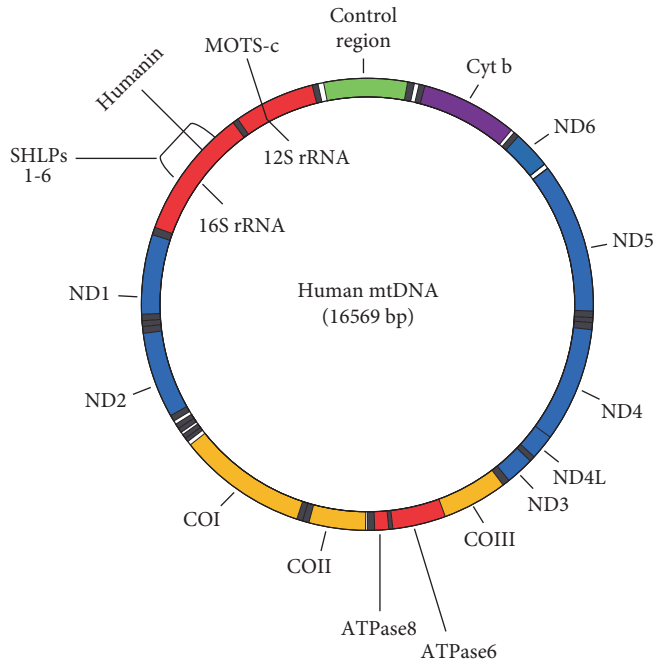

Figure 1: Human mtDNA genome showing location of humanin and SHLPs (16sRNA) and MOTS-c (12S rRNA). Regions for subunits of other proteins are also indicated in the figure. rRNA: ribosomal RNA; ND1 to ND6 and ND4: subunits of NADH dehydrogenase complex (complex 1); COI to COIII: subunits of cytochrome c oxidase (complex 1V); ATP6 and ATP8: subunits of ATP synthase; Cyt b: cytochrome b of CoQ-cytochrome c reductase (complex III).

Table 1: Nomenclature and amino acid sequences of known MDPs.

Name	Sequence	Year discovered	References
HN	MAPRGFSCLLLLTSEIDLPVKRRA	2001, 2003	[25–27]
MOTS-c	MRWQEMGYIFYPRKLR	2015	[28]
SHLP1	MCHWAGGASNTGDARGDVFGKQAG	2016	[16]
SHLP2	MGVKFFTLSTRFFPSVQRAVPLWTNS	2016	[16]
SHLP3	MLGYNFSSFPCGTISIAPGFNFYRLYFIWVNGLAKVVW	2016	[16]
SHLP4	MLEVMFLVNRRGKICRVPFTFFNLSL	2016	[16]
SHLP5	MYCSEVGFCSEVAPTEIFNAGLVV	2016	[16]
SHLP6	MLDQDIPMVQPLLKVRLFND	2016	[16]

number of peptide amino acids compared to cytoplasmic translation of the same gene. Therefore, depending on cytoplasmic versus mitochondrial locale, translation of HN yields either a 24- or 21-amino acid peptide, respectively [30, 31]. Both peptides have been shown to have biological activity [27]. Thirteen humanin-like ORFs were found within the nuclear genome: out of which, 10 were found to be expressed in tissue samples [32]. Additionally, two of these peptides were synthesized and their antiapoptotic properties were established [32].

5. Protective Properties of Humanin in Nonocular Tissues

HN was the first MDP discovered in 2001 by cloning a cDNA library to the 16S rRNA region to screen for molecules conferring neural apoptotic resistance against a mutated amyloid precursor protein (APP) from the unaffected portion of brain tissue of an Alzheimer disease (AD) patient [33, 34]. The peptide was also shown to confer neuroprotection against an array of familial Alzheimer's disease (FAD) genes including presenilin 1, presenilin 2, and mutated APP [25, 33]. HN was independently cloned by two additional groups when screening for various binding factors. Ikonen et al. [26] cloned HN as a binding partner of insulin-like growth factor binding protein-3 (IGFBP-3), while Guo et al. [27] discovered that HN binds to Bax and is a potent cytoprotective agent suppressing apoptosis. By binding to Bax, HN prevents its translocation and suppresses the downstream release of cytochrome c from the mitochondria thereby preventing apoptosis [27]. Additionally, HN binds to and deactivates the proapoptotic BH3 proteins tBid and BimEL [35, 36].

In glial cell lines, HN binding to IGFBP-3 blocks IGFBP-3-mediated apoptosis. However, in neurons, the cytoprotective

capabilities of HN and IGF-1 synergize against Aβ-induced apoptosis [26, 30]. HN binding to IGFBP-3 affects the bioactivity of IGF-1 by increasing clearance without hindering IGFBP-3/IGF-1 binding and reduces circulating levels of IGFBP-3 and IGF-1 [37]. Both IGF-1 and HN inhibit apoptosis, enhance insulin sensitivity, suppress ischemia/reperfusion injury, lower inflammation, and degrade atherosclerotic plaques [37]. Conversely, HN and IGF-1 have opposite effects on longevity and tumorigenesis and both show a decline in expression with aging [37–39].

An age-related decline of HN could play a role in the pathogenesis of age-related diseases including AD and type 2 diabetes mellitus (T2DM) [39]. HN also inhibits pancreatic β-cell apoptosis, improves glucose tolerance, and lowers lymphocyte infiltrates in the nonobese diabetic (NOD) mouse model [40]. HN expression increases in response to stressful stimuli as evident from patients with mitochondrial encephalomyopathy with lactic acidosis and stroke-like episodes (MELAS) and localizes to the mitochondria to presumably increase ATP synthesis and improve cell survival [41].

In addition to FAD genes, HN confers neuroprotection against a variety of other degenerative diseases including spinocerebellar ataxia and Huntington's disease-related polyglutamine toxicity, disorders in which mitochondrial dysfunction has been implicated [30]. As a cytoprotective factor, HN also responded to Aβ and OS in triple transgenic mice by ameliorating cognitive impairment [30, 42]. Atherosclerotic plaques contain oxidized LDL aggregates similar to drusen, and these generate OS insults to the endothelial vasculature and HN suppressed the size of these plaques in ApoE-deficient mice on a high-fat diet [43]. Rat ischemia/reperfusion models also showed attenuated insults from cobalt chloride- ($CoCl_2$-) mediated hypoxia and serum starvation-induced apoptosis by increasing mitochondrial respiration [30, 44]. Undifferentiated rat pheochromocytoma (PC12) cells were rescued from apoptosis under serum starvation conditions by HN and the potent HN analog, HNG [45]. In mouse cerebral artery stroke models, HNG reduced infarct volume by half when administered centrally and had similar effects with systemic injections as well [46].

6. Localization of HN and Its Putative Receptors in RPE Cells

HN is expressed in the cytoplasmic compartments in nonpolarized RPE cells where it is mainly localized in mitochondria [47]. In polarized RPE monolayer cultures which mimic the native and physiological RPE monolayer [48], HN did not exhibit polarized localization and was found in both the apical and basal compartments [47]. The three reported receptors, namely, ciliary neurotrophic factor receptor (CNTFRα), the cytokine receptor (WSX1), and the transmembrane glycoprotein gp130 (gp130) which are essential for the extracellular action of HN, were expressed in RPE cells [47]. All three receptors were expressed in both nonpolarized and polarized hRPE cells. CNTFRα and gp130 showed polarized localization, predominately localized to the apical domain, while WSX1 showed apical as well as basal localization. The binding of HN to heterotrimeric HN receptor (htHNR) results in oligomerization of the receptor subunits and subsequent activation of JAK2 and STAT3 [49–52]. Hashimoto et al. [49] showed that HN induces STAT3 phosphorylation, which was essential for its neuroprotective effects. Glycoprotein 130 is a common element of receptors that belong to the interleukin-6 (IL-6) receptor family and could trigger intracellular signal cascade responsible for (JAK)/STAT and ERK1/2 pathway in neuronal cells [52]. Ciliary neurotrophic factor receptor (CNTFR) is a known IL-6 family cytokine [49]. WSX-1 was found while testing gp130-coupling proteins that co-overexpressed with human gp130 [50]. *In vitro* pulldown analysis indicated that HN binds to CNTFR or WSX-1 [49]. HN treatment induced the dimerization between CNTFR and WSX-1 as well as the dimerization between WSX-1 and gp130. Thus, HN initially induces the dimerization between WSX-1 and CNTFR and then induces the hetero-trimerization of CNTFR/WSX-1/gp130 [49]. In addition, overexpression of CNTFR and/or WSX-1 results in enhanced HN binding to neuronal cells, whereas siRNA-mediated knockdown of both or either component reduces binding. Our study in RPE cells showed that HN activates phosphorylation of STAT3, and incubation with STAT3 inhibitor diminished the protective effect of HN significantly but not completely [47]. Therefore, it has to be reasoned that the receptor-mediated effects of HN peptide only partially contributed to the prevention of cell death. More recent work demonstrates that HN acts through the GP130/IL6ST receptor complex to activate AKT, ERK1/2, and STAT3 signaling pathways [53].

7. Endogenous Expression of HN and Its Functions

There are published reports that HN is expressed endogenously by several cells and tissues in the body such as cardiomyocytes, RPE cells, brain, colon, testis, heart, kidney, skeletal muscle, and liver [47, 54–57]. Further, endogenous HN has been reported to be secreted from cells [25, 29, 47] to the plasma [58–61] and transported to targeted tissues which express HN receptors. Overexpression of HN-protected cells from oxidant insult induced cell death [25, 27, 29]. Further, synthetic HN peptide mimicked the neuroprotection offered by HN-ORF cDNA at concentrations as low as that of secreted HN peptide in the culture medium [25, 29]. In addition, knockdown of endogenous HN by gene silencing correlated with increased sensitivity to oxidative stress- (OS-) induced cell death [27]. Polarization of RPE cells increased endogenous HN levels three-fold over nonpolarized RPE cells [47]. This increase was shown to be correlated with oxidative stress- (OS-) induced cell survival. These studies attest to the importance of HN in cell survival mechanisms.

8. Effects of Oxidative Stress in RPE

The retina is the most vascularized tissue in the human body by mass and is unique in that two independent circulatory networks—the central retinal artery and the choroidal vessels

supply it to maintain its high metabolic demand [62]. As such, RPE cells are highly susceptible to oxidative stress by producing ROS as metabolic byproducts predominantly by robust mitochondrial oxygen consumption during cellular respiration and as a consequence of electron leakage from the respiratory chain enzymes [12]. The vulnerability of RPE cells is also as a result of the large oxygen gradient from the choroid, across the RPE to the outer retina [12]. ROS is also generated by the visual cycle as peroxidation products of photoreceptor polyunsaturated fatty acids and NADPH oxidase-mediated reactions during RPE phagocytosis and recycling of shed POS [12, 63].

Reactive oxygen species are essential physiological signaling molecules modulating gene expression, apoptosis, and proliferation, but are also toxic oxidizers of biomolecules and are linked to many pathologies such as Parkinson disease, AD, atherosclerosis, cancer, diabetes, and age-related diseases [64, 65]. In this regard, the cellular redox status represents a paradox in which an overabundance of oxidizers with insufficient reducing equivalents will accumulate ROS to concentrations that are maladaptive for cell survival by oxidizing and therefore perturbing the structure and function of lipids, proteins, and nucleic acids [21]. Consequently, retinal cells, as with all cells of the body, express enzymatic and nonenzymatic antioxidants and various modalities to repair and or replace oxidized material to circumvent dysfunction and ultimately apoptosis. RPE cells are particularly efficient at maintaining redox homeostasis thanks to, in part, DNA polymerases with sophisticated base excision repair (BER) exonuclease activity and an overabundance of enzymatic and nonenzymatic antioxidants such as reduced GSH and macular pigments that scavenge both photogenerated and nonphotic ROS [12, 66].

As alluded to earlier, the association between AMD and OS comes from biochemical evidence that the toxic, lipid-rich, granules deposited between the RPE and BM are mostly composed of oxidized proteins and lipids. A direct molecular connection between oxidative damage and AMD was established by the finding that carboxyethylpyrrole is elevated in BM and drusen from AMD patients [67]. The multipotent functions of HN and most of the cellular studies have been performed on neuronal cells and AD-related models. Although similarities in the pathogenesis of AD and AMD have been described [68], very little is known on the role of HN in AMD.

9. Exogenous HN Improves Mitochondrial Energetics in Oxidatively Stressed RPE

Due to its high metabolic activity, RPE cells harbor a large number of mitochondria which represent one of the major source of endogenous ROS. Mitochondria are highly susceptible to oxidative damage, and mitochondrial DNA repair in the RPE appears to be relatively very slow [69]. Since RPE cells are postmitotic, damaged mitochondria are not removed as quickly [70] leading to increased ROS production, which may further damage mitochondria [71]. Dysregulated mitochondria result in significantly low energy production and apoptosis, considered one of the initiating factors of AMD [72, 73]. How the MDPs influence the mitochondrial processes was hitherto unknown. Thus, Sreekumar et al. [47] tested HN's potential role in preserving mitochondrial bioenergetics and ROS inhibition in RPE cells. Oxidative stress augmented mitochondrial superoxide production, and HN cotreatment prominently inhibited ROS formation. It is of interest that in cardiac myoblasts stressed with H_2O_2, it was reported that HN analog (HNG) preserved mitochondrial membrane potential and mitochondrial structural integrity and inhibited mitochondrial swelling [74]. These authors further showed that pretreatment with a HN analog exerted cardio protective effects against myocardial ischemia and reperfusion injury in a mouse model [55].

Since it is known that OS affects mitochondria by decreased ATP production, how HN influences mitochondrial bioenergetics needed to be addressed. RPE cells were cotreated with HN (10 and 20 μg) and 150 μM tBH for 24 h. OS induced by tBH significantly decreased mitochondrial respiration, reserve capacity, and ATP production while HN cotreatment dose dependently increased all these parameters thereby restoring mitochondrial functions [47]. Further, it was shown that enhanced bioenergetics is due to increased mitochondrial biogenesis by HN as evidenced by transmission electron microscopy studies and mtDNA copy number [47].

One major consequence of OS is the initiation of cellular senescence. Premature senescence has been suggested as a potentially important pathophysiological mediator of RPE cell atrophy in GA [75, 76]. HN delayed OS-induced premature senescence in RPE cells as evidenced by the regulation of markers of senescence. HN treatment significantly reduced senescence-associated β-Gal-positive cells, *Apo J* transcripts, and $p16^{INK4a}$ expression [47].

10. Effects of ER Stress in RPE and Protection by Exogenous HN

The endoplasmic reticulum (ER) is a large convoluted organelle containing within it the synthetic machinery necessary for producing proteins that it then posttranslationally modifies, folds, and secretes to the Golgi apparatus for further processing [77]. Additional functions include drug detoxification, carbohydrate metabolism, lipid biosynthesis, and regulation of calcium homeostasis as the ER is the major storage depot of intracellular calcium that is essential for calcium-dependent protein folding by ER chaperones [78].

Protein maturation is dependent on the capacity of the ER to fold peptides into their proper tertiary structures, and this requires that the folding within the ER lumen be conducted in an oxidizing environment to facilitate the formation of disulfide bonds [79]. As such, a redox status favoring an oxidizing luminal microenvironment is fundamental for this process. Perturbation of this microenvironment by various insults including viral infections, metabolic disturbances, and OS by excessive ROS results in calcium efflux from the ER and toxic unfolded/misfolded protein

aggregates that increase the ER burden and cause ER stress [80].

To maintain proteostasis and cell function, the ER activates an adaptive quality control measure known as the unfolded protein response (UPR). The UPR is initiated by three independent transmembrane stress transducers: (1) inositol-requiring kinase-1 (IRE1), (2) RNA-activated protein kinase-like ER kinase (PERK), and (3) activating transcription factor-6 (ATF6) [81]. The collective activation of these signaling pathways causes suppression of mRNA translation to prevent further production of unfolded/misfolded proteins, refolding of misfolded proteins by upregulating ER chaperones, and induction of the ER-associated degradation (ERAD) system to eliminate toxic protein aggregates [82]. In this regard, the acute phase of the UPR promotes cell survival when ER stress is salvageable; however, sustained stress will induce caspase activation, mitochondrial dysfunction, and apoptosis to remove pathological cells and spare healthy ones [82–84].

Although the exact stress sensing mechanism of the UPR is yet to be understood, glucose-regulated protein-78 (GRP78), sometimes referred to as immunoglobulin-binding protein (BiP), is a stress-sensitive ER resident chaperone thought to regulate its activation [85]. Normally, GRP78 remains bound to the transmembrane stress transducers within the ER lumen keeping them in an inactive state [85]. The presence of stressful stimuli induces GRP78 to dissociate from the transducers resulting in their dimerization, autophosphorylation, and activation of their respective UPR pathways [86].

If prolonged ER stress exceeds the UPR's adaptive limitations for attenuating ER burden, the IRE1, PERK, and ATF6 prosurvival signals initiate both caspase-dependent and independent programmed cell death (PCD) pathways resulting in mitochondrial dysfunction and apoptosis [81, 83, 84]. Particularly in the retina, IRE1/TNF receptor-associated factor-2 (TRAF2)/apoptosis signal-regulating kinase-1 (ASK1)/c-Jun amino-terminal kinase (JNK) and PERK/eIF2α/ATF4/CHOP can elicit several AMD-related pathways via the induction of VEGF, CHOP, caspase 4, and NF-κB [87].

Only recently, the effect of HN has been studied in the context of ER stress [11]. In human primary RPE cells exposed to multiple ER stressors (tunicamycin, brefeldin A, and thapsigargin), HN pretreatment offered a dose-dependent protection from cell death. The study found that HN treatment downregulated CHOP expression and decreased activated caspase 3 and caspase 4. Further, while TM treatment elevated mitochondrial ROS production and decreased mitochondrial glutathione (GSH), HN cotreatment inhibited ROS formation and restored GSH synthesis under the experimental conditions. While clearly GSH was involved in cellular protection, other antioxidants such as catalase, Trx1, Grx1, and Grx2 and SOD II did not show appreciable change with HN. The protective action of HN was not restricted to RPE cells as the authors showed that HN also protected U-251 glioma cells exposed to TM [11]. A potential role of HN in calcium metabolism in which HN in the ER could regulate intracellular calcium flux has been reported [57].

11. Endoplasmic Reticulum-Mitochondrial Crosstalk

ER stress and OS are participants in an array of physiological and pathophysiological conditions. The interaction between ER and mitochondria is evolving as a crucial factor in the regulation of the dynamic changes in motility, structure, and shape of these organelles. Studies on ER-mitochondria interactions in RPE and their modulation are scarce. In this context, the work of Matsunaga et al. [11] is relevant to further our understanding of ER stress-related mechanisms in the RPE and retina and potential roles of mitochondrial peptides in cellular protection. The study revealed that multiple ER stressors caused cell death by increasing mitochondrial ROS and activating downstream cell death pathways. Furthermore, ER and mitochondria interact both physiologically and functionally at sites called mitochondrial-associated membranes (MAMs) [88]. The contact sites between the ER and mitochondria have been measured to be 10–30 nm wide [89, 90]. MAMs facilitate interorganelle communication between the ER and mitochondria and are critical for lipid synthesis and transport, mitochondrial functions, the maintenance of calcium homeostasis, and apoptosis [91]. Many ER and mitochondria-associated proteins such as chaperones, protein kinases, and proteins regulating mitochondrial dynamics and morphology have been identified in MAMs, suggesting the major involvement of MAMs in all physiological processes [92]. Studies showed that ER Ca^{2+} channels, including the IP3Rs and the mitochondrial voltage-dependent anion channel, are rich in MAMs, which could facilitate Ca^{2+} flow between ER and mitochondria [92]. There is evidence to show that the ER-mitochondria contact sites are involved in autophagosome formation and that many proteins in the MAM compartments are necessary for autophagic vesicle formation [93–95]. In addition, ER-mitochondria contact sites are relevant to mitochondrial biogenesis based on the findings that mitochondrial fission occurs at areas of ER-mitochondria contacts [90, 96]. Further, mitofusin 2, which regulates mitochondrial fusion, is also proposed as a tethering protein that connects ER with mitochondria [97].

Based on our findings, we present a composite scheme that depicts the ER-mitochondrial crosstalk in cellular stress and the protective role played by HN in RPE cell death by ER and oxidant stressors by direct and indirect mechanisms (Figure 2). Both OS and ER stress cause RPE apoptosis by increased generation of ROS, downregulation of mitochondrial GSH, and activation of caspase 3 [11, 47]. Increased ER stress from OS via the crosstalk by MAMs and ER-specific events of caspase 4 and CHOP activation are also shown (Figure 2). Uptake of exogenous HN by RPE mitochondria and the effect of exogenous HN cotreatment with oxidants or ER stressors on the inhibition of apoptotic cell death is illustrated. HN cotreatment inhibits ROS production and upregulates GSH in mitochondria. HN also inhibits caspase 4 and CHOP preventing RPE apoptosis. The known receptors of HN, namely, WSX-1, CNTFR, and gp130 and the inhibition of apoptosis by activation of p-STAT3 are also shown in the figure.

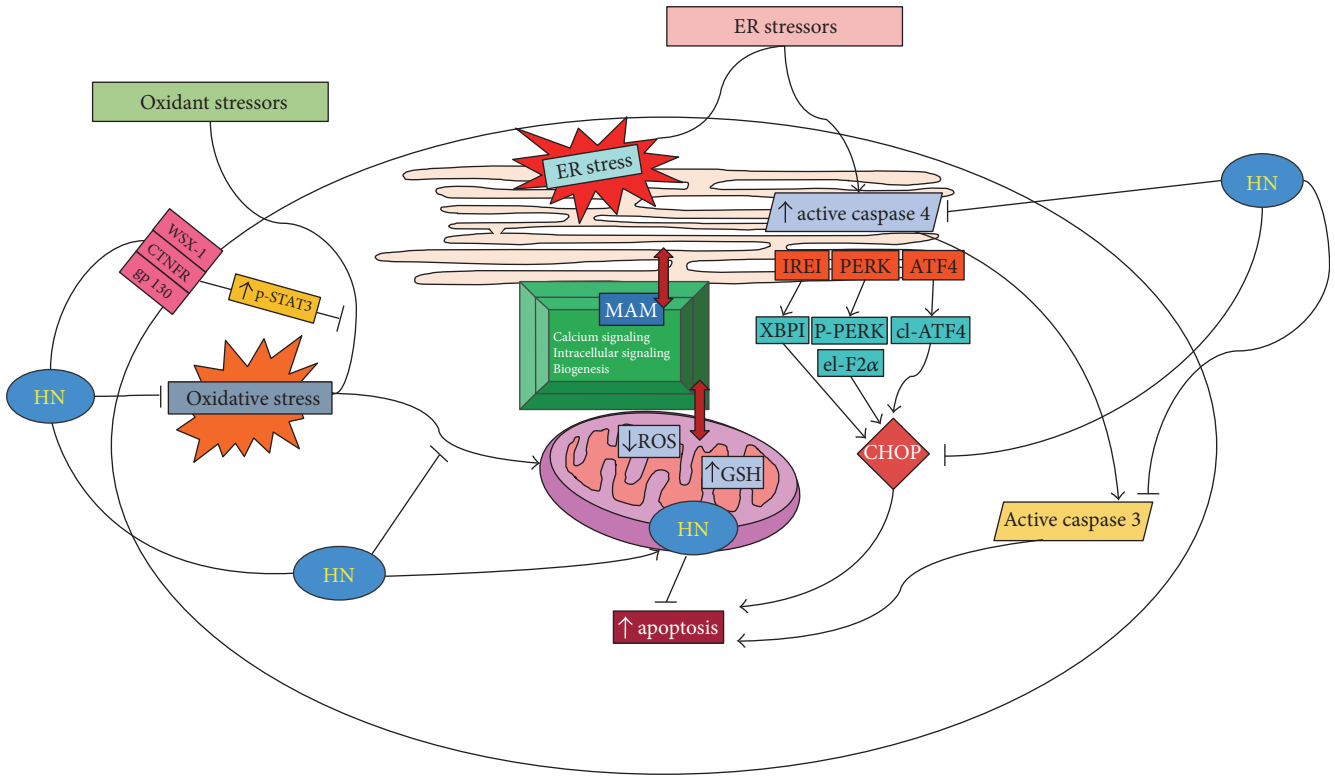

Figure 2: HN inhibits OS and ER stress in RPE by direct and indirect mechanisms. ER and mitochondria are linked through MAMs (mitochondria-associated membranes) which perform a variety of functions; some of which are listed in the figure. ER stress leads to CHOP induction via multiple signaling mechanisms. ER stress also activates procaspase 4 to active caspase 4 which in turn upregulates active caspase 3 leading to increased apoptosis. Exogenous HN's action on the suppression of ER stress-induced apoptosis via inhibition of caspase 4, CHOP, and caspase 3 are also shown in the figure. Exogenous HN is taken up by RPE and gains entry into mitochondria when cotreated with oxidant stressor. HN downregulates cellular OS and decreases mitochondrial ROS and augments mitochondrial GSH. The receptor-mediated pathway of HN preventing oxidant-induced apoptosis via activation of phosphorylated STAT3 is also shown.

12. Future Directions

It would be of great interest to explore proteins and peptides including MDPs that affect ER stress-induced mitochondrial dysfunction and the related pathways participating in the process. On the other hand, the subcellular localization of HN is still under active investigation. We have provided evidence by confocal microscopy that fluorescein-labeled HN was rapidly taken by RPE and colocalized with mitochondria. However, it is not known whether HN is localized in ER compartments and this warrants additional studies. Further, the role of ER stressors on mitochondrial respiration and biogenesis in RPE and the nature of the salutary effects of HN will be an important issue to address. The role of ER stress on pro- and antiapoptotic factors in RPE cells such as Bax and Bcl-2 and the potential effect of HN on these factors remain to be studied. MAMs regulate several calcium-dependent cellular processes, and the movement of calcium between the ER and mitochondria is essential for the execution of both apoptotic [98] and autophagy pathways [99]. As stated earlier, HN was involved in calcium regulation [57], and detailed studies are needed to explore HNs' role in calcium regulation and autophagy under ER stress and OS. Additionally, the potential role of HN in regulating proteins present in MAMs would be of utmost interest to study given the recent studies suggesting the possible role of MAM protein role in mitochondrial dynamics [92]. ER stress and OS form a vicious cycle in human pathologies including AMD, and it would be of interest to determine the role of inflammatory molecules such as NLRP3 in AMD and how HN modulates these effects. Further, the recent discovery of additional MDPs, namely, SHLPs and MOTS-c, provides opportunity for exploration of these new MDPs in the therapy of AMD and related retinal degenerative disorders.

13. Therapeutic Potential of HN and Other MDPs in AMD

Since its discovery, HN has been validated to offer beneficial effects in many disease models, most of which are age-related. The advantage of HN as a therapeutic agent is that it antagonizes against a wide array of insults despite the complex nature of cytotoxic mechanisms. HN being a 24-amino acid peptide has rapid tissue clearance resulting in a very short half-life. To improve the half-life and to permit localized administration, we have suggested that making thermally responsive elastin-like polypeptides (ELP) [100] recombinantly conjugated with HN could be of value. Short peptides are typically proteolytically unstable and are cleared

rapidly from circulation, and the ELP depot protects them from premature proteolysis and increases in vivo bioavailability [101]. Further, ELPs are useful and safe vehicles for both systemic and local drug delivery. Future studies will focus on evaluating the pharmacokinetics of ELP-MDPs for long term use.

14. Conclusions

Many recent studies indicate that ER stress and oxidative stress are highly interconnected biological processes which regulate a wide array of signaling pathways in the cell. Although it is known that both stress processes are closely associated, the mechanisms linking ER stress to OS are not fully explored. A greater understanding of the role of HN and MDPs on their mechanisms of action in the retina under pathophysiological conditions and development of optimal modes of their delivery will be of benefit in combating AMD and other related diseases.

Abbreviations

AD: Alzheimer disease
AMD: Age-related macular degeneration
APP: Amyloid precursor protein
ATP: Adenosine triphosphate
BER: Base excision repair
BM: Bruch membrane
CHOP: C/EBP homologous protein
$CoCl_2$: Cobalt chloride
CNTFR: Ciliary neurotrophic factor receptor
CNV: Choroidal neovascularization
ER: Endoplasmic reticulum
ERAD: ER-associated degradation
ECM: Extracellular matrix
ERK1/2: Extracellular signal-regulated kinase 1/2
FAD: Familial Alzheimer's disease
GWAS: Genome-wide association studies
GA: Geographic atrophy
Gp130: Glycoprotein 130
HN: Humanin
htHNR: Heterotrimeric HN receptor
IGFBP-3: Insulin-like growth factor binding protein-3
MAMs: Mitochondrial-associated membranes
MDP: Mitochondrial-derived peptide
MOTS-c: Mitochondrial open reading frame of the 12S rRNA-c
mtDNA: Mitochondrial DNA
NOD: Nonobese diabetic
nDNA: Nuclear DNA
NUMT: Nuclear mitochondrial DNA transfer
OS: Oxidative stress
PC12: Pheochromocytoma cells
PCD: Programmed cell death
PI3K: Phosphoinositide-3-kinase
ROS: Reactive oxygen species
RPE: Retinal pigment epithelium
SHLPs: Small humanin-like peptides
sORF: Short open reading frame
STAT3: Signal transducer and activator or transcriptor 3
tBH: tert-Butyl hydroperoxide
T2DM: Type 2 diabetes mellitus
UPR: Unfolded protein response
VEGF: Vascular endothelial growth factor.

Conflicts of Interest

The authors declare no conflicts of interest.

Authors' Contributions

Leonid Minasyan and Parameswaran G. Sreekumar contributed equally to the study. David R. Hinton and Ram Kannan are cosenior authors.

Acknowledgments

The authors thank Ernesto Barron and Eric Barron for the help with figures and Jan Lee for secretarial assistance. Work from their laboratory was supported by Grant EY01545 (David R. Hinton) and by Core Grant EY03040 and the Arnold and Mabel Beckman Foundation (David R. Hinton and Ram Kannan).

References

[1] J. Ambati and B. J. Fowler, "Mechanisms of age-related macular degeneration," *Neuron*, vol. 75, no. 1, pp. 26–39, 2012.

[2] K. L. Pennington and M. M. DeAngelis, "Epidemiology of age-related macular degeneration (AMD): associations with cardiovascular disease phenotypes and lipid factors," *Eye and Vision*, vol. 3, no. 1, p. 34, 2016.

[3] R. E. Hogg and U. Chakravarthy, "Visual function and dysfunction in early and late age-related maculopathy," *Progress in Retinal and Eye Research*, vol. 25, no. 3, pp. 249–276, 2006.

[4] J. Z. Nowak, "Age-related macular degeneration (AMD): pathogenesis and therapy," *Pharmacological Reports*, vol. 58, no. 3, pp. 353–363, 2006.

[5] P. T. V. M. D. Jong, "Age-related macular degeneration," *New England Journal of Medicine*, vol. 355, no. 14, pp. 1474–1485, 2006.

[6] R. A. Armstrong and M. Mousavi, "Overview of risk factors for age-related macular degeneration (AMD)," *Journal of Stem Cells*, vol. 10, no. 3, p. 171, 2015.

[7] L. G. Fritsche, W. Igl, J. N. Bailey et al., "A large genome-wide association study of age-related macular degeneration highlights contributions of rare and common variants," *Nature Genetics*, vol. 48, no. 2, pp. 134–143, 2016.

[8] O. Strauss, "The retinal pigment epithelium in visual function," *Physiological Reviews*, vol. 85, no. 3, pp. 845–881, 2005.

[9] S. He, J. Yaung, Y. H. Kim, E. Barron, S. J. Ryan, and D. R. Hinton, "Endoplasmic reticulum stress induced by oxidative stress in retinal pigment epithelial cells," *Graefe's Archive for Clinical and Experimental Ophthalmology*, vol. 246, no. 5, pp. 677–683, 2008.

[10] G. Dou, R. Kannan, and D. R. Hinton, "Endoplasmic reticulum response to oxidative stress in RPE," in *Studies on Retinal and Choroidal Disorders*, pp. 241–258, Humana Press, 2012.

[11] D. Matsunaga, P. G. Sreekumar, K. Ishikawa et al., "Humanin protects RPE cells from endoplasmic reticulum stress-induced apoptosis by upregulation of mitochondrial glutathione," *PLoS One*, vol. 11, no. 10, article e0165150, 2016.

[12] S. G. Jarrett and M. E. Boulton, "Consequences of oxidative stress in age-related macular degeneration," *Molecular Aspects of Medicine*, vol. 33, no. 4, pp. 399–417, 2012.

[13] P. G. Sreekumar, D. R. Hinton, and R. Kannan, "Endoplasmic reticulum-mitochondrial crosstalk: a novel role for the mitochondrial peptide humanin," *Neural Regeneration Research*, vol. 12, no. 1, pp. 35–38, 2017.

[14] S. G. Jarrett, H. Lin, B. F. Godley, and M. E. Boulton, "Mitochondrial DNA damage and its potential role in retinal degeneration," *Progress in Retinal and Eye Research*, vol. 27, no. 6, pp. 596–607, 2008.

[15] M. R. Terluk, R. J. Kapphahn, L. M. Soukup et al., "Investigating mitochondria as a target for treating age-related macular degeneration," *Journal of Neuroscience*, vol. 35, no. 18, pp. 7304–7311, 2015.

[16] L. J. Cobb, C. Lee, J. Xiao et al., "Naturally occurring mitochondrial-derived peptides are age-dependent regulators of apoptosis, insulin sensitivity, and inflammatory markers," *Aging (Albany NY)*, vol. 8, no. 4, p. 796, 2016.

[17] P. F. Chinnery and E. A. Schon, "Mitochondria," *Journal of Neurology, Neurosurgery & Psychiatry*, vol. 74, no. 9, pp. 1188–1199, 2003.

[18] T. R. Mercer, S. Neph, M. E. Dinger et al., "The human mitochondrial transcriptome," *Cell*, vol. 146, no. 4, pp. 645–658, 2011.

[19] J. W. Taanman, "The mitochondrial genome: structure, transcription, translation and replication," *Biochimica et Biophysica Acta (BBA)-Bioenergetics*, vol. 1410, no. 2, pp. 103–123, 1999.

[20] P. Smits, J. Smeitink, and L. van den Heuvel, "Mitochondrial translation and beyond: processes implicated in combined oxidative phosphorylation deficiencies," *Journal of Biomedicine & Biotechnology*, vol. 2010, Article ID 737385, 24 pages, 2010.

[21] M. Valko, D. Leibfritz, J. Moncol, M. T. D. Cronin, M. Mazur, and J. Telser, "Free radicals and antioxidants in normal physiological functions and human disease," *The International Journal of Biochemistry & Cell Biology*, vol. 39, no. 1, pp. 44–84, 2007.

[22] J. Nunnari and A. Suomalainen, "Mitochondria: in sickness and in health," *Cell*, vol. 148, no. 6, pp. 1145–1159, 2012.

[23] S. J. Andrews and J. A. Rothnagel, "Emerging evidence for functional peptides encoded by short open reading frames," *Nature Reviews Genetics*, vol. 15, no. 3, pp. 193–204, 2014.

[24] A. Saghatelian and J. P. Couso, "Discovery and characterization of smORF-encoded bioactive polypeptides," *Nature Chemical Biology*, vol. 11, no. 12, pp. 909–916, 2015.

[25] Y. Hashimoto, T. Niikura, H. Tajima et al., "A rescue factor abolishing neuronal cell death by a wide spectrum of familial Alzheimer's disease genes and Aβ," *Proceedings of the National Academy of Sciences*, vol. 98, no. 11, pp. 6336–6341, 2001.

[26] M. Ikonen, B. Liu, Y. Hashimoto et al., "Interaction between the Alzheimer's survival peptide humanin and insulin-like growth factor-binding protein 3 regulates cell survival and apoptosis," *Proceedings of the National Academy of Sciences*, vol. 100, no. 22, pp. 13042–13047, 2003.

[27] B. Guo, D. Zhai, E. Cabezas et al., "Humanin peptide suppresses apoptosis by interfering with Bax activation," *Nature*, vol. 423, no. 6938, pp. 456–461, 2003.

[28] C. Lee, J. Zeng, B. G. Drew et al., "The mitochondrial-derived peptide MOTS-c promotes metabolic homeostasis and reduces obesity and insulin resistance," *Cell Metabolism*, vol. 21, no. 3, pp. 443–454, 2015.

[29] Y. Yamagishi, Y. Hashimoto, T. Niikura, and I. Nishimoto, "Identification of essential amino acids in Humanin, a neuroprotective factor against Alzheimer's disease-relevant insults," *Peptides*, vol. 24, no. 4, pp. 585–595, 2003.

[30] K. Yen, C. Lee, H. Mehta, and P. Cohen, "The emerging role of the mitochondrial-derived peptide humanin in stress resistance," *Journal of Molecular Endocrinology*, vol. 50, no. 1, pp. R11–R19, 2013.

[31] C. Lee, K. Yen, and P. Cohen, "Humanin: a harbinger of mitochondrial-derived peptides?," *Trends in Endocrinology & Metabolism*, vol. 24, no. 5, pp. 222–228, 2013.

[32] M. Bodzioch, K. Lapicka-Bodzioch, B. Zapala, W. Kamysz, B. Krec-Wilk, and A. Dembinska-Kiec, "Evidence for potential functionality of nuclearly-encoded humanin isoforms," *Genomics*, vol. 94, pp. 247–258, 2009.

[33] Y. Hashimoto, T. Niikura, Y. Ito et al., "Detailed characterization of neuroprotection by a rescue factor humanin against various Alzheimer's disease-relevant insults," *Journal of Neuroscience*, vol. 21, no. 23, pp. 9235–9245, 2001.

[34] V. Maximov, A. Martynenko, G. Hunsmann, and V. Tarantul, "Mitochondrial 16S rRNA gene encodes a functional peptide, a potential drug for Alzheimer's disease and target for cancer therapy," *Medical Hypotheses*, vol. 59, no. 6, pp. 670–673, 2002.

[35] D. Zhai, F. Luciano, X. Zhu, B. Guo, A. C. Satterthwait, and J. C. Reed, "Humanin binds and nullifies Bid activity by blocking its activation of Bax and Bak," *Journal of Biological Chemistry*, vol. 280, no. 16, pp. 15815–15824, 2005.

[36] F. Luciano, D. Zhai, X. Zhu et al., "Cytoprotective peptide humanin binds and inhibits proapoptotic Bcl-2/Bax family protein BimEL," *Journal of Biological Chemistry*, vol. 280, no. 16, pp. 15825–15835, 2005.

[37] J. Xiao, S. J. Kim, P. Cohen, and K. Yen, "Humanin: functional interfaces with IGF-I," *Growth Hormone & IGF Research*, vol. 29, pp. 21–27, 2016.

[38] M. Holzenberger, J. Dupont, B. Ducos et al., "IGF-1 receptor regulates lifespan and resistance to oxidative stress in mice," *Nature*, vol. 421, no. 6919, pp. 182–187, 2003.

[39] R. H. Muzumdar, D. M. Huffman, G. Atzmon et al., "Humanin: a novel central regulator of peripheral insulin action," *PloS One*, vol. 4, no. 7, article e6334, 2009.

[40] P. T. Hoang, P. Park, L. J. Cobb et al., "The neurosurvival factor humanin inhibits β-cell apoptosis via signal transducer and activator of transcription 3 activation and delays and ameliorates diabetes in nonobese diabetic mice," *Metabolism*, vol. 59, no. 3, pp. 343–349, 2010.

[41] S. Kariya, M. Hirano, Y. Furiya, K. Sugie, and S. Ueno, "Humanin detected in skeletal muscles of MELAS patients: a possible new therapeutic agent," *Acta Neuropathologica*, vol. 109, no. 4, pp. 367–372, 2005.

[42] T. Niikura, E. Sidahmed, C. Hirata-Fukae, P. S. Aisen, and Y. Matsuoka, "A humanin derivative reduces amyloid beta accumulation and ameliorates memory deficit in triple transgenic mice," *PLoS One*, vol. 6, no. 1, article e16259, 2011.

[43] Y. K. Oh, A. R. Bachar, D. G. Zacharias et al., "Humanin preserves endothelial function and prevents atherosclerotic plaque progression in hypercholesterolemic ApoE deficient mice," *Atherosclerosis*, vol. 219, no. 1, pp. 65–73, 2011.

[44] J. Men, X. Zhang, Y. Yang, and D. Gao, "An AD-related neuroprotector rescues transformed rat retinal ganglion cells from CoCl2-induced apoptosis," *Journal of Molecular Neuroscience*, vol. 47, no. 1, pp. 144–149, 2012.

[45] S. Kariya, N. Takahashi, N. Ooba, M. Kawahara, H. Nakayama, and S. Ueno, "Humanin inhibits cell death of serum-deprived PC12h cells," *Neuroreport*, vol. 13, no. 6, pp. 903–907, 2002.

[46] X. Xu, C. C. Chua, J. Gao, R. C. Hamdy, and B. H. L. Chua, "Humanin is a novel neuroprotective agent against stroke," *Stroke*, vol. 37, no. 10, pp. 2613–2619, 2006.

[47] P. G. Sreekumar, K. Ishikawa, C. Spee et al., "The mitochondrial-derived peptide humanin protects RPE cells from oxidative stress, senescence, and mitochondrial dysfunction," *Investigative Ophthalmology & Visual Science, 2016*, vol. 57, no. 3, pp. 1238–1253, 2016.

[48] S. Sonoda, C. Spee, E. Barron, S. J. Ryan, R. Kannan, and D. R. Hinton, "A protocol for the culture and differentiation of highly polarized human retinal pigment epithelial cells," *Nature Protocols*, vol. 4, no. 5, pp. 662–673, 2009.

[49] Y. Hashimoto, M. Kurita, S. Aiso, I. Nishimoto, and M. Matsuoka, "Humanin inhibits neuronal cell death by interacting with a cytokine receptor complex or complexes involving CNTF receptor alpha/WSX-1/gp130," *Molecular Biology of the Cell*, vol. 20, no. 12, pp. 2864–2873, 2009.

[50] Y. Hashimoto, M. Kurita, and M. Matsuoka, "Identification of soluble WSX-1 not as a dominant-negative but as an alternative functional subunit of a receptor for an anti-Alzheimer's disease rescue factor humanin," *Biochemical & Biophysical Research Communications*, vol. 389, no. 1, pp. 95–99, 2009.

[51] T. Chiba, M. Yamada, Y. Hashimoto et al., "Development of a femtomolar-acting humanin derivative named colivelin by attaching activity-dependent neurotrophic factor to its N terminus: characterization of colivelin-mediated neuroprotection against Alzheimer's disease-relevant insults in vitro and in vivo," *The Journal of Neuroscience*, vol. 25, no. 44, pp. 10252–10261, 2005.

[52] Y. Hashimoto, H. Suzuki, S. Aiso, T. Niikura, I. Nishimoto, and M. Matsuoka, "Involvement of tyrosine kinases and STAT3 in Humanin-mediated neuroprotection," *Life Sciences*, vol. 77, no. 24, pp. 3092–3104, 2005.

[53] S. J. Kim, N. Guerrero, G. Wassef et al., "The mitochondrial-derived peptide humanin activates the ERK1/2, AKT, and STAT3 signaling pathways and has age-dependent signaling pathways and has age-dependent signaling differences in the hippocampus," *Oncotarget*, vol. 7, no. 30, pp. 46899–46912, 2016.

[54] H. Tajima, T. Niikura, Y. Hashimoto et al., "Evidence for in vivo production of humanin peptide, a neuroprotective factor against Alzheimer's disease-related insults," *Neuroscience Letters*, vol. 324, no. 3, pp. 227–231, 2003.

[55] R. H. Muzumdar, D. M. Huffman, J. W. Calvert et al., "Acute humanin therapy attenuates myocardial ischemia and reperfusion injury in mice," *Arteriosclerosis Thrombosis and Vascular Biology*, vol. 30, no. 10, pp. 1940–1948, 2010.

[56] T. Kin, K. Sugie, M. Hirano, Y. Goto, I. Nishino, and S. Ueno, "Humanin expression in skeletal muscles of patients with chronic progressive external ophthalmoplegia," *Journal of Human Genetics*, vol. 51, no. 6, pp. 555–558, 2006.

[57] A. Knapp, U. Czech, A. Polus, M. Chojnacka, A. Śliwa et al., "Humanin peptides regulate calcium flux in the mammalian neuronal, glial and endothelial cells under stress conditions," *Journal of Cell Science & Therapy*, vol. 3, no. 4, p. 128, 2012.

[58] S. Thummasorn, N. Apaijai, S. Kerdphoo, K. Shinlapawittayatorn, S. C. Chattipakorn, and N. Chattipakorn, "Humanin exerts cardioprotection against cardiac ischemia/reperfusion injury through attenuation of mitochondrial dysfunction," *Cardiovascular Therapeutics*, vol. 34, no. 6, pp. 404–414, 2016.

[59] Y. P. Chin, J. Keni, J. Wan et al., "Pharmacokinetics and tissue distribution of humanin and its analogues in male rodents," *Endocrinology*, vol. 154, no. 10, pp. 3739–3744, 2013.

[60] R. J. Widmer, A. J. Flammer, J. Herrmann et al., "Circulating humanin levels are associated with preserved coronary endothelial function," *American Journal of Physiology-Heart and Circulatory Physiology*, vol. 304, no. 3, pp. H393–H397, 2013.

[61] Y. Lytvyn, J. Wan, V. Lai, P. Cohen, and D. Z. Cherney, "The effect of sex on humanin levels in healthy adults and patients with uncomplicated type 1 diabetes mellitus," *Canadian Journal of Physiology and Pharmacology*, vol. 93, no. 4, pp. 239–243, 2015.

[62] H. Purnyn, "The mammalian retina: structure and blood supply," *Neurophysiology*, vol. 45, no. 3, pp. 266–276, 2013.

[63] P. X. Shaw, T. Stiles, C. Douglas et al., "Oxidative stress, innate immunity, and age-related macular degeneration," *AIMS Molecular Science*, vol. 3, no. 2, pp. 196–221, 2016.

[64] W. Dröge, "Free radicals in the physiological control of cell function," *Physiological Reviews*, vol. 82, no. 1, pp. 47–95, 2002.

[65] A. Phaniendra, D. B. Jestadi, and L. Periyasamy, "Free radicals: properties, sources, targets, and their implication in various diseases," *Indian Journal of Clinical Biochemistry*, vol. 30, no. 1, pp. 11–26, 2015.

[66] J. M. Burke, P. Kaczara, C. Skumatz, M. Zareba, M. W. Raciti, and T. Sarna, "Dynamic analyses reveal cytoprotection by RPE melanosomes against non-photic stress," *Molecular Vision*, vol. 17, pp. 2864–2877, 2011.

[67] J. W. Crabb, M. Miyagi, X. Gu et al., "Drusen proteome analysis: an approach to the etiology of age-related macular degeneration," *Proceedings of the National Academy of Sciences*, vol. 99, no. 23, pp. 14682–14687, 2002.

[68] K. Ohno-Matsui, "Parallel findings in age-related macular degeneration and Alzheimer's disease," *Progress in Retinal and Eye Research*, vol. 30, no. 4, pp. 217–238, 2011.

[69] J. Blasiak, S. Glowacki, A. Kauppinen, and K. Kaarniranta, "Mitochondrial and nuclear DNA damage and repair in age-related macular degeneration," *International Journal of Molecular Sciences*, vol. 14, no. 2, pp. 2996–3010, 2013.

[70] J. Cai, K. C. Nelson, M. Wu, P. Sternberg Jr., and D. P. Jones, "Oxidative damage and protection of the RPE," *Progress in Retinal and Eye Research*, vol. 19, no. 2, pp. 205–221, 2000.

[71] F. Q. Liang and B. F. Godley, "Oxidative stress-induced mitochondrial DNA damage in human retinal pigment epithelial cells: a possible mechanism for RPE aging and age-related macular degeneration," *Experimental Eye Research*, vol. 76, no. 4, pp. 397–403, 2003.

[72] C. L. Nordgaard, P. P. Karunadharma, X. Feng, T. W. Olsen, and D. A. Ferrington, "Mitochondrial proteomics of the retinal pigment epithelium at progressive stages of age-related macular degeneration," *Investigative Ophthalmology & Visual Science*, vol. 49, no. 7, pp. 2848–2455, 2008.

[73] K. Kinnunen, G. Petrovski, M. C. Moe, A. Berta, and K. Kaarniranta, "Molecular mechanisms of retinal pigment epithelium damage and development of age-related macular degeneration," *Acta Ophthalmologica*, vol. 90, no. 4, pp. 299–309, 2012.

[74] L. E. Klein, L. Cui, Z. Gong, K. Su, and R. Muzumdar, "A humanin analog decreases oxidative stress and preserves mitochondrial integrity in cardiac myoblasts," *Biochemical and Biophysical Research Communications*, vol. 440, no. 2, pp. 197–203, 2013.

[75] R. M. Naylor, D. J. Baker, and J. M. van Deursen, "Senescent cells: a novel therapeutic target for aging and age-related diseases," *Clinical Pharmacology and Therapeutics*, vol. 93, no. 1, pp. 105–116, 2013.

[76] M. R. Kozlowski, "RPE cell senescence: a key contributor to age-related macular degeneration," *Medical* Hypotheses, vol. 78, no. 4, pp. 505–510, 2012.

[77] D. Ron and P. Walter, "Signal integration in the endoplasmic reticulum unfolded protein response," *Nature Reviews Molecular Cell Biology*, vol. 8, no. 7, pp. 519–529, 2007.

[78] A. Görlach, P. Klappa, and T. Kietzmann, "The endoplasmic reticulum: folding, calcium homeostasis, signaling, and redox control," *Antioxidants & Redox Signaling*, vol. 8, no. 9-10, pp. 1391–1418, 2006.

[79] B. P. Tu, S. C. Ho-Schleyer, K. J. Travers, and J. S. Weissman, "Biochemical basis of oxidative protein folding in the endoplasmic reticulum," *Science*, vol. 290, no. 5496, pp. 1571–1574, 2000.

[80] G. Jing, J. J. Wang, and S. X. Zhang, "ER stress and apoptosis: a new mechanism for retinal cell death," *Experimental Diabetes Research*, vol. 2012, Article ID 589589, 11 pages, 2012.

[81] M. Gorbatyuk and O. Gorbatyuk, "Review: retinal degeneration: focus on the unfolded protein response," *Molecular Vision*, vol. 19, pp. 1985–1998, 2013.

[82] S. X. Zhang, E. Sanders, S. J. Fliesler, and J. J. Wang, "Endoplasmic reticulum stress and the unfolded protein responses in retinal degeneration," *Experimental Eye Research*, vol. 125, pp. 30–40, 2014.

[83] I. Kim, W. Xu, and J. C. Reed, "Cell death and endoplasmic reticulum stress: disease relevance and therapeutic opportunities," *Nature Reviews Drug Discovery*, vol. 7, no. 12, pp. 1013–1030, 2008.

[84] T. Momoi, "Caspases involved in ER stress-mediated cell death," *Journal of Chemical Neuroanatomy*, vol. 28, no. 1, pp. 101–105, 2004.

[85] A. Bertolotti, Y. Zhang, L. M. Hendershot, H. P. Harding, and D. Ron, "Dynamic interaction of BiP and ER stress transducers in the unfolded-protein response," *Nature Cell Biology*, vol. 2, no. 6, pp. 326–332, 2000.

[86] H. P. Harding, Y. Zhang, A. Bertolotti, H. Zeng, and D. Ron, "Perk is essential for translational regulation and cell survival during the unfolded protein response," *Molecular Cell*, vol. 5, no. 5, pp. 897–904, 2000.

[87] A. Salminen, A. Kauppinen, J. M. Hyttinen, E. Toropainen, and K. Kaarniranta, "Endoplasmic reticulum stress in age-related macular degeneration: trigger for neovascularization," *Molecular Medicine*, vol. 16, no. 11-12, pp. 535–542, 2010.

[88] J. E. Vance, "Phospholipid synthesis in a membrane fraction associated with mitochondria," *The Journal of Biological Chemistry*, vol. 265, no. 3, pp. 7248–7256, 1990.

[89] G. Csordás, C. Renken, P. Várnai et al., "Structural and functional features and significance of the physical linkage between ER and mitochondria," *The Journal of Cell Biology*, vol. 174, no. 7, pp. 915–921, 2006.

[90] J. R. Friedman, L. L. Lackner, M. West, J. R. DiBenedetto, J. Nunnari, and G. K. Voeltz, "ER tubules mark sites of mitochondrial division," *Science*, vol. 334, no. 6054, pp. 358–362, 2011.

[91] A. Raturi and T. Simmen, "Where the endoplasmic reticulum and the mitochondrion tie the knot: the mitochondria-associated membrane (MAM)," *Biochimica et Biophysica Acta*, vol. 1833, no. 1, pp. 213–224, 2013.

[92] A. R. van Vliet, T. Verfaillie, and P. Agostinis, "New functions of mitochondria associated membranes in cellular signaling," *Biochimica et Biophysica Acta*, vol. 1843, no. 10, pp. 2253–2262, 2014.

[93] D. W. Hailey, A. S. Rambold, P. Satpute-Krishnan et al., "Mitochondria supply membranes for autophagosome biogenesis during starvation," *Cell*, vol. 141, no. 4, pp. 656–667, 2010.

[94] M. Hamasaki, N. Furuta, A. Matsuda et al., "Autophagosomes form at ER-mitochondria contact sites," *Nature*, vol. 495, no. 7441, pp. 389–393, 2013.

[95] E. L. Axe, S. A. Walker, M. Manifava et al., "Autophagosome formation from membrane compartments enriched in phosphatidylinositol 3-phosphate and dynamically connected to the endoplasmic reticulum," *The Journal of Cell Biology*, vol. 182, no. 4, pp. 685–701, 2008.

[96] F. Korobova, V. Ramabhadran, and H. N. Higgs, "An actin-dependent step in mitochondrial fission mediated by the ER-associated formin INF2," *Science*, vol. 339, no. 6118, pp. 464–467, 2013.

[97] O. M. de Brito and L. Scorrano, "Mitofusin 2 tethers endoplasmic reticulum to mitochondria," *Nature*, vol. 456, no. 7222, pp. 605–610, 2008.

[98] C. Giorgi, M. R. Wieckowski, P. P. Pandolfi, and P. Pinton, "Mitochondria associated membranes (MAMs) as critical hubs for apoptosis," *Communicative and Integrative Biology*, vol. 4, no. 3, pp. 334-335, 2011.

[99] C. Cardenas, R. A. Miller, I. Smith et al., "Essential regulation of cell bioenergetics by constitutive InsP3 receptor Ca2+ transfer to mitochondria," *Cell*, vol. 142, no. 2, pp. 270–283, 2010.

[100] W. Wang, P. G. Sreekumar, V. Valluripalli et al., "Protein polymer nanoparticles engineered as chaperones protect against apoptosis in human retinal pigment epithelial cells," *Journal of Controlled Release*, vol. 191, pp. 4–14, 2014.

[101] C. A. Gilroy, K. M. Luginbuhl, and A. J. Chilkoti, "Controlled release of biologics for the treatment of type 2 diabetes," *Journal of Controlled Release*, vol. 240, pp. 151–164, 2016.

Hindawi
Oxidative Medicine and Cellular Longevity
Volume 2017, Article ID 7295319, 11 pages
https://doi.org/10.1155/2017/7295319

Research Article

REGγ Contributes to Regulation of Hemoglobin and Hemoglobin δ Subunit

Qiuhong Zuo,[1,2] Shanshan Cheng,[1] Wenxiang Huang,[2] Muhammad Zeeshan Bhatti,[1] Yanyan Xue,[1] Yuanyuan Zhang,[1] Bianhong Zhang,[1] Lei Li,[1] Lin Wu,[1] Junjiang Fu,[3] Jiwu Chen,[1] and Xiaotao Li[1,4]

[1]*Shanghai Key Laboratory of Regulatory Biology, Shanghai Key Laboratory of Brain Functional Genomics (Ministry of Education), Institute of Biomedical Sciences, School of Life Sciences, East China Normal University, 500 Dongchuan Road, Shanghai 200241, China*
[2]*Department of Infectious Diseases, The First Affiliated Hospital of Chongqing Medical University, Chongqing 400016, China*
[3]*Key Laboratory of Epigenetics and Oncology, the Research Center for Preclinical Medicine, Southwest Medical University, Sichuan 646000, China*
[4]*Department of Molecular and Cellular Biology, Dan L. Duncan Cancer Center, Baylor College of Medicine, One Baylor Plaza, Houston, TX 77030, USA*

Correspondence should be addressed to Junjiang Fu; fujunjiang@hotmail.com, Jiwu Chen; jwchen@bio.ecnu.edu.cn, and Xiaotao Li; xiaotaol@bcm.edu

Received 7 December 2016; Revised 22 April 2017; Accepted 8 May 2017; Published 16 July 2017

Academic Editor: Luciano Saso

Hemoglobin (Hb) is a family of proteins in red blood cells responsible for oxygen transport and vulnerable for oxidative damage. Hemoglobin δ subunit (HBD), a member of Hb family, is normally expressed by cells of erythroid lineage. Expression of Hb genes has been previously reported in nonerythroid and hematopoietic stem cells. Here, we report that Hb and HBD can be degraded via REGγ proteasome in hemopoietic tissues and nonerythroid cells. For this purpose, bone marrow, liver, and spleen hemopoietic tissues from *REG*$\gamma^{+/+}$ and *REG*$\gamma^{-/-}$ mice and stable REGγ knockdown cells were evaluated for the degradation of Hb and HBD via REGγ. Western blot and immunohistochemical analyses exhibited downregulation of Hb in REGγ wild-type mouse tissues. This was validated by dynamic analysis following blockade of de novo synthesis of proteins with CHX. Degradation of HBD only occurred in REGγ WT cells but not in REGγN151Y, a dominant-negative REGγ mutant cell. Notably, downregulation of HBD was found in HeLa shN cells with stimulation of phenylhydrazine, an oxidation inducer, suggesting that the REGγ proteasome may target oxidatively damaged Hbs. In conclusion, our findings provide important implications for the degradation of Hb and HBD in hemopoietic tissues and nonerythroid cells via the REGγ proteasome.

1. Introduction

Hemoglobin (Hb) is one of the most abundant proteins in the human body and the major component of erythrocytes. A growing number of studies describe the human red blood cells (RBCs) life span in the circulatory system as approximately 100–120 days. Under the physiology condition, it is estimated that everyday, about 1/120 RBCs are generated and same number of RBCs attempt suicidal cell death or erythrosis in the human body. Eryptosis is characterized by cell shrinkage, cell membrane bleeding, and cell membrane phospholipids scrambling with phosphatidylserine exposure at the cell surface. In this regard, eryptosis is stimulated by an increase in cytosolic Ca^{2+} activity, ceramide, hyperosmotic shock, oxidative stress, energy depletion, hyperthermia, and a wide verity of xenobiotics and endogenous substances [1, 2]. These eryptosis factors also participate in the Hb damage of RBCs as well as in various hemoglobinopathies, which have been observed in Hb damage. Similarly, genetic factors have been implicated in hemoglobinopathies. In view of these

similarities to the physiological and pathological roles of Hb, diminishing the metabolic distribution, the cells have developed a more vulnerable degradation system through which one can recognize damaged or abnormal Hb. Beside these effects, the degradation and removal of damaged/abnormal Hb in RBCs are also assessed by the proteasomal system [3–5]. Research into the molecular mechanism of protein damage of RBCs in human cell line is more fascinating.

Indeed, recent evidence suggests that proteasome exists in various forms and its activity is modulated by multiple activators including 19S, 11S (REG), and PA200. These proteasomes are composed of a 20S core, with three distinct catalytic sites, and proteasomal activators [6, 7]. Furthermore, as it was reported that misfiled protein or short-lived regulatory proteins are mostly degraded in an ATP- and ubiquitin-dependent pathway by the 26S proteasome, composing of the 20S "core" and the 19S regulator cap. In addition, some abnormal proteins can be degraded in an ATP- and ubiquitin-independent pathway by the 11S proteasome, which consists of 20S "core" proteasome and 11S regulator cap, among which REGγ emerges as a biologically important regulatory protein [8–11]. The REG (11S) family protein members include REGα, REGβ, and REGγ, which contribute to almost 35% identical amino acids. The 19S activator contains an ATPase subunit, which degrades proteins in an ATP- and ubiquitin-dependent manner, when bind to the 20S proteasome [7]. In contrast, the REG family mediates protein degradation in an ATP- and ubiquitin-independent manner [6, 7]. Growing amount of evidence suggests that 20S and 26S proteasomes are present in RBCs. These proteasomes are biologically active, with higher 20S proteasome activity than 26S proteasomal activity [3–5]. Therefore, the proteasome activators such as 19S and 11S regulators and their regulation are importance for the homeostasis of RBCs [3, 4]. In fact, Hb degradation of RBCs by proteasome systems is thought to play an important role biochemically and clinically.

In addition, recent studies have shown that REGα/β and 20S proteasome play a role in the oxidized Hb degradation [12]. The precise role of REGγ in the degradation of Hb is still unclear. Despite that human mature RBCs consisting of HbA ($\alpha2\beta2$; 95–98%), HbA2 ($\alpha2\delta2$; 1.5–3.5%), and HbF ($\alpha2\gamma2$; <1%) are well documented for Hb subunits α chain and/or β chain, less studies focus on degradation of Hb δ subunit (HBD). Therefore, we have investigated the role of REGγ proteasome in the degradation of Hb and HBD. Our data provides evidence that REGγ is a regulator for Hb and HBD degradation. The noncanonical proteasomal degradation system (REGγ) identified in this study will shed light on in-depth investigation and understanding the functional pathway of Hb and HBD degradation.

2. Materials and Methods

2.1. Materials. Dulbecco's modified Eagle's medium (DMEM), fetal bovine serum (FBS), and antibiotics (penicillin and streptomycin sulfate) were purchased from Life Technologies Inc. Phenylhydrazine (PHZ) was purchased from Linfeng Chemical Reagent Company (Shanghai, CN). Cycloheximide (CHX) was purchased from Sigma (St. Louis, MO). Anti-REGγ and anti-β-actin antibodies were purchased from Abmart; anti-Hb and human HBD antibodies were purchased from Santa Cruz Biotech Inc.; anti-p21 and anti-Smurf 1 antibodies were purchased from BD Biosciences Inc. (USA). Second antibodies were purchased from LI-COR Biosciences (USA) and/or Abmart.

2.2. Cell Culture. The stable REGγ knockdown HeLa (HeLa shN and shR) cells were previously generated in our laboratory [9, 13, 14]. Cells were routinely grown in Dulbecco's modified Eagle's medium (DMEM) supplemented with 10% FBS and antibiotics (100 mg/ml penicillin and 50 mg/ml streptomycin sulfate) at 37°C with 5% CO_2 atmosphere. The HeLa cells were seeded at 40–50% confluences and split at least twice a week.

2.3. Construct Subcloning (pSG5-HBD Plasmid). The required HBD strain was screened from the library. Taking the human cDNA as a template, RT-PCR amplification was preformed and then cloned into pSG5 vector with HA tag. Briefly, HBD was generated by using the primers HBD-XholI-Forward: 5′-CGACTCGAGATGGTGCATCTG ACTCCTGAG-3′ and HBD-NotI-Reverse: 5′-GAGCGGCC GCTCAATGGTACTTGTGAGCC-3′. PCR analysis was performed with the above specific primers on a PCR Amplifier (Bio-Rad, USA). Each PCR reaction contained 2 μl cDNA-HBD, 1 μl forward primer, 1 μl reverse primer, 1 μl dNTPs, 0.5 μl pFu DNA polymerase, 10× pFu buffer, and 17 μl QH_2O (PCR-grade) in a 25 μl reaction volume. The optimized assay conditions were 95°C for 5 min followed by 32 cycles of amplification (95°C for 45 sec, 52°C for 1 min, and 72°C for 60 sec) and a final extension step at 72°C for 10 min. The amplified product was subjected to agarose gel electrophoresis and the target gene HBD cDNA was extracted by QIAquick Gel Extraction kit (Tiangen Biotech Co. Ltd.) according to the manufacturer's specifications. Then, HBD cDNA was inserted into HA-pSG5 plasmid. The constructs were verified by sequencing.

2.4. Cell Transfection. HeLa cells at 70% confluence were transiently transfected with the plasmids HA-pSG5-HBD, FRT-REGγwt, and FRT-REGγN151Y, using Lipofectamine 2000 transfection reagent (Invitrogen) in accordance with the manufacturer's instructions. The empty vectors such as HA-pSG5-vector and FRT-vector were transfected as controls. Cells were incubated at 37°C in CO_2 incubator; after 6–8 h later, 10% serum growth medium was added to the transfection mixture. Cell extracts were evaluated via Western blot for REGγ and HBD protein expression at 48 h posttransfection.

2.5. Oxidation Analysis. Oxidation analysis was performed for HBD degradation in HeLa shN and shR cells. Briefly, HeLa cells at 70% confluence were transiently transfected with HA-pSG5-HBD plasmid in incubation for 48 h. HeLa shN and shR cells were treated with (5 mM) phenylhydrazine (PHZ) for 0, 1, and 2 h in a time-dependent manner.

2.6. Western Blot Analysis. Western blot was performed using the standard method; cells were cultured to confluence in 6-well plates. The samples were collected with or without plasmids transfection or oxidant reagents; cells were washed with phosphate-buffered saline (PBS) and treated with protein extraction buffer (50 mM Tris-HCl, pH 7.5, 150 mM NaCl, 1% NP-40, 1 mM EDTA, 20 mM Na_3VO_4, and 1 mM PMSF). The sample concentration was measured by BCA protein assay kit (Pierce, USA). Protein samples were subjected to electrophoresis in 10% SDS polyacrylamide gel (SDS-PAGE). Separated proteins were electro blotted to nitrocellulose membranes (Bio-Rad), and the blot was blocked for 1 h at room temperature with blocking buffer (0.1% PBST with 5% fat-free dried milk powder). The blot was then incubated with primary antibodies (1 : 1000 dilutions) at 4°C overnight. The blot was washed with 0.1% TBST 3 times and incubated with secondary antibodies (mouse, rabbit) (1 : 5000 dilution) for 1 h. The blot was washed again 3 times and exposed to Odyssey LI-COR scanner.

2.7. Immunofluorescence (IF) Staining. Sterile slides were inserted into 24-well plates; pretransfected HeLa cells were plated into each well at a concentration of 5×10^4/ml and incubated at 37°C with 5% CO_2 for 24 h. Next, 4% paraformaldehyde was added for 10 min at room temperature for fixation, permeabilized with 0.25% Triton X-100. Then, cells were washed with PBS, three times for 1 min each time, and blocked with 1% BSA for 1 h at room temperature. Subsequently, anti-REGγ and anti-HBD antibodies were incubated at 4°C overnight. Cells were incubated with secondary antibodies Alexa Fluor 488-conjugated goat anti-rabbit IgG and Alexa Fluor 594 goat anti-mouse IgG (Abmart) for 1 h, and nuclei were stained with 4',6-diamidino-2-phenylindole (DAPI). Images of the cells were captured under fluorescence microscopes (LI-COR Bioscience Co.) and analyzed by Image-Pro Plus 6.0 software.

2.8. Animal Care. $REG\gamma^{-/-}$ mice with C57BL/6 genetic background were acquired from Dr. John J. Monaco (University of Cincinnati College of Medicine, Cincinnati) [15]. Our laboratory maintained $REG\gamma^{+/-}$ mice and kept intercrosses between males and females for generation of $REG\gamma^{+/+}$ and $REG\gamma^{-/-}$ mice. Genotyping of $REG\gamma^{+/+}$ and $REG\gamma^{-/-}$ mice was carried out by PCR analysis of genomic DNA as described [15]. All mice were bred in the Animal Core Facility at 20–26°C with 40–70% humidity and 12 h light/dark cycle (07:00–19:00). Standard rodent diet and water were provided ad libitum throughout the study. There were no more than five animals per cage. All mice were sacrificed after feeding for 1 week or 2 weeks. Liver, spleen, and bone marrow tissues were collected form all mice at the same time and paraffin-embedded sections (4 μm thickness) or tissue homogenates were prepared. All procedures were carried out in accordance with the guidelines of the National Institutes of Health Guide for the Care and Use of Laboratory Animals. All the animal experiments were performed according to the approval of the Animal Care Committee of East China Normal University.

2.9. Immunohistochemistry Analysis. Paraffin-embedded sections of liver and spleen tissues from $REG\gamma^{+/+}$ mice and $REG\gamma^{-/-}$ mice were used to perform IHC staining. Tissue sections were deparaffined with xylene and dehydrated with sequential washing of 100%, 95%, 85%, 75%, and 50% ethanol. Endogenous peroxidase activity was quenched using 3% H_2O_2 in methanol for 10 min and then washed three times in PBS. Antigen retrieval was achieved using a water bath heating in citric acid retrieval solution, 0.01 M, pH 7.6, at 100°C for 30 min, followed by cooling at room temperature. Slides were then incubated with anti-HBD antibody (1 : 300) dilutions and anti-REGγ antibody (1 : 500) dilutions at 4°C overnight. Next, the slides were rinsed three times in PBS and incubated in biotin-labeled rabbit anti-rabbit secondary antibodies for 10 min at room temperature. After washing three times with PBS, the staining was performed using diaminobenzidine developing solution. The sections were counter-stained with hematoxylin. We compared IHC staining between $REG\gamma^{+/+}$ and $REG\gamma^{-/-}$ mice liver tissues by percentage of intensity of staining to estimate the changes of HBD expression. Similarly, the difference of HBD expression were compared between $REG\gamma^{+/+}$ and $REG\gamma^{-/-}$ mice spleen tissues. The specimens were then mounted and examined under a light microscope (Model BX-61; Olympus Corp., Tokyo, Japan).

2.10. RT-PCR Analysis. The experiments were conducted with 2-week-old $REG\gamma^{+/+}$ and $REG\gamma^{-/-}$ mice housed in specific pathogen-free conditions and handled according to the ethical and scientific standards by the animal center in the institute (Minhang Laboratory of Animal Center at East China Normal University). Total RNA from bone marrow, spleen, and liver tissues ($REG\gamma^{+/+}$ and $REG\gamma^{-/-}$ mice) were isolated using TRIzol (Invitrogen) following the manufacturer's protocol. Briefly, 1-2 μg of total RNA was reverse-transcribed to cDNA, the final reaction system of 20 μl which contains 1 μl Random Primer, 1-2 μg RNA, 1 μl 10 mM dNTP, and DEPC water. The RT-PCR reaction was performed at 25°C for 10 min, 37°C for 50 min, and 70°C for 15 min. All cDNA samples were stored at −80°C until further analysis. Primer sequences are described as follows: CD163-sense: 5′-TTTGTCAACTTGAGTCCC TTCAC-3′; CD163-antisense: 5′-TCCCGCTACACTTGTT TTCAC-3′; 18S-sense 5′-GGACACG GACAGGATTGA CA-3′; 18S-antisense 5′-GACATCTAAGGGCATCACAG-3′. The primers were synthesized by BioSune Biotechnology (Shanghai) Co. Ltd. The 2 μl of reverse-transcribed cDNA was subjected to quantitative real-time PCR using master mix with SYBR-green (TOYOBO) and the Mx3005P quantitative RT-PCR system (Stratagene). Each reaction system contains 1 μl primer mix, 1 μl cDNA, 7.96 μl miliQ water, 10 μl SYBR green, 0.04 μl 50× ROX to a final volume of 20 μl. Each experiment was performed in duplicates and repeated thrice. The data was normalized to 18S mRNA. The delta threshold cycle value (ΔCt) was calculated using the formula $\Delta Ct = Ct\,gene - Ct\,control$. The fold change was calculated as $2^{-\Delta Ct}$.

2.11. Statistical Analysis. All data is expressed as means ± SD. One-way analysis of variance (ANOVA) or Student's *t*-test

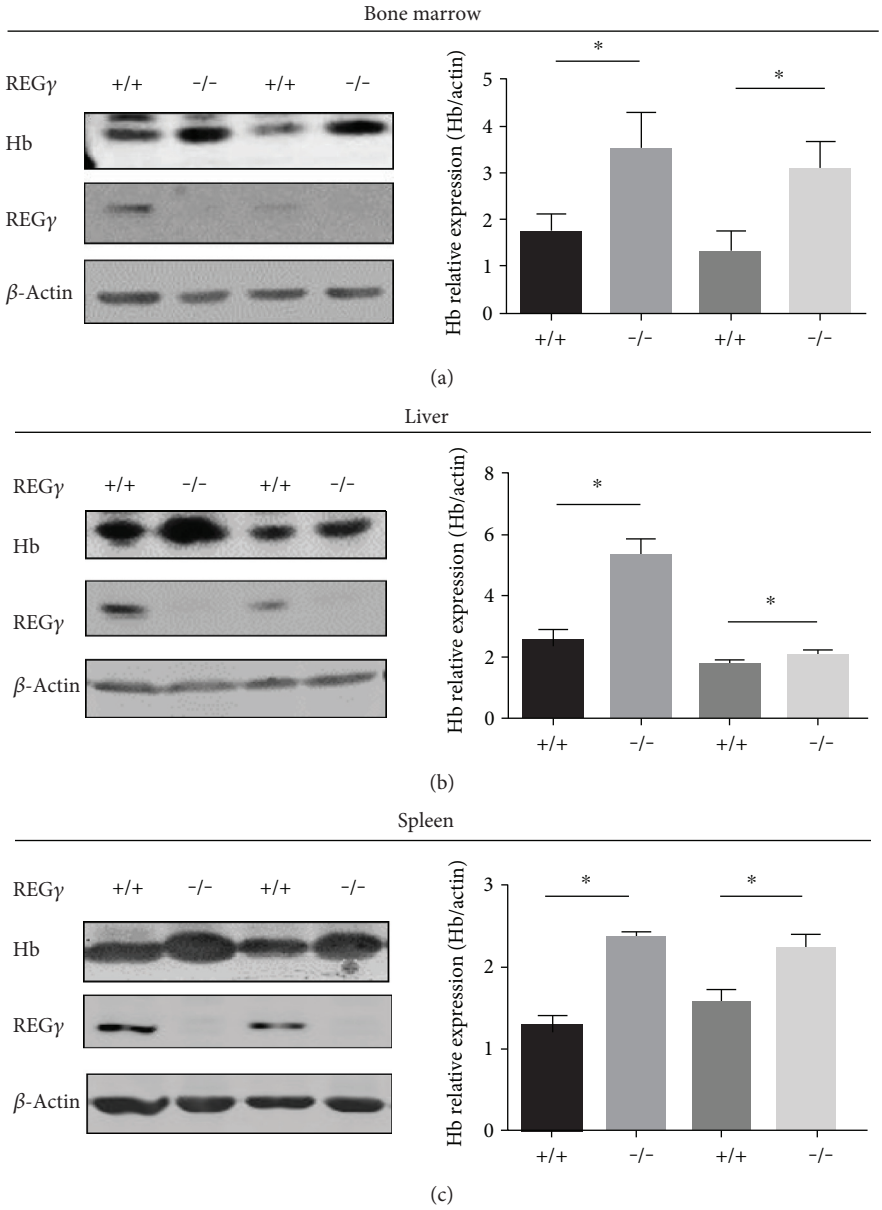

Figure 1: REGγ-mediated Hb degradation in multiple hemopoietic tissues. (a) Hb levels in bone marrow, (b) liver, and (c) spleen tissues from two different $REG\gamma^{+/+}$ and $REG\gamma^{-/-}$ mice. Protein was extracted and analyzed using Western blot against anti-Hb and anti-REGγ antibodies. β-Actin was use as internal control. The quantification analysis was conducted and shown as a graph. Left: Western blot. $n = 3$ represents the number of mice in each genotype. All the mice were sacrificed at age of 1-2 weeks old. Right: quantification analysis. Data are presented as means ± SEM from three independent experiments. $^*p < 0.05$ versus control.

was conducted to find out the significance of variations. A probability level of $p < 0.05$ was selected, indicating statistical significance. All the experiments were repeated in three independent experiments.

3. Results

3.1. REGγ Deficiency Promotes Hb in Mouse Tissues. The REG family member includes REGα and REGβ, as well as 20S proteasome has been shown to induce oxidative Hb degradation in murine embryonic fibroblasts cells [12]. Therefore, we determined whether the other members of REG (11S) proteasome family activator, REGγ, might regulate degradation of oxidized Hb or Hb in REGγ wild-type and knockout mice tissues. We investigated the roles of REGγ-mediated regulation of Hb degradation in $REG\gamma^{+/+}$ and $REG\gamma^{-/-}$ mice tissues (1-2-week-old mice), including the bone marrow, liver, and spleen, since these tissues are associated with removal of aged erythrocytes and clearance of oxidized Hb. We observed that $REG\gamma^{+/+}$ bone marrow tissues exhibited significant downregulation of Hb protein levels by Western blot analysis. In contrast, upregulation of Hb expression was noted in $REG\gamma^{-/-}$ bone marrow tissues (Figure 1(a)). Interestingly, as shown in Figures 1(b) and 1(c), REGγ wild-type tissues from the liver and spleen showed significant decreased Hb protein expression, while

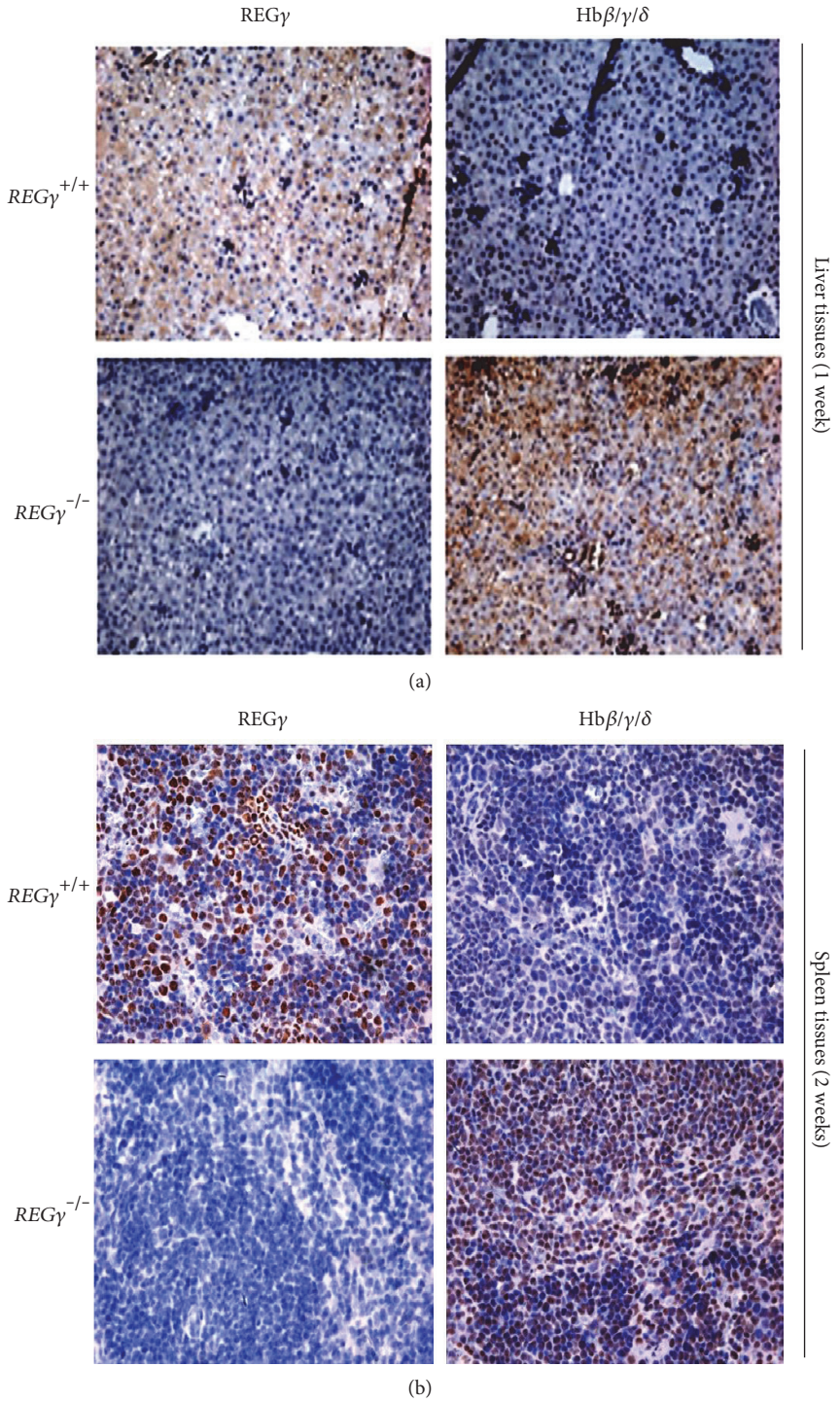

Figure 2: Negative correlation between REGγ and Hb in liver and spleen tissues from REGγ wild-type and knockout neonatal mice. Immunohistochemical staining was performed with anti-REGγ and anti-Hb $\beta/\gamma/\delta$ antibodies in $REG\gamma^{+/+}$ and $REG\gamma^{-/-}$ mice tissues. The tissues for REGγ positive and the Hb positive showed brown granules, respectively. (a) Liver tissues were analyzed for immunohistochemical analysis from one-week-old mice. (b) Spleen tissues from $REG\gamma^{+/+}$ and $REG\gamma^{-/-}$ mice (2 weeks old) were subjected to immunohistochemical analysis. The results of the representative figures were reproduced in three independent experiments.

REGγ knockout mice tissues promoted Hb in both liver and spleen tissues. These results suggest that REGγ plays an important role in the Hb degradation of hemopoietic tissues.

Based on our observation of Hb protein downregulated by REGγ in $REG\gamma^{+/+}$ and $REG\gamma^{-/-}$ mice tissues, we further explored the relationship of REGγ and Hb by performing immunohistochemical staining analysis. We identified liver specimens of one-week-old $REG\gamma^{+/+}$ and $REG\gamma^{-/-}$ mice with anti-REGγ and anti-Hb$\beta/\gamma/\delta$, as shown in Figure 2(a). Results indicated that $REG\gamma^{+/+}$ liver tissues expressed a high

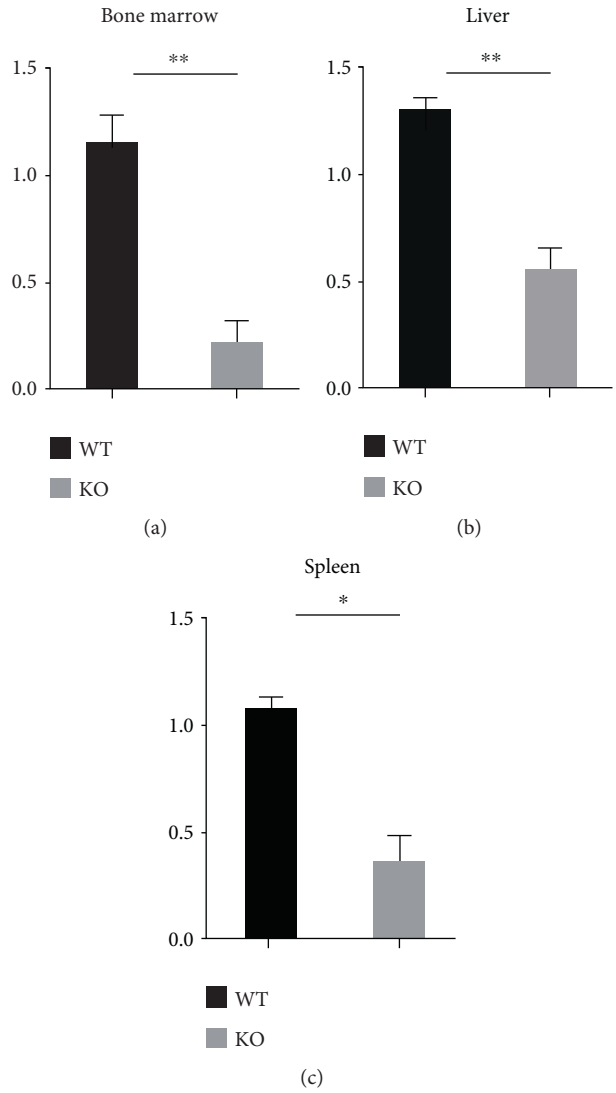

Figure 3: REGγ promotes CD163 expression in mice tissues. mRNA expression of CD163 was measured by qRT-PCR in (a) bone marrow, (b) liver, and (c) spleen tissues from $REG\gamma^{+/+}$ and $REG\gamma^{-/-}$ mice. Data was derived from independent experiments with $n = 6 + 6$ ($REG\gamma^{+/+}$ and $REG\gamma^{-/-}$ mice). Error bars represent mean ± SD; $^{*}p < 0.05$; $^{**}p < 0.01$ versus control, as determined by Student's t-test.

level of REGγ and a low level of Hb. Furthermore, we analyzed spleen tissues from 2-week-old $REG\gamma^{+/+}$ and $REG\gamma^{-/-}$ mice. We observed a high level of REGγ and a low level of Hb in $REG\gamma^{+/+}$ spleen tissues, whereas $REG\gamma^{-/-}$ spleen tissues exhibited a high level of Hb and a low level of REGγ (Figure 2(b)). These results indicate a potentially inverse correlation between REGγ and Hb.

3.2. REGγ Promotes CD163 Expression in Mice Tissues. CD163 is a member of the cysteine-rich scavenger receptor family, and has been identified as an Hb scavenger receptor, mediating uptake of Hb in the circulation system. To elucidate the mechanism underlying interaction between REGγ and CD163 in bone marrow, liver, and spleen tissues from $REG\gamma^{+/+}$ and $REG\gamma^{-/-}$ mice, we evaluated the mRNA expression of CD163 by qRT-PCR analysis. We detected a significant increase of CD163 (4.3-fold change) in REGγ bone marrow tissues as compared to REGγ knockout mice tissues. These results promoted us to test the mRNA level of CD163 in liver and spleen tissues from $REG\gamma^{+/+}$ and $REG\gamma^{-/-}$ mice. We found attenuated mRNA levels of CD163 in liver (1.4-fold change) and spleen (2.2-fold change) tissues from $REG\gamma^{-/-}$ mice, compared with those from $REG\gamma^{+/+}$ mice by qRT-PCR analysis (Figure 3). Overall, CD163 expression was dramatically higher in bone marrow tissues in comparison with liver and spleen tissues. Taken together, this data demonstrated that REGγ mediates a stimulatory effect on Hb degradation through upregulation of CD163 activity in these tissues.

3.3. Hemoglobin δ Subunit (HBD) Regulation in HeLa Cells. HBD typically accounts for approximately 10–30% of total hemoglobin in definitive erythrocytes, and available evidence suggests that it is generally characterized by elevated O_2-binding properties, regulatory changes in intraerythrocytic mechanism. To clarify the function of REGγ in HBD

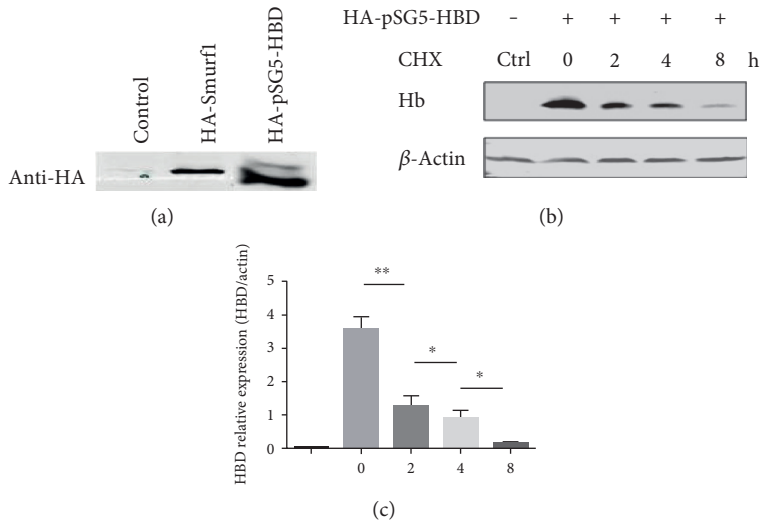

Figure 4: Regulation of endogenous HBD in HeLa cells. (a) HeLa cells were transfected with HA-pSG5-HBD plasmid (1 μg/ml) and HA-Smurf1 (1 μg/ml) as a positive control, using Lipo2000 transfection reagent for 72 h incubation. Total protein extracts were analyzed by Western blot against anti-HA antibody. (b) CHX assay for endogenous degradation. HeLa cells transfected with HA-pSG5-HBD. After 64 h incubation, cells were treated 100 μg/ml of CHX for 0, 2, 4, 6, and 8 h. The total protein extracts were subjected to Western blot analysis. β-Actin was used as loading control. (c) Quantification of CHX-treated Western blot results expressed as the means ± SEM. $^{*}p < 0.05$; $^{**}p < 0.01$ versus control.

degradation, nonblood cells were used for mechanistic studies since they had no endogenous HBD. HBD plasmid was constructed in pSG5 vector with HA tag for the overexpression of HBD, and HA-Smurf1 plasmid was used as control for expression of exogenous DNA. HA-pSG5-HBD was transfected with Lipo2000 reagent for 72 h in HeLa cells and evaluated by Western blot analysis. Results indicated that a significantly increased protein level of HBD was exhibited by the HA-pSG5-HBD-transfected HeLa cells (Figure 4(a)). To further investigate the role of REGγ-mediated degradation of HBD, HeLa cells were treated with CHX (100 μg/ml), an inhibitor for de novo protein synthesis, in a time-dependent manner. Interestingly, we found that CHX treatment dramatically displayed the degradation effects of REGγ on HBD in a time-dependent manner, supporting the hypothesis that HBD is degraded by the REGγ proteasome (Figures 4(b) and 4(c)). These results indicate that REGγ regulates HBD protein stability in HeLa cells.

3.4. REGγ-Mediated Degradation of HBD. To elaborate REGγ-dependent degradation of HBD, we constructed HA-pSG5-HBD, FRT-REGγwt, and FRT-REGγN151Y plasmids, with empty vectors HA-pSG5 and FRT as controls. The pcDNA3.1-p21 plasmid was used as a positive control, since p21 is a known target of REGγ (Figure 5(b)). HBD level was significantly lower in the presence of overexpression of REGγwt, whereas HBD was much higher when the mutant REGγN151Y was exogenously expressed (Figure 5(a)). Notably, the dominant-negative mutant REGγN151Y (with a single amino acid mutation "activation ring" of REGγ) abrogated the proteasome activity, although the binding ability to the proteasome is maintained [15, 16]. As a positive control, p21 showed similar patterns to HBD in the presence of either WT or mutant REGγ (Figure 5(b)). Taken together, these results demonstrate that REGγ is a novel mediator for the degradation of HBD.

3.5. Cellular Location and Expression of HBD in HeLa Cells. Next, we sought to examine the effect of REGγ and HBD on cellular localization and expression by immunofluorescence (IF) staining. HA-pSG5-HBD + FRT-REGγwt and HA-pSG5-HBD + FRT-REGγN151Y plasmids were transiently transfected into HeLa cells, respectively. Results of immunostaining indicated that co-transfection of HA-psG5-HBD (red) and FRT-REGγwt (green) significantly inhibited the expression of HBD in HeLa cells, while FRT-REGγN151Y (green) expressing cells had stabilized expression of HBD (Figure 6(a)). These results demonstrated a critical role of REGγ-mediated regulation of HBD in vitro. Further, quantification of HBD positive cells/total cells expression was quantitated for statistical analysis. We observed that HeLa cells with cotransfection of HA-pSG5-HBD and FRT-REGγwt exhibited reduction in HBD repression. In contrast, cotransfection of HA-pSG5-HBD and FRT-REGγN151Y in HeLa cells displayed elevation in HBD expression level as compared to HA-pSG5-HBD and HA-pSG5 vector-transfected cells (Figure 6(b)). Thus, the immunofluorescence study provides evidence for the relationship between REGγ and HBD.

3.6. REGγ Promotes HBD Degradation under Oxidative Stress. Reactive oxygen species- (ROS-) mediated Hb degradation increase the oxidative damage of erythrocytes via an ATP- and ubiquitin-dependent manner [17, 18]. Interestingly, proteasome activator REGγ has been reported to promote degradation in an ATP- and ubiquitin-independent manner [6, 7] and to mediate oxidative Hb degradation [12].

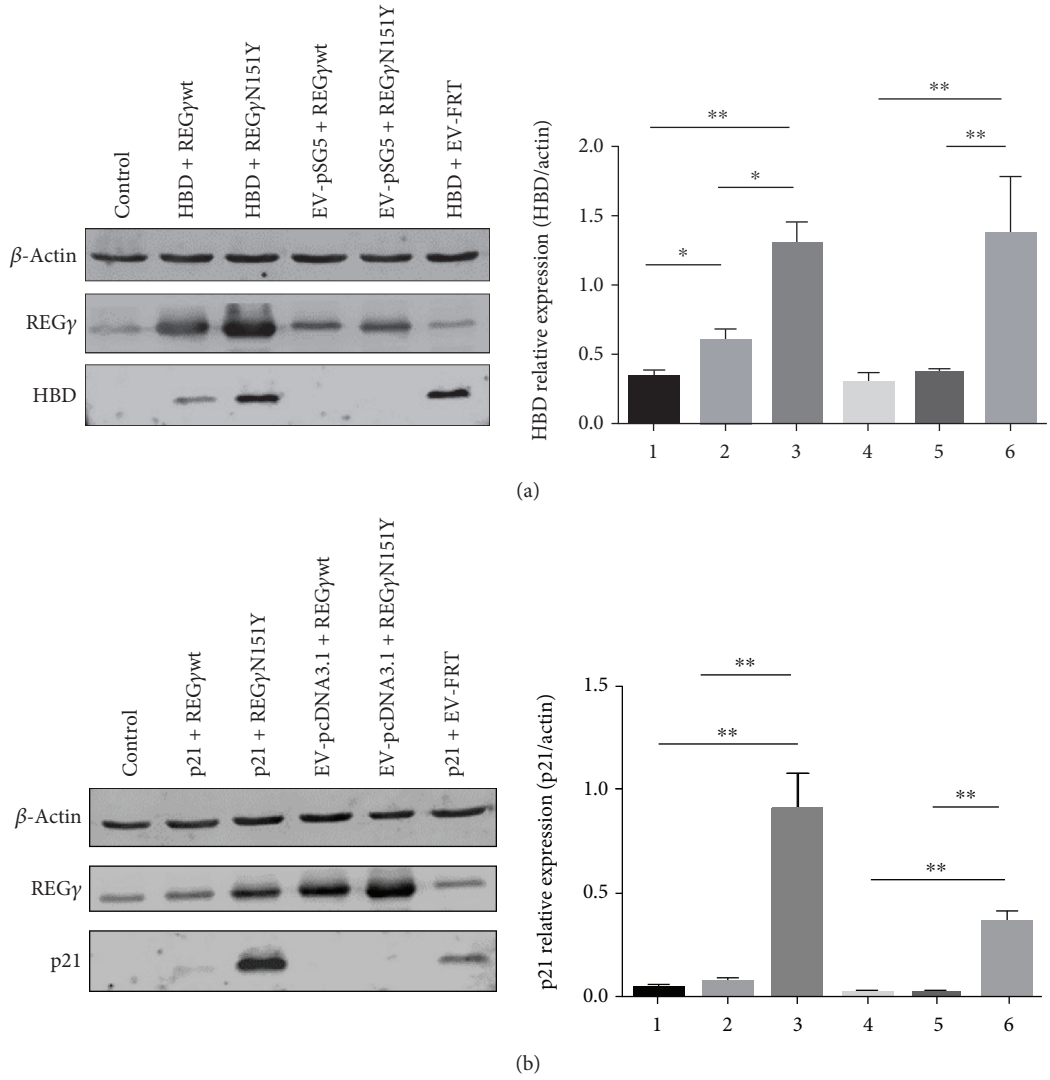

Figure 5: REGγ-mediated degradation of HBD in HeLa cells (a). Cells were transiently transfected with HA-pSG5-HBD (2 μg), FRT-REGγwt (1 μg), FRT-REGγN151Y (1 μg), HA-pSG5 vector (2 μg), and FRT vector (1 μg) using Lipo2000 transfection reagent for 72 h incubation. Protein expression was detected against anti-REGγ, anti-HBD, and anti-β-actin antibodies. Nontransfected HeLa cells were used as a control. (b) HeLa cells were transfected with pcDNA3.1-p21 (2 μg) FRT-REGγwt (1 μg), FRT-REGγN151Y (1 μg), pcDNA3.1 vector (2 μg), and FRT vector (1 μg) using Lipo2000 transfection reagent for 72 h incubation. Protein expressions of indicated antibodies were determined by Western blot analysis. Nontransfected HeLa cells were used as controls. β-Actin was used as loading control. The quantification analysis was conducted and shown as a graph. Left: Western blot. Right: quantification analysis. Data is presented as means ± SEM. $^{*}p < 0.05$; $^{**}p < 0.01$ versus control.

To elucidate the underlying mechanism of REGγ-mediated Hb degradation via oxidative HBD, we utilized stable knockdown REGγ HeLa cells (HeLa shN and shR cells) previously generated in our laboratory. We determined the oxidative effect of HBD degradation in HeLa shN and HeLa shR cells following phenylhydrazine (PHZ) stimulation and overexpression of HBD. We observed that overexpression of HBD in HeLa shN cells showed significant downregulation of HBD by PHZ stimulation in a time-dependent manner. Moreover, overexpressed HBD HeLa shR cells were unable to induce downregulation of HBD with PHZ treatment, as estimated by Western blot analysis (Figure 7). Taken together, our data demonstrate that REGγ induces the degradation of HBD under oxidative stress.

4. Discussion

Hemoglobin is a major protein of erythrocytes (RBCs) responsible for the transport of oxygen (O_2). To maintain maximum O_2-carrying capacity, Hb must be kept under reduced condition known as ferrous (Fe^{2+}) bound state. The oxidation of Hb from ferrous to ferric states is accelerated by reactive oxygen species (ROS) such as superoxide [19] and hydroxyl free radical [20]. The Hb in the aging erythrocytes (RBCs) is mainly scavenged by the CD163 scavenger receptor pathway through monocytes or macrophages [21, 22], while abnormal Hb in the intracellular system is degraded through the proteasomes [23]. In fact, physiological and pathological stresses on the RBCs accelerate the eryptosis

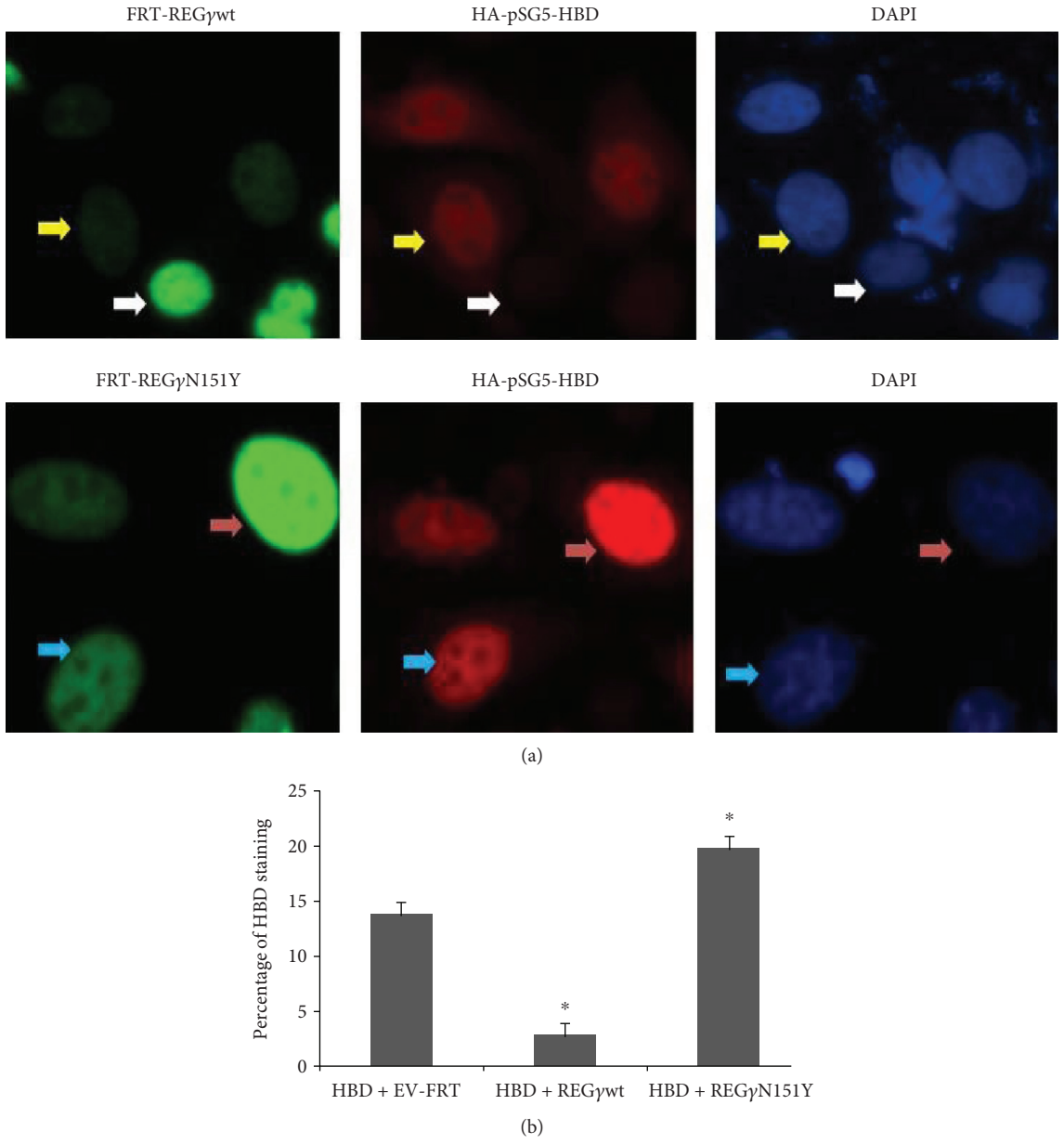

Figure 6: Cellular location and expression of HBD in HeLa cells. (a) Cells were transiently transfected with HA-pSG5-HBD (2 μg) + FRT-REGγwt, HA-pSG5-HBD (2 μg) + FRT-REGγN151Y (1 μg), and HA-pSG5-HBD (2 μg) + HA-pSG5 vector (2 μg). Cells were fixed and immunostained with anti-REGγ (green color) and anti-HBD (red color). Cell nuclei were stained with DAPI staining (blue color). Scale bar: 50 μm. (b) Percentage of HBD expression in HeLa cells with HA-pSG5-HBD + FRT-REGγwt, HA-pSG5-HBD + FRT-REGγN151Y, and HA-pSG5-HBD + HA-pSG5 vector. Each data represents the means of three independent experiments. Bars are the standard errors, $n = 300$. Significance was determined by Student's t-test. $^*p < 0.05$ versus control.

period which possibly led to Hb damage. Further fine-tuning hemoglobin function are oxygen transport, carbon dioxide transport, iron-rich substances, reactive oxygen species (ROS) accumulation, and oxidative damage [19, 20]. Hb binding to the erythrocyte cell membrane has been implicated in senescence and the consequent targeting of the red cell for removal from the circulation by macrophages via phagocytosis. Recent studies demonstrate that oxidized Hb degradation is contributed in the RBC by proteasome and its activators. However, the precise roles of proteasomes in the Hb and Hb subunit degradations within RBCs are still a matter of debate. In the present study, for the first time, the results reported herein clearly demonstrate that REGγ mediates degradation of Hb and HBD in hematopoietic tissues and nonerythroid cells. Specifically, protein level of Hb was detected in hematopoietic tissues from neonatal mice, supporting a broader role of REGγ in the regulation of hemoglobin.

CD163 is an Hb scavenger receptor exclusively expressed in the cell's monocyte/macrophage system. Resident tissue macrophages contain the highest levels of CD163, most notably Kupffer cells in the liver and macrophages within the

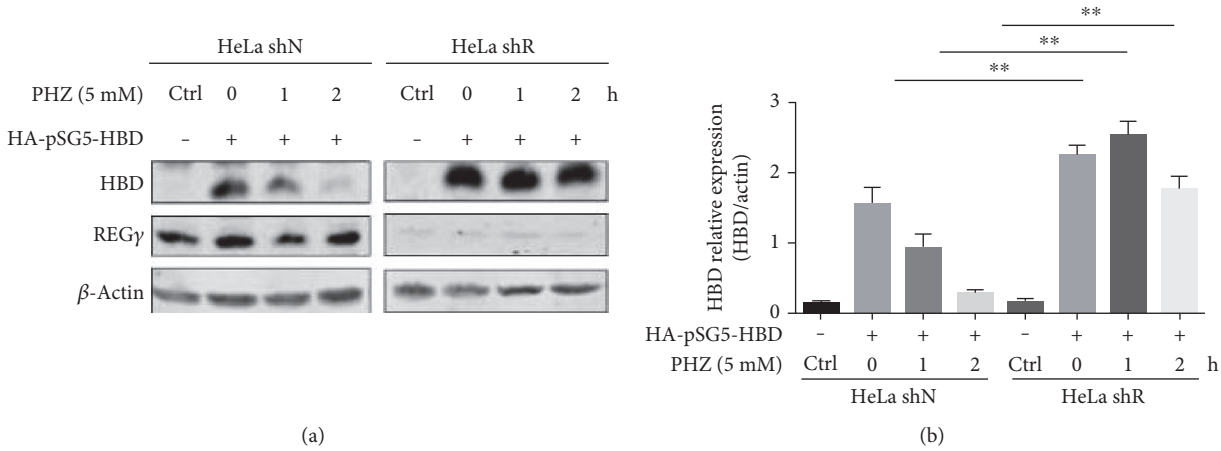

Figure 7: REGγ promotes HBD degradation under oxidative stress. HeLa shN and HeLa shR cells were transfected with or without HA-pSG5-HBD plasmid. Cells were treated with a 5 mM concentration of PHZ for 0, 1, and 2 h. Oxidative stress via PHZ stimulation on HBD in the presence or absence of REGγ was measured by Western blotting against anti-HBD and anti-REGγ antibodies. β-Actin was used as internal control. (b) Quantification of HA-pSG5-HBD- and PHZ-treated Western blot results expressed as the means ± SEM. $^{**}p < 0.01$ versus control.

bone marrow and spleen red pulp [24]. Moreover, the aging erythrocytes are susceptible to recognition by phagocytes and subsequent phagocytosis in the spleen, liver, and bone marrow. Therefore, liver, bone marrow, and spleen tissues are the major sites expressing CD163 and removing aging erythrocytes. Our results showed that CD163 mRNA level was notably decreased in liver, spleen, and bone marrow hemopoietic tissues from REGγ knockout mice. Thus, REGγ positively regulates CD163 gene expression in the hemopoietic tissues, which suggests that REGγ selectively mediated Hb degradation through Hb scavenger receptor pathway. Yet the regulatory mechanisms deserve further studies.

The study of Hb subunit degradation provides new insights to research in Hb degradation. The finding that HBD is a target of REGγ demonstrates a new layer of HB regulation. Despite that HBD variant (HbA_2 or $\alpha_2\delta_2$) is a minor component (2-3%) in the circulating red blood cells, it has important physiological and pathological roles given its unusual elevation in β-thalassemia as a useful clinical diagnostic [24]. HBD also shows high level of gene sequence conservation, possibly due to a regulatory role in the fetal-to-adult switch [25]. We validated degradation of HBD by the REGγ proteasome with dynamic protein stability assays. These results promoted us to determine the protein level of HBD as well as cellular location with or without REGγ overexpression in HeLa cells. We conclude that REGγ appears to be an important factor in the degradation of HBD.

Several studies have shown an apparently increasing rate of proteolysis in RBCs during oxidative stress. Hb is the major RBC protein, which plays a critical role in the modification and proteolytic degradation during oxidative stress. Selectively, oxidative-modified Hb degradation in an ATP- and ubiquitin-independent manner is almost 60–70% due to oxidative damage to the 26S system [26]. Recently, our laboratory has discovered that the intensity of REGγ binding to proteasome was enhanced by mild or severe oxidative stress [7], suggesting that phenylhydrazine-mediated degradation of HBD may be due to strengthened interactions between REGγ and 20S proteasome. The strong oxidative feature of phenylhydrazine has been previously shown to probe hemoglobin oxidative damage. In support of this hypothesis, significant HBD degradation has been observed in phenylhydrazine-treated HeLa shN cells in a time-dependent manner. Therefore, our results indicate that REGγ promotes HBD degradation under oxidative stress.

In conclusion, our study substantiates that REGγ selectively mediates the degradation of Hb and HBD. In fact, the important role of REGγ-mediating Hb and HBD degradation demonstrates an additional pathway for the breakdown of Hb and HBD and provides certain theoretic basis for preventing and curing Hb-related diseases. These results suggest REGγ could be a promising drug target. However, further work is necessary to understand the biological significance and role of REGγ in selective degradation of Hb and HBD.

Conflicts of Interest

The authors declare no conflict of interests.

Authors' Contributions

Jiwu Chen, Junjiang Fu, and Xiaotao Li designed the experiments. Qiuhong Zuo, Shanshan Cheng, Muhammad Zeeshan Bhatti, Yanyan Xue, Yuanyuan Zhang, and Lin Wu conducted the experiments. Qiuhong Zuo, Shanshan Cheng, Muhammad Zeeshan Bhatti, Jiwu Chen, and Xiaotao Li analyzed the data. Lei Li and Bianhong Zhang contributed to the research support. Muhammad Zeeshan Bhatti, Jiwu Chen, Wenxiang Huang, and Xiaotao Li wrote the manuscript. Qiuhong Zuo, Shanshan Cheng, and Wenxiang Huang contributed equally to this work. All authors reviewed the manuscript.

Acknowledgments

This work was supported by the National Basic Research Program of China (2015CB910402 and 2016YFC0902100), the National Natural Science Foundation of China (91629103, 81471066, 31401012, 31200878, 81672883, 81401837, 81261120555, and 31672247), the Science and Technology Commission of Shanghai Municipality (14430712100, 17ZR1407900, and 14ZR1411400), the Shanghai Rising-Star Program (16QA1401500), and the applied Basic Research Program of Science and Technology Department of Sichuan Province (2015JY0038).

References

[1] F. L. Lang and S. M. Qadri, "Mechanisms and significance of eryptosis, the suicidal death of erythrocytes," *Blood Purification*, vol. 33, pp. 125–130, 2012.

[2] F. Lang, E. Lang, and M. Foller, "Physiology and pathophysiology of eryptosis," *Transfusion Medicine and Hemotherapy*, vol. 39, pp. 308–314, 2012.

[3] S. Neelam, D. G. Kakhniashvili, S. Wilkens, S. D. Levene, and S. R. Goodman, "Functional 20S proteasomes in mature human red blood cells," *Experimental Biology and Medicine*, vol. 236, no. 5, pp. 580–591, 2011.

[4] G. Q. Chen, H. Liu, H. J. Zhang, Y. C. Deng, and Z. L. Li, "Proteomic characterization of human erythrocyte 20S proteasome and analysis of species-dependent 20S proteasome heterogeneity," *Chinese Journal of Analytical Chemistry*, vol. 37, no. 12, pp. 1711–1716, 2009.

[5] D. G. Kakhniashvili, L. A. Bulla, and S. R. Goodman, "The human erythrocyte proteome: analysis by ion trap mass spectrometry," *Molecular & Cellular Proteomics*, vol. 3, pp. 501–509, 2004.

[6] J. W. Chen, Q. H. Zuo, L. Ji, and X. T. Li, "The research advances in ubiquitin-independent degradation of proteins," *Progress in Biochemistry and Biophysics*, vol. 38, pp. 593–603, 2011.

[7] Y. Zhang, S. Liu, Q. Zou et al., "Oxidative challenge enhances REGγ-proteasome dependent protein degradation," *Free Radical Biology and Medicine*, vol. 82, pp. 42–49, 2015.

[8] L. Li, D. Zhao, H. Wei et al., "REGγ deficiency promotes premature aging via the casein kinase 1 pathway," *Proceedings of the National Academy of Sciences of the United States of America*, vol. 110, pp. 11005–11010, 2013.

[9] L. Liu, G. Yu, Y. Zhao et al., "REGγ modulates p53 activity by regulating its cellular localization," *Journal of Cell Science*, vol. 123, pp. 4076–4084, 2010.

[10] S. Dong, C. Jia, S. Zhang et al., "The REGγ proteasome regulates hepatic lipid metabolism through inhibition of autophagy," *Cell Metabolism*, vol. 18, pp. 380–391, 2013.

[11] Y. Wu, L. Wang, P. Zhou, G. Wang, and X. Li, "Regulation of REG cellular distribution and function by SUMO modification," *Cell Research*, vol. 21, pp. 807–816, 2011.

[12] A. M. Pickering and K. J. A. Davies, "Differential roles of proteasome and immunoproteasome regulators Pa28$\alpha\beta$, Pa28γ and Pa200 in the degradation of oxidized proteins," *Archives of Biochemistry and Biophysics*, vol. 523, pp. 181–190, 2012.

[13] R. Shringarpure, T. Grune, J. Mehlhase, and K. J. Davies, "Ubiquitin conjugation is not required for the degradation of oxidized proteins by proteasome," *The Journal of Biological Chemistry*, vol. 278, pp. 311–318, 2003.

[14] A. Ali, Z. Wang, J. Fu et al., "Differential regulation of the REGγ–proteasome pathway by p53/TGF-β signalling and mutant p53 in cancer cells," *Nature Communications*, vol. 4, p. 2667, 2013.

[15] X. Li, L. Amazit, W. Long, D. M. Lonard, J. J. Monaco, and B. W. O'Malley, "Ubiquitin- and ATP-independent proteolytic turnover of p21 by the REGgamma-proteasome pathway," *Molecular Cell*, vol. 26, pp. 831–842, 2007.

[16] X. Y. Chen, L. F. Barton, Y. Chi, B. E. Clurmn, and J. M. Robert, "Ubiquitin-independent degradation of cell-cycle inhibitors by the REG γ proteasome," *Molecular Cell*, vol. 26, pp. 843–852, 2007.

[17] A. L. Goldberg and F. S. Boches, "Oxidized proteins in erythrocytes are rapidly degraded by the adenosine triphosphate-dependent proteolytic system," *Science*, vol. 215, pp. 1107–1109, 1982.

[18] J. M. Fagan, L. Waxman, and A. L. Goldberg, "Red blood cells contain a pathway for the degradation of oxidant-damaged hemoglobin that does not require ATP or ubiquitin," *The Journal of Biological Chemistry*, vol. 261, pp. 5705–5713, 1986.

[19] S. M. Sadrzadeh, E. Graf, S. S. Panter, P. E. Hallaway, and J. W. Eaton, "Hemoglobin. A biologic fenton reagent," *The Journal of Biological Chemistry*, vol. 259, pp. 14354–14356, 1984.

[20] H. P. Misra and I. Fridovich, "The generation of superoxide radical during the autoxidation of hemoglobin," *The Journal of Biological Chemistry*, vol. 247, pp. 6960–6962, 1972.

[21] M. J. Nielsen, H. J. Møller, and S. K. Moestrup, "Hemoglobin and heme scavenger receptors," *Antioxidants & Redox Signaling*, vol. 12, pp. 261–274, 2010.

[22] M. J. Nielsen and S. K. Moestrup, "Receptor targeting of hemoglobin mediated by the haptoglobins: roles beyond heme scavenging," *Blood*, vol. 114, pp. 764–771, 2009.

[23] D. S. Schaer, C. A. Schaer, P. W. Buehler et al., "CD163 is the macrophage scavenger receptor fornative and chemically modified hemoglobins in the absence of haptoglobin," *Blood*, vol. 107, pp. 373–380, 2006.

[24] U. Sen, J. Dasgupta, D. Choudhury et al., "Crystal structures of HbA_2 and HbE and modeling of hemoglobin δ_4: interpretation of the thermal stability and the antisickling effect of HbA_2 and identification of the ferrocyanide binding site in Hb," *Biochemistry*, vol. 43, pp. 12477–12488, 2004.

[25] A. Moleirinho, A. M. Lopes, S. Seixas, R. Morales-Hojas, M. J. Prata, and A. Amorim, "Distinctive patterns of evolution of the δ-globin gene (HBD) in primates," *PloS One*, vol. 10, no. 4, article e0123365, 2015.

[26] R. E. Pacifici, Y. KonoSll, and K. J. A. Daviesll, "Hydrophobicity as the signal for radical-modified hemoglobin by complex," *Proteasome the Journal of Biological Chemistry*, vol. 268, pp. 15405–15411, 1993.

Hindawi
Oxidative Medicine and Cellular Longevity
Volume 2017, Article ID 5187102, 12 pages
https://doi.org/10.1155/2017/5187102

Research Article

Neuroprotective and Memory-Enhancing Effect of the Combined Extract of Purple Waxy Corn Cob and Pandan in Ovariectomized Rats

Woranan Kirisattayakul,[1,2] Jintanaporn Wattanathorn,[2,3] Sittichai Iamsaard,[4] Jinatta Jittiwat,[5] Bhalang Suriharn,[6] and Kamol Lertrat[6]

[1]*Department of Physiology and Graduate School (Neuroscience Program), Faculty of Medicine, Khon Kaen University, Khon Kaen 40002, Thailand*
[2]*Integrative Complementary Alternative Medicine Research and Development Center, Khon Kaen University, Khon Kaen 40002, Thailand*
[3]*Department of Physiology, Faculty of Medicine, Khon Kaen University, Khon Kaen 40002, Thailand*
[4]*Department of Anatomy, Faculty of Medicine, Khon Kaen University, Khon Kaen 40002, Thailand*
[5]*Faculty of Medicine, Mahasarakham University, Maha Sarakham 44150, Thailand*
[6]*Faculty of Agriculture, Khon Kaen University, Khon Kaen 40002, Thailand*

Correspondence should be addressed to Jintanaporn Wattanathorn; jintanapornw@yahoo.com

Received 7 March 2017; Accepted 1 June 2017; Published 9 July 2017

Academic Editor: Luciano Saso

The neuroprotectant and memory enhancer supplement for menopause is required due to the side effects of hormone replacement therapy. Since purple waxy corn cob and pandan leaves exert antioxidant and acetylcholinesterase inhibition (AChEI) effects, we hypothesized that the combined extract of both plants (PCP) might provide synergistic effect leading to the improved brain damage and memory impairment in experimental menopause. To test this hypothesis, female Wistar rats were ovariectomized bilaterally and orally given various doses of the functional drink at doses of 20, 40, and 80 mg/kg for 28 days. The animals were assessed nonspatial memory using object recognition test every 7 days throughout the study period. At the end of study, they were assessed with oxidative stress status, AChEI, neuron density, and ERK1/2 signal in the prefrontal cortex (PFC). Interestingly, all doses of PCP increased object recognition memory and neuron density but decreased oxidative stress status in PFC. Low dose of PCP also decreased AChE activity while medium dose of PCP increased phosphorylation of ERK1/2 in PFC. Therefore, the improved oxidative stress status and cholinergic function together with signal transduction via ERK in PFC might be responsible for the neuroprotective and memory-enhancing effects of PCP.

1. Introduction

To date, the number of menopausal women is continually growing. The World Health Organization (WHO) has estimated that the number of menopausal women worldwide will be 1200 million within 2030 [1]. It has been reported that cognitive decline is one of the important symptoms frequently observed especially in premature menopause [2]. Unfortunately, the current therapeutic strategy is still not in satisfaction level. The effect of hormone replacement therapy (HRT) on the cognitive function of menopausal women is controversial [3–7]. In addition, serious adverse effect such as breast cancer risk is reported in HRT [8, 9]. Therefore, the alternative strategy has gained much attention.

Among various alternative strategies, plant-based therapy is very much popular [10]. In the recent years, the use of plant-based food supplement is increased in Thailand [11]. It has been demonstrated that dietary approaches are regarded as the safe and effective preventive intervention against neurodegeneration [12]. A pile of evidence has

revealed that consumption of the polyphenol-rich supplements can enhance memory impairment [13–15]. Recent findings have demonstrated that the purple corn (*Zea mays* Linn., purple color) cob, an agricultural waste, can be served as an important natural resource of polyphenol [16]. It also exhibits potent antioxidant activity and can improve oxidative stress-related disorders [16, 17]. In addition to purple corn cob, pandan (*Pandanus amaryllifolius*), a commonly used culinary plant in Southeast Asia, also possesses high phenolic compound content and exhibits antioxidant activity [18]. An effervescent powder containing pandan also improves oxidative stress-related damage of the pancreas [19]. Based on these pieces of information and synergistic effect according to traditional folklore concept, the protective effect against oxidative stress-related brain damage and functional disorders of the combined extract of purple corn cob and pandan leaves (PCP) in menopausal women has been considered in order to produce an additive value of both plants. Currently, no data concerning this issue are available until now. Therefore, we aimed to determine the neuroprotective and memory-enhancing effects of the combined extract of purple corn cob and pandan leaves in experimental menopause in ovariectomized rats.

2. Materials and Methods

2.1. Chemicals and Reagents. Thiobarbituric acid (TBA), sodium dodecyl sulfate (SDS), glacial acetic acid, N-butanol, pyridine, 1,3,3-tetraethoxypropane (TEP), cytochrome C, xanthine oxidase, xanthine, glutathione reductase, nicotinamide adenine dinucleotide phosphate (NADPH), hydrogen peroxide, superoxide dismutase, glutathione peroxidase, catalase, acetylthiocholine iodide (ATCI), acetylcholinesterase, 5,5′-dithiobis (2-nitrobenzoic acid) (DTNB), cresyl violet, sodium acetate, sodium carbonate, 2,4,6-tripyridyl-striazine (TPTZ), Folin-Ciocalteu reagent, gallic acid, ascorbic acid, Trizma hydrochloride, potassium chloride, 2,2-diphenyl-1-picrylhydrazyl (DPPH), tris-hydrochloride, and sodium carbonate were purchased from Sigma-Aldrich (St. Louis, MO, USA). Chemicals used in Western blot analysis were purchased from Bio-Rad Laboratories. Methanol and acetic acid (HPLC grade) were purchased from Fisher Scientific.

2.2. Plant Material Preparation and Extraction. The cobs of purple waxy corn (*Zea mays*, open-pollinated cultivar) harvested during November–December 2012 were identified and kindly provided by Professor Kamol Lertrat and Assistant Professor Bhalang Suriharn, Department of Plant Science and Agricultural Resources, Faculty of Agriculture, Khon Kaen University, Khon Kaen, Thailand. Pandan (*Pandanus amaryllifolius*) leaves were harvested at the same period as *Z. mays* from the Khon Kaen province. The plant identification was performed by Mister Winai Somprasong, an expert agricultural scientist in the Botany and Plant Herbarium research group, Plant Varieties Protection Division, Ministry of Agriculture and Cooperatives. The cobs of *Z. mays* and the leaves of *P. amaryllifolius* were cleaned and cut into a small pieces; then, they were force dried by using an oven at 60°C overnight. The dried plants (2 kilograms of each plant) were twice extracted with 5 liters of distilled water. The percent yield of *Z. mays* and *P. amaryllifolius* were 2.4 and 8, respectively.

2.3. Preparation of a Polyphenol-Rich Functional Drink. Powder of various ingredients including 2% (*w*/*v*) combined extract of *Z. mays* and *P. amaryllifolius* (a ratio of both extracts was obtained from our unpublished in vitro data which provided optimum potential and under petit patent), 0.75% (*v*/*v*) sucralose, 1% (*v*/*v*) lemonade, 0.025% (*w*/*v*) salt, and 96.225% (*v*/*v*) water. All ingredients were mixed together and filtered through a cheesecloth, and the filtrate was used for further study.

2.4. Determination of Total Phenolic Compound Contents. The determination of total phenolic compounds content was carried out by using the Folin-Ciocalteu method [20]. In brief, an aliquot of combined extract beverage (20 μl) was added to distilled water (1.58 ml) and 50% (*v*/*v*) Folin-Ciocalteu phenol reagent (0.1 ml) (Sigma-Aldrich). After 8 minutes of incubation, 20% sodium carbonate (0.3 ml) was added and mixed well. The mixture was kept in a dark room and incubated for 2 hours at room temperature. The absorbance was measured at 765 nm with a UV-spectrophotometer (Pharmacia LKB-Biochrom4060). Gallic acid at concentrations of 50–600 mg/l were used for preparing the standard calibration curve. The total phenolic compound was expressed as gallic acid equivalents per mg extract (mg/l GAE).

2.5. Assessment of DPPH Inhibition. The scavenging activity against free radicals of the developed drink was assessed via DPPH assessment. Briefly, 0.15 mM DPPH in methanol (0.5 ml) and the functional drink (1 ml) were mixed and incubated at room temperature for 30 minutes. The absorbance was determined at 517 nm with a UV-spectrophotometer (Pharmacia LKB-Biochrom4060). The DPPH radical scavenging activity was calculated using the following equation:

$$\%\text{Inhibition of DPPH} = \left[\left(\frac{\text{Abs control} - \text{Abs sample}}{\text{Abs control}}\right)\right] \times 100. \quad (1)$$

Abs control was the absorbance of methanol plus DPPH reagent while Abs sample was the absorbance of developed drink or standard. The linear portion of percentage inhibition of combined extract beverage was plotted against its concentration. The half maximal inhibitory concentration (IC_{50}) was calculated by using the equation from its graph [21]. All determinations were performed in triplicate.

2.6. Determination of Ferric-Reducing Antioxidant Power (FRAP) Assay. The assessment of ferric-reducing antioxidant power (FRAP) was performed based on the ability of the tested substance to reduce ferric tripyridyl triazine (Fe III TPTZ) complex to ferrous form (intense blue color) at low pH by using a modified method of Benzie and Strin [22]. FRAP reagent was freshly prepared by mixing solution A (300 mM acetate buffer pH 3.6), solution B (10 mM 2,4,6-

tripyridyl-striazine (TPTZ) in 40 mM HCl), and solution C (20 mM ferric chloride) together at a ratio of A : B : C; 10 : 1 : 1, respectively, and kept in water bath at 37°C. The tested substance (50 μl) was added to FRAP reagent (1.45 ml), mixed thoroughly, and incubated at 37°C for 10 minutes. The absorbance was measured with spectrophotometer at 593 nm (Pharmacia LKB-Biochrom4060). FRAP reagent and L-ascorbic acid (100–1000 μM) were used as blank and standard calibration, respectively. Data were expressed as μM L-ascorbic acid equivalent.

2.7. Determination of Anthocyanin Content. Anthocyanin content was determined according to the official method of the Association of Official Analytical Chemists (AOAC) [23]. The tested sample (1 ml) was mixed with 0.025 M potassium chloride pH 1.0 (2 ml) or 0.4 M sodium acetate pH 4.5 (2 ml). After the incubation at room temperature for 10 minutes, the absorbance was determined at 520 and 720 nm using a UV-spectrophotometer (Pharmacia LKB-Biochrom 4060). All assessments were performed as triplicate. Anthocyanin content was calculated and expressed as mg/l cyaniding-3-glucoside equivalent/mg extract (mg/l CGE) as follows:

$$\text{Anthocyanin content} \left(\frac{\text{cyanindin} - 3 - \text{glucoside equivalent, mg}}{\text{l}}\right) = \frac{\left(\text{A} \times \text{MW} \times \text{DF} \times 10^3\right)}{(\varepsilon \times 1)}, \quad (2)$$

where A = (A 520 nm–A 700 nm) pH 1.0 – (A 520 nm–A 700 nm) pH 4.5, MW (molecular weight) = 449.2 g/mol, DF = dilution factor obtained from the study, ε = 26,900 molar extinction coefficient, in l mol^{-1} cm^{-1}, for cyanindin-3-glucoside, 10^3 = factor for conversion from g to mg, and l = path length of the cuvette in cm (1 cm).

2.8. Assessment of Acetylcholinesterase Inhibitory (AChEI) Activity. Inhibition of acetylcholinesterase of the sample was determined according to the method previously described [24] using acetylthiocholine chloride iodide (ATCI) as a substrate. In brief, combined extract beverage (25 μl) was incubated with 15 mM ATCI (25 μl), 3 mM DTNB (5,5′-dithiobis[2-nitrobenzoic acid]) (75 μl), and 50 mM Tris buffer (pH 8) (50 μl) for 5 minutes at room temperature. The absorbance was measured with a microplate reader (iMark™ Microplate Absorbance Reader) at 415 nm before and after adding 0.25 units/ml acetylcholinesterase (AChE) (25 μl) to the mixture. The elevation of yellow color from the reaction was obtained and the percentage inhibition was calculated by comparing the yellow color of extract to a noninhibition well (Tris buffer). All tests were conducted in triplicate.

2.9. Fingerprint Chromatogram Assessment. The fingerprint chromatogram of the developed drink was analyzed by using gradient high-performance liquid chromatography (HPLC) system. High-performance liquid chromatography (HPLC) system consisted of 515 HPLC pump and 2998 photodiode array detector (Water Company, USA). Chromatographic separation was performed using Purospher®STAR, C-18 endcapped (5 μm), LiChroCART®250-4.6, and HPLC-Cartridge, sorbet lot number HX255346 (Merk, Germany) with guard column (Merk, Germany). Methanol (A) and 7.5% acetic acid in deionized (DI) water (B) were used as mobile phases. The gradient elution was carried out at a flow rate of 1.0 ml/min with the following gradient: 0–17 min, 70%A; 18–22 min, 100%A; 23–25, 50%A; and 26–30 min, 60%A. The sample was filtered (0.45 μm, Millipore), and a direct injection of tested sample at the volume of 20 μl on the column was performed. The chromatograms were recorded at 280 nm using a UV detector and data analysis was performed using EmpowerTM3.

2.10. Experimental Animals and Protocols. Female Wistar rats (Laboratory Animal Center, Salaya, Nakhon Pathom, Thailand), weighing 200–250 g, were used as the experimental animals. They were randomly housed 6 per cage in a temperature-controlled room on a 12 h light/dark cycle with ad libitum access to food and water. All procedures in this experiment were strictly performed in accordance with the internationally accepted principles for laboratory use and care of the European Community (EEC directive of 1986; 86/609/EEC). The experiment protocols were approved by the Institutional Animal Care and Unit Committee, Khon Kaen University, Thailand (record number AEKKU 1/2556).

The experimental rats were divided into 8 groups (n = 6/group) as follows:

Group I: Naïve intact group; all rats received no treatment and were served as the control group.

Group II: Sham operation + vehicle; all rats were subjected to sham operation surgery and received distilled water which was served as the vehicle in this study.

Group III: OVX + vehicle; the experimental animals in this group were subjected to bilateral ovariectomy (OVX) and received the vehicle.

Group IV: OVX + donepezil (3 mg/kg BW); the OVX rats were orally given donepezil, an acetylcholinesterase inhibitor, at a dose of 3 mg/kg and were served as the positive control-treated group.

Group V: OVX + isoflavone; all OVX rats were orally given isoflavone, a well-known polyphenol substance with cognitive enhancing, at a dose of 20 mg/kg BW.

Groups VI–VIII: OVX + PCP20, OVX + PCP40, and OVX + PCP80; the OVX rats in these groups received PCP at doses of 20, 40, and 80 mg/kg BW, respectively.

The treatment programs of the assigned substances for rats in groups II–VIII were started since the first day after surgery and were maintained throughout a 28-day experimental period. All treatments were performed once daily in the morning with the total volume of 1.5 ml. The assessment of nonspatial memory was performed every 7 days throughout the study period while the determinations of oxidative stress markers including malondialdehyde (MDA), superoxide dismutase (SOD), catalase (CAT), glutathione peroxidase (GSH-Px), the activity of acetylcholinesterase (AChE), histology, and ERK1/2 expression in the prefrontal cortex were determined at the end of the study.

2.11. Ovariectomized Surgery Procedure. The experimental animal was anesthetized with sodium thiopental at the dose of 60 mg/kg BW via intraperitoneal route prior to the ovariectomy. The ovariectomized (OVX) procedure was performed according to the method which had been previously described [25]. Briefly, the dorsolateral incisions were performed bilaterally, the ovarian blood vessels were tied off, and the ovaries were removed. Then, the skin was sutured and the rat was returned to their cage after postoperation care. Sham operation was carried out with the same procedures except that both the ovaries were kept intact.

2.12. Object Recognition Test. The object recognition test, the common test for evaluating nonspatial memory in rats, was used to assess the effect of PCP on nonspatial memory. This test was performed as previously described elsewhere with minor modification [26]. In brief, each rat was placed in an open field (80 cm long × 50 cm high × 60 cm wide) with two identical objects for 3 minutes (T1) and then was placed back to its home cage. Both objects should be placed in a symmetric position in the central line of the area. Then, the animal was orally given the assigned substance, and 30 minutes later, the second 3-minute trial was performed. In this session, one of the objects was replaced with the novel object which was totally different in shape and size at the same location. During the intertrial interval, the objects and open-field apparatus object were cleaned with 70% ethanol to avoid a confounding error induced by the influence of odor. The amount of time which the rat spent exploring each object was recorded and calculated as a novel object ratio (NOR) as the following equation:

$$\mathrm{NOR} = \frac{(T_{\mathrm{novel}} - T_{\mathrm{familiar}})}{(T_{\mathrm{novel}} + T_{\mathrm{familiar}})}, \quad (3)$$

where T_{novel} = time spent to explore the novel object and T_{familiar} = time spent to explore the familiar object.

2.13. Histological Study. After perfusion, the brains were removed and fixed with 4% paraformaldehyde solution (pH 7.4) at 4°C. Then, they were cryoprotected in formalin-sucrose (30%) for 2-3 days. Serial sections of tissue containing prefrontal cortex were cut frozen on a cryostat (Thermo Scientific™ HM 525 Cryostat) at 20 μm thick and mounted on slides coated with 0.3% aqueous solution of gelatin containing 0.05% aluminum potassium sulfate. To stain with cresyl violet, the slides were air dried; hydrated by successive immersion in 95, 70, and 50% ethanol; stained in 0.5% cresyl violet for 2 min at room temperature; dehydrated by successive immersion in 50, 70, 95, and 100% ethanol and xylene; and mounted with DPX. Three representative slides containing the prefrontal cortex were selected according to the stereotaxic coordinates anteroposterior 2.5–4.5 mm and mediolateral 0.2–1.0 mm from the rat brain atlas [27]. The analysis was performed by a blinded observer. The evaluation was performed via Olympus light microscope model BH-2 (Japan) at 40x magnification. The density of survival neurons in medial prefrontal cortex area (mPFC) was expressed as number of cells/255 μm^2.

2.14. Determination of Extracellular Signal-Regulated Kinase 1/2 (ERK1/2) Expression. The prefrontal cortex was subjected to a 2-minute homogenization in 1/10 (*w*/*v*) M-PER mammalian protein extraction (Pierce Protein Biology Product, Rockford, IL, USA) containing protease inhibitor cocktail (Sigma-Aldrich). Then, it was centrifuged at 14,000*g* for 10 minutes at 4°C. The supernatant was harvested and used for the determination of ERK1/2 expression. Protein concentration of the supernatant was quantified by using NanoDrop instrument (Thermo Fisher Scientific, Wilmington, Delaware USA). Total 30 μg of brain samples were separated by 10% sodium dodecyl sulfate polyacrylamide gel electrophoresis (SDS-PAGE) at 80 V. All protein bands were transferred.

The determination of ERK1/2 protein was performed according to the method previously described with a minor modification [28]. Total of 30 μg of brain samples were separated by 10% sodium dodecyl sulfate polyacrylamide gel electrophoresis (SDS-PAGE) at 80 V. Proteins from the gel were transferred to a nitrocellulose membrane (Bio-Rad Laboratories) and blocked with 5% nonfat dry milk in 0.1% tween 20 tris-buffered saline (TBS-T) for 30 minutes. After the blocking of a membrane, they were incubated with primary antibody which recognized ERK1/2 or monoclonal rabbit antiphosphorylated p44/p42 mitogen-activated protein kinase (MAPK) (Cell Signaling Technology Inc.; dilution, 1 : 1000) for 2 hours at room temperature. Then, they washed and incubated with secondary antibody conjugated with horseradish peroxidase or anti-rabbit IgG, HRP-linked antibody (Cell Signaling Technology Inc.; dilution, 1 : 2000) for 2 hours at room temperature. The band density was detected with an enhanced chemiluminescent (ECL) system (GE Healthcare, Piscataway, NJ). The analysis was performed using ImageQuant TL analysis software (GE Healthcare, Piscataway, NJ). The expression was normalized using antitotal ERK1/2. Data were presented as a relative density to the naïve control.

2.15. Biochemical Assays. The prefrontal cortex, an important area in learning and memory, was isolated and prepared as brain homogenate by subjecting to homogenization with 50 volume of 0.1 M phosphate buffer saline. Then, the homogenate was used for the determination of acetylcholinesterase (AChE) activity and oxidative stress status including malondialdehyde (MDA) level and the activities of superoxide dismutase (SOD), catalase (CAT), and glutathione peroxidase (GSH-Px). Protein concentration was assessed according to the Lowry method [29] and albumin bovine serum (2–20 mg/ml) was used as a standard.

The determination of AChE was carried out to reflect the cholinergic function in OVX rats by the colorimetric method [30]. A reaction mixture of 200 μl of 0.1 mM sodium phosphate buffer (pH 8.0), 10 μl of 0.2 M DTNB (5,5′-dithio-bis-(2-nitrobenzoic acid)), and 20 μl of the sample solution were incubated for 5 minutes, and the absorbance at 415 nm was recorded via microplate reader (iMark Microplate Absorbance Reader). Then, 10 μl of acetylcholine thiochloride (ACTI) was added, incubated for 3 minutes, and recorded the absorbance at 415 nm. The activity of AChE was

calculated according to the equation below and expressed as mmol/min/g protein.

$$\text{AChE activity} = \left(\Delta A/1.36 \times 10^4\right) \times 1/(20/230)C, \quad (4)$$

where ΔA = the difference of absorbance/minute and C = protein concentration of brain homogenate.

MDA level was assessed according to the method of Thiraphatthanavong et al. [31]. In brief, the mixture of 0.1 ml of brain homogenate, 0.1 ml of 8.1% (*w*/*v*) sodium dodecyl sulfate, 0.75 ml of 20% (*v*/*v*) acetic acid pH 3.5, 0.75 ml of 0.8% (*w*/*v*) thiobarbituric acid, and 0.3 ml of distilled water were mixed thoroughly and boiled at 95°C for 1 hour. After cooling, 0.5 ml of water and 2.5 ml of the mixture of n-butanol and pyridine at the ratio of 15 : 1 were added, mixed together, and centrifuged at 4000 rpm for 10 minutes. The pink layer was harvested and determined the optical density at 532 nm. 1,1,3,3-tetramethoxypropane (2–20 nmol) was served as a standard and MDA level was expressed as nmol/mg protein.

SOD assessment was performed according to the method previously described elsewhere [32]. Briefly, 20 μl of brain homogenate was mixed with the mixture which contained 216 mM potassium phosphate buffer (KH_2PO_4), 10.7 mM ethylenediaminetetraacetic acid, 1.1 mM cytochrome C, and 0.54 mM xanthine solution pH 7.4 at the ratio of 25 : 1 : 1 : 50. Then, 20 μl of 0.05 units/ml of xanthine oxidase was added and incubated for 5 minutes at room temperature. The absorbance was measured at 490 nm using microplate reader. SOD enzyme activities at the concentrations of 0–10 units/ml were used as standards, and the results were expressed as units/mg protein.

The activity of catalase (CAT) was evaluated indirectly by measuring the residual H_2O_2 which was titrated by potassium permanganate. In brief, 10 μl of brain homogenate was mixed with 50 μl of 30 mM H_2O_2, 25 μl of 5 N H_2SO_4, and 150 μl of 5 mM $KMnO_4$. The mixture was shaken and the absorbance was measured at 490 nm. CAT enzyme at the concentration range of 0–10 units/ml was used as a standard and the result was expressed as units/mg protein [32].

Glutathione peroxidase activity was assessed using the colorimetric method. In brief, 10 μl of brain homogenate was mixed with the mixture containing 50 μl of 30 mM H_2O_2, 25 μl of 5 N H_2SO_4, and 150 μl of 5 mM $KMnO_4$. The mixture was shaken and the absorbance was measured at 490 nm. The standard calibration curve was prepared by using CAT enzyme at the concentration range of 0–10 units/ml. CAT activity was expressed as units/mg protein [32].

2.16. Statistical Analysis. Data are presented as mean ± standard error of mean (SEM). The statistical analysis of the experiment was carried out using IBM SPSS Statistics (version 21). Data was analyzed using one-way analysis of variance (ANOVA), followed by Tukey's post hoc test. Probability levels less than 0.05 were accepted as significant.

Table 1: The biological activity of PCP including total phenolic compound, anthocyanin content, DPPH radical activity, FRAP activity, and AChEI activity.

Test	PCP	Standard reference
Total phenolic compound (mg/l GAE)	184 ± 1.91	—
Anthocyanin content (mg/l CGE)	25.66 ± 0.32	—
FRAP activity (μM L-ascorbic acid equivalent)	602.40 ± 2.33	—
DPPH radical activity (IC_{50} μg/ml)	56.37 ± 0.45	Ascorbic acid 2.89 ± 0.01
AChEI activity (IC_{50} μg/ml)	1950 ± 16.02	Donepezil 0.51 ± 0.03

3. Results

3.1. Biological Activities of the Combined Extract. Total phenolic compounds and anthocyanin content together with the biological activities including the antioxidant activity (DPPH and FRAP assay) and acetylcholinesterase inhibition activity of the combined extract were evaluated. The results showed that 1 ml of the combined extract contained the total phenolic compounds and anthocyanin contents of 184.00 ± 1.91 mg/l gallic acid equivalent and 25.66 ± 0.32 mg/l cyanidin-3-glucoside equivalent, respectively. IC_{50} of the antioxidant activity via 2,2-diphenyl-1-picrylhydrazyl (DPPH) assay was 56.37 ± 0.45 μg/ml, whereas the antioxidant activity via ferric-reducing antioxidant power (FRAP) assay was 602.40 ± 2.33 μM L-ascorbic acid equivalent. In addition, AChEI activity showed IC_{50} at a concentration of 1950 ± 16.02 μg/ml as shown in Table 1.

3.2. The Fingerprint of the Combined Extract. Figure 1 shows the fingerprint chromatogram of PCP, the combined extract of purple corn cob and pandan leaves. More than 7 different peaks were observed in the chromatogram. Four of them were anthocyanins (peak 2–peak 5) including cyaniding-3-glucoside (peak 2), pelargonidin-3-glucoside (peak 3), cyanidin 3-O-(6″-malonyl-glucoside) (peak 4), and cyaniding-3-o-B-glucopyranoside (peak 5). It was found that the contents of anthocyanins mentioned earlier in PCP were 3.239 ± 0.014, 2.543 ± 0.011, 2.993 ± 0.024, and 2.335 ± 0.006 mg/ml, respectively. In addition to anthocyanins, gallic acid, rutin, and ferulic acid were observed at the concentrations of 0.180 ± 0.001, 0.337 ± 0.001, and 0.341 ± 0.027 mg/ml, respectively.

3.3. Effect of the Combined Extract on Nonspatial Memory in OVX Rats. Memory-enhancing effect of the combined extract on nonspatial memory was shown in Figure 2. It was found that sham operation rats showed no significant change on novel object ratio (NOR). OVX rats treated with vehicle significantly decreased NOR throughout the study period (p value < 0.01, 0.01, 0.05, and 0.05, resp., compared with the sham operation group). OVX rats with isoflavone treatment attenuated the reduction of NOR induced by OVX throughout the study period (p value < 0.01, 0.05, 0.01, and

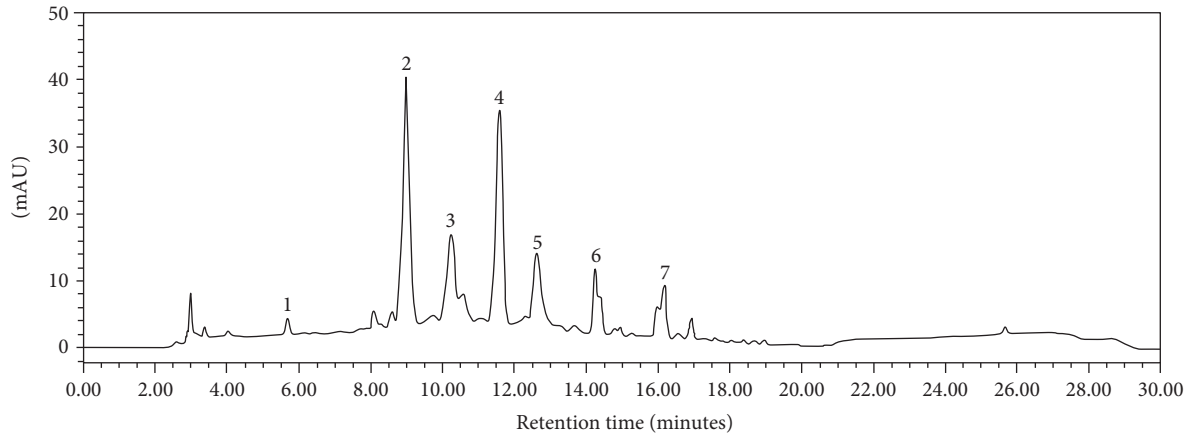

Figure 1: The fingerprint chromatogram of the PCP using HPLC analysis.

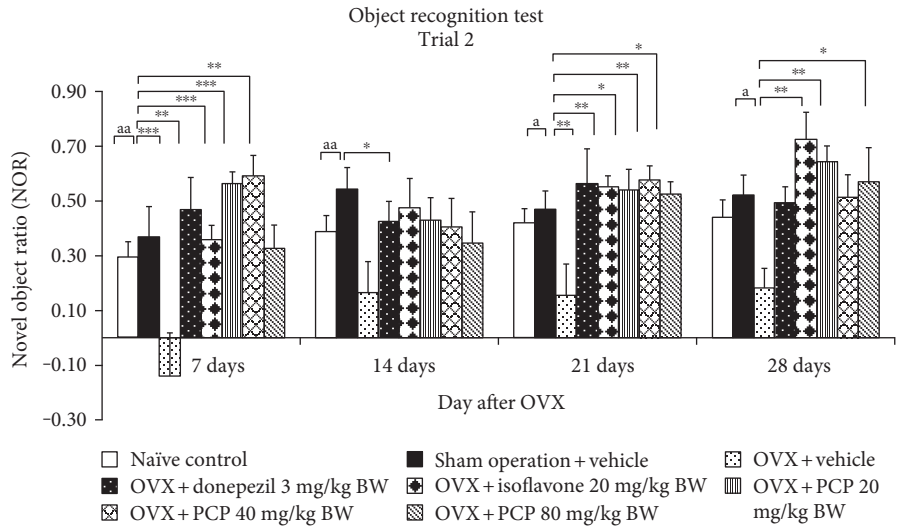

Figure 2: The effect of the PCP on nonspatial memory assessing by the object recognition test ($n = 6$/group). Data were expressed as mean ± SEM. $^{a, aa}p$ value < 0.05, 0.01, respectively, compared with the sham operation group. *, **, $^{***}p$ value < 0.05, 0.01, and 0.001, respectively, compared with the OVX + vehicle-treated group.

0.01, resp., compared with OVX + vehicle). Donepezil also showed the mitigation effect on the reduction of NOR in OVX rats, but significant differences were observed only at 7- and 21-day treatment periods (p value < 0.001 and 0.01, resp., compared with the OVX + vehicle-treated group). The combined extract at doses of 20 and 80 mg/kg BW significantly attenuated the decreased NOR in OVX rats at 7, 21, and 28 days of treatment (p value < 0.001 and 0.01; 0.05 all; and 0.01 and 0.05, resp., compared with the OVX + vehicle-treated group). The significant mitigation effect of PCP at a dose of 40 mg/kg BW on NOR was also observed at 7 and 21 days of treatment (p value < 0.001 and 0.01, resp., compared with the OVX + vehicle-treated group). The increased NOR in the PCP treatment groups were also observed at a 14-day study period, but no significant difference was revealed.

3.4. Histological Change in the Prefrontal Cortex. Based on the previous finding that the prefrontal cortex played a crucial role on working memory in rodents [33], we also investigated the neuron density in this area and results were shown in Figure 3. The current results demonstrated that OVX treated with vehicle significantly reduced the neuron density in PFC (p value < 0.05, compared with the sham operation group). Both donepezil and isoflavone could attenuate the reduction of neuron density in PFC of OVX rats (p value < 0.01 all; compared with the OVX + vehicle-treated group). In addition, combined extract at the dosage range used in this study also significantly attenuated the reduction of neuron density in PFC of OVX rats (p value < 0.01, 0.01, and 0.05; compared with the OVX + vehicle-treated group).

3.5. Biochemical Assays. Table 2 shows the effect of PCP on oxidative stress markers including MDA level and the activities of SOD, CAT, and GSH-Px. Sham operation showed no significant changes of the mentioned parameters. OVX rats which received vehicle significantly increased MDA level (p value < 0.05; compared to the sham operation group) in the prefrontal cortex (PFC). Donepezil treatment

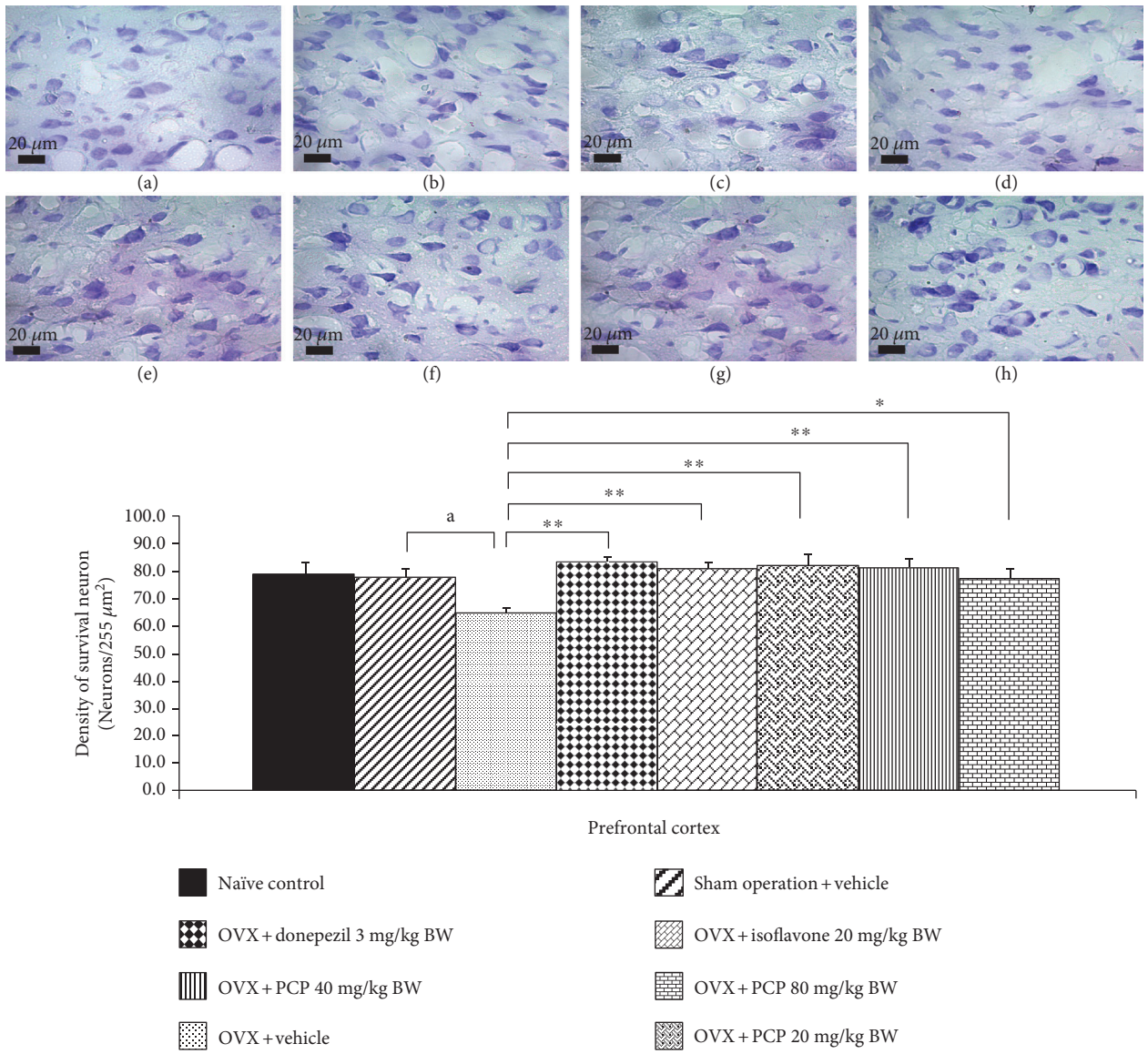

FIGURE 3: The effect of the PCP on the density of survival neurons in medial prefrontal cortex (mPFC) ($n = 6$/group). The upper panel showed the photomicrograph of the coronal section of rat brains in (a) naïve control, (b) sham operation + vehicle, (c) OVX + vehicle, (d) OVX + donepezil, (e) OVX + isoflavone, (f) OVX + PCP 20 mg/kg BW, (g) OVX + PCP 40 mg/kg BW, and (h) OVX + PCP 80 mg/kg BW. Scale bar: 20 μm. The lower panel demonstrated the density of survival neurons of mPFC. ^{a}p value < 0.05, compared with the sham operation group. *, $^{**}p$ value < 0.05 and 0.01, respectively, compared with the OVX + vehicle-treated group. Data were expressed as mean ± SEM.

failed to produce the significant changes on all parameters just mentioned in OVX rats. However, isoflavone significantly decreased MDA level but enhanced SOD activity (p value < 0.05 and 0.01, resp., compared to the OVX + vehicle-treated group). Interestingly, PCP at all doses used in this study significantly decreased MDA level in PFC (p value < 0.001 all; compared to the OVX + vehicle-treated group). The elevation of SOD activity in PFC was observed in OVX rats which received PCP at the concentrations of 20 and 40 mg/kg BW (p value < 0.001 and 0.01, resp., compared with the OVX + vehicle-treated group).

Since the cholinergic system plays a crucial role on learning and memory [34], we also investigated the effect of PCP on the cholinergic system by using the suppression activity of AChE or AChEI activity as an indirect index, and results were shown in Figure 4. It was found that both sham operation and OVX rats which received vehicle failed to produce the significant changes of AChE. The decreased AChE activity was observed in OVX rats which received donepezil and combined extract at the dose of 20 mg/kg BW (p value < 0.05 and 0.01, resp., compared with the OVX rats + vehicle-treated group). When compared with OVX rats which received vehicle, no significant changes of AChE were observed in the other groups.

3.6. ERK1/2 Signaling Pathway. Based on the crucial role of ERK1/2 on the survival neurons and memory enhancement [28], the effect of PCP on the phosphorylation ERK1/2

Table 2: The effect of PCP on oxidative stress markers in the prefrontal cortex ($n = 6$/group).

Treatment	Oxidative stress markers in the prefrontal cortex			
	MDA (nmol/mg protein)	GSH-Px (Units/mg protein)	SOD (Units/mg protein)	CAT (Units/mg protein)
Naïve control	0.073 ± 0.0.001	0.661 ± 0.034	0.567 ± 0.164	2.707 ± 0.234
Sham operation	0.077 ± 0.007	0.576 ± 0.052	0.834 ± 0.256	2.516 ± 0.237
OVX + vehicle	0.095 ± 0.008[a]	0.523 ± 0.034	0.309 ± 0.100	2.684 ± 0.216
OVX + donepezil 3 mg/kg BW	0.090 ± 0.007	0.714 ± 0.047	1.387 ± 0.344	2.650 ± 0.187
OVX + isoflavone 20 mg/kg BW	0.059 ± 0.005*	0.902 ± 0.111	2.220 ± 0.458**	2.130 ± 0.210
OVX + PCP 20 mg/kg BW	0.047 ± 0.012***	0.866 ± 0.186	3.080 ± 0.352***	2.447 ± 0.359
OVX + PCP 40 mg/kg BW	0.034 ± 0.002***	0.799 ± 0.070	2.047 ± 0.184**	2.151 ± 0.160
OVX + PCP 80 mg/kg BW	0.032 ± 0.004***	0.639 ± 0.029	1.068 ± 0.366	1.921 ± 0.092

[a]p value < 0.05, compared with the sham operation group. *, **, ***p value < 0.05, 0.01, and 0.001, respectively, compared with the OVX + vehicle-treated group. Data were expressed as mean ± SEM.

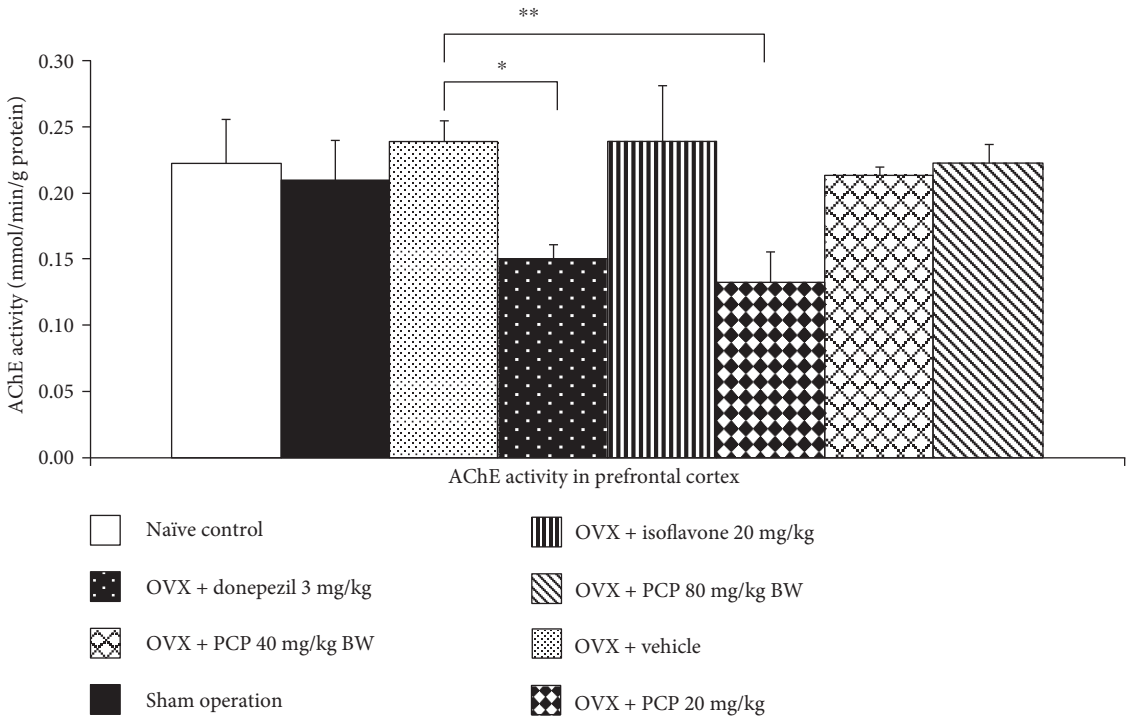

Figure 4: The effect of PCP on the activity of AChE in the prefrontal cortex ($n = 6$/group). *, **p value < 0.05 and 0.01, respectively, compared with the OVX + vehicle-treated group. Data were expressed as mean ± SEM.

was also determined, and results were shown in Figure 5. The current data showed that OVX rats significantly decreased expression of phosphorylation ERK1/2 in PFC (p value < 0.001; compared with the sham operation group). Isoflavone and medium dose of PCP produced the significant attenuation effect induced by OVX (p value < 0.01 and 0.05, resp., compared with the OVX + vehicle-treated group).

4. Discussion

The current data showed that ovariectomy, a widely used model of menopause, increased oxidative stress status, impairment of the cholinergic system, and memory impairment which were in concordance with the previous study [35, 36]. In the present study, it was found that OVX increased MDA without changes of the main scavenger enzymes such as SOD, CAT, and GSH-Px. This was in agreement with the previous study [37]. These results suggested that the elevation of MDA level might occur either via the increased oxidative stress production or via the decreased function of the nonenzymatic antioxidant system. Interestingly, PCP, the combined extract of purple corn cob and pandan leaves attenuated the memory impairment evaluated by using the object recognition test.

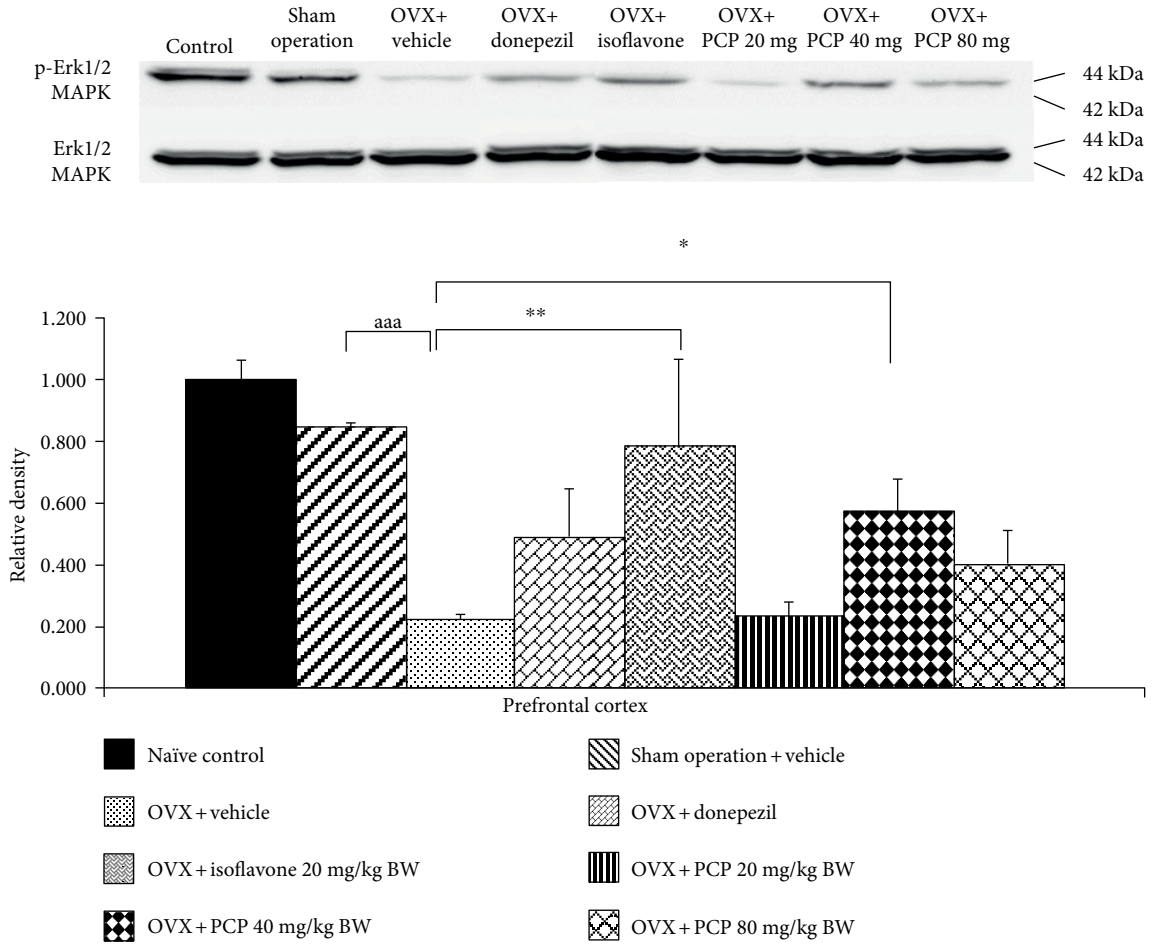

FIGURE 5: The effect of the PCP on the expression of phosphorylation ERK1/2 (p-ERK1/2) protein in the prefrontal cortex ($n = 6$/group). ^{aaa}p value < 0.001, compared with the sham operation group. *, $^{**}p$ value < 0.05 and 0.01, respectively, compared with the OVX + vehicle-treated group. Data were expressed as mean ± SEM.

It has been reported that the prefrontal cortex plays a crucial role on nonspatial memory. Lesion of this area could induce nonspatial memory impairment [38]. In this study, we have found that this impairment was attenuated by both isoflavone and all doses of PCP. The reduction of MDA level which indicated the decreased oxidative stress status and the enhanced neuron density was also observed in OVX rats which received isoflavone and all doses of PCP. Therefore, we suggested that PCP and isoflavone might improve oxidative stress status leading to the enhanced neuron density in PFC resulting in the improved nonspatial memory. The decreased oxidative stress status in PFC observed in this study might occur partly via the enhanced function of a scavenger enzyme especially SOD. Since no closed relationship between the decreased MDA level and the enhanced SOD activity in PFC was observed, other factors such as the decreased nonenzymatic system and the decreased oxidative stress production mentioned earlier might also contribute to the role.

In addition to oxidative stress, the cholinergic system in PFC also plays the crucial role on memory. Depletion of acetylcholine (ACh) together with the elevation of acetylcholinesterase (AChE) in the PFC induces memory impairment both in primates and in rodents [39, 40]. The cognitive-enhancing effect of donepezil, an AChEI, was observed without changes of oxidative stress markers. Our study also demonstrated that both donepezil and low dose of PCP also suppressed AChE activity in PFC. Therefore, the enhanced cholinergic function in PFC by suppressing AChE activity in the mentioned area also contributes to a role on the cognitive-enhancing effect of both substances. It has been reported that polyphenol [14] including anthocyanins [41] can improve memory impairment induced by scopolamine which exerts the effect at muscarinic receptors. Since PCP contains polyphenols and anthocyanins, it is also possible that PCP also exerts its influence on muscarinic receptor. However, this requires further investigation.

Recently, it has been demonstrated that mitogen-activated protein kinase (MAPK) especially ERK1/2 contributes to the pivotal role on learning and memory [42]. The substances which improve ERK signaling also improve the impairment of object recognition memory [43]. Based on this information, we did suggest that the cognitive-enhancing effect of isoflavone and medium dose of PCP might also occur via the enhanced ERK1/2 signaling pathway.

Anthocyanins, a member of flavonoids, have been shown to exert the neuroprotective and cognitive-enhancing effect [44]. Since our fingerprint of PCP showed that the main ingredient in PCP was anthocyanins (peak 2–peak 5), we suggested that the neuroprotective effect and cognitive-enhancing effects of PCP in this study might involve anthocyanins. However, the effect of other ingredients still cannot be omitted.

Our data failed to show a dose-dependent manner of PCP. The possible explanation might be due to the non-simple linear relationship between the concentration of PCP and the observed parameters. Since many factors exert the influences on the observed parameters in this study, no simple linear relationship was observed. In addition, PCP contained many ingredients, so the effect of an active ingredient could be masked by other ingredients.

In this study, we have found that our data showed that although in vitro data showed that IC_{50} of AChEI of PCP was very high, low dose of PCP could exert the cognitive-enhancing effect via the suppression of AChE in the prefrontal cortex while the medium and high doses of PCP failed to exert this effect. The possible explanation might also occur as that mentioned earlier in the lack of a dose-dependent study.

Taken all data together, our study highlights the neuroprotective and cognitive effects of PCP that might occur primarily via the decreased oxidative stress which in turn increased neuron density in the brain especially in PFC, an area playing an important role on learning and memory especially nonspatial memory, resulting in the improved nonspatial memory. However, the improved cholinergic function and signal transduction via ERK1/2 might also exert the roles especially at low and medium doses, respectively.

5. Conclusion

This study is the first study to demonstrate the neuroprotective and cognitive effects of PCP. We have shown that the combined extract of purple corn cob and pandan leaves can be served as functional ingredients for developing neuroprotectant and cognitive enhancer for menopausal women. Therefore, we highlight how to create the value for agricultural waste such as purple corn cob. However, chronic toxicity is required in order to assure the consumption safety before moving forward to a clinical trial study.

Conflicts of Interest

The authors declare that they have no conflicts of interest.

Acknowledgments

This study was supported by the Higher Education Research Promotion and National Research University Project of Thailand, Office of the Higher Education Commission, through the Food and Functional Food Research Cluster of Khon Kaen University, the Integrative Complementary Alternative Medicine Research and Development Center, and the Invitation Research Grant of the Faculty of Medicine (Grant no. IN58219), Khon Kaen University.

References

[1] World Health Organization, *WHO Technical Report Series 866: Research on the Menopause in the 1990s*, WHO Library Cataloguing in Publication Data, Geneva, Switzerland, 1994.

[2] J. R. Sliwinski, A. K. Johnson, and G. R. Elkins, "Memory decline in peri- and post-menopausal women: the potential of mind-body medicine to improve cognitive performance," *Integrative Medicine Insights*, vol. 9, pp. 17–23, 2014.

[3] E. Hogervorst, J. Williams, M. Budge, W. Riedel, and J. Jolles, "The nature of the effect of female gonadal hormone replacement therapy on cognitive function in post-menopausal women: a meta-analysis," *Neuroscience*, vol. 101, no. 3, pp. 485–512, 2000.

[4] M. Sano, "Understanding the role of estrogen on cognition and dementia," *Journal of Neural Transmission Supplementum*, vol. 59, pp. 233–239, 2000.

[5] S. A. Shumaker, C. Legault, L. Kuller et al., "Conjugated equine estrogens and incidence of probable dementia and mild cognitive impairment in postmenopausal women: Women's Health Initiative Memory Study," *The Journal of the American Medical Association*, vol. 291, no. 24, pp. 2947–2958, 2004.

[6] M. A. Espeland, S. R. Rapp, S. A. Shumaker; et al., "Conjugated equine estrogens and global cognitive function in postmenopausal women: Women's Health Initiative Memory Study," *The Journal of the American Medical Association*, vol. 291, no. 24, pp. 2959–2968, 2004.

[7] S. M. Resnick, P. M. Maki, S. R. Rapp et al., "Effects of combination estrogen plus progestin hormone treatment on cognition and affect," *The Journal of Clinical Endocrinology and Metabolism*, vol. 91, no. 5, pp. 1802–1810, 2006.

[8] V. Beral, "Breast cancer and hormone-replacement therapy in the Million Women Study," *Lancet*, vol. 362, no. 9382, pp. 419–427, 2003.

[9] W. Y. Chen, S. E. Hankinson, S. J. Schnitt, B. A. Rosner, M. D. Holmes, and G. A. Colditz, "Association of hormone replacement therapy to estrogen and progesterone receptor status in invasive breast carcinoma," *Cancer*, vol. 101, no. 7, pp. 1490–1500, 2003.

[10] O. H. Franco, R. Chowdhury, J. Troup et al., "Use of plant-based therapies and menopausal symptoms: a systematic review and meta-analysis," *Journal of the American Medical Association*, vol. 315, no. 23, pp. 2554–2563, 2016.

[11] P. Leerasiri, C. Chayachinda, S. Indhavivadhana, T. Wongwananurak, C. Dangrat, and M. Rattanachaiyanont, "Nutritional supplements in health-conscious pre-/post-menopausal Thai women," *Journal of the Medical Association of Thailand*, vol. 93, no. 10, pp. 1128–1136, 2010.

[12] C. W. Cotman, E. Head, B. A. Muggenburg, S. Zicker, and N. W. Milgram, "Brain aging in the canine: a diet enriched in antioxidants reduces cognitive dysfunction," *Neurobiology of Aging*, vol. 23, no. 5, pp. 809–818, 2002.

[13] J. Rubio, W. Qiong, X. Liu et al., "Aqueous extract of black maca (*Lepidium meyenii*) on memory impairment induced by ovariectomy in mice," *Evidence-Based Complementary and Alternative Medicine*, vol. 2011, Article ID 253958, 7 pages, 2011.

[14] Y. S. Juan, S. M. Chuang, Y. L. Lee et al., "Green tea catechins decrease oxidative stress in surgical menopause-induced overactive bladder in a rat model," *BJU International*, vol. 110, no. 6, Part B, pp. E236–E244, 2012.

[15] G. Patki, F. H. Allam, F. Atrooz et al., "Grape powder intake prevents ovariectomy-induced anxiety-like behavior, memory impairment and high blood pressure in female Wistar rats," *PloS One*, vol. 8, no. 9, article e74522, 2013.

[16] F. Ramos-Escudero, A. M. Muñoz, C. Alvarado-Ortíz, Á. Alvarado, and J. A. Yáñez, "Purple corn (*Zea mays* L.) phenolic compounds profile and its assessment as an agent against oxidative stress in isolated mouse organs," *Journal of Medicinal Food*, vol. 15, no. 2, pp. 206–215, 2012.

[17] R. Chaisanam, S. Muchimapura, J. Wattanathorn, W. Thukham-mee, and J. Jittiwat, "Antioxidant and cyclooxygenase-2-inhibiting effect of purple corn cob extract-loaded nanofiber patch on motor recovery in spinal cord injury rats," *North-Eastern Thai Journal of Neuroscience*, vol. 10, no. 4, pp. 14–33, 2015.

[18] S. W. Yan and R. Asmah, "Comparison of total phenolic contents and antioxidant activities of turmeric leaf, pandan leaf and torch ginger flower," *International Food Research Journal*, vol. 17, pp. 417–423, 2010.

[19] T. D. Widyaningsih, I. Z. Zumroh, and N. Rochmawati, "Effect of mixed grass jelly (*Mesona palustris* BL.) and other ingredients effervescent powder in diabetic rats," *International Journal of Technical Research and Applications*, vol. 2, no. 5, pp. 52–55, 2014.

[20] A. L. Waterhouse, "Determination of total phenolics," *Current Protocols in Food Analytical Chemistry*, pp. I1–I8, 2002.

[21] S. Sreelatha and P. R. Padma, "Antioxidant activity and total phenolic content of Moringa oleifera leaves in two stages of maturity," *Plant Foods Human Nutrition*, vol. 64, pp. 303–311, 2009.

[22] I. F. Benzie and J. J. Strin, "The ferric reducing ability of plasma (FRAP) as a measure of antioxidant power: the FRAP assay," *Analytical Biochemistry*, vol. 239, pp. 70–76, 1996.

[23] J. Lee, R. W. Durst, and R. E. Wrolstad, "Determination of total monomeric anthocyanin pigment content of fruit juices, beverages, natural colorants, and wines by the pH differential method: collaborative study," *Journal of AOAC International*, vol. 88, no. 5, pp. 1269–1278, 2005.

[24] M. A. Papandreou, A. Dimakopoulou, Z. I. Linardaki et al., "Effect of a polyphenol-rich wild blueberry extract on cognitive performance of mice, brain antioxidant markers and acetylcholinesterase activity," *Behavioural Brain Research*, vol. 198, no. 2, pp. 352–358, 2009.

[25] S. Sungkamanee, J. Wattanathorn, S. Muchimapura, and W. Thukham-mee, "Antiosteoporotic effect of combined extract of *Morus alba* and *Polygonum odoratum*," *Oxidative Medicine and Cellular Longevity*, vol. 2014, Article ID 579305, 9 pages, 2014.

[26] S. Okuda, B. Roozendaal, and J. L. McGaugh, "Glucocorticoid effects on object recognition memory require training-associated emotional arousal," *Proceedings of the National Academy of Sciences of the United States of America*, vol. 101, no. 3, pp. 853–858, 2004.

[27] G. Paxinos and C. Watson, *The Rat Brain in Stereotaxic Coordinates*, Elsevier, Amsterdam, 2009.

[28] J. Lu, D. M. Wu, Y. L. Zheng, B. Hu, and Z. F. Zhang, "Purple sweet potato color alleviates D-galactose-induced brain aging in old mice by promoting survival of neurons via PI3K pathway and inhibiting cytochrome C-mediated apoptosis," *Brain Pathology*, vol. 20, no. 3, pp. 598–612, 2010.

[29] O. H. Lowry, N. J. Rosebrough, A. L. Farr, and R. J. Randall, "Protein measurement with the folin phenol reagent," *Journal of Biological Chemistry*, vol. 193, no. 1, pp. 265–275, 1951.

[30] G. L. Ellman, K. D. Courtney, V. Andres Jr, and R. M. Feather-Stone, "A new and rapid colorimetric determination of acetylcholinesterase activity," *Biochemical Pharmacology*, vol. 7, pp. 88–95, 1961.

[31] P. Thiraphatthanavong, J. Wattanathorn, S. Muchimapura et al., "Preventive effect of *Zea mays* L. (purple waxy corn) on experimental diabetic cataract," *BioMed Research International*, vol. 2014, Article ID 507435, 8 pages, 2014.

[32] W. Kirisattayakul, J. Wattanathorn, T. Tong-Un, S. Muchimapura, P. Wannanon, and J. Jittiwat, "Cerebroprotective effect of Moringa oleifera against focal ischemic stroke induced by middle cerebral artery occlusion," *Oxidative Medicine and Cellular Longevity*, vol. 2013, Article ID 951415, 10 pages, 2013.

[33] S. M. Courtney, L. Petit, J. V. Haxby, and L. G. Ungerleider, "The role of prefrontal cortex in working memory: examining the contents of consciousness," *Philosophical Transactions of the Royal Society B*, vol. 353, no. 1377, pp. 1819–1829, 1998.

[34] A. Blokland, "Acetylcholine: a neurotransmitter for learning and memory?" *Brain Research Review*, vol. 21, no. 3, pp. 285–300, 1995.

[35] M. Ulas and M. Cay, "The effects of 17beta-estradiol and vitamin E treatments on oxidative stress and antioxidant levels in brain cortex of diabetic ovariectomized rats," *Acta Physiologica Hungarica*, vol. 97, no. 2, pp. 208–215, 2010.

[36] M. Singh, E. M. Meyer, W. J. Millard, and J. W. Simpkins, "Ovarian steroid deprivation results in a reversible learning impairment and compromised cholinergic function in female Sprague-Dawley rats," *Brain Research*, vol. 644, no. 2, pp. 305–312, 1994.

[37] M. Da Silva Morrone, C. E. Schnorr, G. A. Behr et al., "Oral administration of curcumin relieves behavioral alterations and oxidative stress in the frontal cortex, hippocampus, and striatum of ovariectomized Wistar rats," *The Journal of Nutritional Biochemistry*, vol. 32, pp. 181–188, 2016.

[38] C. T. Curtis, "The effects of prefrontal lesions on working memory performance and theory," *Cognitive, Affective & Behavioral Neuroscience*, vol. 4, no. 4, pp. 528–539, 2004.

[39] Z. Alrefaie, "Vitamin D3 improves decline in cognitive function and cholinergic transmission in prefrontal cortex of streptozotocin-induced diabetic rats," *The Medical Journal of Cairo University*, vol. 81, no. 2, pp. 25–31, 2013.

[40] Y. Chudasama, J. W. Dalley, F. Nathwani, P. Bouger, T. W. Robbins, and F. Nathwani, "Cholinergic modulation of visual attention and working memory: dissociable effects of basal forebrain 192-IgG-saporin lesions and intraprefrontal infusions of scopolamine," *Learning & Memory*, vol. 11, no. 1, pp. 78–86, 2004.

[41] J. M. Gutierres, F. B. Carvalho, M. R. Schetinger et al., "Protective effects of anthocyanins on the ectonucleotidase activity in the impairment of memory induced by scopolamine in adult rats," *Life Sciences*, vol. 91, no. 23-24, pp. 1221–1228, 2012.

[42] K. P. Giese and K. Mizuno, "The roles of protein kinases in learning and memory," *Learning & Memory*, vol. 20, no. 10, pp. 540–552, 2013.

[43] B. González, M. Raineri, J. L. Cadet, E. García-Rill, F. J. Urbano, and V. Bisagno, "Modafinil improves methamphetamine-induced object recognition deficits and restores prefrontal cortex ERK signaling in mice," *Neuropharmacology*, vol. 87, no. 1, pp. 188–197, 2014.

[44] P. Kaewkaen, T. Tong-Un, J. Wattanathorn, S. Muchimapura, W. Kaewrueng, and S. Wongcharoenwanakit, "Mulberry fruit extract protects against memory impairment and hippocampal damage in animal model of vascular dementia," *Evidence-Based Complementary and Alternative Medicine*, vol. 2012, Article ID 263520, 9 pages, 2012.

Hindawi
Oxidative Medicine and Cellular Longevity
Volume 2017, Article ID 5205471, 17 pages
https://doi.org/10.1155/2017/5205471

Research Article

Curcumin Protects Skin against UVB-Induced Cytotoxicity via the Keap1-Nrf2 Pathway: The Use of a Microemulsion Delivery System

Maya Ben Yehuda Greenwald,[1,2,3,4] Marina Frušić-Zlotkin,[1] Yoram Soroka,[1] Shmuel Ben Sasson,[4] Ronit Bitton,[5,6] Havazelet Bianco-Peled,[2,3] and Ron Kohen[1]

[1]*The Institute for Drug Research, School of Pharmacy, The Hebrew University of Jerusalem, 9112100 Jerusalem, Israel*
[2]*Department of Chemical Engineering, Technion-Israel Institute of Technology, Technion City, 3200003 Haifa, Israel*
[3]*The Russell Berrie Nanotechnology Institute and Technion-Israel Institute of Technology, 32000 Haifa, Israel*
[4]*Department of Developmental Biology and Cancer Research, The Hebrew University Medical School, Ein-Karem Campus, 9112100 Jerusalem, Israel*
[5]*Department of Chemical Engineering, Ben-Gurion University of the Negev, 8410501 Beer-Sheva, Israel*
[6]*Ilse Katz Institute for Nanoscale Science and Technology, 8410501 Beer-Sheva, Israel*

Correspondence should be addressed to Ron Kohen; ronk@ekmd.huji.ac.il

Received 24 October 2016; Revised 19 March 2017; Accepted 16 April 2017; Published 5 July 2017

Academic Editor: Luciano Saso

Curcumin was found to be beneficial in treating several skin pathologies and diseases, providing antioxidant protection due to its reducing properties and its electrophilic properties (the ability to activate the Nrf_2 pathway and induce phase II cytoprotective enzymes). Nevertheless, clinical applications of curcumin are being hampered by its insufficient solubility, chemical instability, and poor absorption, leading to low efficacy in preventing skin pathologies. These limitations can be overcome by using a nanotechnology-based delivery system. Here, we elucidated the possibility of using curcumin encapsulated in a microemulsion preserving its unique chemical structure. We also examined whether curcumin microemulsion would reduce UVB-induced toxicity in skin. A significant curcumin concentration was found in the human skin dermis following topical application of a curcumin microemulsion. Moreover, curcumin microemulsion enhanced the reduction of UV-induced cytotoxicity in epidermal cells, paving the way for other incorporated electrophiles in encapsulated form protecting skin against stress-related diseases.

1. Introduction

The concept that antioxidants can protect cells and organs against oxidative stress has been established in numerous basic and clinical studies [1]. Nevertheless, nowadays, it has become evident that antioxidants of low molecular weight cannot protect the living organism against continuous stress and sometimes can even be deleterious [2]. Oxidants (electrophiles), on the other hand, were recently shown to be compounds capable of inducing cellular-protecting enzymes such as the phase II enzymes when provided in moderate concentrations. One of the basic factors activated when an electrophile is present is the transcription factor nuclear factor (erythroid-derived 2)-like 2, an NF-E2-related factor 2 (Nrf2), which is responsible for the induction of a variety of cytoprotective genes [3]. Regulated by the Keap1 metalloprotein, Nrf2 is capable of inducing a large number of genes encoding antioxidant enzymes and genes enabling homeostasis and controlling processes involved in the pathology of many diseases (e.g., immune and inflammatory responses, tissue remodeling and fibrosis, carcinogenesis, and metastasis) [4, 5]. Nrf2 plays a vital and crucial role in the maintenance of skin homeostasis and repair and regeneration in various disease states of the skin [6]. However, acute and chronic Nrf2 activation in a healthy epidermis resulted in a negative effect on skin integrity [6]. Endogenous Nrf2 has the ability to protect skin against UV irradiation [6]. Nrf2 is also capable of decreasing symptoms of skin photoaging (e.g., wrinkle

formation, loss of skin flexibility) [6]. The pharmacological activation of Nrf2 was proven to provide protection against various toxic compounds responsible for a reduction in skin toxicity [6]. The role of Nrf2 in the prevention of skin carcinogenesis has been demonstrated in various research models [6]. Nrf2 is a key element in the prevention of chemically induced tumor formation and promotion [6]. Moreover, Nrf2 activation reduced solar-simulated UV radiation tumor formation in hairless mice [6]. Nrf2 also demonstrated its essentiality in the healing process of full-thickness wounds and in the recovery and repair of an epidermal barrier defect [6]. There are compelling evidences demonstrating Nrf2 activation as a promising strategy for the treatment of atopic dermatitis, psoriasis, and epidermal blistering diseases (e.g., Hailey-Hailey disease) [6]. Nrf2 activation in vitiligo vulgaris pigment disorder was investigated as a potential strategy to prevent the development of the disorder and treatment [6]. It was also suggested that activation of Nrf2 is important for the treatment of patients suffering from allergic skin inflammation (e.g., allergic contact dermatitis) [6].

Curcumin (1,7-bis(4-hydroxy 3-methoxy phenyl)-1,6-heptadiene-3,5-dione) is a natural polyphenol from the powdered rhizome of the medicinal plant *Curcuma longa* (also known as turmeric) [7]. It is an amphipathic molecule with polar-central and flanking regions that are separated by a lipophilic methine segment [8]. Curcumin contains seven chemical functional groups (see curcumin chemical structure in the Supplementary Data (Figure S1) available online at https://doi.org/10.1155/2017/5205471) [8]. Among others, curcumin contains phenolic groups and thus can act as a reducing antioxidant and directly scavenge oxygen-centered reactive intermediates [8, 9]. Curcumin also displays oxidant activity partly due to its Michael acceptor functionalities. As such, curcumin is capable of inducing the activation of the Keap1-Nrf_2-EpRE pathway [9]. The unique chemical attributes of curcumin (e.g., log *P* ensuring curcumin's accessibility to its molecular targets, the capacity to undergo H-bonding and hydrophobic interactions, and activity as a Michael acceptor) are responsible for curcumin's pleiotropic biological activity [8]. These include curcumin's bifunctional antioxidant properties, anti-inflammatory activity, anticancer effects, wound healing, and antimicrobial effects [8–14]. Therefore, curcumin was suggested for the treatment of various disorders like cancer and proinflammatory chronic diseases [8–14]. Skin, being an interface between the environment and the body, suffers from chronic oxidative stress resulting from exposure to environmental toxicants including chemical and physical pollutants, ionization, and UV radiation [15]. The resulting oxidative stress in skin may be involved in the pathogenesis of a number of skin disorders including some types of cutaneous malignancy and photosensitivity diseases [15]. Curcumin, due to its pleiotropic behavior, was found to be beneficial in treating several skin pathology disorders and diseases (e.g., psoriasis, scleroderma, and skin cancer) [8–14, 16–19]. Moreover, drug development studies were carried out where curcumin analogues were designed and synthesized due to curcumin's antiangiogenic activities [13]. The role of curcumin in treating various skin pathologies and disorders and Nrf2 involvement is summarized in Table 1.

However, the pharmacokinetics of curcumin are unsatisfactory due to its chemical instability, scarce solubility in aqueous solutions, deficient absorption, rapid metabolism, and systemic elimination [8, 20]. Therefore, curcumin suffers from poor bioavailability and its clinical application is restricted [8, 20]. Moreover, no double-blinded, placebo-controlled clinical trial of curcumin has been successful [21]. A reasonable approach to overcome these limitations could be to encapsulate curcumin into delivery systems of different characteristics [22, 23]. In addition, a topical delivery system for local administration of curcumin mat results in an increase in curcumin bioavailability [21]. There are compelling evidences supporting this approach. It was shown that topical application of curcumin exhibited a more pronounced effect on wound healing compared to its oral administration due to a superior accessibility of curcumin at the wound site [10]. One of the leading vehicles for dermal drug delivery is microemulsions [24]. Microemulsions are isotropic colloidal nano-formulations, composed of water, oil, and surfactants [25]. These vehicles are thermodynamically stable and form almost spontaneously (without any energy input) to a transparent or slightly opalescent formulation of low viscosity [25]. The use of microemulsions offers many advantages including enhancement of drug solubility, protection of labile drugs, controlled drug release, augmentation in the rate and extent of absorption, and a decrease in patient side effects [24]. In addition, it has been shown that microemulsions significantly increase bioavailability compared with classical delivery systems such as emulsions, gels, and solutions [24].

Incorporating curcumin into a microemulsion may improve its water solubility and bioavailability and hence lead to better efficacy [21]. Until now, little work has focused on topical microemulsion delivery systems containing curcumin aimed at treating skin conditions [26–29]. Nanoformulations of curcumin might potentially improve the infiltration of curcumin into cutaneous cells [10]. Indeed, studies to date support this claim [26–29]; Lin et al. developed curcumin encapsulated in an oil-in-water microemulsion system and investigated its phase diagram and stability [29]. In vitro skin permeation assays have demonstrated time-dependent increases in permeated curcumin in stable microemulsion formulations. Enhanced skin permeability of curcumin encapsulated in microemulsions was also reported by Liu and Chang [28]. The vehicle composition significantly influenced curcumin solubility and skin permeability [28]. Teichmann et al. incorporated curcumin in an oil-in-water microemulsion and in an amphiphilic cream [30]. A deeper part of the stratum corneum was accessible, and significantly smaller amounts of curcumin were found on the skin surface following microemulsion application. Furthermore, curcumin was detected in hair follicles, indicating that the microemulsion penetrated into the complete follicular infundibula [30]. Liu and Huang demonstrated that the antimicrobial activity of curcumin-loaded myristic acid microemulsions against the skin pathogen *Staphylococcus epidermidis* was 12 times higher than

Table 1: Curcumin's role in treating various skin pathologies and disorders and the interconnectedness with Nrf2 [8–14, 16–19].

Skin pathology/disorder	Effect of curcumin treatment	Nrf2 involvement
Inflammatory diseases (e.g., psoriasis, atopic dermatitis, contact dermatitis, acne, rosacea, and erythroderma)	Inflammatory reduction via (1) Inhibition of NF-κB transcription factor and reducing the production of TNF-α, IL-1, and interferon-γ (2) Scavenging reactive oxygen species (3) Modulating production of antioxidant enzymes	+
Scleroderma	Antifibrotic effect via suppressing TGF-β	+
Vitiligo vulgaris	Protection against disease progression via (1) An increase in MAPK/ERK phosphorylation and inhibition of apoptosis (2) An increase in total antioxidant capacity and a decrease in intracellular reactive oxygen species generation (3) Improving mitochondrial activity	+
Wound healing	Enhancing effective wound healing in three stages (a) Inflammation (see above) (b) Proliferation (1) Enhancing fibroblast migration, granulation tissue formation, collagen deposition, and re-epithelialization (2) Apoptosis in the early stage of wound healing resulting in removal of nondesirable inflammatory cells from the wound site (c) Remodeling (1) Enhancing wound closure via the production of TGF-β1 and fibronectin resulting in increased migration and proliferation of fibroblasts	+
Aging	Delay the aging process via induction of Keap1-Nrf2-EpRE and phosphatidylinositol 3-kinase/Akt pathways	+
Carcinogenesis	Anticarcinogenic activity in different stages of cancer (a) Transformation of normal cells into tumor cells: curcumin inhibits NF-κB and its target genes like COX-2 and *cyclin* D1 and induces apoptosis via activation of caspase-3, caspase-8, and Fas receptor (b) Tumor growth and progression: curcumin inhibits mTOR signaling resulting in blocking of tumor progression (c) Tumor promotion: curcumin inhibits 12-o-tetradecanoylphorbol-(TPA-) induced tumor promotion and TPA-induced tumor markers via modulation of transmembrane signal transduction via protein kinase	+

that of curcumin dissolved in dimethyl sulfoxide (DMSO) [26]. Yutani et al. assessed the distribution of polyphenols in skin from a di-2-ethylhexyl sodium sulfosuccinate (Aerosol OT) microemulsion and detected enhanced intradermal delivery [27].

In the present study, we hypothesize that incorporating curcumin into a topical microemulsion delivery system will preserve its unique chemical structure allowing it to induce the Keap1-Nrf_2-EpRE pathway more efficiently than the unformulated curcumin. This hypothesis holds an additional rationale; it was shown that chronic and enhanced activation of the Keap1-Nrf_2-EpRE pathway in the epidermis suffers from several detrimental complications including defects in the epidermal barrier, inflammation, and induced keratinocyte hyperproliferation [31]. Thus, precise and temporary activation of the Keap1-Nrf_2-EpRE in skin is essential [32].

Here, we suggest to expand our prior work demonstrating the feasibility of encapsulating Nrf2-activating agent into a delivery system. We have previously shown that three members of the nitroxide family representing synthetic stable radicals were encapsulated into a microemulsion delivery system resulting in enhanced Nrf2 activation, protection against UVB-induced injury, and relief in inflamed skin condition [33]. While encapsulating these synthetic antioxidants with diverse lipophilicity and ability to shuttle between the nitroxide radical, the reduced hydroxylamine, and the oxidized oxoammonium cation formed by one- and two-electron transfer reactions [33] (i.e., members of the nitroxide family) may be challenging, the case of encapsulating the natural polyphenol curcumin into a microemulsion delivery system holds different challenges since curcumin is prone to oxidative degradation and has low solubility in aqueous solution [8, 20].

In order to investigate our hypothesis, curcumin was incorporated into a microemulsion delivery system and microemulsion nanometric structure was evaluated using dynamic light scattering (DLS), small-angle light scattering (SAXS), and cryo-transmission electron microscopy (cryo-TEM) measurements. Moreover, the antioxidant activity of curcumin incorporated into the microemulsion was evaluated

in vitro using oxygen radical absorbance capacity assay (ORAC), luminol-dependent chemiluminescence (LDCL) assay, and 2-diphenyl-lpicrylhydrazyl (DPPH) radical assay. The capability of a curcumin-loaded microemulsion to induce the Keap1-Nrf2-EpRE pathway was evaluated in keratinocyte culture and in human skin. Human skin organ culture was used to access the reduced UVB-induced cytotoxicity resulting from topical application of the curcumin-loaded microemulsion.

2. Material and Methods

*Similar material and methods were used in [33].

2.1. Microemulsion Preparation. Microemulsions were prepared by first mixing the surfactants lauric acid (pKa = 5.3 at room temperature, Sigma-Aldrich, Israel), Span® 20 (sorbitan laurate, Sigma-Aldrich, Israel), and Tween® 80 (polysorbate 80, Sigma-Aldrich, Israel) with isopropyl myristate (IPM, Sigma-Aldrich, Israel). Upon receiving a transparent blend of surfactants and oil, curcumin (Sigma-Aldrich, Israel) was added to the solution and then mixed until completely dissolved. This step was followed by a dropwise addition of double-distilled water (DDW; pH = 6.8 ± 0.2). Solutions were allowed to equilibrate for 24 h to obtain a clear oil-in-water microemulsion. The ratio of Tween 80® : Span 20 : lauric acid : IPM : curcumin was 33.3 : 1.6 : 1 : 5 : 1.3 and kept constant throughout the study. The final concentrations (%*w*/*w*) in the microemulsion were 26.8 : 1.3 : 0.8 : 4 : 1 : 66.1 for Tween 80, Span 20, lauric acid, isopropyl myristate, curcumin, and water, respectively. tert-Butylhydroquinone (tBHQ) and trolox were purchased from Sigma-Aldrich, Israel.

2.2. Dynamic Light Scattering (DLS). DLS measurements on microemulsions (microemulsions were diluted to 1 : 100 with DDW; the final curcumin concentration was 0.01% *w*/*w* (0.27 mM)) were performed using a Zetasizer Nano Series (Malvern) and analyzed using Zetasizer software. The droplet diameter was calculated from the diffusion coefficient, using Stokes-Einstein equation [34].

2.3. Cryogenic Transmission Electron Microscopy (Cryo-TEM). Cryo-TEM specimens were prepared in a controlled environment box using a vitrification robot (Vitrobot). 60 μL of the microemulsion (the final curcumin concentration was 1% *w*/*w* (27.1 mM)) was dropped onto a glow-discharged TEM grid (300-mesh Cu Lacey substrate; Ted Pella Ltd.). Excess was automatically blotted with a filter paper, and the specimen was rapidly plunged into liquid ethane and transferred to liquid nitrogen where it was kept until used. Specimens were analyzed below −175°C using an FEI Tecnai 12G^2 TWIN TEM operated at 120 kV in a low-dose mode and with a few micrometers under focus to increase phase contrast. Images were recorded with a Gatan charge-coupled device camera (model 794) and examined using Digital Micrograph software, Version 3.1.

2.4. Small-Angle X-ray Scattering (SAXS). SAXS experiments were performed on microemulsions without further manipulations (the final curcumin concentration was 1% *w*/*w* (27.1 mM)) using a small-angle diffractometer (a Molecular Metrology SAXS system with Cu Kα radiation from a sealed microfocus tube (MicroMax-002+S), two Göbel mirrors, and three-pinhole slits; the generator was powered at 45 kV and 0.9 mA). Scattering patterns were recorded by a 20 × 20 cm two-dimensional position-sensitive wire detector (gas-filled proportional type of Gabriel design with 200 μm resolution) that was positioned 150 cm behind the sample. Scattered intensity $I(q)$ was recorded in the interval $0.07 < q < 2.7\,\text{nm}^{-1}$, where q is the scattering vector defined as $q = (4\pi/\lambda)\sin(\Theta)$, where 2Θ is the scattering angle and λ is the radiation wavelength (0.1542 nm). Microemulsions were sealed in a thin-walled capillary (glass) of about 2 mm diameter and 0.01 mm wall thickness. Experiments were performed under vacuum at ambient temperature. Scattering curves were adjusted for counting time and sample absorption.

2.5. Spectrofluorometer Measurements. Curcumin location in the microemulsion was investigated using the fluorescent probe method [35], which can sense the microenvironment of the probe from changes in the intensity and wavelength of the emission peak. Curcumin's emission properties highly depend on its specific microenvironment; therefore, curcumin could be used directly as a probe [8, 36]. Curcumin was dissolved in different microemulsion components to a final concentration of 0.007% *w*/*w* (1.9 μM), and fluorescence measurements were obtained using a Jobin Yvon Horiba Fluoromax 4 spectrofluorometer. The excitation source was a xenon arc lamp. The excitation and emission slit widths were 5 nm. Excitation was set at 450 nm, and emission was scanned from 460 nm to 600 nm.

2.6. Voltammetric Measurements of Reducing Power. The overall reducing power of microemulsions (the final curcumin concentrations were as follows (%*w*/*w*): 0 (empty microemulsion), 0.25 (6.8 mM), 0.5 (13.9 mM), 0.75 (20.4 mM), and 1 (27.1 mM)) was examined using a cyclic voltammeter (Electrochemical Analyzer, CH Instruments, Austin, TX, USA). Samples were placed in a well with three electrodes: a glassy carbon, with a working electrode of 3.3 mm diameter; an Ag/AgCl reference electrode; and a platinum wire as an auxiliary electrode [37]. Potential was applied to the working electrode at a constant rate (100 mV/s) receiving cyclic voltammogram. Cyclic voltammogram was composed of two parameters: the peak potential (Ep(a)), which reflects the ability to donate electrons, and the anodic current (AC), which correlates with the concentrations of these compounds [38]. Reducing power was determined from the cyclic voltammogram. The working electrode was tested prior to each series of measurements, by performing a cyclic voltammogram of 1 mm potassium ferricyanide in PBS.

2.7. Oxygen Radical Absorbance Capacity Assay (ORAC). ORAC assay adapted to fluorescein labeling [39] was used to determine the total antioxidant capacity of curcumin-loaded microemulsions (the final curcumin concentrations were as follows (%*w*/*w*): 0 (empty microemulsion), 0.25 (6.8 mM),

0.5 (13.9 mM), 0.75 (20.4 mM), and 1 (27.1 mM)). Analysis was performed using 2, 2′-azobis(2-amidinopropane) dihydrochloride (AAPH) as a peroxyl generator. This assay is a kinetic assay which measures the loss of fluorescein fluorescence over time due to peroxyl radical formed by AAPH, enabling evaluation of antioxidant protection. Measurements were performed on a Fluostar Galaxy plate reader (BMG, Offenburg, Germany) equilibrated at 37°C, with excitation and emission set up at 485 nm and 520 nm, respectively. Trolox was used as a calibration standard. Reagents were prepared in phosphate buffer (pH 7.4). 40 μL samples were pipetted into a 96-well plate. Fluorescein was added to a final concentration of 96 nM. ORAC fluorescence was read every 2 min for 70 min. Oxidation resulting from peroxyl radical started immediately following AAPH addition. Total antioxidant capacity was calculated by measuring the area below the kinetic curve [39].

2.8. Quantification of Oxidant-Scavenging Abilities (OSA) by a Luminol-Dependent Chemiluminescence (LDCL) Assay. A highly sensitive luminol-dependent chemiluminescence-inducing cocktail [40] was employed to quantify the OSA of microemulsions (the final curcumin concentrations were as follows (%*w*/*w*): 0 (empty microemulsion), 0.25 (6.8 mM), 0.5 (13.9 mM), 0.75 (20.4 mM), and 1 (27.1 mM)). Briefly, the following were added into 850 μL of Hanks' balanced salt solution (HBSS) (pH 7.4): 10 μL of luminol (1 mM), H_2O_2 (100 mM), sodium selenite (IV) (2 mM), and CoCl2·6H2O (II) (1 mM). This cocktail produces an immediate wave of light due to peroxide and hydroxyl radical. Light quenching by microemulsions indicates the degree of their oxidant-scavenging ability.

Light quenching was measured as counts per minute by a Lumac 2500 Luminometer (Landgraaf, The Netherlands).

2.9. Quantification of Oxidant-Scavenging Abilities (OSA) by the 2-diphenylpicrylhydrazyl (DPPH) Radical Assay. Modified DPPH assay [41] was used to determine the oxidant-scavenging ability of curcumin-loaded microemulsion (the final curcumin concentrations were as follows (%*w*/*w*): 0 (empty microemulsion), 0.25 (6.8 mM), 0.5 (13.9 mM), 0.75 (20.4 mM), and 1 (27.1 mM)). 2,2-diphenylpicrylhydrazyl (DPPH) free radical was used as a probe; upon reduction, this stable, purple, free radical changed its color to a yellow diphenylpicryl hydrazine. Briefly, 10 μL of microemulsions was mixed with 20 μL of a DPPH solution (10 mM in absolute methanol). One minute later, 800 μL of absolute methanol was added. The reaction mixtures were centrifuged at 425 ×g for 2 min, and the change in absorption at 517 nm using a Whittaker microplate reader 2001 was determined. Oxidant-scavenging ability is expressed in terms of micromole equivalents of trolox per 100 grams of sample.

2.10. Cell Culture. Immortalized human keratinocytes, HaCaT cells [42], were grown in Dulbecco's Modified Eagle's Medium (DMEM, Biological Industries, Beit Haemek, Israel) containing 4.5 g/L D-glucose and supplemented with 10% fetal bovine serum, 1 mM L-glutamine, 100 U/mL penicillin, and 100 U/mL streptomycin in DMEM. The cultures were maintained in an incubator at 37°C in a humidified atmosphere of 5% CO_2. Cells were subcultured twice weekly at a 1 : 10 ratio using a trypsin-EDTA (0.05%) solution (Biological Industries, Beit Haemek, Israel) as a detaching agent.

2.11. Human Skin Organ Culture. Human skin was obtained with informed consent from 20- to 60-year-old healthy women, who had gone through breast or abdomen reduction. Testing was performed according to the Declaration of Helsinki and approved by the Hadassah University Hospital Ethics Committee, #0639-12-HMO. Skin was cut into pieces of approximately 0.5 × 0.5 cm and cultured, dermal side down and epidermal side up, in 35 mm diameter petri dishes containing DMEM (Dulbecco's Modified Eagle's Medium, Biological Industries, Beit Haemek, Israel) at 37°C, under 5% CO_2. 4 μL of curcumin-loaded microemulsion (the final curcumin concentration was 1%*w*/*w* (27.1 mM)) was applied to the air-exposed epidermis 24 h before irradiation as described below. The samples were incubated for another 24 h for apoptosis determination. The epidermis was separated from the dermis by 1 min heating in phosphate-buffered saline (PBS) at 56°C and apoptosis was examined.

2.12. Dermal Absorption of Curcumin: An Ex Vivo Model Using Human Skin Organ Culture. Microemulsion penetration was investigated using Franz-type diffusion cells (PermeGear Inc., Hellertown, PA, USA) with a diffusion area of 1 cm^2 and an acceptor compartment of 8 mL containing fetal bovine serum and PBS (pH 7.4) (1 : 9, *v*/*v*). Skin was mounted on Franz-type diffusion cells, epidermal side up, and dermal side facing the receptor compartment. Diffusion cells were kept at 32°C. 100 μL of different treatments (the final curcumin concentration was 1%*w*/*w* (27.1 mM)) was applied to the mounted skin. Following 24 h incubation, skin was removed and washed three times using a cotton cloth containing ethanol and the viable epidermis was separated from the dermis. Separation of the full epidermis from the dermis was achieved by heat shock treatment; skin was placed for 30 seconds at 55–60°C followed by 1 min at 4°C, both in PBS. Curcumin was extracted from the separated layers with DMSO. The extraction was performed by incubation in a shaker (60 ×g) until all curcumin were released (24 h). Finally, 100 μL from the receptor fluids was collected. Curcumin existence in skin layers and in the acceptor compartment was determined by measuring fluorescence excitation at 485/40 nm and emission at 528/20 nm, using a BioTek microplate reader (BioTek Instruments Inc., Winooski, VT).

2.13. Skin Exposure to UVB Irradiation. Prior to irradiation, culture medium was removed and skin was washed with PBS to remove all traces of treatments. PBS was added to cover the dermis, and the sample was irradiated with a UVB source (VL-6.M lamp, emission spectrum 280–350 nm, emission peak 312 nm, filter size 145 × 48 mm; Vilber Lourmat, Torcy, France) at 300 mJ/cm^2. Immediately following irradiation, PBS was replaced by human skin organ culture medium (see above) and skin was incubated for an additional 24 h.

2.14. Apoptosis Determination by Caspase-3 Activity Assay. The epidermis was incubated in 100 μL PBS containing

2.5 μM Ac-DEVD-AMC as a substrate, with 0.02% Triton X-100 and 10 mM DTT, at 37°C in a 96-well plate [43]. Fluorescence of the released coumarin derivative was measured at 390/435 nm, using a Fluostar-BMG spectrofluorometer (Offenburg, Germany). Caspase-3 activity was calculated over 40 min in a linear range from the fluorescence versus time slope. Results were normalized relative to the control group.

2.15. Viability Measurements through Mitochondrial Assay. Cytotoxicity of treated cell culture (HaCaT cells) was evaluated by the MTT method described elsewhere [44]. Treatments (empty microemulsion, curcumin-loaded microemulsion, and curcumin dissolved in DMSO) according to dilutions in increasing curcumin concentrations (0–3 μM) were added to 24-microwell plates containing cell cultures of 30,000 cells/mL. After 24 h, cell survival was evaluated by measuring the absorbance at 540 nm, using a Whittaker microplate reader 2001. The percentage of cell survival was normalized relative to the control group.

2.16. Keap1-Nrf$_2$-EpRE Pathway Activation. Real-time PCR of Nrf$_2$ and enzyme expression after treatments (microemulsions, free curcumin, and catalase; Sigma-Aldrich, Israel) were measured in cell culture. Subconfluent cells were treated and harvested at the desired times after treatment (see below). In the case of catalase treatments, catalase (300 U/mL) was coadministered simultaneously with the other treatments. Total RNA from cell culture was extracted according to tri-reagent protocol (Sigma). Reverse transcription was performed as previously described [45]. Aliquots of cDNA culture were subjected to real-time PCR using PerfeCTa SYBR Green SuperMix, Low ROX (Quanta Biosciences Inc.), Stratagene real-time PCR machine, and oligonucleotide sets (see oligonucleotide sequence in the Supplementary Data). In all cases, the samples were normalized relative to GAPDH expression.

2.17. Statistical Analysis. Experiments were performed independently at least three times. For oxidant-scavenging ability assays, each experiment included three repetitions ($n = 3$). For organ culture experiments, experiments were performed with three different donors. Each independent experiment included four repetitions, with four skin pieces being processed in parallel. Data were expressed as mean ± standard errors of the mean (SEM) or standard deviation of the mean (STDEV) as specified. Statistical significance of differences was determined using one-way ANOVA, followed by Kruskal-Wallis test. The significance threshold was set at $P < 0.05$.

3. Results and Discussion

3.1. Design of Curcumin-Loaded Microemulsion. The usage of microemulsions for dermal delivery offers several advantages. Few mechanisms of activity were suggested in order to elucidate microemulsion penetration ability. High solubilization capacity of the drug in the microemulsion may increase its activity towards the skin by raising the drug gradient across the skin [46] and may favor skin partition [47]. Microemulsion ingredients also have a pivotal role in the beneficial dermal delivery; surfactants and cosurfactants are often penetration enhancers resulting in the decrease in the diffusional barrier of the stratum corneum [48]. Moreover, microemulsions may have a beneficial hydration effect on the stratum corneum, influencing permeation ability [49]. Therefore, o/w microemulsions were designed. Ingredients were carefully chosen for their biocompatibility and lack of toxicity, and the usage of alcohol as a cosurfactant due to toxicity and irritancy issues [50] was denied. Nonionic surfactants were selected due to their activity as solubilizing agents and their effects on the skin barrier function [25]. The stabilization of the microemulsion was achieved using a mixture of surfactants with different HLB values. Figure 1(a) demonstrates the ability to form an empty microemulsion formulation. Next, curcumin incorporation in the empty microemulsion formulation without disrupting its phase consistency was tested. As mentioned above, increasing curcumin's solubility would enhance its dermal delivery. Curcumin which is highly insoluble in water was solubilized in the microemulsion (Figure 1(b)). Microemulsions demonstrated stability; visual evaluation following accelerated conditions (40 ± 3°C) in darkness for 24 months revealed a transparent and isotropic behavior. Microemulsion particle size was similar to that of the freshly prepared samples with the same monomodal size distribution pattern.

3.2. Reduction of Cytotoxicity Using Curcumin-Loaded Microemulsions Compared to Free Curcumin in Keratinocyte. Curcumin has poor solubility in water, yet good solubility in dimethyl sulfoxide (DMSO) and chloroform [8]. Due to the low aqueous solubility of curcumin, some researchers dissolve it in base medium; however, this approach does not address the alkaline decomposition of curcumin: degradation products including ferulic acid and feruloylmethane [8]. Therefore, through all of this study, curcumin dissolved in DMSO was used as a control. DMSO curcumin solutions are termed in the following as free curcumin.

Cytotoxicity of an empty microemulsion, curcumin-loaded microemulsion, and free curcumin in DMSO in immortal human keratinocyte cells (HaCaT) was measured by the MTT assay. Figure 2 shows cell viability (%) following 24 h treatment. Axis x represents the treatment concentration in the cell culture (%). As can be seen, the viability of HaCaT cells exposed to an empty microemulsion at a concentration of 0.11% (v/v) or less was greater than 80%. Introduction of cells into a microemulsion at a concentration of 0.15% (v/v) significantly reduced cell viability (~50%). This decline in cell viability could be derived from the surfactants composing the microemulsion. It has been shown that all nonionic surfactants are capable of causing cell damage due to destruction of the cell membrane and its solubilization, in a concentration-dependent manner [51]. In particular, it has been shown that Tween 80 can cause cellular damage [52]. Consistent with our results (see above), it has also been shown that Tween 80 used at a concentration above 0.03% (v/v) reduced cell viability [52]. However, incorporation of curcumin into the microemulsion mitigated this cytotoxicity

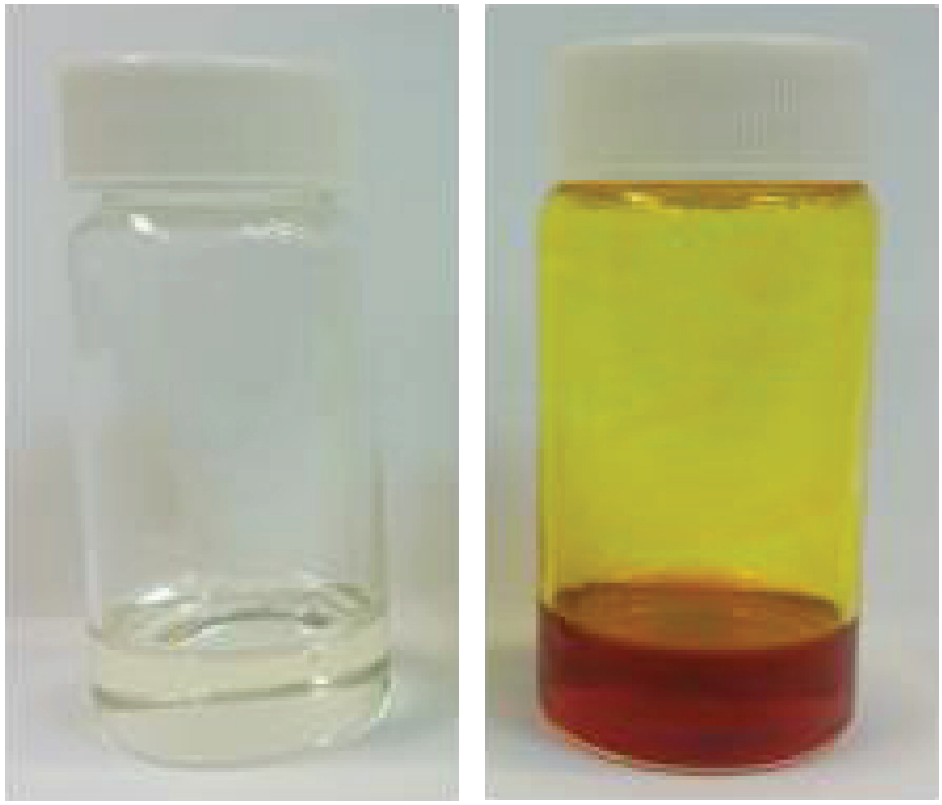

(a) (b)

Figure 1: Images of (a) clear empty microemulsion and (b) curcumin-loaded microemulsion.

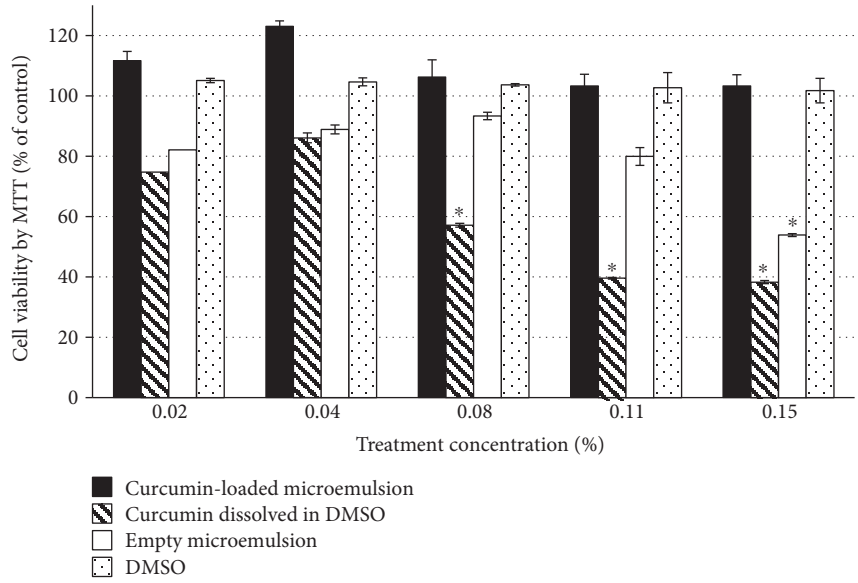

Figure 2: HaCaT cell viability as measured by MTT (in percentage) after 24 h treatment. Cell viability was expressed as the percentage of the untreated control (dashed line) as the function of treatment concentration. Average values are presented in the figure with standard deviation of the mean ($^*P < 0.05$).

resulting in cell survival. Introducing free curcumin (curcumin dissolved in DMSO) demonstrates cytotoxicity at a concentration of 0.08% (*v*/*v*), indicating the curcumin-loaded microemulsion's preference in terms of cytotoxicity.

3.3. Structural Investigation. One of the main challenges in incorporating curcumin into a microemulsion is avoiding the interruption of microemulsion structure [53]. Cryo-TEM micrographs of the empty microemulsion and

Table 2: Diameters (averaged by volume) of empty microemulsion and microemulsion containing curcumin, as measured by dynamic light scattering. Standard deviation is specified ($N = 6$).

	Diameter (nm)
Empty microemulsion	6.75 ± 2.9
Microemulsion containing curcumin	9.33 ± 3.6

curcumin-loaded microemulsions are presented in the Supplementary Data (Figure S2). Both microemulsions demonstrate a level of order of the closely packed droplets with a diameter of about 10 nm. The dimension of microemulsion's spherical droplet was further evaluated using dynamic light scattering (DLS) measurements. As can be seen in Table 2, there is no significant difference between the size of the droplets in the empty microemulsion and that in the curcumin-loaded microemulsion. Additional nanostructure information was obtained using small-angle X-ray scattering. SAXS plots are presented in the Supplementary Data (Figures S3), demonstrating a broad peak at $q \approx 0.07\,A^{-1}$, which corresponds to a structure with a dimension of about 9 nm according to Bragg's law, in agreement with DLS measurements and cryo-TEM images. Further analysis was done by fitting the core and shell model, which is frequently used to describe micelles and microemulsions [53]. In the case of oil-in-water microemulsions, the core is the hydrophobic component and the surfactants comprise the shell. Table 3 reveals the best-fit parameters for the core and shell model (see Supplementary Data, Eq. 1-2), with 95% confidence bounds of the fit. The oil component (IPM) in the microemulsion has a strong influence on the microemulsion's formation and stability (data is not shown). Thus, density of the core was calculated from the oil properties (IPM) and kept constant. The shell in this model is composed from the surfactant mixture. The incorporation of curcumin into the microemulsion might affect the shell density of the microemulsion. Data in Table 3 demonstrate no significant difference in the core and shell radius between the empty microemulsion and the microemulsion containing curcumin. However, the shell density of the curcumin-loaded microemulsion is higher than the shell density of the empty microemulsion, hinting at curcumin's location in the microemulsion.

The complete model used in this study was the core and shell, with a normal size distribution of the core. Small deviations of the model from the experimental data could originate from the droplet not being ideally spherical or from the nature of the shell, which is not constant in density due to radial concentration gradients.

Curcumin's location inside the microemulsion and its interaction with the other ingredients seem to be of major importance since its mobility in the vehicle can be affected and may influence its delivery [54]. Therefore, the location of curcumin within the microemulsion was examined using the fluorescent probe method. This method can detect the microenvironment near a substance and is commonly used for revealing phase changes and structure of microemulsions and micelles [35]. Curcumin's emission properties highly depend on its specific microenvironment (e.g., polar and nonpolar solvents) [8, 36]. Therefore, curcumin can be used as a probe and directly monitor the polarity of its surroundings instead of using a probe, pointing out its site in the microemulsion. The fluorescence curves of curcumin in different solvents (background of the corresponding solvent was subtracted) are presented in the Supplementary Data (Figure S4). The wavelength of the peak is dependent on the solvent; the peak in DDW (524 nm) shifts in IPM (463-464 nm). The peak of curcumin in the microemulsion is at a wavelength of 509 nm, similar to the peak of curcumin in Tween 80 (504 nm), suggesting that the microenvironment of curcumin is alike in both the microemulsion and Tween 80 and that curcumin is located in the Tween 80 layer of the droplets. This is consistent with other studies that show that the drug is in the interface of microemulsion [53]. In addition, this data are also in agreement with SAXS data presented in Table 3 supporting curcumin's location in the surfactant shell.

Table 3: Best-fit parameters for the core and shell model (Eq. 1-2), with 95% confidence bounds of the fit. Rc is the radius of the core, Rs is the radius of the droplet, and σ is the standard deviation of Rc ($N = 4$).

Parameter	Empty microemulsion	Microemulsion containing curcumin
Rc (nm)	3.85 ± 0.04	3.87 ± 0.07
Rs (nm)	5.39 ± 0.07	5.17 ± 0.04
Shell density (el/nm^3)	36.34 ± 1.24	48.19 ± 2.08
σ	0.57 ± 0.02	0.61 ± 0.02

3.4. Curcumin-Loaded Microemulsions Maintain Oxidant-Scavenging Ability In Vitro. Maintaining the oxidant-scavenging ability of curcumin loaded in microemulsions is crucial for its utilization. Therefore, antioxidant capacity was evaluated by a variety of methods on curcumin-loaded microemulsions in five increasing curcumin concentrations (%w/w): 0 (empty microemulsion), 0.25 (6.8 mM), 0.5 (13.9 mM), 0.75 (20.4 mM), and 1 (27.1 mM). Oxygen radical absorbance capacity (ORAC) assay measures the degree of inhibition of peroxyl radical-induced oxidation by the compounds of interest, expressed in trolox equivalents (y-axis). Figure 3(a) demonstrates the protection of the curcumin-loaded microemulsions against the free radical. As can be seen, the microemulsion with an increased curcumin concentration demonstrates a linear trend with ORAC values expressed in trolox equivalents ($\mathrm{ORAC} = 17.451c - 3.9076$, where c is the curcumin concentration in mM, coefficient of determination ($R^2 = 0.99$)). Free curcumin (curcumin dissolved in DMSO) in increasing concentrations also demonstrates a linear trend with ORAC value ($\mathrm{ORAC} = 19.463c - 16.702$, $R^2 = 0.99$). Thus, curcumin-loaded microemulsions demonstrate improved protection against peroxyl radicals relative to trolox (~17.5 times more). Similar behavior is observed for free curcumin (~19.5).

The LDCL assay is based on the ability of an antioxidant agent to quench the luminescence generated by a "cocktail of oxidants." Figure 3(b) shows that while the luminescence induced by the "cocktail" is kept steady at a high level for 2.5 min, the addition of curcumin-loaded microemulsions dramatically affects the luminescence observed. The sharp and steady decline in luminescence due to the consumption of the bulk of oxidants generated yields a curve of light emission. Figure 3(d) demonstrates similar behavior for free curcumin (curcumin dissolved in DMSO). From calculating the area under the curve for a curcumin-loaded microemulsion and free curcumin, it can be concluded that the scavenging ability of a curcumin-loaded microemulsion is not significantly different than that of free curcumin.

Using cyclic voltammetry, the oxidation potentials of a curcumin-loaded microemulsion and free curcumin were measured. Two oxidation potentials were observed corresponding to two electron-donating centers in the curcumin molecule. Table 4 summarizes the oxidation potentials of a curcumin-loaded microemulsion and free curcumin. Figure 3(c) shows the anodic current at oxidation potential of 407 mV and 473 mV for free curcumin and for curcumin-loaded microemulsions, respectively. As expected, an increase in curcumin concentration resulted in an increased anodic current both for the curcumin-loaded microemulsions and for free curcumin. The anodic current drop for a curcumin-loaded microemulsion in the highest curcumin concentration might be explained by other processes involved apart from curcumin diffusion (e.g., interaction with surfactants and oils). This observation is consistent with other works [55].

The DPPH assay measures the hydrogen atom (or one electron)-donating activity and hence evaluates the antioxidant activity due to free radical scavenging. Expressed as trolox equivalents, Figure 3(e) shows that free curcumin and the curcumin-loaded microemulsions display similar antioxidant activity.

The redox assay presented here indicates that the oxygen-scavenging ability of curcumin-loaded microemulsions is similar to that of free curcumin. However, taking into consideration that curcumin dissolved in DMSO showed cytotoxicity (even in low concentrations), curcumin-loaded microemulsions may provide improved protection against free radicals without raising cytotoxicity issues. These experiments demonstrate preservation of curcumin phenolic group's activity. Thus, curcumin-loaded microemulsions can scavenge directly and potently oxygen-centered reactive intermediates.

3.5. Microemulsions Containing Curcumin Enhance the Activation of the Keap1-Nrf$_2$-EpRE Pathway in Keratinocyte. Cellular redox homeostasis guarantees a suitable cell response to a variety of exogenous or endogenous stimuli [56]. Upon disrupting this gentle balance, reactive oxygen species which can activate proliferative and cell-survival signaling [56] can alter apoptotic pathways that may be involved in the pathogenesis of a number of skin disorders including photosensitive diseases and some types of cutaneous malignancy [15]. One of the central players involved in the redox homeostasis maintenance is the transcription factor Nrf$_2$, a central key target for skin protection and cancer prevention [31]. As mentioned above, curcumin is capable of activating the Keap1-Nrf2-EpRE pathway [9]. Therefore, the effects of microemulsions on the activation of the Keap1-Nrf$_2$-EpRE pathway were examined using real-time PCR. The mRNA expression of a few phase II enzymes was examined: (catalase (EC 1.11.1.6), glutathione S-transferase (EC 2.5.1.18), superoxide dismutase (EC 1.15.1.1), glutathione reductase (EC 1.8.1.7), NAD(P)H dehydrogenase [quinone] 1 (EC 1.6.5.2), and glutamate-cysteine ligase (EC 6.3.2.2) [5]. Although the relative mRNA expression of most of these enzymes was not significantly affected, the relative mRNA expression of HO-1, a known phase II enzyme, was significantly induced. HO-1 regulates the level of intracellular heme by catalyzing the oxidative degradation of heme to biliverdin, iron, and carbon monoxide, resulting in cytoprotective, antiapoptotic, and anti-inflammatory effects on various experimental models [57]. HO-1 levels are associated with the proliferating epidermis [58].

Figure 4 demonstrates relative mRNA expression of HO-1 6, 12, and 24 h after treatments. As can be seen, the most significant relative mRNA expression increase occurs following 6 h treatment with a microemulsion containing curcumin. Empty microemulsion and free curcumin also exhibit activation of the Keap1-Nrf$_2$-EpRE pathway. As can be seen, following 6 h treatment, microemulsion containing curcumin has a synergistic effect. The observation that the empty micreomulsion is capable of activating the Keap1-Nrf2-EpRE pathway can be explained by the nanodroplets composing it. It was shown that fibers and particles may activate the Keap1-Nrf2-EpRE pathway via production of reactive oxygen species [43], and we assume that the microemulsion nanodroplets operate similarly. Alternatively, the oxidation status of the micreomulsion might generate reactive oxygen species capable of activating the pathway.

Overall, our results demonstrate the advantage of curcumin-loaded microemulsions over free curcumin. Microemulsion containing curcumin enhanced the Keap1-Nrf$_2$-EpRE pathway in an epidermal cell culture with a 180% increase over free curcumin. It is worth noting that tert-butylhydroquinone (tBHQ), a synthetic electrophile known for its ability in activating the Keap1-Nrf2-EpRE pathway in epidermal cell culture [59], induced the relative mRNA expression of HO-1 following 6 h treatment (50 μM) similar to the curcumin-loaded microemulsions (3.5 ± 0.7 fold change). Treatment with DMSO had no effect.

3.6. Microemulsion Containing Curcumin Induced Activation of the Keap1-Nrf$_2$-EpRE Pathway in Keratinocyte: Mechanism of Action. Polyphenols in general and curcumin in particular, under in vitro conditions, in the presence of oxygen and metal ions, may exhibit pro-oxidant activity [60]. Polyphenols can undergo autoxidation involving oxygen consumption generating $O_2^{\cdot -}$, hydrogen peroxide (H_2O_2), semiquinones, and quinones [61]. Hydrogen peroxide (H_2O_2) production by polyphenols in culture media was well demonstrated [61]. H_2O_2 is an important mild oxidant capable of

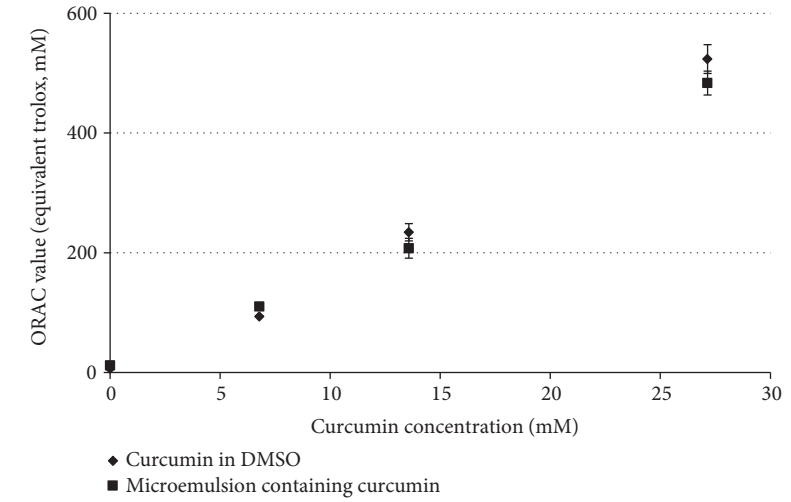

(a)

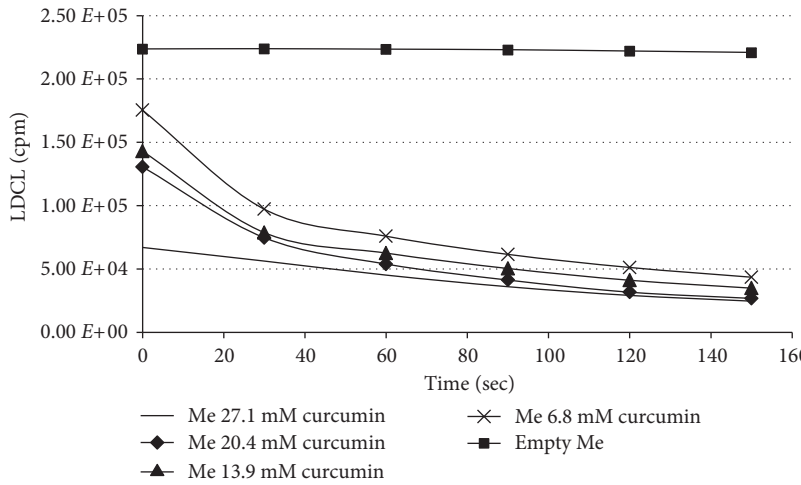

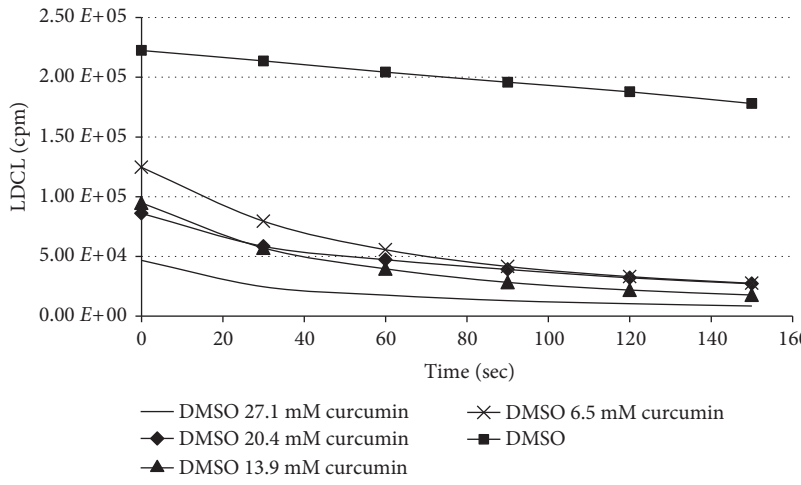

(b)

Figure 3: Continued.

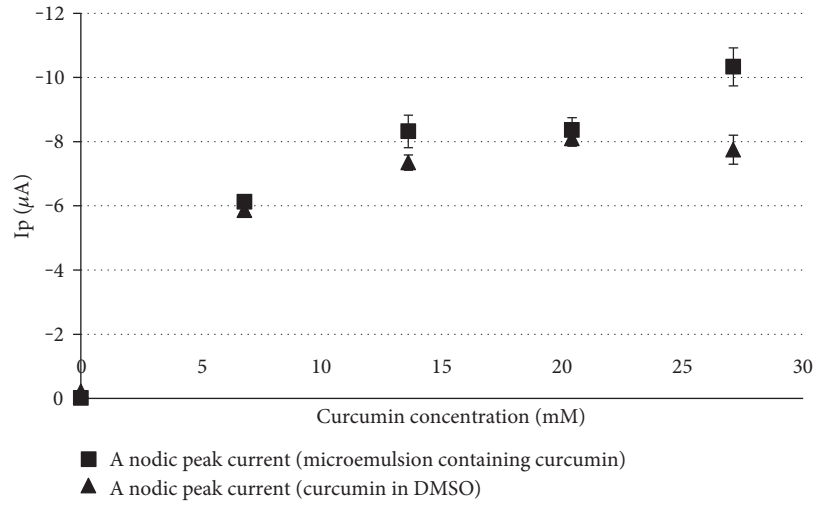

(c)

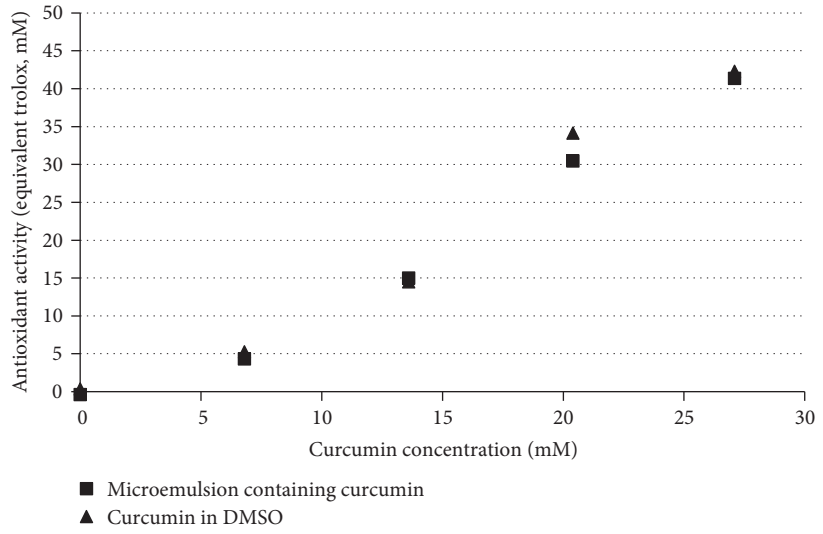

(d)

Figure 3: (a) ORAC value (equivalent trolox, mM) versus curcumin concentration for (■) curcumin-loaded microemulsion and (✦) curcumin dissolved in DMSO, (b) LDCL generated by "cocktail," for curcumin-loaded microemulsion (b) and curcumin dissolved in DMSO (d) containing in increasing concentration (-) 27.1 mM curcumin, (✦) 20.4 mM curcumin, (▲) 13.9 mM curcumin, (×) 6.8 mM curcumin, and (■) microemulsion without curcumin (microemulsion and DMSO, respectively). Statistical analysis indicated significantly higher antioxidant activity indicated by a decrease in LDCL ($P < 0.01$). (c) Typical anodic peak as measured by cyclic voltammetry for (✦) curcumin dissolved in DMSO (1st oxidation potential, 407 mV) and (■) curcumin-loaded microemulsion (1st oxidation potential, 473 mV) in increasing curcumin concentrations. (e) Antioxidant activity of (✦) curcumin dissolved in DMSO and (■) curcumin-loaded microemulsion as measured by the DPPH assay and expressed in trolox equivalents.

Table 4: Oxidation potential of microemulsion containing curcumin and curcumin in DMSO is measured by cyclic voltammetry.

	1st oxidation potential (mV)	2nd oxidation potential (mV)
Microemulsion containing curcumin	473	701
Curcumin dissolved in DMSO	407	702

reacting with cysteines and therefore is capable of inducing several transcription factors involved in cell replication, regulation of metabolism, apoptosis, and necrosis [62]. It is worth noting that H_2O_2 is electronically neutral and can freely diffuse through cellular membranes [63].

An important question regarding the mechanism of activity by which the curcumin-loaded microemulsion operates in keratinocyte is whether curcumin's phenolic groups preserve their activity following incorporation into microemulsions and moreover whether curcumin retains its pro-oxidative activity. It has been shown that curcumin

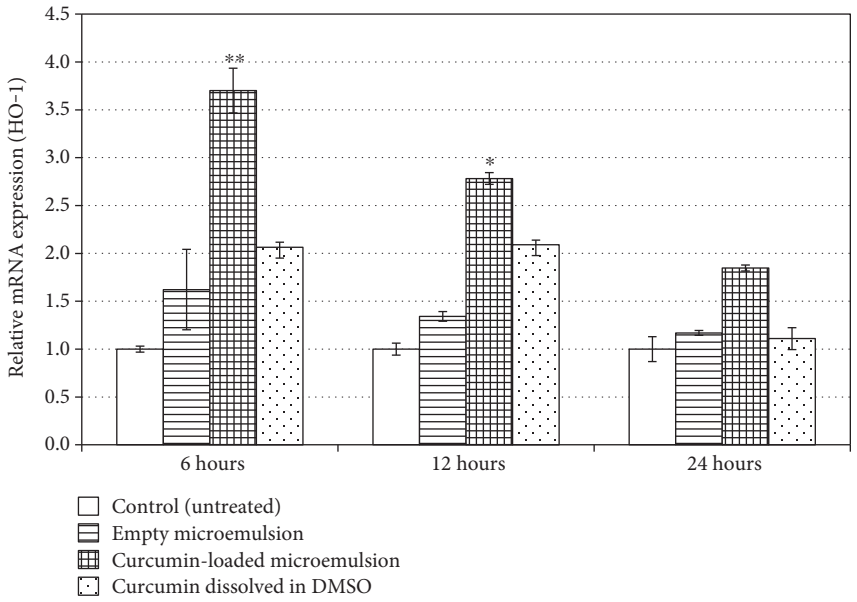

Figure 4: Activation of the Keap1-Nrf$_2$-EpRE pathway following 6 h, 12 h, and 24 h treatments. mRNA expression determined by real-time PCR. GAPDH mRNA expression was used for normalization, and the basal mRNA normalized expression was considered 1. Average values are presented in the figure with standard deviation of the mean ($^*P < 0.05$, $^{**}P < 0.01$).

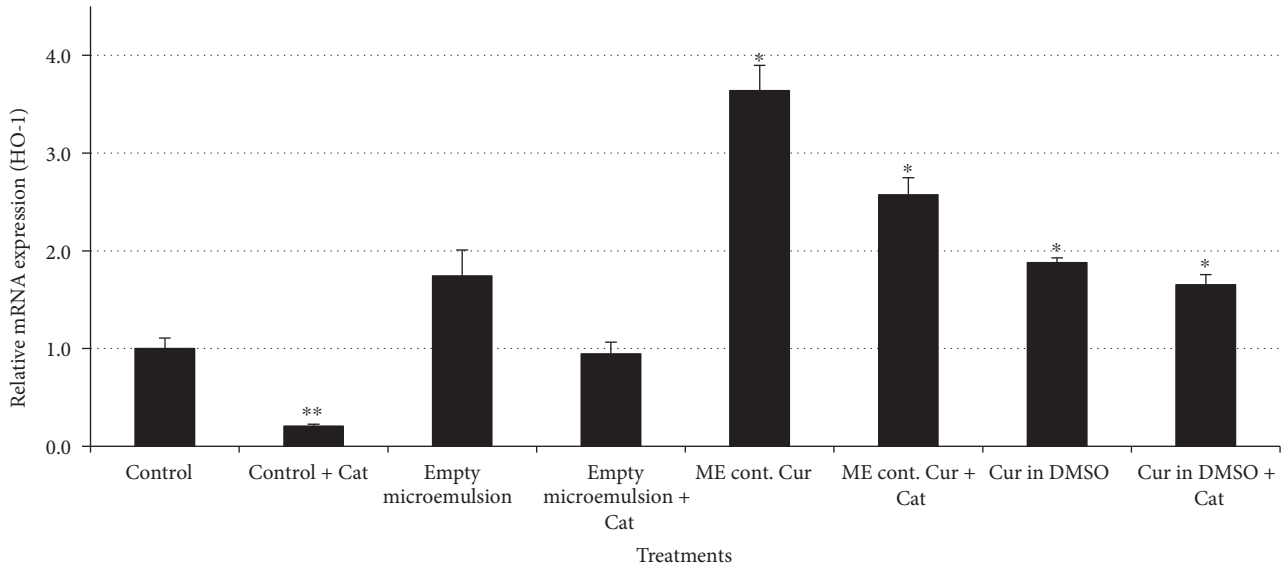

Figure 5: Activation of the Keap1-Nrf$_2$-EpRE pathway following treatment with microemulsions (empty ME or ME containing curcumin) and free curcumin in the absence or presence of catalase (Cat, 300 U/mL). mRNA expression determined by real-time PCR. GAPDH mRNA expression was used for normalization, and the basal mRNA normalized expression was considered 1. Average values are presented in the figure with standard deviation of the mean ($^*P < 0.05$, $^{**}P < 0.01$).

generated extracellular H_2O_2 in cell growth medium during autoxidation [60]. Therefore, it can be speculated that activation of the Keap1-NRF$_2$-EpRE system is partially mediated by extracellular H_2O_2 production by curcumin [9]. In order to test this hypothesis, microemulsions and free curcumin were applied to keratinocyte in the presence of the enzyme catalase. H_2O_2 is decomposed by catalase to water and oxygen [60].

Therefore, H_2O_2 involvement is expected to be abrogated following catalase addition. As can be seen in Figure 5, introduction of catalase (300 U/mL) to microemulsions decreased the relative mRNA expression of HO-1 indicating lower activation of the Keap1-Nrf$_2$-EpRE pathway. Catalase addition to the empty microemulsion decreased the relative mRNA expression of HO-1 from ~1.75-fold to ~0.95-fold, similar to that to the control group. This decrease demonstrated H_2O_2 production by the microemulsion and involvement in activation of the Keap1-Nrf$_2$-EpRE pathway under experimental conditions. Curcumin-loaded

microemulsions increased the relative mRNA expression of HO-1 by ~3.65-fold. As can be seen, following catalase addition, the induction was lowered to ~2.57-fold indicating that ~30% of this microemulsion's activity resulted from H_2O_2 involvement and the other ~70% is related to microemulsion penetration ability and curcumin's pro-oxidative activity.

It can be speculated that a few factors contribute to HO-1 induction: microemulsion's skin penetration, H_2O_2 involvement in curcumin phenolic groups, and the pro-oxidant activity of curcumin. Although we realize that this summation is not perfectly accurate, it is interesting to evaluate and quantify the significance of each of these contributing factors. Therefore, an assumption that the different contributions are additives was made and a rough estimation was obtained. Free curcumin treatment induced relative mRNA expression of HO-1 to increase by ~1.9-fold; following catalase addition, the induction decreased into ~1.65-fold, indicating ~12.2% H_2O_2 involvement and ~87.8% curcumin pro-oxidant activity. By comparing the free curcumin following catalase addition and the microemulsion containing curcumin following catalase addition, H_2O_2 extracellular involvement is eliminated and emphasizes the microemulsion's contribution to the means of penetration. Both treatments resulted in the induction of relative mRNA expression of HO-1 by ~1.65- and ~2.57-fold, respectively, caused by the penetration ability and curcumin's pro-oxidative activity. Since curcumin's pro-oxidative activity is exactly the same, it can be concluded that the penetration ability of the microemulsion in comparison to that in DMSO is higher by ~156% in keratinocyte. Another interesting result is the sharp decrease in relative mRNA expression of HO-1 in the control group with catalase addition, indicating H_2O_2 involvement in the basal state. It was shown that reactive oxygen species is formed in the cellular medium [64]; catalase addition can deplete reactive oxygen species production and therefore decrease phase II detoxification enzyme expression.

3.7. Evaluation of Dermal Absorption of Curcumin-Loaded Microemulsions in an Ex Vivo Model Using Human Skin Organ Culture. The skin constitutes a barrier between the body and the environment [15]. It preserves homeostasis by avoiding water loss via evaporation and protects against the environment by preventing penetration of exogenous substances [15]. Skin layers which are continuously renewed enable efficient protection against the penetration of external substances, especially thanks to the stratum corneum [65]. The outermost stratum corneum layer, despite its thickness of only 15–20 μm [25], regulates the barrier properties of the skin by regulating the fluxes of chemicals and water between the environment and the organism [66]. Moreover, the hermetic barrier of the stratum corneum makes topical application challenging in spite of the large available surface area, relative low enzymatic degradation, and long application time [67].

A prerequisite for the success of a dermatological drug, primarily, is its ability to penetrate through or into the skin in sufficient quantities to achieve the desired effect. A curcumin-loaded microemulsion was applied to human skin organ culture in Franz-type diffusion cells in order to perform and evaluate microemulsion's penetration ability. Curcumin was analyzed separately in the epidermis and dermis. Figure 6 demonstrates extracted curcumin (μg/cm^2) from the epidermis (Figure 6(a) and dermis (Figure 6(b)) of human skin following topical applications. As can be seen in Figure 6(a), a significant elevation in curcumin compared to the control group (untreated skin) was observed only for application of free curcumin. However, Figure 6(b), which demonstrates curcumin's quantity in the human skin dermis, reveals that curcumin-loaded microemulsions and free curcumin (curcumin dissolved in DMSO) both penetrated the dermis by a significantly similar and elevated quantity compared to the control group (untreated skin). The observation that free curcumin was found in the epidermis is consistent with DMSO's skin adsorption enhancement properties [68]. DMSO, a polar and aprotic molecule, is one of the most efficient transdermal delivery agents [69]. However, due to its side effects (including erythema, scaling, and contact urticaria) and its potential toxicity, DMSO is rarely used as a transdermal delivery agent [69]. The ability of microemulsions to penetrate skin may be attributed to the use of penetration enhancers in the formulation, for example, isopropyl myristate, Tween 80, and Span 20 [25]. The observation that curcumin-loaded microemulsions penetrated the skin and reached the dermis in a similar quantity as free curcumin without any cytotoxicity highlights microemulsion superiority. It is worth mentioning that a similar level of fluorescence was observed in the untreated skin (control group) and in the empty microemulsion and DMSO treatments, which can be explicated by the basal levels of skin autofluorescence [44].

3.8. Reduction of UVB Cytotoxicity Using Curcumin-Loaded Microemulsions in Human Skin Organ Culture. Skin exposure to environmental stressors (e.g., UVB) may cause injury to epidermal cells through enhanced production of reactive oxygen species, thus leading to a variety of skin pathologies [15]. One of the approaches that was suggested to enable skin protection was the use of various nontoxic antioxidants which displayed efficacy in cell culture systems and animal models [15]. However, absolute efficacy in humans was not well demonstrated [15]. Topical application of Keap1-Nrf$_2$-EpRE-inducing agents may present a protective strategy to reduce UVB-induced skin injury. Indeed, it has been shown that UVB-induced damage to skin cells can be efficiently limited by Keap1-Nrf$_2$-EpRE-inducing agents [6]. A curcumin-loaded microemulsion was applied to human skin organ culture in order to perform and evaluate the microemulsion's ability to impede UVB-induced cell toxicity in the epidermis via Keap1-Nrf$_2$-EpRE activation. Elevated HO-1 levels following 24 h incubation with the curcumin-loaded microemulsion were observed using immunohistochemical staining (indication for Keap1-Nrf$_2$-EpRE pathway activation) as presented in the Supplementary Data (Figure S5). Following treatment and 24 h incubation, skin was irradiated and apoptosis was then monitored by caspase-3 activity assay. UVB irradiation caused a ~17-fold increase in caspase-3 activity indicating an increase in epidermal cell

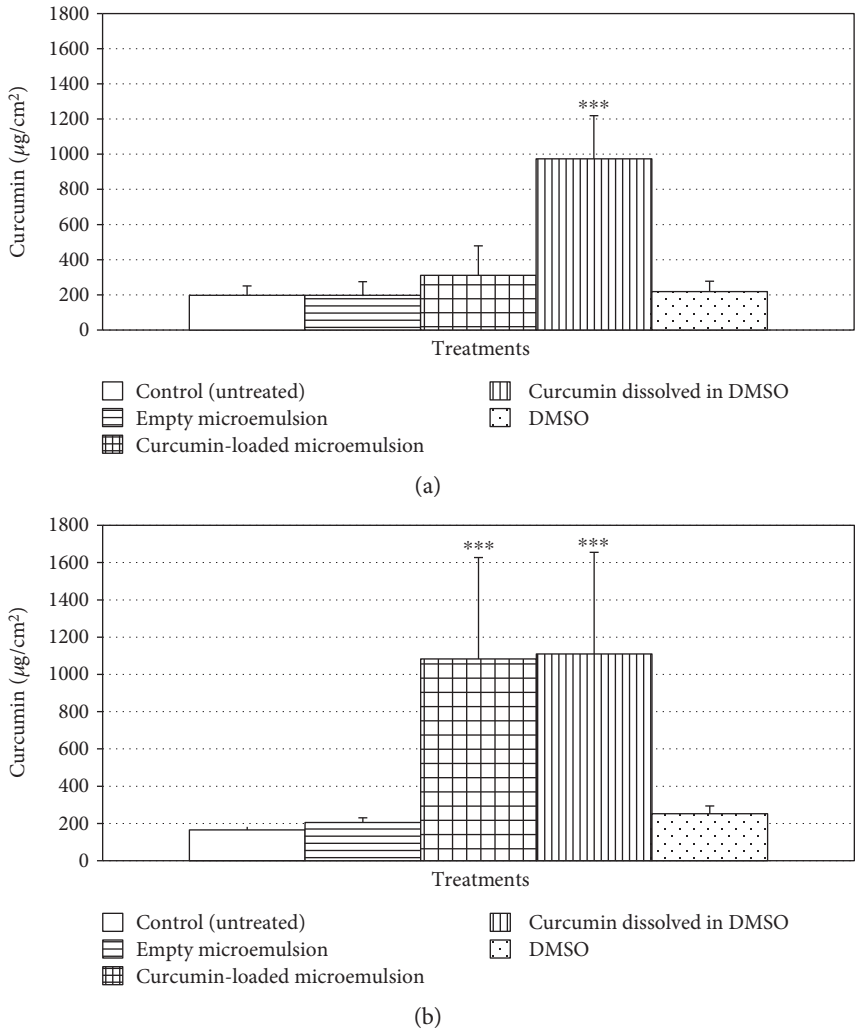

Figure 6: Dermal absorption evaluation of curcumin-loaded microemulsion in (a) the human skin epidermis and in (b) human skin dermis. Average values are presented in the figure with standard deviation of the mean (***$P < 0.001$).

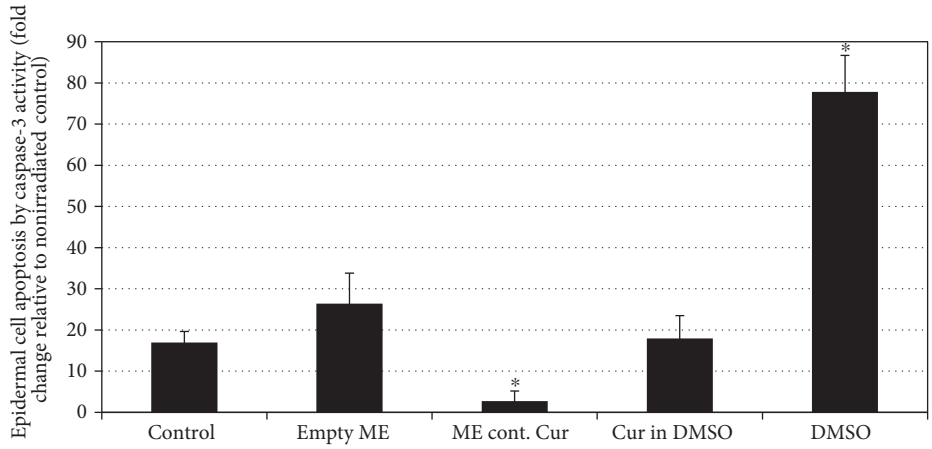

Figure 7: Organ cultures were treated with microemulsions for 24 h and then irradiated with UVB at 300 mJ/cm^2, and cell apoptosis was evaluated by caspase-3 activity assay 24 h after irradiation. Data were normalized on the basis of untreated (control), nonirradiated skin (equal to 1). Average values are presented in the figure with standard deviation of the mean (*$P < 0.05$).

apoptosis. On the other hand, the prior application of a curcumin-loaded microemulsion reversed this trend, with only ~2.7-fold increase in caspase-3 activity in the same conditions (Figure 7). The previous application of free curcumin or an empty microemulsion did not affect caspase-3 activity significantly. However, DMSO, as expected, increased capsase-3 activity by ~78-fold. These results demonstrate an intense effect of a curcumin-loaded microemulsion to restrain UV-induced cytotoxicity in epidermal cells.

It is worth noting that curcumin's preventive effect against UVB-induced damage in skin might also be the consequence of molecular events such as downregulation of cell proliferative controls, involving thymine dimer, apoptosis, transcription factor NF-κB, and inflammatory responses or upregulation of p53, and these different contributions need to be further revealed [70].

4. Conclusions

The work presented in this study supports the usage of curcumin-loaded microemulsions for treating oxidative stress-related conditions in skin. The incorporation of curcumin in a microemulsion, from a structural point of view, resulted in a stable nanometric-size microemulsion composed of core and shell droplets. Curcumin-loaded microemulsions maintained curcumin's activity as a reactive oxygen species scavenger. Moreover, curcumin-loaded microemulsions enabled an efficient Keap1-Nrf_2-EpRE pathway activation.

Curcumin-loaded microemulsions promoted a powerful effect on the reduction of UV-induced cytotoxicity in epidermal cells. This work provided insights regarding the mechanism of activity in which curcumin-loaded microemulsions operate and thus supports our suggested strategy for ameliorating skin injuries and damages.

Abbreviations

ME: Microemulsion
SOD1: Superoxide dismutase
Nrf2: Nuclear factor (erythroid-derived 2)-like 2, NF-E2-related factor
EpRE: Electrophile response element
HO-1: Heme oxygenase-1 or haem oxygenase-1
GAPDH: Glyceraldehyde 3-phosphate dehydrogenase
NQO1: NAD(P)H dehydrogenase [quinone] 1
ROS: Reactive oxygen species
tBHQ: tert-Butylhydroquinone.

Conflicts of Interest

The authors report no conflicts of interest. Ron Kohen is affiliated with the Bloom Center of Pharmacy and is the incumbent of the Richard and Jean Zarbin Chair in Medical Studies at the Hebrew University of Jerusalem.

Authors' Contributions

The authors alone are responsible for the content and writing of the article.

Acknowledgments

The authors thank Yael Levi-Kalisman for her assistance in obtaining cryo-TEM images. This work was funded by the David and Ines Myers Fund of Cleveland, Ohio, USA.

References

[1] R. Rn and C. Bosco, "Oxidative stress and protective effects of polyphenols: comparative studies in human and rodent kidney. A review," *Comparative Biochemistry and Physiology Part C: Toxicology & Pharmacology*, vol. 142, no. 3, pp. 317–327, 2006.

[2] S.-K. Myung, W. Ju, B. Cho et al., "Efficacy of vitamin and antioxidant supplements in prevention of cardiovascular disease: systematic review and meta-analysis of randomised controlled trials," *British Medical Journal*, vol. 346, p. f10, 2013.

[3] G. Tsuji, M. Takahara, H. Uchi et al., "Identification of ketoconazole as an AHR-NRF2 activator in cultured human keratinocytes: the basis of its anti-inflammatory effect," *Journal of Investigative Dermatology*, vol. 132, no. 1, pp. 59–68, 2012.

[4] B. M. Hybertson, B. Gao, S. K. Bose, and J. M. McCord, "Oxidative stress in health and disease: the therapeutic potential of Nrf2 activation," *Molecular Aspects of Medicine*, vol. 32, no. 4, pp. 234–246, 2011.

[5] G. P. Sykiotis and D. Bohmann, "Stress-activated cap'n'collar transcription factors in aging and human disease," *Science Signaling*, vol. 3, no. 112, p. re3, 2010.

[6] M. Schafer and S. Werner, "NRF2-a regulator of keratinocyte redox signaling," *Free Radical Biology and Medicine*, vol. 88, Part B, pp. 243–252, 2015.

[7] A. Goel and B. B. Aggarwal, "Curcumin, the golden spice from Indian saffron, is a chemosensitizer and radiosensitizer for tumors and chemoprotector and radioprotector for normal organs," *Nutrition and Cancer*, vol. 62, no. 7, pp. 919–930, 2010.

[8] M. Heger, R. F. van Golen, M. Broekgaarden, and M. C. Michel, "The molecular basis for the pharmacokinetics and pharmacodynamics of curcumin and its metabolites in relation to cancer," *Pharmacological Reviews*, vol. 66, no. 1, pp. 222–307, 2013.

[9] A. T. Dinkova-Kostova and P. Talalay, "Direct and indirect antioxidant properties of inducers of cytoprotective proteins," *Molecular Nutrition & Food Research*, vol. 52, Supplement 1, pp. S128–SS38, 2008.

[10] D. Akbik, M. Ghadiri, W. Chrzanowski, and R. Rohanizadeh, "Curcumin as a wound healing agent," *Life Sciences*, vol. 116, no. 1, pp. 1–7, 2014.

[11] J. L. Arbiser, N. Klauber, R. Rohan et al., "Curcumin is an in vivo inhibitor of angiogenesis," *Molecular Medicine*, vol. 4, no. 6, p. 376–383, 1998.

[12] S. S. Bhandarkar and J. L. Arbiser, *Curcumin as an Inhibitor of Angiogenesis. The Molecular Targets and Therapeutic Uses of Curcumin in Health and Disease*, pp. 185–195, Springer, Boston, MA, 2007.

[13] T. P. Robinson, R. B. Hubbard, T. J. Ehlers, J. L. Arbiser, D. J. Goldsmith, and J. P. Bowen, "Synthesis and biological evaluation of aromatic enones related to curcumin," *Bioorganic & Medicinal Chemistry*, vol. 13, no. 12, pp. 4007–4013, 2005.

[14] R. L. Thangapazham, S. Sharad, and R. K. Maheshwari, "Skin regenerative potentials of curcumin," *BioFactors*, vol. 39, no. 1, pp. 141–149, 2013.

[15] D. R. Bickers and M. Athar, "Oxidative stress in the pathogenesis of skin disease," *Journal of Investigative Dermatology*, vol. 126, no. 12, pp. 2565–2575, 2006.

[16] G. Kuttan, K. B. H. Kumar, C. Guruvayoorappan, and R. Kuttan, *Antitumor, Anti-Invasion, and Antimetastatic Effects of Curcumin. The Molecular Targets and Therapeutic Uses of Curcumin in Health and Disease*, pp. 173–184, Springer, Boston, MA, 2007.

[17] V. P. Menon and A. R. Sudheer, *Antioxidant and Anti-Inflammatory Properties of Curcumin. The Molecular Targets and Therapeutic Uses of Curcumin in Health and Disease*, pp. 105–125, Springer, Boston, MA, 2007.

[18] K. Song, S. Peng, Z. Sun, H. Li, and R. Yang, "Curcumin suppresses TGF-β signaling by inhibition of TGIF degradation in scleroderma fibroblasts," *Biochemical and Biophysical Research Communications*, vol. 411, no. 4, pp. 821–825, 2011.

[19] R. L. Thangapazham, A. Sharma, and R. K. Maheshwari, *Beneficial Role of Curcumin in Skin Diseases. The Molecular Targets and Therapeutic Uses of Curcumin in Health and Disease*, pp. 343–357, Springer, Boston, MA, 2007.

[20] P. Anand, A. B. Kunnumakkara, R. A. Newman, and B. B. Aggarwal, "Bioavailability of curcumin: problems and promises," *Molecular Pharmaceutics*, vol. 4, no. 6, pp. 807–818, 2007.

[21] K. M. Nelson, J. L. Dahlin, J. Bisson, J. Graham, G. F. Pauli, and M. A. Walters, "The essential medicinal chemistry of curcumin: miniperspective," *Journal of Medicinal Chemistry*, vol. 60, no. 5, pp. 1620–1637, 2017.

[22] M. Mouslmani, J. M. Rosenholm, N. Prabhakar, M. Peurla, E. Baydoun, and D. Patra, "Curcumin associated poly (allylamine hydrochloride)-phosphate self-assembled hierarchically ordered nanocapsules: size dependent investigation on release and DPPH scavenging activity of curcumin," *RSC Advances*, vol. 5, no. 24, pp. 18740–18750, 2015.

[23] D. Patra and F. Sleem, "A new method for pH triggered curcumin release by applying poly (l-lysine) mediated nanoparticle-congregation," *Analytica Chimica Acta*, vol. 795, pp. 60–68, 2013.

[24] R. H. H. Neubert, "Potentials of new nanocarriers for dermal and transdermal drug delivery," *European Journal of Pharmaceutics and Biopharmaceutics*, vol. 77, no. 1, pp. 1–2, 2011.

[25] A. Kogan and N. Garti, "Microemulsions as transdermal drug delivery vehicles," *Advances in Colloid and Interface Science*, vol. 123, pp. 369–385, 2006.

[26] C. H. Liu and H. Y. Huang, "Antimicrobial activity of curcumin-loaded myristic acid microemulsions against *Staphylococcus epidermidis*," *Chemical and Pharmaceutical Bulletin*, vol. 60, no. 9, pp. 1118–1124, 2012.

[27] R. Yutani, S. Y. Morita, R. Teraoka, and S. Kitagawa, "Distribution of polyphenols and a surfactant component in skin during Aerosol OT microemulsion-enhanced intradermal delivery," *Chemical and Pharmaceutical Bulletin*, vol. 60, no. 8, pp. 989–994, 2012.

[28] C. H. Liu and F. Y. Chang, "Development and characterization of eucalyptol microemulsions for topic delivery of curcumin," *Chemical and Pharmaceutical Bulletin*, vol. 59, no. 2, pp. 172–178, 2011.

[29] C. C. Lin, H. Y. Lin, H. C. Chen, M. W. Yu, and M. H. Lee, "Stability and characterisation of phospholipid-based curcumin-encapsulated microemulsions," *Food Chemistry*, vol. 116, no. 4, pp. 923–928, 2009.

[30] A. Teichmann, S. Heuschkel, U. Jacobi et al., "Comparison of stratum corneum penetration and localization of a lipophilic model drug applied in an o/w microemulsion and an amphiphilic cream," *European Journal of Pharmaceutics and Biopharmaceutics*, vol. 67, no. 3, pp. 699–706, 2007.

[31] M. Schafer, H. Farwanah, A. H. Willrodt et al., "Nrf2 links epidermal barrier function with antioxidant defense," *EMBO Molecular Medicine*, vol. 4, no. 5, pp. 364–379, 2012.

[32] T. A. Beyer, U. Auf dem Keller, S. Braun, M. Schafer, and S. Werner, "Roles and mechanisms of action of the Nrf2 transcription factor in skin morphogenesis, wound repair and skin cancer," *Cell Death & Differentiation*, vol. 14, no. 7, pp. 1250–1254, 2007.

[33] M. Ben Yehuda Greenwald, M. Frusic-Zlotkin, Y. Soroka et al., "Nitroxide delivery system for Nrf2 activation and skin protection," *European Journal of Pharmaceutics and Biopharmaceutics*, vol. 94, pp. 123–134, 2015.

[34] A. Shukla and R. H. H. Neubert, "Diffusion behavior of pharmaceutical O/W microemulsions studied by dynamic light scattering," *Colloid and Polymer Science*, vol. 284, no. 5, pp. 568–573, 2006.

[35] G. B. Behera, B. K. Mishra, P. K. Behera, and M. Panda, "Fluorescent probes for structural and distance effect studies in micelles, reversed micelles and microemulsions," *Advances in Colloid and Interface Science*, vol. 82, no. 1, pp. 1–42, 1999.

[36] D. Patra and C. Barakat, "Synchronous fluorescence spectroscopic study of solvatochromic curcumin dye," *Spectrochimica Acta Part a: Molecular and Biomolecular Spectroscopy*, vol. 79, no. 5, pp. 1034–1041, 2011.

[37] Y. Abramov, J. G. Schenker, A. Lewin, S. Friedler, B. Nisman, and V. Barak, "Endocrinology: plasma inflammatory cytokines correlate to the ovarian hyperstimulation syndrome," *Human Reproduction*, vol. 11, no. 7, pp. 1381–1386, 1996.

[38] R. Kohen and I. Gati, "Skin low molecular weight antioxidants and their role in aging and in oxidative stress," *Toxicology*, vol. 148, no. 2, pp. 149–157, 2000.

[39] J. R. Cronin, "The biochemistry of alternative medicine: comparing antioxidant values with the ORAC method," *Alternative & Complementary Therapies*, vol. 10, no. 3, pp. 167–170, 2004.

[40] I. Ginsburg, M. Sadovnic, M. Oron, and R. Kohen, "Novel chemiluminescence-inducing cocktails, part II: measurement of the anti-oxidant capacity of vitamins, thiols, body fluids, alcoholic beverages and edible oils," *Inflammopharmacology*, vol. 12, no. 4, pp. 305–320, 2004.

[41] M. S. Blois, "Antioxidant determinations by the use of a stable free radical," *Nature*, vol. 181, no. 4617, pp. 1199–1200, 1958.

[42] P. Boukamp, R. T. Petrussevska, D. Breitkreutz, J. Hornung, A. Markham, and N. E. Fusenig, "Normal keratinization in a spontaneously immortalized aneuploid human keratinocyte cell line," *The Journal of Cell Biology*, vol. 106, no. 3, pp. 761–771, 1988.

[43] M. Frusic-Zlotkin, R. Pergamentz, B. Michel et al., "The interaction of pemphigus autoimmunoglobulins with epidermal cells: activation of the fas apoptotic pathway and the use of caspase activity for pathogenicity tests of pemphigus patients," *Annals of the New York Academy of Sciences*, vol. 1050, no. 1, pp. 371–379, 2005.

[44] M. Portugal-Cohen, Y. Soroka, M. Frusic-Zlotkin et al., "Skin organ culture as a model to study oxidative stress, inflammation and structural alterations associated with UVB10 induced photodamage," *Experimental Dermatology*, vol. 20, no. 9, pp. 749–755, 2011.

[45] J. Sambrook DWR and D. W. Russell, *Molecular Cloning: A Laboratory Manual Cold Spring Harbour*, Cold Spring Harbour Laboratory Press, New York, 2001.

[46] V. Singh, H. Sharma, R. Veerma, A. Javed, and M. Singh, "Topical non steroidal anti inflammatory drug (NSAIDs) microemulsions: rationale, review and future prospective," *Asian Journal of Pharmaceutics*, vol. 7, no. 1, p. 1, 2014.

[47] M. Kreilgaard, "Influence of microemulsions on cutaneous drug delivery," *Advanced Drug Delivery Reviews*, vol. 54, Supplement 1, pp. S77–S98, 2002.

[48] Y. S. Rhee, J. G. Choi, E. S. Park, and S. C. Chi, "Transdermal delivery of ketoprofen using microemulsions," *International Journal of Pharmaceutics*, vol. 228, no. 1, pp. 161–170, 2001.

[49] M. Changez and M. Varshney, "Aerosol-OT microemulsions as transdermal carriers of tetracaine hydrochloride," *Drug Development and Industrial Pharmacy*, vol. 26, no. 5, pp. 507–512, 2000.

[50] M. J. Lawrence and G. D. Rees, "Microemulsion-based media as novel drug delivery systems," *Advanced Drug Delivery Reviews*, vol. 45, no. 1, pp. 89–121, 2000.

[51] C. Korzeniewski and D. M. Callewaert, "An enzyme-release assay for natural cytotoxicity," *Journal of Immunological Methods*, vol. 64, no. 3, pp. 313–320, 1983.

[52] S. Roohinejad, D. Middendorf, D. J. Burritt, U. Bindrich, D. W. Everett, and I. Oey, "Capacity of natural β-carotene loaded microemulsion to protect Caco-2 cells from oxidative damage caused by exposure to H_2O_2," *Food Research International*, vol. 66, pp. 469–477, 2014.

[53] A. S. Narang, D. Delmarre, and D. Gao, "Stable drug encapsulation in micelles and microemulsions," *International Journal of Pharmaceutics*, vol. 345, no. 1, pp. 9–25, 2007.

[54] M. Lapteva and Y. N. Kalia, "Microstructured bicontinuous phase formulations: their characterization and application in dermal and transdermal drug delivery," *Expert Opinion on Drug Delivery*, vol. 10, no. 8, pp. 1043–1059.

[55] G. Chen, Y. Chen, N. Yang, X. Zhu, L. Sun, and G. Li, "Interaction between curcumin and mimetic biomembrane," *Science China Life Sciences*, vol. 55, no. 6, pp. 527–532, 2013.

[56] D. Trachootham, W. Lu, M. A. Ogasawara, N. R. D. Valle, and P. Huang, "Redox regulation of cell survival," *Antioxidants & Redox Signaling*, vol. 10, no. 8, pp. 1343–1374, 2008.

[57] Y. M. Kim, H. O. Pae, J. E. Park et al., "Heme oxygenase in the regulation of vascular biology: from molecular mechanisms to therapeutic opportunities," *Antioxidants & Redox Signaling*, vol. 14, no. 1, pp. 137–167, 2011.

[58] R. M. Tyrrell, "Solar ultraviolet A radiation: an oxidizing skin carcinogen that activates heme oxygenase-1," *Antioxidants & Redox Signaling*, vol. 6, no. 5, pp. 835–840, 2004.

[59] F. Lieder, F. Reisen, T. Geppert et al., "Identification of UV43 protective activators of nuclear factor erythroid-derived 2-related factor 2 (Nrf2) by combining a chemical library screen with computer-based virtual screening," *Journal of Biological Chemistry*, vol. 287, no. 39, pp. 33001–33013, 2012.

[60] H. Erlank, A. Elmann, R. Kohen, and J. Kanner, "Polyphenols activate Nrf2 in astrocytes via H_2O_2, semiquinones, and quinones," *Free Radical Biology and Medicine*, vol. 51, no. 12, pp. 2319–2327, 2011.

[61] L. H. Long, M. V. Clement, and B. Halliwell, "Artifacts in cell culture: rapid generation of hydrogen peroxide on addition of (−)-epigallocatechin, (−)-epigallocatechin gallate, (+)-catechin, and quercetin to commonly used cell culture media," *Biochemical and Biophysical Research Communications*, vol. 273, no. 1, pp. 50–53, 2000.

[62] S. G. Rhee, "Cell signaling. H_2O_2, a necessary evil for cell signaling," *Science*, vol. 312, no. 5782, pp. 1882–1883, 2006.

[63] G. P. Bienert, J. K. Schjoerring, and T. P. Jahn, "Membrane transport of hydrogen peroxide," *Biochimica et Biophysica Acta (BBA)-Biomembranes*, vol. 1758, no. 8, pp. 994–1003, 2006.

[64] A. Balcerczyk, A. Grzelak, S. Kozio, R. Bae, and G. Bartosz, "Formation of reactive oxygen species in cellular media," *Current Topics in Biophysics*, vol. 29, no. 1-2, pp. 109–111, 2005.

[65] M. A. Bolzinger, S. P. Briançon, J. Pelletier, and Y. Chevalier, "Penetration of drugs through skin, a complex rate-controlling membrane," *Current Opinion in Colloid & Interface Science*, vol. 17, no. 3, pp. 156–165, 2012.

[66] J. Hadgraft and R. H. Guy, *Transdermal Drug Delivery: Developmental Issues and Research Initiatives*, Marcel Dekker Inc, New York, 1989.

[67] M. R. Prausnitz and R. Langer, "Transdermal drug delivery," *Nature Biotechnology*, vol. 26, no. 11, pp. 1261–1268, 2008.

[68] S. G. Elfbaum and K. Laden, "The effect of dimethyl sulfoxide on percutaneous absorption: a mechanistic study. Part III," *Journal of the Society of Cosmetic Chemists*, vol. 19, no. 13, pp. 841–847, 1968.

[69] S. Kwak and M. Lafleur, "Effect of dimethyl sulfoxide on the phase behavior of model stratum corneum lipid mixtures," *Chemistry and Physics of Lipids*, vol. 161, no. 1, pp. 11–21, 2009.

[70] K. D. Tsai, J. C. Lin, S. M. Yang et al., "Curcumin protects against UVB-Induced skin cancers in SKH-1 hairless mouse: analysis of early molecular markers in carcinogenesis," *Evidence-Based Complementary and Alternative Medicine*, vol. 2012, Article ID 593952, 11 pages, 2012.

Hindawi
Oxidative Medicine and Cellular Longevity
Volume 2017, Article ID 3034245, 15 pages
https://doi.org/10.1155/2017/3034245

Review Article

Cardiovascular Mitochondrial Dysfunction Induced by Cocaine: Biomarkers and Possible Beneficial Effects of Modulators of Oxidative Stress

Manuela Graziani,[1,2] Paolo Sarti,[3] Marzia Arese,[3] Maria Chiara Magnifico,[3] Aldo Badiani,[1,4] and Luciano Saso[1]

[1]*Department of Physiology and Pharmacology "Vittorio Erspamer", Sapienza University of Rome, Rome, Italy*
[2]*Drug Addiction and Clinical Pharmacology Unit, University Hospital Umberto I, Sapienza University of Rome, Rome, Italy*
[3]*Department of Biochemical Sciences "Alessandro Rossi Fanelli", Sapienza University of Rome, Rome, Italy*
[4]*Sussex Addiction Research and Intervention Centre (SARIC), School of Psychology, University of Sussex, Brighton BN1 9RH, UK*

Correspondence should be addressed to Manuela Graziani; manuela.graziani@uniroma1.it

Received 1 December 2016; Revised 8 March 2017; Accepted 26 March 2017; Published 16 May 2017

Academic Editor: Daniela Giustarini

Cocaine abuse has long been known to cause morbidity and mortality due to its cardiovascular toxic effects. The pathogenesis of the cardiovascular toxicity of cocaine use has been largely reviewed, and the most recent data indicate a fundamental role of oxidative stress in cocaine-induced cardiovascular toxicity, indicating that mitochondrial dysfunction is involved in the mechanisms of oxidative stress. The comprehension of the mechanisms involving mitochondrial dysfunction could help in selecting the most appropriate mitochondria injury biological marker, such as superoxide dismutase-2 activity and glutathionylated hemoglobin. The potential use of modulators of oxidative stress (mitoubiquinone, the short-chain quinone idebenone, and allopurinol) in the treatment of cocaine cardiotoxic effects is also suggested to promote further investigations on these potential mitochondria-targeted antioxidant strategies.

1. Introduction

Cocaine (COC) use has long been known to cause morbidity and mortality due to its cardiovascular toxic effects [1, 2]. COC can induce coronary and systemic vasoconstriction and arrhythmias, such as atrial and ventricular fibrillation [3], contraction band necrosis, atherosclerosis, and chest pain [4] as well as acute myocardial infarction [5], up to weeks after last consumption [6], even in presence of normal coronary arteries [7].

The pathogenesis of cardiovascular toxicity related to COC use has been reviewed recently [8–10]. Direct (block of voltage-dependent K^+ and Na^{++} channels) and indirect (actions of catecholamines and their oxidation products on α- and β-adrenergic receptors) are suspected to be the primary pathogenic mechanisms.

The fundamental role of oxidative stress (OS) in COC-induced cardiovascular toxicity is well established [8, 11]. Moreover, formation and accumulation of reactive oxygen species (ROS) as a consequence of α- and β-adrenergic receptors stimulation [12, 13], as well as of enzymatic or non-enzymatic catabolism of catecholamines [14, 15], have been demonstrated in cardiac and vascular cells. Mitochondrial dysfunction leading to the production of ROS is implicated in cardiovascular toxicity [16, 17]. Furthermore, a number of drugs (e.g., anticancer drugs, antiviral drugs, oral antidiabetic drugs, and recreational drugs) have been demonstrated to induce toxic effects as a consequence of mitochondrial dysfunctions [18]. An important contribution of mitochondria in COC-induced OS and ROS production has been shown in experimental in vivo models [19, 20] and in the culture of rat cardiomyocytes [21]. In cardiomyocytes, the

mitochondria themselves could become the target of COC-induced OS, due to ROS accumulation.

A better understanding of the role of mitochondrial dysfunction in COC-induced cardiovascular toxicity will help to select the most appropriate biological markers and to develop novel mitochondria-targeted antioxidant strategies. The purpose of the present paper is to review the state-of-the-art study of mitochondrial involvement in ROS production associated to COC-induced cardiovascular toxicity. In particular, we focused on the identification of possible biological markers of OS and the possible beneficial effects of OS modulators.

2. Mitochondrial Toxicity and Molecular Targets

The molecular mechanisms by which drugs of abuse, COC particularly, attack tissues' integrity is an issue of paramount importance. Pioneering experiments carried out using epithelial cell cultures [22] or animal models, such as mice [23, 24], have clearly suggested an involvement of mitochondrial chemistry based on the impairment of the respiratory chain with the rise of cytotoxic (ROS) species.

2.1. Mitochondrial Energy Production and Electron Transport Chain. In cells, most of the ATP is synthesized by the mitochondria via a proton electrochemical potential gradient, $\Delta\mu H^+$ [25]. Under physiological conditions, the mitochondria are maintained operative by a resident mitochondrial DNA in synergy with nuclear DNA, both regulating fusion and fission and mitophagy dynamics of the organelles [26] and, indeed, the expression and activity of the respiratory chain electron transfer (eT) complexes. These complexes, at the level of the inner mitochondrial membrane, either collide among themselves randomly [27], the hypothesis later on reconsidered by [28], or are organised in supramolecular structures of the individual complexes [29]. Relevant to cell bioenergetics, the structural stability of the supercomplexes and the functional performance of the respiratory chain both have been shown to be modulated by the mitochondrial membrane potential [30] and the protein complexes phosphorylation. In addition and possibly related to the cocaine-dependent chemistry involving the proteo-membrane complexes, the functional performance of the supercomplexes has been shown to strongly depend on the membrane lipid composition and lipid peroxidation [31]. Regardless of whether organised as individual entities or as supercomplexes, the respiratory chain components enable the redox chemistry and the H^+ translocation across the inner mitochondrial membrane to occur, ensuring the built up and maintenance of the proton-electrochemical gradient used by the mitochondrial ATPase to synthesize the ATP [25, 32].

Relevant to the COC-induced chemistry, the mitochondrial function appears affected both directly, particularly at the level of complex I [33], and indirectly, due to production of reactive oxygen and nitrogen species (ROS and RNS), both strongly affecting mitochondrial complex IV and permeability and fluidity of the membranes. The mitochondrial ATP synthesis depends on the cell metabolism, and the functional status of the molecular machinery is modulated at several levels, principally by the energetic demand and by the substrates availability; in this context, Ca^{2+} plays a crucial role.

2.2. Mitochondria and Ca^{2+} Homeostasis. In the frame of the molecular changes induced by COC, it is worth to recall its interference with the cell integrated Ca^{2+} signaling and homeostasis, whose network although intensively studied is still only partly understood [34]. A complex set of equilibria and chemical reactions tightly controls the flux of Ca^{2+} within all cell organelles and among specific molecular components of the extracellular and the intracellular cell compartments [34–37].

In the extracellular space, Ca^{2+} concentration is in the mM range, whereas in the cytoplasm of a resting cell is $\sim 10^2$ nM [38]. The large concentration gradient is maintained by a dynamic equilibrium, involving a finely integrated Ca^{2+} controlling molecular machinery [34, 39] including a variety of plasma membrane Ca^{2+} channels, receptors, exchangers, pumps, binding proteins, chaperons, and transporters (Figure 1).

In the cell, the intracellular Ca^{2+} ions are accumulated into specific cell compartments, the so-called Ca^{2+} stores. These are the endoplasmic/sarcoplasmic reticulum (ER, for simplicity), the mitochondria, and to some extent the Golgi apparatus, together with the cell nucleus and other organelles, such as the lysosomes and peroxisomes. The Ca^{2+} concentration in the stores may rise up to 1 or 2 orders of magnitude (1–10 μM) higher than that in the cytoplasm, the value depending on the actual cell compartment, and its functional state [40–42].

The mitochondria and ER are responsible for the accumulation in the stores of most Ca^{2+} contributing, respectively, to microcompartmentalization of up to 25% and 75% Ca^{2+}. These compartments are tightly interconnected at specialised sites named *mitochondrial-associated membranes* (MAM). At this level, the side-by-side proximity between ER and the mitochondria allows the transfer of Ca^{2+} ions to the mitochondria from proteins and chaperons of the ER. This process occurs via specific channels such as the inositol-tri-phosphate receptors and the ryanodine receptors. At the level of the outer mitochondrial membrane (OMM), Ca^{2+} ions are transported from the cytoplasm into the intermembrane space (IMS) through the voltage-dependent anion channel (VDAC): this reaction uses ATP; thus, once promoted, ATP synthesis is stimulated. The transport, across the inner membrane of Ca^{++} from the IMS to the mitochondrial matrix, is mainly contributed by the mitochondrial calcium uniporter (MCU), an ion channel that selectively drives the Ca^{2+} entry into the matrix. Transport occurs in synergy with two complexes named the mitochondrial Ca^{2+} uptake 1 (MICU1) and the mitochondrial Ca^{2+} uptake 2 (MICU2), together setting the threshold for the Ca^{2+} uniporter activity, also mediated by the essential MCU regulator (EMRE) [43]. It is worthy to point out that the mitochondrial Ca^{2+} loading and its back release to ER take part in the physiological, vital ion-buffering system, while the mitochondrial Ca^{2+} overloading most often paves the way to apoptosis or even to cell irreversible damage.

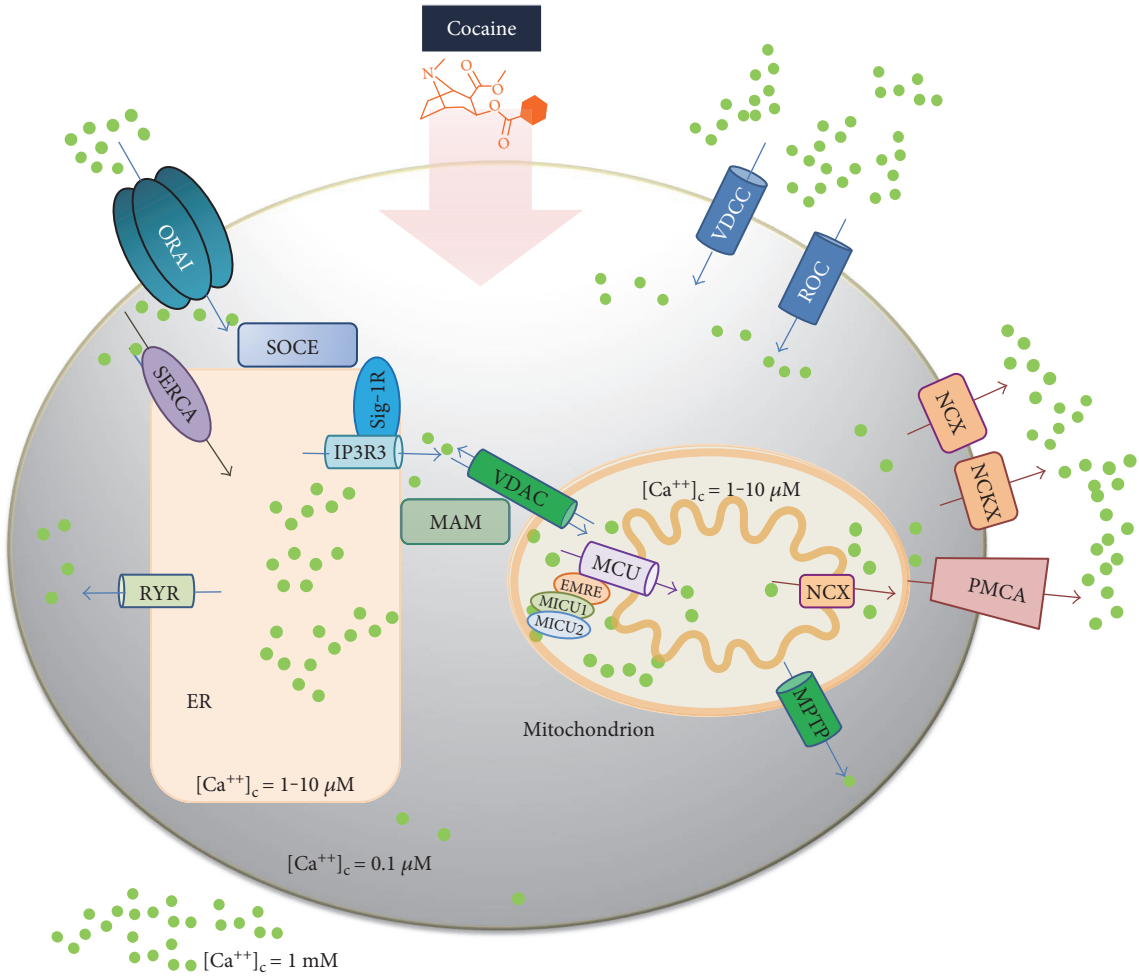

Figure 1: Main players of the cell Ca^{2+} molecular machinery as putative cocaine targets. Ideal intracellular Ca^{2+} concentration is maintained through complex equilibria among the extracellular space (1 mM), the cytoplasm (0.1 μM), and the cellular stores (1.0–10 μM), such as the mitochondrion, the endoplasmic reticulum (ER), the Golgi apparatus, and nucleus. The ion trafficking occurs via a variety of selective membrane channels, Ca^{2+}-binding proteins and transporters and ion exchangers and receptors, altogether responsible for Ca^{2+} import, export, and homeostasis. Import occurs at the level of (i) cell plasma membrane through the calcium release-activated Ca^{2+} channel protein 1 (ORAI1), the store-operated calcium entry channels (SOCE), and specific receptor-operated channels (ROC) such as AMPA, NMDA, TRPC, and the voltage-dependent calcium channels (VDCC); (ii) endoplasmic reticulum (ER) through the sarco/endoplasmic reticulum calcium ATPase (SERCA); (iii) mitochondria intermembrane space through the voltage-dependent anion channel (VDAC); and (v) in the matrix by the mitochondrial uniporter (MCU), in synergy with the mitochondrial calcium uptake (MICU) system. Extrusion occurs at the level of (i) cell plasma membrane mainly by the plasma membrane calcium ATPase (PMCA) and the sodium calcium exchangers (NCX) also potassium-dependent (NCKX) and (ii) the ER by the ryanodine (RYR) and the inositol 1,4,5-trisphosphate receptors (I P3R), as well as by the mitochondrial permeability transition pore (MPTP).

Uncontrolled mitochondrial Ca^{2+} accumulation rapidly induces, in fact, a decrease of the mitochondrial membrane potential ($\Delta\Psi$) leading to pathological production of ROS, RNS with opening of the mitochondrial permeability transition pore (MPTP), and release of cytochrome *c* and other proapoptotic components. The Ca^{2+} extrusion into the extracellular compartment, therefore, is also under tight control: it occurs via (i) the plasma membrane-associated Ca^{2+} ATPase pump (PMCA), extruding against an unfavourable electrochemical gradient, 1 Ca^{2+} ion per hydrolysed ATP and (ii) the potassium-independent Na^{+}/Ca^{2++} exchanger (NCX) and the potassium-dependent exchanger (NCKX) [44].

According to recent reports [45, 46], COC interferes with the intracellular Ca^{2+} distribution and trafficking. The interference has been proposed to occur at the level of the store-operated calcium entry (SOCE) system and particularly at the sigma-1 receptor site (Sig-1R) [47]. This is an intracellular chaperone embedded in the endoplasmic reticulum and is responsible for Ca^{2+} loading into the intracellular stores, the mitochondria included. The functional activity of Sig-1R was shown to be depressed by COC with impairment of the Ca^{2+} equilibrium among the cell cytoplasm and stores [40, 48]. It is worth noticing that the inhibition of SOCE via COC binding at the Sig-1R [45], if confirmed, might lead to even opposite pathophysiological effects. Depending on the extent of binding and duration of SOCE inhibition, the electrophoretic transfer of the positively charged Ca^{2+} in the mitochondrial matrix could, initially, lead to a slight

depression of the mitochondrial $\Delta\Psi$, counterbalanced by stimulation of ATP synthesis. No wonder, therefore, the COC induced mitochondrial Ca^{2+} loading might be overlooked. On the opposite, the persistence of the mitochondrial Ca^{2+} loading leads to the opening of the MPTP and triggers the apoptotic programme, with release of cytochrome *c* and other proapoptotic components [34, 37, 49–52]. Accordingly, COC-treated rat astroglioma cells had shown a dose-dependent manner depression of mitochondrial $\Delta\Psi$ and a disruption of cell morphology [53].

2.3. Mitochondria, ROS, and RNS Production in the Pathogenesis of Cardiovascular Toxicity. Cardiomyocytes undergo incessant contractions, their mitochondria requiring a regular supply of O_2 and reducing substrates. Normally, during mitochondrial respiration, the vast majority of O_2 is reduced to water via the electron transfer (eT) chain ($4e^-$/O atom), and only a small oxygen amount (0.1–2%) undergoes a 1- or 2-electron reduction, with formation of highly reactive partially reduced species, among which H_2O_2 and the superoxide radical ion ($O_2^{-\cdot}$) are the best representatives. These, when produced at sub-μmolar, nanomolar levels contribute to the formation of the cellular pool of physiological ROS that plays crucial signaling roles in a variety of conditions. Similarly, under normal conditions, also a number of more or less stable nitrogen oxides can be detected in the cells and tissues (RNS). These include nitric oxide (NO) and peroxynitrite ($ONOO^-$), that is, highly reactive species responsible, particularly the latter, for cell redox reactions that are often highly detrimental, such as protein nitrosation and membrane nitration. Among them, NO is present in the environment at up to nanomolar concentrations, as produced by the cell constitutive NOSs (eNOS and nNOS).

When present in large excess by the inducible iNOS ($\geq\mu$M), NO is a potent inhibitor of the mitochondrial respiration [54]. Noticeably, in the presence of enough O_2 ($5 \div 20\,\mu$M) and a suitable electron flux through the respiratory chain sustained by the mitochondrial substrates and reduced cytochrome *c*, the presence of nanomolar NO does not depress (significantly) cell respiration. Interestingly, from the bioenergetics signaling point of view, under these conditions, the apparent affinity for O_2 ($K_{M,\,O2}$) of cytochrome *c* oxidase (CcOX) rises [55], and the mitochondria become sensitive to the O_2 concentration, thus ready to shift to glycolytic production of ATP [56, 57]. Under persistent hypoxic conditions, when the mitochondrial respiratory chain experiences for longer times a too low (insufficient) O_2 concentration, a different landscape could be depicted. The rapid activation of constitutive NOS is observed together with the rise of NO concentration, whose increase, however, induces a depression to the oxidative phosphorylation due to, particularly, the inhibition of not only complex IV but also to some extent of complex I [57]. As observed in neurons, glycolysis takes place to compensate for the decreased ATP synthesis, a finding not directly shown, however, in cardiomyocytes. In addition, the cell environment turns acidic facilitating the conversion of nitrite (NO_2^-) into nitric oxide. NO, in the presence of O_2^-, at a diffusion-limited rate [58], forms the highly cell detrimental peroxynitrite, $ONOO^-$, initiating and sustaining a vicious circle that leads to permanent blockage of the mitochondrial eT [59, 60]. At this point, the reaction mechanisms controlling the cell steady-state level of ROS and RNS might become severely insufficient.

In summary, due to complex I inhibition by COC, the cardiomyocytes are likely called to face in rapid sequence, though not necessarily in this chronological order, hypoxia and cell acidification and rise of ROS/RNS species. As a consequence, cell survival might be at risk and cell death committed. Most frequently, the chemical species formed are strong oxidizing agents such as hydrogen peroxide, hypochlorous acid and peroxynitrite ion, and some of them are radical, for example, the nitric oxide and superoxide anion or the hydroxyl radical. Pathophysiologically relevant, not only cardiomyocytes but also the endothelial cells and the leucocytes, activated during the oxidative burst and the inflammation response, are responsible for the environmental physicochemical change and the uncontrolled ROS and RNS production. Altogether, the events point to excess ROS/RNS as being responsible for the production of cell detrimental effects, thus linking together, at the mitochondrial level, the OS, the early inflammation response, and cell death.

2.4. Crosstalk between the NO Chemistry and Cocaine. NO is actively produced by the NOSs [61] or it is chemically generated all throughout our organism. Three NOS isoforms have been identified and named after the cell tissues where they were first detected: the endothelial NOS (eNOS) from the endothelium, the neuronal NOS (nNOS) from the nervous system, and the inducible NOS (iNOS) from immunocompetent cells. These three isoforms share a substantial sequence homology (50–60%) and some basic features such as one catalytic Fe metal, the cofactors, and the substrates' binding sites. The expression and activity of the iNOS strongly depend on cell stressors but are independent on cell pCa^{2+} whereas eNOS and nNOS, both constitutive enzymes, are finely regulated by the concentration of cytosolic Ca^{2+}. Relevant to the NO chemistry, COC is known to react also with the NMDA receptor [62], whose activation is induced via Ca^{2+} rise, activity of nNOS, and NO production [63] (Figure 2); a pathway was also reported for morphine [55].

NOSs use arginine and O_2 as substrates. The affinity for O_2 is not equally distributed among the NOS isoforms. The eNOS shows the highest affinity (K_M~5 μM), comparable to that of the mitochondrial CcOX, while nNOS and iNOS have a lower O_2 affinity [57, 64].

Under hypoxic conditions, therefore, the O_2 availability can limit the enzymatic production of NO by the NOSs. During hypoxia, maintenance of the NO homoeostasis may require the release of NO from bulk nitrosothiols, or at the expenses of metal ions (Fe^{2+} and Cu^+) bound to proteins or free in solution. These ions catalyze the reduction of nitrite to NO and particularly at acidic pH and under hypoxic conditions [65].

In agreement with previous reports [66–71], the involvement of the NO chemistry in the development of COC addiction has been recently confirmed by the results of the selective 7-nitroindazole (7-N) inhibition of nNOS, induced on Wistar rats. The animals when preliminarily treated with

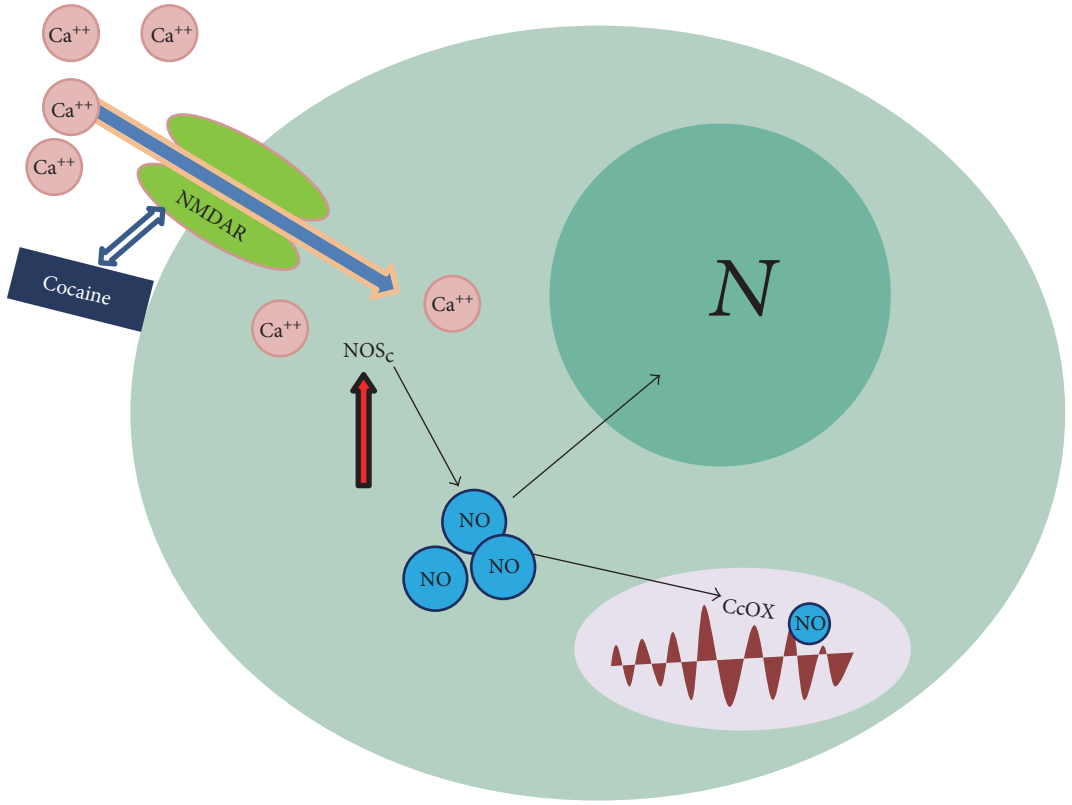

Figure 2: NMDA-receptor targeting by cocaine (hypothesis). The scheme is drawn by analogy to the functional effects observed at the level of the cell nitric oxide chemistry and detected when treating glioma cells in culture with morphine [55]. It shows the activation of the cocaine-mediated NMDA-R, leading to cytoplasmic Ca^{++} rise, activation of the constitutive NOS, and release of NO, targeting mitochondrial respiratory chain complexes.

7-N showed a significant attenuation of the COC withdrawal symptoms, and their brain-isolated synaptosomes displayed both the reversal of the drug mitochondrial depression and the decrease of GSH levels [72]. The fundamental role of mitochondrial GSH in protecting membrane functions was also observed in an experimental model of COC-induced hepatotoxicity in rats [73].

In humans, PET measurements performed using C-11-COC have shown in the early 90s that COC redistributes in most organs and tissues although following different kinetics (from seconds to several minutes) [74]. Redistribution likely includes the skin, and heavy COC abusers often display unpleasant skin signs, whose molecular mechanisms, however, are still mostly obscure. In this framework, it may be worthy to recall that the systemic administration of COC to male Sabra rats, thereafter subjected to skin biopsies, was able to rise the iNOS and xanthine oxidase (XO) activity prevented by specific inhibitors, such as the L-nitroso-arginine methyl-ester (L-NAME) and the oxypurinol (OP), respectively; the same authors reported similar results using human keratinocytes in culture [75]. The proposition put forward was that the oxidative-oxynitrosative damage was bound to the skin accumulation of superoxide and nitric oxide radicals, readily forming peroxynitrite [58] and lipoperoxides, along with a marked decrease of ROS/RNS scavengers such as reduced glutathione (GSH) and ascorbic acid (AA) [75]. This hypothesis appears fully consistent with the suggestion that the COC oxidative metabolites, and among them particularly, the nitrogen N-derivatives, are involved in the adverse biological effects observed in the human body, at least when chronically exposed to COC [76].

3. Mitochondria and Cocaine-Induced Cardiovascular Toxicity

As mentioned above, the role of mitochondria in the pathogenesis of COC-induced cardiovascular toxicity is well recognized [8, 20, 21, 33, 77]. COC may induce mitochondrial dysfunction in cardiomyocytes and in endothelial cells, based on direct and indirect mechanisms (Figure 3). Owing to its pathophysiological relevance at both cardiomyocytes and endothelial level, it may be worth to summarize the evidence supporting the hypothesis that COC is likely responsible for a specific mitochondrial impairment.

3.1. Cardiomyocytes. Notably, stimulation (and overstimulation) of β-adrenergic receptors (β-AR) triggers the release of Ca^{2+} in the mitochondria [78]. Indeed, stimulation of β-adrenergic receptors increases Ca^{2+} levels in the cytosol, through the activation of protein kinase A (PKA): increased cytosolic Ca^{2+} leads in turn to phosphorylation of Ca^{2+}-protein substrates and to the transfer of Ca^{2+} into the mitochondria [79]. As mentioned above (Section 2.2), excess mitochondrial Ca^{2+} impairs ATP production, causing nitro-oxidative stress

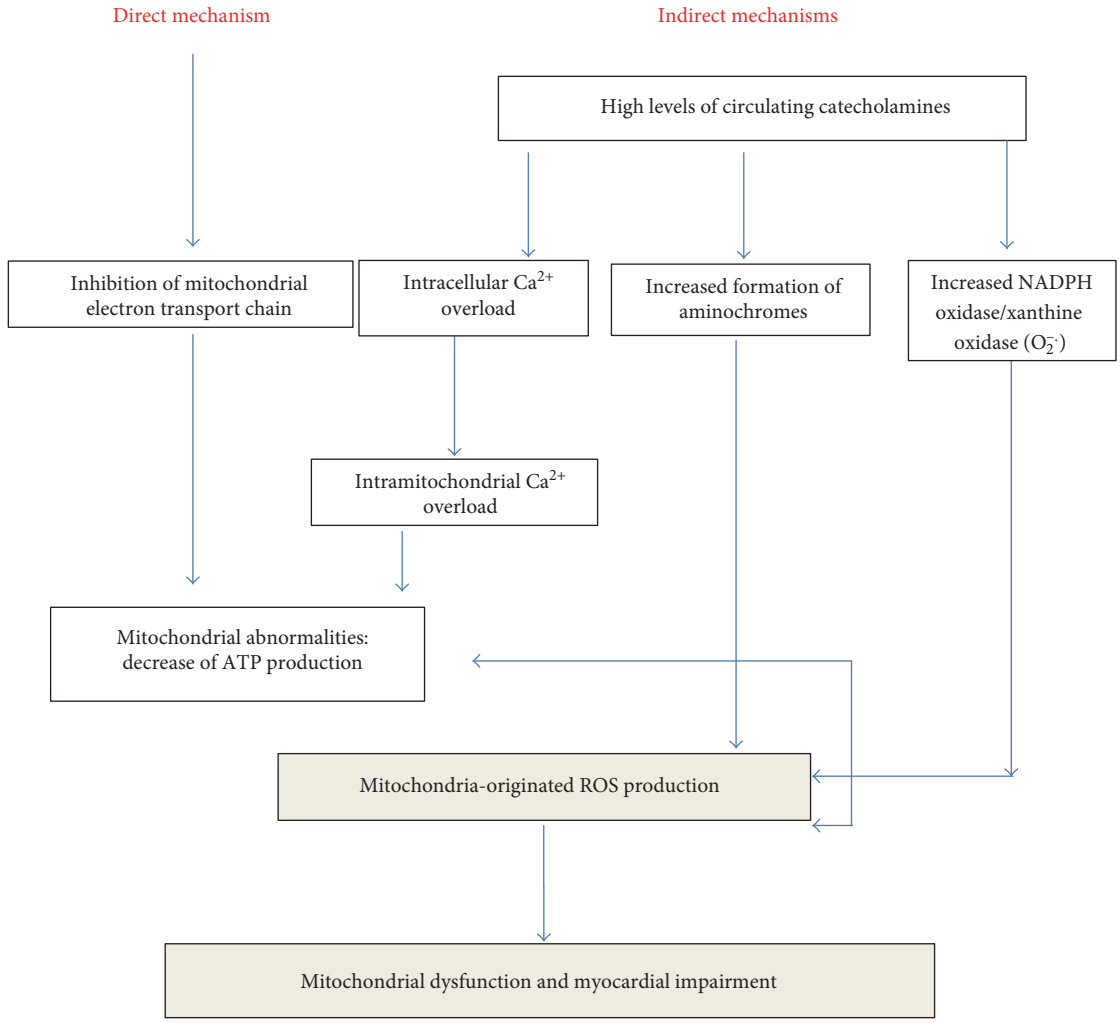

Figure 3: Cocaine-induced mitochondrial dysfunction.

with changes in permeability of the mitochondrial membrane, altogether leading to structural degeneration of cardiomyocytes [9, 80, 81]. Overproduction of mitochondrial ROS/RNS is in fact responsible for the massive opening of MPTP [16, 82] resulting in a further dysfunctional and structural degeneration of these organelles.

As already mentioned in Section 2.1 in isolated brain and liver mitochondria [83] and in culture rat myocardial cells, COC at high concentration had shown to inhibit complex I (NADH dehydrogenase) activity [33] leading in turn to inhibition of ATP synthesis. Accordingly, Fantel and colleagues [84] demonstrated a COC inhibitory effect on mitochondria respiration in rat embryo tissues. Importantly, in a model of myocardial ischemia-reperfusion, it has been demonstrated that a reduction in complex I activity may enhance ROS production by complex III [85].

A further mitochondrial role in COC myocyte toxicity is suggested by experimental studies, in which a mitochondria-dependent apoptosis was observed [77, 86, 87]. Indeed, in chronic COC-treated rats [77] and in cultured fetal [87] and adult [86] myocytes, COC induced apoptosis. The cytotoxic effects on cardiomyocytes were related to the release of cytochrome *c* from the mitochondria with activation of caspase-9 and caspase-3, whose inhibition blocked cell apoptosis [87]. Accordingly, a COC-induced apoptosis associated with the release of cytochrome *c* was observed also in cultured bovine coronary artery endothelial cells [88]. Interestingly, from the mechanistic point of view, in experiments carried out using adult rat ventricular cardiac myocytes, the caspase inhibition decreased the β-AR-stimulated apoptosis [86].

Apoptosis activation was also observed in the cerebral cortex of human COC addicts [89]. The postmortem brain study showed a significant reduction in the content of mitochondrial cytochrome *c* in prefrontal cortex: the authors suggest that the downregulation of cytochrome *c* could represent the induction of a counter regulatory adaptation to brain apoptotic effects induced by COC via mitochondria oxidative stress.

As mentioned above (Section 2.3), the accumulation of ROS/RNS is an important event by which COC may induce mitochondrial dysfunction with subsequent cardiotoxicity. Although the extent of mitochondrial dysfunction produced by COC is still unknown, it is generally accepted that the mitochondria are the main source of ROS production [90, 91] meantime being targets of the oxidative stress.

COC-induced ROS production may occur by mechanisms different from electron leak at the sites of the respiratory chain complexes, namely, by

(i) formation of $O_2^{-\cdot}$, during catecolamine oxidation (intramitochondria redox cycling),

(ii) synthesis of H_2O_2 by monoamine oxidase (MAO), during oxidative deamination of catecholamines (outer membrane of mitochondria),

(iii) ROS-induced ROS mitochondria formation [92].

Thus, ROS formation has been associated with COC-induced catecholamine release [8, 93].

As noted, a crucial role in COC-induced toxicity is played by transformation of catecholamines into aminochromes, that is, the oxidative catecholamine metabolites [93]. Indeed, when the level of catecholamines rises and the enzymes responsible for their catabolism become less efficient, as it might likely occur during COC abuse, catecholamines can undergo oxidation [14, 94] with formation of aminochromes (adrenochrome, dopachrome, and noradrenochrome); these molecules are very active from the redox cycling point of view. In bovine heart, it has been demonstrated that adrenochrome is reduced into semiquinone by mitochondrial complex I [95] inducing in cardiomyocyte mitochondria the formation of $O_2^{-\cdot}$ [9, 94, 96].

Genova and coworkers [97] had shown that mitocondrial complex I is involved both in initial generation of superoxide and in the reduction of adrenochrome to its semiquinone form. Furthermore, the superoxide anion $O_2^{-\cdot}$ in turn increases the adrenaline oxidation rate [14, 97]. Thus, the mitochondria, on one side, are largely responsible for cardiomyocyte oxidative stress, while on the other side, they are themselves targets of the stress. In addition, it is worth mentioning that the adrenochrome inhibits the oxidative phosphorylation of cardiac mitochondria [98] and leads to further enhancement of mitochondrial impairment.

Also MAO, flavin enzymes located in the outer membrane of mitochondria, are responsible for oxidative deamination of catecholamines, resulting in synthesis of H_2O_2 leading in turn to highly reactive HO· [93, 99]. Accordingly, in an experimental model in rats, it has been demonstrated that myocardial oxidative stress could be partially prevented by MAO inhibitors [100].

A further contribution to the stimulation of COC-induced mitochondrial ROS production may be derived from NADPH oxidase (Nox) and XO activity, also contributing to ROS generation in cardiac tissue [8, 13]. Indeed, the α1-adrenoceptor stimulation increases the activation of Nox [13, 101] which in turn produces $O_2^{-\cdot}$.

In an in vivo model of COC-induced diastolic dysfunction, it has been shown that 7 days of COC administration induces an increase of mitochondrial ROS production in cardiac fibers, with uncoupling of mitochondrial respiration [20]. It is worth noticing that over a similar period of incubation COC administration induces also the activation of Nox and XO, whose functional onset might precede mitochondrial failure [102]; this finding suggests that it is the ROS production by the Nox and XO that first triggers the ROS production by mitochondria not vice-versa [19].

Accordingly with this hypothesis, it has been suggested that MitoQ [20] and allopurinol [19] treatments may prevent oxidative stress and attenuate COC-induced cardiotoxicity.

3.2. Endothelial Cells. In endothelial cells, the mitochondrial content is reduced, compared to other cell lines [103, 104]. Thus, by comparison with cardiac myocytes and other cell types characterized by higher energy requirements, one might expect, from the quantitative point of view (only), a relatively smaller production by mitochondria of COC-induced reactive species. This notwithstanding ROS production by endothelial cell and their contribution to development of heart disease [104] has been demonstrated in rat [105] and in mouse [106] models. In cultured endothelial cells used as experimental models of ischemia/reperfusion, extensive amounts of ROS were observed [107].

The pro-oxidant activity of XO has been observed [108], and XO from endothelial vasculature has been proposed as the main ROS enzymatic source [93]; accordingly, patients with ischemic cardiomyopathy oxypurinol-induced inhibition of XO had shown improved myocardial contractility [109]. In endothelial cells, the activity of XO increases in I/R and it is a source of O_2 when in the presence of high levels of hypoxanthine.

4. Possible Biomarkers of Cocaine-Induced Oxidative Stress

Notably, biological markers (biomarkers) may be useful to quantify biological processes, disease state, or therapy prediction and therapeutic tools [110, 111]. The increase in understanding mechanisms of oxidative stress in drug [8, 112, 113] and alcohol [114, 115] addiction has led to identify oxidative stress markers, that, although not validated and specific, could help to evaluate oxidative status in drug abusers, both in acute and chronic use and in withdrawal syndrome [116, 117]. In Table 1, the proposed peripheral biomarkers of OS and relative references are listed.

In a recent study [117], it has been suggested that thiobarbituric acid reactive substances (TBARS) and brain-derived neurotrophic factor (BDNF) could be biomarkers for evaluation of severity of crack COC use. Furthermore, the authors found in male crack COC users a positive correlation between TBARS levels and severity of abuse during withdrawal syndrome. Notably, TBARS are an aspecific biomarker of peripheral oxidative stress, consisting of a quantification method for malondialdehyde (MDA) and stabile product of lipid peroxidation [118, 119]. Accordingly with clinical data, experimental studies in rats showed an increase in MDA levels in the heart, both after COC self-administration and extinction training [120] and after COC injection [121, 122].

Conversely, in a clinical study aimed at evaluating total antioxidant capacity in COC and methamphetamine subjects [123], no difference was found in MDA blood levels with respect to control. One possible explanation is that discrepancy in results may be due to differences in some

Table 1: Peripheral biomarkers of cocaine-induced oxidative stress.

Markers	Sample	Note	References
MDA	Plasma	Aspecific biomarker of lipid peroxidation	[117, 120–123]
TBARS	Plasma	Aspecific biomarker of lipid peroxidation	[117, 128]
BDNF	Plasma	Negative correlation with severity of cocaine use	[117, 128]
Glutathionylated Hb	Plasma (RBC)	Increased levels in oxidative stress conditions (i.e., cigarette smokers)	[113, 140]
SOD	Plasma (RBC)	Decreased levels of activity	[120–122, 131]

BDNF: malodialdehyde; TBARS: thiobarbituric acid reactive substances; BDNF: brain-derived neurotrophic factor; Hb: hemoglobin; RBC: red blood cells; SOD: superoxide dismutase.

characteristics of participants. Indeed, Sordi and coworkers [117] included subjects ($N = 49$) positive for current COC use, while in the study from Walker and coworkers [123], patients ($N = 126$) had used COC within 60 days prior to the test and almost 23% were positive for use. It can be suggested that the oxidative damage of lipids produced by current COC use, counteracting by antioxidant defense (see below), may shift towards antioxidant systems when the subjects became progressively abstinent.

Even though TBARS are neither specific nor quantitative [119], given that MDA plasma levels showed an increase in acute myocardial infarction [124, 125] and also in brain illnesses such as Parkinson's [126] and Alzheimer's [127] diseases, this biomarker may be useful to assess relative level of lipid peroxidation in COC abusers.

An increase in BDNF levels among crack users with respect to control subjects was also found [117, 128]. The function of this peripheral brain injury biomarker in drug-induced neuroadaptation is well known [129], and recent clinical data in chronic schizophrenia patients [130] showed that both BDNF and OS may be involved in the pathophysiology of this disease, suggesting an interaction mechanism between oxidative damage and neurotrophin dysfunction. Further investigations implicating these two peripherally measured biomarkers should contribute to understand the relative implication and interaction of oxidative stress and neurotrophic factors in disorders.

5. Antioxidant Defense System Biomarkers of Cocaine Oxidative Stress

Blood peripheral biomarkers of antioxidant enzymes were evaluated in a population of COC user [123], ($N = 126$; 18% abstinent for 1 month and more prior to the inclusion). The results showed no differences in the activities of glutathione peroxidase and catalase between COC user and control subjects, whereas a significant reduction in the SOD activity was observed in erythrocytes.

Accordingly, in a rat model of COC-induced heart injury, Moritz and coworkers [122] had shown that COC long-term administration caused a significant decrease in SOD activity; a biphasic trend in SOD concentration in rat spleen was observed after chronic COC administration in vivo [131] since that, after an early peak, SOD was significantly depleted 24 hours after COC treatment.

Notably SOD are an ubiquitous family of enzymes [132, 133] in which actually three distinct isoforms has been identified in humans. SOD1 (Cu/ZnSOD) is the major intracellular form of SOD, accounting for almost 80% of total SOD protein and is localized to the outer mitochondrial membrane, while SOD2 (MnSOD) is localized exclusively in the mitochondrial matrix [134, 135] and is expressed in the heart, lung, liver, and blood cells. SOD3 is the major SOD of human extracellular matrix of different tissues, mainly expressed in the lung and scarcely in the brain [136].

In the rat liver, SOD1/Cu, Zn was found in the mitochondrial intermembrane space and SOD2 was found in the matrix and also in the inner membrane [137]. Recent experimental data in rats [120] indicate no changes in SOD activity (irrespective of the isozyme subclass) in peripheral organs such as the heart and the liver, both during COC self-administration and during extinction phase (10 days). Conversely, a significant enhancement in SOD activity was found in the hippocampus and in the kidney. The authors suggest that different changes in the activity of SOD in rat brain structures and peripheral tissues may reflect differences in OS status and that increases in the SOD enzymatic activity could correspond to a reduction in MDA concentrations.

Due to its exclusive nuclear-encoded localization in the mitochondrial matrix, SOD2 is considered the main mitochondria antioxidant defense against toxic effects of ROS. So it can be suggested that evaluation of activity of SOD with respect to its isozyme subclasses could be a more specific biomarkers of mitochondrial oxidative stress. A further attention to different isozyme overexpression in specific cell types and tissues may achieve a contribution to better identify specific targets of oxidative stress.

Another peripheral biological marker that might reflect oxidative status in tissues is the level of glutathionylated hemoglobin (Hb). The role of the mechanism of S-glutathionylation (i.e., the conjugation of glutathione to protein cysteine residues catalyzed by glutathione S-transferase P) in response to oxidative stress in drug addiction was discussed in a recent review [113]. Protein S-glutathionylation can be considered a protective mechanism associated with elevated oxidative stress in alcohol, heroin, and also in COC abuse. In preclinical studies, acute and chronic COC treatment, but not withdrawal, had shown to increase brain formation of glutathionylated protein and a decrease in expression of GSH-S-transferase P [138, 139]. Notably most of the glutathionylated proteins are intracellular [110]; to date, in human, the extent of glutathionylation in some pathologies (i.e., diabetes mellitus, hyperlipidemia, and uremia) can be measured only in blood [140], since in red blood cells Hb accounts for 97% of protein composition [141]. Importantly, increased levels of glutathionylated Hb were observed in

Table 2: Potential therapeutic use of selective antioxidant compounds for cocaine-induced mitochondrial impairment.

Antioxidant compounds	Mechanism of action	References
MitoQ	Inhibition of XO activity and protection of mitochondria membrane potential	[20, 47, 148]
Idebenone (short chain quinone)	Transferring of electron in mitochondrial respiratory chain from cytoplasm to complex III (bypass deficiency in complex I)	[149–152]
Allopurinol	Inhibition of XO activity and consequent rescue of in ATP production	[19, 153–155]

cigarette smokers [142, 143] suggesting that its quantification can be used as a low-invasive clinical biomarker of oxidative stress-associated diseases. To our best of knowledge, no clinical data are present in literature regarding glutathionylated Hb in COC addicts.

In conclusion, we further retain that in studies concerning the evaluation of oxidative stress in drug abuse and clinical relevance of relative biomarkers it is important to take into account factors that could significantly influence both oxidative state and antioxidant defense. Physiological (e.g., age, gender, body weight, diet, and lifestyle) and pathologic factors (psychiatric comorbidity, cardiovascular and metabolic illnesses and their relative severity, etc.) as well as drug abuse history [age of onset, duration, polydrug abuse, tobacco smoking, alcohol use, and prevalence of current use (i.e., during last month)] could affect total oxidative state. Only early patient stratification based on their profile could help to identify the most appropriate panels of both diagnostic and prognostic biomarkers and conduct to optimal management for the patients.

6. Modulators of Oxidative Stress in Mitochondrial Protection: Future Direction

The use of antioxidants as therapeutic tools is still controversial [8, 144, 145]. In a recent review on potential use of modulators of OS in treatment of COC cardiotoxic effects, Graziani and coworkers [8] underlies that both preclinical and clinical data in literature has not yet been adduced to argue conclusive evidence.

However, the fundamental role of mitochondria in COC-induced OS strongly suggests that mitochondria-targeted intervention could become a pharmacological strategy to prevent and to treat this kind of damage. In Table 2, selective antioxidant compounds for potential therapeutic use in COC toxicity are reported.

In an experimental model of COC-induced cardiac dysfunction, *MitoQ* (mitoubiquinone) had shown to limit COC-induced left ventricular dysfunction [20]. Accordingly, in vitro studies [146, 147] of rat-stretched cardiomyocytes showed that MitoQ could prevent both mitochondrial damage and increase in XO activity and protect mitochondrial membrane potential. MitoQ is actually the most studied mitochondria-targeted antioxidant therapeutic compound [148] and some human studies have confirmed its efficacy in some cardiovascular pathologies, such as hypertension, and drug toxicity (alcohol, adriamycin) [47]. To our best of knowledge, no human studies are present in literature on the potential effects of MitoQ in treatment of COC-induced mitochondria toxicity.

On the basis of the abovementioned mechanisms of mitochondria dysfunction induced by COC, other therapeutic tools may be hypothesized.

The short-chain quinone *idebenone* has been also suggested to be beneficial in mitochondrial dysfunction [149] due to its antioxidant effects [150]. Idebenone proved to rescue ATP levels under conditions of impaired complex I transferring electron in mitochondrial respiratory chain from complex III [151]. The COC toxic effect of inhibition of the activity of mitochondrial complex I [33] may be reversed by some short-chain quinones. Consistent with this capacity of ATP activity rescue, idebenone should be investigated as a possible treatment for COC-induced dysfunction in mitochondrial respiratory chain [152].

In an experimental model of COC-induced diastolic dysfunction, XO activity inhibition by *allopurinol* [19] had preserved both left ventricular systolic and the decrease in ATP production, confirming the contribution of COC-induced mitochondrial ROS production in cardiac tissue. The protective role of allopurinol was confirmed in human and rat left ventricular (LV) myocytes with volume overload where the increase in ATP demand and the concurrent XO-mediated ROS can decrease mitochondrial respiration and contractile function [153] and in remodeling processes after experimental myocardial infarction [154]. To date, some clinical data appear to suggest that pharmacological XO inhibition could represent potential tools for the treatment of human cardiomyopathy [155]. The safety profile of (the old) allopurinol underlies the possibility of testing this XO inhibitor for further therapeutic interventions.

7. Conclusion

In the present paper, the role of cardiovascular mitochondria in COC-induced OS and ROS production was reported. Preclinical and clinical data underlie the fundamental participation of mitochondrial dysfunction to pathogenesis of COC-induced cardiovascular toxicity. As a consequence, possible biological peripheral markers of OS mitochondrial injury may be proposed. Both the antioxidant defense system biomarkers SOD2/MnSOD and glutathionylated Hb appear to be appropriate peripheral biomarkers of oxidative stress: since clinical data in COC and psychotropic drug users are inadequate to draw any conclusion, it could suggest that additional studies in this population subjects may be performed. Even in the case of potential therapeutic effects of mitochondrial protection, further studies on the proposed antioxidant drugs (MitoQ, idebenone, and allopurinol) will be crucial to assess their effectiveness or inability to counteract mitochondrial dysfunctions induced by cocaine.

Abbreviations

AA: Ascorbic acid
β-AR: β-Adrenergic receptors
BDNF: Brain-derived neurotrophic factor
CcOX: Cytochrome c oxidase
COC: Cocaine
$\Delta\Psi$: Mitochondrial membrane potential
eNOS: Endothelial NOS
ER: Endoplasmic/sarcoplasmic reticulum
eT: Electron transfer
GSH: Glutathione
Hb: Hemoglobin
H_2O_2: Hydrogen peroxide
HO·: Hydroxyl radical
HO: Heme oxygenase
iNOS: Inducible NOS
IMS: Intermembrane space
L-NAME: L-Nitroso-arginine methyl-ester
MAM: Mitochondrial-associated membranes
MAO: Monoamine oxidase
MDA: Malondialdehyde
MCU: Mitochondrial calcium uniporter
MICU1: Mitochondrial Ca^{2+} uptake 1
MICU2: Mitochondrial Ca^{2+} uptake 2
MitoQ: Mitoubiquinone
MPTP: Mitochondrial permeability transition pore
NAC: N-Acetylcysteine
nNOS: Neuronal NOS
NO·: Nitric oxide
Nox: NADPH oxidase
NMDA: N-Methyl-D-aspartate
NOS: NO synthase
$O_2^{-\cdot}$: Superoxide anion
OMM: Outer mitochondrial membrane
ONOO-: Peroxynitrite ion
OP: Oxypurinol
OS: Oxidative stress
OXPHOS: Oxidative phosphorylation
PKA: Protein kinase A
PMCA: Plasma membrane associated Ca^{2+} ATPase pump
RNS: Reactive nitrogen species
ROS: Reactive oxygen species
Sig-1R: Sigma-1 receptor site
SOCE: Store-operated calcium entry
SOD: Superoxide dismutase
TBARS: Thiobarbituric acid reactive substances
XO: Xanthine oxidase
EMRE: Essential MCU regulator
VDAC: Voltage-dependent anion channel
NCX: Potassium-independent Na^+/Ca^{2++} exchanger
NCKX: Potassium-dependent Na^+/Ca^{2++} exchanger
7-N: 7-Nitroindazole.

Conflicts of Interest

The authors declare that there is no conflict of interests regarding the publication of this paper.

References

[1] D. L. Coleman, T. F. Ross, and J. L. Naughton, "Myocardial ischemia and infarction related to recreational cocaine use," *The Western Journal of Medicine*, vol. 136, no. 5, pp. 444–446, 1982.

[2] R. Virmani, M. Robinowitz, J. E. Smialek, and D. F. Smyth, "Cardiovascular effects of cocaine: an autopsy study of 40 patients," *American Heart Journal*, vol. 115, no. 5, pp. 1068–1076, 1988.

[3] R. A. Lange, R. G. Cigarroa, C. W. Yancy Jr et al., "Cocaine-induced coronary-artery vasoconstriction," *The New England Journal of Medicine*, vol. 321, no. 23, pp. 1557–1562, 1989.

[4] S. Maraj, V. M. Figueredo, and D. Lynn Morris, "Cocaine and the heart," *Clinical Cardiology*, vol. 33, no. 5, pp. 264–269, 2010.

[5] J. E. Weber, C. R. Chudnofsky, M. Boczar, E. W. Boyer, M. D. Wilkerson, and J. E. Hollander, "Cocaine-associated chest pain: how common is myocardial infarction?" *Academic Emergency Medicine*, vol. 7, no. 8, pp. 873–877, 2000.

[6] R. Khan, S. Arshed, W. Jehangir, S. Sen, and A. Yousif, "Cocaine-induced delayed myocardial infarction complicated by apical thrombus," *Journal of Clinical Medicine Research*, vol. 8, no. 1, pp. 59–61, 2016.

[7] A. Sarkar, A. Pande, G. N. Chandra, and I. Ahmed, "Acute myocardial infarction in a young cocaine addict with normal coronaries: time to raise awareness among emergency physicians," *Indian Journal of Critical Care Medicine*, vol. 17, no. 1, pp. 56–58, 2013.

[8] M. Graziani, L. Antonilli, A. R. Togna, M. C. Grassi, A. Badiani, and L. Saso, "Cardiovascular and hepatic toxicity of cocaine: potential beneficial effects of modulators of oxidative stress," *Oxidative Medicine and Cellular Longevity*, vol. 2016, no. 33, p. 8408479, 2016.

[9] L. Liaudet, B. Calderari, and P. Pacher, "Pathophysiological mechanisms of catecholamine and cocaine-mediated cardiotoxicity," *Heart Failure Reviews*, vol. 19, no. 6, pp. 815–824, 2014.

[10] B. G. Schwartz, S. Rezkalla, and R. A. Kloner, "Cardiovascular effects of cocaine," *Circulation*, vol. 122, no. 24, pp. 2558–2569, 2010.

[11] D. Cerretani, V. Fineschi, S. Bello, I. Riezzo, E. Turillazzi, and M. Neri, "Role of oxidative stress in cocaine-induced cardiotoxicity and cocaine-related death," *Current Medicinal Chemistry*, vol. 19, no. 33, pp. 5619–5623, 2012.

[12] D. C. Andersson, J. Fauconnier, T. Yamada et al., "Mitochondrial production of reactive oxygen species contributes to the beta-adrenergic stimulation of mouse cardiomycytes," *The Journal of Physiology*, vol. 589, no. Pt 7, pp. 1791–1801, 2011.

[13] L. Xiao, D. R. Pimentel, J. Wang, K. Singh, W. S. Colucci, and D. B. Sawyer, "Role of reactive oxygen species and NAD(P)H oxidase in alpha(1)-adrenoceptor signaling in adult rat cardiac myocytes," *American Journal of Physiology. Cell Physiology*, vol. 282, no. 4, pp. C926–C934, 2002.

[14] V. M. Costa, R. Silva, L. M. Ferreira et al., "Oxidation process of adrenaline in freshly isolated rat cardiomyocytes: formation of adrenochrome, quinoproteins, and GSH adduct," *Chemical Research in Toxicology*, vol. 20, no. 8, pp. 1183–1191, 2007.

[15] M. Neri, D. Cerretani, A. I. Fiaschi et al., "Correlation between cardiac oxidative stress and myocardial pathology due to acute and chronic norepinephrine administration in

rats," *Journal of Cellular and Molecular Medicine*, vol. 11, no. 1, pp. 156–170, 2007.

[16] H. Pei, Y. Yang, H. Zhao et al., "The role of mitochondrial functional proteins in ROS production in ischemic heart diseases," *Oxidative Medicine and Cellular Longevity*, vol. 2016, p. 5470457, 2016.

[17] D. B. Zorov, C. R. Filburn, L. O. Klotz, J. L. Zweier, and S. J. Sollott, "Reactive oxygen species (ROS)-induced ROS release: a new phenomenon accompanying induction of the mitochondrial permeability transition in cardiac myocytes," *The Journal of Experimental Medicine*, vol. 192, no. 7, pp. 1001–1014, 2000.

[18] Z. V. Varga, P. Ferdinandy, L. Liaudet, and P. Pacher, "Drug-induced mitochondrial dysfunction and cardiotoxicity," *American Journal of Physiology. Heart and Circulatory Physiology*, vol. 309, no. 9, pp. H1453–H1467, 2015.

[19] A. Vergeade, P. Mulder, C. Vendeville, R. Ventura-Clapier, C. Thuillez, and C. Monteil, "Xanthine oxidase contributes to mitochondrial ROS generation in an experimental model of cocaine-induced diastolic dysfunction," *Journal of Cardiovascular Pharmacology*, vol. 60, no. 6, pp. 538–543, 2012.

[20] A. Vergeade, P. Mulder, C. Vendeville-Dehaudt et al., "Mitochondrial impairment contributes to cocaine-induced cardiac dysfunction: prevention by the targeted antioxidant MitoQ," *Free Radical Biology & Medicine*, vol. 49, no. 5, pp. 748–756, 2010.

[21] C. Yuan and D. Acosta Jr., "Cocaine-induced mitochondrial dysfunction in primary cultures of rat cardiomyocytes," *Toxicology*, vol. 112, no. 1, pp. 1–10, 1996.

[22] R. L. Grant and D. Acosta Jr., "A digitized fluorescence imaging study on the effects of local anesthetics on cytosolic calcium and mitochondrial membrane potential in cultured rabbit corneal epithelial cells," *Toxicology and Applied Pharmacology*, vol. 129, no. 1, pp. 23–35, 1994.

[23] F. Leon-Velarde, L. Huicho, and C. Monge, "Effects of cocaine on oxygen consumption and mitochondrial respiration in normoxic and hypoxic mice," *Life Sciences*, vol. 50, no. 3, pp. 213–218, 1992.

[24] B. G. Devi and A. W. Chan, "Impairment of mitochondrial respiration and electron transport chain enzymes during cocaine-induced hepatic injury," *Life Sciences*, vol. 60, no. 11, pp. 849–855, 1997.

[25] P. Mitchell, "Coupling of phosphorylation to electron and hydrogen transfer by a chemi-osmotic type of mechanism," *Nature*, vol. 191, no. 4784, pp. 144–148, 1961.

[26] R. A. Gottlieb and D. Bernstein, "Mitochondrial remodeling: rearranging, recycling, and reprogramming," *Cell Calcium*, vol. 60, no. 2, pp. 88–101, 2016.

[27] D. E. Green and A. Tzagoloff, "The mitochondrial electron transfer chain," *Archives of Biochemistry and Biophysics*, vol. 116, no. 1, pp. 293–304, 1966.

[28] C. R. Hackenbrock, B. Chazotte, and S. S. Gupte, "The random collision model and a critical assessment of diffusion and collision in mitochondrial electron transport," *Journal of Bioenergetics and Biomembranes*, vol. 18, no. 5, pp. 331–368, 1986.

[29] M. L. Genova and G. Lenaz, "Functional role of mitochondrial respiratory supercomplexes," *Biochimica et Biophysica Acta*, vol. 1837, no. 4, pp. 427–443, 2014.

[30] M. E. Dalmonte, E. Forte, M. L. Genova, A. Giuffrè, P. Sarti, and G. Lenaz, "Control of respiration by cytochrome c oxidase in intact cells: role of the membrane potential," *The Journal of Biological Chemistry*, vol. 284, no. 47, pp. 32331–32335, 2009.

[31] G. Lenaz and M. L. Genova, "Structure and organization of mitochondrial respiratory complexes: a new understanding of an old subject," *Antioxidants & Redox Signaling*, vol. 12, no. 8, pp. 961–1008, 2010.

[32] J. R. Friedman and J. Nunnari, "Mitochondrial form and function," *Nature*, vol. 505, no. 7483, pp. 335–343, 2014.

[33] C. Yuan and D. Acosta Jr., "Effect of cocaine on mitochondrial electron transport chain evaluated in primary cultures of neonatal rat myocardial cells and in isolated mitochondrial preparations," *Drug and Chemical Toxicology*, vol. 23, no. 2, pp. 339–348, 2000.

[34] R. J. Kaufman and J. D. Malhotra, "Calcium trafficking integrates endoplasmic reticulum function with mitochondrial bioenergetics," *Biochimica et Biophysica Acta*, vol. 1843, no. 10, pp. 2233–2239, 2014.

[35] M. Brini, T. Calì, D. Ottolini, and E. Carafoli, "Neuronal calcium signaling: function and dysfunction," *Cellular and Molecular Life Sciences*, vol. 71, no. 15, pp. 2787–2814, 2014.

[36] R. M. Case, D. Eisner, A. Gurney, O. Jones, S. Muallem, and A. Verkhratsky, "Evolution of calcium homeostasis: from birth of the first cell to an omnipresent signalling system," *Cell Calcium*, vol. 42, no. 4-5, pp. 345–350, 2007.

[37] P. Pinton, C. Giorgi, R. Siviero, E. Zecchini, and R. Rizzuto, "Calcium and apoptosis: ER-mitochondria Ca2+ transfer in the control of apoptosis," *Oncogene*, vol. 27, no. 50, pp. 6407–6418, 2008.

[38] A. Görlach, K. Bertram, S. Hudecova, and O. Krizanova, "Calcium and ROS: a mutual interplay," *Redox Biology*, vol. 6, pp. 260–271, 2015.

[39] M. J. Berridge, M. D. Bootman, and H. L. Roderick, "Calcium signalling: dynamics, homeostasis and remodelling," *Nature Reviews. Molecular Cell Biology*, vol. 4, no. 7, pp. 517–529, 2003.

[40] X. Tang, Y. X. Luo, H. Z. Chen, and D. P. Liu, "Mitochondria, endothelial cell function, and vascular diseases," *Frontiers in Physiology*, vol. 5, p. 175, 2014.

[41] S. Patergnani, J. M. Suski, C. Agnoletto et al., "Calcium signaling around mitochondria associated membranes (MAMs)," *Cell Communication and Signaling: CCS*, vol. 9, no. 1, p. 19, 2011.

[42] S. Marchi, S. Patergnani, and P. Pinton, "The endoplasmic reticulum-mitochondria connection: one touch, multiple functions," *Biochimica et Biophysica Acta*, vol. 1837, no. 4, pp. 461–469, 2014.

[43] M. Ahuja and S. Muallem, "The gatekeepers of mitochondrial calcium influx: MICU1 and MICU2," *EMBO Reports*, vol. 15, no. 3, pp. 205–206, 2014.

[44] D. Krizaj and D. R. Copenhagen, "Compartmentalization of calcium extrusion mechanisms in the outer and inner segments of photoreceptors," *Neuron*, vol. 21, no. 1, pp. 249–256, 1998.

[45] G. C. Brailoiu, E. Deliu, L. M. Console-Bram et al., "Cocaine inhibits store-operated Ca2+ entry in brain microvascular endothelial cells: critical role for sigma-1 receptors," *The Biochemical Journal*, vol. 473, no. 1, pp. 1–5, 2016.

[46] J. A. Rosado, "Sigma-1 receptors: a new pathway for the modulation of store-operated calcium entry," *The Biochemical Journal*, vol. 473, no. 3, pp. e9–e10, 2016.

[47] R. A. Smith and M. P. Murphy, "Animal and human studies with the mitochondria-targeted antioxidant MitoQ," *Annals of the new York Academy of Sciences*, vol. 1201, no. 1, pp. 96–103, 2010.

[48] G. Szabadkai and M. R. Duchen, "Mitochondria: The hub of cellular Ca2+ signaling," *Physiology (Bethesda)*, vol. 23, no. 2, pp. 84–94, 2008.

[49] I. Kruman, Q. Guo, and M. P. Mattson, "Calcium and reactive oxygen species mediate staurosporine-induced mitochondrial dysfunction and apoptosis in PC12 cells," *Journal of Neuroscience Research*, vol. 51, no. 3, pp. 293–308, 1998.

[50] K. Lynch, G. Fernandez, A. Pappalardo, and J. J. Peluso, "Basic fibroblast growth factor inhibits apoptosis of spontaneously immortalized granulosa cells by regulating intracellular free calcium levels through a protein kinase Cdelta-dependent pathway," *Endocrinology*, vol. 141, no. 11, pp. 4209–4217, 2000.

[51] S. Orrenius, B. Zhivotovsky, and P. Nicotera, "Regulation of cell death: the calcium-apoptosis link," *Nature Reviews. Molecular Cell Biology*, vol. 4, no. 7, pp. 552–565, 2003.

[52] B. Tombal, S. R. Denmeade, and J. T. Isaacs, "Assessment and validation of a microinjection method for kinetic analysis of [Ca2+]i in individual cells undergoing apoptosis," *Cell Calcium*, vol. 25, no. 1, pp. 19–28, 1999.

[53] R. B. Badisa, S. F. Darling-Reed, and C. B. Goodman, "Cocaine induces alterations in mitochondrial membrane potential and dual cell cycle arrest in rat c6 astroglioma cells," *Neurochemical Research*, vol. 35, no. 2, pp. 288–297, 2010.

[54] P. Sarti, A. Giuffrè, M. C. Barone, E. Forte, D. Mastronicola, and M. Brunori, "Nitric oxide and cytochrome oxidase: reaction mechanisms from the enzyme to the cell," *Free Radical Biology & Medicine*, vol. 34, no. 5, pp. 509–520, 2003.

[55] D. Mastronicola, E. Arcuri, M. Arese et al., "Morphine but not fentanyl and methadone affects mitochondrial membrane potential by inducing nitric oxide release in glioma cells," *Cellular and Molecular Life Sciences*, vol. 61, no. 23, pp. 2991–2997, 2004.

[56] M. Arese, M. C. Magnifico, D. Mastronicola et al., "Nanomolar melatonin enhances nNOS expression and controls HaCaT-cells bioenergetics," *IUBMB Life*, vol. 64, no. 3, pp. 251–258, 2012.

[57] P. Sarti, E. Forte, A. Giuffre, D. Mastronicola, M. C. Magnifico, and M. Arese, "The chemical interplay between nitric oxide and mitochondrial cytochrome c oxidase: reactions, effectors and pathophysiology," *International Journal of Cell Biology*, vol. 2012, p. 571067, 2012.

[58] P. Pacher, J. S. Beckman, and L. Liaudet, "Nitric oxide and peroxynitrite in health and disease," *Physiological Reviews*, vol. 87, no. 1, pp. 315–424, 2007.

[59] G. C. Brown and A. Vilalta, "How microglia kill neurons," *Brain Research*, vol. 1628, no. Pt B, pp. 288–297, 2015.

[60] A. Galkin and S. Moncada, "S-nitrosation of mitochondrial complex I depends on its structural conformation," *The Journal of Biological Chemistry*, vol. 282, no. 52, pp. 37448–37453, 2007.

[61] D. J. Stuehr and C. F. Nathan, "Nitric oxide. A macrophage product responsible for cytostasis and respiratory inhibition in tumor target cells," *The Journal of Experimental Medicine*, vol. 169, no. 5, pp. 1543–1555, 1989.

[62] P. I. Ortinski, "Cocaine-induced changes in NMDA receptor signaling," *Molecular Neurobiology*, vol. 50, no. 2, pp. 494–506, 2014.

[63] P. Sarti, E. Lendaro, R. Ippoliti, A. Bellelli, P. A. Benedetti, and M. Brunori, "Modulation of mitochondrial respiration by nitric oxide: investigation by single cell fluorescence microscopy," *The FASEB Journal*, vol. 13, no. 1, pp. 191–197, 1999.

[64] C. N. Hall and J. Garthwaite, "What is the real physiological NO concentration in vivo?" *Nitric Oxide*, vol. 21, no. 2, pp. 92–103, 2009.

[65] J. O. Lundberg, E. Weitzberg, and M. T. Gladwin, "The nitrate-nitrite-nitric oxide pathway in physiology and therapeutics," *Nature Reviews. Drug Discovery*, vol. 7, no. 2, pp. 156–167, 2008.

[66] Y. Itzhak, "Modulation of the PCP/NMDA receptor complex and sigma binding sites by psychostimulants," *Neurotoxicology and Teratology*, vol. 16, no. 4, pp. 363–368, 1994.

[67] Y. Itzhak, "Attenuation of cocaine kindling by 7-nitroindazole, an inhibitor of brain nitric oxide synthase," *Neuropharmacology*, vol. 35, no. 8, pp. 1065–1073, 1996.

[68] M. A. Balda, K. L. Anderson, and Y. Itzhak, "Adolescent and adult responsiveness to the incentive value of cocaine reward in mice: role of neuronal nitric oxide synthase (nNOS) gene," *Neuropharmacology*, vol. 51, no. 2, pp. 341–349, 2006.

[69] F. J. Nasif, X. T. Hu, O. A. Ramirez, and M. F. Perez, "Inhibition of neuronal nitric oxide synthase prevents alterations in medial prefrontal cortex excitability induced by repeated cocaine administration," *Psychopharmacology*, vol. 218, no. 2, pp. 323–330, 2011.

[70] S. Liddie, M. A. Balda, and Y. Itzhak, "Nitric oxide (NO) signaling as a potential therapeutic modality against psychostimulants," *Current Pharmaceutical Design*, vol. 19, no. 40, pp. 7092–7102, 2013.

[71] A. Frustaci, M. A. Russo, E. Morgante et al., "Oxidative myocardial damage in human cocaine-related cardiomyopathy," *European Journal of Heart Failure*, vol. 17, no. 3, pp. 283–290, 2015.

[72] V. Vitcheva, R. Simeonova, M. Kondeva-Burdina, and M. Mitcheva, "Selective nitric oxide synthase inhibitor 7-nitroindazole protects against cocaine-induced oxidative stress in rat brain," *Oxidative Medicine and Cellular Longevity*, vol. 2015, p. 157876, 2015.

[73] A. Masini, D. Gallesi, F. Giovannini, T. Trenti, and D. Ceccarelli, "Membrane potential of hepatic mitochondria after acute cocaine administration in rats—the role of mitochondrial reduced glutathione," *Hepatology*, vol. 25, no. 2, pp. 385–390, 1997.

[74] N. D. Volkow, J. S. Fowler, A. P. Wolf et al., "Distribution and kinetics of carbon-11-cocaine in the human body measured with PET," *Journal of Nuclear Medicine*, vol. 33, no. 4, pp. 521–525, 1992.

[75] M. Portugal-Cohen, R. Numa, R. Yaka, and R. Kohen, "Cocaine induces oxidative damage to skin via xanthine oxidase and nitric oxide synthase," *Journal of Dermatological Science*, vol. 58, no. 2, pp. 105–112, 2010.

[76] P. Kovacic, "Unifying mechanism for bacterial cell signalers (4,5-dihydroxy-2,3-pentanedione, lactones and oligopeptides): electron transfer and reactive oxygen species. Practical medical features," *Medical Hypotheses*, vol. 69, no. 5, pp. 1105–1110, 2007.

[77] C. M. Liou, S. C. Tsai, C. H. Kuo, H. Ting, and S. D. Lee, "Cardiac Fas-dependent and mitochondria-dependent apoptosis after chronic cocaine abuse," *International Journal of Molecular Sciences*, vol. 15, no. 4, pp. 5988–6001, 2014.

[78] B. J. Borkowski, Y. Cheema, A. U. Shahbaz, S. K. Bhattacharya, and K. T. Weber, "Cation dyshomeostasis and cardiomyocyte necrosis: the Fleckenstein hypothesis revisited," *European Heart Journal*, vol. 32, no. 15, pp. 1846–1853, 2011.

[79] D. M. Bers, "Cardiac excitation-contraction coupling," *Nature*, vol. 415, no. 6868, pp. 198–205, 2002.

[80] J. J. Lemasters, T. Qian, C. A. Bradham et al., "Mitochondrial dysfunction in the pathogenesis of necrotic and apoptotic cell death," *Journal of Bioenergetics and Biomembranes*, vol. 31, no. 4, pp. 305–319, 1999.

[81] M. U. Khan, Y. Cheema, A. U. Shahbaz et al., "Mitochondria play a central role in nonischemic cardiomyocyte necrosis: common to acute and chronic stressor states," *Pflügers Archiv*, vol. 464, no. 1, pp. 123–131, 2012.

[82] A. I. Tarasov, E. J. Griffiths, and G. A. Rutter, "Regulation of ATP production by mitochondrial Ca(2+)," *Cell Calcium*, vol. 52, no. 1, pp. 28–35, 2012.

[83] T. Cunha-Oliveira, L. Silva, A. M. Silva, A. J. Moreno, C. R. Oliveira, and M. S. Santos, "Mitochondrial complex I dysfunction induced by cocaine and cocaine plus morphine in brain and liver mitochondria," *Toxicology Letters*, vol. 219, no. 3, pp. 298–306, 2013.

[84] A. G. Fantel, C. V. Barber, M. B. Carda, R. W. Tumbic, and B. Mackler, "Studies of the role of ischemia/reperfusion and superoxide anion radical production in the teratogenicity of cocaine," *Teratology*, vol. 46, no. 3, pp. 293–300, 1992.

[85] Q. Chen, A. K. Camara, D. F. Stowe, C. L. Hoppel, and E. J. Lesnefsky, "Modulation of electron transport protects cardiac mitochondria and decreases myocardial injury during ischemia and reperfusion," *American Journal of Physiology. Cell Physiology*, vol. 292, no. 1, pp. C137–C147, 2007.

[86] A. Remondino, S. H. Kwon, C. Communal et al., "Beta-adrenergic receptor-stimulated apoptosis in cardiac myocytes is mediated by reactive oxygen species/c-Jun NH2-terminal kinase-dependent activation of the mitochondrial pathway," *Circulation Research*, vol. 92, no. 2, pp. 136–138, 2003.

[87] Y. Xiao, J. He, R. D. Gilbert, and L. Zhang, "Cocaine induces apoptosis in fetal myocardial cells through a mitochondria-dependent pathway," *The Journal of Pharmacology and Experimental Therapeutics*, vol. 292, no. 1, pp. 8–14, 2000.

[88] J. He, Y. Xiao, C. A. Casiano, and L. Zhang, "Role of mitochondrial cytochrome c in cocaine-induced apoptosis in coronary artery endothelial cells," *The Journal of Pharmacology and Experimental Therapeutics*, vol. 295, no. 3, pp. 896–903, 2000.

[89] M. Alvaro-Bartolome, R. La Harpe, L. F. Callado, J. J. Meana, and J. A. García-Sevilla, "Molecular adaptations of apoptotic pathways and signaling partners in the cerebral cortex of human cocaine addicts and cocaine-treated rats," *Neuroscience*, vol. 196, pp. 1–15, 2011.

[90] A. J. Kowaltowski, N. C. de Souza-Pinto, R. F. Castilho, and A. E. Vercesi, "Mitochondria and reactive oxygen species," *Free Radical Biology & Medicine*, vol. 47, no. 4, pp. 333–343, 2009.

[91] D. B. Zorov, M. Juhaszova, and S. J. Sollott, "Mitochondrial reactive oxygen species (ROS) and ROS-induced ROS release," *Physiological Reviews*, vol. 94, no. 3, pp. 909–950, 2014.

[92] D. B. Zorov, M. Juhaszova, and S. J. Sollott, "Mitochondrial ROS-induced ROS release: an update and review," *Biochimica et Biophysica Acta*, vol. 1757, no. 5-6, pp. 509–517, 2006.

[93] V. M. Costa, F. Carvalho, M. L. Bastos, R. A. Carvalho, M. Carvalho, and F. Remiao, "Contribution of catecholamine reactive intermediates and oxidative stress to the pathologic features of heart diseases," *Current Medicinal Chemistry*, vol. 18, no. 15, pp. 2272–2314, 2011.

[94] A. Bindoli, M. P. Rigobello, and D. J. Deeble, "Biochemical and toxicological properties of the oxidation products of catecholamines," *Free Radical Biology & Medicine*, vol. 13, no. 4, pp. 391–405, 1992.

[95] A. Bindoli, D. J. Deeble, M. P. Rigobello, and L. Galzigna, "Direct and respiratory chain-mediated redox cycling of adrenochrome," *Biochimica et Biophysica Acta*, vol. 1016, no. 3, pp. 349–356, 1990.

[96] G. S. Behonick, M. J. Novak, E. W. Nealley, and S. I. Baskin, "Toxicology update: the cardiotoxicity of the oxidative stress metabolites of catecholamines (aminochromes)," *Journal of Applied Toxicology*, vol. 21, Suppl 1, pp. S15–S22, 2001.

[97] M. L. Genova, N. M. Abd-Elsalam, M. E. El Sayed et al., "Redox cycling of adrenaline and adrenochrome catalysed by mitochondrial complex I," *Archives of Biochemistry and Biophysics*, vol. 447, no. 2, pp. 167–173, 2006.

[98] G. M. Taam, S. Takeo, A. Ziegelhoffer, P. K. Singal, R. E. Beamish, and N. S. Dhalla, "Effect of adrenochrome on adenine nucleotides and mitochondrial oxidative phosphorylation in rat heart," *The Canadian Journal of Cardiology*, vol. 2, no. 2, pp. 88–93, 1986.

[99] N. Kaludercic, J. Mialet-Perez, N. Paolocci, A. Parini, and F. Di Lisa, "Monoamine oxidases as sources of oxidants in the heart," *Journal of Molecular and Cellular Cardiology*, vol. 73, pp. 34–42, 2014.

[100] H. C. Stanton and A. Schwartz, "Effects of a hydrazine monoamine oxidase inhibitor (phenelzine) on isoproterenol-induced myocardiopathies in the rat," *The Journal of Pharmacology and Experimental Therapeutics*, vol. 157, no. 3, pp. 649–658, 1967.

[101] M. Isabelle, C. Monteil, F. Moritz et al., "Role of alpha1-adrenoreceptors in cocaine-induced NADPH oxidase expression and cardiac dysfunction," *Cardiovascular Research*, vol. 67, no. 4, pp. 699–704, 2005.

[102] M. Isabelle, A. Vergeade, F. Moritz et al., "NADPH oxidase inhibition prevents cocaine-induced up-regulation of xanthine oxidoreductase and cardiac dysfunction," *Journal of Molecular and Cellular Cardiology*, vol. 42, no. 2, pp. 326–332, 2007.

[103] E. Barth, G. Stämmler, B. Speiser, and J. Schaper, "Ultrastructural quantitation of mitochondria and myofilaments in cardiac muscle from 10 different animal species including man," *Journal of Molecular and Cellular Cardiology*, vol. 24, no. 7, pp. 669–681, 1992.

[104] S. M. Davidson, "Endothelial mitochondria and heart disease," *Cardiovascular Research*, vol. 88, no. 1, pp. 58–66, 2010.

[105] S. Serpillon, B. C. Floyd, R. S. Gupte et al., "Superoxide production by NAD(P)H oxidase and mitochondria is increased in genetically obese and hyperglycemic rat heart and aorta before the development of cardiac dysfunction. The role of glucose-6-phosphate dehydrogenase-derived NADPH," *American Journal of Physiology. Heart and Circulatory Physiology*, vol. 297, no. 1, pp. H153–H162, 2009.

[106] R. M. Lebovitz, H. Zhang, H. Vogel et al., "Neurodegeneration, myocardial injury, and perinatal death in mitochondrial superoxide dismutase-deficient mice," *Proceedings of the National Academy of Sciences of the United States of America*, vol. 93, no. 18, pp. 9782–9787, 1996.

[107] D. N. Granger and P. R. Kvietys, "Reperfusion injury and reactive oxygen species: the evolution of a concept," *Redox Biology*, vol. 6, pp. 524–551, 2015.

[108] J. M. McCord, R. S. Roy, and S. W. Schaffer, "Free radicals and myocardial ischemia. The role of xanthine oxidase," *Advances in Myocardiology*, vol. 5, pp. 183–189, 1985.

[109] S. Baldus, K. Müllerleile, P. Chumley et al., "Inhibition of xanthine oxidase improves myocardial contractility in patients with ischemic cardiomyopathy," *Free Radical Biology & Medicine*, vol. 41, no. 8, pp. 1282–1288, 2006.

[110] J. Frijhoff, P. G. Winyard, N. Zarkovic et al., "Clinical relevance of biomarkers of oxidative stress," *Antioxidants & Redox Signaling*, vol. 23, no. 14, pp. 1144–1170, 2015.

[111] WHO, *Biomarkers in Risk Assessment: Validity and Validation*, WHO, Geneva, Switzerland, 2001.

[112] H. Solhi, A. Malekirad, A. Mohammad Kazemifar, and F. Sharifi, "Oxidative stress and lipid peroxidation in prolonged users of methamphetamine," *Drug Metabolism Letters*, vol. 7, no. 2, pp. 79–82, 2014.

[113] J. S. Womersley and J. D. Uys, "S-Glutathionylation and redox protein signaling in drug addiction," *Progress in Molecular Biology and Translational Science*, vol. 137, pp. 87–121, 2016.

[114] J. A. Hernandez, R. C. Lopez-Sanchez, and A. Rendon-Ramirez, "Lipids and oxidative stress associated with ethanol-induced neurological damage," *Oxidative Medicine and Cellular Longevity*, vol. 2016, p. 1543809, 2016.

[115] T. A. Zima, L. Fialová, O. Mestek et al., "Oxidative stress, metabolism of ethanol and alcohol-related diseases," *Journal of Biomedical Science*, vol. 8, no. 1, pp. 59–70, 2001.

[116] M. C. Huang, C. H. Chen, F. C. Peng, S. H. Tang, and C. C. Chen, "Alterations in oxidative stress status during early alcohol withdrawal in alcoholic patients," *Journal of the Formosan Medical Association*, vol. 108, no. 7, pp. 560–569, 2009.

[117] A. O. Sordi, F. Pechansky, F. H. Kessler et al., "Oxidative stress and BDNF as possible markers for the severity of crack cocaine use in early withdrawal," *Psychopharmacology*, vol. 231, no. 20, pp. 4031–4039, 2014.

[118] D. Del Rio, A. J. Stewart, and N. Pellegrini, "A review of recent studies on malondialdehyde as toxic molecule and biological marker of oxidative stress," *Nutrition, Metabolism, and Cardiovascular Diseases*, vol. 15, no. 4, pp. 316–328, 2005.

[119] E. Niki, "Lipid peroxidation products as oxidative stress biomarkers," *BioFactors*, vol. 34, no. 2, pp. 171–180, 2008.

[120] L. Pomierny-Chamioło, A. Moniczewski, K. Wydra, A. Suder, and M. Filip, "Oxidative stress biomarkers in some rat brain structures and peripheral organs underwent cocaine," *Neurotoxicity Research*, vol. 23, no. 1, pp. 92–102, 2013.

[121] V. Fineschi, G. Baroldi, F. Centini et al., "Markers of cardiac oxidative stress and altered morphology after intraperitoneal cocaine injection in a rat model," *International Journal of Legal Medicine*, vol. 114, no. 6, pp. 323–330, 2001.

[122] F. Moritz, C. Monteil, M. Isabelle et al., "Role of reactive oxygen species in cocaine-induced cardiac dysfunction," *Cardiovascular Research*, vol. 59, no. 4, pp. 834–843, 2003.

[123] J. Walker, T. Winhusen, J. M. Storkson et al., "Total antioxidant capacity is significantly lower in cocaine-dependent and methamphetamine-dependent patients relative to normal controls: results from a preliminary study," *Human Psychopharmacology*, vol. 29, no. 6, pp. 537–543, 2014.

[124] F. Freitas, N. Brucker, J. Durgante et al., "Urinary 1-hydroxypyrene is associated with oxidative stress and inflammatory biomarkers in acute myocardial infarction," *International Journal of Environmental Research and Public Health*, vol. 11, no. 9, pp. 9024–9037, 2014.

[125] I. L. Megson, S. J. Haw, D. E. Newby, and J. P. Pell, "Association between exposure to environmental tobacco smoke and biomarkers of oxidative stress among patients hospitalised with acute myocardial infarction," *PLoS One*, vol. 8, no. 12, article e81209, 2013.

[126] C. C. de Farias, M. Maes, K. L. Bonifácio et al., "Highly specific changes in antioxidant levels and lipid peroxidation in Parkinson's disease and its progression: disease and staging biomarkers and new drug targets," *Neuroscience Letters*, vol. 617, pp. 66–71, 2016.

[127] M. Schrag, C. Mueller, M. Zabel et al., "Oxidative stress in blood in Alzheimer's disease and mild cognitive impairment: a meta-analysis," *Neurobiology of Disease*, vol. 59, pp. 100–110, 2013.

[128] J. C. Narvaez, P. V. Magalhães, G. R. Fries et al., "Peripheral toxicity in crack cocaine use disorders," *Neuroscience Letters*, vol. 544, pp. 80–84, 2013.

[129] J. C. Narvaez, P. V. Magalhães, G. R. Fries et al., "Repeated exposure to cocaine differently modulates BDNF mRNA and protein levels in rat striatum and prefrontal cortex," *The European Journal of Neuroscience*, vol. 26, no. 10, pp. 2756–2763, 2007.

[130] X. Y. Zhang, D. C. Chen, Y. L. Tan et al., "The interplay between BDNF and oxidative stress in chronic schizophrenia," *Psychoneuroendocrinology*, vol. 51, pp. 201–208, 2015.

[131] R. Pacifici, A. I. Fiaschi, L. Micheli et al., "Immunosuppression and oxidative stress induced by acute and chronic exposure to cocaine in rat," *International Immunopharmacology*, vol. 3, no. 4, pp. 581–592, 2003.

[132] C. He, P. C. Hart, D. Germain, and M. G. Bonini, "SOD2 and the mitochondrial UPR: partners regulating cellular phenotypic transitions," *Trends in Biochemical Sciences*, vol. 41, no. 7, pp. 568–577, 2016.

[133] I. N. Zelko, T. J. Mariani, and R. J. Folz, "Superoxide dismutase multigene family: a comparison of the CuZn-SOD (SOD1), Mn-SOD (SOD2), and EC-SOD (SOD3) gene structures, evolution, and expression," *Free Radical Biology & Medicine*, vol. 33, no. 3, pp. 337–349, 2002.

[134] A. Y. Andreyev, Y. E. Kushnareva, and A. A. Starkov, "Mitochondrial metabolism of reactive oxygen species," *Biochemistry (Mosc)*, vol. 70, no. 2, pp. 200–214, 2005.

[135] M. Che, R. Wang, X. Li, H. Y. Wang, and X. S. Zheng, "Expanding roles of superoxide dismutases in cell regulation and cancer," *Drug Discovery Today*, vol. 21, no. 1, pp. 143–149, 2016.

[136] S. L. Marklund, "Extracellular superoxide dismutase in human tissues and human cell lines," *The Journal of Clinical Investigation*, vol. 74, no. 4, pp. 1398–1403, 1984.

[137] A. Okado-Matsumoto and I. Fridovich, "Subcellular distribution of superoxide dismutases (SOD) in rat liver: Cu,Zn-SOD in mitochondria," *The Journal of Biological Chemistry*, vol. 276, no. 42, pp. 38388–38393, 2001.

[138] R. López-Pedrajas, D. T. Ramírez-Lamelas, B. Muriach et al., "Cocaine promotes oxidative stress and microglial-macrophage activation in rat cerebellum," *Frontiers in Cellular Neuroscience*, vol. 9, p. 279, 2015.

[139] J. D. Uys, L. Knackstedt, P. Hurt et al., "Cocaine-induced adaptations in cellular redox balance contributes to enduring behavioral plasticity," *Neuropsychopharmacology*, vol. 36, no. 12, pp. 2551–2560, 2011.

[140] P. Ghezzi, "Protein glutathionylation in health and disease," *Biochimica et Biophysica Acta*, vol. 1830, no. 5, pp. 3165–3172, 2013.

[141] W. A. Kleinman, D. Komninou, Y. Leutzinger et al., "Protein glutathiolation in human blood," *Biochemical Pharmacology*, vol. 65, no. 5, pp. 741–746, 2003.

[142] H. J. Chen, W. P. Lin, S. D. Chiu, and C. H. Fan, "Multistage mass spectrometric analysis of human hemoglobin glutathionylation: correlation with cigarette smoking," *Chemical Research in Toxicology*, vol. 27, no. 5, pp. 864–872, 2014.

[143] J. E. Muscat, W. Kleinman, S. Colosimo et al., "Enhanced protein glutathiolation and oxidative stress in cigarette smokers," *Free Radical Biology & Medicine*, vol. 36, no. 4, pp. 464–470, 2004.

[144] O. Firuzi, R. Miri, M. Tavakkoli, and L. Saso, "Antioxidant therapy: current status and future prospects," *Current Medicinal Chemistry*, vol. 18, no. 25, pp. 3871–3888, 2011.

[145] L. Saso and O. Firuzi, "Pharmacological applications of antioxidants: lights and shadows," *Current Drug Targets*, vol. 15, no. 13, pp. 1177–1199, 2014.

[146] J. D. Gladden, B. R. Zelickson, C. C. Wei et al., "Novel insights into interactions between mitochondria and xanthine oxidase in acute cardiac volume overload," *Free Radical Biology & Medicine*, vol. 51, no. 11, pp. 1975–1984, 2011.

[147] D. M. Yancey, J. L. Guichard, M. I. Ahmed et al., "Cardiomyocyte mitochondrial oxidative stress and cytoskeletal breakdown in the heart with a primary volume overload," *American Journal of Physiology. Heart and Circulatory Physiology*, vol. 308, no. 6, pp. H651–H663, 2015.

[148] R. A. Smith and M. P. Murphy, "Mitochondria-targeted antioxidants as therapies," *Discovery Medicine*, vol. 11, no. 57, pp. 106–114, 2011.

[149] M. Erb, B. Hoffmann-Enger, H. Deppe et al., "Features of idebenone and related short-chain quinones that rescue ATP levels under conditions of impaired mitochondrial complex I," *PLoS One*, vol. 7, no. 4, article e36153, 2012.

[150] A. Mordente, G. E. Martorana, G. Minotti, and B. Giardina, "Antioxidant properties of 2,3-dimethoxy-5-methyl-6-(10-hydroxydecyl)-1,4-benzoquinone (idebenone)," *Chemical Research in Toxicology*, vol. 11, no. 1, pp. 54–63, 1998.

[151] V. Giorgio, V. Petronilli, A. Ghelli et al., "The effects of idebenone on mitochondrial bioenergetics," *Biochimica et Biophysica Acta*, vol. 1817, no. 2, pp. 363–369, 2011.

[152] A. Sadakierska-Chudy, M. Frankowska, and M. Filip, "Mitoepigenetics and drug addiction," *Pharmacology & Therapeutics*, vol. 144, no. 2, pp. 226–233, 2014.

[153] J. D. Gladden, B. R. Zelickson, J. L. Guichard et al., "Xanthine oxidase inhibition preserves left ventricular systolic but not diastolic function in cardiac volume overload," *American Journal of Physiology. Heart and Circulatory Physiology*, vol. 305, no. 10, pp. H1440–H1450, 2013.

[154] N. Engberding, S. Spiekermann, A. Schaefer et al., "Allopurinol attenuates left ventricular remodeling and dysfunction after experimental myocardial infarction: a new action for an old drug?" *Circulation*, vol. 110, no. 15, pp. 2175–2179, 2004.

[155] T. P. Cappola, D. A. Kass, G. S. Nelson et al., "Allopurinol improves myocardial efficiency in patients with idiopathic dilated cardiomyopathy," *Circulation*, vol. 104, no. 20, pp. 2407–2411, 2001.

Hindawi
Oxidative Medicine and Cellular Longevity
Volume 2017, Article ID 9808520, 13 pages
https://doi.org/10.1155/2017/9808520

Research Article

Cytoprotective Mechanisms Mediated by Polyphenols from Chilean Native Berries against Free Radical-Induced Damage on AGS Cells

Felipe Ávila,[1] Cristina Theoduloz,[2] Camilo López-Alarcón,[3] Eva Dorta,[3] and Guillermo Schmeda-Hirschmann[4]

[1]*Escuela de Nutrición y Dietética, Facultad de Ciencias de la Salud, Universidad de Talca, 3460000 Talca, Chile*
[2]*Laboratorio de Cultivo Celular, Facultad de Ciencias de la Salud, Universidad de Talca, 3460000 Talca, Chile*
[3]*Departamento de Química Física, Facultad de Química, Pontificia Universidad Católica de Chile, 7820436 Santiago, Chile*
[4]*Laboratorio de Química de Productos Naturales, Instituto de Química de Recursos Naturales, Universidad de Talca, 3460000 Talca, Chile*

Correspondence should be addressed to Felipe Ávila; favilac@utalca.cl

Received 16 November 2016; Revised 1 March 2017; Accepted 16 March 2017; Published 2 May 2017

Academic Editor: Luciano Saso

The prevalence of cytoprotective mechanisms induced by polyphenols such as activation of intracellular antioxidant responses (ICM) and direct free radical scavenging was investigated in native Chilean species of strawberries, raspberries, and currants. Human gastric epithelial cells were co- and preincubated with polyphenolic-enriched extracts (PEEs) from Chilean raspberries (*Rubus geoides*), strawberries (*Fragaria chiloensis* ssp. *chiloensis* f. *chiloensis*), and currants (*Ribes magellanicum*) and challenged with peroxyl and hydroxyl radicals. Cellular protection was determined in terms of cell viability, glyoxalase I and glutathione s-transferases activities, and carboxymethyl lysine (CML) and malondialdehyde levels. Our results indicate that cytoprotection induced by ICM was the prevalent mechanism for *Rubus geoides* and *F. chiloensis*. This agreed with increased levels of glyoxalase I and glutathione S-transferase activities in cells preincubated with PEEs. ORAC index indicated that *F. chiloensis* was the most efficient peroxyl radical scavenger. Moreover, ICM mediated by *F. chiloensis* was effective in protecting cells from CML accumulation in contrast to the protective effects induced by free radical scavenging. Our results indicate that although both polyphenol-mediated mechanisms can exert protective effects, ICM was the most prevalent in AGS cells. These results suggest a potential use of these native berries as functional food.

1. Introduction

Oxidative stress has been implied in the etiology of numerous diseases as well as in the ageing process [1–3]. The balance established in terms of the relative amounts of antioxidants and reactive species (reactive oxygen and nitrogen species and electrophilic molecules) plays a pivotal role in the cellular integrity and functionality [4]. Antioxidants and reactive species can have an exogenous or endogenous origin, dietary intake being the most important source of exogenous antioxidants [5]. It has been suggested that the intake of dietary antioxidants is inversely associated with the development of chronic diseases, which currently constitute the main cause of mortality worldwide [6]. In fact, dietary interventions in humans, as well as in vitro studies, have shown evidence regarding the beneficial effects on the health related to the consumption of berries [7]. These effects have been mainly attributed to their content of polyphenols, which can protect biological systems against the damage induced by numerous agents, including free radicals [8, 9]. Cellular protection mediated by polyphenols against free radical-induced damage can be exerted by different mechanisms, including scavenging of free radicals by direct reactions, metal ion complexation with a consequent inhibition of the free radicals generated through Fenton-type reactions, and activation of the intracellular signaling cascades

that result in activation of detoxifying enzymes or repression of pro-oxidant proteins [10–12]. In addition, during the last years, it has been suggested that, under physiological conditions and in vivo, the main protective mechanism associated with polyphenols arising from dietary sources involves activation of transcription factors that regulate the expression and activity of antioxidant and detoxifying systems in cells [12]. This concept agrees with the relative low bioavailability of polyphenols (implying very low systemic concentrations) and would explain the lack of correlation between their in vitro antioxidant capacity and their protective effects on cellular cultures (which imply cellular responses) [10].

On the other hand, human gastric epithelial cells are constantly exposed to an oxidative environment produced by the intake of reactive species (generated during thermal processing of foods) as well as by the oxidative reactions that take place during the processes associated with food digestion [13]. These cells are also exposed to polyphenols arising from foods, which have not been previously metabolized by the liver or colonic microflora [14]. In this sense, gastric epithelial cells constitute a unique model in which different mechanisms of cytoprotection mediated by polyphenols could be active. The human gastric adenocarcinoma cell line (AGS) consists of mucus-secreting epithelial cells presenting several characteristics of normal gastric epithelial cells and a good power of differentiation [15]. For this reason, they have been widely used to evaluate the antioxidant activity of several lentil cultivars [9, 16]. In fact, we have recently reported that polyphenolic-enriched extracts (PEEs) from Chilean native berries, including *Rubus geoides* and *Ribes magellanicum* (Figure S1 in Supplementary Material available online at https://doi.org/10.1155/2017/9808520), present a significant cytoprotective activity against H_2O_2 and methylglyoxal-induced damage of AGS cells [16]. The Chilean native berries selected for this study are wild relatives of the widely cultivated and consumed strawberries, raspberries, and currants. The PEEs of these species have also shown a high scavenging capacity of stable free radicals such as DPPH and ABTS [9, 16]. However, evidence aiming to elucidate the main mechanisms involved in the protection of gastric human cells mediated by polyphenols against the damage inflicted by free radicals is lacking.

It has been reported that numerous polyphenols are able to activate transcription factors including the nuclear factor-erythroid 2 p45 (Nrf2) [17, 18], which is involved in the control of the expression of detoxifying enzymes such as glutathione S-transferases [19] and glyoxalase I [20], inducing protective effects against oxidative stress [21]. Cellular activation of Nrf2 and the subsequent expression of detoxifying enzymes have shown to occur in a period of hours, and consequently, most responses associated to intracellular antioxidant response activation involves 16–24 hours of incubations [9, 22]. Such time frame contrasts with the kinetic of reactions between free radicals and polyphenols which typically involves rate constants in the range of $10^9\,M^{-1}\,s^{-1}$ (towards hydroxyl radicals) [11] to $10^3\,M^{-1}\,s^{-1}$ (towards superoxide radical anion) [23].

To get more insights regarding the protection afforded by polyphenols from the South American relatives of commercial berries on AGS cells exposed to a free radical source, in the present work, we have addressed studies aimed to assess the cytoprotective mechanisms mediated by the polyphenols contained in the Chilean native raspberry *Rubus geoides*, the native currant *Ribes magellanicum*, and the Chilean strawberry *Fragaria chiloensis* ssp. *chiloensis* f. *chiloensis*.

2. Materials and Methods

2.1. Chemicals. 2,2′-Azobis(2-methyl-propionamidine) dihydrochloride (AAPH), copper sulphate, Chelex® 100 sodium, quercetin, thiobarbituric acid, trichloroacetic acid, Amberlite XAD-7, sodium bicarbonate, methylglyoxal, glutathione (reduced form), 1-chloro-2,4-dinitrobenzene (CDNB), L-glutamine, and CelLytic™ M were purchased from Sigma-Aldrich (St. Louis, MO, USA). Pierce™ BCA Protein Assay Kit was obtained from Thermo Scientific (Rockford, IL, USA). Hydrogen peroxide (30%), HCl, methanol, and formic acid were purchased from Merck (Darmstadt, Germany). MTT was obtained from Calbiochem (Darmstadt, Germany). Fetal bovine serum (FBS), antibiotics, and culture media were purchased from Invitrogen (Grand Island, New York, USA). Ultrapure water was obtained using a Barnstead EasyPure water filter system (Thermo Scientific, Dubuque, IA, USA).

2.2. Polyphenolic-Enriched Extracts (PEEs). The Chilean berries included two collections from the native raspberry *Rubus geoides*, one of them from southern Chile (Las Raices) and the second one from Tierra del Fuego, Patagonia (Lago Blanco), the native currant *Ribes magellanicum* from Araucanía, southern Chile, and the Chilean strawberry *Fragaria chiloensis* ssp. *chiloensis* f. *chiloensis* was cultivated in central Chile (Figure S1). The study was performed with the polyphenolic-enriched extracts (PEEs) of the fruits. The PEEs were obtained according to the methodology previously reported [9, 24–26]. Briefly, the fruits were homogenized and extracted with a MeOH : formic acid 99 : 1 (*v*/*v*) mixture and the solution was taken to dryness under reduced pressure. The extract was resuspended in water and loaded on a preconditioned Amberlite XAD-7 resin. The resin was washed with distilled water, and the polyphenols were desorbed with MeOH to afford after concentration under reduced pressure and lyophilization of the phenolic-enriched extracts (PEEs). The chemical characterization of the PEEs has been reported as follows: *Ribes magellanicum* [16, 24], *Rubus geoides* [9], and *Fragaria chiloensis* ssp. *chiloensis* f. *chiloensis* [25, 26].

2.3. AGS Cell Culture. Human epithelial gastric cells (AGS) (ATCC CRL-1739) were grown as monolayers in HAM F-12 medium containing 1 mM L-glutamine and 1.5 g/L sodium bicarbonate, supplemented with 10% FBS, 100 IU/mL penicillin, and 100 μg/mL streptomycin. Cells were grown in a humidified incubator with 5% CO_2 in air at 37°C. For the subsequent experiments, cells were plated at a density of 2.5×10^4 cells/mL.

2.4. Cell Viability Determination. Cell viability was determined by means of the MTT reduction assay [15].

Cytoprotection against free radical-induced damage was assessed by coincubation and preincubation models, according to the procedure described next. All the analyses were performed according to the following common procedures: untreated cells were used as 100% viability controls. Cells coincubated or preincubated with quercetin (6 μg/mL) were used as positive controls [27]. Cells treated with the free radicals served as damage controls. Each concentration was tested in quintuplicate, and experiments were repeated two times using different cell preparations. Results are expressed as percentage of the 100% viability control.

2.4.1. Coincubation Model (Free Radical Scavenging). Confluent cultures of AGS cells were coincubated during 30 min or 60 min with the free radicals (see Section 2.5) together with different final concentrations of the PEEs as follows. For *R. geoides* and *R. magellanicum*, the concentrations are as follows: 0, 15.6, 31.3, 62.5, and 125 μg/mL; for *F. chiloensis*: 0, 7.8, 15.6, 31.3, and 62.5 μg/mL. The PEEs and the free radical sources were prepared freshly in a medium without antibiotics or FBS. At the end of the stress induction, the medium was removed by vacuum aspiration and replaced by complete medium (containing 10% of FBS). Cells were left to recover for 24 hours and cell viability was determined.

2.4.2. Preincubation Model (Intracellular Antioxidant Responses). Confluent cultures of AGS cells were preincubated during 16 h with different concentrations of the PEEs as described in Section 2.4.1. The extracts were dissolved in complete medium supplemented with 2% FBS. At the end of the incubation, culture medium was completely removed by vacuum aspiration. Then, the cells were submitted to the free radical-induced stress (see Section 2.5) using the radical sources freshly prepared in a medium without antibiotics or FBS. After the stress induction, the medium was removed by vacuum aspiration and replaced by complete medium (containing 10% of FBS). Cells were left to recover for 24 hours and cell viability was determined.

2.4.3. Challenge with Hydroxyl Radical. Hydroxyl radicals were generated through a Fenton-type reaction [28]. Cell culture medium (HAM-F12), without FBS or antibiotics, was pretreated with Chelex to decrease the concentration of trace metals that could be present in the media. For cell viability analyses, the reaction was generated with different concentrations of hydrogen peroxide (0.5, 1, 1.5, and 2 mM) and different concentrations of $CuSO_4$ (ranging from 0.2 μM to 410 μM). Controls incubated only with $CuSO_4$ or hydrogen peroxide were also performed. Confluent cells were co- or preincubated with the different PEEs during 30 minutes at 37°C. Cells were left to recover incubating with complete medium (containing 10% of FBS) during 24 hours, and the effects were determined by means of MTT analysis according to the procedure described in Section 2.4.

2.4.4. Peroxyl Radicals. Peroxyl radicals were generated by the thermal decomposition of 2,2′-azobis(2-methylpropionamidine) dihydrochloride (AAPH) [29]. Cell culture medium (HAM-F12), without FBS or antibiotics, was pretreated with Chelex. The cytotoxicity elicited by peroxyl radicals was evaluated, incubating during 60 minutes confluent AGS cells with different concentrations of AAPH (0.78 to 400 mM). Then, the solution was removed and cells were left to recover during 24 hours with FBS at 10%. Cell viability analyses were performed according to the procedure described in Section 2.4.

2.5. Enzymatic Activity Determination. AGS cells were seeded in 75 cm^2 culture flasks until confluence. Then, cells were co- or preincubated (see Sections 2.4.1 and 2.4.2) with the PPEs from the selected species as follows: *R. geoides* (Las Raices) 62.5 μg/mL, *R. geoides* (Lago Blanco) 125 μg/mL, *R. magellanicum* 31.3 μg/mL, and *F. chiloensis* 62.5 μg/mL. At the end of the experiments, cells were collected using a cell scraper. Cells were centrifuged at 3500 rpm during 10 minutes to remove the culture medium. The pellet was kept at −80°C until analyses. On the day of the corresponding analysis, cells were lysed by adding 100 μL of CelLytic and debris was removed by centrifugation at 10,000 rpm during 10 minutes. Protein concentration was determined by means of the bicinchoninic acid (BCA) method [30].

2.5.1. Glutathione S-Transferases. The enzymatic activity of glutathione S-transferases (GST) was quantified according to the method of Habig and Jakoby [31]. The reaction mixture of 1 mL included 1 mM of 1-chloro-2,4-dinitrobenzene (CDNB), 1 mM of reduced glutathione, and 15 μg of protein from treated cell extracts in 100 mM phosphate buffer pH 6.5. The reaction was initiated by the addition of the cell extract, and it was monitored by following the rate of the formation of the adduct glutathione-DNB (GS-DNB) at 340 nm. The initial rates were obtained from the slopes of plots of GS-DNB concentration (using an extinction coefficient of 0.0096 $\mu M^{-1}\,cm^{-1}$ at 340 nm) against time. The GST activity was expressed as a percentage, considering 100% as the slope of the controls (cells treated with medium only).

2.5.2. Glyoxalase I (GLOI). The enzymatic activity of glyoxalase I was determined spectrophotometrically, according to the protocol of Thornalley, with minor modifications [32]. Methylglyoxal (2 mM) was incubated during 5 minutes with reduced glutathione (2 mM) at pH 6.6 and 25 ± 2°C to produce a hemithioacetal by a nonenzymatic reaction. Then, 30 μg of cellular protein extract was added and the increase in the absorbance due to S-D-lactoylglutathione formation was registered at 240 nm ($\varepsilon_{240} = 2.86\,mM^{-1}\,cm^{-1}$). The activities were assessed determining the initial rates of the S-D-lactoylglutathione formation. The GLOI activity was expressed as a percentage, considering 100% as the slope of the controls (cells treated with medium only).

2.6. Oxygen Radical Absorbance Capacity (ORAC). Fluorescein- and pyrogallol red-based ORAC assays (ORAC-FL and ORAC-PGR) were determined according to Cao et al. [29] and Lopez-Alarcón and Lissi [33], respectively. A reaction mixture containing fluorescein (FL, 70 nM final concentration) or pyrogallol red (PGR, 5 μM final concentration) was prepared in phosphate buffer (75 mM, pH 7.4), with or without the PEEs (50 μg/mL, final concentration). The fluorescence (FL, $\lambda_{em} = 515$ nm; $\lambda_{ex} = 493$ nm) or the absorbance

(PGR, $\lambda = 540$ nm) decay was measured using a multimode microplate reader (Synergy HTX; Biotek Instruments, Winooski, VT, USA). Stock solutions of the PEEs were prepared in ethanol at 5 mg/mL. The solutions were preincubated for 30 min at 37°C. The AAPH solution (10 mM final concentration) was added and the fluorescence (F) or absorbance (A) were registered every 30 s for 180 min. Data were plotted as F/F_0 or A/A_0 as a function of time. The area under the curve (AUC) of F/F_0 or A/A_0 was calculated. Plots and integration data were obtained using MicroCal Origin® 7.0 software (Boston, MA, USA). AUC data were used to obtain ORAC values, according to the equation described next. All experiments were carried out in triplicate.

$$\text{ORAC} = \frac{[\text{AUC} - \text{AUC}^0]}{[\text{AUC}_{\text{Trolox}} - \text{AUC}^0]} f[\text{Trolox}], \quad (1)$$

where AUC corresponds to the experiments performed in the presence of the tested samples, integrating between time zero and the time corresponding to 80% of FL or PGR consumption; AUC^0 corresponds to control experiments (in the absence of samples); $\text{AUC}_{\text{Trolox}}$ corresponds to experiments in the presence of Trolox; f is the dilution factor (ratio between the final volume of the AAPH-FL or AAPH-PGR solutions and the added sample volume); and [Trolox] is the Trolox concentration (mM).

2.7. Thiobarbituric Acid Reactive Species (TBAR) Determination. The TBAR determination was carried out according to [34]. Briefly, a mixture of 20% (*w*/*v*) trichloroacetic acid and 0.8% (*w*/*v*) thiobarbituric acid was prepared in 0.25 N HCl (color reagent). The PEE from *F. chiloensis* (62.5 μg/mL) was selected for this assay. Cells were grown until confluence in 5 cm diameter Petri dishes (19.6 cm^2), treated under both schemes of co- and preincubations with the PEE, and challenged with AAPH 168 mM during 1 h. At the end of the incubation, the medium was removed by vacuum aspiration. One mL of the color reagent was added and cells were scrapped-off immediately and homogenized. Samples were quantitatively transferred into a glass vial and hermetically sealed with a vial crimper (Chromatography Research Supplies, USA) and then boiled during 45 min. Samples were allowed to cool-down to room temperature and centrifuged at 10,000 rpm for 10 min. The absorbance of the supernatant was measured at 535 nm, and the MDA concentration was calculated using the molar extinction coefficient of the MDA-TBA_2 complex of $1.49 \times 10^5\ \text{M}^{-1}\,\text{cm}^{-1}$. The results were expressed as nmol of MDA/mg of protein. Additional control plates with AGS cells were cultivated simultaneously to determine the protein concentration.

2.8. Carboxymethyl Lysine Determination. The PEE from *F. chiloensis* (62.5 μg/mL) was added to a confluent culture of cells grown in 75 cm^2 culture flasks. Cells were treated under both schemes of co- and preincubations with the PEE and challenged with AAPH 168 mM during 1 h. Then, the medium was removed by vacuum aspiration and cells were left to recover for 24 h with complete medium. At the end of the incubation, the medium was removed by vacuum aspiration and cells were scrapped-off in PBS. Cells were centrifuged at 3500 rpm for 10 min, and the pellet was resuspended in CelLytic. Protein concentration was determined by the BCA method [30]. Twenty μg of each sample was boiled for 5 minutes in Laemmli sample buffer and loaded onto 12% (*w*/*v*) SDS-PAGE gels. Electrophoresis was performed at 100 V for 1-2 hours. Then, proteins were electrotransferred onto a Hybond nitrocellulose membrane (GE Healthcare) during 1 h at 100 V. The membrane was blocked with PBS containing 1% BSA and 0.1% Tween 20. Membranes were incubated with anti-CML primary antibody, at a dilution of 1/1000, and washed 3 times with PBS and then incubated with HRP-conjugated secondary antibody. Membranes were revealed with the ECL. Signal intensities were quantified with ImageJ software (NIH).

2.9. Statistical Analysis. Statistical differences between different treatments and their respective control were determined by one-way analysis of variance (ANOVA) followed by Dunnett's multiple comparison test. The level of significance was set at $P < 0.05$. All statistical analyses were carried out using the software SPSS 14.0 for Windows (IBM, Armonk, NY, USA).

3. Results

The ability of polyphenols from Chilean native berries to protect AGS cells against free radical-induced damage was assessed using two different approaches, namely, activation of intracellular antioxidant mechanisms and direct free radical scavenging. The former was assessed by preincubating AGS cells with PPEs during 16 hours and subsequently (after washing cycles) exposing the cells to a challenge by free radical source. In the case of the studies about the free radical scavenging and/or metal-chelating activity of PPEs, AGS cells were simultaneously incubated with each PEE and the free radical sources (coincubation). The protective effects were evaluated using two different sources of free radicals: AAPH and $\text{H}_2\text{O}_2/\text{CuSO}_4$ (Fenton-type reaction).

In the absence of a free radical source, viability of AGS cells was not affected by pre- or coincubations with the different PPEs (15–125 μg/mL) (data not shown). But, in the absence of PPEs, when AGS cells were exposed to different doses of free radicals generated by thermal decomposition of AAPH, cell viability showed an IC_{50} value of 168 mM. Figure 1 shows the cellular viability for AGS cells challenged with AAPH (168 mM) and the protective effects of coincubations and preincubations with quercetin (positive control) or PEEs from the Chilean native berries *R. geoides*, *R. magellanicum*, and *F. chiloensis*. The addition of different concentrations of all the extracts (co- and preincubated) to AGS cell cultures induced a statistically significant cytoprotection ($P < 0.05$) against the challenge with AAPH-derived peroxyl radicals (Figures 1(a), 1(b), 1(c), and 1(d)). The Chilean strawberry *Fragaria chiloensis* was the most efficient species against free radical damage induced by AAPH, considering that its cytoprotective activity was exerted at lower concentrations of the PEEs (Figures 1(a) and 1(c)).

Figure S2 shows the effect of different concentrations of Cu^{2+} (added as CuSO_4) in cell viability in the presence and

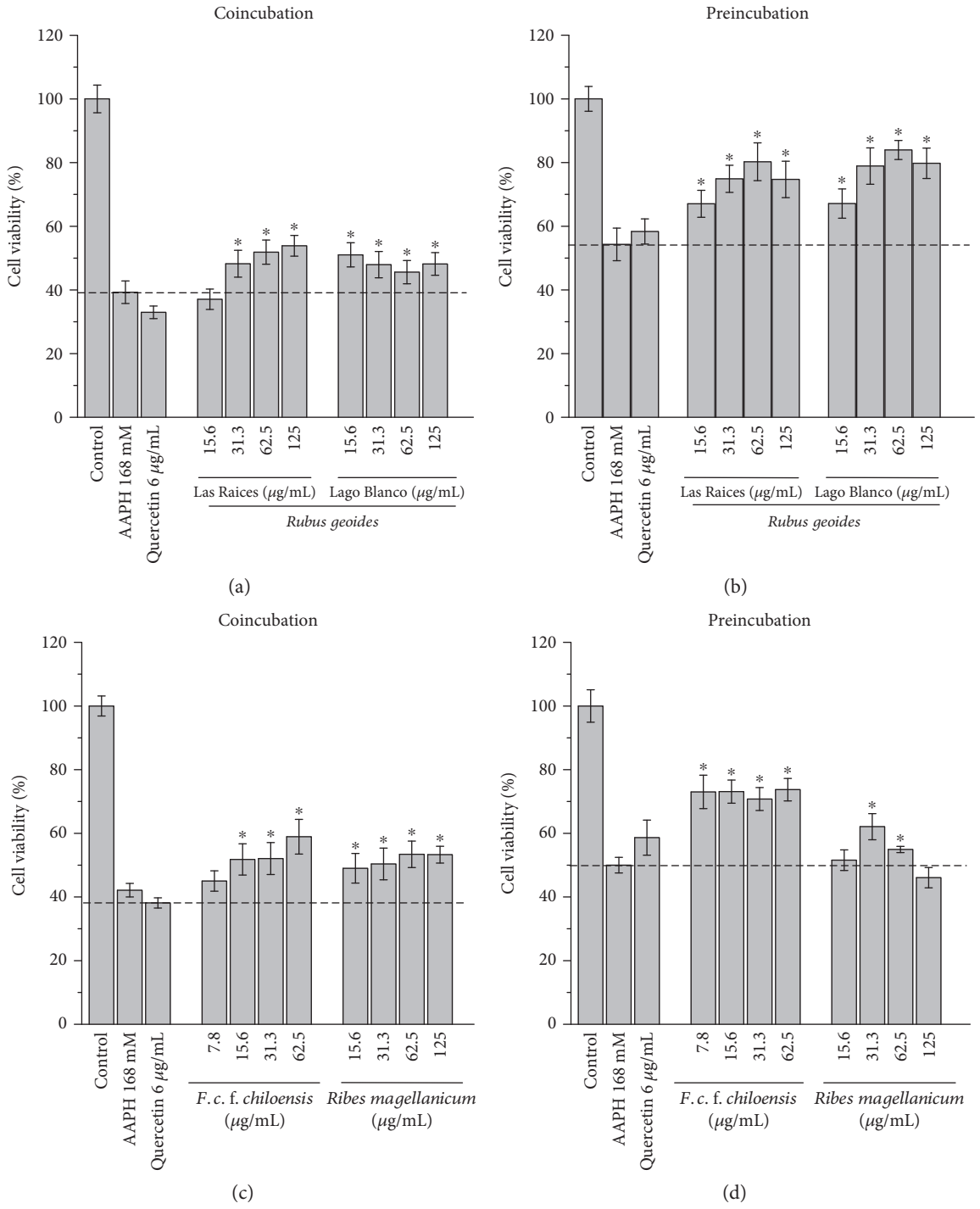

Figure 1: Effects of the PEEs on cell viability of AGS cells challenged with peroxyl radicals (AAPH, 168 mM). (a) Cytoprotective effects of the PEEs from *R. geoides* (Las Raices and Lago Blanco) in the coincubation model. (b) Cytoprotective effects of the PEEs from *R. geoides* (Las Raices and Lago Blanco) in the preincubation model. (c) Cytoprotective effects of the PEEs from *F. chiloensis* and *R. magellanicum* in the coincubation model. (d) Cytoprotective effects of the PEEs from *F. chiloensis* and *R. magellanicum* in the preincubation model.

absence of H_2O_2 (1.5 mM). It was found that, in the absence of H_2O_2, Cu^{2+} at 410 μM did not affect the cell viability. However, in the presence of H_2O_2, cell viability decreased to 54.3 ± 6.6% (Figure S2). On the other hand, 1.5 mM H_2O_2 (in the absence of Cu^{2+}) decreased cell viability by 14.3 ± 4% (data not shown). Figure 2 shows that $H_2O_2 + Cu^{2+}$ induce a significant decrease in the cell viability compared to the H_2O_2 controls (in the absence of Cu^{2+}). Therefore, cytotoxic effects induced by $H_2O_2 + Cu^{2+}$ can be attributed not only to free radicals but also in less degree to H_2O_2. Figures 2(a), 2(b), 2(c), and 2(d) show the protective effects of co- and preincubations with PEEs from *R. geoides*, *R. magellanicum*, and *F.*

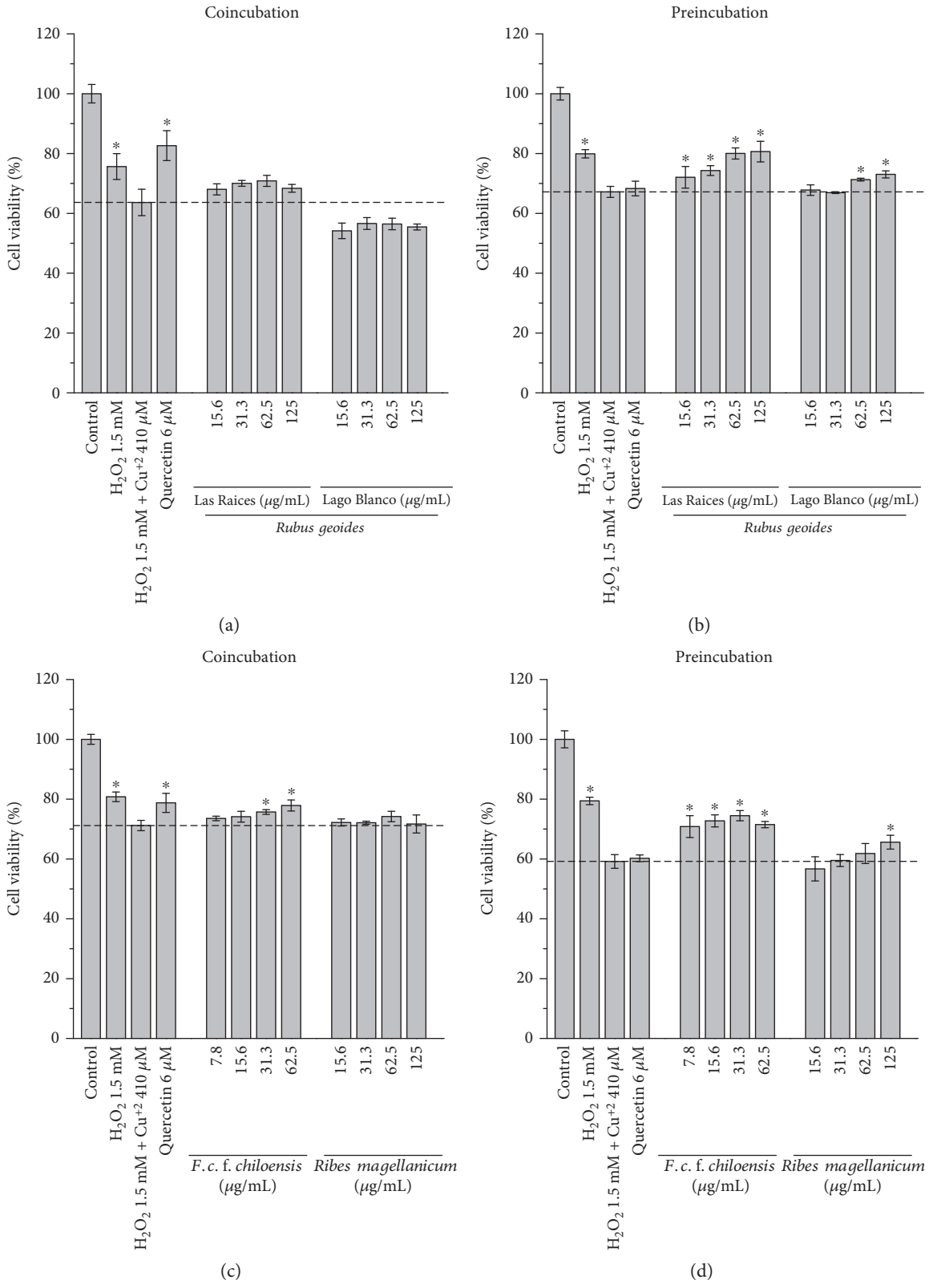

Figure 2: Effects of the PEEs in cell viability of AGS cells challenged with H_2O_2 (1.5 mM) + Cu^{2+} (410 μM). (a) Cytoprotective effects of the PEEs from *Rubus geoides* (Las Raices and Lago Blanco) in the coincubation model. (b) Cytoprotective effects of the PEEs from *R. geoides* (Las Raices and Lago Blanco) in the preincubation model. (c) Cytoprotective effects of the PEEs from *Fragaria chiloensis* and *Ribes magellanicum* in the coincubation model. (d) Cytoprotective effects of the PEEs from *F. chiloensis* and *R. magellanicum* in the preincubation model.

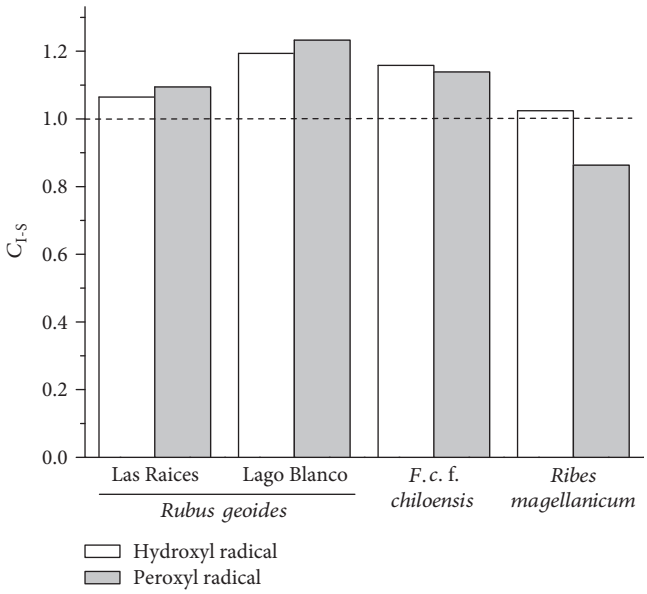

Figure 3: Ratio between normalized areas of cell viability plots for AGS cells preincubated with the PEEs over normalized area of AGS cells coincubated with PEEs and challenged with peroxyl radicals (AAPH, 168 mM) and hydroxyl radicals (H_2O_2, 1.5 mM + Cu^{2+}, 410 μM).

chiloensis against the damage induced by free radicals generated from the redox couple $H_2O_2 + Cu^{2+}$. The positive control quercetin induced significant cytoprotection in the coincubation model, but not in the preincubation conditions (Figure 2). The protective effect of all the PEEs against the damage induced by $H_2O_2 + Cu^{2+}$ was more efficient in the preincubation model than in the coincubation model. In the *F. chiloensis*, PEE presented a significant protection in the model of coincubation. To determine the prevalence of the cytoprotective mechanisms, the area under the curve was calculated using the cell viability plots against the different concentrations of the PEEs. The area under the curve was calculated by normalizing the ratio of the cell viability over cytotoxicity induced by the stressor agent. We defined the coefficient $C_{I\text{-}S}$ (intracellular-scavenging) as the area under the curve of the protective effects induced by intracellular antioxidant mechanisms over the area under the curve of protective effects induced by extracellular scavenging. Therefore, when $C_{I\text{-}S} = 1$, cytoprotective effects of intracellular antioxidant mechanisms will be the same as that of direct scavenging; when $C_{I\text{-}S} < 1$, cytoprotective effects of scavenging will prevail over those exerted by intracellular activation; and when $C_{I\text{-}S} > 1$, cytoprotective effects of intracellular activation will prevail over those exerted by a direct scavenging of free radicals (or chelating effect on Cu^{2+}). Figure 3 shows the ratio $C_{I\text{-}S}$ obtained by the analysis of the protection of the different PEEs against damage mediated by AAPH and $H_2O_2 + Cu^{2+}$. It can be observed that for hydroxyl radicals the prevalent cytoprotective mechanism was the intracellular activation of antioxidant responses. This fact was also observed when peroxyl radicals were used as the stressor agent, except with the native currant *R. magellanicum*. In this case, the prevalent mechanism was the free radical scavenging.

To verify the differences in both cytoprotective mechanisms induced by pre- and coincubations, the enzymatic activities of Nrf2-regulated enzymes were determined for both models with the PEEs without free radical challenge. Glutathione S-transferases and glyoxalase I activities were quantified after 30 minutes of incubation (coincubation model) or after 16 hours of incubation (preincubation model) in AGS cells. The concentrations were chosen considering (1) the most effective ones for the protection against peroxyl radicals and (2) those concentrations that presented statistically significant protection with both incubation models. Figure 4(a) shows that *R. geoides* (Las Raices and Lago Blanco samples) did not present significant differences with the control, whereas *F. chiloensis* and *R. magellanicum* presented a decrease of 25.2% and 34.5%, respectively, in the activities of glutathione S-transferases after coincubation. Figure 4(c) shows that coincubation with *R. magellanicum* and *R. geoides* (Las Raices and Lago Blanco) decreases significantly the activity of glyoxalase I by 38.2, 15.8, and 21.9%, respectively. Coincubation with *F. chiloensis* did not present significant differences when compared with the control. Figures 4(b) and 4(c) show that preincubation of AGS cells with all PEEs elicits a significant increase in the activity of the enzymes glutathione S-transferase and glyoxalase I compared with the control.

With the aim to determine the effectiveness of each PEEs in the free radical scavenging process, in vitro assays were performed by means of the ORAC methods, using fluorescein and pyrogallol red as the target molecules. ORAC fluorescein (ORAC-FL) provides information about the stoichiometry of the reaction between the free radicals produced by AAPH thermal decomposition, and ORAC red pyrogallol (ORAC-PGR) indicates the reactivity of a sample towards such free radicals. Table 1 depicts that the order of the antioxidant capacity of all the PEEs was the same in both methods, however, showing higher differences in the PGR-based methodology. The efficiency in the free radical scavenging was *F. chiloensis* > *R. magellanicum* > *Rubus* (Lago Blanco sample) > *Rubus* (Las Raices sample) (Table 1). *Fragaria chiloensis* was selected to perform further analyses considering its better efficiency to induce cytoprotection through intracellular antioxidant mechanisms and free radical scavenging.

The protective effects exerted by polyphenols from *F. chiloensis* in AGS cells in the co- and preincubation models challenged with AAPH (168 mM) were assessed using markers of oxidative stress such as the advanced glycation end product carboxymethyl lysine (CML) in proteins and thiobarbituric acid reactive substances (TBARs). Representative blots of CML under the different treatments described before are shown in Figure 5. The panel C displays a densitometric analysis of CML levels detected by immunochemical means (Figure 5). A slight increase of $4.3 \pm 0.4\%$ and $10.3 \pm 0.2\%$ in the CML levels was observed for samples incubated with peroxyl radicals for coincubation and preincubation, respectively, when compared to control experiments. On the other hand,

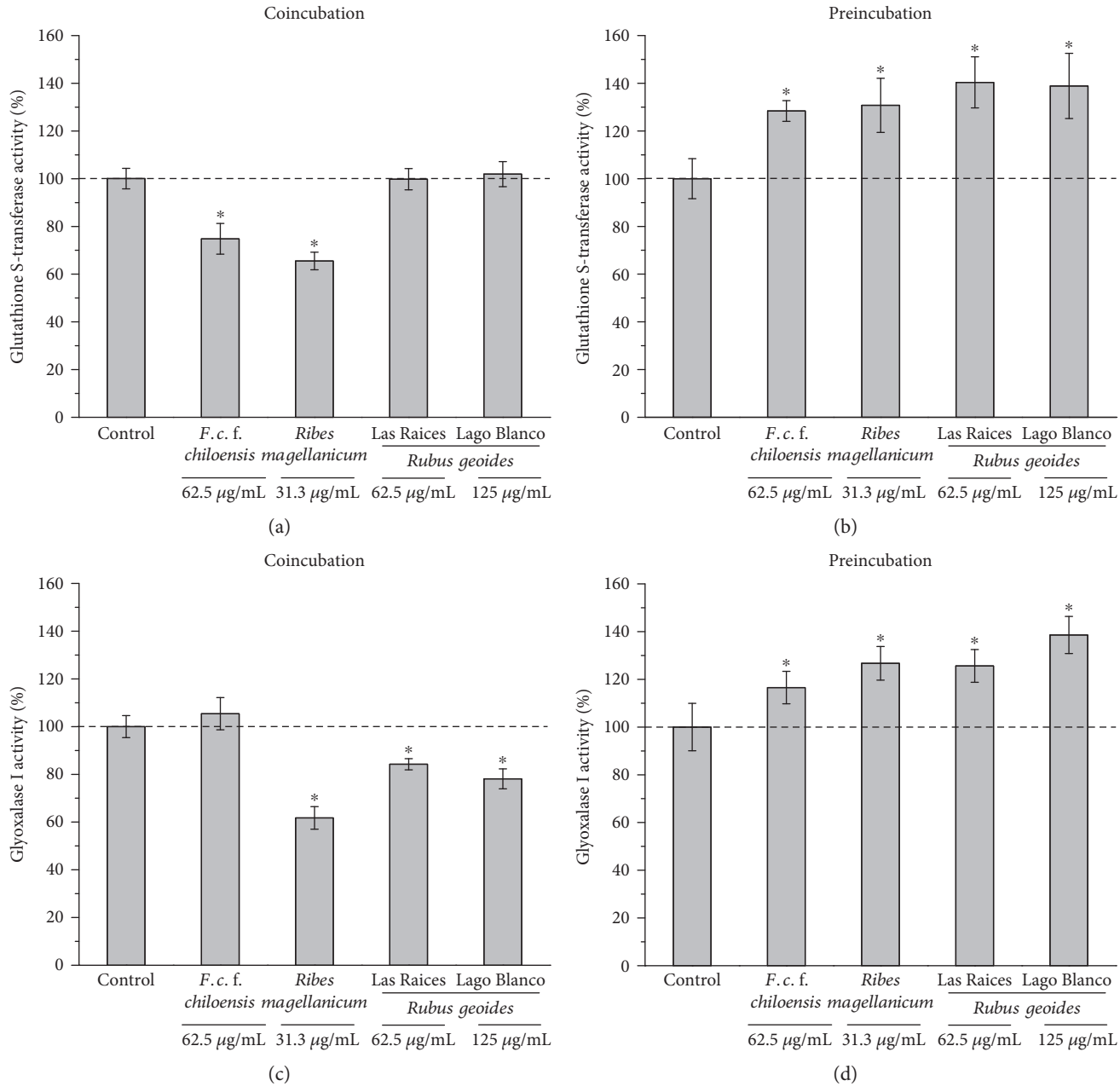

Figure 4: Effects of the PEEs in the enzymatic activity of glutathione S-transferases and glyoxalase I in AGS cells. (a) Glutathione S-transferase activity after coincubation of AGS with PEEs. (b) Glutathione S-transferase activity after preincubation of AGS cells with PEEs. (c) Glyoxalase I activity after coincubation of AGS with PEEs. (d) Glyoxalase I activity after preincubation of AGS with PEEs.

we have only detected a significant decrease of CML levels in cells preincubated with the PEE from *F. chiloensis*. The levels of CML decrease in $20.9 \pm 2.7\%$ and $31.2 \pm 4.9\%$ when compared with the untreated and AAPH controls, respectively.

Figures 5(d) and 5(e) show the TBAR levels in AGS cells exposed to peroxyl radicals and submitted to co- and preincubation with the PEE from *F. chiloensis*. Figure 5(d) presents an increase of 358.7% in the levels of MDA when AGS cells were coincubated with the free radicals only. On the other hand, when cells were coincubated with the PEE, the increase in MDA was only 95%. The inhibition of the MDA levels induced by the PEE in the model of coincubation was statistically significant when compared with the peroxyl radical control ($P < 0.05$).

In the presence of AAPH, when cells were treated employing the preincubation model, in comparison with control experiments, an increase of 178.8% in the MDA levels was observed (Figure 5(e)). When AGS cells were preincubated with the PEE and posteriorly challenged with AAPH-derived peroxyl radicals, an increment of 171.2% was observed (Figure 5(e)). Therefore, employing the preincubation approach, no significant decrease in the MDA levels was detected in the presence of PEEs.

Table 1: Oxygen radical absorbance capacity (ORAC) of polyphenolic-enriched extracts from the selected native species using as free radical target fluorescein (FL) and red pirogallol (PGR).

Sample	ORAC-FL (mmol TE[a]/L)	ORAC-PGR (mmol TE[a]/L)
Rubus geoides (Las Raices)	4.26 ± 0.2	1.99 ± 0.4
Rubus geoides (Lago Blanco)	4.36 ± 0.4	3.55 ± 0.3
Fragaria chiloensis	7.16 ± 0.1	10.56 ± 1.1
Ribes magellanicum	5.11 ± 0.7	7.19 ± 0.1

[a]Trolox equivalents.

4. Discussion

It has been established that one of the main sites of the biological action of polyphenols is the stomach [35]. For instance, polyphenols from coffee and red wine can exert their antioxidant effects at the stomach cavity during postprandial processes decreasing the levels of plasmatic malondialdehyde [36–38]. On the other hand, lipid peroxidation reactions produced during digestion are favored due to the acidic environment of the stomach [13]. This fact could increase the potential damage mediated by free radicals, which have been proposed to play a relevant role in numerous diseases including stomach ulcers and cancer [39]. Polyphenols can induce protective effects against free radical-induced damage by multiple mechanisms including metal-ion complexation, free radical scavenging, and activation of intracellular detoxifying mechanisms [40, 41]. However, the prevalence of the protective mechanisms induced by polyphenols in epithelial gastric human cells has been poorly understood.

In this work, we assessed the prevalence of protective mechanisms mediated by polyphenols against the damage induced by free radicals generated by the redox couple $H_2O_2 + Cu^{2+}$ and thermal decomposition of AAPH, which produce hydroxyl [28] and peroxyl radicals [29], respectively.

Considering that free radical scavenging occurs typically in seconds (lifetime of peroxyl radicals in tissues has been estimated to be 7 s) [42] and the activation of intracellular protective mechanisms comprises several hours [43], we have hypothesized that coincubations of AGS cells with the PEEs and the free radical sources might reflect protective effects by a direct free radical scavenging and/or metal chelation reactions. On the other hand, preincubations (16 h) of cells with the PEEs and a subsequent challenge with free radicals would indicate protective effects mediated by intracellular antioxidant mechanisms.

Cell viability of AGS cells pre- and coincubated with the different PEEs and exposed to AAPH-derived peroxyl radicals indicates that both mechanisms can induce significant protective effects (Figure 1). This fact agrees with numerous reports as well as with the bimolecular rate constants for the reactions between peroxyl radicals and linoleic acid or peroxyl radicals and chlorogenic acid ($1 \cdot 10^2\,M^{-1}\,s^{-1}$ and $1.28 \cdot 10^5\,M^{-1}\,s^{-1}$, resp.) [23]. This allows the possibility of competitive reactions between cell components, such as membrane lipids and the polyphenols. To determine the prevalence of the main protective mechanisms induced by the studied PEEs, we used the ratio between the area under the curve of cytoprotection mediated by intracellular antioxidant mechanisms over the direct free radical scavenging (evaluated from coincubation conditions) (Figure 3). The analysis of the obtained data indicated that intracellular antioxidant mechanism (ICM) was the prevalent protective mechanism induced by polyphenols from the Chilean raspberry *R. geoides* (Las Raices and Lago Blanco samples) and the native strawberry *F. chiloensis*, with 9.5, 23.9, and 13.9%, respectively (Figure 3). Interestingly, only the polyphenols from the currant *Ribes magellanicum* showed that the direct free radical scavenging was the main protective mechanism with a 13.7% over ICM (Figure 3).

Employing the mixture H_2O_2/Cu^{2+} instead of AAPH-derived peroxyl radicals, the study of the cytoprotective effects mediated by PEEs showed, for the extracts of all berries species, that ICM was the prevalent cytoprotective mechanism. It is noteworthy that only the polyphenol employed as control (quercetin) and the extract of *F. chiloensis* presented a significant protection of AGS cells against the oxidative stress induced by H_2O_2/Cu^{2+} in the coincubation model. This is probably due to Cu^{2+} chelation, considering that complexation of Cu^{2+} by quercetin has been reported [44]. This fact is in agreement with the kinetics of the reactions mediated by hydroxyl radicals, which typically present second-order rate constants of $\sim 10^9\,M^{-1}\,s^{-1}$ (close to diffusion limit) [23], and thus, a protection elicited by scavenging of hydroxyl radicals by polyphenols could not be expected. This behavior validates our findings with peroxyl radicals and provides empirical evidence indicating that polyphenols from our berries as well as vegetables and other fruits could not induce an efficient protection by means of the scavenging of hydroxyl radical [45].

To test the hypothesis that co- and preincubations of AGS cells with polyphenols and free radicals involve different mechanisms of cellular protection, we determined the enzymatic activity of Nrf2-regulated enzymes, which constitute one of the final outcomes of the Nrf2 downstream [45]. The transcription factor Nrf2 coordinates the expression of detoxifying enzymes for survival and defense in stressful conditions [45, 46]. For this purpose, the enzymatic activities of the detoxifying enzymes glyoxalase I (GLOI) and glutathione S-transferases (GST) were assessed. Co- and preincubations were performed with the concentrations of the PEEs that presented the best cytoprotective effects against peroxyl radicals. We observed that only preincubations with the PEEs induced a significant increase in the activity of both enzymes (Figure 4), whereas coincubations did not induce significant changes and even a decrease in the enzymatic activities was observed with some species (Figures 4(a) and 4(c)). A lag period of time between the initiation of the oxidative stress and the expression of Nrf2-regulated enzymes has also been reported in AGS cells stressed with H_2O_2, which have shown to increase the expression of the enzyme heme oxygenase-1 at least after 3 h poststress [43]. A time-dependent Nrf2-regulated response in the expression of glyoxalase I (with a maximum at 18 h after treatment) has also been reported for HepG2 hepatocytes incubated with the microbial

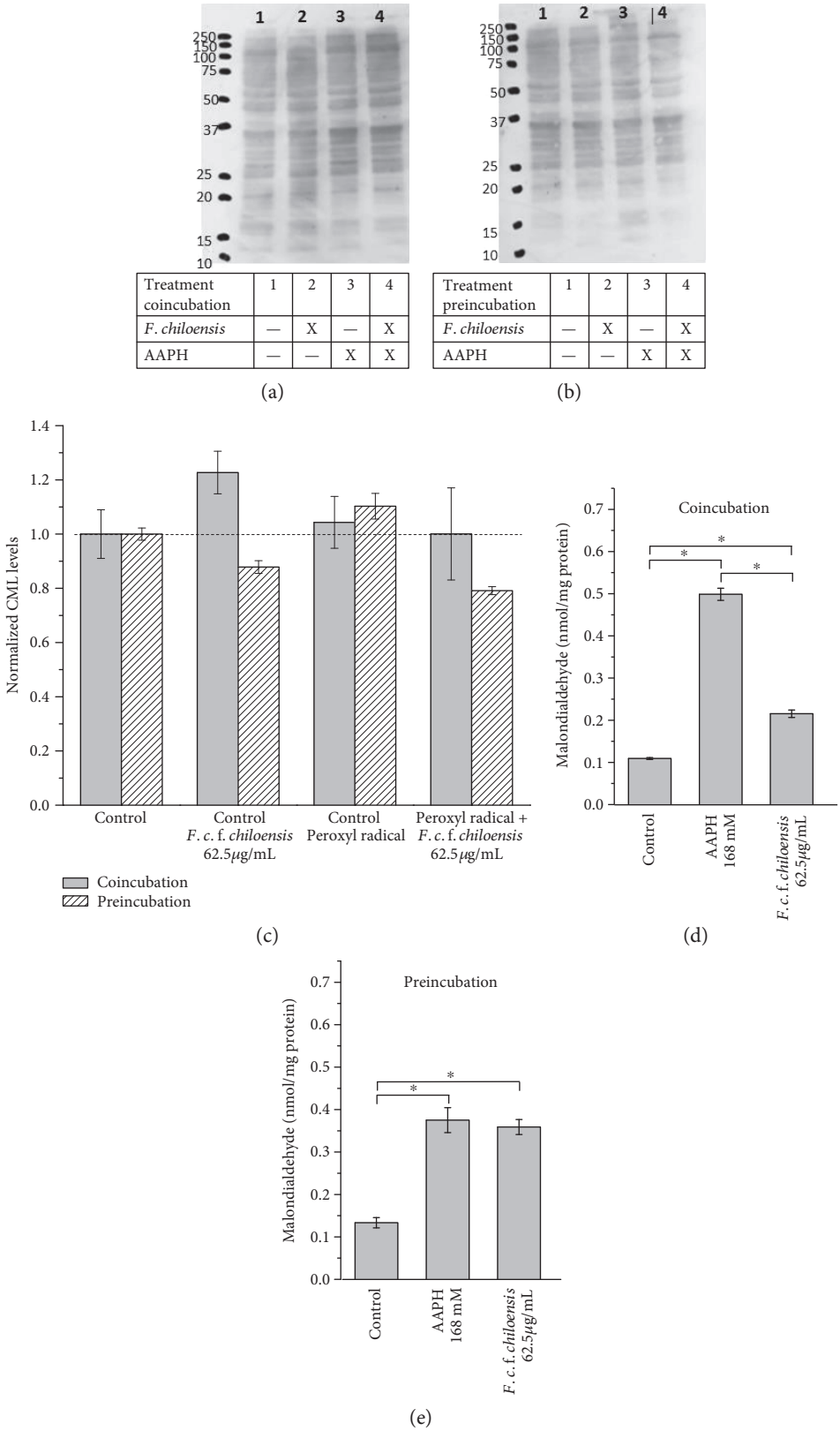

Figure 5: Effect of the PEE from *F. chiloensis* on oxidative stress markers. (a) and (b) Western blots showing the levels of carboxymethyl lysine (CML) in proteins from AGS cells co- and preincubated and challenged with peroxyl radicals (AAPH, 168 mM), respectively. (c) Densitometric analysis of CML levels obtained from the Western blots. (d) and (e) Thiobarbituric acid reactive substances expressed as malondialdeyde concentration (nmol/mg protein) in AGS cells co- and preincubated with the PEE from *F. chiloensis* and challenged with peroxyl radicals (AAPH, 168 mM).

compound monascin [47]. We have previously reported that preincubations (24 h) of AGS cells with the PEEs from *Rubus geoides* induce an increase in the levels of intracellular glutathione as well as protective effects against hydrogen peroxide and methylglyoxal [9].

The efficiency of the PEEs on the free radical scavenging mechanism was evaluated employing ORAC methods, using as target molecules fluorescein (ORAC-FL) and red pyrogallol (ORAC-PGR). ORAC-FL has been related to the stoichiometry of the reaction between AAPH-derived peroxyl radicals and the antioxidant compound, while ORAC-PGR has been associated with the reactivity (rate of reaction) of polyphenols towards such free radicals [33]. The PEE from *F. chiloensis* presented the highest value of ORAC-FL and ORAC-PGR, indicating that the PEE from this species was the most efficient to inactivate peroxyl radicals in terms of the stoichiometry of the reaction as well as in terms of the reactivity of its polyphenolic compounds. The phenolic composition of the PEEs from *R. geoides*, *Ribes* spp., and *F. chiloensis* has been previously reported. The PEEs from the selected berries present antioxidant activity, but the chemical composition of the fruit phenolics is very different, as can be expected from different fruit (berries) species [9, 16, 24–26]. The PEE of *Fragaria chiloensis* presents hydrolizable and condensed tannins as well as flavonoids, while *Ribes* spp. are rich in anthocyanins, caffeoylquinic acids, and flavonoids and *Rubus geoides* yielded flavonoid glycosides and tannins [9, 16, 24–26].

Considering that the PEE from *F. chiloensis* was the most efficient sample to scavenge peroxyl radicals and also presented a high protection mediated by ICM, we selected this species to carry out additional experiments. We evaluated the cytoprotective effect of the PEE from *F. chiloensis* using two different oxidative stress markers, namely, carboxymethyl lysine (CML) and TBAR levels in both experimental models. Carboxymethyl lysine results from the nonenzymatic posttranslational modification occurring in proteins and is one of the most abundant advanced glycation end products in the human body [48]. Carboxymethyl lysine levels have shown to be increased in aged tissues, constituting a marker of occurrence of glycoxidative reactions during aging [49–52]. This compound can be generated intracellularly by direct reaction with glyoxal, which can be detoxified intracellularly by the glyoxalase system (comprised by glyoxalase I and glyoxalase II) [53]. Consequently, a decrease in glyoxalase I activity has been associated with increased CML levels [54]. We have found that the PEE from *F. chiloensis*, in the preincubation model, was able to protect AGS cells from the glycoxidative damage reducing the CML relative levels, compared with the peroxyl radical control (Figures 5(a), 5(b), and 5(c)). This result agrees with the increased levels of electrophile-detoxifying enzymes such as GLOI and GST after preincubation with the PEE from *F. chiloensis* (Figure 4). This constitutes an interesting finding, considering that the overexpression of GLOI has been shown to increase the longevity of the nematode *C. elegans* [54] and to retard the senescence of renal proximal tube epithelial cells [55].

The effect of peroxidative damage to lipids was determined using the TBAR method (Figures 5(d) and 5(e)). Only the coincubation model presented a significant decrease of malondialdehyde levels, implying an inhibition of lipid peroxidation process. It has been reported that Nrf2 activation mediated by lucidine in human keratinocytes (HaCaT) cells can induce a decrease in MDA levels induced by the presence of AAPH [56]. The differences observed in the work of Kumar et al. [56] and our results are probably due to different experimental designs. Such authors treated the HaCaT cells with AAPH during 6 h, a time that should be enough for MDA diffusion from the cell membrane and to be detoxified intracellularly. We incubated with AAPH during 1 h and immediately analyzed the levels of MDA. Nonetheless, our results indicate that despite the effectiveness of coincubation in reducing the MDA levels due to the fast kinetics of free radical scavenging mechanisms, the most relevant cytoprotective mechanism induced by the PEEs from the selected native berries was achieved by intracellular antioxidant mechanisms.

5. Conclusions

Our results with the Chilean berries show the potential of these native fruits as sources of natural antioxidants exerting protective effects on AGS cells against free radical-induced damage. Such effect is related to a direct scavenging activity of polyphenols towards free radicals and also to the modulation of pivotal intracellular mechanisms. However, our results clearly demonstrate that the intracellular antioxidant response activation is the main mechanism accounting the protective effect of Chilean berries. To the best of our knowledge, this work is the first attempt for developing a model to study the prevalence of cytoprotective mechanisms mediated by polyphenols against the damage induced by free radicals in cell cultures. Establishing the differences in the prevalence of protective mechanisms induced by polyphenols may be useful in the design of novel strategies to maximize the efficiency of healthy effects mediated by dietary polyphenols.

Abbreviations

AAPH: 2,2′-Azobis(2-methyl-propionamidine) dihydrochloride
AGS cells: Human gastric adenocarcinoma cell line
CML: Carboxymethyl lysine
GLOI: Glyoxalase I
GST: Glutathione S-transferases
ICM: Intracellular antioxidant mechanisms
Nrf2: Nuclear factor-erythroid 2 p45
ORAC: Oxygen radical absorbance capacity
PEEs: Polyphenolic-enriched extracts
TBARs: Thiobarbituric acid reactive species.

Conflicts of Interest

On behalf of all authors, the corresponding author states that there is no conflict of interest.

Acknowledgments

The authors are grateful to FONDECYT Project nos. 1120096, 1141142, 11160749, and 11150657. The PIEI-QUIM-BIOL and the PIEI-ES from the Universidad de Talca are also kindly acknowledged. The authors wish to thank Dr. Felipe Jimenez-Aspee and Mrs. Samanta Thomas-Valdés for the preparation of the phenolic-enriched extracts.

References

[1] E. R. Stadtman, "Protein oxidation in aging and age-related diseases," *Annals of the New York Academy of Sciences*, vol. 928, pp. 22–38, 2001.

[2] V. Cachofeiro, M. Goicochea, S. G. de Vinuesa, P. Oubina, V. Lahera, and J. Luno, "Oxidative stress and inflammation, a link between chronic kidney disease and cardiovascular disease," *Kidney International*, vol. 74, no. 111, pp. S4–S9, 2008.

[3] M. A. Baraibar, L. Liu, E. K. Ahmed, and B. Friguet, "Protein oxidative damage at the crossroads of cellular senescence, aging, and age-related diseases," *Oxidative Medicine and Cellular Longevity*, vol. 2012, Article ID 919832, p. 8, 2012.

[4] D. Trachootham, W. Lu, M. A. Ogasawara, N. R.-D. Valle, and P. Huang, "Redox regulation of cell survival," *Antioxidants and Redox Signaling*, vol. 10, no. 8, pp. 1343–1374, 2008.

[5] J. Bouayed and T. Bohn, "Exogenous antioxidants—double-edged swords in cellular redox state: health beneficial effects at physiologic doses versus deleterious effects at high doses," *Oxidative Medicine and Cellular Longevity*, vol. 3, no. 4, pp. 228–237, 2010.

[6] K. B. Pandey and S. I. Rizvi, "Plant polyphenols as dietary antioxidants in human health and disease," *Oxidative Medicine and Cellular Longevity*, vol. 2, no. 5, pp. 270–278, 2009.

[7] J. M. Alvarez-Suarez, F. Giampieri, S. Tulipani et al., "One-month strawberry-rich anthocyanin supplementation ameliorates cardiovascular risk, oxidative stress markers and platelet activation in humans," *The Journal of Nutritional Biochemistry*, vol. 25, no. 3, pp. 289–294, 2014.

[8] E. A. Lapshina, M. Zamaraeva, V. T. Cheshchevik et al., "Cranberry flavonoids prevent toxic rat liver mitochondrial damage in vivo and scavenge free radicals in vitro," *Cell Biochemistry and Function*, vol. 33, no. 4, pp. 202–210, 2015.

[9] F. Jiménez-Aspee, C. Theoduloz, F. Ávila et al., "The Chilean wild raspberry (*Rubus geoides* Sm.) increases intracellular GSH content and protects against H_2O_2 and methylglyoxal-induced damage in AGS cells," *Food Chemistry*, vol. 194, pp. 908–919, 2016.

[10] C. López-Alarcón and A. Denicola, "Evaluating the antioxidant capacity of natural products: a review on chemical and cellular-based assays," *Analytica Chimica Acta*, vol. 763, pp. 1–10, 2013.

[11] C. C. Winterbourn, "Reconciling the chemistry and biology of reactive oxygen species," *Nature Chemical Biology*, vol. 4, no. 5, pp. 278–286, 2008.

[12] H. J. Forman, K. J. Davies, and F. Ursini, "How do nutritional antioxidants really work: nucleophilic tone and para-hormesis versus free radical scavenging in vivo," *Free Radical Biology & Medicine*, vol. 66, pp. 24–35, 2014.

[13] J. Kanner and T. Lapidot, "The stomach as a bioreactor: dietary lipid peroxidation in the gastric fluid and the effects of plant-derived antioxidants," *Free Radical Biology & Medicine*, vol. 31, no. 11, pp. 1388–1395, 2001.

[14] G. Graziani, G. D'Argenio, C. Tuccillo et al., "Apple polyphenol extracts prevent damage to human gastric epithelial cells in vitro and to rat gastric mucosa in vivo," *Gut*, vol. 54, no. 2, pp. 193–200, 2005.

[15] F. Cheli and A. Baldi, "Nutrition-based health: cell-based bioassays for food antioxidant activity evaluation," *Journal of Food Science*, vol. 76, no. 9, pp. R197–R205, 2011.

[16] F. Jiménez-Aspee, C. Theoduloz, M. N. Vieira et al., "Phenolics from the Patagonian currants *Ribes* spp.: isolation, characterization and cytoprotective effect in human AGS cells," *Journal of Functional Foods*, vol. 26, pp. 11–26, 2016.

[17] A. Aboonabi and I. Singh, "Chemopreventive role of anthocyanins in atherosclerosis via activation of Nrf2–ARE as an indicator and modulator of redox," *Biomedicine & Pharmacotherapy*, vol. 72, pp. 30–36, 2015.

[18] A. Speciale, S. Anwar, R. Canali et al., "Cyanidin-3-O-glucoside counters the response to TNF-alpha of endothelial cells by activating Nrf2 pathway," *Molecular Nutrition & Food Research*, vol. 57, no. 11, pp. 1979–1987, 2013.

[19] C. Gorrini, I. S. Harris, and T. W. Mak, "Modulation of oxidative stress as an anticancer strategy," *Nature Reviews. Drug Discovery*, vol. 12, no. 12, pp. 931–947, 2013.

[20] M. Xue, N. Rabbani, H. Momiji et al., "Transcriptional control of glyoxalase 1 by Nrf2 provides a stress-responsive defence against dicarbonyl glycation," *Biochemical Journal*, vol. 443, no. 1, pp. 213–222, 2012.

[21] L.-O. Klotz, C. Sánchez-Ramos, I. Prieto-Arroyo, P. Urbánek, H. Steinbrenner, and M. Monsalve, "Redox regulation of FoxO transcription factors," *Redox Biology*, vol. 6, pp. 51–72, 2015.

[22] K. L. Wolfe and R. H. Liu, "Cellular antioxidant activity (CAA) assay for assessing antioxidants, foods, and dietary supplements," *Journal of Agricultural and Food Chemistry*, vol. 55, no. 22, pp. 8896–8907, 2007.

[23] Y. Kono, K. Kobayashi, S. Tagawa et al., "Antioxidant activity of polyphenolics in diets: rate constants of reactions of chlorogenic acid and caffeic acid with reactive species of oxygen and nitrogen," *Biochimica et Biophysica Acta-General Subjects*, vol. 1335, no. 3, pp. 335–342, 1997.

[24] F. Jiménez-Aspee, S. Thomas-Valdés, A. Schulz, A. Ladio, C. Theoduloz, and G. Schmeda-Hirschmann, "Antioxidant activity and phenolic profiles of the wild currant *Ribes magellanicum* from Chilean and Argentinean Patagonia," *Food Science & Nutrition*, vol. 4, no. 4, pp. 595–610, 2016.

[25] M. J. Simirgiotis, C. Theoduloz, P. D. S. Caligari, and G. Schmeda-Hirschmann, "Comparison of phenolic composition and antioxidant properties of two native Chilean and one domestic strawberry genotypes," *Food Chemistry*, vol. 113, no. 2, pp. 377–385, 2009.

[26] M. J. Simirgiotis and G. Schmeda-Hirschmann, "Determination of phenolic composition and antioxidant activity in fruits, rhizomes and leaves of the white strawberry (Fragaria chiloensis spp. chiloensis form chiloensis) using HPLC-DAD–ESI-MS and free radical quenching techniques," *Journal of Food Composition and Analysis*, vol. 23, no. 6, pp. 545–553, 2010.

[27] X. Li, T. Zheng, S. Sang, and L. Lv, "Quercetin inhibits advanced glycation end product formation by trapping methylglyoxal and glyoxal," *Journal of Agricultural and Food Chemistry*, vol. 62, no. 50, pp. 12152–12158, 2014.

[28] J. A. Simpson, K. H. Cheeseman, S. E. Smith, and R. T. Dean, "Free-radical generation by copper ions and hydrogen peroxide. Stimulation by Hepes buffer," *Biochemical Journal*, vol. 254, no. 2, pp. 519–523, 1988.

[29] G. Cao, H. M. Alessio, and R. G. Cutler, "Oxygen-radical absorbance capacity assay for antioxidants," *Free Radical Biology and Medicine*, vol. 14, no. 3, pp. 303–311, 1993.

[30] P. K. Smith, R. I. Krohn, G. T. Hermanson et al., "Measurement of protein using bicinchoninic acid," *Analytical Biochemistry*, vol. 150, no. 1, pp. 76–85, 1985.

[31] W. H. Habig and W. B. Jakoby, "Assays for differentiation of glutathione S-transferases," *Methods in Enzymology*, vol. 77, pp. 398–405, 1981, Academic Press.

[32] P. J. Thornalley, "Modification of the glyoxalase system in human red blood cells by glucose in vitro," *Biochemical Journal*, vol. 254, no. 3, pp. 751–755, 1988.

[33] C. Lopez-Alarcon and E. Lissi, "A novel and simple ORAC methodology based on the interaction of pyrogallol red with peroxyl radicals," *Free Radical Research*, vol. 40, no. 9, pp. 979–985, 2006.

[34] A. Linden, M. Gulden, H. J. Martin, E. Maser, and H. Seibert, "Peroxide-induced cell death and lipid peroxidation in C6 glioma cells," *Toxicology in Vitro*, vol. 22, no. 5, pp. 1371–1376, 2008.

[35] J. Kanner, S. Gorelik, S. Roman, and R. Kohen, "Protection by polyphenols of postprandial human plasma and low-density lipoprotein modification: the stomach as a bioreactor," *Journal of Agricultural and Food Chemistry*, vol. 60, no. 36, pp. 8790–8796, 2012.

[36] S. Gorelik, M. Ligumsky, R. Kohen, and J. Kanner, "A novel function of red wine polyphenols in humans: prevention of absorption of cytotoxic lipid peroxidation products," *The FASEB Journal*, vol. 22, no. 1, pp. 41–46, 2008.

[37] R. Sirota, S. Gorelik, R. Harris, R. Kohen, and J. Kanner, "Coffee polyphenols protect human plasma from postprandial carbonyl modifications," *Molecular Nutrition & Food Research*, vol. 57, no. 5, pp. 916–919, 2013.

[38] S. Gorelik, M. Ligumsky, R. Kohen, and J. Kanner, "The stomach as a "bioreactor": when red meat meets red wine," *Journal of Agricultural and Food Chemistry*, vol. 56, no. 13, pp. 5002–5007, 2008.

[39] A. Bhattacharyya, R. Chattopadhyay, S. Mitra, and S. E. Crowe, "Oxidative stress: an essential factor in the pathogenesis of gastrointestinal mucosal diseases," *Physiological Reviews*, vol. 94, no. 2, pp. 329–354, 2014.

[40] J.-M. Lü, P. H. Lin, Q. Yao, and C. Chen, "Chemical and molecular mechanisms of antioxidants: experimental approaches and model systems," *Journal of Cellular and Molecular Medicine*, vol. 14, no. 4, pp. 840–860, 2010.

[41] S. J. S. Flora, "Structural, chemical and biological aspects of antioxidants for strategies against metal and metalloid exposure," *Oxidative Medicine and Cellular Longevity*, vol. 2, no. 4, pp. 191–206, 2009.

[42] J. M. Gebicki, "Oxidative stress, free radicals and protein peroxides," *Archives of Biochemistry and Biophysics*, vol. 595, pp. 33–39, 2016.

[43] S. Piccirillo, G. Filomeni, B. Brune, G. Rotilio, and M. R. Ciriolo, "Redox mechanisms involved in the selective activation of Nrf2-mediated resistance versus p53-dependent apoptosis in adenocarcinoma cells," *The Journal of Biological Chemistry*, vol. 284, no. 40, pp. 27721–27733, 2009.

[44] H. El Hajji, E. Nkhili, V. Tomao, and O. Dangles, "Interactions of quercetin with iron and copper ions: complexation and autoxidation," *Free Radical Research*, vol. 40, no. 3, pp. 303–320, 2006.

[45] N. Li, J. Alam, M. I. Venkatesan et al., "Nrf2 is a key transcription factor that regulates antioxidant defense in macrophages and epithelial cells: protecting against the proinflammatory and oxidizing effects of diesel exhaust chemicals," *Journal of Immunology*, vol. 173, no. 5, pp. 3467–3481, 2004.

[46] M. K. Kwak, N. Wakabayashi, K. Itoh, H. Motohashi, M. Yamamoto, and T. W. Kensler, "Modulation of gene expression by cancer chemopreventive dithiolethiones through the Keap1-Nrf2 pathway. Identification of novel gene clusters for cell survival," *The Journal of Biological Chemistry*, vol. 278, no. 10, pp. 8135–8145, 2003.

[47] W. H. Hsu, B. H. Lee, Y. Y. Chang, Y. W. Hsu, and T. M. Pan, "A novel natural Nrf2 activator with PPARgamma-agonist (monascin) attenuates the toxicity of methylglyoxal and hyperglycemia," *Toxicology and Applied Pharmacology*, vol. 272, no. 3, pp. 842–851, 2013.

[48] R. D. Semba, E. J. Nicklett, and L. Ferrucci, "Does accumulation of advanced glycation end products contribute to the aging phenotype?" *The Journals of Gerontology. Series A, Biological Sciences and Medical Sciences*, vol. 65, no. 9, pp. 963–975, 2010.

[49] C. E. Finch and E. M. Crimmins, "Constant molecular aging rates vs. the exponential acceleration of mortality," *Proceedings of the National Academy of Sciences of the United States of America*, vol. 113, no. 5, pp. 1121–1123, 2016.

[50] G. Viteri, G. Carrard, I. Birlouez-Aragon, E. Silva, and B. Friguet, "Age-dependent protein modifications and declining proteasome activity in the human lens," *Archives of Biochemistry and Biophysics*, vol. 427, no. 2, pp. 197–203, 2004.

[51] L. Gorisse, C. Pietrement, V. Vuiblet et al., "Protein carbamylation is a hallmark of aging," *Proceedings of the National Academy of Sciences of the United States of America*, vol. 113, no. 5, pp. 1191–1196, 2016.

[52] M. Hamelin, C. Borot-Laloi, B. Friguet, and H. Bakala, "Increased level of glycoxidation product N(epsilon)-(carboxymethyl) lysine in rat serum and urine proteins with aging: link with glycoxidative damage accumulation in kidney," *Archives of Biochemistry and Biophysics*, vol. 411, no. 2, pp. 215–222, 2003.

[53] S. Radjei, B. Friguet, C. Nizard, and I. Petropoulos, "Prevention of dicarbonyl-mediated advanced glycation by glyoxalases: implication in skin aging," *Biochemical Society Transactions*, vol. 42, no. 2, pp. 518–522, 2014.

[54] M. Morcos, X. Du, F. Pfisterer et al., "Glyoxalase-1 prevents mitochondrial protein modification and enhances lifespan in *Caenorhabditis elegans*," *Aging Cell*, vol. 7, no. 2, pp. 260–269, 2008.

[55] Y. Ikeda, R. Inagi, T. Miyata et al., "Glyoxalase I retards renal senescence," *The American Journal of Pathology*, vol. 179, no. 6, pp. 2810–2821, 2011.

[56] K. J. Kumar, H. L. Yang, Y. C. Tsai et al., "Lucidone protects human skin keratinocytes against free radical-induced oxidative damage and inflammation through the up-regulation of HO-1/Nrf2 antioxidant genes and down-regulation of NF-kappaB signaling pathway," *Food and Chemical Toxicology*, vol. 59, pp. 55–66, 2013.

Hindawi
Oxidative Medicine and Cellular Longevity
Volume 2017, Article ID 8634249, 17 pages
https://doi.org/10.1155/2017/8634249

Review Article

Opuntia spp.: Characterization and Benefits in Chronic Diseases

María del Socorro Santos Díaz,[1] Ana-Paulina Barba de la Rosa,[2] Cécile Héliès-Toussaint,[3,4] Françoise Guéraud,[3,4] and Anne Nègre-Salvayre[4,5]

[1]*Facultad de Ciencias Químicas, Universidad Autonoma de San Luis Potosí, San Luis Potosí, SLP, Mexico*
[2]*Instituto Potosino de Investigación Científica y Tecnológica (IPICyT), San Luis Potosi, SLP, Mexico*
[3]*Toxalim (Research Center in Food Toxicology), INRA, ENVT, INP-Purpan, UPS, Toulouse, France*
[4]*University of Toulouse, Toulouse, France*
[5]*INSERM U 1048, Toulouse, France*

Correspondence should be addressed to Anne Nègre-Salvayre; anne.negre-salvayre@inserm.fr

Received 2 January 2017; Accepted 14 March 2017; Published 9 April 2017

Academic Editor: Liudmila Korkina

Opuntia species have been used for centuries as food resources and in traditional folk medicine for their nutritional properties and their benefit in chronic diseases, particularly diabetes, obesity, cardiovascular diseases, and cancer. These plants are largely distributed in America, Africa, and the Mediterranean basin. *Opuntia* spp. have great economic potential because they grow in arid and desert areas, and *O. ficus-indica*, the domesticated *O.* species, is used as a nutritional and pharmaceutical agent in various dietary and value-added products. Though differences in the phytochemical composition exist between wild and domesticated (*O. ficus-indica*) *Opuntia* spp., all *Opuntia* vegetatives (pear, roots, cladodes, seeds, and juice) exhibit beneficial properties mainly resulting from their high content in antioxidants (flavonoids, ascorbate), pigments (carotenoids, betalains), and phenolic acids. Other phytochemical components (biopeptides, soluble fibers) have been characterized and contribute to the medicinal properties of *Opuntia* spp. The biological properties of *Opuntia* spp. have been investigated on cellular and animal models and in clinical trials in humans, allowing characterization and clarification of the protective effect of *Opuntia*-enriched diets in chronic diseases. This review is an update on the phytochemical composition and biological properties of *Opuntia* spp. and their potential interest in medicine.

1. Introduction

Long historical and worldwide use of medicinal plants and phytochemicals has demonstrated the efficacy of traditional medicine to prevent the onset and progression of chronic diseases. In Mexico, among the number of plants identified and used in folk medicine, *Opuntia* species (spp.) exhibit a lot of beneficial properties and high biotechnological potential. They grow in dry desert area where hard environmental conditions prevail, and they have been used for centuries as food resources and in folk medicine for the treatment of chronic diseases (obesity, cardiovascular and inflammatory diseases, diabetes, and gastric ulcer) and many other illnesses [1]. Some species such as *O. ficus-indica* are cultivated for economical and medicinal purposes in Mexico area. Though differences in the phytochemical composition exist between domesticated and wild *Opuntia* spp., the presence of antioxidants (flavonoids, ascorbate), pigments (carotenoids, betalains such as indicaxanthin), or phenolic acids has been reported in all *Opuntia* products, including seeds, roots, pears, cladodes, or juice. Antioxidants could be responsible for the nutritional and protective benefit of *Opuntia*-enriched diets in chronic diseases, in which inflammation and oxidative stress play a major involvement. Other plant materials such as biopeptides or soluble fibers have been characterized and contribute to the medicinal properties of *Opuntia* spp. This review is an update on the active compounds and the biological and medical benefit of wild and domesticated *Opuntia* spp. in chronic diseases.

2. *Opuntia* History and Production

2.1. Opuntia History. Plants are classified as succulent when they exhibit pronounced water storage in one or more organs. The Opuntioid cacti represent the most spectacular species of succulent plants, which are characterized by a shallow root system that permits rapid water uptake; a thick, waxy cuticle that prevents excessive water loss; and crassulacean acid metabolism (CAM), an alternative photosynthetic pathway, that allows plants to uptake atmospheric CO_2 at night when water loss is minimized [2]. Opuntioid cacti are recognized as ideal crops for arid regimes because they are extremely efficient at generating biomass under water-deficient conditions [3].

Opuntia spp. is one of the most diverse and widely distributed genus in America [4], but the highest richness of wild species are found in Mexico, as at least 126 species with different degrees of domestication have been observed [5]. There are evidences that during the process of *Opuntia* domestication, the continuous and systematic gather of cladodes and fruit favored the development of exceptional features, with the purpose to adapt plants to successfully live in human-made environment and maximize yield or any given selected feature [6, 7].

Wild species of the *Opuntia* genus have been grouped in one line of domestication processes where the wildest species are *O. streptacantha* and *O. hyptiacantha*. Others species are semidomesticated like *O. megacantha* and *O. albicarpa* [5]. As a result of domestication, the *Opuntia* fruit has been enhanced in flavor, size, shape, pulp texture, and decreased seed hardness and quantity. Regarding cladodes, changes occurred in shape, color, earliness, flavor, texture, and mucilage quantity and quality [5]. *O. ficus-indica* is a long-domesticated cactus crop that is important in agricultural economies throughout arid and semiarid parts of the world. It has been proposed that *O. ficus-indica* is a spineless cultivar derived from *O. megacantha*, a native species from central Mexico [8, 9]. Bayesian phylogenetic analysis of nrITS DNA sequences indicates that the center of domestication for this species is located in central Mexico [10].

The easy of clonal *Opuntia* propagation probably explains why it is easily distributed worldwide. Evidence exists for the use of *Opuntia* as human food since at least 9000 years ago [11] or even as early as 12,000 years ago [8, 12].

In the recorded history of the Old World, *O. ficus-indica* was certainly known at the beginning of the 16th century [6, 7] and it is believed that this species accompanied Columbus in his first return to Lisbon in 1493 [4], placing *O. ficus-indica* in the Caribbean by at least the late 1400s. The plants are also recorded in cultivation in Tlaxcala, Mexico, in 1519. *O. ficus-indica* fruits and shoots were also reportedly consumed by the Maya of southeastern Mexico [8]. There is also some evidence for the use of *O. ficus-indica* by the Nazca of Peru [13]. The succulent, ever-fresh cladodes were certainly a novelty to late 15th century and later Europeans [14].

Actually, *O. ficus-indica* is as important as corn and tequila agave in the agricultural economy of modern Mexico [15] and represents important food and feed resources. Its economic importance has gradually increased around the world as a health-promoting food [16]. *O. ficus-indica* is grown for the large, sweet fruits (often called "tunas"), which are available in local and commercial markets worldwide [17]. In addition, the young cladodes (stem segments) of *O. ficus-indica* are harvested as a vegetable crop (often called nopalitos). Other uses have been reported, including as a binding and waterproofing agent in adobe and its medicinal properties [18, 19]. *O. ficus-indica*, along with other Opuntia and Nopalea species, has been grown from pre-Columbian times as a host plant for cochineal insects (*Dactylopiuscoccus*) for the production of valuable, vivid red and purple dyes [4, 20].

Interest in health care among consumers is increasing steadily and has expanded to dietary intake, and as a result, the food industry has started to produce new food types based on "nopalitos" to reflect this change in consumerism [18].

2.2. Opuntia Production. *Opuntia* plants produce edible stems known as pads, vegetable, cladodes, nopales, or pencas. The tender young part of the cactus stem, young cladode or "nopalitos", is frequently consumed as vegetable in salads, while the cactus pear fruit is consumed as a fresh fruit. Mexico and Italy are the main producer countries and consumers, from the approximately 590,000 ha cultivated worldwide, México accounts for 70% and Italy for 3.3%. Under optimal conditions, the annual production in Mexico can reach 350,000 tons [5].

Nowadays, *Opuntia* plants are grown in more than 30 countries; Chile and South Africa are producers with 1500 ha and 1000 ha, respectively. Israel and Colombia account for with 300 ha cultivated. In the US, California is the leading state with 200 ha cultivated producing 4000 tons of dry matter.

3. Cladodes Chemical Composition

Opuntia spp. have a high nutritional value, mainly due to their mineral, protein, dietary fiber, and phytochemical contents [21]. Table 1 indicates the chemical composition of some wild and domesticated species (*O. ficus-indica*). The main constituent of *O. ficus-indica* cladodes is water (80–95%), followed by carbohydrates (3–7%), fibers (1-2%), and proteins (0.5–1%). However, the chemical composition of cladodes is modified by maturity stage, harvest season, environmental conditions, postharvest treatment, and type of species [22–24]. In some wild species such as *O. robusta* (Tapon) and Blanco, 17.4 to 19% proteins can be reached [22]. *O. leucotricha* (Duraznillo) yield high-quality cladodes, since the pericarp can be easily removed and will neither fall apart during boiling nor release mucilage [21].

It is well known that *Opuntia* cladodes are a good source of dietary fibers [25], which may help in reducing body weight by binding to dietary fat and increasing its excretion [26]. This may explain why cladodes are considered as hypolipidemic.

Opuntia cladodes contain higher calcium (Ca) contents relative to vegetables, fruits, and nuts [24, 27, 28]. Table 2

Table 1: Chemical composition of wild and domesticated species in Mexico and other countries.

Species	Composition (%)				Phenolic acids[c]	Flavonoids[d]
	Protein	Fat	CF	Ash		
O. streptacantha[a]	11.2	0.73	7.3	12.6	56.8	18.0
O. hyptiacantha[a]	11.0	0.80	6.5	15.1	33.4	17.1
O. megacantha[a]	10.7	0.69	6.5	13.6	44.7	16.8
O. albicarpa[a]	11.6	0.75	6.5	13.2	40.8	17.2
O. ficus-indica[a]	11.2	0.69	5.9	14.4	40.1	19.4
O. humifusa[b]	4.7	1.25	50.3	2.0	—	—

[a]Astello-Garcia et al. [28]; [b]Jun et al. [131]; [c]as mmol of gallic acid/g sample; [d]as mmol of quercetin/g sample; CF: crude fiber.

Table 2: Mineral composition of wild and domesticated species in Mexico and other countries.

Species	Mineral (mg/100 g sample)					
	K	Ca	Na	P	Fe	Mn
O. streptacantha[a]	2213	667	70	0.09	2.9	16.5
O. hyptiacantha[a]	2690	740	87	0.09	3.9	9.8
O. megacantha[a]	1960	683	137	0.08	5.1	13.3
O. albicarpa[a]	1956	647	77	0.09	0.7	24.1
O. ficus-indica[a]	2403	627	63	0.09	8.6	13.8
O. humifusa[b]	1269	1968	nd	1110	nd	1411

[a]Astello-Garcia et al. [28]; [b]Jun et al. [131]; nd: not determined.

shows the mineral composition of wild and domesticated *Opuntia* spp.

Calcium content seems higher in *Opuntia* spp. than in other plants such as spinach (1151 mg/100 g), lettuce (703 mg/100 g), cabbage (511 mg/100 g), and broccoli (43 mg/100 g). Aguilera-Barreiro et al. [29] reported that consumption of cactus improves the bone mineral density in women with low bone mass.

The *Opuntia* spp. cladodes are also widely known for their strong viscous materials and hydrophilic polysaccharides of large molecular weight due to their great capacity to absorb and retain water [21]. The soluble dietary fiber and calcium contents of *Opuntia* spp. cladodes are considered to be very important elements for their physical properties because the main cell wall polysaccharide consists of low methoxyl pectin [19].

3.1. Total Phenolic and Flavonoid Content in Opuntia spp. It is well known that the secondary metabolite accumulation depends on biotic and abiotic factors. Since *Opuntia* spp. used in this study were cultivated under the same environmental conditions, then the differences in the amount of metabolites should be related to each species biochemical characteristics. Table 3 shows the content of phenolic acids and flavonoids present in wild and domesticated *Opuntia* spp.

The beneficial properties of *Opuntia* spp. are related to their content in chemical compounds as minerals, polyphenols, vitamins, polyunsaturated fatty acids, and amino acids, as recently reviewed by El-Mostafa et al. [30]. *O. ficus-indica* is the most domesticated and studied species, and several reports describe the main compounds found in cladodes, flowers, and fruits [21, 30, 31]. However, other *Opuntia* spp. used in folk medicine are important sources of bioactive compounds. In this chapter, we report the antioxidant composition (phenolic acids, flavonoids, betalains, and vitamins) of wild *Opuntia* spp. and the most recent information related to *O. ficus-indica*.

3.1.1. Phenolic Compounds. The phenolic compounds are important antioxidants since phenoxy radical intermediates (PO) are relatively stable due to resonance and act as terminators of propagation route by reacting with other free radicals. On the other hand, the phenolic hydroxyl groups can donate a hydrogen atom or an electron to a free radical conferring radical scavenging activities. They also extended conjugated aromatic system to delocalize an unpaired electron. Some phenolic compounds with dihydroxy groups can conjugate transition metals, preventing metal-induced free radical formation [32].

The total phenolic compound content in *Opuntia* spp. is quite variable and is affected by the maturity stage, harvest season, environmental conditions, postharvest treatment, and species (Table 3). It has been reported that *O. ficus-indica* fruits contain 218 mg GAE/100 g FW [30], but the wild species *O. stricta* also exhibited high concentrations of these metabolites (204 mg GAE/100 g FW), followed by *O. undulata*, *O. megacantha*, *O. streptacantha*, and *O. dinellii* (164.6, 130, 120, and 117 mg/100 g FW pear, respectively) [33–36]. Important differences in the content of flavonoids among species are described, ranging between 9.8 (in *O. stricta*) and 50.24 (in *O. megacantha*) mg QE/100 g FW [33, 34].

In relation to the color of fruits, variations on metabolite contents can be observed. Purple fruits of *O. ficus-indica* cultivated in Italy, Spain, USA, Tunisia, and Saudi Arabia contain higher levels of phenolics (89–218.8 mg GAE/100 g FW) than the orange fruits (69.8 mg GAE/100 g FW) [33, 37–40]. However, the Mexican cultivars, *O. megacantha* (orange fruits), *O. streptacantha*, and *O. robusta* (purple fruits), exhibited a similar phenolic compound concentration (120–140 mg GAE/100 g FW) [34].

Pads are also source of polyphenols. It has been reported that *O. violacea*, *O. megacantha*, *O. atropes*, and *O. albicarpa* contain high concentration of phenolic acids (17.8–20 mg GAE/g DW), while *O. rastrera* and *O. undulata* present the lowest values (0.39–0.95 mg GAE/g DW) [22]. A recent comparative analysis realized with 15 *Opuntia*

Table 3: Content of antioxidants compounds present in *Opuntia* species.

Species	Region	Tissue	Chemical compound	Concentration	Reference
O. albicapa	México	Pads (Cristalino cultivar)	Total phenolic acids	5.83–18 mg GAE/g DW	[22, 28]
			Total flavonoids	2.5–5.62 mg QE/g DW	[22, 28]
		Fruits (Reyna cultivar)	Total betalains	1 mg/100 g FW	[34]
			Ascorbic acid	1.8 mg/100 FW	[34]
O. atropes	México	Pads (Blanco cultivar)	Total phenolic acids	5.2 mg GAE/g DW	[22]
			Total flavonoids	9.7 mg QE/g DW	[22]
O. dinellii	Spain	Pads	Total phenolic acids	16.1 mg GAE/100 g FW	[52]
		Fruits	Total phenolic acids	117 mg QE/100 g FW	[35]
			Ascorbic acid	29.7 mg/100 g FW	[35]
	Taiwan	Fruits	Total phenolic acids	91 (juice) and 133 (peel) mg GAE/100 g FW	[132]
			Total flavonoids acids	32.5 (juice), 29.2 (peel) mg GAE/100 g FW	[132]
			Catechin	22.7 (juice), 18 (peel) mg/100 g FW	[132]
			Epicatechin	10.9 (juice), 17.1 (peel) mg/100 g FW	[132]
			p-Coumaric acid	0.6 (peel) mg/100 g FW	[132]
			Ferulic acid	4 mg/100 g FW (peel)	[132]
			Quercetin	4.6 mg/100 g FW (peel)	[132]
	Egypt	Fruit	Betacyanins	0.54 mg/100 mg DW	[36]
			Isorhamnetin-3-O-rutinoside	56 μg/100 mg DW	[36]
O. ficus-indica	México	Pads	Total phenolic acids	6.8–18 mg GAE/g DW	[22, 28]
			Total flavonoids	5.3–6.1 mg QE/g DW	[28]
			Quercetin 3-O-rhamnosyl-(1-2)-[rhamnosyl-(1-6)]-glucoside	nq	[28]
	Spain	Pads	Total phenolic acids	128.8 mg GAE/100 g FW	[133]
	Italy	Fruits	Total phenolic acids	89.2 mg GAE/100 g FW	[40]
			Total betacyanins	39.3 mg/100 g FW	[40]
	Portugal	Fruit	Ferulic acid glucoside, piscidic acid, isorhamnetinpentosyl-rutinoside, isorhamnetinpentosyl-glucoside, isorhamnetinpentosyl-rhamnoside	nq	[42]
O. hyptiacantha	México	Pads	Total phenolic acids	5.39–6.14 mg GAE/g DW	[28]
			Total flavonoids	4.86–5.62 mg QE/g DW	[28]
O. leucotricha	Mexico	Pads (Duraznillo cultivar)	Total phenolic acids	3 mg GAE/g DW	[22]
			Total flavonoids	1.8 mg QE/g DW	[22]
O. lindheimeri	Mexico	Pads	Total phenolic acids	0.75 mg GAE/g DW	[134]
			Kaempferol	1.8 μg/g DW	[134]
	USA	Fruits	Kaempferol	1.1 μg/g FW	[37]
			Quercetin	90.5 μg/g FW	[37]
			Isorhamnetin	1.9 μg/g FW	[37]
			Ascorbic acid	121 μg/g FW	[37]

Table 3: Continued.

Species	Region	Tissue	Chemical compound	Concentration	Reference
O. megacantha	México	Pads	Total phenolic acids	6.7–19.5 mg GAE/g DW	[22, 28]
			Total flavonoid	3.2–5.62 mg QE/g DW	[22, 28]
		Fruit (Naranjona cultivar)	Total betalains	2.2 mg/100 g FW	[34]
	Argentina	Fruits	Total phenolic acids	36 mg GAE/100 g FW	[135]
			Total betalains	27 μg/g FW	[135]
	Morocco	Fruits	Total flavonoids	50.24 μg QE/g FW	[136]
			Total betalains	29.9 μg/g FW	[136]
O. rastrera	Mexico	Pads	Total phenolic acids	0.39 mg/g DW	[134]
			Kaempferol	28.9 μg/g DW	[134]
			Isorhamnetin	199.8 μg/g DW	[134]
			Isorhamnetin-glucosyl-rhamnoside	nq	[134]
			Isorhamnetin + hexose + pentose	nq	[134]
O. robusta	México	Pads (Tapon cultivar)	Total phenolic acids	2 mg GAE/g DW	[22]
			Total flavonoids	3.8 mg QE/g DW	[22]
		Pads (Gavia cultivar)	Total phenolic acids	0.561 mg GAE/g DW	[134]
		Fruit (Camuesa cultivar)	Total betalains	6.8 mg/100 g FW	[34]
			Ascorbic acid	6 mg/100 g FW	[34]
		Pads (Tapon cultivar)	Total phenolic acids	0.39 mg GAE/g DW	[134]
			Kaempferol	45.6 μg/g DW	[134]
			Isorhamnetin	99.58 μg/g DW	[30]
O. streptacantha	Mexico	Pads	Total phenolic acids	0.66–11.07 mg GAE/g DW	[28, 134]
			Total flavonoids	4.92–5.74 mg QE/g DW	[28]
			Kaempferol	42.2 μg/g DW	[134]
			Isorhamnetin	58.9 μg/g DW	[134]
			Kaempferol 3-O-arabinofuranoside	nq	[28]
		Fruit (Cardona cultivar)	Total betalains	3.5 mg/100 g FW	[34]
	USA	Fruit (red-skinned)	Kaempferol	3.8 μg/g FW	[37]
			Quercetin	51 μg/g FW	[37]
			Ascorbic acid	815 μg/g FW	[37]
O. stricta	Spain	Fruits	Total phenolic acids	204.4 GAE/100 g FW	[33]
			Total betalains	80.1 mg/100 g FW	[33]
			Ascorbic acid	23.3 mg/100 g FW	[33]
			Quercetin	87.5 μg/g FW	[33]
			Isorhamnetin	50.3 μg/g FW	[33]
			Kaempferol	7.7 μg/g FW	[33]
			Luteolin	15.6 μg/g FW	[33]
	USA	Fruits	Total flavonoids	9.8 μg/g FW	[37]
			Quercetin	9.8 μg/g FW	[37]
			Ascorbic acid	437 μg/g FW	[37]

Table 3: Continued.

Species	Region	Tissue	Chemical compound	Concentration	Reference
O. undulata	Mexico	Pads	Total phenolic acids	0.95 mg GAE/g DW	[134]
			Kaempferol	12.9 μg/g DW	[134]
			Isorhamnetin	326.9 μg/g DW	[134]
			Isorhamnetin-glucosyl-rhamnosyl-rhamnoside	nq	[134]
			Isorhamnetin + 1 hexose + 1 methylpentose + pentose	nq	[134]
			Kaempferol-glucosylrhamnoside	nq	[134]
	Spain	Fruits	Total phenolic acids	164.6 mg GAE/g FW	[33]
			Total betalains	42.4 mg/100 g FW	[33]
			Total flavonoids	51.1 μg/g FW	[33]
			Quercetin	30 μg/g FW	[33]
			Isorhamnetin	9.6 μg/g FW	[33]
			Kaempferol	5.6 g/g FW	[33]
			Luteolin	5.9 μg/g FW	[33]
O. violacea	México	Pads (Morado cultivar)	Total phenolic acids	20 mg GAE/g DW	[22]
			Total flavonoids	3.5 mg QE/g DW	[22]

nq: not quantified.

cultivars from *O. streptacantha*, *O. hyptiacantha*, *O. megacantha*, *O. albicarpa*, and *O. ficus-indica*, cultivated under the same environmental conditions and at the same developmental stage, showed that metabolite content in cladodes was independent of domestication grade. Thus, differences depend basically on the biochemical characteristics of each species [28].

Flowers and peels could exhibit a higher phenolic content than fruits and pads with about 45.7 g/100 g FW, so it is recommended to exploit these materials to obtain biocompounds with antioxidant characteristics [30, 36].

The phenolic profile in *Opuntia* is complex with more than 30 compounds identified in cladodes of different species [21, 22, 28, 31], more than 20 in seeds, and 44 compounds in juices [41, 42]. The most common compounds present in *Opuntia* tissues from wild and cultivated species include kaempferol, quercetin, isorhamnetin, and isorhamnetin glucosides (Table 3). Kaempferol 3-O-arabinofuranoside was detected only in *O. streptacantha*, quercetin 3-O-rhamnosyl-(1-2)-[rhamnosyl-(1-6)]-glucoside was detected only in *O. ficus-indica* cladodes [28], and isorhamnetin-3-O-rutinoside was present in the juice and peel from *O. dilleni* [36]. The rare piscidic acid and derivatives, restricted to plants exhibiting crassulacean acid metabolism and succulence, were detected in juices from *O. ficus-indica* [42]. In seeds, sinapoyl-glucose, sinapoyl-diglucoside, three isomers of feruloyl-sucrose, catechin, rutin, and quercetin derivatives were detected [43]. Taurine, an unusual sulfonic acid, was identified in Sicilian and African cultivars [31].

3.1.2. Betalains. Betalains are water-soluble molecules with two or three nitrogen atoms and about 55 structures known, including the red-violet betacyanins and the yellow-orange betaxanthins. Their characteristic is the N-heterocyclic nature with betalamic acid being their common biosynthetic precursor. Aldimine formation with *cyclo*-Dopa yields the betanidin aglycone that is usually conjugated with glucose and sometimes with glucuronic acid. On the other hand, betaxanthins are conjugates of betalamic acid with amino acids or amines [44].

Betalains are excellent radical scavengers with an antioxidant activity 3-4 times higher than ascorbic acid, rutin, and catechin [45], twice higher than that measured for pear, apple, tomato, banana, and white grape, and from the same order as pink grapefruit, red grape, and orange [46]. The monophenol nature of betanin and reducing intermediates during the oxidation process may confer to the molecule a higher H-atom or electron donation potential. In the case of betaxanthins, the antioxidant power has been linked to the presence of one or two phenolic hydroxy groups in their structure. Betacyanins also have a potential to inhibit NO or nitrogen radical species due to the presence of a catechol group in betanidin structure [47, 48].

In the literature, it is reported that fruits of cactus pear contain different betalains whose concentration depends on species, cultivar, and geographic region. The betacyanins identified in *Opuntia* fruits include betanidin, betanin, isobetanin, isobetanidin, neobetanin, phyllocactin, and gomphrenin I [3, 4, 24–26]. *O. streptacantha* (Cardona cultivar), (Rojalisa cultivar), and *O. megacantha* (Naranjona cultivar) contain traces of betanidin 5-O-β-sophoroside [34].

The presence of conjugates of betalamic acid with several amino acids is reported in pears, corresponding to miraxanthine II (aspartic acid), indicaxanthin (proline), vulgaxantin I (glutamine), vulgaxantin II (glutamic acid), vulgaxantin III (asparagin), vulgaxantin IV (leucine), portulacaxanthin I

(tyrosine), portulacaxanthin III (lysine), ɣ-aminobutyric acid-betaxanthin, serine-betaxanthin, valine-betaxanthin, isoleucine-betaxanthin, isoproline-betaxanthin, phenylalanine-betaxanthin, histidine-betaxanthin, phenethylamine-betaxanthin, and muscaaurin [42, 46–52]. Using cactus pears as a betalain source is of great interest because they are highly flavored, with better nutritional properties than red beetroot.

3.2. Vitamins. The main vitamins present in *Opuntia* spp. include vitamin E, vitamin C, vitamin K, and tocopherols [30]. The vitamin levels depend on the cultivar type. In *O. ficus-indica*, Italian varieties exhibit values ranging 30–36 mg Vit C/100 g FW in fruits [40, 49, 52]; in *O. ficus-indica* and *O. streptacantha* (red-skinned), *O. stricta* (yellow-skinned), *O. undulata, O. dinellii*, and *O. lindheimeri* (purple-skinned) cultivated in Texas, the values range from 12.1 to 81.5 mg Vit C/100 g, while in *O. dillenii* and *O. ficus-indica* cultivars from Tenerife, the concentration ranged from 17 to 29.7 mg/100 g, respectively [35, 37]. Usually, the highest ascorbic acid content is present in red-skinned fruits (815 mg/g FW) and the highest carotenoid content in yellow-skinned fruits (23.7 mg/g FW) [35].

Although other compounds present in the various *Opuntia* parts may exhibit antioxidant properties, most reports suggest that polyphenols, betalains, and vitamins are the main compounds involved in their biological properties. Beside the use of pads or fruits, the seeds and peels have a high promising potential for the development of new nutraceutic products.

4. Biological and Medical Properties of *Opuntia* spp. in Chronic Diseases

Opuntia extracts have been used since centuries for nutritional and medical purposes, and their therapeutical interest has recently been made clear by in vitro and in vivo scientific studies [30]. We report here the protective properties of various *Opuntia* spp. in the development of atherosclerosis and cardiovascular diseases, diabetes, obesity, and cancer.

4.1. Opuntia spp. in Cardiovascular Diseases. Atherosclerosis and its related cardiovascular complications are the leading worldwide cause of death related to chronic diseases [53]. Since the beginning of the last decade, even if the cardiovascular mortality rates tend to slightly decline in western countries, they are fastly increasing in the developing world. In Mexico, the mortality due to coronary artery diseases (CAD) strongly increased in the last 30 years, representing more than 11% of deaths in the country by 2006 [54]. The lifelong risk factors for CAD in Mexico have been studied and are similar to those reported in Western countries, that is, hypertension, high cholesterol levels, smoking, diabetes, and obesity [55, 56]. Interestingly, CAD and risk factors such as diabetes were rare in Mexico before the second half of the twentieth century, suggesting that lifestyle changes including nutritional habits have contributed to the increased cardiovascular risk in this country [56]. Strategies focusing on changing lifestyles are thus becoming a priority, with particular focus on smoking and dietary habits. In this context, there is an increasing interest for the nutritional benefit of *Opuntia* spp. to prevent the development of CAD. The antiatherogenic properties of *Opuntia* spp. result from their high antioxidant (polyphenols) content which could decrease lipid peroxidation, an important risk factor in atherosclerosis [57], and also from dietary fibers and proteins, which exhibit lipid-lowering properties, in humans and in animals.

4.1.1. Cholesterol-Lowering properties of Opuntia. Several reports point out the antioxidant and antiatherogenic properties of *Opuntia* spp. [57]. First, the consumption of *Opuntia* juice and fruits naturally prevents oxidative stress and improves the redox status in healthy humans [58]. Budinski et al. [59] reported that the regular consumption of prickly pears from *O. robusta,* by patients affected with familial heterozygous hypercholesterolemia, significantly lowered the plasma levels of LDL cholesterol and the plasma and urine content of 8-epi-prostaglandin $F_2\alpha$, a F2 isoprostane produced through the peroxidation of arachidonic acid. No modifications were observed on HDL and triglycerides [59]. Likewise, the consumption by women affected with metabolic syndrome, of dried leaves from *O. ficus-indica* as dietary supplement, showed a rapid increase in circulating HDL cholesterol level concomitantly with a decrease in LDL cholesterol and (slightly) in triglycerides, indicating that the plant exerts an hypocholesterolemic effect [60]. These lipid-lowering properties were confirmed by studies on mice fed with a hypercholesterolemic diet. When the animals were supplemented with a methanolic extract from *O. joconostle* (polyphenol enriched) seeds, they exhibited a marked reduction in circulating LDL cholesterol and triglyceride levels, by comparison with animals fed with a placebo [61].

The lipid-lowering properties of *Opuntia* spp. are not well clarified. Antioxidants block lipid peroxidation, but have usually no effect on plasma lipid profiles, except grape polyphenols (such as resveratrol), which decrease plasma triglyceride levels and alter the metabolism of VLDL [62]. In *Opuntia*, the lipid-lowering properties may rather result from their content in dietary fibers, as supported by data from Wolfram et al. [63]. These authors reported that prickly pears from *O. robusta* lower the cholesterol levels in hyperlipemic nondiabetic human patients. They concluded that the protective effect of *Opuntia* prickly pear may result from pectin, a soluble fiber [63]. The mechanism elicited by pectin could evoke an alteration of hepatic cholesterol metabolism without affecting cholesterol absorption [64, 65]. Likewise, glycoprotein isolated from *O. ficus-indica* var. *saboten* MAKINO (an *Opuntia* variety used in folk medicine in Korea) exerts potent antioxidant and hypolipidemic properties evidenced by a protective effect on mice treated with triton WR-1339, an inhibitor of lipoprotein lipase [66]. It is to note that the ingestion of *Opuntia* prickly pears also improves the platelet function and haemostatic balance, thus contributing to prevent the atherosclerotic risk [63].

4.1.2. Antiatherogenic Properties of Opuntia spp. The early stages of atherosclerosis development are characterized by the retention in the intima of LDL, which undergo oxidation upon the attack of their polyunsaturated fatty acid content by

environmentally produced reactive oxygen species (ROS), [67–70]. Several ROS-producing systems are involved in the LDL oxidation process, among them the activation of NADPH oxidase NOX2 [71], through a mechanism implicating the scavenger receptor LOX-1 [72]. Oxidized LDL initiate inflammatory processes in the vascular wall, leading to the recruitment of monocytes/macrophages and the accumulation of foam cells, and finally to the formation of the fatty streaks which are the early atherosclerotic lesions [69, 70]. Beside their role in fatty streak formation, oxidized LDL behave as strong cytotoxines for vascular cells [70, 73]. Lipid oxidation products (LPO) formed during the onset of LDL oxidation are detected responsible for the proapoptotic and proinflammatory properties of oxidized LDL [70, 74]. Furthermore, aldehydic LPO such as hydroxynonenal (HNE), malondialdehyde (MDA), or acrolein form adducts on proteins generating their progressive dysfunction and contributing to inflammation and apoptosis [74].

Most antioxidants are antiatherogenic as they neutralize the formation of ROS by vascular cells and exhibit anti-inflammatory and antiapoptotic properties against the effects of oxidized LDL on vascular cells [70]. Our group recently compared the antiatherogenic properties of *Opuntia* powders obtained from the cladodes of five different wild spp. (*O. streptacantha* var. *cardona*, *tuna loca*, *O. hyptiacantha*, and *O. megacantha*), medium (*O. albicarpa*), and domesticated (*O. ficus-indica*) [75]. Precisely, the effect of cladodes was tested on oxidation of LDL evoked by murine endothelial cells (an in vitro model mimicking the mechanism of LDL oxidation occurring in vivo in the vascular wall). Cladode powdered and solubilized in the culture medium dose-dependently inhibited LDL oxidation and the subsequent formation of foam cells by macrophages, which suggests that *Opuntia* spp. could inhibit the early steps of atherogenesis [75]. This inhibitory effect of *Opuntia* spp. involves an inhibition of NADPH oxidase (NOX2) resulting in a decreased generation of intracellular and extracellular superoxide anion ($O_2^{\cdot}$-), a main ROS involved in the LDL oxidation process [75, 76]. No major difference of protection was observed between wild and domesticated *Opuntia* spp. Likewise, *Opuntia* spp. inhibit the nuclear translocation of the redox-sensitive transcription factor NFκB and the subsequent expression of ICAM-1 and VCAM-1 adhesion molecules [76, 77] and thus exhibit anti-inflammatory properties resulting from their inhibitory effect on cellular ROS production. Additionally, wild *O. streptacantha* and domesticated *O. ficus-indica* inhibit the toxicity of cell-oxidized LDL [75, 76] and oxidized lipids such as 7-ketocholesterol [78] through mechanisms implicating an inhibition of intracellular oxidative stress and subsequent cytosolic calcium deregulation [78].

In vivo studies on apoE-KO mice, which spontaneously develop atherosclerotic lesions in basal diet conditions, indicated that the supplementation of the diet in *O. streptacantha* or *O. ficus-indica* powdered cladodes (10 mg/kg during 15 weeks) significantly reduced the development of atherosclerotic lesions [76]. In addition, the lowering effect of *Opuntia* spp. on LDL oxidation was supported by a decrease in HNE-adduct accumulation in the intima [76]. In contrast to the data reported by Osorio-Esquivel et al. [61], the intake of *O. streptacantha* or *O. ficus-indica* cladodes did not reduce the plasma cholesterol level [56]. This discrepancy may result from the diet (basal or cholesterol-enriched) or from the *Opuntia* components (cladodes versus seeds). Nevertheless, both lipid-lowering and antioxidant properties of the different wild and domesticated *Opuntia* spp. may support their efficacy to prevent or slow down atherosclerotic lesion development and subsequent cardiovascular diseases.

4.2. Opuntia spp. in Diabetes. Type 2 diabetes mellitus (T2DM) is a multifactorial disease including genetic determinants of individual susceptibility and environmental lifestyle factors. It is considered as a major health problem worldwide, with an increasing incidence and invalidating long-term complications, affecting macro- and microvasculature, kidney, heart, nerves, or eyes [79].

Several reports in diabetic patients and animals point out the antihyperglycemic and antihyperinsulinemic properties of *Opuntia* spp. The dietary intake of nopal (*O. ficus-indica*) improves the postprandial response of glucose, insulin, glucose-dependent insulinotropic peptide (GIP) index, and the glucagon-like peptide 1 (GLP-1) index on T2DM patients after consumption of a high-carbohydrate or high-soy-protein breakfast [80]. The hypoglycemic efficacy could be higher after heating *Opuntia* extracts, as reported by Frati-Munari et al. [81], in patients consuming broiled *O. streptacantha* extracts. Likewise, glycemia and glycated hemoglobin are lowered to normal values in rats rendered diabetic after treatment by streptozotocin (STZ) and supplemented with an extract of *O. fuliginosa* prickly pear [82]. Likewise, *O. humifusa* stems promote a blood glucose and cholesterol decrease in STZ-treated rats [83].

In a recent study, Andrade-Cetto et al. [84] indicated that *O. streptacantha* extracts do not reduce glycemia in STZ-treated rats when compared to the control but exhibit an antihyperglycemic effect when administered before an oral glucose tolerance test (OGTT). A similar result was observed in obese prediabetic patients (men and women) treated for 16 weeks with OpunDia™ (a mixture of *O. ficus-indica* cladode and fruit extracts), that is, a net blood glucose decrease when the mixture was given before OGTT, suggesting that *Opuntia* spp. intake may reduce blood glucose in postprandial conditions [85].

The hypoglycemic mechanism evoked by *Opuntia* spp. ingestion could be due to dietary fibers such as pectin and mucilage [81], which may slow down the absorption of glucose by increasing the viscosity of food in the gut [86, 87]. Likewise, polysaccharides isolated from *O. ficus-indica* or *O. streptacantha* could exert a hypoglycemic effect in diabetic mice [88]. The hydrolysis of disaccharide has been proposed to explain the hypoglycemic effect of *O. streptacantha*, via an inhibition of α-glucosidase inhibitors (AGIs) or through a barrier function. However, this hypothesis was not verified [89]. Another hypothesis is that *Opuntia* spp. stimulate insulin secretion via a direct action on pancreatic beta cells [90], a mechanism also observed after exercise in healthy subjects and involved in fast glycogen resynthesis [91]. In addition, the antioxidant properties of *Opuntia* spp. could play a role in the prevention of cardiovascular complications due to

T2DM. Indeed, oxidative stress plays a pivotal role in the pathophysiology of T2DM, particularly in the development of accelerated atherosclerosis lesions and cardiovascular diseases which represent a main complication in diabetes [92]. *Opuntia* spp. may exert an inhibitory effect on the oxidative environment generated by hyperglycemia, via their antioxidant components, and as suggested by a recent report by Berraaouan et al. [93] who showed that cactus pear seed oil from *O. ficus-indica* L. Mill. prevents the development of alloxan-induced diabetes in mice by quenching the generation of ROS. Though the protective mechanisms are not yet clarified, all these reports confirm that *Opuntia* spp. extracts exhibit antihyperglycemic and antidiabetic properties.

4.3. Opuntia spp. in Obesity. Obesity is becoming a major public health concern all over the world. Worldwide obesity has more than doubled since 1980 with approximately 66 million obese individuals in the world [94]. The obesity prevalence has increased significantly as a result of rapid urbanization and improvement in socioeconomic conditions. In Mexico, the prevalence of obesity in adults is 32% (with a higher prevalence in females) and is about 15% in children. Mexico faces a challenging situation with one of the highest and most rapidly increasing prevalence of obesity. Thus, researchers, clinicians, and people looking to reduce body weight are always in search of solutions.

The complex pathogenesis of obesity indicates the need of different intervention strategies to confront this problem with a simple drug therapy that is more acceptable to patients. It is difficult for patients to follow diets and exercises that would improve their symptoms. Therefore, investigation of new efficient agents is an important medical field for research. Herbal supplements and diet-based therapies for weight loss are among the most common, complementary, and alternative medicine modalities. The demand for weight-loss products based on plants has increased during the last decade. This demand clearly indicates that medicinal plants for the treatment of obesity represent a current topic of interest. *O. ficus-indica* fruits, stems, seeds, and cladodes have been traditionally used in folk medicine to prevent and cure chronic diseases. Therefore, clinical pharmacologic interest in the efficacy and safety of the phytochemicals present in the genus *Opuntia* has grown during recent years due to the realization that many people self-medicate using this plant [30, 95, 96]. Different approaches can be used, including in vitro on cellular models, in vivo by the use of animal models such as mice or rats fed diets enriched with *Opuntia* extracts, and human clinical trials.

4.3.1. Cellular Models for In Vitro Analysis of Opuntia Effects. Adipogenesis is a complex process that includes coordinated changes in adipocytes morphology, hormone sensitivity, and gene expression. Adipocytes play a central role in the maintenance of lipid homeostasis and energy balance by storing triglycerides or releasing free fatty acids in response to changes in energy demand. Obesity is not only caused by adipose tissue hypertrophy but also by adipose tissue hyperplasia, which triggers the transformation of preadipocytes into adipocytes. Adipocyte dysfunction is strongly associated with the development of obesity. Many studies have shown that *Opuntia* extracts such as the flavonoid kaempferol or isorhamnetin can suppress lipid accumulation or inhibit adipogenesis through adipogenic-responsible genes down-regulation [97, 98]. The use of cellular models allows a better knowledge of the gene regulations and the metabolic pathways in which plant extracts could interfere.

4.3.2. Animal Models. The use of animal models with diet-induced obesity helped to evaluate the nutritional values and some biological parameters of cactus seed supplements [99, 100], dehydrated *O. ficus-indica* cladodes [101, 102], or a combination of pre-Hispanic Mexican diet including nopal and nopal seeds [103] on rat models. These studies have shown that supplementation of diet with *O. ficus-indica* seed powder may have a favorable effect on the serum lipid profile and glucose, linked with beneficial effects on atherosclerosis, diabetes, and obesity [99, 100]. It exerts a favorable impact on insulin sensitivity through the regulation of genes involved in adipocyte differentiation [102], it attenuates hepatic steatosis in obese Zucker (fa/fa) rats [101], and it decreases metabolic and cognitive abnormalities and gut microbiota dysbiosis caused by a high-fat diet in rats [103]. To determine the metabolic effect of an *O. ficus-indica* extract on a mouse model of diet-induced obesity [104], the extract was added to a high-fat diet and administered to mice for 12 weeks. Mice fed with the high-fat diet supplemented with *O. ficus-indica* extract gained less body weight and exhibited significantly lower circulating cholesterol, LDL cholesterol, and HDL cholesterol, when compared to mice fed with the high-fat diet alone. In this study, the *O. ficus-indica* extract prevented the development of metabolic abnormalities associated with diet-induced obesity [104]. Thus, the use of different animal models provided many clues to the potential effects of *Opuntia* extracts in terms of energy metabolism, gene regulation, and insulin and glucose pathways regulation, suggesting that cactus pears, given in different ways in the diet, could be efficient in human treatment of obesity.

4.3.3. Clinical Trials. Antiobesity agents obtained from natural products are gaining more and more interest in the scientific community, and some of their active compounds have reached clinical trials.

In their double-blind, randomized, placebo-controlled clinical investigation, Grube et al. [105] used Litramine, a natural fiber complex derived from *O. ficus-indica*, associated with a hypocaloric diet, plus moderate physical activity (30 minutes walking or cycling). In a 12-week treatment on a panel of 125 overweight and obese volunteers, they were able to show a weight loss of at least 5% of the volunteers' initial body weight compared to placebo. They showed significantly greater reduction in BMI (body mass index), body fat composition, and waist circumference. Importantly, they noticed that Litramine fibers complement was well tolerated and that no adverse reactions were reported. These results suggest that the natural fiber complex Litramine can be effective in promoting weight loss. To go further, Uebelhack et al. [26] and Chong et al. [106] determined that *Opuntia*-derived fibers bind to dietary fat and increase its excretion and thus

reduce its absorption; this leads to a lower energy intake and weight loss. The safety assessment also revealed minimal concerns as Litramine is well tolerated, unlike lipase inhibitors usually used as weight loss complements acting on the inhibition of enzymes responsible for the digestion of long-chain triglycerides that present gastrointestinal negative side effects up to possible liver damages. Another point to notice is that acute and chronic effects of OpunDia induced a significant decrease in blood glucose concentrations after acute administration of 400 mg OpunDia 30 minutes before a 75 g glucose load. In the chronic phase of the study, supplementation of OpunDia for 16 weeks significantly lowered glucose concentrations (as described above), supporting the use of *O. ficus-indica* for blood glucose management [85].

The meta-analysis from Onakpoya et al. [107] reveals that even if many works report positive effects concerning *Opuntia*, whatever the mode of administration, randomized clinical trials do not indicate that supplementation with *O. ficus-indica* generates statistically significant effects on body weight and waist circumference. These conclusions may be due to the inconsistent quality of recording and high heterogeneity observed in some analyses, which makes the meta-analysis difficult to interpret. However, the results also suggest that *O. ficus-indica* ingestion results in significant reduction in body mass index, body fat percentage, and circulating triglycerides. Thus, larger well-controlled randomized clinical trials examining the effects of *O. ficus-indica* on body composition and metabolic parameters are required to conclude on the effects on body parameters. However, consumption of fruits is widely recommended for healthy lifestyle, and intake of cactus pears takes part in a well-balanced diet. This type of dietary recommendations could be adapted to different ethnic groups by incorporation of native food, known for a long time to have beneficial medical properties. Indeed, individuals at risk for diabetes, obesity, or cardiovascular diseases will prefer to include local, beneficial food in their diet as a way to improve the biochemical and clinical abnormalities associated with metabolic syndrome [108]. To achieve the potential benefits associated with the concept of local beneficial food, it should include an approach taking into account the genetic variation of the population as nutrigenetics [108].

Finally, in many countries, these "antiobesity agents" are marked as food supplements, which are exempted of strict licensing regulations routinely imposed on synthetic drugs or medicinal products before releasing them onto the market. Then, the abuse and overdose of these products are common practices, as consumers believe that increasing consumption of these products will increase weight loss and treatment efficacy [96].

Thus, even if the meta-analysis of Onakpoya et al. [107] reveals a need for more studies to be conclusive, it seems that the genus *Opuntia* is rich in healing properties and could be of beneficial interest in weight loss and possibly in dealing with chronic diseases such as metabolic syndrome.

4.4. Opuntia spp. in Cancer. Numerous studies have demonstrated the cytotoxic effects of various parts of *Opuntia*, namely the prickly pears (fruits), with or without peels and seeds, the cladodes or stems, and even the roots, on cancerous cell lines.

Antunes-Ricardo et al. [109] evaluated the cytotoxic effects of *O. ficus-indica* cladode flour extracts (var. Jalpa) or of purified isorhamnetin glycosides on two models of human colon cancer cell lines, namely, HT-29 and Caco2, representing apoptosis-resistant and apoptosis-susceptible cell lines, respectively, while normal fibroblasts (NIH 3T3) were used as controls. These authors reported that cladode flour extract and purified isorhamnetin glycosides were more cytotoxic to HT-29 cells than to Caco2 or to controls, with an effect of the glycosylation pattern. These effects were related to apoptosis induction through caspase cascade, which plays a central role in apoptosis pathways. Naselli et al. [110] studied the effect of *O. ficus-indica* fruit aqueous extract and its betalain pigment indicaxanthin on the proliferation of the human colon cancer cell line Caco2. These authors showed a dose-dependent apoptotic effect on proliferating cells, while no effect was reported on differentiated cells. In this study, indicaxanthin presented an epigenomic effect on the tumor suppressor gene p16INK4a, through demethylation of its promoter and activation of its expression. Sreekanth et al. [111] reported that betanin, extracted from *O. ficus-indica* fruits, was able to inhibit the growth of the human chronic myeloid leukemia cell line K562, through apoptotic intrinsic pathway.

Chavez-Santoscoy et al. [112] tested the cytotoxic effect of filtered juices from prickly pears of various species of *Opuntia* on several cancer lines. The PC3 prostate and the Caco2 colon cell lines were the most affected, while the growth of the mammary MCF-7 and the hepatic HepG2 cell lines was diminished at a lesser extent. Normal fibroblasts were used as controls. The most cytotoxic species on cancer cells was *O. rastrera rastrero* that presented at the same time the best antioxidant content and capacity among the various species tested. In contrast, Kim et al. [113] showed that extracts from *O. humifusa* cladodes were able to induce apoptosis in MCF-7 cells and human colon SW-480 cells. Water-partitioned fractions of fruits and stems of *O. humifusa* were reported to suppress the growth of U87MG glioblastoma cells, in association to an increase in ROS production in the cells [114]. The same team reported a similar effect on HeLa cervical carcinoma cells, while normal fibroblasts were unaffected [115]. Serra et al. [116] showed that polyphenol-rich juice concentrates of various *Opuntia* were cytotoxic to HT-29 colon cancer cell lines, but not to Caco2, while natural extracts from juice residues (peels and seeds) were reported to be more effective than juice concentrates to induce a cell-cycle arrest in the same cells. Interestingly, this effect paralleled an increase of ROS in the cells, which suggests a ROS-induced cell death probably due to the pro-oxidant effects of the extracts. This pro-oxidant effect has been also reported for ovarian cancer cells by Feugang et al. [117], when compared to normal or immortalized cells. The use of pertinent controls, that is, cells of the same type with the same genetic background, is essential to conclude about the potentially beneficial effect of compounds. To be qualified as protective towards cancer, (phyto)-compounds need to be more cytotoxic to cancer cells than to their normal

counterparts. In addition, Keller et al. [75] reported a protective effect of various *Opuntia* cladode flour towards the cytotoxic effect of 4-hydroxynonenal, a dietary lipid oxidation product possibly involved in the promoting effect of red meat on colon cancer. This protective effect was observed only on normal epithelial mouse colon cells, but not on the same cells bearing the Apc mutation, which is a frequent and early event in human colorectal carcinogenesis. Both normal and preneoplastic cells were immortalized cells obtained by crossing of normal or Min mice that carry the Apc mutation, with Immortomouse® mice.

However, in vivo studies are important to confirm those effects evidenced in vitro. Zou et al. [118] showed that *Opuntia* pear aqueous extracts suppressed tumor growth in nude mice, in an extent similar to the one these authors observed with the synthetic retinoid N-(4-hydroxyphernyl) retinamide (4-HPR) used as a chemopreventive model compound. A protective effect of *O. humifusa* was also reported by Hahm et al. on HeLa cells xenografts [115]. Some authors reported an effect of *O. ficus-indica* cladode extracts on oxidative stress and genotoxicity induced in vivo by the mycotoxins zearalenone and aflatoxin B1 [119–121]. Most of the time, *Opuntia* extracts were given intraperitoneally. More studies are needed to confirm the protective effects of *Opuntia* spp., testing those compounds in a more physiological way or for instance by oral route that will take into account the digestibility and bioavailability of such compounds. In this spirit, *O. humifusa* fruit lyophilized powder given in the pelleted diet was reported to be protective in two different animal models of skin carcinogenesis, together with a reduction of skin lipid peroxidation and skin inflammation [122, 123].

Taken together, all these studies show that *Opuntia* spp., as fruits, fruit juice, or nopal (*Opuntia* cladodes or stems), could provide an interesting anticancer strategy.

4.5. Opuntia spp. in Skin Wound Healing. As the largest organ of the human body and its location at the interface of the organism and the external environment, the skin has major protective properties, including a permeability barrier function, the maintenance of body temperature, and a role as a defense system against physical aggressions, ultraviolet (UV) radiations, microorganisms, and xenobiotics. The skin has also antioxidant and repair functions allowing removal of the damaged biomolecules, thereby preventing their accumulation and promoting wound healing.

The wound healing process is complex and fragile. It can be altered in various pathological situations (diabetes and arterial and metabolic diseases and infections and aging) and by multiple local and systemic factors among them (hypoxia and oxidative stress, decreased immune responses, infectious agents, inflammatory cytokines, metalloprotease activation, etc.); this leads to nonhealing chronic wounds [124]. Nopal and other *Opuntia* spp. extracts have long been used in traditional medicine for the treatment of burns, skin disorders, and wound healing, and the recent demonstration of their efficacy at the molecular and cellular levels justifies their use in nowadays dermatologic preparations [125].

Several recent studies point out the wound healing properties of *O. ficus-indica* cladode extracts. Using keratinocytes stimulated by benzopyrene or TNF-α, Nakahara et al. showed that *O. ficus-indica* cladode extracts may protect the epidermal barrier and the keratinocyte function by upregulating the expression of filaggrin and loricrin, two proteins present in differentiated keratinocytes and corneocytes. The protective effect of the extract is characterized by an inhibition of ROS production evoked by the inflammatory agents. This could result from the activation of the aryl hydrocarbon receptor, which in turn activates the transcription factor Nrf2 and subsequently the antioxidant NAD(P)H: quinone oxidoreductase 1 [126]. The cicatrizing properties of *O. ficus-indica* cladodes may involve both high molecular weight polysaccharide components such as a linear galactan polymer and a highly branched xyloarabinan, as well as low molecular weight components such as lactic acid, D-mannitol, piscidic, eucomic, and 2-hydroxy-4-(4′-hydroxyphenyl)-butanoic acids. These extracts could fasten cell regeneration on a scratched keratinocytes monolayer, suggesting that *O. ficus-indica* components exhibit high anti-inflammatory and high wound healing properties [127]. Likewise, polysaccharides extracted from cactus pear of *O. ficus-indica* stimulate the proliferation of fibroblasts and keratinocytes [128]. Among the protective agents present in the extracts, isorhamnetin glycoside components, such as diglycoside isorhamnetin-glucosyl-rhamnoside (IGR), could inhibit COX-2 and the production of TNF-α and IL-6 as well as the generation of nitric oxide (NO) evoked by lipolysaccharide (LPS) [129]. Moreover, cladode extracts from *O. humifusa* (Raf.) may regulate the production of hyaluronic acid (HA) by increasing the expression of HA synthase in keratinocytes exposed to UV-B treatment. Conversely, treatment using cladode extracts from *O. humifusa* could decrease the UV-B increased expression of hyaluronidase. Interestingly, the same protective effect on HA was observed in SKH-1 hairless mice exposed to UV-B, indicating that cladode extracts from *O. humifusa* have strong skin care capacities [130]. Altogether, these reports point out the ability of *Opuntia* spp. to accelerate wound healing and their potential interest as cotreatment of skin complications in diabetes and other pathologies characterized by a defective wound healing.

5. Conclusion and Future Directions

The vegetative parts of wild and domesticated *Opuntia* spp. have been used for centuries for nutritional and medicine purposes and are traditionally considered healthy nutritional sources for preventing chronic diseases such as diabetes, cardiovascular diseases, metabolic syndrome, obesity, or aging, as well as infectious or neurodegenerative diseases. Since several years, scientific research has been interested in deepening the knowledge on these plants, in order to better understand their nutritional and therapeutic properties. Moreover, there is also an interest in their development for economical purposes, as they easily grow in arid desert area. As reviewed in this article, a number of scientific studies have analyzed the *Opuntia* properties, particularly their phytochemical composition in fibers, antioxidants, vitamins, and protective peptides. Some of the biological processes evoked by the different *Opuntia* parts have been identified through

in vitro studies and in vivo approaches, based on animal models and clinical trials. These studies emphasize their lipid-lowering, antidiabetic, and antiatherogenic properties, as well as their ability to slow down tumoral cell proliferation. Additional studies could be required to standardize the properties and the safety of *Opuntia* spp., knowing that their properties may differ as function of the different wild or domesticated species and the vegetative parts may exhibit variations in their phytochemical composition and properties. Nonetheless, it is likely that *Opuntia* spp. can be considered efficient functional food or nutraceuticals, able to prevent or slow down chronic disease development and promote a better health, quality of life, and longevity.

Abbreviations

4-HPR:	N-(4-Hydroxyphernyl) retinamide
AGIs:	α-Glucosidase inhibitors
BMI:	Body mass index
CAD:	Cardioartery diseases
CAM:	Crassulacean acid metabolism
FW:	Fresh weight
GAE:	Gallic acid equivalents
GIP:	Glucose-dependent insulinotropic peptide
GLP-1:	Glucagon-like peptide 1
HDL:	High-density lipoprotein
HNE:	4-Hydroxy-2-nonenal
ICAM-1:	Intercellular adhesion molecule
LDL:	Low-density lipoprotein
LOX-1:	Lectin-like oxidized low-density lipoprotein receptor-1
LPO:	Lipid oxidation products
MDA:	Malondialdehyde
NO:	Nitric oxide
NOX2:	NADPH oxidase 2
O.:	*Opuntia*
OGTT:	Oral glucose tolerance test
Opuntia spp.:	*Opuntia* species
QE:	Quercetin equivalent
ROS:	Reactive oxygen species
STZ:	Streptozotocin
T2DM:	Type 2 diabetes mellitus
VCAM-1:	Vascular cell adhesion protein 1
VLDL:	Very low-density lipoprotein.

Conflicts of Interest

The authors declare that there is no conflict of interest regarding the publication of this paper.

Acknowledgments

This work was funded by the INSERM, INRA, University of Toulouse and by the bilateral French/Mexican ANR (French National Research Agency)/CONACYT (National Council of Science and Technology of Mexico) project BIOPUNTIA (ANR-2010-INTB-1702).

References

[1] J. E. Young, X. Zhao, E. E. Carey, R. Welti, S.-S. Yang, and W. Wang, "Phytochemical phenolics in organically grown vegetables," *Molecular Nutrition & Food Research*, vol. 49, no. 12, pp. 1136–1142, 2005.

[2] R. M. Ogburn and E. J. Edwards, "The ecological water-use of succulent plants," *Advances in Botanical Research*, vol. 55, pp. 179–255, 2010, Academic Press.

[3] C. Hecht-Buchholz, M. Kluge, and I. P. Ting, "Crassulacean Acid Metabolism. Analysis of an Ecological Adaptation," in *Ecological Studies*, W. D. Billings, F. Golley, O. L. Lage and J. S. Olson Hrsg, Eds., vol. 30 of Analysis and Synthesis, pp. 609-610, Springer-Verlag, Berlin-Heidelberg-New York, 1980.

[4] E. F. Anderson, *The Cactus Family*, Timber Press, Portland, Or, 2001.

[5] J. A. Reyes-Agüero and J. R. Aguirre Rivera, "Agrobiodiversity of cactus pear (Opuntia, Cactaceae) in the meridional highlands plateau of Mexico," *Journal of Natural Resources and Development*, vol. 1, pp. 1–8, 2011.

[6] A. Casas and G. Barrera, "Mesoamerican domestication and diffusion," in *Cacti: Biology Uses*, P. S. Nobel, Ed., pp. 143–162, University of California Press, Berkeley, 2002.

[7] A. Casas, B. Pickersgill, J. Caballero, and A. ValienteBanuet, "Ethnobotany and domestication in xoconochtli, Stenocereus stellatus (Cactaceae), in the Tehuacan Valley and La Mixteca Baja, Mexico," *Economic Botany*, vol. 51, no. 3, pp. 279–292, 1997.

[8] M. P. Griffith, "The origins of an important cactus crop, Opuntia ficus-indica (Cactaceae): new molecular evidence," *American Journal of Botany*, vol. 91, no. 11, pp. 1915–1921, 2004.

[9] M. Labra, F. Grassi, M. Bardini et al., "Genetic relationships in Opuntia Mill. genus (Cactaceae) detected by molecular marker," *Plant Science*, vol. 165, no. 5, pp. 1129–1136, 2003.

[10] M. Arakaki, P.-A. Christin, R. Nyffeler et al., "Contemporaneous and recent radiations of the world's major succulent plant lineages," *Proceedings of the National Academy of Sciences*, vol. 108, no. 20, pp. 8379–8384, 2011.

[11] R. Kiesling, "Origin, domestication and distribution of Opuntia ficus-indica," *Journal of the Professional Association for Cactus Development*, vol. 3, pp. 50–59, 1998.

[12] E. O. Callen, "Analysis of the Tehuacan coprolites," in *Prehistory Tehuacan Val.*, D. S. Byers, Ed., pp. 261–289, University of Texas Press, Austin, Texas, USA, 1967.

[13] O. Sejuro, *Plantas medicinales utilizadas por los curanderos de Nasca: registro gráfico botánico*, CONCYTEC, Mexico, 1990.

[14] R. Donkin, "Spanish red-ethnogeographical study of cochineal and Opuntia cactus," *Transactions of the American Philosophical Society*, vol. 67, pp. 5–84, 1977.

[15] P. F. Barrientos, *El nopal y su utilizacion en Mexico*, La Sociedad Mexicana de Historia Natural, Mexico City, Mexico, 1966.

[16] M. A. Anaya-Perez, "History of the use of opuntia as forage in Mexico," in *Cactus Opuntia Spp Forage*, C. Mondragon-Jacobo, S. Perez-Gonzalez, E. R. Arias and S. G. Sanchez, Eds., pp. 5–12, FAO, Rome, Italy, 2001.

[17] P. Inglese, F. Basile, and M. Schirra, "Cactus pear fruit production," in *Cacti: Biology Uses*, P. S. Nobel, Ed., pp. 163–183, University of California Press, Berkeley, 2002.

[18] C. Saenz-Hernandez, J. Corrales-Garcia, and G. Aquino-Perez, "Nopalitos, mucilage, fiber and cochineal," in *Cacti: Biology Uses*, P. S. Nobel, Ed., pp. 311–234, University of California Press, Berkeley, 2002.

[19] A. Cardenas, W. M. Arguelles, and F. M. Goycoolea, "On the possible role of Opuntia ficus-indica mucilage in lime mortar performance in the protection of historical buildings," *Journal of the Professional Association for Cactus Development*, vol. 3, pp. 64–71, 1998.

[20] P. S. Nobel, E. De la Barrera, D. W. Beilman, J. H. Doherty, and B. R. Zutta, "Temperature limitations for cultivation of edible cacti in California," *Madrono*, vol. 49, no. 4, pp. 228–236, 2002.

[21] F. C. Stintzing and R. Carle, "Cactus stems (Opuntia spp.): a review on their chemistry, technology, and uses," *Molecular Nutrition & Food Research*, vol. 49, no. 2, pp. 175–194, 2005.

[22] T. Guevara-Figueroa, H. Jimenez-Islas, M. L. Reyes-Escogido et al., "Proximate composition, phenolic acids, and flavonoids characterization of commercial and wild nopal (Opuntia spp.)," *Journal of Food Composition and Analysis*, vol. 23, no. 6, pp. 525–532, 2010.

[23] M. Contreras-Padilla, E. Perez-Torrero, M. I. Hernandez-Urbiola et al., "Evaluation of oxalates and calcium in nopal pads (Opuntia ficus-indica var. redonda) at different maturity stages," *Journal of Food Composition and Analysis*, vol. 24, no. 1, pp. 38–43, 2011.

[24] M. I. Hernandez-Urbiola, E. Perez-Torrero, and M. E. Rodriguez-Garcia, "Chemical analysis of nutritional content of prickly pads (Opuntia ficus indica) at varied ages in an organic harvest," *International Journal of Environmental Research and Public Health*, vol. 8, no. 5, pp. 1287–1295, 2011.

[25] C. Beatriz Pena-Valdivia, C. Trejo, V. B. Arroyo-Pena, A. B. Sanchez Urdaneta, and R. Balois Morales, "Diversity of unavailable polysaccharides and dietary fiber in domesticated nopalito and cactus pear fruit (Opuntia spp.)," *Chemistry & Biodiversity*, vol. 9, no. 8, pp. 1599–1610, 2012.

[26] R. Uebelhack, R. Busch, F. Alt, Z.-M. Beah, and P.-W. Chong, "Effects of cactus fiber on the excretion of dietary fat in healthy subjects: a double blind, randomized, placebo-controlled, crossover clinical investigation," *Current Therapeutic Research, Clinical and Experimental*, vol. 76, no. C, pp. 39–44, 2014.

[27] E. Ramirez-Moreno, C. Diez Marques, M. C. Sanchez-Mata, and I. Goni, "In vitro calcium bioaccessibility in raw and cooked cladodes of prickly pear cactus (Opuntia ficus-indica L. Miller)," *LWT- Food Science and Technology*, vol. 44, no. 7, pp. 1611–1615, 2011.

[28] M. G. Astello-Garcia, I. Cervantes, V. Nair et al., "Chemical composition and phenolic compounds profile of cladodes from Opuntia spp. cultivars with different domestication gradient," *Journal of Food Composition and Analysis*, vol. 43, pp. 119–130, 2015.

[29] M. de los Angeles Aguilera-Barreiro, J. Alberto Rivera-Marquez, H. Miguel Trujillo-Arriaga, J. Alfredo Tamayo y Orozco, E. Barreira-Mercado, and M. E. Rodriguez-Garcia, "Intake of dehydrated nopal (Opuntia ficus indica) improves bone mineral density and calciuria in adult Mexican women," *Food & Nutrition Research*, vol. 57, no. 1, p. 19106, 2013.

[30] K. El-Mostafa, Y. El Kharrassi, A. Badreddine et al., "Nopal cactus (Opuntia ficus-indica) as a source of bioactive compounds for nutrition, health and disease," *Molecules*, vol. 19, no. 9, pp. 14879–14901, 2014.

[31] F. C. Stintzing, K. M. Herbach, M. R. Mosshammer et al., "Color, betalain pattern, and antioxidant properties of cactus pear (Opuntia spp.) clones," *Journal of Agricultural and Food Chemistry*, vol. 53, no. 2, pp. 442–451, 2005.

[32] J. Dai and R. J. Mumper, "Plant phenolics: extraction, analysis and their antioxidant and anticancer properties," *Molecules*, vol. 15, no. 10, pp. 7313–7352, 2010.

[33] J. A. Fernández-López, L. Almela, J. M. Obón, and R. Castellar, "Determination of antioxidant constituents in cactus pear fruits," *Plant Foods for Human Nutrition*, vol. 65, no. 3, pp. 253–259, 2010.

[34] E. Castellanos-Santiago and E. M. Yahia, "Identification and quantification of betalains from the fruits of 10 mexican prickly pear cultivars by high-performance liquid chromatography and electrospray ionization mass spectrometry," *Journal of Agricultural and Food Chemistry*, vol. 56, no. 14, pp. 5758–5764, 2008.

[35] E. M. Diaz Medina, E. M. Rodriguez Rodriguez, and C. D. Romero, "Chemical characterization of Opuntia dillenii and Opuntia ficus indica fruits," *Food Chemistry*, vol. 103, no. 1, pp. 38–45, 2007.

[36] T. E. Moussa-Ayoub, E.-S. A. Abd El-Hady, H. T. Omran, S. K. El-Samahy, L. W. Kroh, and S. Rohn, "Influence of cultivar and origin on the flavonol profile of fruits and cladodes from cactus Opuntia ficus-indica," *Food Research International*, vol. 64, pp. 864–872, 2014.

[37] J. O. Kuti, "Antioxidant compounds from four Opuntia cactus pear fruit varieties," *Food Chemistry*, vol. 85, no. 4, pp. 527–533, 2004.

[38] N. Yeddes, J. Chérif, S. Guyot, H. Sotin, and M. Ayadi, "Comparative study of antioxidant power, polyphenols, flavonoids and betacyanins of the peel and pulp of three Tunisian Opuntia forms," *Antioxidants*, vol. 2, no. 2, pp. 37–51, 2013.

[39] E.-S. S. Abdel-Hameed, M. A. Nagaty, M. S. Salman, and S. A. Bazaid, "Phytochemicals, nutritionals and antioxidant properties of two prickly pear cactus cultivars (Opuntia ficus indica Mill.) growing in Taif, KSA," *Food Chemistry*, vol. 160, pp. 31–38, 2014.

[40] C. Albano, C. Negro, N. Tommasi et al., "Betalains, phenols and antioxidant capacity in cactus pear [Opuntia ficus-indica (L.) Mill.] fruits from Apulia (South Italy) genotypes," *Antioxidants*, vol. 4, no. 2, pp. 269–280, 2015.

[41] N. Chougui, A. Tamendjari, W. Hamidj et al., "Oil composition and characterisation of phenolic compounds of Opuntia ficus-indica seeds," *Food Chemistry*, vol. 139, no. 1–4, pp. 796–803, 2013.

[42] A. Mata, J. P. Ferreira, C. Semedo, T. Serra, C. M. M. Duarte, and M. R. Bronze, "Contribution to the characterization of Opuntia spp. juices by LC-DAD-ESI-MS/MS," *Food Chemistry*, vol. 210, pp. 558–565, 2016.

[43] M. S. Tounsi, I. Ouerghemmi, R. Ksouri, W. A. Wannes, I. Hammrouni, and B. Marzouik, "HPLC-determination of phenolic composition and antioxidant capacity of cactus prickly pears seeds," *Asian Journal of Chemistry*, vol. 23, no. 3, pp. 1006–1010, 2011.

[44] F. C. Stintzing and R. Carle, "Betalains - emerging prospects for food scientists," *Trends in Food Science and Technology*, vol. 18, no. 10, pp. 514–525, 2007.

[45] Y. Z. Cai, M. Sun, and H. Corke, "Characterization and application of betalain pigments from plants of the Amaranthaceae," *Trends in Food Science and Technology*, vol. 16, no. 9, pp. 370–376, 2005.

[46] D. Strack, T. Vogt, and W. Schliemann, "Recent advances in betalain research," *Phytochemistry*, vol. 62, no. 3, pp. 247–269, 2003.

[47] F. Gandía-Herrero, J. Escribano, and F. García-Carmona, "The role of phenolic hydroxy groups in the free radical scavenging activity of betalains," *Journal of Natural Products*, vol. 72, no. 6, pp. 1142–1146, 2009.

[48] J. Taira, E. Tsuchida, M. C. Katoh, M. Uehara, and T. Ogi, "Antioxidant capacity of betacyanins as radical scavengers for peroxyl radical and nitric oxide," *Food Chemistry*, vol. 166, pp. 531–536, 2015.

[49] D. Butera, L. Tesoriere, F. Di Gaudio et al., "Antioxidant activities of sicilian prickly pear (Opuntia ficus indica) fruit extracts and reducing properties of its betalains: betanin and indicaxanthin," *Journal of Agricultural and Food Chemistry*, vol. 50, no. 23, pp. 6895–6901, 2002.

[50] S. P. Chauhan, N. R. Sheth, I. S. Rathod, B. N. Suhagia, and R. B. Maradia, "Analysis of betalains from fruits of Opuntia species," *Phytochemistry Reviews*, vol. 12, no. 1, pp. 35–45, 2013.

[51] M. R. Castellar, F. Solano, and J. M. Obón, "Betacyanin and other antioxidants production during growth of Opuntia stricta (Haw.) fruits," *Plant Foods for Human Nutrition*, vol. 67, no. 4, pp. 337–343, 2012.

[52] A. Piga, A. Del Caro, I. Pinna, and M. Agabbio, "Changes in ascorbic acid, polyphenol content and antioxidant activity in minimally processed cactus pear fruits," *LWT-Food Science and Technology*, vol. 36, no. 2, pp. 257–262, 2003.

[53] S. Mendis, P. Puska, and B. Norrving, *Global Atlas on Cardiovascular Disease Prevention and Control*, World Health Organization, World Heart Federation, World Stroke Organization, World Health Organization in collaboration with the World Heart Federation and the World Stroke Organization, Geneva, 2011.

[54] T. Rodríguez, M. Malvezzi, L. Chatenoud et al., "Trends in mortality from coronary heart and cerebrovascular diseases in the Americas: 1970-2000," *Heart*, vol. 92, no. 4, pp. 453–460, 2006.

[55] H. Schargrodsky, R. Hernández-Hernández, B. M. Champagne et al., "CARMELA: assessment of cardiovascular risk in seven Latin American cities," *The American Journal of Medicine*, vol. 121, no. 1, pp. 58–65, 2008.

[56] B. Acosta-Cázares and J. Escobedo-de la Peña, "High burden of cardiovascular disease risk factors in Mexico: an epidemic of ischemic heart disease that may be on its way?" *American Heart Journal*, vol. 160, no. 2, pp. 230–236, 2010.

[57] U. Osuna-Martínez, J. Reyes-Esparza, and L. Rodríguez-Fragoso, "Cactus (Opuntia ficus-indica): a review on its antioxidants properties and potential pharmacological use in chronic diseases," *Natural Products Chemistry & Research*, vol. 2, no. 6, p. 153, 2014.

[58] L. Tesoriere, D. Butera, A. M. Pintaudi, M. Allegra, and M. A. Livrea, "Supplementation with cactus pear (Opuntia ficus-indica) fruit decreases oxidative stress in healthy humans: a comparative study with vitamin C," *The American Journal of Clinical Nutrition*, vol. 80, no. 2, pp. 391–395, 2004.

[59] A. Budinsky, R. Wolfram, A. Oguogho, Y. Efthimiou, Y. Stamatopoulos, and H. Sinzinger, "Regular ingestion of Opuntia robusta lowers oxidation injury," *Prostaglandins, Leukotrienes, and Essential Fatty Acids*, vol. 65, no. 1, pp. 45–50, 2001.

[60] E. Linarès, C. Thimonier, and M. Degre, "The effect of NeOpuntia on blood lipid parameters—risk factors for the metabolic syndrome (syndrome X)," *Advances in Therapy*, vol. 24, no. 5, pp. 1115–1125, 2007.

[61] O. Osorio-Esquivel, A. Ortiz-Moreno, L. Garduño-Siciliano, V. B. Alvarez, and M. D. Hernández-Navarro, "Antihyperlipidemic effect of methanolic extract from Opuntia joconostle seeds in mice fed a hypercholesterolemic diet," *Plant Foods for Human Nutrition*, vol. 67, no. 4, pp. 365–370, 2012.

[62] T. L. Zern, R. J. Wood, C. Greene et al., "Grape polyphenols exert a cardioprotective effect in pre- and postmenopausal women by lowering plasma lipids and reducing oxidative stress," *The Journal of Nutrition*, vol. 135, no. 8, pp. 1911–1917, 2005.

[63] R. M. Wolfram, H. Kritz, Y. Efthimiou, J. Stomatopoulos, and H. Sinzinger, "Effect of prickly pear (Opuntia robusta) on glucose- and lipid-metabolism in non-diabetics with hyperlipidemia—a pilot study," *Wiener Klinische Wochenschrift*, vol. 114, no. 19-20, pp. 840–846, 2002.

[64] F. Garcia-Diez, V. Garcia-Mediavilla, J. E. Bayon, and J. Gonzalez-Gallego, "Pectin feeding influences fecal bile acid excretion, hepatic bile acid and cholesterol synthesis and serum cholesterol in rats," *The Journal of Nutrition*, vol. 126, no. 7, pp. 1766–1771, 1996.

[65] P. Gunness and M. J. Gidley, "Mechanisms underlying the cholesterol-lowering properties of soluble dietary fibre polysaccharides," *Food & Function*, vol. 1, no. 2, pp. 149–155, 2010.

[66] P.-S. Oh and K.-T. Lim, "Glycoprotein (90 kDa) isolated from Opuntia ficus-indica var. saboten MAKINO lowers plasma lipid level through scavenging of intracellular radicals in triton WR-1339-induced mice," *Biological & Pharmaceutical Bulletin*, vol. 29, no. 7, pp. 1391–1396, 2006.

[67] D. Steinberg, "Low density lipoprotein oxidation and its pathobiological significance," *The Journal of Biological Chemistry*, vol. 272, no. 34, pp. 20963–20966, 1997.

[68] U. P. Steinbrecher, "Receptors for oxidized low density lipoprotein," *Biochimica et Biophysica Acta*, vol. 1436, no. 3, pp. 279–298, 1999.

[69] A. J. Lusis, "Atherosclerosis," *Nature*, vol. 407, pp. 233–241, 2000.

[70] R. Salvayre, A. Negre-Salvayre, and C. Camaré, "Oxidative theory of atherosclerosis and antioxidants," *Biochimie*, vol. 125, pp. 281–296, 2016.

[71] H. Cai, "NAD(P)H oxidase-dependent self-propagation of hydrogen peroxide and vascular disease," *Circulation Research*, vol. 96, pp. 818–822, 2005.

[72] M. Chen, T. Masaki, and T. Sawamura, "LOX-1, the receptor for oxidized low-density lipoprotein identified from endothelial cells: implications in endothelial dysfunction and atherosclerosis," *Pharmacology & Therapeutics*, vol. 95, no. 1, pp. 89–100, 2002.

[73] D. P. Hajjar and M. E. Haberland, "Lipoprotein trafficking in vascular cells. Molecular Trojan horses and cellular

saboteurs," *The Journal of Biological Chemistry*, vol. 272, no. 37, pp. 22975–22978, 1997.

[74] A. Negre-Salvayre, N. Auge, V. Ayala et al., "Pathological aspects of lipid peroxidation," *Free Radical Research*, vol. 44, no. 10, pp. 1125–1171, 2010.

[75] J. Keller, C. Camaré, C. Bernis et al., "Antiatherogenic and antitumoral properties of Opuntia cladodes: inhibition of low density lipoprotein oxidation by vascular cells, and protection against the cytotoxicity of lipid oxidation product 4-hydroxynonenal in a colorectal cancer cellular model," *Journal of Physiology and Biochemistry*, vol. 71, no. 3, pp. 577–587, 2015.

[76] S. Garoby-Salom, F. Guéraud, C. Camaré et al., "Dietary cladode powder from wild type and domesticated Opuntia species reduces atherogenesis in apoE knock-out mice," *Journal of Physiology and Biochemistry*, vol. 72, no. 1, pp. 59–70, 2016.

[77] C. Gentile, L. Tesoriere, M. Allegra, M. A. Livrea, and P. D'Alessio, "Antioxidant betalains from cactus pear (Opuntia ficus-indica) inhibit endothelial ICAM-1 expression," *Annals of the New York Academy of Sciences*, vol. 1028, no. 1, pp. 481–486, 2004.

[78] L. Tesoriere, A. Attanzio, M. Allegra, C. Gentile, and M. A. Livrea, "Phytochemical indicaxanthin suppresses 7-ketocholesterol-induced THP-1 cell apoptosis by preventing cytosolic Ca(2+) increase and oxidative stress," *The British Journal of Nutrition*, vol. 110, no. 2, pp. 230–240, 2013.

[79] A. Negre-Salvayre, R. Salvayre, N. Augé, R. Pamplona, and M. Portero-Otín, "Hyperglycemia and glycation in diabetic complications," *Antioxidants & Redox Signaling*, vol. 11, no. 12, pp. 3071–3109, 2009.

[80] P. López-Romero, E. Pichardo-Ontiveros, A. Avila-Nava et al., "The effect of nopal (Opuntia ficus indica) on post-prandial blood glucose, incretins, and antioxidant activity in Mexican patients with type 2 diabetes after consumption of two different composition breakfasts," *Journal of the Academy of Nutrition and Dietetics*, vol. 114, no. 11, pp. 1811–1818, 2014.

[81] A. C. Frati-Munari, B. E. Gordillo, P. Altamirano, and C. R. Ariza, "Hypoglycemic effect of Opuntia streptacantha Lemaire in NIDDM," *Diabetes Care*, vol. 11, no. 1, pp. 63–66, 1988.

[82] A. TrejoGonzalez, G. GabrielOrtiz, A. M. PueblaPerez et al., "A purified extract from prickly pear cactus (Opuntia fuliginosa) controls experimentally induced diabetes in rats," *Journal of Ethnopharmacology*, vol. 55, no. 1, pp. 27–33, 1996.

[83] S.-W. Hahm, J. Park, and Y.-S. Son, "Opuntia humifusa stems lower blood glucose and cholesterol levels in streptozotocin-induced diabetic rats," *Nutrition Research*, vol. 31, no. 6, pp. 479–487, 2011.

[84] A. Andrade-Cetto and H. Wiedenfeld, "Anti-hyperglycemic effect of Opuntia streptacantha Lem," *Journal of Ethnopharmacology*, vol. 133, no. 2, pp. 940–943, 2011.

[85] M. P. Godard, B. A. Ewing, I. Pischel, A. Ziegler, B. Benedek, and B. Feistel, "Acute blood glucose lowering effects and long-term safety of OpunDia supplementation in pre-diabetic males and females," *Journal of Ethnopharmacology*, vol. 130, no. 3, pp. 631–634, 2010.

[86] K. Shapiro and W. C. Gong, "Natural products used for diabetes," *Journal of the American Pharmaceutical Association*, vol. 42, no. 2, pp. 217–226, 2002.

[87] J. L. J. Lopez, "Use of Opuntia cactus as a hypoglycemic agent in managing type 2 diabetes mellitus among Mexican American patients," *Nutrition Bytes*, vol. 12, no. 1, 2007, December 2016, http://escholarship.org/uc/item/555845bf.

[88] F. J. Alarcon-Aguilar, A. Valdes-Arzate, S. Xolalpa-Molina et al., "Hypoglycemic activity of two polysaccharides isolated from Opuntia ficus-indica and O. streptacantha," *Proceedings of the Western Pharmacology Society*, vol. 46, pp. 139–142, 2003.

[89] J. Becerra-Jiménez and A. Andrade-Cetto, "Effect of Opuntia streptacantha Lem. on alpha-glucosidase activity," *Journal of Ethnopharmacology*, vol. 139, no. 2, pp. 493–496, 2012.

[90] V. Butterweck, L. Semlin, B. Feistel, I. Pischel, K. Bauer, and E. J. Verspohl, "Comparative evaluation of two different Opuntia ficus-indica extracts for blood sugar lowering effects in rats," *Phytotherapy Research*, vol. 25, no. 3, pp. 370–375, 2011.

[91] L. Deldicque, K. Van Proeyen, M. Ramaekers, I. Pischel, H. Sievers, and P. Hespel, "Additive insulinogenic action of Opuntia ficus-indica cladode and fruit skin extract and leucine after exercise in healthy males," *Journal of the International Society of Sports Nutrition*, vol. 10, no. 1, p. 45, 2013.

[92] F. Giacco and M. Brownlee, "Oxidative stress and diabetic complications," *Circulation Research*, vol. 107, no. 9, pp. 1058–1070, 2010.

[93] A. Berraaouan, Z. Abderrahim, M. Hassane, L. Abdelkhaleq, A. Mohammed, and B. Mohamed, "Evaluation of protective effect of cactus pear seed oil (Opuntia ficus-indica L. MILL.) against alloxan-induced diabetes in mice," *Asian Pacific Journal of Tropical Medicine*, vol. 8, no. 7, pp. 532–537, 2015.

[94] WHO, "Obesity and Overweight, WHO," (n.d.). December 2016, http://www.who.int/mediacentre/factsheets/fs311/en/.

[95] S. Hasani-Ranjbar, Z. Jouyandeh, and M. Abdollahi, "A systematic review of anti-obesity medicinal plants - an update," *Journal of Diabetes and Metabolic Disorders*, vol. 12, no. 1, p. 28, 2013.

[96] A. J. Alonso-Castro, F. Domínguez, J. R. Zapata-Morales, and C. Carranza-Álvarez, "Plants used in the traditional medicine of Mesoamerica (Mexico and Central America) and the Caribbean for the treatment of obesity," *Journal of Ethnopharmacology*, vol. 175, pp. 335–345, 2015.

[97] Y.-J. Lee, H.-S. Choi, M.-J. Seo, H.-J. Jeon, K.-J. Kim, and B.-Y. Lee, "Kaempferol suppresses lipid accumulation by inhibiting early adipogenesis in 3T3-L1 cells and zebrafish," *Food & Function*, vol. 6, no. 8, pp. 2824–2833, 2015.

[98] J. Lee, E. Jung, J. Lee et al., "Isorhamnetin represses adipogenesis in 3T3-L1 cells," *Obesity*, vol. 17, no. 2, pp. 226–232, 2009.

[99] M. Ennouri, H. Fetoui, E. Bourret, N. Zeghal, and H. Attia, "Evaluation of some biological parameters of Opuntia ficus indica. 1. Influence of a seed oil supplemented diet on rats," *Bioresource Technology*, vol. 97, no. 12, pp. 1382–1386, 2006.

[100] M. Ennouri, H. Fetoui, E. Bourret, N. Zeghal, F. Guermazi, and H. Attia, "Evaluation of some biological parameters of Opuntia ficus indica. 2. Influence of seed supplemented diet on rats," *Bioresource Technology*, vol. 97, no. 16, pp. 2136–2140, 2006.

[101] S. Morán-Ramos, A. Avila-Nava, A. R. Tovar, J. Pedraza-Chaverri, P. López-Romero, and N. Torres, "Opuntia ficus indica (nopal) attenuates hepatic steatosis and oxidative stress in obese Zucker (fa/fa) rats," *The Journal of Nutrition*, vol. 142, no. 11, pp. 1956–1963, 2012.

[102] J. Kang, J. Lee, D. Kwon, and Y. Song, "Effect of Opuntia humifusa supplementation and acute exercise on insulin sensitivity and associations with PPAR-γ and PGC-1α protein expression in skeletal muscle of rats," *International Journal of Molecular Sciences*, vol. 14, no. 4, pp. 7140–7154, 2013.

[103] A. Avila-Nava, L. G. Noriega, A. R. Tovar et al., "Food combination based on a pre-hispanic Mexican diet decreases metabolic and cognitive abnormalities and gut microbiota dysbiosis caused by a sucrose-enriched high-fat diet in rats," *Molecular Nutrition & Food Research*, vol. 61, no. 1, 2016.

[104] C. Rodríguez-Rodríguez, N. Torres, J. A. Gutiérrez-Uribe et al., "The effect of isorhamnetin glycosides extracted from Opuntia ficus-indica in a mouse model of diet induced obesity," *Food & Function*, vol. 6, no. 3, pp. 805–815, 2015.

[105] B. Grube, P.-W. Chong, K.-Z. Lau, and H.-D. Orzechowski, "A natural fiber complex reduces body weight in the overweight and obese: a double-blind, randomized, placebo-controlled study," *Obesity*, vol. 21, no. 1, pp. 58–64, 2013.

[106] P.-W. Chong, K.-Z. Lau, J. Gruenwald, and R. Uebelhack, "A review of the efficacy and safety of Litramine IQP-G-002AS, an *Opuntia ficus-indica* derived fiber for weight management," *Evidence-Based Complementary and Alternative Medicine*, vol. 2014, Article ID 943713, p. 6, 2014.

[107] I. J. Onakpoya, J. O'Sullivan, and C. J. Heneghan, "The effect of cactus pear (Opuntia ficus-indica) on body weight and cardiovascular risk factors: a systematic review and meta-analysis of randomized clinical trials," *Nutrition*, vol. 31, no. 5, pp. 640–646, 2015.

[108] M. Guevara-Cruz, A. R. Tovar, C. A. Aguilar-Salinas et al., "A dietary pattern including nopal, chia seed, soy protein, and oat reduces serum triglycerides and glucose intolerance in patients with metabolic syndrome," *The Journal of Nutrition*, vol. 142, no. 1, pp. 64–69, 2012.

[109] M. Antunes-Ricardo, B. E. Moreno-García, J. A. Gutiérrez-Uribe, D. Aráiz-Hernández, M. M. Alvarez, and S. O. Serna-Saldivar, "Induction of apoptosis in colon cancer cells treated with isorhamnetin glycosides from Opuntia ficus-indica pads," *Plant Foods for Human Nutrition*, vol. 69, no. 4, pp. 331–336, 2014.

[110] F. Naselli, L. Tesoriere, F. Caradonna et al., "Anti-proliferative and pro-apoptotic activity of whole extract and isolated indicaxanthin from Opuntia ficus-indica associated with re-activation of the onco-suppressor p16(INK4a) gene in human colorectal carcinoma (Caco-2) cells," *Biochemical and Biophysical Research Communications*, vol. 450, no. 1, pp. 652–658, 2014.

[111] D. Sreekanth, M. K. Arunasree, K. R. Roy, T. Chandramohan Reddy, G. V. Reddy, and P. Reddanna, "Betanin a betacyanin pigment purified from fruits of Opuntia ficus-indica induces apoptosis in human chronic myeloid leukemia cell line-K562," *Phytomedicine*, vol. 14, no. 11, pp. 739–746, 2007.

[112] R. A. Chavez-Santoscoy, J. A. Gutierrez-Uribe, and S. O. Serna-Saldívar, "Phenolic composition, antioxidant capacity and in vitro cancer cell cytotoxicity of nine prickly pear (Opuntia spp.) juices," *Plant Foods for Human Nutrition*, vol. 64, no. 2, pp. 146–152, 2009.

[113] J. Kim, S. Y. Soh, J. Shin, C.-W. Cho, Y. H. Choi, and S.-Y. Nam, "Bioactives in cactus (Opuntia ficus-indica) stems possess potent antioxidant and pro-apoptotic activities through COX-2 involvement," *Journal of the Science of Food and Agriculture*, vol. 95, no. 13, pp. 2601–2606, 2014.

[114] S.-W. Hahm, J. Park, and Y.-S. Son, "Opuntia humifusa partitioned extracts inhibit the growth of U87MG human glioblastoma cells," *Plant Foods for Human Nutrition*, vol. 65, no. 3, pp. 247–252, 2010.

[115] S.-W. Hahm, J. Park, S.-Y. Oh et al., "Anticancer properties of extracts from Opuntia humifusa against human cervical carcinoma cells," *Journal of Medicinal Food*, vol. 18, no. 1, pp. 31–44, 2015.

[116] A. T. Serra, J. Poejo, A. A. Matias, M. R. Bronze, and C. M. M. Duarte, "Evaluation of Opuntia spp. derived products as antiproliferative agents in human colon cancer cell line (HT29)," *Food Research International*, vol. 54, no. 1, pp. 892–901, 2013.

[117] J. M. Feugang, F. Ye, D. Y. Zhang et al., "Cactus pear extracts induce reactive oxygen species production and apoptosis in ovarian cancer cells," *Nutrition and Cancer*, vol. 62, no. 5, pp. 692–699, 2010.

[118] D. Zou, M. Brewer, F. Garcia et al., "Cactus pear: a natural product in cancer chemoprevention," *Nutrition Journal*, vol. 4, no. 1, p. 25, 2005.

[119] L. Zourgui, E. E. Golli, C. Bouaziz, H. Bacha, and W. Hassen, "Cactus (Opuntia ficus-indica) cladodes prevent oxidative damage induced by the mycotoxin zearalenone in Balb/C mice," *Food and Chemical Toxicology*, vol. 46, no. 5, pp. 1817–1824, 2008.

[120] L. Zorgui, I. Ayed-Boussema, Y. Ayed, H. Bacha, and W. Hassen, "The antigenotoxic activities of cactus (Opuntia ficus-indica) cladodes against the mycotoxin zearalenone in Balb/c mice: prevention of micronuclei, chromosome aberrations and DNA fragmentation," *Food and Chemical Toxicology*, vol. 47, no. 3, pp. 662–667, 2009.

[121] D. Brahmi, C. Bouaziz, Y. Ayed, H. Ben Mansour, L. Zourgui, and H. Bacha, "Chemopreventive effect of cactus Opuntia ficus indica on oxidative stress and genotoxicity of aflatoxin B1," *Nutrition and Metabolism*, vol. 8, no. 1, p. 73, 2011.

[122] J.-A. Lee, B.-G. Jung, and B.-J. Lee, "Inhibitory effects of Opuntia humifusa on 7, 12-dimethyl- benz[a]anthracene and 12-O-tetradecanoylphorbol-13- acetate induced two-stage skin carcinogenesis," *Asian Pacific Journal of Cancer Prevention*, vol. 13, no. 9, pp. 4655–4660, 2012.

[123] J.-A. Lee, B.-G. Jung, T.-H. Kim, S.-G. Lee, Y.-S. Park, and B.-J. Lee, "Dietary feeding of Opuntia humifusa inhibits UVB radiation-induced carcinogenesis by reducing inflammation and proliferation in hairless mouse model," *Photochemistry and Photobiology*, vol. 89, no. 5, pp. 1208–1215, 2013.

[124] S. Guo and L. A. DiPietro, "Factors affecting wound healing," *Journal of Dental Research*, vol. 89, no. 3, pp. 219–229, 2010.

[125] R. C. Ribeiro, S. M. A. G. Barreto, E. A. Ostrosky, P. A. da Rocha-Filho, L. M. Veríssimo, and M. Ferrari, "Production and characterization of cosmetic nanoemulsions containing Opuntia ficus-indica (L.) Mill extract as moisturizing agent," *Molecules*, vol. 20, no. 2, pp. 2492–2509, 2015.

[126] T. Nakahara, C. Mitoma, A. Hashimoto-Hachiya et al., "Antioxidant Opuntia ficus-indica extract activates AHR-NRF2 signaling and upregulates filaggrin and loricrin expression in human keratinocytes," *Journal of Medicinal Food*, vol. 18, no. 10, pp. 1143–1149, 2015.

[127] A. M. Deters, U. Meyer, and F. C. Stintzing, "Time-dependent bioactivity of preparations from cactus pear (Opuntia ficus indica) and ice plant (Mesembryanthemum crystallinum) on human skin fibroblasts and keratinocytes," *Journal of Ethnopharmacology*, vol. 142, no. 2, pp. 438–444, 2012.

[128] F. Di Lorenzo, A. Silipo, A. Molinaro et al., "The polysaccharide and low molecular weight components of Opuntia ficus indica cladodes: structure and skin repairing properties," *Carbohydrate Polymers*, vol. 157, pp. 128–136, 2017.

[129] M. Antunes-Ricardo, J. A. Gutiérrez-Uribe, C. Martínez-Vitela, and S. O. Serna-Saldívar, "Topical anti-inflammatory effects of isorhamnetin glycosides isolated from Opuntia ficus-indica," *BioMed Research International*, vol. 2015, Article ID 847320, p. 9, 2015.

[130] K. Park, H.-S. Choi, Y. H. Hong, E. Y. Jung, and H. J. Suh, "Cactus cladodes (Opuntia humifusa) extract minimizes the effects of UV irradiation on keratinocytes and hairless mice," *Pharmaceutical Biology*, vol. 55, no. 1, pp. 1032–1040, 2017.

[131] H.-I. Jun, M.-N. Cha, E.-I. Yang, D. G. Choi, and Y.-S. Kim, "Physicochemical properties and antioxidant activity of Korean cactus (Opuntia humifusa) cladodes," *Horticulture, Environment and Biotechnology*, vol. 54, no. 3, pp. 288–295, 2013.

[132] S.-F. Chang, C.-L. Hsieh, and G.-C. Yen, "The protective effect of Opuntia dillenii haw fruit against low-density lipoprotein peroxidation and its active compounds," *Food Chemistry*, vol. 106, no. 2, pp. 569–575, 2008.

[133] L. P. Méndez, F. T. Flores, J. D. Martín, E. M. Rodríguez Rodríguez, and C. Díaz Romero, "Physicochemical characterization of cactus pads from Opuntia dillenii and Opuntia ficus indica," *Food Chemistry*, vol. 188, pp. 393–398, 2015.

[134] L. Santos-Zea, J. A. Gutierrez-Uribe, and S. O. Serna-Saldivar, "Comparative analyses of total phenols, antioxidant activity, and flavonol glycoside profile of cladode flours from different varieties of Opuntia spp," *Journal of Agricultural and Food Chemistry*, vol. 59, no. 13, pp. 7054–7061, 2011.

[135] Y. S. Coria Cayupan, M. J. Ochoa, and M. A. Nazareno, "Health-promoting substances and antioxidant properties of Opuntia sp. fruits. Changes in bioactive-compound contents during ripening process," *Food Chemistry*, vol. 126, no. 2, pp. 514–519, 2011.

[136] Z. Bouzoubaâ, Y. Essoukrati, S. Tahrouch, A. Hatimi, S. Gharby, and H. Harhar, "Phytochemical study of prickly pear from southern Morocco," *Journal of the Saudi Society of Agricultural Sciences*, vol. 15, no. 2, pp. 155–161, 2016.

Hindawi
Oxidative Medicine and Cellular Longevity
Volume 2017, Article ID 8356175, 13 pages
https://doi.org/10.1155/2017/8356175

Research Article

A Single Zidovudine (AZT) Administration Delays Hepatic Cell Proliferation by Altering Oxidative State in the Regenerating Rat Liver

Armando Butanda-Ochoa,[1] Diego Rolando Hernández-Espinosa,[2] Marisela Olguín-Martínez,[1] Lourdes Sánchez-Sevilla,[1] Mario R. Rodríguez,[2] Benito Chávez-Rentería,[3] Alberto Aranda-Fraustro,[3] and Rolando Hernández-Muñoz[1]

[1]*Departamento de Biología Celular y Desarrollo, Instituto de Fisiología Celular, Universidad Nacional Autónoma de México (UNAM), 04510 Ciudad de México, Mexico*
[2]*Departamento de Neurodesarrollo y Fisiología, Instituto de Fisiología Celular, Universidad Nacional Autónoma de México (UNAM), 04510 Ciudad de México, Mexico*
[3]*Departamento de Patología Instituto Nacional de Cardiología "Ignacio Chávez", 14080 Ciudad de México, Mexico*

Correspondence should be addressed to Rolando Hernández-Muñoz; rhernand@correo.ifc.unam.mx

Received 12 December 2016; Revised 1 February 2017; Accepted 21 February 2017; Published 5 April 2017

Academic Editor: Luciano Saso

The 3′-azido-3′-deoxythymidine or Zidovudine (AZT) was the first antiretroviral drug used in the treatment of HIV patients, which has good effectiveness but also hepatotoxic side effects that include cell cycle arrest and oxidative/nitrative mitochondrial damage. Whether such an oxidative damage may affect the proliferative-regenerative capacity of liver remains to be clearly specified at doses commonly used in the clinical practice. In this study, we described the oxidative-proliferative effect of AZT administered at a common clinical dose in rat liver submitted to 70% partial hepatectomy (PH). The results indicate that AZT significantly decreased DNA synthesis and the number of mitosis in liver subjected to PH in a synchronized way with the promotion of organelle-selective lipid peroxidation events (especially those observed in plasma membrane and cytosolic fractions) and with liver enzyme release to the bloodstream. Then at the dose used in clinical practice AZT decreased liver regeneration but stimulates oxidative events involved during the proliferation process in a way that each membrane system inside the cell preserves its integrity in order to maintain the cell proliferative process. Here, the induction of large amounts of free ammonia in the systemic circulation could become a factor capable of mediating the deleterious effects of AZT on PH-induced rat liver regeneration.

1. Introduction

According to the World Health Organization at the end of 2015 there were 36.7 million persons infected with HIV in the world (see Progress Report at http://www.who.int/hiv/data/en/) and 1.1 million people are dead because of HIV. The common treatment for those patients is the administration of antiretroviral nucleosides (18.2 million of patients were medicated with them in the middle of 2016 and that number is expected to increase to 30 million in 2020). Among them, the 3′-azido-3′-deoxythymidine or Zidovudine (AZT) was the first antiretroviral drug used [1, 2] and its therapeutic effect includes the blockade of the cytopathic effect and the inhibition of the viral reverse transcriptase activity [3–5]. This antiretroviral agent shows good effectiveness but also unfortunate (concentration and time of exposure dependent) side effects. The specific molecular structure of AZT can contribute to carcinogenesis causing DNA damage. The initial phosphorylation to give AZT 5′-monophosphate is performed by thymidine kinase 1 (TK1), constituting the key regulatory step in AZT metabolism and the activity of this cytosolic TK1 is dependent on the cell cycle progression (in comparison to the mitochondrial TK2 that is not relevant in cell proliferation) [6]. The AZT-5′-triphosphate formed can

be incorporated into nuclear DNA instead of the thymidine nucleotide [7, 8]. This DNA damage is repaired through the Nucleotide Excision Repair (NER) pathways [9] and it also involves cell cycle arrest by increasing the expression of phosphorylated checkpoint kinase 1 and 2 [10].

Once AZT is transported into the mitochondria [11, 12], the AZT-5′-triphosphate formed inside [8, 13] impairs the bioenergetics and increments H_2O_2 production, when glutamate/malate were used as substrates. Indicating a severe effect at the level of respiratory complex-I [14], particularly at the sub-complex-Iβ [15]. The enhanced H_2O_2 content induces a large increase in reactive oxygen species (ROS) and peroxynitrite production that causes single strand DNA breaks, lipid peroxidation, protein oxidation/nitration, and mitochondrial DNA (mtDNA) oxidation [16, 17]. Experimental evidence indicates that these prooxidative effects of AZT (or AZT-5′-triphosphate) are more related to mtDNA depletion than premature chain termination of mtDNA synthesis caused by inhibition of mitochondrial DNA-polymerase-γ [17–19]. AZT also increases lactate production but it is unclear whether it is due to poly-ADP ribose polymerase activation caused by ROS production, by direct inhibition of NADH oxidation into the mitochondria or both [16, 18]. In cardiac cells the ROS production caused by AZT also have epigenetic effects by altering the expression of 95 genes and reducing DNA methylation probably by reducing S-adenosylmethionine abundance that, in turns, reduces available substrates for new DNA methylation [19].

Based upon the aforementioned, hepatotoxicity is one of the most common adverse side effects associated with AZT involved in the oxidative/nitrative mitochondrial impairment already described, which also promotes fat accumulation by increasing fat synthesis and suppressing its degradation pathway [20] causing hepatocellular damage manifested as macro- and microvacuolar steatosis [21]. Whether such oxidative damage may affect one of the major intrinsic properties of the liver cells which is to proliferate, in order to regenerate the whole hepatic tissue, remains to be more clearly and widely understood particularly at doses commonly used in the clinical practice. In this regard, it is known that, depending on its concentration and the cell type experimentally used, AZT promotes cell cycle arrest and alters gene expression for TK1 [8, 22]. On the other hand, there is in vivo experimental evidence suggesting that lipid peroxidation (LP), induced by ROS, plays a role during the liver proliferative process [23]. In fact, it has been proposed that controlled peroxidative modifications of membranes could be playing a role in the early steps of liver regeneration and that a decrease in the magnitude or in the time-course of this partial hepatectomy (PH) induced an increase in lipid peroxidation (LP), as it occurs after administration of α-tocopherol, that could promote an early termination of the intracellular preparative events required for the replicative phase during the surgical-induced liver proliferation [23, 24].

Based on the anterior, it is possible that, at a dose commonly used in clinical practice, AZT may alter the proliferative potential of the liver and this may involve some selective alterations in the oxidative events that occurred during PH-induced rat liver regeneration. In vivo data presented here contribute to having a wider and closer approximation to understand the hepatotoxicity induced by a single clinically-used dose of AZT, especially with regard to how this antiretroviral alters the intrinsic capacity of the liver to regenerate and how such alterations may be related to other hepatocellular oxidative events. Therefore, in the present study, we described the liver oxidative-proliferative effects of a single clinical AZT administration to rats subjected to 70% PH.

2. Methods

2.1. Materials. The [^{3}H]-Thymidine (specific activity 2 Ci/mmol) was purchased from Perkin Elmer. Other reagents were obtained from Sigma Chemical Co. (St Louis MO) or JT Baker Chemicals.

2.2. Animals and Treatments. Male Wistar rats (of ~250 g weight) were fed ad libitum and maintained under a 12-hour light/dark period. Thereafter the animals were treated according to the next experimental groups: Sham, Sham + AZT, PH alone, and PH + AZT. The Sham (control) group were the laparotomized rats that received the AZT vehicle (0.9% NaCl) immediately after surgery and the Sham + AZT group were orally administered (using a gastric cannula) with 5 mg/Kg of body-weight AZT (a dose commonly used in the clinical practice). The PH group were those animals subjected to two-thirds (~70%) liver resection as described by Higgins and Anderson [25]. The PH + AZT group were those animals that were also orally administered with a single dose of 5 mg/Kg of body-weight AZT. Each experimental group comprised four animals that were independently analyzed per experimental time-point ($n = 4$). All surgical procedures were performed at about 9-10 AM, and rats were euthanized at 6, 12, 24, 48, or 72 h after surgery always under sedation with an overdose of sodium pentobarbital. All procedures were done in accordance with the *Mexican Federal Regulations for Animal Care and Experimentation* (Ministry of Agriculture, SAGARPA, NOM-062-ZOO-1999).

2.3. Isolation of Subcellular Fractions. Around 4 g of liver tissue was homogenized in 8 mL of Buffer A (225 moles/L sucrose, 10 mmol/L Tris-HCl, and 0.3 mmol/L EDTA, pH 7.4; thereafter, the homogenate was centrifuged at 1,800 g 15 min at 4°C. From here, the mitochondrial, cytosolic, and microsomal fractions were obtained and purified as described in detail by Aguilar-Delfín et al. [23]. To isolate the plasma membranes, this subcellular fraction was achieved by centrifuging through Percoll gradient, as described by Loten and Redshaw-Loten [26]. Finally, the nuclear fraction was isolated according to Sindić et al. [27]; briefly: 4 g of liver tissue was homogenized in 8 mL of buffer B (10 mmol/L HEPES pH 7.5, 5 mmol/L $MgCl_2$, 25 mmol/L KCl); then, 1.4 mL of buffer C (10 mmol/L HEPES pH 7.5, 2 mmol/L $MgCl_2$, and 2.4 mol/L sucrose) was added and mixed by inversion, followed by addition of another 26 mL of buffer D (10 mmol/L HEPES pH 7.5, 2 mmol/L $MgCl_2$, and 2.3 mol/L sucrose). The whole mixture was placed on 7.5 mL of cold buffer D and spun at 120,000 g for 45 min. The final pellet was resuspended in 0.5 mL of buffer A (10 mmol/L HEPES pH 7.5,

2 mmol/L $MgCl_2$ 0.25 mol/L sucrose). All isolated subcellular fractions were kept at −20°C until used.

2.4. Parameters Indicative of Liver Cell Proliferation. The cytosolic activity of thymidine kinase (TK) was assayed according to Sauer and Wilmanns [28]; briefly: cytosolic samples were incubated with a reaction mixture consisting in 0.2 mol/L Tris-HCl pH 8.0, 10 mmol/L EDTA, 20 mmol/L $MgCl_2$, 40 mmol/L ATP, 450 μmol/L thymidine, and 4.5 μCi [^{3}H]-Thymidine for one hour at 37°C. After stopping the reaction, samples were spun and the supernatant was filtered (with Grade DE81 ion exchange DEAE-cellulose Whatman paper) and washed with 1 mM ammonium formate. The filter papers were dried and placed in 10 mL of Tritosol scintillation liquid and counted for dpm. Mitotic index was assessed with an optical microscope (Olympus, CH-30) taking into account the number of mitotic cells in 20 microscopic fields with a 40x objective.

2.5. Caspase-3 Activity Assay. After treatment, the tissue was lysed in Caspase Assay Buffer (50 mmol/L HEPES pH 7.4, 100 mmol/L NaCl, 0.1% CHAPS, 1 mmol/L EDTA, 10% glycerol, and 10 mmol/L DTT). Equal amounts of homogenate extract (300 μg of protein) from each sample were analyzed. The assay was carried out by adding 100 μmol/L of Ac-DEVD-AMC (Sigma Chemical Co.) at 37°C. The amount of fluorescent product was monitored continuously for 60 min with a spectrofluorometer (FLx800 BIO-TEK Instruments, Winooski, VT, USA) at an excitation wavelength of 355 nm and an emission wavelength of 460 nm [29]. Data were analyzed using the KC JUNIOR software (BIO-TEK Instruments, Winooski, VT, USA), normalized to fluorescence levels in vehicle-treated cells, and expressed as relative units of fluorescence (RUF).

2.6. Parameters Indicative of Oxidant Stress in Lipids and Proteins. The amount of some LP by-products, mainly malondialdehyde (MDA), conjugated dienes, and the protein carbonyl content (protein oxidation) were determined as previously reported, in detail [30]. In the case of the protein-attached carbonyl groups (oxidized proteins), the denaturalized proteins with trichloroacetic acid were stained with 2,4-dinitrophenylhydrazine and further precipitated with 6 mol/L guanidine dissolved in 20 mmol/L KH_2PO_4 and further measured at 375 nm and finally calculated by its absorption coefficient, according to Levine et al. [31].

2.7. Determination of Blood Levels for MDA and Free Ammonia and the Serum Enzyme Activities. Heparin-anticoagulated blood was obtained from the experimental groups, and the serum was rapidly separated. Aliquots of serum and red blood cells (RBC) package were placed in ice-cold perchloric acid (8% w/v, final concentration). In neutralized perchloric extracts, the levels of MDA [30], free ammonia [32], and those of urea [33] were determined. In serum, the following enzyme activities were quantified: lactic dehydrogenase (LDH; EC 1.1.1.27), alanine aminotransferase (ALT; EC 2.6.1.2), and ornithine carbamoyltransferase (OCT; EC 2.1.3.3) by the methods described elsewhere [33]. As to Arginase (ARG; EC 3.5.3.1), this enzymatic activity was quantified according to Iyamu et al. [34].

2.8. Statistics. All results expressed as means ± error standard (SE) were analyzed using two-way analysis of variance, followed by pairwise comparisons (Tukey's-test). For individual comparisons, statistical analysis was performed using unpaired Student's t-test. In all cases, $p < 0.01$ was considered to be statistically significant.

3. Results

3.1. Effect of AZT Administration on the Liver Proliferative Profile. In the proliferating tissue, the activity of cytosolic thymidine kinase 1 (TK1) usually increases to provide thymidine triphosphate for its incorporation during DNA synthesis. Here, the PH represented a physical and chemical stimulus for cell proliferation that leads TK1 activity to reach its maximum value at 24 h after surgery (Figure 1(a)). The expression and activity of cytosolic TK1 is cell cycle dependent and its increment meant that hepatocytes population was prepared for DNA synthesis-phase and, a day after (48 h after surgery), the whole cell cycle process was culminated producing a maximal number of mitotic cells (Figure 1(b)). After PH, the administered AZT (PH + AZT) induced a significant decrease (~3-fold) on the 24 h activity peak of TK1 that was sustained 24 h more and finally reached the basal levels of the Sham and Sham + AZT control groups at 72 h after surgery (data not shown); therefore, AZT significantly decreased the activity of TK1, hence promoting a partial inhibition on DNA synthesis. The same happened with the number of mitotic cells as well (Figure 1(b)); the rate of mitotic images was very scanty in the sham-control group, which was unmodified by the treatment with AZT. On the contrary, in animals subjected to PH and administered with AZT (PH + AZT), we noted an almost 3-fold decrease in cell mitosis (48 h after surgery) when compared with the group of PH alone (Figure 1(b)). This partial inhibition of rat liver regeneration induced by the administration of AZT to PH-rats was not apparently accompanied by a stimulated apoptosis, since the cytosolic caspase-3 activity remained without significant changes in those PH-animals treated with AZT (Figure 1(c)).

3.2. Effect of AZT Administration on the Liver Profile for Lipoperoxidative Events and Oxidation of Proteins in Subcellular Fractions. The AZT promotes oxidative stress that alters cell physiology in different ways. Experimental evidence has associated lipid peroxidation to the proliferative process during liver regeneration [23]; the results obtained here indicate that oral administration of AZT alters the pattern of lipid peroxidation according to each specific cellular fraction isolated from livers submitted to a proliferative stimulus such as 70% PH. In plasma membranes, LP (MDA and conjugated dienes) significantly initiated at 12 h after surgery and then decreased over time, while AZT administration induced an earlier LP (at 6 h after surgery) that was maintained until 12 h after surgery and then decreased thereafter (Figure 2(a)). The magnitude of MDA production is expected to correlate with

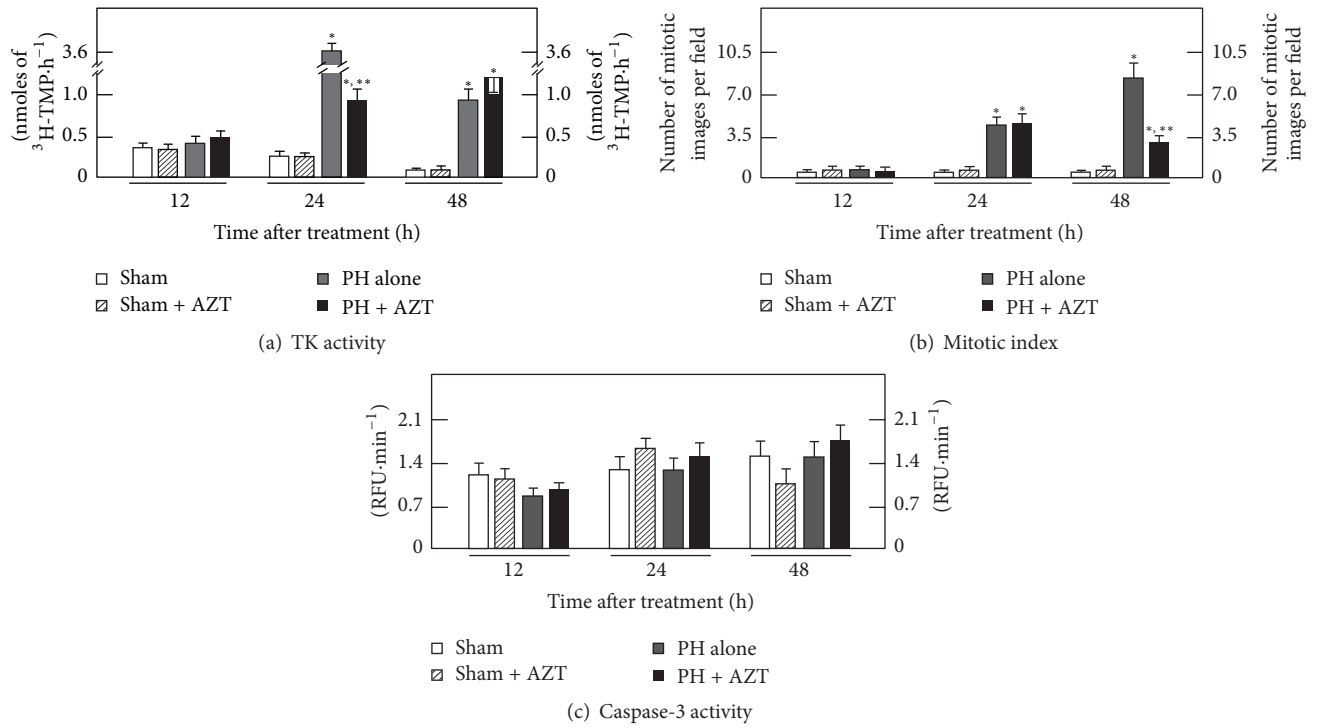

Figure 1: Effects of AZT administration on some parameters indicative of cell proliferation and apoptosis at various times after 70%-PH. Results are expressed as mean ± SE for four independent determinations per experimental point for panel (a). The activity of TK expressed as nmoles of formed [3H]-TMP·h^{-1}·mg^{-1} of cytosolic protein, in panel (b). The number of mitotic cells per microscopic field, as well as the cytosolic activity of caspase-3 (apoptosis) expressed as Relative Fluorescence Units (RFU)·min^{-1}·mg^{-1} of protein (panel (c)). Symbols for the experimental groups at the bottom of each figure. Statistical significance: $^*p < 0.01$ against Sham-operated (control) rats, and $^{**}p < 0.01$ versus the PH group.

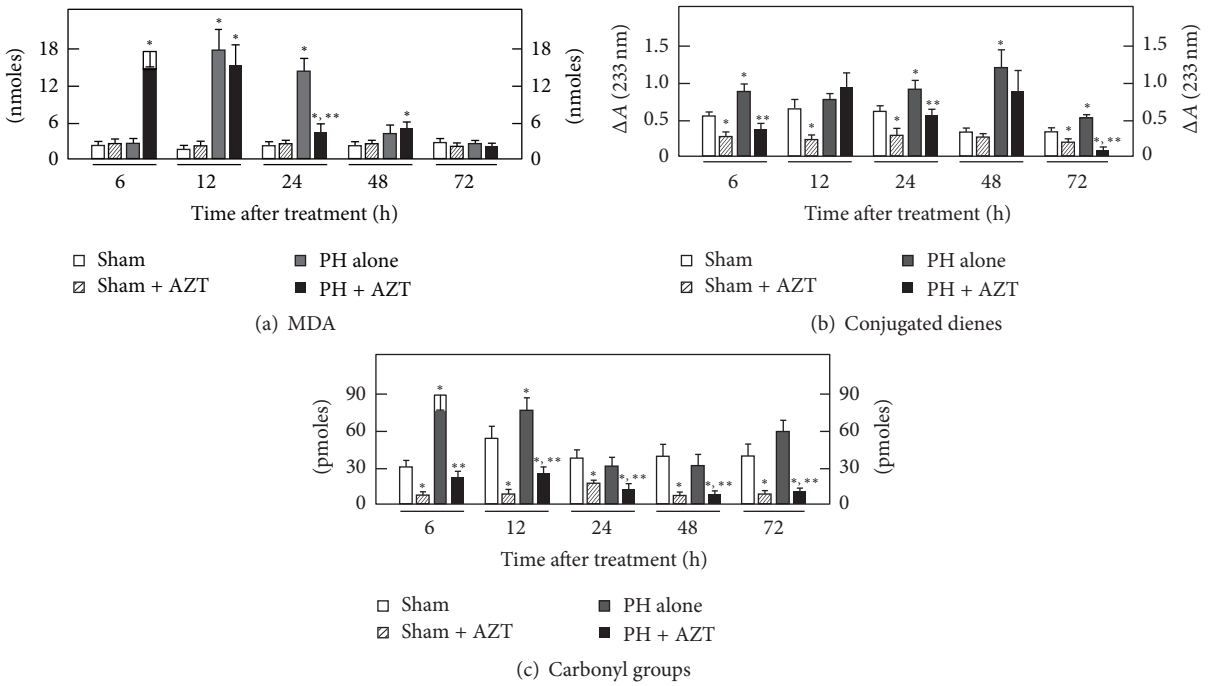

Figure 2: Effects of AZT on parameters indicative of oxidant stress in plasma membranes obtained from livers at various times after 70% PH. Results are expressed as mean ± SE for four independent determinations per experimental point as nmoles·mg^{-1} of protein in panels (a) and (b), or in pmoles·mg^{-1} of protein (panel (c)). Symbols for the experimental groups at the bottom of each figure and the statistical significance as indicated in Figure 1.

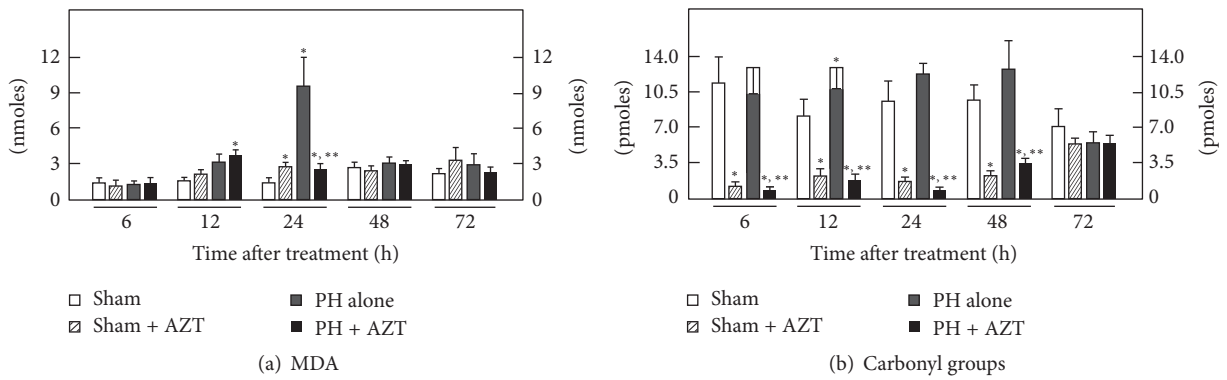

Figure 3: Effects of AZT on parameters indicative of oxidant stress in the cytosolic fraction obtained from livers at various times after 70% PH. Results are expressed as mean ± SE for four independent determinations per experimental point as nmoles·mg^{-1} of protein in panels (a) and (b), or in pmoles·mg^{-1} of protein (panel (c)). Symbols for the experimental groups at the bottom of each figure and the statistical significance as indicated in Figure 1.

conjugated dienes content, since the double conjugated bonds located along the carbon chains of lipids represent reactive (oxidable) sites for oxygen peroxides [35, 36]; therefore, when the conjugated dienes are consumed by reacting with ROS-derived peroxides, the amount of MDA and other final LP by-products will consequently increase. During the times considered in this study, control plasma membranes exhibited a basal conjugated dienes content which was significantly increased by PH along the times tested (Figure 2(b)). On the contrary, those PH-rats treated with AZT depicted lower values of conjugated dienes in plasma membranes, when compared with the group of PH alone (Figure 2(b)). Here, it should be noticed that, at 6 or 12 h after surgery, when the rate of MDA was high for plasma membranes in the PH + AZT group, the corresponding conjugated dienes levels were decreased in this experimental group.

The content of carbonyl groups indicates the rate of protein oxidation associated with an oxidative surround. In plasma membranes, administration of AZT after PH significantly decreased the levels of carbonyl groups through the times studied compared to those in the PH alone group, where we found an increase at 6 h, which diminished up to 48 h, returning to control values thereafter (Figure 2(c)). Together, these data indicated that in plasma membrane AZT influences the occurrence of oxidative events, mainly in the rate of LP, which occurred at earlier times after surgery rather than changing the magnitude of protein oxidation as a response to liver cell proliferation.

Cytosolic LP was maximally increased showing a major peak at 24 h after surgery that returned to control values thereafter. AZT administration practically avoided the PH-induced increase in cytosolic LP (Figure 3(a)). When the amount of carbonyl groups was examined in the liver cytosolic fractions from PH-rats, we detected only a modest transient increase of oxidized proteins at 12 h after PH. On the contrary, AZT administration elicited a drastic protective effect on cytosolic protein oxidation in Sham-operated control animals and, when administered to PH-rats, the nucleoside was also able to significantly decrease the content of protein's carbonyl groups in the cytosolic fraction obtained from these animals (Figure 3(b)).

As to mitochondrial LP (MDA and conjugated dienes), PH had not significant changes in this parameter and neither had AZT administration after PH at 24 h (Figure 4(a)), and we did not find significant changes in the content of conjugated dienes in these experimental groups (Figure 4(b)). However, the amount of mitochondrial protein carbonyl groups was indeed modified by AZT administration (Figure 4(c)); whereas PH alone did not induce significant changes in this parameter, AZT administration promoted significantly lower levels of mitochondrial carbonyl groups along all the times tested (Figure 4(c)). Data indicated that under proliferative conditions AZT did not promote evident oxidative events (not for lipids or for proteins) in the hepatic mitochondrion.

In the microsomal fraction, PH alone did not increase the rate of LP, as assessed by MDA content, but AZT enhanced this LP by-product at 6 and 72 h after surgery in animals subjected to PH, when compared to those with PH alone (Figure 5(a)). Whereas PH alone did not significantly modify microsomal content of conjugated dienes, AZT changed this parameter at the same experimental times (6 and 72 h after surgery, resp.) but in an opposite manner (Figure 5(b)). The carboxyl content in the microsomal fraction obtained from PH-animals only showed an early significant increase (6 h after surgery). Despite the scanty early (6 h) effects of PH in this parameter, the concomitant administration of AZT strongly decreased the rate of oxidized proteins in both sham-control and PH along the times tested (Figure 5(c)).

Regarding the nuclear fraction, PH alone promoted an early increase (6 h) in the amount of MDA, which rapidly decreased thereafter (Figure 6(a)) and was not accompanied by significant changes in the nuclear content for conjugated dienes (Figure 6(b)). The AZT treatment after PH elicited a significant lipid peroxidative effect at 24 and 72 h, respectively (Figure 6(a)), which was also associated with an active formation of conjugated dienes at the same experimental post-PH times (Figure 6(a)).

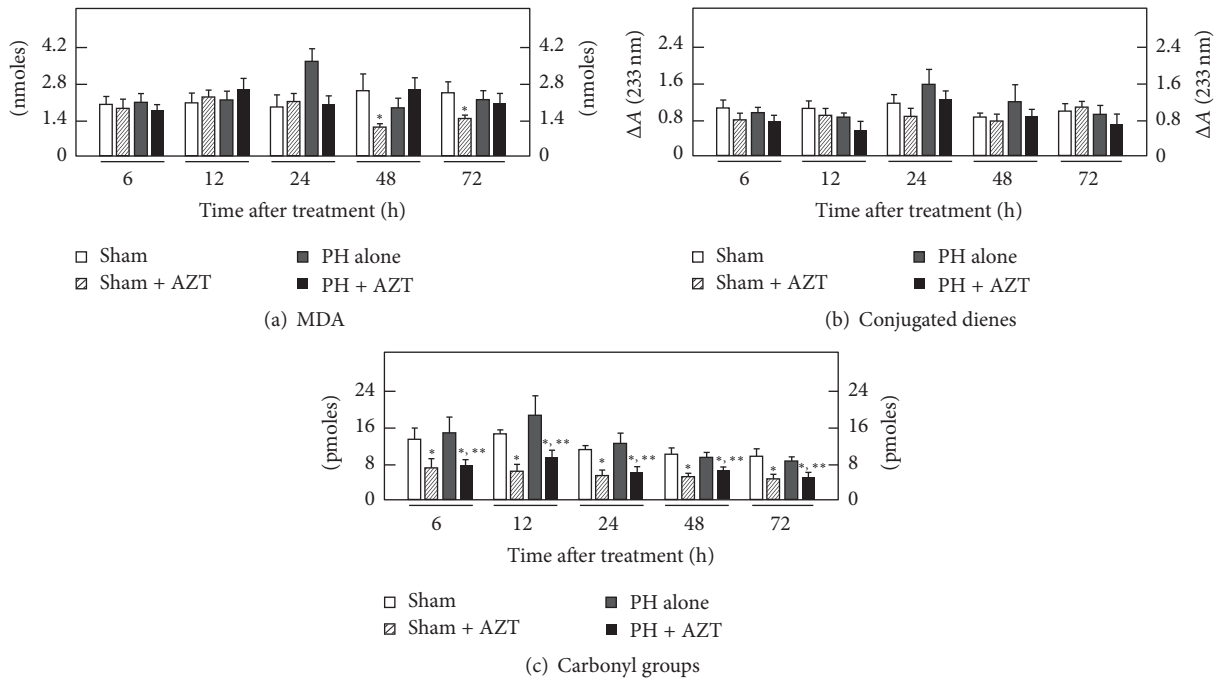

Figure 4: Effects of AZT on parameters indicative of oxidant stress in isolated mitochondria obtained from livers at various times after 70% PH. Results are expressed as mean ± SE for four independent determinations per experimental point as nmoles·mg^{-1} of protein in panels (a) and (b), or in pmoles·mg^{-1} of protein (panel (c)). Symbols for the experimental groups at the bottom of each figure and the statistical significance as indicated in Figure 1.

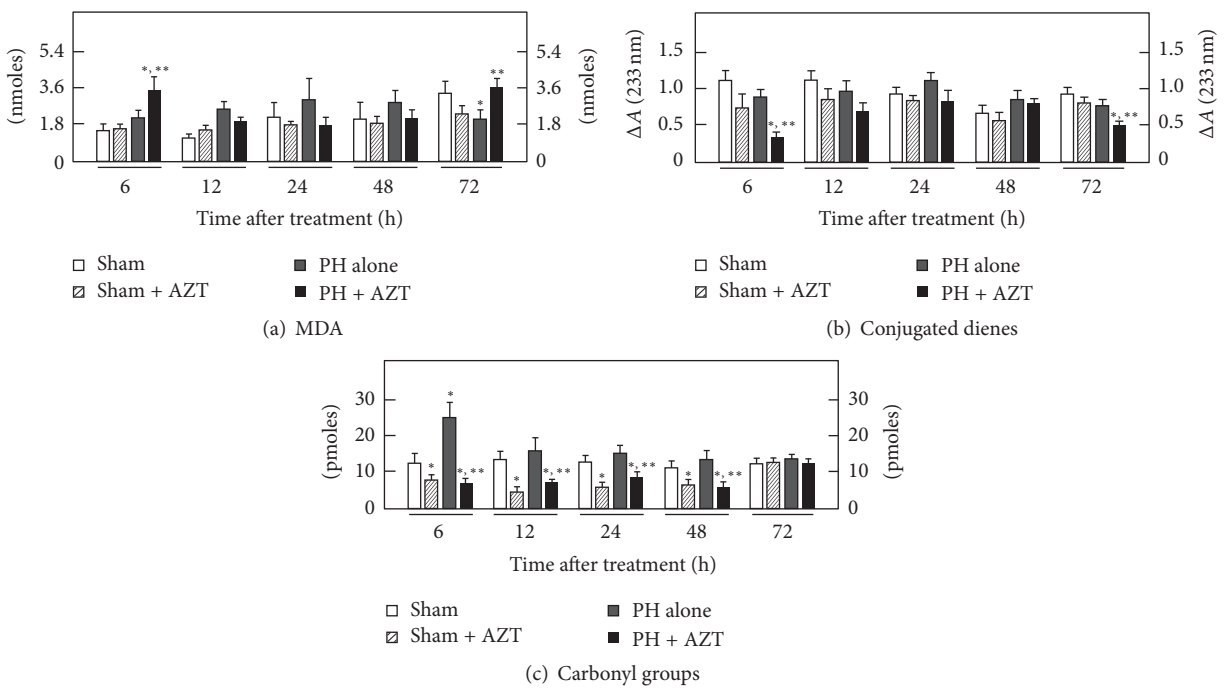

Figure 5: Effects of AZT on parameters indicative of oxidant stress in microsomes (Endoplasmic Reticulum) obtained from livers at various times after 70% PH. Results are expressed as mean ± SE for four independent determinations per experimental point as nmoles·mg^{-1} of protein in panels (a) and (b), or in pmoles·mg^{-1} of protein (panel (c)). Symbols for the experimental groups at the bottom of each figure and the statistical significance as indicated in Figure 1.

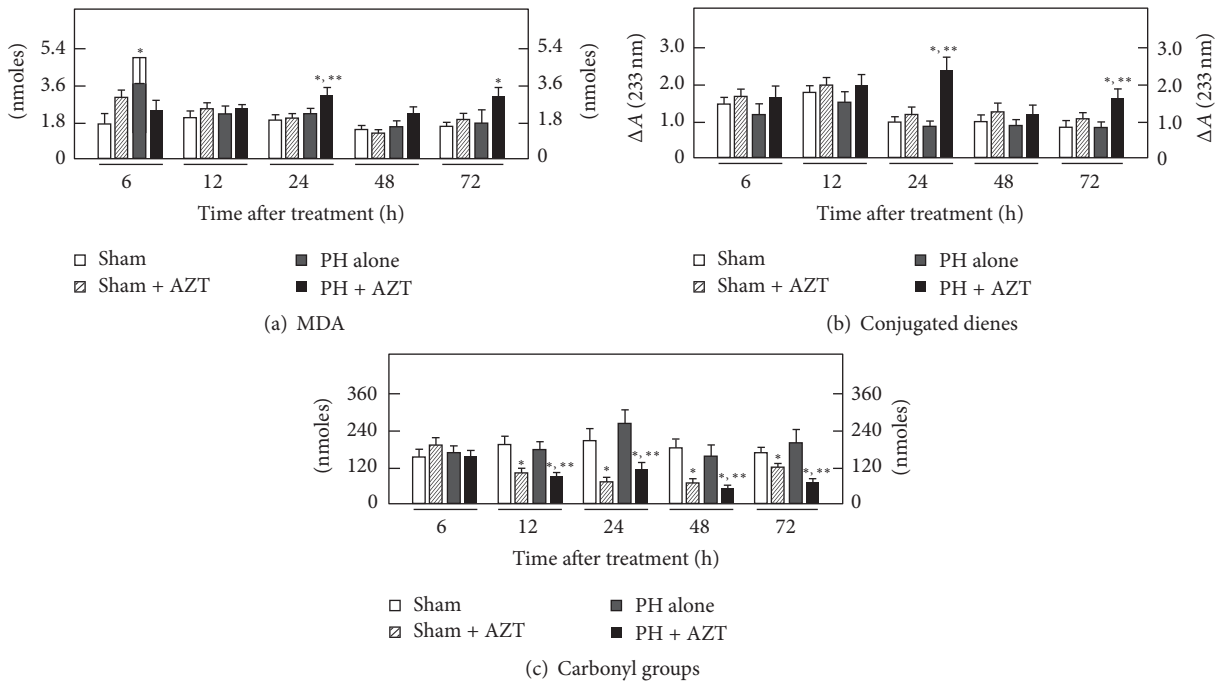

Figure 6: Effects of AZT on parameters indicative of oxidant stress in nuclei obtained from livers at various times after 70% PH. Results are expressed as mean ± SE for four independent determinations per experimental point as nmoles·mg^{-1} of protein in panels (a) to (c). Symbols for the experimental groups at the bottom of each figure and the statistical significance as indicated in Figure 1.

In agreement with the absence of effects on parameters indicative of LP, PH alone did not induce significant changes in the nuclear content of protein carbonyl groups (Figure 6(c)). On the contrary, in this subcellular fraction, the administration of AZT also exerted an important "protective" effect on nuclear protein oxidation in either control (Sham + AZT) or hepatectomized (PH + AZT) animals, practically at all postsurgery times tested (Figure 6(c)). It is noteworthy to mention that these organelle-selective peroxidation changes, already described, were not associated with apoptotic events as indicated by caspase-3 activity, which was not changed by either PH alone or AZT administration (Figure 1(c)).

3.3. Effect of AZT Administration on the Serum Enzyme Activity. Clinical practice uses some enzyme serum activity levels as indicative of liver damage, despite their levels inside the organ are not changing [37]. As previously reported [38] after PH, the serum activities of LDH, ALT, and OCT were significantly increased in a synchronized manner to DNA synthesis and mitosis showing the main peaks at 24 h after surgery and completely normalizing three days after the surgery (Figures 7(a) and 7(b)). When AZT was administered, the serum LDH activity was indeed early increased (12 h) and remained high in animals subjected to PH, whereas the profile for serum ALT induced by PH was not significantly modified by the nucleoside administration (Figure 7(a)). Regarding the OCT activity, the AZT induced an early (12 h) and drastic increase of the serum activity of this enzyme, which decreased thereafter, in a different pattern when compared to PH-animals receiving only the vehicle (Figure 7(b)). Moreover, another hepatic enzyme also involved in the cytoplasmic component of the urea cycle, namely, ARG, also shown changes in its "release" after PH. The partial removal of the liver was also accompanied by gradual increase in the serum activity of ARG, peaking at 24 h after PH, which was also altered by the administration of AZT to these animals in a similar fashion than that recorded for the activity of OCT (Figure 7(b)). Therefore, the administration of the nucleoside readily affected the magnitude and time-course of the pattern of serum enzyme activities induced by PH, which was not recorded in the control animals. As a whole, AZT indeed modified the coordinated pattern of enzyme's release elicited by the PH.

3.4. Effect of AZT Administration on Blood Levels of MDA, Ammonia, and Urea. As another parameter of liver damage, we looked for possible peroxidative events in blood compartments, serum, and RBC. In serum, PH induced a discrete increase in the MDA level (compared to control groups) only at 48 h, and the administration of AZT showed a lower value, but similar to the control ones at that time. In RBC, PH also elicited a first augmentation of MDA at 12 h, which decayed in the next twelve hours after PH, raising again at 48 h after surgery (Figures 8(a) and 8(b)). The AZT administration promoted a distinct MDA pattern in RBC from PH-animals, represented by a progressive decrement of this LP by-product throughout the times tested, even reaching MDA levels far lower than that of controls (Figures 8(a) and 8(b)). It is interesting to notice that the presence of AZT in RBC may induce oxidative events temporarily independent from liver proliferation, since the Sham + AZT group showed a sustained significant enhancement of oxidative by-products

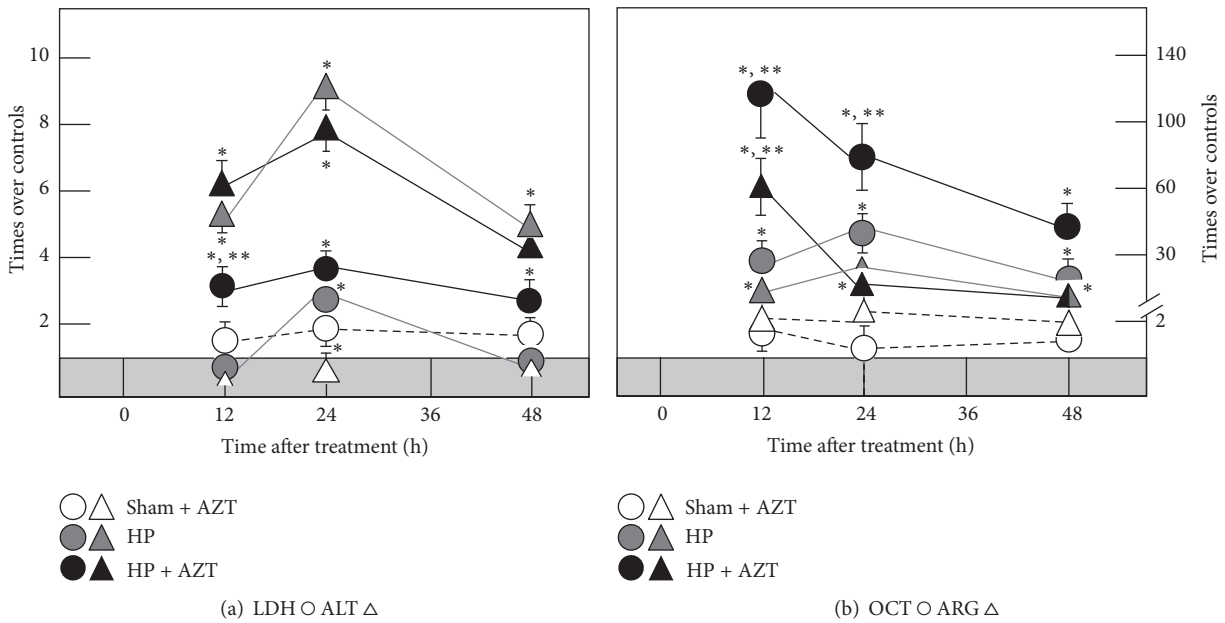

Figure 7: Effects of AZTon serum enzyme activities in samples obtained at several times after 70% PH. Results of serum enzyme activities are expressed as mean ± SE mean of four independent determinations per experimental point. In both panels, the shadowed horizontal bar represents the range of serum enzyme activities for controls (Sham): ALT 20 ± 3, LDH 570 ± 90, OCT 2.1 ± 0.3, and Arginase, 4.5 ± 0.7 IU/L. Symbols for the experimental groups at the bottom of each figure. Statistical significance as indicated in Figure 1.

levels when compared with Sham controls alone throughout this range of posttreatment time.

Blood ammonia levels can reflect liver dysfunction, which results from a compromised hepatic handling for this cation, that is, liver injury (Figures 8(c) and 8(d)). The serum levels of ammonia were maintained within the normal range and even decreased at 24 h after PH (Figure 8(c)). During PH-induced rat liver regeneration, RBC levels of ammonia almost disappeared, suggesting that an increment in blood ammonia may be an adverse effect on the "primed" liver cell proliferation promoted by PH (Figure 8(d)). In fact, a single administration of AZT induced a drastic increase of ammonia levels in both serum and RBC from sham-control and PH-rats (Figure 8(d)). Therefore, the partial inhibition in PH-induced rat liver regeneration caused by treatment with AZT was also associated with a clear hyperammonemia present in these animals, besides the alterations found in the oxidant status (Figures 2 to 6). In order to determine whether the AZT-induced increase in blood levels of ammonia was due to a defective liver ureagenesis, we also measured this nitrogen by-product in the blood compartments from our experimental groups (Figures 8(e) and 8(f)). Despite the fact that AZT administration elicited high blood levels, the nucleoside did not significantly modify serum and RBC levels of urea in control-laparotomized rats (Figures 8(e) and 8(f)). On the other hand, whereas PH alone did not change levels of blood urea, the administration of AZT significantly diminished serum levels of urea in PH-animals at 24 and 48 h after surgery (Figure 8(e)), contrasting with an unexpected and drastic accumulation of urea in RBC from the PH + AZT group (Figure 8(f)). Indeed, these results indicated that animals subjected to PH and administered with AZT had similar values for urea per mL of whole blood (3.7±0.5 against 3.1 ± 0.4 μmoles·mL^{-1} of blood, at 24 h after PH). Therefore, the augmented levels of ammonia in the blood of animals treated with a single AZT dose did not seem to be due to an ineffective liver production of urea induced by the nucleoside.

4. Discussion

Liver regeneration must undergo changes in major metabolic pathways in order to achieve DNA replication, cell division, and restitution of liver mass [39]. Hence, synthesis of thymidine triphosphate from thymidine by the cytosolic TK1 activity evidences an active DNA synthesis after PH; then the surgery represented a proliferative physical stimulus that promoted the DNA synthesis until a 24 h maximum peak which was followed by another mitosis peak a day later (Figures 1(a) and 1(b)). Here, AZT administration promoted a similar ~3-fold decrease on TK1 activity (associated with DNA synthesis) and on the number of mitosis (cell divisions). This effect on proliferative response is in accordance with a previous report [9] where it has been shown that, depending on its concentration, AZT arrests the hepatic cell cycle promoting phosphorylation of checkpoints 1 and 2 proteins that are involved in cell cycle regulation at the S-phase. Therefore, the mitotic rate occurred as an evident consequence of the surgical stimulus but at the dose administered here the azido-deoxynucleoside made the number of mitotic cell divisions significantly decreased (Figure 1(b)), due to a decreased DNA synthesis. However, it has to keep in mind that, under our experimental conditions, the AZT administration still allowed an evident TK1 activity compared to the control groups,

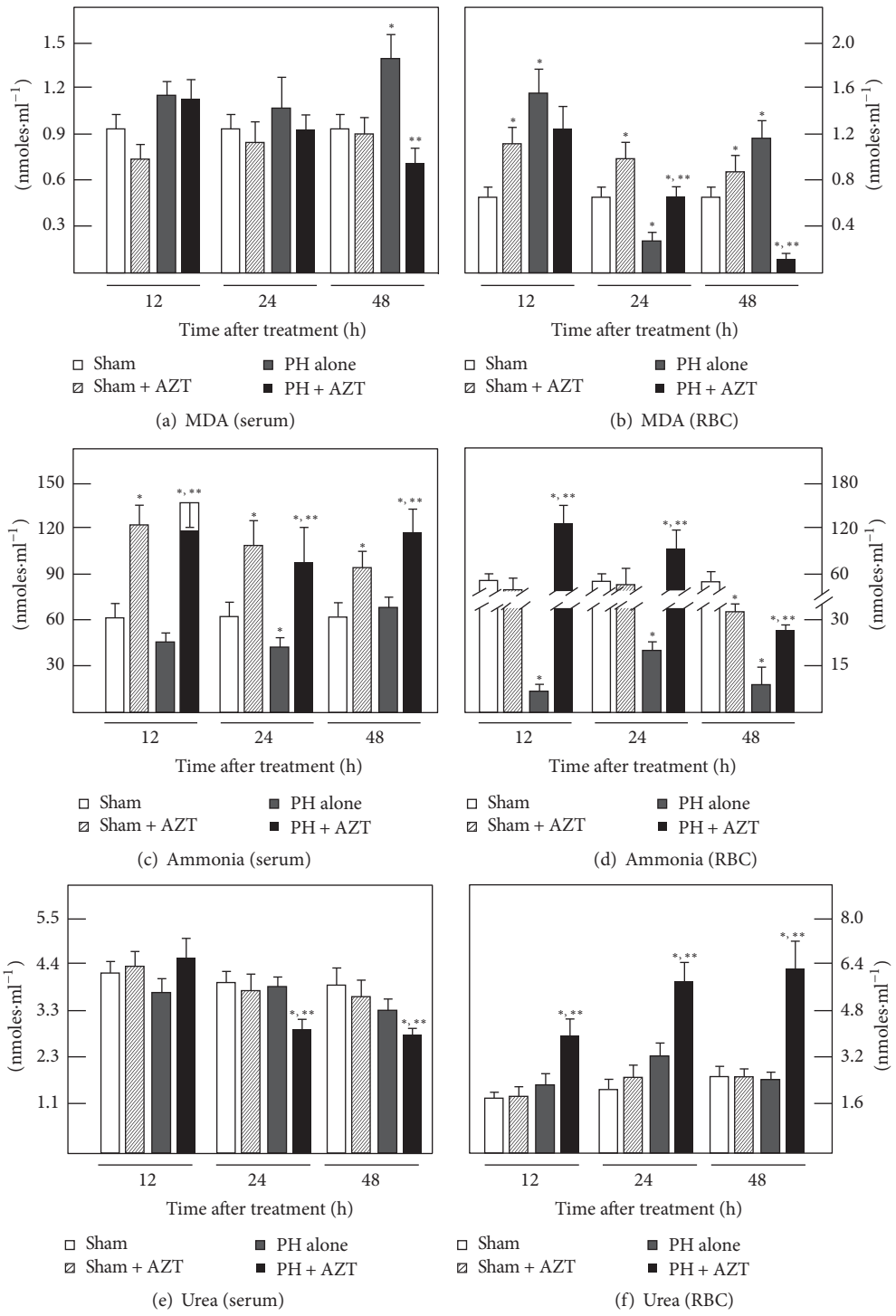

Figure 8: Effects of AZTon blood levels for MDA, ammonia, and urea in samples obtained at several times after 70% PH. Results of serum enzyme activities are expressed as mean ± SE mean of four independent determinations per experimental point. Symbols for the experimental groups at the bottom of each figure. Statistical significance as indicated in Figure 1.

which entailed a significant but discrete liver cell mitosis 24 h after the S-phase. Thus, at the clinical dose used, AZT deeply reduced the enzyme activity but did not induce its complete inhibition nor in the DNA synthesis or the mitotic cell division. Hence, under our experimental conditions, the cell cycle arrest induced by AZT may be partial, and further information must be generated in that direction. It is also interesting that the AZT-induced reduction on liver cell proliferation was not accompanied by apoptotic events mediated by caspases.

After PH, lipid peroxidative events are associated with and synchronized to proliferation but in an organelle-selective way [23]. The administration of AZT promotes an early (6–12 h) peroxidative stimulus that may represent a change in fluidity of plasma membrane [40] that prepares a posterior enzyme release to the extracellular space. In plasma membrane peroxidation of lipids is chemically preferred over proteins due to their structural double conjugated bonds that constitute reactive sites for peroxide species [36, 37]. Then, lipids of plasma membrane may represent constitutive scavengers that selectively avoid protein peroxidation. In the cytoplasmic space, where lipids and proteins are not organized and compacted as in intracellular membranes, their conjugated dienes do not have the same chemical potential to react with peroxide species. In the case of PH-induced rat liver regeneration, the LP events occurred only as a major transient event during the first 24 h of the proliferative process, and the rate of proteins oxidation was not significantly modified or even avoided when AZT was administered. Under these conditions, the effect of the administered AZT contrasted with the scheme observed for plasma membrane where AZT administration induced an early LP.

Apparently, the transient peroxidation occurred in cytosol and the change in plasma membrane fluidity (because of early LP) allows the release of active enzymes (Figure 7) that may constitute extrahepatic signals that may stimulate retrograde signals for some other organs that may contribute to the whole liver regeneration process as suggested by previous data obtained by our group [37, 38], where enzyme release under proliferative conditions was not associated with liver damage or necrosis. AZT seems to promote an early 6 h postsurgery change in plasma membrane fluidity, which was previous to the premature release of some liver enzymes (Figure 7) that may represent a signal involved in a decreased DNA synthesis and a lower mitotic response.

In the mitochondria, the proliferative conditions did not stimulate the peroxidative events (not for lipids neither for proteins) at a significant level even in the presence of AZT. Apparently, cell proliferation represents a stimulus that permits cell homeostasis to establish a control that prevails over the free radical-peroxidative uncontrolled chain reactions in order to preserve mitochondria structure and function, since it constitutes the main energy source for cell division. Therefore, it was not expected that AZT promoted the formation of any oxidative products in the mtDNA, such as the well-known 8-oxo-deoxyguanosine, previously reported [17].

The release into the blood of enzymes located at the mitochondrial compartment, such as OCT, did occur at high levels and at early times (before DNA synthesis and mitosis peaks) probably because of the high demand for extrahepatic retrograde signals. Besides, since the hepatic cells are being physically stimulated to proliferate and, so far, no ammonia production has been reported in blood cells, it is also possible that such mitochondrial enzyme release may be involved in some alterations of the urea cycle that generated the high levels of ammonia detected in the blood of PH and more notoriously in PH + AZT rats. Somehow the accumulated ammonia may be expulsed from the mitochondria to the bloodstream representing a possible source of the great ammonia levels observed in the serum and RBC of rats subjected to PH and particularly subjected to PH and AZT administration. However, a previous report from our group showed that despite the effect of PH in dragging out enzymes by in vitro perfusing the proliferating liver, the rate of urea cycle to remove ammonia is not adversely affected [32]. Moreover, despite AZT significantly increased blood levels of ammonia in control and PH-rats, this nucleoside did not reduce the amount of urea in the whole blood, but rather did change its distribution in the blood compartments (Figure 8). We ignore the physiological meaning of the differential distribution of these nitrogen-compounds in the blood compartments but, in the present study, we cannot explain the AZT-induced hyperammonemia as a consequence of a diminished liver capacity for removing this cation through forming urea. Another possibility is that AZT is altering glutamine metabolism by increasing its deamination to glutamic acid, with the corresponding production of ammonia overwhelming urea cycle; however, this hypothesis remains to be tested.

In the microsomal fraction, the activity of different metabolic enzymes depends on the integrity of membrane [41]. The increment induced by PH in lipid peroxidation correlates with a decrease in the activity of cytochrome P450E1 (CYP2E1) previously reported [42] and agrees with the gradual reduction of protein oxidation over the time. The clinical dose administration of AZT gradually reduced lipid peroxidation events and maintained far low the rate of protein oxidation during the proliferative process. In fact, the integrity of microsomal membrane and metabolic enzymes has to be preserved in order to generate the adequate reductive biochemical surround required to transform the azido-deoxynucleoside into the 3′-azido-3′-deoxy-5′-O-β-D-glucopyranuronosylthymidine (GAZT) and then to the final reduced 3′-amino-3′-deoxythymidine (AMT) by NADPH-cytochrome P450 reductase and cytochrome b5 [43–45].

Under proliferative conditions the integrity of the nucleus was practically preserved. Protein oxidation was very low in the presence of AZT. Then, it seems that AZT might exert a kind of "antioxidant" effect, mainly in this subcellular fraction. Indeed, in the presence of AZT, final LP by-products (MDA, for instance) were not completed and some conjugated double bonds were left unreacted as observed at 24 h when lipid peroxidation raised very discretely and conjugated dienes were above the control group receiving AZT. This would suggest that adequate conditions for cell proliferation demand the preservation of nuclear integrity.

Persistent slight or modest increments in blood ammonia level resulting from continuous intravenous infusion of the cation depressed hepatic TK1 and ornithine decarboxylase activities, as regenerative enzymes after 30% or 70% PH.

Specifically, TK1 activity was similarly depressed by the large transient amounts of ammonia but it was less affected by the persistent smaller amounts [46]. These data strongly indicated that ammonia can exert deleterious effects on rat liver regeneration. In this study, administration of AZT to both control Sham-operated rats and PH-animals induced a drastic elevation of blood ammonia levels in either controls and PH-animals (Figures 8(c) and 8(d)). In this regard, despite the fact that AZT does not generate ammonia during its catabolism, the fact that this cation increases mainly in those animals undergoing PH can be considered as a noxious factor that is promoting adverse actions on the rat liver regeneration induced by PH.

5. Conclusion

The present model was designed to test the possible adverse effects of AZT administered at clinical dosing, as an attempt to resemble what happens with patients that need to be treated with antiretroviral drugs and also have a liver compromised to regenerate, as this can be expected in patients infected with HIV and coinfected with viral hepatitis (HBV or HCV). In this model, administration of a single AZT dose used here decreased parameters indicative of liver cell proliferation in animals subjected to 70% PH, which coincided with alterations in the PH-induced patterns of LP which are shown to be characteristics during rat liver regeneration induced by the surgery. Then the administered dose of AZT used in clinical practice decreased liver regeneration that correlated with a constant "antioxidant" effect on the rate of protein oxidation in most of the subcellular fractions tested, which highlights the importance of preserving the functional integrity of all those proteins involved in this cell proliferative process. Moreover, the induction of large amounts of free ammonia in the systemic bloodstream could become a factor capable of mediating the deleterious effects of AZT on PH-induced rat liver regeneration. The fact that the production of the ammonia-removing molecule, urea, was not significantly affected by the administration of AZT raises the need of exploring the effects of AZT on liver nitrogen metabolism that could be involved in the pharmacological effects of this nucleoside used in the antiretroviral therapy for patients undergoing HIV infection.

Conflicts of Interest

Authors declare that they do not have any conflicts of interest.

Authors' Contributions

Armando Butanda-Ochoa and Rolando Hernández-Muñoz conceived the original idea, performed the biochemical determinations, analyzed data, and wrote the manuscript. Diego Rolando Hernández-Espinosa, Marisela Olguín-Martínez, Lourdes Sánchez-Sevilla, and Mario R. Rodríguez performed biochemical assays and analyzed the experimental data; Alberto Aranda-Fraustro and Benito Chávez-Rentería performed microscope preparations and the whole histological analysis, including quantitation of mitotic index.

Acknowledgments

The present research was partially supported by a grant from the PAPIIT-DGAPA, UNAM # IN202014, and from Consejo Nacional de Ciencia y Tecnología (CONACyT).

References

[1] M. A. Fischl, D. D. Richman, M. H. Grieco et al., "The efficacy of azidothymidine (AZT) in the treatment of patients with AIDS and AIDS-related complex. A double-blind, placebo-controlled trial," *New England Journal of Medicine*, vol. 317, no. 4, pp. 185–191, 1987.

[2] D. D. Richman, M. A. Fischl, M. H. Grieco et al., "The toxicity of azidothymidine (AZT) in the treatment of patients with AIDS and AIDS-related complex. A double-blind, placebo-controlled trial," *New England Journal of Medicine*, vol. 317, no. 4, pp. 192–197, 1987.

[3] H. Mitsuya, K. J. Weinhold, P. A. Furman et al., "3'-Azido-3'-deoxythymidine (BW A509U): an antiviral agent that inhibits the infectivity and cytopathic effect of human T-lymphotropic virus type III/lymphadenopathy-associated virus in vitro," *Proceedings of the National Academy of Sciences of the United States of America*, vol. 82, no. 20, pp. 7096–7100, 1985.

[4] P. A. Furman, J. A. Fyfe, M. H. St Clair et al., "Phosphorylation of 3'-azido-3'-deoxythymidine and selective interaction of the 5'-triphosphate with human immunodeficiency virus reverse transcriptase," *Proceedings of the National Academy of Sciences of the United States of America*, vol. 83, no. 21, pp. 8333–8337, 1986.

[5] Y. C. Cheng, G. E. Dutschman, K. F. Bastow, M. G. Sarngadharan, and R. Y. Ting, "Human immunodeficiency virus reverse transcriptase. General properties and its interactions with nucleoside triphosphate analogs," *Journal of Biological Chemistry*, vol. 262, no. 5, pp. 2187–2189, 1987.

[6] S. Aufderklamm, T. Todenhöfer, G. Gakis et al., "Thymidine kinase and cancer monitoring," *Cancer Letters*, vol. 316, no. 1, pp. 6–10, 2012.

[7] A. Zeller, J. Koenig, G. Schmitt, T. Singer, and M. Guérard, "Genotoxicity profile of Azidothymidine in vitro," *Toxicological Sciences*, vol. 135, no. 2, pp. 317–327, 2013.

[8] J.-L. Fang, T. Han, Q. Wu et al., "Differential gene expression in human hepatocyte cell lines exposed to the antiretroviral agent zidovudine," *Archives of Toxicology*, vol. 88, no. 3, pp. 609–623, 2014.

[9] Q. Wu, F. A. Beland, C.-W. Chang, and J.-L. Fang, "Role of DNA repair pathways in response to zidovudine-induced DNA damage in immortalized human liver THLE2 cells," *International Journal of Biomedical Science*, vol. 9, no. 1, pp. 18–25, 2013.

[10] J.-L. Fang and F. A. Beland, "Long-term exposure to zidovudine delays cell cycle progression, induces apoptosis, and decreases telomerase activity in human hepatocytes," *Toxicological Sciences*, vol. 111, no. 1, pp. 120–130, 2009.

[11] Y. Lai, C.-M. Tse, and J. D. Unadkat, "Mitochondrial expression of the human equilibrative nucleoside transporter 1 (hENT1) results in enhanced mitochondrial toxicity of antiviral drugs," *Journal of Biological Chemistry*, vol. 279, no. 6, pp. 4490–4497, 2004.

[12] R. Govindarajan, G. P. H. Leung, M. Zhou, C.-M. Tse, J. Wang, and J. D. Unadkat, "Facilitated mitochondrial import of antiviral and anticancer nucleoside drugs by human equilibrative

nucleoside transporter-3," *American Journal of Physiology—Gastrointestinal and Liver Physiology*, vol. 296, no. 4, pp. G910–G922, 2009.

[13] E. S. Arnér and S. Eriksson, "Mammalian deoxyribonucleoside kinases," *Pharmacology & Therapeutics*, vol. 67, no. 2, pp. 155–186, 1995.

[14] J. Pupure, M. A. S. Fernandes, M. S. Santos et al., "Mitochondria as the target for mildronate's protective effects in azidothymidine (AZT)-induced toxicity of isolated rat liver mitochondria," *Cell Biochemistry and Function*, vol. 26, no. 5, pp. 620–631, 2008.

[15] L. F. Pereira, M. B. M. Oliveira, and E. G. S. Carnieri, "Mitochondrial sensitivity to AZT," *Cell Biochemistry and Function*, vol. 16, no. 3, pp. 173–181, 1998.

[16] E. Szabados, G. M. Fischer, K. Toth et al., "Role of reactive oxygen species and poly-ADP-ribose polymerase in the development of AZT-induced cardiomyopathy in rat," *Free Radical Biology and Medicine*, vol. 26, no. 3-4, pp. 309–317, 1999.

[17] J. García de la Asunción, M. L. Del Olmo, F. V. Pallardó, and J. Viña, "Zidovudine (AZT) causes an oxidation of mitochondrial DNA in mouse liver," *Hepatology*, vol. 29, no. 3, pp. 985–987, 1999.

[18] K. C. Lund, L. L. Peterson, and K. B. Wallace, "Absence of a universal mechanism of mitochondrial toxicity by nucleoside analogs," *Antimicrobial Agents and Chemotherapy*, vol. 51, no. 7, pp. 2531–2539, 2007.

[19] C. A. Koczor, Z. Jiao, E. Fields, R. Russ, T. Ludaway, and W. Lewis, "AZT-induced mitochondrial toxicity: an epigenetic paradigm for dysregulation of gene expression through mitochondrial oxidative stress," *Physiological Genomics*, vol. 47, no. 10, pp. 447–454, 2015.

[20] A. Banerjee, M. A. Abdelmegeed, S. Jang, and B.-J. Song, "Zidovudine (AZT) and hepatic lipid accumulation: implication of inflammation, oxidative and endoplasmic reticulum stress mediators," *PLOS ONE*, vol. 8, no. 10, Article ID e76850, 2013.

[21] P. Chariot, I. Drogou, I. D. Lacroix-Szmania et al., "Zidovudine-induced mitochondrial disorder with massive liver steatosis, myopathy, lactic acidosis, and mitochondrial DNA depletion," *Journal of Hepatology*, vol. 30, no. 1, pp. 156–160, 1999.

[22] R. Sun, S. Eriksson, and L. Wang, "Zidovudine induces down-regulation of mitochondrial deoxynucleoside kinases: implications for mitochondrial toxicity of antiviral nucleoside analogs," *Antimicrobial Agents and Chemotherapy*, vol. 58, no. 11, pp. 6758–6766, 2014.

[23] I. Aguilar-Delfín, F. López-Barrera, and R. Hernández-Muñoz, "Selective enhancement of lipid peroxidation in plasma membrane in two experimental models of liver regeneration: partial hepatectomy and acute CCl4 administration," *Hepatology*, vol. 24, no. 3, pp. 657–662, 1996.

[24] C. Trejo-Solís, V. Chagoya De Sánchez, A. Aranda-Fraustro, L. Sánchez-Sevilla, C. Gómez-Ruíz, and R. Hernández-Muñoz, "Inhibitory Effect of Vitamin E Administration on the Progression of Liver Regeneration Induced by Partial Hepatectomy in Rats," *Laboratory Investigation*, vol. 83, no. 11, pp. 1669–1679, 2003.

[25] G. M. Higgins and R. M. Anderson, "Experimental pathology of the liver- restoration of the liver of the white rat following partial surgical removal," *Archives of Pathology*, vol. 12, pp. 186–202, 1931.

[26] E. G. Loten and J. C. Redshaw-Loten, "Preparation of rat liver plasma membranes in a high yield," *Analytical Biochemistry*, vol. 154, no. 1, pp. 183–185, 1986.

[27] A. Sindić, A. Aleksandrova, A. P. Fields, S. Volinia, and H. Banfić, "Presence and activation of nuclear phosphoinositide 3-kinase C2β during compensatory liver growth," *Journal of Biological Chemistry*, vol. 276, no. 21, pp. 17754–17761, 2001.

[28] H. Sauer and W. Wilmanns, "Thymydine kinase," in *Methods of Enzymatic Analysis*, H. U. Bergmeyer, J. Bergmeyer, and M. Grassl, Eds., pp. 468–473, Chemie, Deerfield Beach, Fla, USA, 1984.

[29] A. Valencia and J. Morán, "Role of oxidative stress in the apoptotic cell death of cultured cerebellar granule neurons," *Journal of Neuroscience Research*, vol. 64, no. 3, pp. 284–297, 2001.

[30] R. Hernandez-Munoz, C. Montiel-Ruiz, and O. Vazquez-Martinez, "Gastric mucosal cell proliferation in ethanol-induced chronic mucosal injury is related to oxidative stress and lipid peroxidation in rats," *Laboratory Investigation*, vol. 80, no. 8, pp. 1161–1169, 2000.

[31] R. L. Levine, D. Garland, C. N. Oliver et al., "Determination of carbonyl content in oxidatively modified proteins," *Methods in Enzymology*, vol. 186, pp. 464–478, 1990.

[32] H. U. Bergmeyer and H. O. Beutler, "Ammonia," in *Methods in Enzymatic Analysis*, H. U. Bergmeyer, J. Bergmeyer, and M. Grassl, Eds., vol. 7, pp. 454–461, Chemie, Deerfield Beach, Fla, USA, 1984.

[33] L. Kerscher and J. Ziegenhorn, "Urea," in *Methods in Enzymatic Analysis*, H. U. Bergmeyer, J. Bergmeyer, and M. Grassl, Eds., vol. 7, pp. 444–453, Chemie, Deerfield Beach, Fla, USA, 1984.

[34] E. W. Iyamu, T. Asakura, and G. M. Woods, "A colorimetric microplate assay method for high-throughput analysis of arginase activity in vitro," *Analytical Biochemistry*, vol. 383, no. 2, pp. 332–334, 2008.

[35] L. J. Marnett, "Lipid peroxidation—DNA damage by malondialdehyde," *Mutation Research*, vol. 424, no. 1-2, pp. 83–95, 1999.

[36] D. A. Pratt, K. A. Tallman, and N. A. Porter, "Free radical oxidation of polyunsaturated lipids: new mechanistic insights and the development of peroxyl radical clocks," *Accounts of Chemical Research*, vol. 44, no. 6, pp. 458–467, 2011.

[37] M. L. Contreras-Zentella and R. Hernández-Muñoz, "Is liver enzyme release really associated with cell necrosis induced by oxidant stress?" *Oxidative Medicine and Cellular Longevity*, vol. 2016, Article ID 3529149, 12 pages, 2016.

[38] J. Díaz-Juárez, L. Rivera-Valerdi, D. E. Bernal-Cerrillo, and R. Hernández-Muñoz, "Predominance of released mitochondrial enzymes by partial hepatectomy-induced rat regenerating liver is controlled by hemodynamic changes and not related to mitochondrial damage," *Scandinavian Journal of Gastroenterology*, vol. 41, no. 2, pp. 223–233, 2006.

[39] S. J. Forbes and P. N. Newsome, "Liver regeneration—mechanisms and models to clinical application," *Nature Reviews Gastroenterology & Hepatology*, vol. 13, no. 8, pp. 473–485, 2016.

[40] G. Bruscalupi, G. Curatola, G. Lenaz et al., "Plasma membrane changes associated with rat liver regeneration," *Biochimica et Biophysica Acta*, vol. 597, no. 2, pp. 263–273, 1980.

[41] J. Högberg, A. Bergstrand, and S. V. Jakobsson, "Lipid peroxidation of rat–liver microsomes: its effect on the microsomal membrane and some membrane–bound microsomal enzymes," *European Journal of Biochemistry*, vol. 37, no. 1, pp. 51–59, 1973.

[42] J. Gutiérrez-Salinas, L. Miranda-Garduño, E. Trejo-Izquierdo et al., "Redox state and energy metabolism during liver regeneration: alterations produced by acute ethanol administration," *Biochemical Pharmacology*, vol. 58, no. 11, pp. 1831–1839, 1999.

[43] Š. Bezek, M. Kukan, and P. Bohov, "Hepatobiliary disposition of 3′–Azido–3′–deoxythymidine (AZT) in the rat: effect of phenobarbitone induction," *Journal of Pharmacy and Pharmacology*, vol. 46, no. 7, pp. 575–580, 1994.

[44] J. F. Rajaonarison, B. Lacarelle, A. Durand, and J. Catalin, "In vitro metabolism of zidovudine in man," *Therapie*, vol. 48, no. 4, pp. 341–343, 1993.

[45] X.-R. Pan-Zhou, E. Cretton-Scott, X.-J. Zhou, M.-X. Yang, J. M. Lasker, and J.-P. Sommadossi, "Role of human liver P450s and cytochrome b5 in the reductive metabolism of 3'-azido-3'-deoxythymidine (AZT) to 3'-amino-3'-deoxythymidine," *Biochemical Pharmacology*, vol. 55, no. 6, pp. 757–766, 1998.

[46] L. Zieve, "Regenerative enzyme activity of the liver after partial hepatectomy or toxic injury depressed by continuous NH4+ infusion," *Journal of Laboratory and Clinical Medicine*, vol. 114, no. 5, pp. 527–530, 1989.

Hindawi
Oxidative Medicine and Cellular Longevity
Volume 2017, Article ID 9172741, 11 pages
https://doi.org/10.1155/2017/9172741

Research Article

4-Hydroxynonenal Contributes to Angiogenesis through a Redox-Dependent Sphingolipid Pathway: Prevention by Hydralazine Derivatives

Caroline Camaré,[1,2] Corinne Vanucci-Bacqué,[3] Nathalie Augé,[1,2] Mélanie Pucelle,[1,2] Corinne Bernis,[1,2] Audrey Swiader,[1,2] Michel Baltas,[3] Florence Bedos-Belval,[3] Robert Salvayre,[1,2] and Anne Nègre-Salvayre[1]

[1]*INSERM I2MC, UMR-1048, Toulouse, France*
[2]*Université Paul Sabatier Toulouse III, Toulouse, France*
[3]*CNRS UMR 5068, Laboratoire de Synthèse et Physico-Chimie de Molécules d'Intérêt Biologique, Toulouse, France*

Correspondence should be addressed to Anne Nègre-Salvayre; anne.negre-salvayre@inserm.fr

Received 5 January 2017; Accepted 1 March 2017; Published 5 April 2017

Academic Editor: Liudmila Korkina

The neovascularization of atherosclerotic lesions is involved in plaque development and may contribute to intraplaque hemorrhage and plaque fragilization and rupture. Among the various proangiogenic agents involved in the neovascularization process, proatherogenic oxidized LDLs (oxLDLs) contribute to the formation of tubes *via* the generation of sphingosine 1-phosphate (S1P), a major mitogenic and proangiogenic sphingolipid mediator. In this study, we investigated whether 4-hydroxynonenal (4-HNE), an aldehydic lipid oxidation product abundantly present in oxLDLs, contributes to their proangiogenic properties. Immunofluorescence analysis of human atherosclerotic lesions from carotid endarterectomy showed the colocalization of HNE-adducts with CD31, a marker of endothelial cells, suggesting a close relationship between 4-HNE and neovessel formation. In vitro, low 4-HNE concentration (0.5–1 μM) elicited the formation of tubes by human microvascular endothelial cells (HMEC-1), whereas higher concentrations were not angiogenic. The formation of tubes by 4-HNE involved the generation of reactive oxygen species and the activation of the sphingolipid pathway, namely, the neutral type 2 sphingomyelinase and sphingosine kinase-1 (nSMase2/SK-1) pathway, indicating a role for S1P in the angiogenic signaling of 4-HNE. Carbonyl scavengers hydralazine and bisvanillyl-hydralazone inhibited the nSMase2/SK1 pathway activation and the formation of tubes on Matrigel® evoked by 4-HNE. Altogether, these results emphasize the role of 4-HNE in the angiogenic effect of oxLDLs and point out the potential interest of pharmacological carbonyl scavengers to prevent the neovascularization process.

1. Introduction

Angiogenesis, that is, the formation of new capillaries from preexisting blood vessels, is required for embryonic vascular development and wound healing and is involved in the pathophysiology of various diseases, such as diabetic retinopathy, cancer, and atherosclerosis [1]. In human normal arteries, the adventitial vasa vasorum constitute a microvascular network that supplies oxygen and nutrients to the outer part of the arterial wall. In contrast, the inner part of the arterial wall does not contain (or only few) capillaries and is fed by diffusion from the lumen [2]. Angiogenesis from vasa vasorum may be induced by an increased thickness of the vascular wall. In atherosclerotic lesions, the relative local hypoxia, which results from insufficient oxygen and nutrient diffusion and from the enhanced demand due to increased metabolism of inflammatory cells, activates the HIF/VEGF pathway and the subsequent angiogenic response [3–7]. Interestingly, in atherosclerosis prone areas of coronary arteries, hypercholesterolemia induces neovascularization in

the very early steps of intima hyperplasia, before the thickening of the vascular wall [8, 9]. This suggests that, beside the activation of hypoxia-inducible transcription factors that enhance the expression of angiogenic factors [10, 11], some stimuli associated with hypercholesterolemia during early steps of atherosclerosis may induce an angiogenic signaling.

Atherosclerosis is a long and complex multifactorial process which involves several classical pathogenic events, including endothelial activation and injury, leukocyte recruitment and activation, oxidative stress, LDL oxidation and modification, macrophagic foam cell formation, local inflammation, smooth muscle cell migration and proliferation, and extracellular matrix (ECM) synthesis [12–16]. Early atherosclerotic lesions are characterized by clusters of lipid-laden macrophagic cells that form the fatty streaks, whereas advanced atherosclerotic plaques are constituted by a central core containing extracellular lipids (mainly cholesterol) and cell debris, surrounded by macrophagic cells and a collagenous fibrous cap [17, 18].

In atherosclerotic prone areas, activated vascular and inflammatory cells induce a local oxidative stress and LDL oxidation. In vitro, oxidized lipids exhibit a variety of biological properties, suggesting their potential role in the progression of atherosclerotic lesions [14, 19–22]. Various oxidized lipids are generated during the peroxidation of polyunsaturated fatty acids, in particular the unsaturated aldehyde 4-hydroxynonenal (4-HNE), which is highly reactive with thiol and amino groups and forms adducts with proteins and other cellular components [23–25]. 4-HNE-adducts are abundant in the center of the plaque and in macrophagic cells of human carotid atherosclerotic lesions [26, 27].

As atherosclerotic neovascularization develops mainly in lipid-rich atheromatous and inflammatory areas, this suggests that the association of atheromatous lipids with local inflammation may play a role in angiogenesis. Oxidized phospholipids exhibit proinflammatory [28] and proangiogenic properties [29]. Oxidation derivatives of arachidonic acid may act as initiators of atherogenesis and trigger endothelial cell proliferation and capillary network formation [30]. Oxidized LDLs (oxLDLs) exhibit a dual dose-dependent angiogenic effect, since low oxLDL concentrations are angiogenic, while higher concentrations are not angiogenic and are rather cytotoxic [31–35]. The angiogenic effect of oxLDLs is mediated by their binding to LOX-1 that triggers the activation of signaling pathways involving NAD(P)H oxidase, p38-MPAK, PI3 kinase/Akt/eNOS, and neutral sphingomyelinase-2/sphingosine kinase-1/sphingosine-1-phosphate (nSMase2/SK1/S1P) [31, 33, 35, 36] and the expression of angiogenic genes (e.g., VEGFR-2, PDGFR, NOTCH-1, and NRP-1) [29, 34].

Low concentration of 4-HNE upregulates VEGF expression and thus potentially induces angiogenesis, in retinal pigment epithelial cells [37]. In contrast, higher 4-HNE concentration upregulates chondromodulin-1 and inhibits angiogenesis [38].

We aimed to evaluate whether 4-HNE exerts a pro- or antiangiogenic effect on cultured endothelial cells, to investigate the 4-HNE-induced angiogenic signaling and to prevent the angiogenic effect by carbonyl scavengers and signaling inhibitors.

2. Methods

2.1. Chemicals. Matrigel was from BD Biosciences (Le-Pont-de-Claix, France). Calcein-AM bioreagent, trolox, diphenylene iodonium (DPI), GW4869, Vas2870, and hydralazine were from Sigma, and 4-HNE was from Calbiochem, [methyl-^{14}C]choline-sphingomyelin was from Perkin-Elmer. 5- (and 6-)Carboxy-2′,7′-dichlorodihydrofluorescein diacetate (H2DCFDA), was from Molecular Probes (Invitrogen France). The anti-CD31 was from Abcam, the anti-4-HNE Michael adducts were from Calbiochem, the anti-LOX-1 antibody (aLox1 Ab) was from R&D Systems, and the anti-CD68 was from Thermo Fisher Scientific. Alexa Fluor 488-conj-ugated and Alexa Fluor 546-conjugated secondary antibodies were from Invitrogen. Cell culture reagents and other materials were from WWR or Sigma. Bisvanillin (BV) and bisvanillyl-hydralazone (BVH) were synthesized as reported [39].

2.2. Cell Culture. Human microvascular endothelial cells (HMEC-1) (CDC, Dr. Candal, Atlanta, US) were grown in MCDB131 culture medium supplemented with 10% heat inactivated fetal bovine serum (FBS), 100 U/ml penicillin, and 100 μg/ml streptomycin.

2.3. LDL Isolation and Oxidation Parameters. LDLs were prepared by ultracentrifugation of pool of human sera and mildly oxidized by UV irradiation [35, 36]. The extent of LDL oxidation was monitored by the determination of the thiobarbituric reactive substance (TBARS) content, using the fluorimetric procedure of Yagi [40]. The 4-HNE-adduct content was determined by ELISA (OxiSelect™ HNE Adduct Competitive ELISA Kit, Cell Biolabs Inc.), in the conditions of the manufacturer.

Under standard conditions, these oxLDLs contained 78–97 nmol lipid hydroperoxide/mg apoB, 10–15 nmol 4-HNE/mg apoB, and 8.7 nmol TBARS/mg apoB.

2.4. Intracellular ROS Determination. Intracellular ROS generated in cells upon treatment by oxLDL or 4-HNE were evaluated by measuring the oxidation of H_2DCFDA-AM [35, 36]. 30 min before the end of the experiment, the probe was added to the culture medium (5 μM final concentration) of HMEC-1 previously seeded on 96-well microplates. Cells were carefully washed twice with phosphate buffered saline (PBS), then 0.2 ml fresh PBS was added to each well, and the fluorescence of CFDA was measured using a fluorescence microplate reader TECAN® (excitation/emission 495/525 nm). The data are expressed as ratio of fluorescence/fluorescence of the unstimulated control.

2.5. Determination of nSMase2 and SK1 Activities. The activity of nSMase2 was measured using radiolabeled [methyl-^{14}C]choline-sphingomyelin (Perkin-Elmer), and SK1 activity was determined in HMEC-1 lysed in ice-cold lysis buffer, after incubation with [^{33}P]ATP (Perkin-Elmer), as reported

[35, 36]. The [^{33}P]-labeled-S1P was extracted, isolated by TLC, and counted by liquid scintillation.

Protein concentration was determined using the Bradford reagent (Bio-Rad).

2.6. Capillary Tube Formation. HMEC-1 were seeded (30,000 cells/well) in MCDB131 supplemented with 0.1% FCS (negative control) on 24-well plates coated with Matrigel and incubated with 4-HNE freely added to the culture medium at the indicated concentrations and the pharmacological agents, when indicated. After 24 h at 37°C, the cells were labeled with Calcein-AM (1 μM, 30 minutes) and observed by fluorescence microscopy (exc. 496/em. 516, resp.), under the previously used conditions [35]. The number of capillary tubes (linked cells) was counted and reported to the total cell number.

2.7. Immunofluorescence and Immunohistochemistry. Serial 3 μm thin sections of human advanced carotid plaques obtained after endarterectomy (Cardiovascular Surgery Department, CHU Toulouse) were characterized by hemalun/eosin staining and were incubated with the antibodies, anti-CD31, anti-4-HNE Michael adducts, and anti-CD68, and revealed using either avidin-biotin horseradish peroxidase visualization system (Vectastain, ABC Kit Elite, Vector Laboratories) or Alexa Fluor 488-conjugated and Alexa Fluor 546-conjugated secondary antibodies and confocal microscopy (Zeiss 780).

2.8. Statistical Analyses. The results are presented as mean ± SEM of n experiments. Statistical significance was estimated by analysis of variance (SigmaStat 3.5, Systat Software). When test for normality and equal variance (Kolmogorov–Smirnov) was passed, differences between means values were evaluated byone-way ANOVA (several experimental groups) followed by multiple comparisons by the Holm–Sidak test. Values of $P < 0.05$ were considered significant.

3. Results

3.1. 4-HNE and Neovascularization in Human Atherosclerotic Plaques. Immunohistological studies of human atherosclerotic lesions of carotid endarterectomy show a staining for 4-HNE-adducts localized in areas labeled for CD68 (Figure 1(a)), thus suggesting that 4-HNE is generated in inflammatory areas. Confocal immunofluorescence shows that CD31-positive tubular capillary structures are surrounded by areas stained for 4-HNE-adducts (Figure 1(b), upper panels). Sometimes, 4-HNE is colocalized with CD31 (Figure 1(b), lower panels), thus suggesting that a relationship may exist between 4-HNE and angiogenesis. This led us to investigate whether 4-HNE exhibits an angiogenic effect in a model system of HMEC-1 grown on Matrigel.

3.2. Pro- and Antiangiogenic Effect of 4-HNE on HMEC-1 Grown on Matrigel. We used the HMEC-1 cell line in angiogenesis experiments, because these endothelial cells of microvascular origin are immortalized and stable over time, in contrast to primary endothelial cells (e.g., HUVEC), which originate from multiple donors and exhibit phenotypic changes and limited lifespan.

4-HNE exhibited a biphasic dose-dependent effect on tube formation by HMEC-1 cells grown on Matrigel (Figure 2(a)). Under the conditions used in Figure 2, the highest angiogenic effect was observed at low concentration, between 0.5 and 1 μM of 4-HNE. At concentrations higher than 1 μM, the angiogenic effect decreased and was below the baseline at 10 μM. The toxic effect evaluated by morphological apoptosis was detected at 10 μM and higher concentrations (Figure 2(b)).

3.3. Intracellular ROS Mediate 4-HNE-Induced Tube Formation by HMEC-1 on Matrigel. 4-HNE is one of the major RCCs present in oxLDLs that also exhibit angiogenic properties at low concentration [31, 35, 36]. This led us to investigate whether the same angiogenic signaling pathways were involved in 4-HNE tube formation. Low concentration of 4-HNE triggered a rise of intracellular ROS that peaked 30 min after 4-HNE addition to the culture medium (Figure 3(a)). 4-HNE-induced ROS were involved in the angiogenic response, as shown by the inhibitory effect of the cell-permeant antioxidant Trolox and the NADPH oxidase inhibitors DPI and Vas2870 that blocked both ROS generation and tube formation (Figures 3(b) and 3(c)). The inhibition of intracellular ROS and tube formation by DPI and Vas2870 suggest that ROS are generated by a NADPH oxidase, like those triggered by oxLDLs, but through a different mechanism. It may be noted that low oxLDL concentration triggers similar signaling and angiogenic effect through a LOX-1-dependent mechanism [31, 35], but, under the experimental conditions used here, 4-HNE-induced ROS signaling and tube formation were not inhibited by anti-LOX-1 antibody (Figures 3(b) and 3(c)), while oxLDL-induced capillary tube was inhibited by anti-LOX-1 antibody (Figure 3(d)).

3.4. 4-HNE Activates the Neutral Sphingomyelinase-2/Sphingosine Kinase-1 Pathway. As oxLDLs trigger a redox-dependent activation of the neutral sphingomyelinase2/sphingosine kinase-1 pathway (nSMase2/SK1 pathway) which is involved in oxLDL-induced angiogenesis [35, 36], we investigated whether the sphingolipid signaling pathway is implicated in 4-HNE-induced angiogenesis. As shown in Figure 4(a), incubation of HMEC-1 with 4-HNE (0.5 μM) elicits nSMase2 activation, peaking at 90 min, dependent on ROS generation, and inhibited by trolox. Moreover, as expected, nSMase2 activation was inhibited by GW4869, a well-known nSMase2 inhibitor (Figure 4(b)). 4-HNE induced SK1 activation that peaked at 90–120 min (Figure 4(c)). In agreement with the previously reported signaling cascade that coordinates the activation of nSMase2 and SK1 [41], SK1 activation was blocked by trolox that acts upstream from nSMase2, by GW4869 that inhibits nSMase2 but has no direct inhibitory effect on SK1 and by DMS which is a classical inhibitor of SK1 (Figure 4(d)). Interestingly, SK1 inhibition by GW4869 or by DMS was associated with the inhibition of capillary tube formation evoked by 4-HNE (Figures 4(d) and 4(e)), which is consistent with a role of SK1 in S1P generation, in agreement with oxLDL-induced angiogenesis [35, 36].

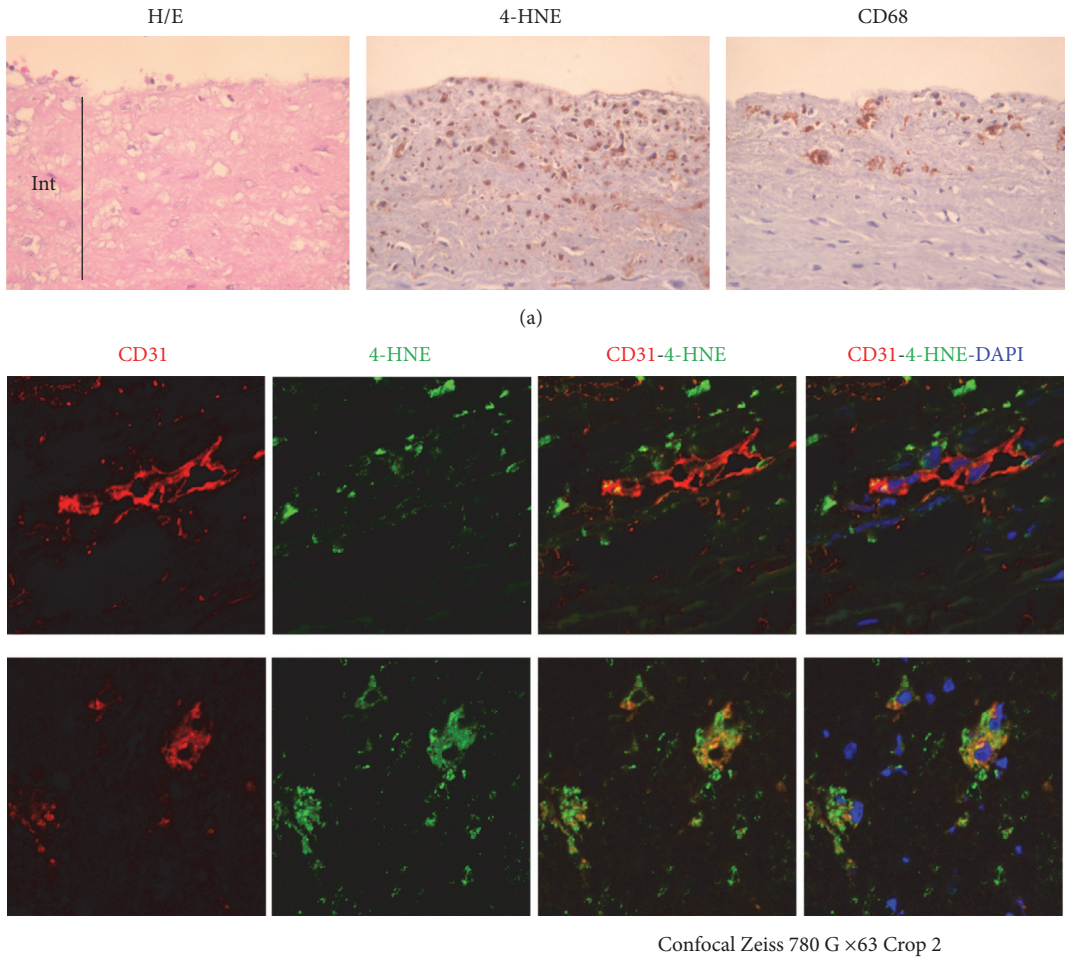

Figure 1: *4-HNE is colocalized with CD31 in human atherosclerotic lesions*. Paraffin sections of human carotid plaques from endarterectomy were analyzed. In (a), hematoxylin/eosin (H/E) staining and immunostaining for 4-HNE-adduct (HNE) and CD68 expression. In (b), immunofluorescence analysis of 4-HNE-adduct expression (green) and CD31 (red), with nuclei counterstaining by DAPI. Int: intima. These pictures are representative of analysis for 3 separate advanced carotid plaques.

3.5. 4-HNE-Induced Tube Formation Is Blocked by Hydralazine (Hdz) and Bisvanillyl-Hydralazone (BVH). Hydralazine (Hdz) is used for medical purposes as an antihypertensive drug and in combination with isosorbide dinitrate (BiDil) for the treatment of heart failure [42]. Its antiatherogenic effect has been evaluated in several hypercholesterolemic mice models [43–46]. We recently synthesized a new hydralazine derivative, the bisvanillyl-hydralazone (BVH) (Figure 5(a)), which associates antioxidant (bisvanillin) and carbonyl scavenger (hydralazine) activities and prevents both the carbonyl stress and fatty streaks formation in apoE−/− mice [39]. This led us to evaluate whether these carbonyl scavengers may prevent the angiogenic response triggered by 4-HNE in our experimental model system. Both Hdz and BVH inhibited the 4-HNE-induced ROS rise, SK1 activation, and the tube formation by HMEC-1 (Figures 5(b)–5(d)). These data suggest that Hdz may prevent the oxidative stress triggered by 4-HNE and the angiogenic response of endothelial cells.

4. Discussion

The data reported in this manuscript show that a low concentration of 4-HNE may stimulate the formation of capillary tubes by HMEC-1 on Matrigel. The angiogenic effect of 4-HNE is mediated through a signaling pathway involving ROS generation and the subsequent activation of the sphingolipid pathway (nSMase2/SK1/S1P). These effects of 4-HNE can be blocked by antioxidants and by inhibitors of the nSMase2/SK1 pathway and are prevented by carbonyl scavengers such as Hdz and BVH.

The highly reactive 4-HNE is generated during lipid peroxidation of n-6 polyunsaturated fatty acids (PUFAs) under various physio(patho)logical conditions [23]. In advanced atherosclerotic lesions, 4-HNE-adducts accumulate in atheromatous areas [26, 27]. Oxidized lipids present in these areas [21] induce a sustained ER stress in vascular cells [27, 46], alter autophagy and efferocytosis, and reduce the mobility of lipid-laden macrophages that are trapped in the lesion [14].

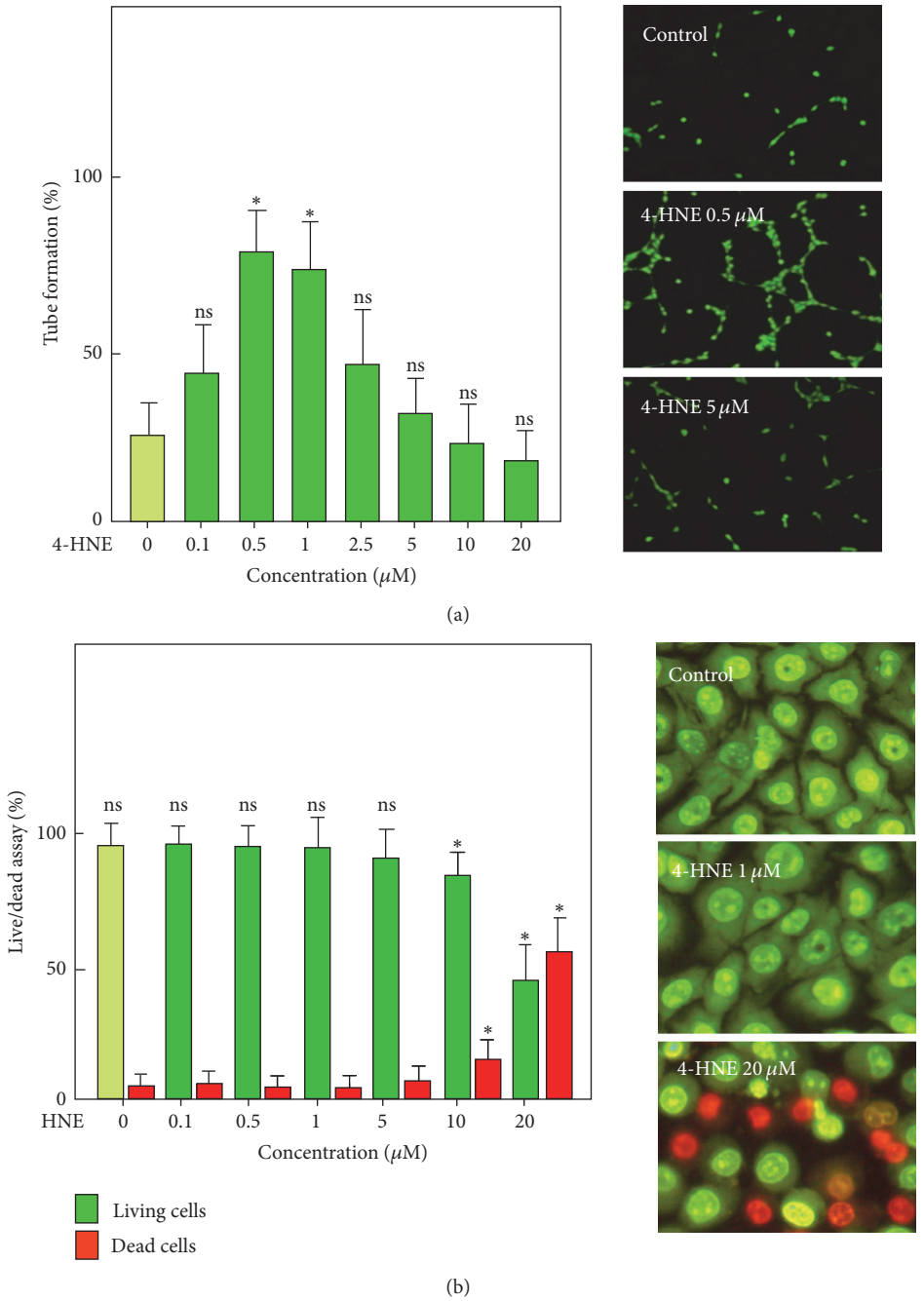

Figure 2: *Dual effect of 4-HNE on neocapillary formation by HMEC-1.* (a) Dose-response effect of 4-HNE on capillary tubes formed by HMEC-1. Cells were grown on Matrigel in MCDB131 culture medium supplemented with 0.1% FBS and PBS (negative control) or 4-HNE (in PBS) varying from 0.1 to 20 μM. After 18 h incubation, the cells were stained with calcein (1 μmol/1, 30 min) and photographed (Nikon Coolpix 995 camera) under a fluorescence microscope. Tube formation was expressed as linked cells per 100 cells. Results are means ± SEM of 6 to 8 experiments. Right panel, representative pictures of the experiments. $^{*}P < 0.05$; ns: not significant. (b) Live-dead experiment on HMEC-1 stimulated by increasing 4-HNE concentrations and performed using the fluorescent DNA probes, permeant green Syto13 (0.6 μM) and nonpermeant red propidium iodide (1 μM). The results are expressed as the number (%) of living, apoptotic, or necrotic cells versus total cells. Right panels, representative pictures of fluorescence microscopy of HMEC-1, incubated for 18 h without (control) or with 4-HNE 1 μM or 20 μM. Means ± SEM of 3 experiments. $^{*}P < 0.05$; ns: not significant.

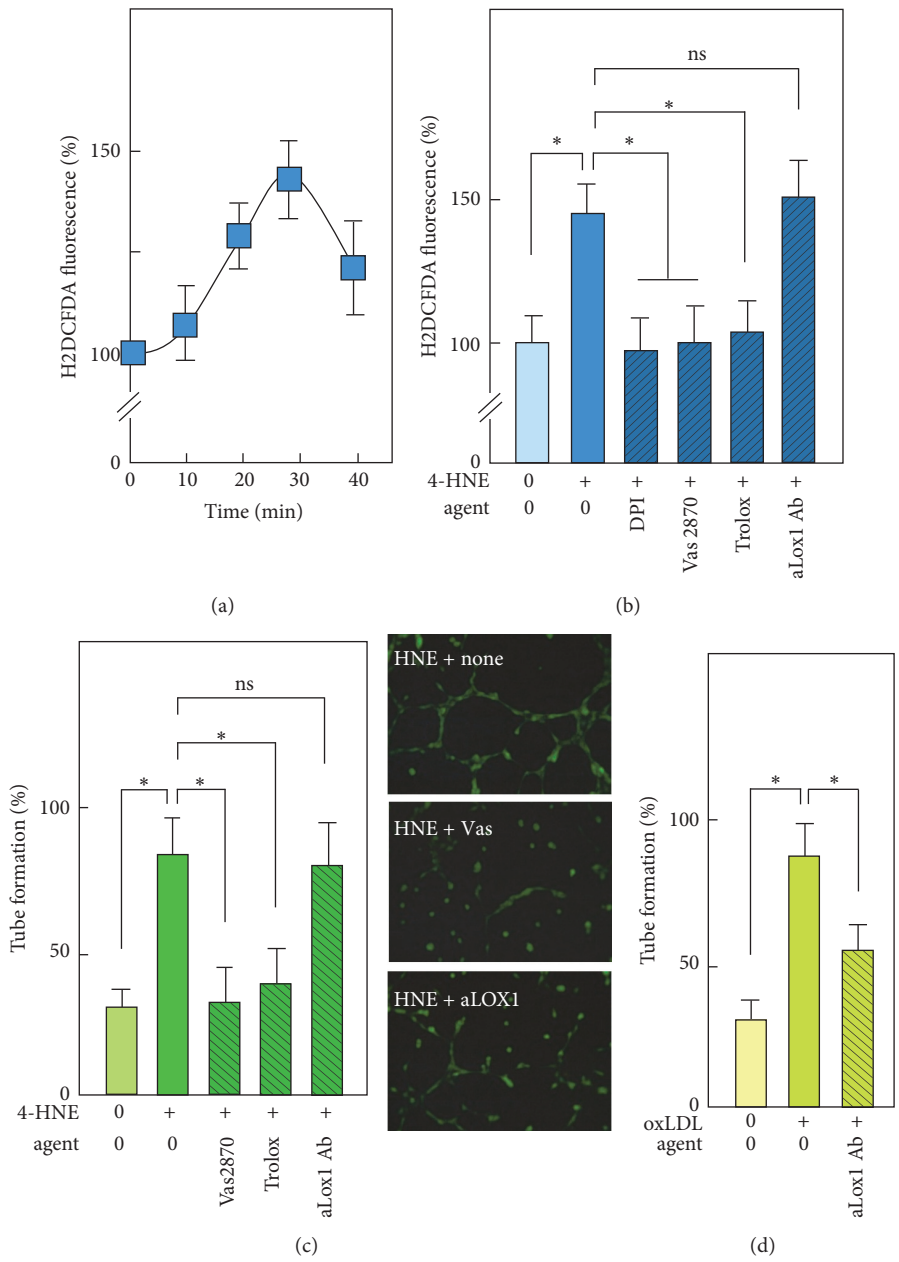

Figure 3: *Implication of ROS in tube formation by 4-HNE.* (a) Time-course of intracellular ROS production evoked by 4-HNE (0.5 μM) in HMEC-1 and measured fluorometrically using the H2DCFDA probe (5 μM final concentration). Results are expressed as % of the unstimulated control. (b) Effect of the antioxidant trolox (10 μM) and of NADPH oxidase inhibitors DPI and Vas2870 (10 μM each) and of the anti-Lox-1 antibody (5 μg/ml) on ROS generated by HMEC-1 after 30 min of contact with 4-HNE (0.5 μM). (c) Effect of trolox, DPI, and Vas2870 and anti-Lox-1 antibody, on tube formation elicited by 4-HNE (0.5 μM). Representative pictures of tube formation in the presence of 4-HNE (0.5 μM) and without (none) or with inhibitors Vas2870 (Vas) or anti-Lox-1 Ab (aLox1). (d) Effect of the anti-Lox-1 Ab on tube formation elicited by oxLDL (20 μg/ml). Note that the anti-Lox-1 Ab has no effect on tubes formed by 4-HNE-stimulated HMEC-1 but inhibits tubes formed by oxLDL-stimulated cells. These data are means ± SEM of 5 separate experiments. $^*P < 0.05$; ns: not significant.

In these areas, neovascularization developed by sprouting angiogenesis from adventitial vasa vasorum invades progressively the atherosclerotic area and takes part in the progression of lesions and complications observed in unstable plaques, such as hemorrhages and rupture [4–7, 47]. Neovascularization may be induced by classical angiogenic pathways, such as hypoxia/HIF/VEGF in the hypoxic thickened intima, and by other atherosclerotic factors, such as inflammation, oxidative stress, and oxidized lipids [36]. RCC-adducts, including 4-HNE-adducts, are highly concentrated in the necrotic lipidic center of the plaque, where lipids are not cleared and autooxidize [27, 48].

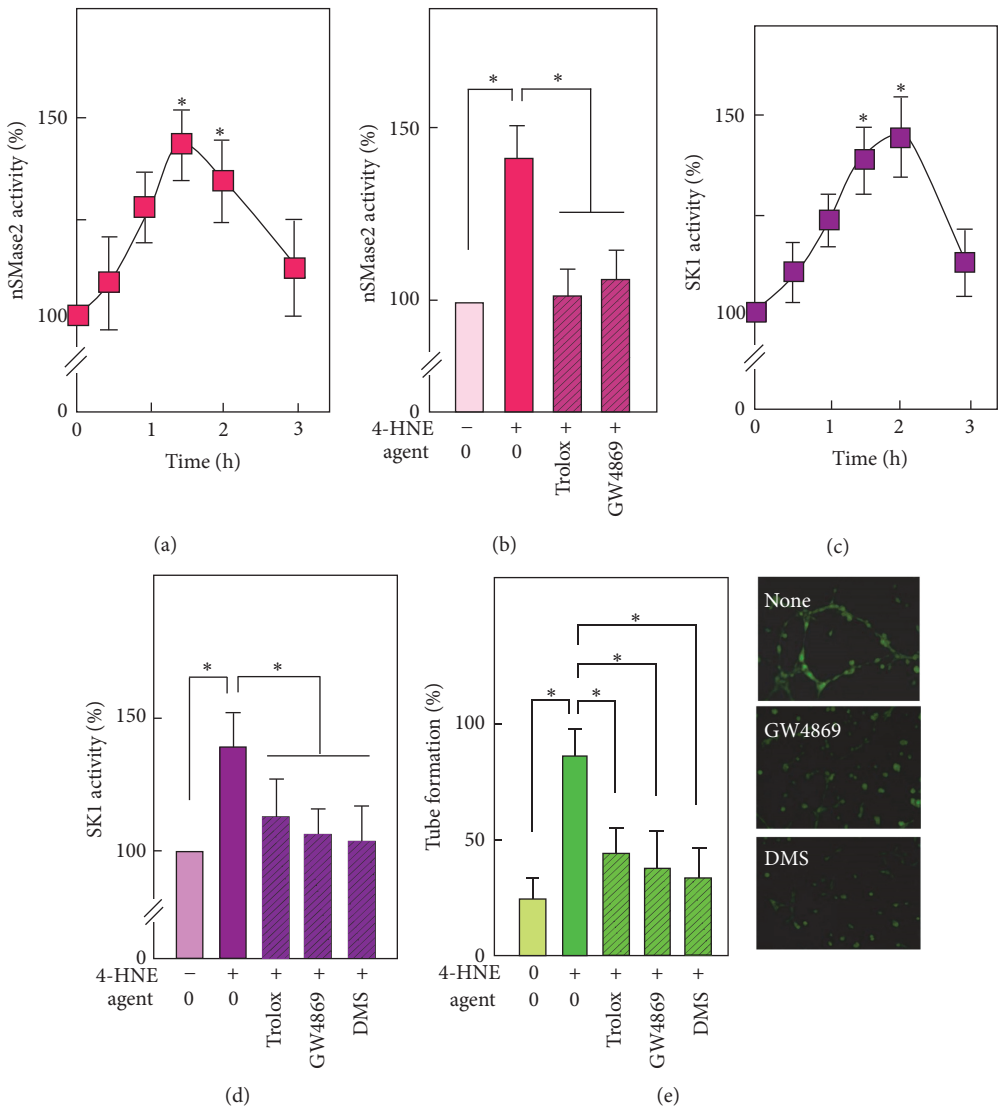

Figure 4: *Implication of nSMase2 and SK1 in tube formation elicited by 4-HNE.* ((a), (b)) Time-course of nSMase2 activation by 4-HNE (0.5 μM) (a) and inhibitory effect of trolox (10 μM) and of the nSMase2 inhibitor GW4869 (5 μM) on nSMase2 activation induced by 4-HNE (b) after 90 min incubation. (c), (d) Time-course of SK1 activation by 4-HNE (0.5 μM) (c) and effect of trolox, GW4869 and of the SK1 inhibitor DMS (1 μM) on SK1 activation by 4-HNE (d), measured after 90 min incubation. (e) Effect of trolox, GW4869, and DMS on capillary tube formation on Matrigel elicited by 4-HNE (0.5 μM). Means ± SEM. $^*P < 0.05$; ns: not significant.

At the periphery of the lesions, the density of 4-HNE-adducts is lower, but the fluorescent detection shows a faint staining for 4-HNE-adducts, particularly around CD31 positive cells that form tubular capillary structures (Figure 1). This is consistent with experiments on cell culture showing the angiogenic effect of low 4-HNE concentrations. Similarly, immunohistochemical studies of human aorta revealed the presence of 4-HNE-adducts at low concentration in early atherosclerotic lesions [26], while neovascularization is present at early stages of coronary artery disease and is associated with epicardial endothelial dysfunction [49]. Moreover, in experimental hypercholesterolemia in pigs, coronary neovascularization occurs very early in atherogenesis, prior to endothelial dysfunction [8, 9]. This suggests that the local hemodynamic stress associated with hypercholesterolemia may induce neovascularization, before intimal thickening and local hypoxia, in atherosclerotic prone areas, where inflammation and oxidative stress initiate lipid peroxidation [14, 26, 50]. It is thought that lipid peroxidation occurring in vivo in early atherosclerotic lesions is a slow process that generates low levels of 4-HNE. This is consistent with the angiogenic effect of very low 4-HNE concentration in our HMEC-1/Matrigel system. Interestingly, similar concentration of 4-HNE (0.1 to 1 μM) promotes VEGF expression and secretion in retinal pigment epithelial cells that induce a paracrine angiogenic response [37]. However, under our standard experimental conditions (cell culture in normoxia), HMEC-1 do not release VEGF (or only very low level)

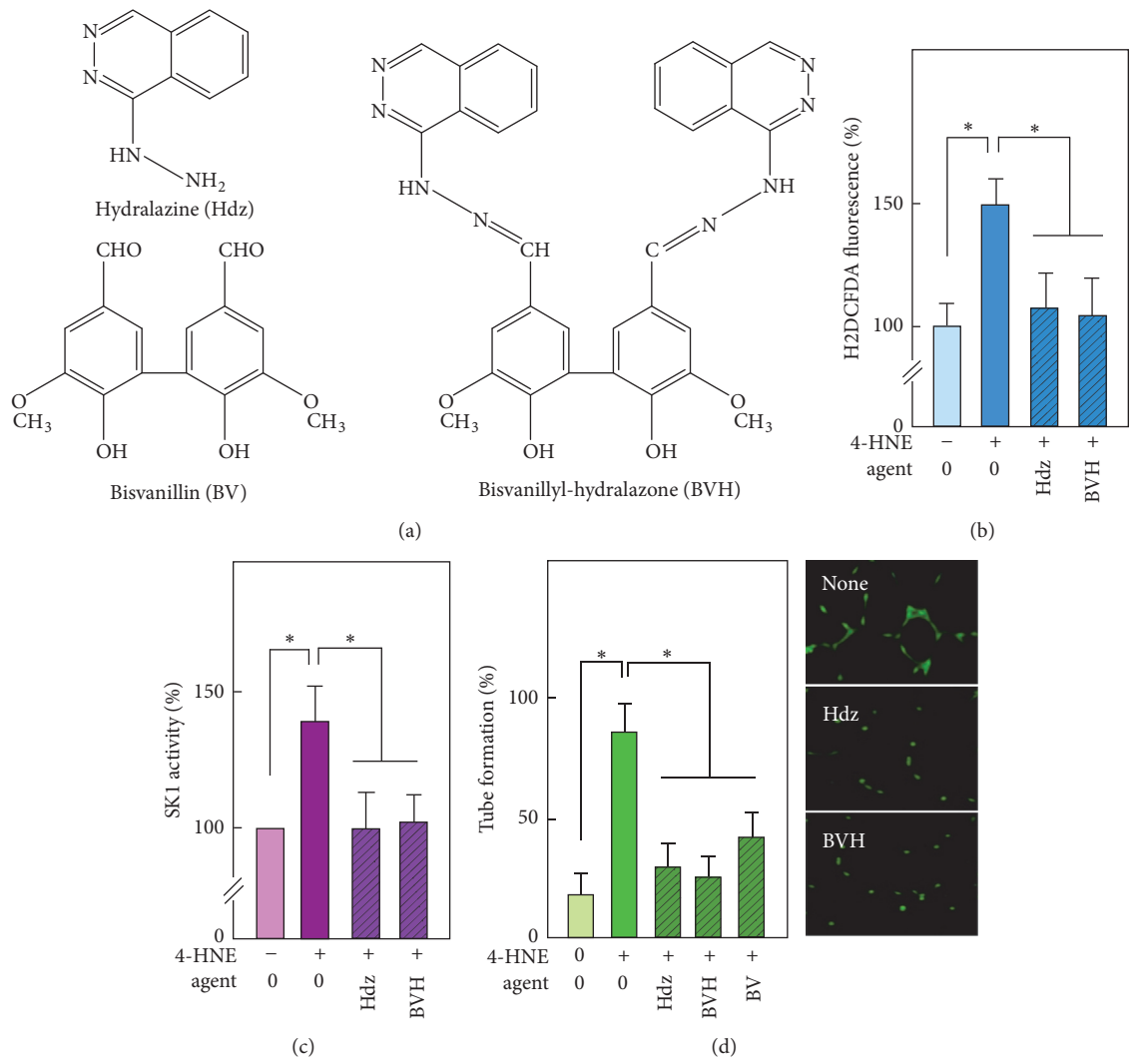

Figure 5: *Effect of hydralazine and BVH on the angiogenic signaling of 4-HNE*. (a) Chemical structures of hydralazine (Hdz), bisvanillin (BV), and bisvanillyl-hydralazone (BVH). (b) Effect of Hdz and BVH (10 μM each), on ROS generated by HMEC-1 after 30 min of contact with 4-HNE (0.5 μM). (c) Effect of Hdz and BVH (10 μM each), on SK1 activation by 4-HNE, measured after 90 min incubation. (d) Effect of Hdz, BVH, and BV (10 μM each) on tube formation elicited by 4-HNE (0.5 μM). These data are means ± SEM of 4 separate experiments. $^*P < 0.05$; ns: not significant.

and the angiogenic effect cannot be attributed to a VEGF-mediated autocrine angiogenic response. This led us to investigate another angiogenic mechanism by analogy with that involved in oxLDL-induced angiogenesis by HMEC-1 [35]. Low concentrations of oxLDLs trigger capillary tube formation by endothelial cells on Matrigel and angiogenesis in vivo in the Matrigel plug assay [31, 35]. This angiogenic effect of oxLDLs is mediated, at least in part, through LOX-1 and NADPH oxidase activation [31, 35], but our data show that the angiogenic effect of free 4-HNE does not require LOX-1. This is consistent with the specificity of LOX-1 for modified lipoproteins and 4-HNE-modified proteins [51]. Thus, 4-HNE can react with cellular proteins or peptides either at the plasma membrane or inside the cell, as previously reported [24, 52–54]. However, in the reported experiments, the 4-HNE-induced tube formation is not inhibited by anti-LOX-1 blocking Ab, suggesting that the binding of 4-HNE-modified proteins with LOX-1 is not involved in the angiogenic response to 4-HNE. In our model, ROS induced by 4-HNE are generated by a NADPH oxidase, as suggested by the inhibitory effect of DPI and Vas2870 and in agreement with the 4-HNE-induced activation of NADPH oxidase, which is mediated through lipoxygenase activation in macrophages [55].

ROS generated upon 4-HNE stimulation act as an intracellular signaling that activates the nSMase2/SK1 pathway. This role of ROS in nSMase2 activation is consistent with the redox-dependent activation of nSMase2 induced by TNF-alpha [56], daunorubicin [57], H2O2 [41, 58], and oxLDLs [35]. These data are consistent with the inhibitory effect of trolox and of NADPH oxidase inhibitors, DPI and Vas2870 that concomitantly block the intracellular ROS rise, and

the activation of nSMase2 and SK1, which also inhibit the activation of the nSMase2/SK1 pathway by oxLDLs [35]. Interestingly, nSMase2 inhibition, either by antioxidants and NADPH oxidase inhibitors or by the specific nSMase2 inhibitor GW4869, inhibits in turn SK1 and angiogenesis. This suggests that nSMase2 plays a crucial role in 4-HNE-induced angiogenesis, as also supported by the angiogenic effect of low C6 ceramide concentration on HMEC-1 grown on Matrigel [36]. Moreover, these data show that SK1 activation depends on nSMase2, since SK1 activation by 4-HNE is blocked when nSMase2 is inhibited, supporting a coordinated signaling cascade as previously reported [41]. Interestingly, although the starting point of angiogenic signaling triggered by oxLDLs and free 4-HNE is not similar (dependent versus independent from LOX-1), these atherogenic compounds trigger an intracellular signaling that induces ROS generation and activation of the nSMase2/SK1 pathway. This is consistent with reports showing that cellular stresses inducing ROS generation activate the sphingolipid pathway [41], which is involved in physiological and pathological vascular biology by regulating endothelial integrity, migration and proliferation, angiogenesis, vascular tone, and leukocyte recruitment [59–62].

Finally, the angiogenic effect of 4-HNE depends on SK1 activation, since its inhibition blocks tube formation, in agreement with the angiogenic effect of S1P [63–65] and with oxLDL-induced angiogenesis [35]. Under the culture conditions used here, 4-HNE did not elicit any significant expression of VEGF, like that observed with oxLDLs. However crosstalks between the SK1/S1P and the VEGF/VEGFR pathways have been reported in the angiogenic effect of S1P and VEGF [66–68] and oxLDLs [35].

Another aim of this study was to investigate the antiangiogenic properties of hydralazine (Hdz), an antihypertensive drug with carbonyl scavenger activity, and of its derivative bisvanillyl-hydralazone (BVH), in which hydralazine is covalently bound to bisvanillin, a phenolic antioxidant. These compounds exhibit a potent antiatherogenic effect in the apoE−/− murine model of atherosclerosis [30, 39]. We report here that both Hdz and BVH prevent the angiogenic effect of 4-HNE. Hdz is a potent carbonyl scavenger that reacts rapidly with 4-HNE and prevents the formation of 4-HNE-protein adducts [30]. BVH, which is constituted by two molecules of Hdz associated with the antioxidant BV, is able to scavenge 4-HNE and block intracellular ROS generated by cells [39]. In our experimental model system, both Hdz and BVH prevent almost completely the angiogenic effect of 4-HNE.

In conclusion, our data emphasize the role of 4-HNE in the formation of tubes evoked by oxidized LDL and suggest that, in vivo, these oxidized lipids may contribute to the neovascularization of atherosclerotic lesions, particularly at the periphery of the plaque where their concentration is lower. In contrast, higher 4-HNE concentration in the lipid core could contribute to the apoptosis of neovessels, thereby promoting intraplaque hemorrhage and plaque rupture. In this context, it could be of interest to evaluate in vivo the ability of pharmacological carbonyl scavengers to prevent the formation of neovessels together with the reduction of atherosclerosis progression.

Abbreviations

BV: Bisvanillin
BVH: Bisvanillyl-hydralazone
DMS: Dimethyl sphingosine
FBS: Fetal bovine serum
Hdz: Hydralazine
HMEC-1: Human microvascular endothelial cell
4-HNE: 4-Hydroxynonenal
oxLDL: Oxidized LDL
nSMase2: Neutral type 2-sphingomyelinase
RCC: Reactive carbonyl compound
SK1: Sphingosine kinase-1
S1P: Sphingosine 1-phosphate
VEGF: Vascular endothelial growth factor.

Conflicts of Interest

The authors declare that there are no conflicts of interest regarding the publication of this paper.

Acknowledgments

This work was supported by INSERM (Institut National de la Santé et de la Recherche Médicale), ANR-Carina (ANR-12-BSV1-0016-01), IdEx Emergence Call-PALMA 2015, and Université Paul Sabatier Toulouse III.

References

[1] P. Carmeliet and R. K. Jain, "Molecular mechanisms and clinical applications of angiogenesis," *Nature*, vol. 473, no. 7347, pp. 298–307, 2011.

[2] M. J. Mulligan-Kehoe and M. Simons, "Vasa vasorum in normal and diseased arteries," *Circulation*, vol. 129, no. 24, pp. 2557–2566, 2014.

[3] K. Sueishi, Y. Yonemitsu, K. Nakagawa, Y. Kaneda, M. Kumamoto, and Y. Nakashima, "Atherosclerosis and angiogenesis. Its pathophysiological significance in humans as well as in an animal model induced by the gene transfer of vascular endothelial growth factor," *Annals of the New York Academy of Sciences*, vol. 811, pp. 311–324, 1997.

[4] F. D. Kolodgie, H. K. Gold, A. P. Burke et al., "Intraplaque hemorrhage and progression of coronary atheroma," *The New England Journal of Medicine*, vol. 349, no. 24, pp. 2316–2325, 2003.

[5] R. Khurana, M. Simons, J. F. Martin, and I. C. Zachary, "Role of angiogenesis in cardiovascular disease: a critical appraisal," *Circulation*, vol. 112, no. 12, pp. 1813–1824, 2005.

[6] P. R. Moreno, K.-R. Purushothaman, M. Sirol, A. P. Levy, and V. Fuster, "Neovascularization in human atherosclerosis," *Circulation*, vol. 113, no. 18, pp. 2245–2252, 2006.

[7] K. S. Moulton, "Angiogenesis in atherosclerosis: gathering evidence beyond speculation," *Current Opinion in Lipidology*, vol. 17, no. 5, pp. 548–555, 2006.

[8] H. M. Kwon, G. Sangiorgi, E. L. Ritman et al., "Enhanced coronary vasa vasorum neovascularization in experimental hypercholesterolemia," *Journal of Clinical Investigation*, vol. 101, no. 8, pp. 1551–1556, 1998.

[9] J. Herrmann, L. O. Lerman, M. Rodriguez-Porcel et al., "Coronary vasa vasorum neovascularization precedes epicardial

endothelial dysfunction in experimental hypercholesterolemia," *Cardiovascular Research*, vol. 51, no. 4, pp. 762–766, 2001.

[10] M. Ushio-Fukai and R. W. Alexander, "Reactive oxygen species as mediators of angiogenesis signaling. Role of NAD(P)H oxidase," *Molecular and Cellular Biochemistry*, vol. 264, no. 1-2, pp. 85–97, 2004.

[11] M. Shibuya, "VEGF-dependent and -independent regulation of angiogenesis," *BMB Reports*, vol. 41, pp. 278–286, 2008.

[12] R. Ross, "The pathogenesis of atherosclerosis: a perspective for the 1990s," *Nature*, vol. 362, no. 6423, pp. 801–809, 1993.

[13] M. S. Brown and J. L. Goldstein, "Lipoprotein metabolism in the macrophage: implications for cholesterol deposition in atherosclerosis," *Annual Review of Biochemistry*, vol. 52, pp. 223–261, 1983.

[14] D. Steinberg, S. Parthasarathy, T. E. Carew, J. C. Khoo, and J. L. Witztum, "Beyond cholesterol: modifications of low-density lipoprotein that increase its atherogenicity," *New England Journal of Medicine*, vol. 320, no. 14, pp. 915–924, 1989.

[15] A. J. Lusis, "Atherosclerosis," *Nature*, vol. 407, no. 6801, pp. 233–241, 2000.

[16] P. Libby and P. Theroux, "Pathophysiology of coronary artery disease," *Circulation*, vol. 111, no. 25, pp. 3481–3488, 2005.

[17] H. C. Stary, "Changes in components and structure of atherosclerotic lesions developing from childhood to middle age in coronary arteries," *Basic Research in Cardiology*, vol. 89, pp. 17–32, 1994.

[18] E. Falk, M. Nakano, J. F. Bentzon, A. V. Finn, and R. Virmani, "Update on acute coronary syndromes: the pathologists' view," *European Heart Journal*, vol. 34, no. 10, pp. 719–728, 2013.

[19] G. M. Chisolm and D. Steinberg, "The oxidative modification hypothesis of atherogenesis: an overview," *Free Radical Biology and Medicine*, vol. 28, no. 12, pp. 1815–1826, 2000.

[20] D. Harrison, K. K. Griendling, U. Landmesser, B. Hornig, and H. Drexler, "Role of oxidative stress in atherosclerosis," *American Journal of Cardiology*, vol. 91, no. 3, pp. 7A–11A, 2003.

[21] R. Stocker and J. F. Keaney Jr., "Role of oxidative modifications in atherosclerosis," *Physiological Reviews*, vol. 84, no. 4, pp. 1381–1478, 2004.

[22] R. Salvayre, A. Negre-Salvayre, and C. Camaré, "Oxidative theory of atherosclerosis and antioxidants," *Biochimie*, vol. 125, pp. 281–296, 2016.

[23] H. Esterbauer, R. J. Schaur, and H. Zollner, "Chemistry and biochemistry of 4-hydroxynonenal, malonaldehyde and related aldehydes," *Free Radical Biology and Medicine*, vol. 11, no. 1, pp. 81–128, 1991.

[24] A. Negre-Salvayre, C. Coatrieux, C. Ingueneau, and R. Salvayre, "Advanced lipid peroxidation end products in oxidative damage to proteins. Potential role in diseases and therapeutic prospects for the inhibitors," *British Journal of Pharmacology*, vol. 153, no. 1, pp. 6–20, 2008.

[25] J. P. Castro, T. Jung, T. Grune, and W. Siems, "4-Hydroxynonenal (HNE) modified proteins in metabolic diseases," *Free Radical Biology and Medicine*, 2016.

[26] G. Jürgens, Q. Chen, H. Esterbauer, S. Mair, G. Ledinski, and H. P. Dinges, "Immunostaining of human autopsy aortas with antibodies to modified apolipoprotein B and apoprotein(a)," *Arteriosclerosis and Thrombosis*, vol. 13, no. 11, pp. 1689–1699, 1993.

[27] M. Sanson, N. Augé, C. Vindis et al., "Oxidized LDL trigger endoplasmic reticulum stress in vascular cells: prevention by ORP-150 expression," *Circulation Research*, vol. 104, pp. 328–336, 2009.

[28] A. D. Watson, N. Leitinger, M. Navab et al., "Structural identification by mass spectrometry of oxidized phospholipids in minimally oxidized low density lipoprotein that induce monocyte/endothelial interactions and evidence for their presence in vivo," *Journal of Biological Chemistry*, vol. 272, no. 21, pp. 13597–13607, 1997.

[29] V. N. Bochkov, M. Philippova, O. Oskolkova et al., "Oxidized phospholipids stimulate angiogenesis via autocrine mechanisms, implicating a novel role for lipid oxidation in the evolution of atherosclerotic lesions," *Circulation Research*, vol. 99, no. 8, pp. 900–908, 2006.

[30] B. Kiec-Wilk, A. Polus, U. Razny, U. Cialowicz, and A. Dembinska-Kiec, "Modulation of endothelial cell proliferation and capillary network formation by the ox-LDL component: 1-palmitoyl-2-archidonoyl-sn-glycero-3- phosphocholine (ox-PAPC)," *Genes and Nutrition*, vol. 6, no. 4, pp. 347–351, 2011.

[31] A. Dandapat, C. Hu, L. Sun, and J. L. Mehta, "Small concentrations of OXLDL induce capillary tube formation from endothelial cells via LOX-1-dependent redox-sensitive pathway," *Arteriosclerosis, Thrombosis, and Vascular Biology*, vol. 27, no. 11, pp. 2435–2442, 2007.

[32] Y. Wu, Q. Wang, L. Cheng, J. Wang, and G. Lu, "Effect of oxidized low-density lipoprotein on survival and function of endothelial progenitor cell mediated by p38 signal pathway," *Journal of Cardiovascular Pharmacology*, vol. 53, no. 2, pp. 151–156, 2009.

[33] S. Yu, S. L. Wong, C. W. Lau, Y. Huang, and C.-M. Yu, "Oxidized LDL at low concentration promotes in-vitro angiogenesis and activates nitric oxide synthase through PI3K/Akt/eNOS pathway in human coronary artery endothelial cells," *Biochemical and Biophysical Research Communications*, vol. 407, no. 1, pp. 44–48, 2011.

[34] M. Khaidakov, S. Mitra, X. Wang et al., "Large impact of low concentration oxidized LDL on angiogenic potential of human endothelial cells: a microarray study," *PLoS ONE*, vol. 7, no. 10, Article ID e47421, 2012.

[35] C. Camaré, M. Trayssac, B. Garmy-Susini et al., "Oxidized LDL-induced angiogenesis involves sphingosine 1-phosphate: prevention by anti-S1P antibody," *British Journal of Pharmacology*, vol. 172, no. 1, pp. 106–118, 2015.

[36] C. Camaré, N. Augé, M. Pucelle et al., "The neutral sphingomyelinase-2 is involved in angiogenic signaling triggered by oxidized LDL," *Free Radical Biology and Medicine*, vol. 93, pp. 204–216, 2016.

[37] R. Vatsyayan, P. C. R. Lelsani, P. Chaudhary, S. Kumar, S. Awasthi, and Y. C. Awasthi, "The expression and function of vascular endothelial growth factor in retinal pigment epithelial (RPE) cells is regulated by 4-hydroxynonenal (HNE) and glutathione S-transferaseA4-4," *Biochemical and Biophysical Research Communications*, vol. 417, no. 1, pp. 346–351, 2012.

[38] D. Stagos, H. Zhou, D. Ross, and V. Vasiliou, "4-HNE inhibits tube formation and up-regulates chondromodulin-I in human endothelial cells," *Biochemical and Biophysical Research Communications*, vol. 379, no. 3, pp. 654–658, 2009.

[39] B. Bouguerne, N. Belkheiri, F. Bedos-Belval et al., "Antiatherogenic effect of bisvanillyl-hydralazone, a new hydralazine derivative with antioxidant, carbonyl scavenger, and antiapoptotic properties," *Antioxidants and Redox Signaling*, vol. 14, no. 11, pp. 2093–2106, 2011.

[40] K. Yagi, "Lipid peroxides and human diseases," *Chemistry and Physics of Lipids*, vol. 45, no. 2–4, pp. 337–351, 1987.

[41] C. Cinq-Frais, C. Coatrieux, M.-H. Grazide et al., "A signaling cascade mediated by ceramide, src and PDGFRβ coordinates the activation of the redox-sensitive neutral sphingomyelinase-2 and sphingosine kinase-1," *Biochimica et Biophysica Acta—Molecular and Cell Biology of Lipids*, vol. 1831, no. 8, pp. 1344–1356, 2013.

[42] M. S. Carmody and J. R. Anderson, "BiDil (isosorbide dinitrate and hydralazine): a new fixed-dose combination of two older medications for the treatment of heart failure in black patients," *Cardiology in Review*, vol. 15, no. 1, pp. 46–53, 2007.

[43] J. Chen, P. J. Kuhlencordt, J. Astern, R. Gyurko, and P. L. Huang, "Hypertension does not account for the accelerated atherosclerosis and development of aneurysms in male apolipoprotein E/endothelial nitric oxide synthase double knockout mice," *Circulation*, vol. 104, no. 20, pp. 2391–2394, 2001.

[44] S. Wassmann, T. Czech, M. Van Eickels, I. Fleming, M. Böhm, and G. Nickenig, "Inhibition of diet-induced atherosclerosis and endothelial dysfunction in apolipoprotein E/angiotensin II type 1A receptor double-knockout mice," *Circulation*, vol. 110, no. 19, pp. 3062–3067, 2004.

[45] D. Weiss and W. R. Taylor, "Deoxycorticosterone acetate salt hypertension in apolipoprotein E-/- mice results in accelerated atherosclerosis: The role of angiotensin II," *Hypertension*, vol. 51, no. 2, pp. 218–224, 2008.

[46] S. Galvani, C. Coatrieux, M. Elbaz et al., "Carbonyl scavenger and antiatherogenic effects of hydrazine derivatives," *Free Radical Biology and Medicine*, vol. 45, no. 10, pp. 1457–1467, 2008.

[47] J.-B. Michel, J. L. Martin-Ventura, A. Nicoletti, and B. Ho-Tin-Noé, "Pathology of human plaque vulnerability: mechanisms and consequences of intraplaque haemorrhages," *Atherosclerosis*, vol. 234, no. 2, pp. 311–319, 2014.

[48] W. Palinski, M. E. Rosenfeld, S. Ylä-Herttuala et al., "Low density lipoprotein undergoes oxidative modification in vivo," *Proceedings of the National Academy of Sciences of the United States of America*, vol. 86, no. 4, pp. 1372–1376, 1989.

[49] B.-J. Choi, Y. Matsuo, T. Aoki et al., "Coronary endothelial dysfunction is associated with inflammation and vasa vasorum proliferation in patients with early atherosclerosis," *Arteriosclerosis, Thrombosis, and Vascular Biology*, vol. 34, no. 11, pp. 2473–2477, 2014.

[50] C. Napoli, F. P. D'Armiento, F. P. Mancini et al., "Fatty streak formation occurs in human fetal aortas and is greatly enhanced by maternal hypercholesterolemia. Intimal accumulation of LDL and its oxidation precede monocyte recruitment into early atherosclerotic lesions," *The Journal of Clinical Investigation*, vol. 100, no. 11, pp. 2680–2690, 1997.

[51] R. Yoshimoto, Y. Fujita, A. Kakino, S. Iwamoto, T. Takaya, and T. Sawamura, "The discovery of LOX-1, its ligands and clinical significance," *Cardiovascular Drugs and Therapy*, vol. 25, no. 5, pp. 379–391, 2011.

[52] I. Suc, O. Meilhac, I. Lajoie-Mazenc et al., "Activation of EGF receptor by oxidized LDL," *The FASEB Journal*, vol. 12, no. 9, pp. 665–671, 1998.

[53] I. Escargueil-Blanc, R. Salvayre, N. Vacaresse et al., "Mildly oxidized LDL induces activation of platelet-derived growth factor β-receptor pathway," *Circulation*, vol. 104, no. 15, pp. 1814–1821, 2001.

[54] S. J. Chapple, X. Cheng, and G. E. Mann, "Effects of 4-hydroxynonenal on vascular endothelial and smooth muscle cell redox signaling and function in health and disease," *Redox Biology*, vol. 1, no. 1, pp. 319–331, 2013.

[55] M. R. Yun, H. M. Park, K. W. Seo, S. J. Lee, D. S. Im, and C. D. Kim, "5-Lipoxygenase plays an essential role in 4-HNE-enhanced ROS production in murine macrophages via activation of NADPH oxidase," *Free Radical Research*, vol. 44, no. 7, pp. 742–750, 2010.

[56] S. Jayadev, H. L. Hayter, N. Andrieu et al., "Phospholipase A2 is necessary for tumor necrosis factor α-induced ceramide generation in L929 cells," *The Journal of Biological Chemistry*, vol. 272, no. 27, pp. 17196–17203, 1997.

[57] V. Mansat-De Mas, C. Bezombes, A. Quillet-Mary et al., "Implication of radical oxygen species in ceramide generation, c-Jun N- terminal kinase activation and apoptosis induced by daunorubicin," *Molecular Pharmacology*, vol. 56, no. 5, pp. 867–874, 1999.

[58] M. Levy, S. S. Castillo, and T. Goldkorn, "nSMase2 activation and trafficking are modulated by oxidative stress to induce apoptosis," *Biochemical and Biophysical Research Communications*, vol. 344, no. 3, pp. 900–905, 2006.

[59] T. Hla, "Signaling and biological actions of sphingosine 1-phosphate," *Pharmacological Research*, vol. 47, no. 5, pp. 401–407, 2003.

[60] S. Spiegel and S. Milstien, "Sphingosine-1-phosphate: an enigmatic signalling lipid," *Nature Reviews Molecular Cell Biology*, vol. 4, no. 5, pp. 397–407, 2003.

[61] G. Daum, A. Grabski, and M. A. Reidy, "Sphingosine 1-phosphate: a regulator of arterial lesions," *Arteriosclerosis, Thrombosis, and Vascular Biology*, vol. 29, no. 10, pp. 1439–1443, 2009.

[62] S. M. Pitson, "Regulation of sphingosine kinase and sphingolipid signaling," *Trends in Biochemical Sciences*, vol. 36, no. 2, pp. 97–107, 2011.

[63] M.-J. Lee, S. Thangada, K. P. Claffey et al., "Vascular endothelial cell adherens junction assembly and morphogenesis induced by sphingosine-1-phosphate," *Cell*, vol. 99, no. 3, pp. 301–312, 1999.

[64] O.-H. Lee, Y.-M. Kim, Y. M. Lee et al., "Sphingosine 1-phosphate induces angiogenesis: its angiogenic action and signaling mechanism in human umbilical vein endothelial cells," *Biochemical and Biophysical Research Communications*, vol. 264, no. 3, pp. 743–750, 1999.

[65] F. Wang, J. R. Van Brooklyn, J. P. Hobson et al., "Sphingosine 1-phosphate stimulates cell migration through a G(i)-coupled cell surface receptor. Potential involvement in angiogenesis," *The Journal of Biological Chemistry*, vol. 274, no. 50, pp. 35343–35350, 1999.

[66] T. Tanimoto, Z. G. Jin, and B. C. Berk, "Transactivation of VEGFR Flk-1/KDR is involved in sphingosine 1-phosphate-stimulated phosphorylation of Akt and eNOS," *The Journal of Biological Chemistry*, vol. 277, pp. 42997–43001, 2002.

[67] J. Igarashi, P. A. Erwin, A. P. V. Dantas, H. Chen, and T. Michel, "VEGF induces S1P1 receptors in endothelial cells: Implications for cross-talk between sphingolipid and growth factor receptors," *Proceedings of the National Academy of Sciences of the United States of America*, vol. 100, no. 19, pp. 10664–10669, 2003.

[68] S.-S. Chae, J.-H. Paik, M. L. Allende, R. L. Proia, and T. Hla, "Regulation of limb development by the sphingosine 1-phosphate receptor S1p1/EDG-1 occurs via the hypoxia/VEGF axis," *Developmental Biology*, vol. 268, no. 2, pp. 441–447, 2004.

Hindawi
Oxidative Medicine and Cellular Longevity
Volume 2017, Article ID 4069839, 15 pages
https://doi.org/10.1155/2017/4069839

Research Article

Dihydropyridine Derivatives as Cell Growth Modulators In Vitro

Imanta Bruvere,[1] Egils Bisenieks,[1] Janis Poikans,[1] Janis Uldrikis,[1] Aiva Plotniece,[1] Karlis Pajuste,[1] Martins Rucins,[1] Brigita Vigante,[1] Zenta Kalme,[1] Marina Gosteva,[1] Ilona Domracheva,[1] Astrida Velena,[1] Tea Vukovic,[2] Lidija Milkovic,[2] Gunars Duburs,[1] and Neven Zarkovic[2]

[1]*Latvian Institute of Organic Synthesis, 21 Aizkraukles Str., Riga LV-1006, Latvia*
[2]*Laboratory for Oxidative Stress, Rudjer Boskovic Institute, Bijenicka 54, 10000 Zagreb, Croatia*

Correspondence should be addressed to Astrida Velena; astrida@osi.lv and Neven Zarkovic; zarkovic@irb.hr

Received 9 December 2016; Accepted 20 February 2017; Published 3 April 2017

Academic Editor: Serafina Perrone

The effects of eleven 1,4-dihydropyridine derivatives (DHPs) used alone or together with prooxidant anticancer drug doxorubicin were examined on two cancer (HOS, HeLa) and two nonmalignant cell lines (HMEC, L929). Their effects on the cell growth (^{3}H-thymidine incorporation) were compared with their antiradical activities (DPPH assay), using well-known DHP antioxidant diludine as a reference. Thus, tested DHPs belong to three groups: (1) antioxidant diludine; (2) derivatives with pyridinium moieties at position 4 of the 1,4-DHP ring; (3) DHPs containing cationic methylene onium (pyridinium, trialkylammonium) moieties at positions 2 and 6 of the 1,4-DHP ring. Diludine and DHPs of group 3 exerted antiradical activities, unlike compounds of group 2. However, novel DHPs had cell type and concentration dependent effects on ^{3}H-thymidine incorporation, while diludine did not. Hence, IB-32 (group 2) suppressed the growth of HOS and HeLa, enhancing growth of L929 cells, while K-2-11 (group 3) enhanced growth of every cell line tested, even in the presence of doxorubicin. Therefore, growth regulating and antiradical activity principles of novel DHPs should be further studied to find if DHPs of group 2 could selectively suppress cancer growth and if those of group 3 promote wound healing.

1. Introduction

Growth modulation, that is, proliferation induction or decline, is fundamental for cellular metabolic processes both in the health and in disease, as well in pharmaceutical interventions. Particularly regenerative medicine needs nontoxic proliferation inducers for cell, tissue, and organ regeneration. On the other side, proliferation inhibitors are necessary for the prevention and inhibition of uncontrolled growth of cancer cells. Recently [1] it was found that same 1-benzyl substituted 1,4-dihydropyridines (1,4-DHPs), activating SIRT1, are proliferation inhibitors in the cancer cells and on the contrary proliferation promoters in the wound healing. Direction of the search of the compounds acting in dual mode seems to be perspective.

Cellular redox signaling, including oxidative stress (OS) related events, is connected with genetic and epigenetic regulatory systems. Reactive oxygen species (ROS) and lipid peroxidation products are not only cytotoxic but may also perform and modulate signal transduction in cells. Accordingly, antioxidants (AOs) and radical scavengers may be considered as modifiers of cellular redox signaling, as well as genetic and epigenetic events, and thus 1,4-dihydropyridines being a group of synthetic antioxidants could be used for modulation of cellular redox signaling. Oxidative stress may have at least dual effects on cell proliferation and growth: anticancer-like effects as well as protumorigenic effects. The last ones are primarily related to induction of oxidative DNA lesions (8-OH-G) and consequential increase of DNA mutation frequency. These undesirable changes may, if not repaired, lead to genome instability and an increased rate of cellular proliferation [2]. Antineoplastic (anticarcinogenic, antitumorigenic) effects of OS have been closely linked to cellular processes of senescence and apoptosis, two major molecular mechanisms that counteract tumor development [3]. Which of these two actions will dominate depends on

many factors including the metabolic status of the cell, as recently reviewed [4]. Accordingly, many AOs, for instance, curcumin [5], may be antineoplastic and cytotoxic by targeting mitochondria, affecting p53-related signaling and blocking NF-kappa B activation. A number of other curcumin targets include the aryl hydrocarbon receptor, cytochrome P450, glutathione S-transferase, serine/threonine kinases, transcription factors, cyclooxygenase, ornithine decarboxylase, nitric oxide synthase, matrix metalloproteinases, and tyrosine kinases. Some of these targets are characteristic also for DHPs antioxidant action [6].

Some of the amphiphilic compounds possessing self-assembling properties and forming nanoparticles in an aqueous medium could form stable liposomes [7–10] which are suitable as gene (pDNA) delivery agents in vitro, while the cytotoxicity and antiradical activity (ARA) of these amphiphilic 1,4-DHP derivatives were determined, too [10].

Biological activity of some of these compounds was previously studied (for antioxidant **diludine** ([11], see as cited in [6]), amphiphilic 1,4-DHP derivative, MDR modifier and suitable gene (plasmid DNA) delivery agent in vitro **K-2-11** [10], neuromodulator **AP-12** [12, 13], and also close compound **Z41-74** [14] (see also *Discussion* part)). However, physiological activity profile for most of mentioned compounds has not been still determined and published.

Presented work includes studies about a set of 11 original 1,4-dihydropyridine derivatives (comprising different substituents at positions 4, 2, and 6 or 3 and 5, containing neutral or cationic moieties, with diverse lipophilic or amphiphilic properties).

The studied eleven DHP derivatives could be divided into 3 groups considering structure fragments (see Figure 1, Table 1):

(1) 1.4-Unsubstituted 1,4-DHP (I, compound (1) in Table 1)

(2) 1,4-DHPs comprising N-quaternized pyridine moiety at position 4 of the DHP ring (II, compounds (2)–(4) in Table 1)

(3) 1,4-DHPs containing cationic onium methylene moieties at positions 2 and 6 of the DHP cycle (III, compounds (5)–(11) in Table 1) (in this set previously reported compound (12) (**Z41-74**) was included for more detailed analysis of relationships)

These DHPs were studied as potential cell proliferation modulators in two normal (human mammary epithelial cells HMEC and murine fibroblasts L929) and in two malignant cell lines (human osteosarcoma HOS and human cervical carcinoma HeLa). The effects of tested DHPs occurred if they were used alone or together with the well-known anticancer, prooxidant drug doxorubicin. Namely, doxorubicin causes long-lasting stimulation of ROS generation and OS in cancer cells and in cardiomyocytes [15]. Therefore, it is assumed that certain antioxidants (including DHPs) may influence the undesired side effects of doxorubicin, like cardiotoxicity. Some suggestions about DHP structure-activity relationships and selectivity on the above-mentioned cell lines are proposed.

2. Materials and Methods

All DHP derivatives (see further as listed in Table 1 and given in the *Results and Discussion* part) provided for the cell proliferation evaluation and used in this study have been synthesized in the Laboratory of Membrane active compounds of the Latvian Institute of Organic Synthesis (Latvian IOS).

Compound **AP-12** was obtained following an already reported method [16]; **A2-15** was obtained according to procedure described by Makarova et al. [17]; compounds **K-2-11**, **IOS-10003**, **D-3-59-1,** and **K2-71** were obtained following an already reported method [10]; compound **IOS-10004** was obtained based on analogy by reported method [10]; compounds **V-1-32** and **V-1-41** were obtained according to procedure described by [18]; compound **IB-32** was obtained according to procedure described by [19].

2.1. Antiradical (Free Radical Scavenging) Activity (ARA). ARA data were obtained spectrophotometrically using decoloration reaction ability with 1,1-diphenyl-2-picrylhydrazyl (DPPH) as a free radical scavenger [20], adapted for DHPs [10, 16]. An aliquot (0.5 mL) of the tested 1,4-DHP derivative solution in EtOH was added to 3 mL of freshly prepared DPPH solution in EtOH (0.1 mM). The final concentration of the tested compounds was 0.086 mM and the ratio of the tested compound and DPPH was equimolar. The solution was incubated for 30 min in the dark and changes in the optical density of solution were measured at 517 nm using a UV/Vis Camspec M501 spectrometer (UK). Each assay was performed in triplicate.

The scavenging activity was defined as the decrease in sample absorbance versus absorbance of DPPH standard solutions. Results were expressed as a percentage (%) of the DPPH free radical scavenging, which is defined by the following formula:

$$\text{ARA } (\%) = \frac{A_{\text{control}} - A_{\text{sample}}}{A_{\text{control}}} \times 100, \quad (1)$$

where A_{control} is the absorbance of the standard solution of DPPH and A_{sample} is the absorbance value for the sample.

2.2. Basal Cytotoxicity Test. The Neutral Red Uptake (NRU) Assay was performed according to the standard protocol of [21] modified by NICEATM-ECVAM (Committee on the Validation of Alternative Methods (ICCVAM) of National Toxicology Program (NTP) Interagency Center for the Evaluation of Alternative Methods (NICEATM)) validation study [22]. The NRU cytotoxicity assay procedure is based on the ability of viable cells to incorporate and bind neutral red, a supravital dye. 3T3 (Mouse Swiss Albino embryo fibroblast) cells (purchased from ATCC®) (9000 cells/well) were placed into 96-well plates for 24 h in Dulbecco's modified Eagle's medium (DMEM) containing 5% fetal bovine serum and then exposed to the test compound over a range of eight concentrations (1000, 316, 100, 31, 10, 3, and 1 μg/mL) for 24 h. Untreated cells were used as a control. After 24 h, the medium was removed from all plates. Then, 250 μL of neutral

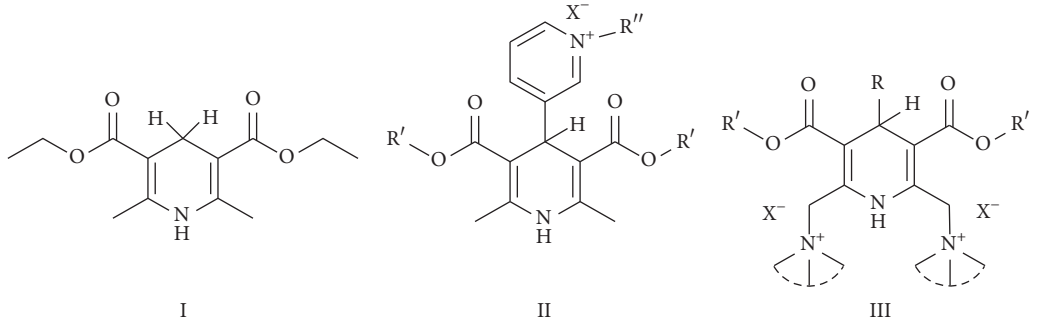

I II III

Figure 1: Core structures of studied 1,4-DHP derivatives (for details see Table 1).

red solution was added (0.05 mg/mL NR in DMEM, 24 h, preincubated at 37°C and then filtered before use through 0.22 μm syringe filter). Plates were incubated for 3 h and then cells were washed three times with PBS. The dye within viable cells was released by extraction with a mixture of acetic acid, ethanol, and water (1 : 50 : 49). Absorbance of neutral red was measured using spectrophotometer multiplate reader (TECAN, Infinite M1000) at 540 nm. The optical density (OD) was calculated using the formula: OD (treated cells) $*$ 100/OD (control cells). The IC_{50} values were calculated using the program Graph Pad Prism® 3.0.

2.3. Estimation of LD_{50} from IC_{50} Values. Data from the in vitro tests were used for estimating the starting dose for acute oral systemic toxicity tests in rodents (mice, rat). The in vivo starting dose is an estimated LD_{50} value calculated by inserting the in vitro IC_{50} value into a regression formula: log LD_{50} (mM/kg) = 0.439 log IC_{50} (mM) + 0.621 [23]. The value is recalculated to mg/kg and compounds are evaluated in accordance with 4 toxicity categories [24]: category 1: $LD_{50} \leq$ 5 mg/kg (highly toxic); category 2: 5 < $LD_{50} \leq$ 50 mg/kg (moderately toxic); category 3: 50 < $LD_{50} \leq$ 300 mg/kg (slightly toxic); category 4: 300 < $LD_{50} \leq$ 2,000 mg/kg (practically nontoxic). Using an alternative in vitro method allows comparisons of possible toxicity of new compounds and selecting compounds for further study vastly reducing the number of animal experiments.

Radioactive thymidine assay was used for quantification of *cell proliferation modulation* properties of DHPs.

2.4. ^3H-Thymidine Assay. To test the effects of DHPs on the growth of different types of cells in vitro we used the ^3H-thymidine incorporation assay reflecting the DNA synthesis (i.e., the cell growth) of murine skin fibroblasts L929 cell line (NCTC clone 929 [L cell, L-929, derivative of Strain L] (ATCC CCL-1™)), human endothelial cells HMEC-1 (ATCC CRL-3243™), human cervical carcinoma HeLa (ATCC CCL-2™), and human osteosarcoma cell line HOS (ATCC CRL-1543™), which in vitro grows resembling osteoblast cells.

For the ^3H-thymidine incorporation assay, the cells were seeded in microtiter plates (TPP, Swiss) at a density of 6 × 10^4 cells/well and were treated with DHPs at three various stepwise concentrations: 1 μg/mL, 10 μg/mL, and 100 μg/mL (approximately molar concentrations (~1 μM, ~10 μM, ~100 μM) could be calculated from molecular mass data presented in the Table 1). Stock solutions of the compounds were obtained, diluting 5 mg of each compound in absolute ethanol to get concentration of 10 mg/mL. Some of the substances were not completely soluble; therefore in this case 5–10% DMSO were added.

After 1 h preincubation, ^3H-thymidine (methyl-^3H-thymidine, 25 Ci/mmol, Amersham) diluted with medium at a 1 : 25 ratio was added and the cells were cultured in humidified atmosphere containing 5% CO_2 in DMEM culture medium supplemented with 5% fetal calf serum (Sigma, USA) for the following 24 h. After that, the cells were washed by cell harvester (Scatron, Norway) over a filter and the radioactivity of incorporated ^3H-thymidine was detected in a beta-counter (Beckman LS 100C). Each group of cultures comprised four samples.

Control cells were equally cultured but without the presence of DHPs.

In the experiments with doxorubicin (Sigma) its stock solution concentration was 1 mg/mL (the 1 mg content diluted in 1 mL H_2O). Three doxorubicin concentrations used were 0.1 μg/mL, 0.5 μg/mL, and 1 μg/mL.

Dilution of stock solutions was made as follows.

Stock solutions in concentration 10 mg/mL were further diluted in DMEM to final concentrations 1, 10, and 100 μg/mL. The rest of the solutions were stored at +4°C in plastic micro tubes with screw caps and used in next experiments.

The cells are plated in 96-well plates; cell cultures were incubated in DMEM media, containing 2.5% FCS, 2 × 10^6 cells count in 6 mL DMEM (0.3 mL FCS) (each well of the plate was filled with 1–5 × 10^4 cells (depending on the cell line) in 90 μL cultured medium). After 4 h the cells were treated with the DHPs, while 1 h after that doxorubicin was added. The radioactive thymidine was added to cultures and left again for additional 24 h to incorporate ^3H-thymidine, when the assay was performed on beta-counter (Beckman LS 100C).

Incubation was performed as follows.

Incubation and its duration (added volume)

(1) cell culture → 4-5 h (100 μL)

(2) DHPs, DOXO → 24 h (100 μL (50 + 50 μL))

(3) ^3H TIM ☢ → 24 h (20 μL)

Table 1: Studied 1,4-dihydropyridine derivatives, their chemical structures, molecular weight (M_w) values, LD_{50} values (on NIH 3T3, normal mice embryonal fibroblast cells), and antiradical activity (ARA) determined by DPPH assay. The untreated level of the DPPH radical is designated as 100%. Data are presented as mean ± SD.

Number	Compound	Chemical structures	M_w	LD_{50} mg/kg	ARA ± SD %
		Group I			
(1)	**Diludine**	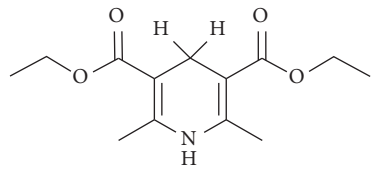	253.30	>2000 (>7.9 mmol/kg) (32,000 mg/kg, mice, ip)	40.5 ± 3.0
		Group II			
(2)	**AP-12**	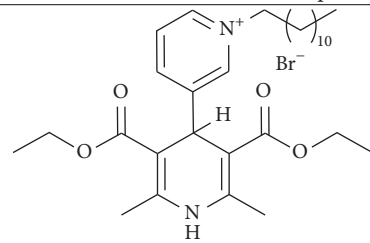	579.61	692	0
(3)	**IB-32**	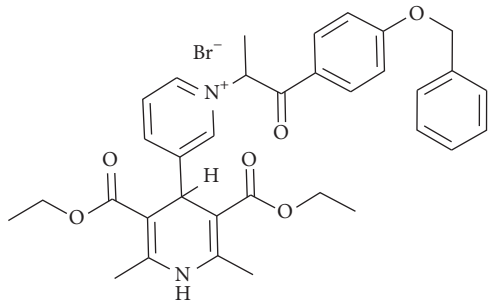	649.57	520	0
(4)	**A2-15**	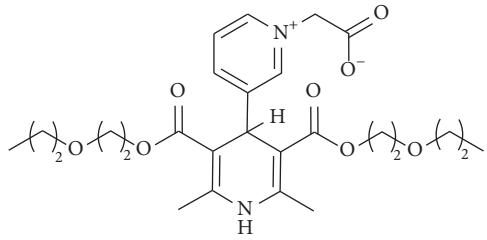	505.56	>2000 (>3.9 mmol/kg)	0
		Group III			
(5)	**V-1-32**	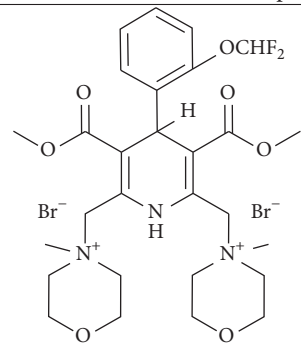	727.43	1706	95.1 ± 0.2

Table 1: Continued.

Number	Compound	Chemical structures	M_w	LD_{50} mg/kg	ARA ± SD %
(6)	**IOS-10003**	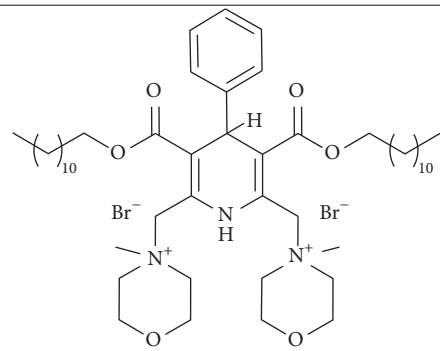	970.01	NA	95.1 ± 0.2
(7)	**IOS-10004**	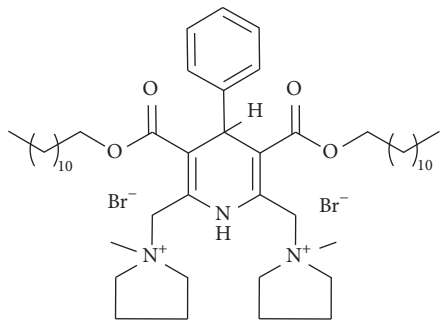	938.01	NA	54.0 ± 0.3
(8)	**V-1-41**	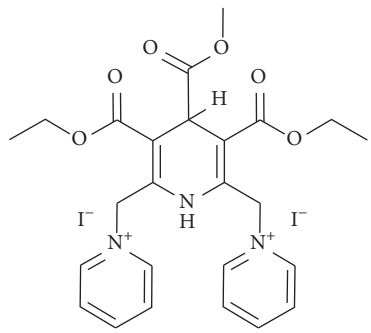	721.32	>2000	70.7 ± 0.9
(9)	**K-2-11**	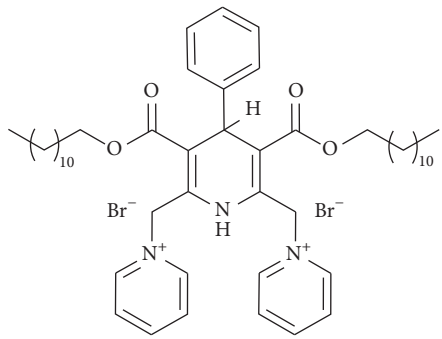	925.91	1482	39.5 ± 0.3

Table 1: Continued.

Number	Compound	Chemical structures	M_w	LD_{50} mg/kg	ARA ± SD %
(10)	**D-3-59-1**	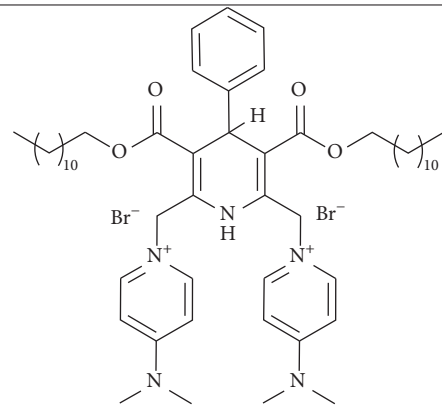	1012.05	1706	27.5 ± 0.2
(11)	**K2-71**	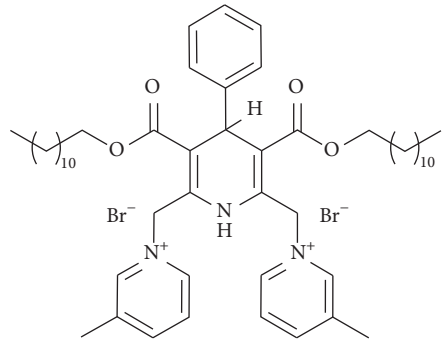	953.98	463 ± 19 (0.9 ± 0.09 mmol/kg)	39.0 ± 2.7
(12)	**Z41-74** [14]	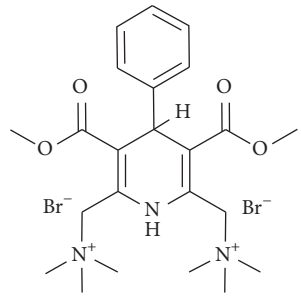	577.35	2425	16.1 ± 0.7

NA: not applicable (the data are absent).

Three identical repeated experiments were done for each treatment protocol of each cell line used.

3. Results

List of studied eleven 1,4-dihydropyridine derivatives, their structural formulas, molecular weight data, LD_{50} values in mg/kg (on NIH 3T3 cells), and antiradical activity data (DPPH assay, in %) (ARA) and data for previously reported compound **Z41-74** for more detailed analysis of relationships are given in Table 1.

The respective estimated LD_{50} values (see Table 1) for tested 1,4-DHP derivatives are different. Some of the listed compounds have the medium toxicity, some low according to 4 toxicity categories. Compounds **IB-32**, **AP-12**, and **K2-71** (in the lesser extent **K-2-11**, **D-3-59-1**) exerted toxicity, which could be classified as dangerous, while other compounds **diludine**, **A2-15**, and **V-1-41** could be classified as nontoxic DHPs.

3.1. Antiradical Activity (ARA) of Various DHPs. Relative antiradical activity (ARA, expressed in %) was determined using DPPH method [10, 20], for DHPs chosen upon the results of cytotoxicity assays to be tested further in the cell growth experiments.

Thus, a wide range of ARA, from relative high and significant ARA for compounds **IOS-10003**, **IOS-10004**, **V-1-41**, to the absence of ARA, as for compounds **AP-12**, **A2-15**, and **IB-32**, were revealed (see Table 1).

Medium ARA values were obtained for compounds **K-2-11** and **diludine**, 40.5 and 39.5%, respectively.

One can notice that all studied compounds possessing cationic (onium: trimethylammonium, methylcycloalkylammonium, or pyridinium) substituents at 2 and 6 methylene of the DHP cycle have more or less significant ARA.

In case of 2,6-methylmorpholiniummethylene substituents (compounds **IOS-10003** and **V-1-32**) the highest ARA are detected (95% for each other).

Electron-donating substituents' containing pyridiniomethylene moieties at positions 2 and 6 of the 1,4-DHP diminished the ARA (compound **D-3-59-1**), while DHPs have shown ARA also in case of absence of electron-withdrawing cationic groups at positions 2 and 6 of the 1,4-DHP cycle (**diludine**). It should be mentioned here that corresponding 4-phenyl analogue was practically inactive (see [6]).

As showed in the previous studies, compound **Z41-74** stimulated HOS cell growth [14]. This compound has trimethylammoniomethylene substituents at positions 2 and 6 of the DHP cycle and is relative structural analogue of compounds **V-1-32**, **IOS-10003** and **IOS-10004** with saturated cationic heterocyclic moieties at positions 2 and 6 of the DHP cycle. However compound **Z41-74** possesses lower antiradical activity (16%), perhaps due to aliphatic (uncyclic) trimethylammonio part in molecule.

There are 3 compounds with cationic N-quaternized pyridinium moiety at position 4 of the 1,4-DHP cycle, **A2-15** and **AP-12**, that have shown perspective as bifunctional growth modulating agent compound **IB-32**, lacking ARA. These compounds lack cationic moieties at position 2 and 6 capable of forming labile hydrogen atom.

A group comprising compounds **V-1-32** and **V-1-41** (see Table 1) having both 2,6-pyridiniomethylene substituents, but with different variations at position 4 of the 1,4-DHP cycle, gave relatively high values of ARA (68.8% and 70.7% correspondingly). Therefore substituent in position 4 seems to have less decisive effect than do variations at positions 2 and 6 of the 1,4-DHP molecule. Their influence on normal and on tumor cells was less manifested; there was no difference in case of normal cell growth and in case of **V-1-32**, either on HOS or on HeLa cells growth (except 100 μg/mL concentration which slightly retarded cell proliferation). Nevertheless, compound **V-1-41** increased growth of HeLa cells and HOS cells indicating it could be used to study further altered mechanisms of the malignant cell growth.

These compounds have shown low toxicity (1706 mg/kg and >2000 mg/kg correspondingly) and did not suppress growth of any cell type even at the concentration 100 μg/mL.

These compounds have structure similarities with compounds **IOS-10003** (versus **V-1-32**) and **K-2-11** (versus **V-1-41**) that also share similar biological activities, although one can notice some minor differences.

3.2. Dependence of the Cell Growth Regulating Activities of the DHP Derivatives on Their Structure and Concentrations Used. The data regarding 1,4-DHPs growth modulating activities were obtained using the ^{3}H-thymidine incorporation assay reflecting the cellular DNA synthesis (i.e., the cell growth). Different types of cells in vitro were used: murine skin fibroblasts L929 cell line (Figure 2), human endothelial cells HMEC (Figure 3), human osteosarcoma cell line HOS, which in vitro grows resembling osteoblast cells (Figure 4), and human cervical carcinoma HeLa (Figure 5). Concentration/activity and structure/activity relationship of tested 11 DHP derivatives are

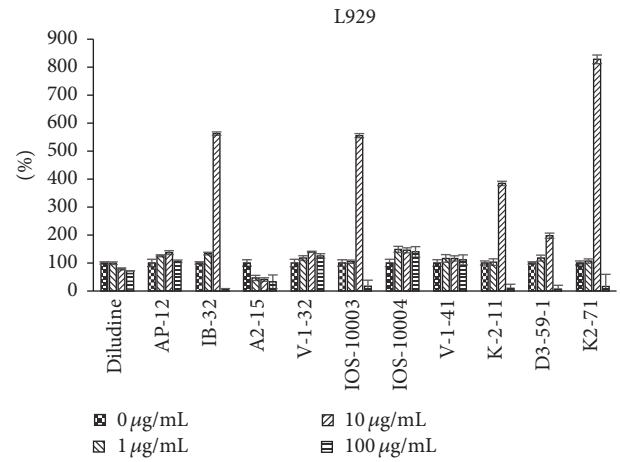

Figure 2: Dependence of proliferation modulation activity (expressed as ^{3}H-thymidine incorporation, in percentage (y-axis) of the respective, untreated control) on chemical structure and concentration of eleven DHP compounds on L929 cells.

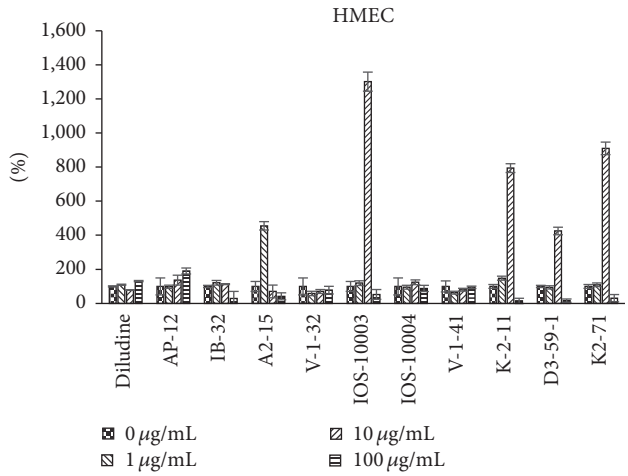

Figure 3: Dependence of proliferation modulation activity (expressed as ^{3}H-thymidine incorporation, in % of control, y-axis) on chemical structure and concentration of eleven DHP compounds on HMEC cells.

presented in Figures 2–5. In Figures 2–5 on ordinate axis the value of proliferation activity as percentage of the untreated controls is given. Three stepwise concentrations were used: 1 μg/mL, 10 μg/mL, and 100 μg/mL. Since the different experiments had different control levels of incorporation to compile the data of 3 experiments it was calculated. Data are presented as mean ± SD.

Further proliferation modulation activity of some DHPs is compared with DOXO activity (see Figure 6).

All tested DHPs exerted cell type-dependent and concentration dependent effects, as quantified by the ^{3}H-thymidine incorporation (DNA synthesis) of the cultured cells (see Figures 2–5). Nonlinear dependence of effect on the concentrations of compounds used was observed. Medium concentrations of DHP derivatives showed usually the most pronounced effects, except usually cytotoxic effects of the

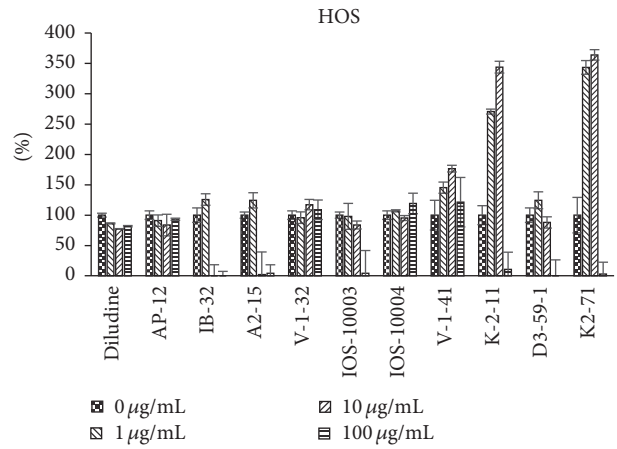

Figure 4: Dependence of proliferation modulation activity (expressed as ^{3}H-thymidine incorporation, in % of control, y-axis) on chemical structure and concentration of eleven DHP compounds on HOS cells.

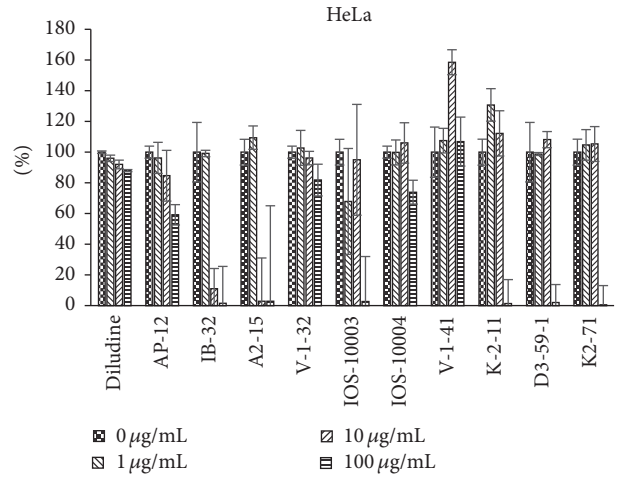

Figure 5: Dependence of proliferation modulation activity (expressed as ^{3}H-thymidine incorporation, in % of control, y-axis) on chemical structure and concentration of eleven DHP compounds on HeLa cells.

highest concentrations (see Figures 2–5). The more effective one was concentration 10 μg/mL (for compound **K-2-11**, on all four cell lines, for **IOS-10003,** on L929 and HeLa cells). The highest concentration 100 μg/mL was however manifold less effective than 10 μg/mL or even cytotoxic (in the case of **K-2-11**, on HeLa cells).

While all 4 substituted 1,4-DHPs, except **diludine**, were completely abolishing the ^{3}H-thymidine incorporation by L929 cells if used at 100 μg/mL concentration indicating even cytotoxic activities of DHPs, the **K-2-11**, **D3-59-1,** and in particular **IB-32** and **IOS-10003** on the other hand strongly enhanced the growth of these fibroblasts, but only if used at 10 μg/mL concentration. However, compound **IB-32** did not show such growth enhancing effect for any other cell line used. Actually compound **IB-32** was toxic at 10 μg/mL concentration for HOS and for HeLa cells. Opposite to that, compound **K-2-11** enhanced the growth of every cell line tested, if used at 10 μg/mL concentration. The most pronounced stimulating effect of compound **K-2-11** was observed for HMEC endothelial cells (Figure 3), while for HeLa cells it was more or less enhancing (Figure 5). It should also be mentioned that growth stimulating effects of compound **K-2-11** obtained at 10 μg/mL concentration were changed into strong suppression, that is, cytotoxicity in case of 100 μg/mL concentration of **K-2-11**.

The most similar effects to those of derivative **K-2-11** were effects of compound **K2-71**, with only exception of the even higher efficiency of compound **K2-71** in case of L929 cells stimulation (Figure 2). Compound **K2-71** was efficient DHP stimulating L929, also HOS and HMEC cells (Figures 3 and 4) even more than compound **K-2-11**, while for all cell lines tested it was toxic if used at 100 μg/mL concentration.

Interestingly, the well-known DHP antioxidant **diludine** did not exert as strong effects as did the other DHPs; even in case of 100 μg/mL concentration **diludine** did not show strong toxicity as did the other DHPs tested.

As in case of other physiological activities (antihypertensive, anticancer, etc.), substituents at positions 4, 2 and 6, and 3 and 5 of the 1,4-DHP cycle and also the lipophilicity of the molecule have important effects on the antiproliferative activity of 1,4-dihydropyridine derivatives. Regarding structure-activity relationships, present work claims the importance of hetaryl substituents at position 4 of the DHPs (compound **IB-32**, see Table 1) (analogous as given in [25]). Active are aryl (phenyl-) substituents too (see Table 1).

The length of alkyl chains of substituents at positions 3 and 5 may be shorter (methyl or ethyl esters), medium (propoxyethoxy ester), or prolonged (till C-12: dodecyl ester), substituents at positions 2 and 6 may be charged bilaterally. The charge in position four seems to be important, while activity is present both for lipophilic compounds (low activity for **diludine**, see Table 1), and, especially, for amphiphilic compounds too, analogues of **K-2-11**.

Compound **V-1-32** containing N-methylmorpholiniomethylene substituent at positions 2 and 6 analogue comprising 4-[2′-difluoromethoxyphenyl] moiety and shorter (methyl) alkyl chains in ester groups at substituents 3 and 5, as well as **V-1-41** (which is structural analogue of known compound **Z41-74** comprising methoxycarbonyl group (**V-1-41**) at position 4 of the 1,4-DHP cycle instead of phenyl group (**Z41-74**)) with pyridiniomethylene substituents at positions 2 and 6, only insignificantly influences normal and tumor cell proliferation.

On the contrary, DHP derivative **K-2-11** possessing ARA properties [10] significantly increased proliferation of HOS cells at 10 μg/mL concentration. The data obtained for HeLa cells are contradictory: 10 μg/mL concentrations increased HeLa cells proliferation almost 10 times, but some experiments revealed absence of statistically significant increase of HeLa cells proliferation. Compound **K-2-11** increased also proliferation of normal cells (cell lines HMEC and L929). At the concentration 100 μg/mL the growth of cells was suppressed, including also tumor cell lines HeLa and HOS. Cytotoxicity on normal cells is low: NIH 3T3 is 1482 mg/kg (see Table 1).

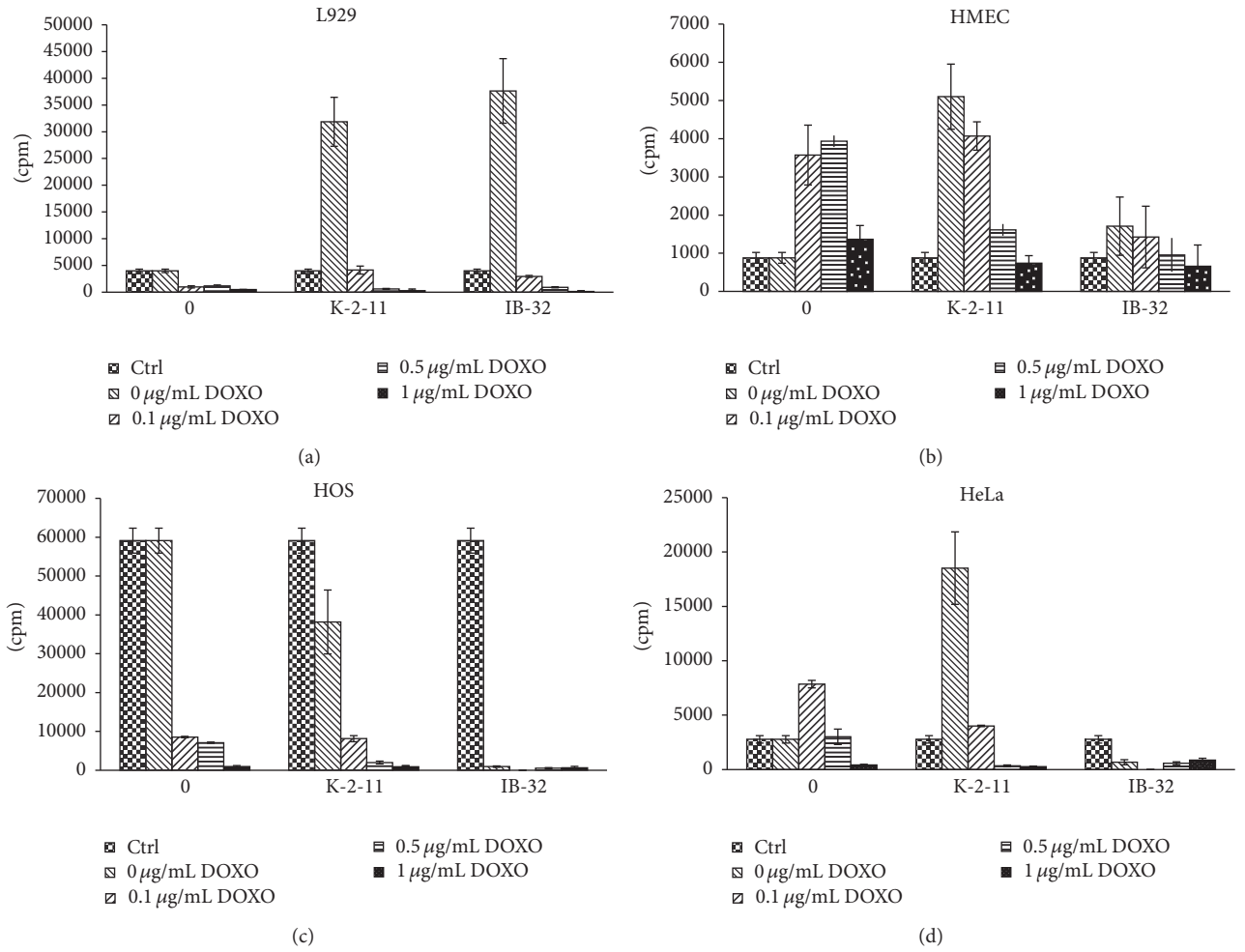

Figure 6: (a) Proliferation modulation activity of DOXO (columns 0) and of DHP derivatives **K-2-11** and **IB-32** (10 μg/mL) alone and in the presence of DOXO on L929 cells (expressed as ^{3}H-thymidine incorporation, in CPM, y-axis). Control cells (Ctrl) without DOXO (0 μg/mL) are presented in the 1st bar of each column. First column (0): control cells treated with DOXO, without DHPs. Added DOXO concentrations were expressed as μg/mL: 0.1 μg/mL, 0.5 μg/mL, and 1 μg/mL. Results were expressed as mean values of counts per minute (CPM) ± SD. (b) Proliferation modulation activity of DOXO (columns 0) and of DHP derivatives **K-2-11** and **IB-32** (10 μg/mL) alone and in the presence of DOXO on HMEC cells (expressed as ^{3}H-thymidine incorporation, in CPM, y-axis). (c) Proliferation modulation activity of DOXO (columns 0) and of DHP derivatives **K-2-11** and **IB-32** (10 μg/mL) alone and in the presence of DOXO on HOS cells (expressed as ^{3}H-thymidine incorporation, in CPM, y-axis). (d) Proliferation modulation activity of DOXO (columns 0) and of DHP derivatives **K-2-11** and **IB-32** (10 μg/mL) alone and in the presence of DOXO on HeLa cells (expressed as ^{3}H-thymidine incorporation, in CPM, y-axis).

Compound **K2-71** containing 3-methylpyridiniomethylene substituents at positions 2 and 6 is a close relative (homologue) of compound **K-2-11**. It has medium ARA (~39%), low cytotoxicity, and enhanced growth of normal cells at concentration of 10 μg/mL, stimulating also HOS cells (at 1 and 10 μg/mL), but not HeLa cells, while at 100 μg/mL growth of all cell types was suppressed.

Compound **IOS-10003** is intriguing compound: it has high ARA (~95%) [10]. It is effective proliferation promoter at 10 μg/mL for the L929 cells (Figure 2) and in HMEC cells (Figure 3). At 100 μg/mL concentration proliferation of L929 and HMEC was suppressed significantly similar to malignant HOS and HeLa cells.

Compounds **V-1-32** and **V-1-41** have similar and also different structural parameters comparing to **IOS-10003** (versus **V-1-32**) and **K-2-11** (versus **V-1-41**), so also properties are at the same time similar in some sense, but one can also notice difference. Compounds **V-1-32** and **V-1-41** possess high ARA (95.1 and 70.7% correspondingly); nevertheless their influence on normal and tumor cells growth was less manifested. There was no effect on normal cells growth; and in case of compound **V-1-32** there was also no influence on HOS and HeLa cell growth. However, compound **V-1-41** increased the growth of HeLa and HOS cells. Both compounds have low cytotoxicity (1706 mg/kg and >2000 mg/kg correspondingly). They did not suppress growth of any cell line even at concentration 100 μg/mL.

Similarly, compound **A2-15** (one representative from compounds group II (**A2-15**, **AP-12**, and **IB-32**, but without ARA)) was mainly inert regarding studied cell lines. Concerning compound **AP-12** one can mention its enhancing effect on HMEC cells growth and diminishing effect for the

growth of HeLa cells at 10 μg/mL and 100 μg/mL concentrations.

On the contrary, **IB-32** revealed quite unique properties, enhancing growth of normal cells (especially L929) and sharp diminishing or completely stopping the growth of HOS and HeLa cells (at concentrations 10 μg/mL and 100 μg/mL). For L929 cells activity of compound **IB-32** was remarkable in the same activity range as for compound **K-2-11** (Figures 2 and 6(a)), being more efficient with DOXO concentration 0.1 μg/mL.

The activities of remaining 5 compounds (**V-1-32**; **V-1-41**; **IOS-10004**; **A2-15**; **AP-12**) only insignificantly prevailed over control levels (without DHPs addition). Accordingly, we can define following groups of compounds concerning their influence on tested cell cultures:

(1) Compounds significantly enhancing growth of cultured cells in case of

  (1a) Both normal and tumor cells: **K-2-11** (ARA 39.5%)

  (1b) Only normal cells: growth of tumor cells may be suppressed: **AP-12** (lacked ARA), **IB-32** (also lacked ARA), and **IOS-10003** (ARA 95.1%)

  (1c) Only tumor cells: **V-1-41** (ARA 70.7%)

(2) Compounds revealing minor deviations on normal and tumor cells growth: **V-1-32** (ARA 95.1%), **IOS-10004** (ARA 54.1%), **A2-15** (ARA close to 0%), and **AP-12** (ARA close to 0%)

3.3. Proliferation Modulation Activity of DHPs in Combination with Doxorubicin. The anticancer drug doxorubicin (DOXO) was used at ranging concentrations: 0.1 μg/mL, 0.5 μg/mL, and 1 μg/mL to test additional effects of compounds **K-2-11** and **IB-32** (see Figures 6(a)–6(d)). In the experiments with DOXO (see Figures 6(a)–6(d)) final concentration of both 1,4-DHP derivatives (**K-2-11** and **IB-32**) was 10 μg/mL. Both compounds are representatives of 2 different groups of DHPs studied (**IB-32**: II group, **K-2-11**: III group).

Addition of DOXO itself reduced the growth of most cells (not significantly in case of HMEC cells), if used at high concentrations, while it surprisingly enhanced both normal cell line HMEC and cancerous cell line HeLa if used at lower concentrations.

On the contrary, the growth enhancing effects of compound **IB-32** were more selective; that is, they were observed only for normal cell lines L929 and HMEC, while **IB-32** entirely retarded growth of tumor cells HOS and HeLa. Compound **K-2-11** alone stimulated growth of normal (L929 and HMEC) cell lines but also of tumor (HeLa) cells; in case of HOS cells reduction of the cell growth was observed.

4. Discussion

4.1. Is Growth Regulating/Antiproliferative Activity Related to Antioxidant and/or Antiradical Properties of DHP Compounds? Previously ARA was found only for a part of the 11 compounds set: for **diludine** (see [6]) and **K-2-11**, **Z41-74** [10, 14].

Comparison of proliferation modulation direction and strength of cationic moieties containing compounds **Z41-74** (see Table 1), compound, relative to **K-2-11**, **IOS-10003** [10], and **V-1-32** and **V-1-41** (see Table 1), and their dependence on ARA or AOA of these compounds was performed.

Compound **Z41-74** increased HOS cells growth attenuating lipid peroxidation effects [14]; it has low antiradical activity (16.1%).

Compounds having almost identical ARA had however different effects on cell proliferation. Archetype of DHP compounds, Hantzsch ester **diludine**, which is claimed as possessing remarkable AOA and ARA (ARA $\approx$ 41% in this study, see also appropriate citations in [6]) revealed almost inert attitude to normal and tumor cell proliferation. Compound **K-2-11** has almost identical ARA (ARA $\approx$ 40%); nevertheless it had significant influence on cell proliferation (HMEC, L929, HOS, and also HeLa). This may indicate that antioxidant properties of mentioned compounds (and probably other DHPs) are not the most relevant ones for their growth regulating effects.

Compound **IOS-10003** has high ARA (93.9%, see Table 1 and text of Section 3.2.); nevertheless it in general had very poor influence on normal and on tumor cells proliferation. Its effects were concentration dependent. So, it increased HMEC cell proliferation only at concentration 10 μg/mL and decreased L929 cells proliferation at 10 μg/mL and 100 μg/mL concentration. It also slightly reduced HOS cells proliferation at all studied concentrations. Nevertheless influence on HeLa cells was more remarkable; at 10 μg/mL concentration, proliferation rate was increased more than twice, while at 100 μg/mL HeLa proliferation was stopped. At 100 μg/mL for all cell types a decrease of proliferation was noticed.

We assume that hormetic redox signaling that is influenced by cellular stress could be important for the biological effects of DHPs, causing their biphasic dose-response relationship, manifested by low-dose stimulation and a high-dose inhibition of the cell growth, which seems to be true for most antioxidants [26, 27].

However, it seems there is no obvious relationship of ARA and influence of DHPs on cell proliferation, and the probability of the prediction of proliferation/regeneration inhibition or stimulation by DHPs using AOA or ARA activity as a criterion is the open question.

According to the ^{3}H-thymidine incorporation data obtained using 11 DHPs to treat 4 cell lines we can conclude that the most effective growth enhancing DHP was **K-2-11**, which enhanced the growth of all cell lines, usually for 3-fold, being the most effective in case of HMEC cells (8-fold increase) and the least effective in case of HeLa cells (only about 20% increase). The highest growth enhancing capacity of **K-2-11** was also supported by its efficiency even at 1 μg/mL concentration. Interestingly, similar to **K-2-11**, **K2-71**, **D3-59-1**, and **IB-32** had strongest growth enhancing effects exerted at 10 μg/mL concentration, which was even stronger than in case of **K-2-11**, but just of one cell line for each of these DHPs. Hence, **K2-71** and **D3-59-1** were the most potent growth stimulators for the HMEC cell line, while **IB-32** enhanced

only L292 murine fibroblasts. While it is not likely that such a specificity of IB-32 for L929 cells was due to the murine origin of these cells, we can assume that it rather reflects certain fibroblast cell growth enhancing capacity of **IB-32**. To verify this assumption additional fibroblast cell lines should be tested, since such an effect might be relevant for the possible use of **IB-32** to promote the wound healing, yet bearing a risk of the scar formation. It is certainly interesting that **K2-71** did not stimulate only the growth of L929 fibroblasts, so further comparisons between these two DHPs might help elucidating their activity principles.

The fact that most of the growth enhancing DHPs had strongest effects for human endothelial cells (HMEC) might indicate their possibly beneficial effects to support recovery of the damaged blood vessels or the neovascularization. That could be especially valuable for the promotion of the wound healing but could perhaps represent certain risk for the enhancement of the tumor neovascularization; therefore such effects should be further studied, too.

However, it is certain that none of these DHPs bears significant risk for enhancement of the cancer cell growth because none of them supported HeLa cell growth, while they all entirely abolished the growth of all cell lines tested if used at 100 μM concentration, except **diludine**. The growth enhancement of human osteosarcoma cells (HOS) observed upon **K-2-11** and **K2-71** does not necessarily have to be negative, because HOS cells are considered to be the osteoblast-like cells and are therefore used often to evaluate the growth of bone cells.

Since most of the DHPs used might be considered also as potential antioxidants, while their effect of the cell growth is cell type and concentration dependent, it is possible to assume that they could affect the cellular redox signaling, either directly or indirectly affecting the redox signaling pathways. Of particular interest for further studies would be analysis of potential interference of DHPs with lipid peroxidation, notably with 4-hydroxynonenal (HNE), which is considered to act as second messenger of free radicals and as growth regulating factor showing effects similar to the effects of the DHPs tested [4, 28–30].

It could be proposed that there can be also different additional factors (binding with some nuclear factors and/or receptors, modulation of gene and protein expression) relevant for the results obtained. Thus, some water-soluble 1,4-dihydropyridine derivatives without Ca^{2+}-antagonist activity, having proteolysis promoting activities, upregulate Psma6 mRNA expression in kidneys of intact and diabetic rats [31].

It should be mentioned also that in [32] instead of prooxidant toxicity of DOXO new alternative mechanism of doxorubicin antitumor effect is proposed, notably enhancement of de novo synthesis of ceramide, which in turn activates transcription factor CREB3L1. DOXO stimulates proteolytic cleavage of membrane-bound precursor of CREB3L1 by Site 1 Protease and Site 2 Protease, allowing the NH(2)-terminal domain of CREB3L1 to enter the nucleus and activate transcription of genes which encode inhibitors of the cell cycle, including p21. As mentioned above [31], water-soluble DHPs have proteolysis promoting activity. This property as one of the possible parts in cell growth regulating mechanism further should be examined and verified (maybe it is not only the case for water-soluble DHPs) for proliferation modulating DHPs tested in present study.

4.2. The Sensitivity (or Selectivity) of the Used Cell Lines toward Various DHP. The sensitivity (or selectivity) of the two normal cell lines (human endothelial cells HMEC and murine fibroblasts L929) and the two cancerous cell lines (human osteosarcoma HOS and human cervical carcinoma HeLa) toward proliferative/antiproliferative activity of DHPs both when used alone or in combination with DOXO appeared to be cell type different.

Namely, if the results obtained are analyzed according to the cell type used, it could observed that the most sensitive ones for the growth enhancing effects of the DHPs were human endothelial cells HMEC, while DHPs had hardly any stimulating effects for human cervical carcinoma cells HeLa.

Using L929 cell culture (Figure 2), it was found that compound **K-2-11** stimulates proliferation rate about 8 times. In case of **IB-32** (10 μg/mL) the stimulation is about 9.5 times. In presence of 0.1 μg/mL DOXO stimulation of cell proliferation was inhibited. It is also worth mentioning that **IB-32** has shown growth stimulating effects only for L929 murine fibroblasts, while it was the most effective DHP suppressing the growth of HOS and HeLa cells even if used at 10 μg/mL concentration, unlike the other tested 1,4-DHP derivatives which were effective only at 100 μg/mL concentration.

In case of HMEC cell line (see Figure 6(b)) stimulation of proliferation was observed mainly for compound **K-2-11**, as well as in presence of DOXO at 0.1 μg/mL.

As shown by Figure 6(c), compound **IB-32** inhibited HOS cell proliferation better than DOXO at 0.1 μg/mL and even 0.5 μg/mL. Therefore, this compound seems to be very potent proliferation inhibitor and perspective anticancer drug. Compound **K-2-11** per se partially inhibits HOS cells proliferation and enhances inhibition of HOS cells proliferation in combination with 0.5 μg/mL DOXO.

Compound **K-2-11** stimulated proliferation (Figure 6(d)) of HeLa cells (both if used alone, without DOXO, and if used in the presence of 0.1 μg/mL DOXO). That makes it less likely to be proposed as anticancer proliferation modifier. Surprisingly, DOXO too at 0.1 μg/mL stimulated proliferation rate.

On the contrary compound **IB-32** inhibited proliferation of HeLa cells both by itself and in the presence of DOXO.

4.3. Revealing Physiological Effects of Tested DHPs in relation to Their Growth Regulating Effects. Our present data are complementary to those previously obtained and to the results of other researchers concerning antioxidant, antiradical properties and growth regulating (proliferation modifying, both of normal and of cancer cell lines), as well as anticancer, MDR reversing, and other activities of studied DHP derivatives and their close analogues.

Growth regulation through redox signaling seems however not the only possible activity principles of the DHPs, although some other growth regulating mechanisms (apoptotic and antiapoptotic) could be also influenced by DHPs

active as proliferation modulating agents. Namely, it was shown that the type of substituents at positions 1 and 4, 2 and 6, or 3 and 5 and also the lipophilicity of the molecule have substantial effects on the proliferation modulation and anticancer activity of 1,4-dihydropyridine derivatives [1].

Antioxidant **diludine** enhances growth performance of domestic animals, poultry, and fish; therefore it is claimed as functional growth enhancer in vivo (see [6]). However, **diludine** was until now never examined in cell proliferation experiments (on these four cell lines), so these data indicated it is probably metabolized/activated to become a growth promotor in vivo.

Diludine and water-soluble dihydroisonicotinic acid derivatives reveal antimutagenic and anticlastogenic properties and accelerate repair of oxidant and ionising radiation generated DNA damage (see Duburs et al.'s [33]).

Three water-soluble 1,4-dihydroisonicotinic acid derivatives were tested using ^{3}H-thymidine incorporation and trypan blue assay for liver cells growth and viability [34]. All three substances caused a dose-dependent decrease in ^{3}H-thymidine incorporation, but in different concentration ranges. Classical antioxidant Trolox caused very rapid decline in ^{3}H-thymidine incorporation. Thus, depending on the structure and concentration, the cited 1,4-DHP derivatives variously affected thymidine incorporation, cell proliferation, and growth, connected with OS and other metabolic influences. Maybe further derivatization of the tested DHPs (**AP-12** and **IB-32**) with water-soluble substituents could be worthwhile. Compounds **K-2-11** and **K2-71**, as well as **IOS-10003**, **IOS-10004**, and **A2-15** have water-soluble properties.

Dual effects of a water-soluble 1,4-DHP compound (sodium 3,5-bis-ethoxycarbonyl-2,6-dimethyl-1,4-dihydropyridine-4-carboxylate) in X-irradiated *L5178Y cells* (*murine lymphoma sublines*, double strand break (DSB) repair competent *LY-R* and radiosensitive *LY-S* cells) are reported by Dalivelya et al. [35]. Decreased fixation of radiation inflicted DNA damage by increasing the rate of DNA repair and enhancing the efficiency of checkpoint control were postulated as activity principles of this DHP. However direct confirmation of this assumption is necessary. Ryabokon et al. [36] found that 1,4-DHP derivative reduces DNA damage and stimulates DNA repair in human cells in vitro.

Amphiphilic DHP compound **K-2-11** is claimed to be a multidrug resistance (MDR) reverser [37]. MDR often develops in cancer cells to different chemotherapeutic drugs and is essential factor in the failure of various chemotherapies [25], including those based on DOXO. In the last two decades some 1,4-DHPs and structurally related compounds were discovered and approved as effective reversers of resistance to doxorubicin, daunomycin, vinblastine, and vincristine, as other anticancer drugs [25, 38, 39]. The presence of a hetaryl group at position 4of DHP is claimed as effectively increasing MDR-inhibiting activity [25]. MDR modulating activity was found for near DHP analogues, thieno[2,3-b]pyridines too [40].

Compound **K-2-11** was tested [37] on MDR1-expressing mouse lymphoma cells and their parental control. **K-2-11** enhanced the cytotoxic effects of doxorubicin, both in the MDR and in parental cell line, while **K-2-11** alone did not affect cell viability. Our data however suggest that compound **K-2-11** could per se modulate proliferation activity, as well in the presence of DOXO (in HMEC and HeLa cells, see Figures 6(b) and 6(d)). Compound **K-2-11** also acted as an antioxidant, reducing the cellular generation of reactive oxygen species (ROS). It is assumed that 1,4-DHP derivative **K-2-11** blocks P-gp activity; thus cancer cells stay more chemosensitive due to DOXO retention in the cells. Compound **K-2-11** could suppress also increase of ROS (caused by DOXO and further doxorubicin semiquinone radical initiated reduction of molecular oxygen and generation of superoxide radical, which initiates ROS production chain reaction), preventing in this way NF-κB activation that could consequently lead to a normal expression of MDR1 and antiapoptosis genes, restoring chemosensitivity of cancer cells.

The ability of compound **K-2-11** to modulate the growth the of cells found on MDR1-expressing mouse lymphoma cells and their parental control [37] was also confirmed in current study (see Table 1, Figures 6(a)–6(d)). Unfortunately **K-2-11** several times enhanced the HeLa cell growth, thus reducing its attractiveness to some extent (Figure 6(d)).

A novel *amphiphilic (lipophilic)* 1,4-dihydropyridine derivative **AP-12** (see Table 1) was studied in the present article as proliferation modifier in the above-mentioned cell systems. Recently, Jansone et al., 2016 [13], have described memory-improving, anxiolytic effects of this compound in transgenic AD model (TgAPPSweDI) male mice. It was also shown [12] that this compound crosses the blood-brain barrier and blocks neuronal (neuroblastoma) and vascular (vascular smooth muscle cell line) calcium channels, exerting Ca^{2+} antagonistic properties, and changed brain protein expression (as postsynaptic membrane protein Homer-1), with a particular focus on those of the GABAergic system, and improved behavior. Previously direct correlation between the length of the alkyl chain substituent at structurally related N-quaternized 4-β-pyridyl-l,4-dihydropyridines and their improved "membranotropic" effects was noticed, such as incorporation in the liposomal membranes and bilayer fluidity could be one of essential activity principles of this DHP [41].

Compound **Z41-74** (as well as another *lipophilic* DHP compound neuroprotectant **cerebrocrast**) was previously tested for the influence on HOS (human osteosarcoma) cell line [14]. Both compounds **Z41-74** and **cerebrocrast** caused increased metabolic rate and growth of these cells, even attenuating suppressive effects of lipid peroxidation. Herewith we must say that HOS cells are known not only as sarcoma, but also as a model osteoblast cells, due to their growth features in vitro.

It must be also mentioned that recently SIRT1 activation and promotion of wound healing (proliferation) of normal cells and contrary suppression of tumor cell proliferation were found for some lipophilic 1-benzyl substituted 1,4-DHPs [1], similar to our data obtained concerning N-unsubstituted dually acting DHP compound **IB-32**.

Antihypertensive DHPs are structural analogues of compounds surveyed in the present study as proliferation modifiers. Antiproliferative effect for these compounds was reported as structure (substituent type and length, stereochemistry of substances) and concentration dependent,

as well as being connected with lipophilicity parameters. Thus, *lipophilic* DHP calcium channel blockers **lacidipine** and **amlodipine** reduced carotid intima-media thickness by decreasing proliferative effect of oxidized low-density lipoprotein (ox-LDL) (antiproliferative effect against pro-proliferative effect of ox-LDL), whereas **(*S*-)-amlodipine** had no antiproliferative effect. ROS-MAPKs (Mitogen Activated Protein Kinases) pathway might be involved in the mechanism [42, 43]. Antihypertensive DHP drug **azelnidipine** (AZL, CS-905) being antioxidant compound inhibited mesangial cell proliferation induced by highly concentrated insulin (INS) [44]. INS-increased phosphorylation of extracellular signal-regulated kinase (MAPK/ERK) 1/2 was inhibited by 0.1 μM AZL. At the same concentration AZL blocked intracellular ROS production more effectively than 0.1 μM nifedipine. Azelnidipine inhibits insulin-induced mesangial cell proliferation by inhibiting the production of ROS. Thus, AZL is considered to be administered for diabetic nephropathy.

Evaluation of DHP antihypertensive drug **nifedipine** effects on *Saccharomyces cerevisiae* was recently performed [45]. Surprisingly, **nifedipine** exercised a toxic effect on *Saccharomyces cerevisiae* shown through measuring the following parameters: the cell proliferation, respiratory activity, and the level of some OS biomarkers (CAT, MDA).

Effects of some structurally different 1,4-DHP Ca antagonists (four commercial 4-nitrophenyl 1,4-DHP derivatives: **nimodipine**, **nicardipine**, **nifedipine**, and **niludipine**, two originated from LIOS 1,4-DHPs, **cerebrocrast** and **etaftoron**, as well as *two metabolites* of **cerebrocrast**) were studied on rat spleen lymphocyte activation and proliferation in vitro following stimulation with the mitogens: concanavalin A and recombinant interleukin-2 (IL-2), as well as insulin and insulin antibodies [46]. Ca^{2+} antagonists in a concentration range of 10 μM and higher are known to suppress Ca transport into the lymphocyte cytosol, changing a normal response of lymphocytes to mitogens and antigens and so inhibiting their proliferation, as well as IL-2-induced cell proliferation, and their receptor expression on the surface of lymphocytes without cell cytotoxicity. Contrary results with DHP compounds were found at lower concentrations. Authors concluded that in low concentrations (0.1 μM to 1 nM) the tested 1,4-DHP Ca antagonists, especially **cerebrocrast**, stimulated the process of rat spleen lymphocyte proliferation and DNA synthesis [46].

5. Conclusions

Some of the studied DHP compounds showed remarkable proliferation regulation properties alone or in combination with anticancer drug doxorubicin (DOXO). They were found to show different concentration-dependence and selectivity for the tested four cell lines (two normal (HMEC, L929) and two malignant (HOS, HeLa)) treated. Nonlinear dose-activity dependence and even bifunctional effects depending on substance concentration were observed for some DHPs, while most of them suppressed the cell growth if used at high concentration.

Compound **IB-32**, also **AP-12** and **IOS-10003**, has shown promising dual activity, proliferation inhibition on cancer cell line and proliferation stimulating effect on normal cell line. Mentioned compounds comprise long alkyl (or aralkyl) chains. Therefore, further search of the dual acting compounds seems to be perspective.

There was no obvious relationship of antiradical activity of the tested DHPs and their influence on cell proliferation observed. Finally, it can be concluded that well-known antioxidant DHP **diludine** was the least effective DHP used, although it is well known for its numerous beneficial effects, so we assume that some of the other DHPs tested might allow development of novel biomedical remedies.

Abbreviations

DHP(s): 1,4-Dihydropyridine(s)
OS: Oxidative stress
AO: Antioxidant
AOA: Antioxidant activity
ROS: Reactive oxygen species
ARA: Antiradical activity
DOXO: Doxorubicin
pDNA: Plasmid DNA
SIRT1: Sirtuin 1
L929: Murine skin fibroblasts
HMEC: Human mammary epithelial cells
HOS: Human osteosarcoma cells
HeLa: Human epitheloid cervix carcinoma cells
FCS: Fetal calf serum
DMEM: Dulbecco's modified Eagle's medium.

Conflicts of Interest

The authors declare there are no conflicts of interest regarding the publication of this paper.

Acknowledgments

Authors from Latvian IOS acknowledge Latvian Council of Science, National Research Programme PUBLIC HEALTH/Biomedicine of the Republic of Latvia, as well as projects NFI/R/2014/051 and INNOVABALT (REGPOT–CT-2013-316149) project for financial support, and administration of the institute for technical support. Authors acknowledge Brigita Chekavichus, Ph.D., Inese Reine, M.S., and Dainis Kaldre, Ph.D., for provided DHPs, and Zaiga Ogle, M.S., for graphical support. The support of Cooperation in European System of Science and Technology (COST) Domain of Chemistry, Molecular Sciences and Technologies (CMST) (COST B35) was of highest importance for dissemination of results and discussions regarding topic of this paper.

References

[1] S. Valente, P. Mellini, F. Spallotta et al., "1,4-Dihydropyridines active on the SIRT1/AMPK pathway ameliorate skin repair and mitochondrial function and exhibit inhibition of proliferation

in cancer cells," *Journal of Medicinal Chemistry*, vol. 59, no. 4, pp. 1471–1491, 2016.

[2] R. Visconti and D. Grieco, "New insights on oxidative stress in cancer," *Current Opinion in Drug Discovery and Development*, vol. 12, no. 2, pp. 240–245, 2009.

[3] S. Reuter, S. C. Gupta, M. M. Chaturvedi, and B. B. Aggarwal, "Oxidative stress, inflammation, and cancer: how are they linked?" *Free Radical Biology and Medicine*, vol. 49, no. 11, pp. 1603–1616, 2010.

[4] R. Novak Kujundžić, N. Žarković, and K. Gall Trošelj, "Pyridine nucleotides in regulation of cell death and survival by redox and non-redox reactions," *Critical Reviews in Eukaryotic Gene Expression*, vol. 24, no. 4, pp. 287–309, 2014.

[5] T.-H. Leu and M.-C. Maa, "The molecular mechanisms for the antitumorigenic effect of curcumin," *Current Medicinal Chemistry - Anti-Cancer Agents*, vol. 2, no. 3, pp. 357–370, 2002.

[6] A. Velena, N. Zarkovic, K. Gall Troselj et al., "1,4-dihydropyridine derivatives: dihydronicotinamide analogues—model compounds targeting oxidative stress," *Oxidative Medicine and Cellular Longevity*, vol. 2016, Article ID 1892412, 35 pages, 2016.

[7] Z. Hyvönen, A. Plotniece, I. Reine, B. Chekavichus, G. Duburs, and A. Urtti, "Novel cationic amphiphilic 1,4-dihydropyridine derivatives for DNA delivery," *Biochimica et Biophysica Acta - Biomembranes*, vol. 1509, no. 1-2, pp. 451–466, 2000.

[8] Z. Hyvönen, M. Ruponen, S. Rönkkö, P. Suhonen, and A. Urtti, "Extracellular and intracellular factors influencing gene transfection mediated by 1,4-dihydropyridine amphiphiles," *European Journal of Pharmaceutical Sciences*, vol. 15, no. 5, pp. 449–460, 2002.

[9] A. Plotniece, K. Pajuste, D. Kaldre et al., "Oxidation of cationic 1,4-dihydropyridine derivatives as model compounds for putative gene delivery agents," *Tetrahedron*, vol. 65, no. 40, pp. 8344–8349, 2009.

[10] K. Pajuste, Z. Hyvönen, O. Petrichenko et al., "Gene delivery agents possessing antiradical activity: self-assembling cationic amphiphilic 1,4-dihydropyridine derivatives," *New Journal of Chemistry*, vol. 37, no. 10, pp. 3062–3075, 2013.

[11] G. Duburs, J. Zilbers, A. Velēna, A. Kumerova, and G. Tirzītis, "Multistage studies of control of peroxidation processes in biological membranes with antioxidants of 1,4-dihydropyridine series," *Izvestija Akademii Nauk Latvijskoj SSR, Serija B*, vol. 7, no. 336, pp. 65–68, 1975 (Russian).

[12] B. Jansone, I. Kadish, T. Van Groen et al., "A novel 1,4-dihydropyridine derivative improves spatial learning and memory and modifies brain protein expression in wild type and transgenic APPSweDI mice," *PLoS ONE*, vol. 10, no. 6, Article ID e0127686, 2015.

[13] B. Jansone, I. Kadish, T. van Groen et al., "Memory-enhancing and brain protein expression-stimulating effects of novel calcium antagonist in Alzheimer's disease transgenic female mice," *Pharmacological Research*, vol. 113, pp. 781–787, 2016.

[14] T. Lovaković, M. Poljak-Blazi, G. Duburs et al., "Growth modulation of human cells in vitro by mild oxidative stress and 1,4-dihydropyridine derivative antioxidants," *Collegium Antropologicum*, vol. 35, no. 1, pp. 137–141, 2011.

[15] S. Zhou, C. M. Palmeira, and K. B. Wallace, "Doxorubicin-induced persistent oxidative stress to cardiac myocytes," *Toxicology Letters*, vol. 121, no. 3, pp. 151–157, 2001.

[16] M. Rucins, D. Kaldre, K. Pajuste et al., "Synthesis and studies of calcium channel blocking and antioxidant activities of novel 4-pyridinium and/or N-propargyl substituted 1,4-dihydropyridine derivatives," *Comptes Rendus Chimie*, vol. 17, no. 1, pp. 69–80, 2014.

[17] N. V. Makarova, A. Plotnietse, G. Tirzitis, I. Turovskii, and G. Dubur, "Some transformations of N-ethoxycarbonyl-methylpyridinium bromides with a pyridyl or 1,4-dihydropyridyl substituent at position 3," *Chemistry of Heterocyclic Compounds*, vol. 33, no. 2, pp. 175–183, 1997.

[18] M. Petrova, R. Muhamadejev, B. Vigante et al., "Intramolecular C-H$\cdots$O hydrogen bonding in 1,4-dihydropyridine derivatives," *Molecules*, vol. 16, no. 9, pp. 8041–8052, 2011.

[19] G. Duburs, J. Klovins, I. Bruvere et al., "1,4-Dihydropyridine-4-yl pyridinyo derivatives as new agoallosteric modulators of adenosine A2A receptor," Latvian Patent. Application demand P-13-02, 2013.

[20] A. Abdelwahed, I. Bouhlel, I. Skandrani et al., "Study of antimutagenic and antioxidant activities of Gallic acid and 1,2,3,4,6-pentagalloylglucose from Pistacia lentiscus. Confirmation by microarray expression profiling," *Chemico-Biological Interactions*, vol. 165, no. 1, pp. 1–13, 2007.

[21] W. S. Stokes, S. Casati, J. Strickland, and M. Paris, "Neutral red uptake cytotoxicity tests for estimating starting doses for acute oral toxicity tests," *Current Protocols in Toxicology*, vol. 36, pp. 20.4.1–20.4.20, 2008.

[22] NIEHS (National Institute of Environmental Health Sciences), "ICCVAM test method evaluation report: in vitro cytotoxicity test methods for estimating starting doses for acute oral systemic toxicity tests," NIH Publication no. 07-4519, NIEHS, Research Triangle Park, NC, USA, 2006, http://iccvam.niehs.nih.gov/docs/acutetox_docs/BRD_TMER/TMERmain_Nov2006.pdf.

[23] ICCVAM, *Background Review Document: In Vitro Basal Cytotoxicity Test Methods for Estimating Acute Oral Systemic Toxicity*, National Institute for Environmental Health Sciences, Research Triangle Park, NC, USA, 2006, http://iccvam.niehs.nih.gov/methods/acutetox/inv_nru_brd.htm.

[24] EU legislation Dangerous Substances Directive (Directive 67/548/EEC), and the Dangerous Preparations Directive (Directive 1999/45/EC).

[25] S. Sepehri, H. P. Sanchez, A. Fassihi, and A. Fassihi, "Hantzsch-type dihydropyridines and biginelli-type tetrahydropyrimidines: a review of their chemotherapeutic activities," *Journal of Pharmacy and Pharmaceutical Sciences*, vol. 18, no. 1, pp. 1–52, 2015.

[26] V. Calabrese, C. Cornelius, A. Trovato-Salinaro et al., "The hormetic role of dietary antioxidants in free radical-related diseases," *Current Pharmaceutical Design*, vol. 16, no. 7, pp. 877–883, 2010.

[27] B. Poljsak and I. Milisav, "The neglected significance of 'antioxidative stress'," *Oxidative Medicine and Cellular Longevity*, vol. 2012, Article ID 480895, 12 pages, 2012.

[28] N. Zarkovic, Z. Ilic, M. Jurin, R. J. Schaur, H. Puhl, and H. Esterbauer, "Stimulation of HeLa cell growth by physiological concentrations of 4-hydroxynonenal," *Cell Biochemistry and Function*, vol. 11, no. 4, pp. 279–286, 1993.

[29] M. Jaganjac, T. Čačev, A. Čipak, S. Kapitanović, K. G. Trošelj, and N. Žarković, "Even stressed cells are individuals: second messengers of free radicals in pathophysiology of cancer," *Croatian Medical Journal*, vol. 53, no. 4, pp. 304–309, 2012.

[30] L. Milkovic, W. Siems, R. Siems, and N. Zarkovic, "Oxidative stress and antioxidants in carcinogenesis and integrative therapy of cancer," *Current Pharmaceutical Design*, vol. 20, no. 42, pp. 6529–6542, 2014.

[31] K. Ošiņa, E. Rostoka, J. Sokolovska et al., "1,4-dihydropyridine derivatives without Ca2+-antagonist activity up-regulate Psma6 mRNA expression in kidneys of intact and diabetic rats," *Cell Biochemistry and Function*, vol. 34, no. 1, pp. 3–6, 2016.

[32] A. G. Patel and S. H. Kaufmann, "How does doxorubicin work?" *Elife*, vol. 1, Article ID e00387, 2012.

[33] G. Duburs, B. Vigante, A. Plotniece et al., "Dihydropyridine derivatives as bioprotectors," *Chimica Oggi*, vol. 26, no. 2, pp. 68–70, 2008.

[34] S. Borovic, G. Tirzitis, D. Tirzite et al., "Bioactive 1,4-dihydroisonicotinic acid derivatives prevent oxidative damage of liver cells," *European Journal of Pharmacology*, vol. 537, no. 1–3, pp. 12–19, 2006.

[35] O. Dalivelya, N. Savina, T. Kuzhir, I. Buraczewska, M. Wojewódzka, and I. Szumiel, "Effects of an antimutagen of 1,4-dihydropyridine series on cell survival and DNA damage in L5178Y murine sublines," *Nukleonika*, vol. 51, no. 3, pp. 141–146, 2006.

[36] N. I. Ryabokon, R. I. Goncharova, G. Duburs, and J. Rzeszowska-Wolny, "A 1,4-dihydropyridine derivative reduces DNA damage and stimulates DNA repair in human cells in vitro," *Mutation Research*, vol. 587, no. 1-2, pp. 52–58, 2005.

[37] M. Cindric, A. Cipak, J. Serly et al., "Reversal of multidrug resistance in murine lymphoma cells by amphiphilic dihydropyridine antioxidant derivative," *Anticancer Research*, vol. 30, no. 10, pp. 4063–4069, 2010.

[38] L. Capolongo, N. Amboldi, D. Ballinari et al., "Reversal of multidrug resistance by new dihydropyridines with low calcium antagonist activity," *Acta Oncologica*, vol. 33, no. 7, pp. 787–791, 1994.

[39] S. Tasaka, H. Ohmori, N. Gomi et al., "Synthesis and structure-activity analysis of novel dihydropyridine derivatives to overcome multidrug resistance," *Bioorganic and Medicinal Chemistry Letters*, vol. 11, no. 2, pp. 275–277, 2001.

[40] A. Krauze, S. Grinberga, L. Krasnova et al., "Thieno[2,3-b]pyridines—a new class of multidrug resistance (MDR) modulators," *Bioorganic and Medicinal Chemistry*, vol. 22, no. 21, pp. 5860–5870, 2014.

[41] D. Tirzite, J. Koronova, and A. Plotniece, "Influence of some quaternised 1,4-dihydropyridine derivatives on liposomes and erythrocyte membranes," *Biochemistry and Molecular Biology International*, vol. 45, no. 4, pp. 849–856, 1998.

[42] I. T. Mak, P. Boehme, and W. B. Weglicki, "Protective effects of calcium channel blockers against free radical-impaired endothelial cell proliferation," *Biochemical Pharmacology*, vol. 50, no. 9, pp. 1531–1534, 1995.

[43] J. Zou, Y. Li, H.-Q. Fan, and J.-G. Wang, "Effects of dihydropyridine calcium channel blockers on oxidized low-density lipoprotein induced proliferation and oxidative stress of vascular smooth muscle cells," *BMC Research Notes*, vol. 5, article no. 168, 2012.

[44] S. Manabe, T. Okura, T. Fukuoka, and J. Higaki, "Antioxidative effects of azelnidipine on mesangial cell proliferation induced by highly concentrated insulin," *European Journal of Pharmacology*, vol. 567, no. 3, pp. 252–257, 2007.

[45] C. Asma and D. M. Reda, "Evaluation of dihydropyridine calcium antagonist effects on the stress bioindicator organism *Saccharomyces cerevisiae*," *Annals of Biological Research*, vol. 4, no. 10, pp. 40–46, 2013.

[46] J. Briede, D. Daija, E. Bisenieks et al., "Effects of some 1,4-dihydropyridine Ca antagonists on the blast transformation of rat spleen lymphocytes," *Cell Biochemistry & Function*, vol. 17, no. 2, pp. 97–105, 1999.

Hindawi
Oxidative Medicine and Cellular Longevity
Volume 2017, Article ID 8940321, 13 pages
https://doi.org/10.1155/2017/8940321

Research Article

A Clinically Relevant Variant of the Human Hydrogen Sulfide-Synthesizing Enzyme Cystathionine β-Synthase: Increased CO Reactivity as a Novel Molecular Mechanism of Pathogenicity?

João B. Vicente,[1] Henrique G. Colaço,[2] Francesca Malagrinò,[3,4] Paulo E. Santo,[1,5] André Gutierres,[1] Tiago M. Bandeiras,[1,5] Paula Leandro,[6] José A. Brito,[1] and Alessandro Giuffrè[3]

[1]*Instituto de Tecnologia Química e Biológica António Xavier, Universidade Nova de Lisboa, Oeiras, Portugal*
[2]*Instituto Gulbenkian da Ciência, Oeiras, Portugal*
[3]*CNR Institute of Molecular Biology and Pathology, Rome, Italy*
[4]*Department of Biochemical Sciences, Sapienza University of Rome, Rome, Italy*
[5]*Instituto de Biologia Experimental e Tecnológica, Oeiras, Portugal*
[6]*Research Institute for Medicines and Department of Biochemistry and Human Biology, Faculty of Pharmacy, University of Lisbon, Lisbon, Portugal*

Correspondence should be addressed to João B. Vicente; jvicente@itqb.unl.pt and Alessandro Giuffrè; alessandro.giuffre@uniroma1.it

Received 9 December 2016; Revised 10 January 2017; Accepted 16 January 2017; Published 22 March 2017

Academic Editor: Steven McAnulty

The human disease classical homocystinuria results from mutations in the gene encoding the pyridoxal 5′-phosphate- (PLP-) dependent cystathionine β-synthase (CBS), a key enzyme in the transsulfuration pathway that controls homocysteine levels, and is a major source of the signaling molecule hydrogen sulfide (H_2S). CBS activity, contributing to cellular redox homeostasis, is positively regulated by S-adenosyl-L-methionine (AdoMet) but fully inhibited upon CO or NO• binding to a noncatalytic heme moiety. Despite extensive studies, the molecular basis of several pathogenic *CBS* mutations is not yet fully understood. Here we found that the ferrous heme of the reportedly mild p.P49L CBS variant has altered spectral properties and markedly increased affinity for CO, making the protein much more prone than wild type (WT) CBS to inactivation at physiological CO levels. The higher CO affinity could result from the slightly higher flexibility in the heme surroundings revealed by solving at 2.80-Å resolution the crystallographic structure of a truncated p.P49L. Additionally, we report that p.P49L displays impaired H_2S-generating activity, fully rescued by PLP supplementation along the purification, despite a minor responsiveness to AdoMet. Altogether, the results highlight how increased propensity to CO inactivation of an otherwise WT-like variant may represent a novel pathogenic mechanism in classical homocystinuria.

1. Introduction

Hydrogen sulfide (H_2S) has emerged as a key signaling molecule in human physiology and pathophysiology, being implicated in the regulation of several processes such as neuromodulation, angiogenesis, vasorelaxation, bioenergetics/respiration, cell survival, and proliferation [1–4]. The gas has a pivotal role in the control of cellular redox homeostasis and prevention of oxidative stress, modulating the expression of key antioxidant enzymes [2]. Similarly to other relevant gaseous signaling molecules like CO and NO•, at low concentrations H_2S can exert cytoprotective effects or become cytotoxic at higher concentrations.

At least three human enzymes have been identified as key endogenous sources of H_2S: cystathionine β-synthase (CBS) and cystathionine γ-lyase (CSE), both occurring in

the transsulfuration pathway of methionine metabolism and mercaptopyruvate sulfurtransferase (MST) [1]. Beyond enabling conversion of homocysteine to cysteine through their historically recognized canonical activities, CBS and CSE catalyze a number of "alternative" reactions leading to H_2S synthesis, which has brought these enzymes into the limelight [1, 5, 6]. Indeed, a growing number of human pathologies, from cardiovascular and neurodegenerative diseases to different cancer types, are reportedly associated with disturbances of H_2S metabolism related to CBS, CSE, and/or MST [7]. CBS, in particular, has been shown to be overexpressed in colorectal, ovarian, and breast cancer, among other cancer types (reviewed in [8, 9]), as well as in neurodegenerative diseases, such as amyotrophic lateral sclerosis [10]. The enzyme is therefore currently recognized as a drug target [8].

CBS catalyzes the condensation of homocysteine and serine (or cysteine) leading to formation of cystathionine and H_2O (or H_2S). The human enzyme is a 551-amino acid protein with a central catalytic domain, harboring a pyridoxal 5′-phosphate (PLP) cofactor, flanked by a C-terminal domain with a binding site for the allosteric positive regulator s-adenosyl-L-methionine (AdoMet) and an N-terminal domain, harboring a hexacoordinate heme with C52 and H65 as endogenous Fe ligands [11]. Structural studies have shown that whereas the AdoMet-binding domain occludes the substrate entry site in the catalytic core, AdoMet binding induces a conformational change clearing the path for substrates to access the active site [11–13]. In the presence of AdoMet enzymatic activity thus increases 2–5-fold, as measured with isolated proteins and bacterial or human cell lysates. Another interesting regulatory mechanism concerns the B-type heme moiety in the N-terminal domain. While the enzyme is fully active when the heme is in the oxidized state, reduction to the ferrous state negatively impacts enzyme activity, possibly through a ligand exchange mechanism involving the replacement of C52 by a yet unknown neutral ligand [14, 15]. Such change in the Fe coordination is accompanied by a notable shift in the CBS heme Soret band from 449 to 424 nm, leading to an inactive protein species commonly referred to as "C-424" [15]. Even more striking is that binding of NO• or CO to the ferrous heme results in enzyme inhibition [16–20], with different lines of evidence pointing to a physiological role of this regulatory mechanism in vivo [21–27]. According to structural and mutagenesis studies, changes in the heme redox and ligation state are communicated to the PLP active site through α-helix 8 [15, 28, 29]. This regulatory mechanism places CBS at the crossroad between the signaling pathways of the three gasotransmitters (H_2S, CO, and NO•) in human physiology [30]. More recently, it has been shown that AdoMet enhances CBS sensitivity to CO and NO•, further highlighting an intricate interplay between the three domains in the protein [20].

Classical homocystinuria (OMIM #236200) is an inborn error of metabolism associated with mutations in the *CBS* gene. With a variable incidence of 1 : 1,800 to 1 : 900,000, classical homocystinuria is biochemically detected by markedly high homocysteine and methionine levels in plasma and urine, with clinical presentation involving mental impairment, vascular complications, dislocated lenses, and skeletal abnormalities [31]. Notably, elevated homocysteine levels are associated with oxidative stress conditions, well known to contribute to the onset and progress of a broad spectrum of diseases. Thus far, besides dietary methionine restriction, the major therapeutic approach for classical homocystinuria consists of administration of pyridoxine (vitamin B6), a precursor of the PLP cofactor [31], although a significant part of patients (approximately half) do not respond to this treatment [32]. The vast majority of the mutations identified in patients with classical homocystinuria are missense mutations resulting in single amino acid substitutions. Whereas most mutations affect the enzyme folding and/or activity [15, 28, 33–39], some of them have been shown to affect enzyme regulation by AdoMet, pointing to such dysregulation as a new pathogenic mechanism in classical homocystinuria [40]. The fact that several variants have impaired activity due to protein misfolding is underlined by the demonstration that some of them are amenable to be functionally rescued by chemical chaperones [34, 36, 38, 39, 41, 42]. A novel therapeutic approach is currently under development based on enzyme replacement therapy using PEGylated recombinant CBS, which has been shown to afford a marked decrease in circulating homocysteine in a mouse model of homocystinuria [43]. This therapeutic approach might be particularly relevant for PLP-unresponsive patients.

The 146 C>T transition in exon 1 of the *CBS* gene generates the clinically relevant p.P49L variant, identified in patients with classical homocystinuria [44–46]. The mutation results in mild to moderate symptoms and sporadic responsiveness to vitamin B6 treatment. When assayed in cell extracts or after purification, the protein variant shows impaired or wild type- (WT-) like canonical activity in the absence or presence of PLP in the assays, respectively, and milder to normal responsiveness to AdoMet [36, 37, 39, 40]. These findings point to defects in PLP incorporation, although the protein variant as purified after recombinant expression in *Escherichia coli* in the presence of suitable chemical chaperones at optimal concentrations exhibits unaffected PLP and heme incorporation, and unperturbed circular dichroism (CD) or UV-visible absorption spectra in the oxidized state [39].

Herein we demonstrate that the p.P49L variant of human CBS displays H_2S-synthesizing activity largely sensitive to PLP supplementation along the protein purification. The crystallographic structure of a truncated version of CBS p.P49L, devoid of the C-terminal AdoMet binding domain, reveals no major differences at the level of the PLP catalytic site with respect to the WT but slightly increased protein flexibility in the heme surroundings. As a novel finding we report a markedly increased CO affinity of p.P49L as compared to the wild type enzyme, *en route* to enzyme inactivation. The obtained functional and structural data are discussed in light of the proposal that in pathogenic variants of human CBS increased reactivity towards exogenous ligands, such as CO, represents a further molecular mechanism at the basis of classical homocystinuria.

2. Materials and Methods

2.1. Protein Expression and Purification. Recombinant full-length human CBS p.P49L was expressed and purified as previously described for WT CBS [19] in either the absence or presence of 20 μM PLP, using the herein named pET28b-CBS-p.P49L vector generated in [40]. With this vector as template, site-directed mutagenesis was employed to obtain also a truncated form of the protein (denoted by CBS$\Delta_{409-551}$ p.P49L) devoid of the C-terminal 143 residues corresponding to the AdoMet-binding domain. The 1227G>A mutant (cDNA numbering) carrying a premature stop codon at position 409 was generated from pET28b-CBS-p.P49L using the XL Quick Change Kit (Agilent) and the primers 5′-GAAGAAGCCCTGGTGATGGCACCTCCGTG (forward) and 5′-CACGGAGGTGCCATCACCAGGGCTTCTTC (reverse). All vectors were checked for the correct mutation by DNA sequencing. Expression and purification of CBS$\Delta_{409-551}$ p.P49L were carried out as described in [20].

Purity of the isolated proteins was assessed by SDS-PAGE and their concentration was determined by the Bradford method [47], whereas the heme concentration in the isolated oxidized proteins was determined using $\varepsilon_{428\,nm}$ = 92,700 M^{-1} cm^{-1} [48].

Unless otherwise stated, the experiments were carried out in 50 mM KPi buffer, 300 mM KCl, 10% glycerol, 100 μM EDTA, pH 7.0 (buffer A).

2.2. H_2S Synthesis Assays. H_2S production by recombinant human CBS variants was measured at 37°C, either by amperometry using a H_2S-selective electrode (World Precision Instruments) or by the lead acetate method [5]. Purified CBS (0.5–1 μM) was incubated for 10 minutes with 50 μM PLP, 260 U/ml catalase, and 0.4–2.0 mM homocysteine in the absence or presence of 0.5 mM AdoMet, after which 10 mM cysteine was added to trigger the reaction. Amperometric assays were performed using an ISO-H2S-2 hydrogen sulfide sensor coupled to an Apollo 4000 Free Radical Analyzer (World Precision Instruments). After recording H_2S production for 3 minutes, the electrode was internally calibrated by adding 4 μM NaHS (corresponding to 2 μM H_2S at pH 7.0). Finally, 50 μM *o*-acetylserine and 200 nM *Entamoeba histolytica o*-acetylserine sulfhydrylase were added to the reaction mixture to remove H_2S from solution and bring the signal back to baseline [49]. Activity assays by the lead acetate method were carried out in a thermostated cuvette under stirring, according to [5]. Lead acetate (400 μM) was added to the reaction mix prior to cysteine addition and H_2S production monitored at 390 nm in an Agilent Cary-60 spectrophotometer.

2.3. CO Titrations. UV-visible absorption spectra of oxidized and reduced CBS p.P49L and WT were recorded in an Agilent Cary-60 spectrophotometer. Anaerobic titrations of reduced CBS p.P49L with CO were performed at 20°C in an Agilent Cary-60 or a Shimadzu UVPC-1800 spectrophotometer. Gas exchange was prevented either by filling the quartz cuvette and sealing it with a rubber-cap or by adding mineral oil on top of the aqueous medium. Anaerobic conditions were ensured by nitrogen flushing and addition of glucose oxidase (4 units·ml^{-1}), catalase (13 μg·ml^{-1}), superoxide dismutase (12 units·ml^{-1}), and glucose (3 mM) to scavenge contaminant oxygen, hydrogen peroxide, and superoxide anion. CBS p.P49L and WT (1.4–1.6 μM in heme) were reduced with 90 μM sodium dithionite, diluted from a 45 mM stock solution (quantitated using $\varepsilon_{314\,nm}$ = 8,043 M^{-1}·cm^{-1} [50]). CO stock solutions were prepared by equilibrating thoroughly degassed buffer A with the pure gas at 1 atm, yielding 1 mM CO at 20°C. After each CO addition with gas-tight Hamilton syringes, the spectral changes were visually inspected in real time and a new addition was immediately made when no more changes were observed.

According to [16, 19, 20, 51], two apparent K_d (K_{d1} and K_{d2}) were used to satisfactorily fit the CO affinity data. The K_{d1} and K_{d2} values were obtained by fitting the data to (1), where P_L is the concentration of CO-bound CBS p.P49L, P_T and L_T are, respectively, the total CBS p.P49L and CO concentrations, and α_1 and α_2 are, respectively, the protein fractions binding CO at higher (K_{d1}) and lower (K_{d2}) affinity.

$$PL = \frac{\alpha_1\left[(P_T + L_T + K_{d1}) - \sqrt{(P_T + L_T + K_{d1})^2 - 4P_TL_T}\right] + \alpha_2\left[(P_T + L_T + K_{d2}) - \sqrt{(P_T + L_T + K_{d2})^2 - 4P_TL_T}\right]}{2}. \quad (1)$$

2.4. Stopped-Flow Measurements. Time-resolved absorption spectroscopy experiments were carried out in a thermostated stopped-flow instrument (DX.17MV, Applied Photophysics), equipped with a photodiode-array (light path, 1 cm). To avoid light-induced artifacts, the intensity of the white-light incident beam was decreased and a filter cutting UV light at $\lambda < 360$ nm was employed. Absorption spectra were recorded with an acquisition time of 10 ms per spectrum according to a logarithmic time scale. All reactions were carried out at 25°C in buffer A. CBS p.P49L was thoroughly flushed with nitrogen, after which glucose oxidase (4 units·ml^{-1}), catalase (13 μg·ml^{-1}), superoxide dismutase (12 units·ml^{-1}), and glucose (3 mM) were added to scavenge oxygen, hydrogen peroxide, and superoxide anion. The protein was then placed on ice, protected from light to prevent possible damaging photoreactions. When indicated, CBS p.P49L was incubated with AdoMet for ≥10 minutes, prior to reduction with 90 μM sodium dithionite. CO association kinetics were studied by mixing in the stopped-flow apparatus reduced CBS p.P49L, in the absence or presence of AdoMet, with CO solutions and the spectra recorded over time. CO dissociation kinetics were evaluated by mixing the Fe(II)-CO adduct of CBS p.P49L

with NO• stock solutions, prepared by equilibrating degassed ultra-pure water with NO• gas at 1 atm, further kept on ice protected from light.

2.5. Spectral Data Analysis. CO affinity titrations and CO binding and dissociation kinetic data were analyzed with the software MATLAB (Mathworks). Global fit analysis of spectral data was performed by singular value decomposition analysis combined with curve fitting [52].

2.6. Protein Crystallization. Initial crystallization screenings for $CBS\Delta_{409–551}$ p.P49L were performed in 96-well plates at 293 K using a Cartesian mini-Bee nanoliter-drop dispensing robot (Genomic Solutions). These screenings allowed for the identification of one hit for $CBS\Delta_{409–551}$ p.P49L from the JCSGplus™ screen (Molecular Dimensions): G10 (0.15 M KBr, 30% w/v PEG 2000 MME). Crystals were optimized at the microliter scale using sitting-drop vapor diffusion with a drop composition of 0.5 μl protein solution (27.4 mg·ml^{-1} in buffer A with 20 μM PLP) and 0.5 μl reservoir solution (0.15 M NaBr, 35% PEG 2000 MME) equilibrated against 500 μl precipitant solution in the well. Dark orange colored small needles as well as big rod-shaped crystals appeared after 12 h at 20°C.

2.7. Data Processing and Refinement. Cryoprotection conditions for diffraction experiments were achieved by transferring the crystals to a 5 μl drop of 35% (w/v) PEG 2000 MME, 5% (v/v) glycerol, and 0.15 M NaBr. The crystals were flash-cooled by quick plunging into liquid nitrogen. A single crystal was used for data collection under a nitrogen-gas stream (Oxford Cryosystems 700) on beamline ID30A-3 at the ESRF synchrotron (Grenoble, France) using a PILATUS 6 M detector (Dectris) at a wavelength of 0.9677 Å. After indexing and calculation of a data collection strategy using *EDNA* [53], a wedge of 360° of data was collected using a fine-slicing strategy (0.1° rotation per image). The data set was indexed and integrated with *XDS* [54], the space group assignment was performed with *POINTLESS* [55], and scaling was performed with *AIMLESS* [56], all within the *autoPROC* data-processing pipeline [57]. At this stage an R_{free}-flag set was created corresponding to 5% of the measured reflections of the data set. Crystals belonged to the monoclinic space group *P*1 with unit cell parameters a = 86.2 Å, b = 86.8 Å, c = 97.8 Å, α = 102.6°, β = 103.1°, and γ = 111.2°. Data were truncated at 2.80 Å. Data reduction and refinement statistics are depicted in Table 1. The structure of the $CBS\Delta_{409–551}$ p.P49L variant was solved by molecular replacement using PDB entry 1JBQ devoid of any solvent and cofactors as search model using *phaser* [58] within the *PHENIX* software suite of programs [59]. Based on the Matthews coefficient, the search was performed for six molecules. Automated model building was performed using the *AutoBuild* wizard [60], also within *PHENIX*. Initial refinement rounds were carried out with *BUSTER-TNT* [61] using the macro that accounts for missing parts of the model ("-L"). At this point, electron density features attributed to the heme moieties were easily identified. Iterative cycles of manual model building and refinement were carried out with *COOT* [62] and *BUSTER-TNT* until convergence. Validation was performed with *RAMPAGE* [63] and *MolProbity* [64] as implemented in *PHENIX*.

Table 1: Data reduction and refinement statistics of CBS p.P49L structure.

	p.P49L CBS variant
PDB entry	5MMS
Data collection	
Synchrotron	ESRF (Grenoble, France)
Beamline	ID30A-3
Wavelength (Å)	0.968
Space group	*P*1
Unit cell	
a, b, c (Å)	86.2, 86.8, 97.8
α, β, γ (°)	102.7, 103.1, 111.2
Resolution range[a] (Å)	76.35–2.80 (2.90–2.80)
Total number of reflections	121227 (1141)
Number of unique reflections	58862 (571)
Completeness (%)	98.5 (95.6)
Multiplicity	2.1 (2.0)
$\langle I/\sigma(I)\rangle$	4.8 (1.5)
R_{meas}[b] (%)	17.4 (68.7)
R_{pim}[c] (%)	11.2 (45.1)
$CC_{1/2}$[d] (%)	97.6 (62.1)
Wilson B-factor (Å^2)	41.8
Refinement	
R_{cryst}[e] (%)	18.2 (27.2)
R_{free}[f] (%)	22.1 (33.1)
Number of non-H atoms	16452
Protein	15916
Ligands	351
Waters	185
r.m.s.d bonds (Å)	0.010
r.m.s.d. angles (°)	1.12
Protein residues	2077
Ramachandran plot	
Most favoured (%)	96.6
Allowed (%)	3.2
Outliers (%)	0.3
Rotamer outliers (%)	0.3
Clashscore	0.46
MolProbity score[g]	0.88
B-factors (Å^2)	45.4
Protein	41.3
Ligands	29.7

[a]Information in parenthesis refers to the last resolution shell. [b]$R_{meas} = \Sigma_{hkl}(n/n-1)^{1/2}\Sigma_i|I_{hkl,j} - \langle I_{hkl,j}\rangle|/\Sigma_{hkl}\Sigma_j I_{hkI,j}$, where n_h denotes multiplicity and j the j-th reflection hkl. [c]$R_{pim} = \Sigma_{hkl}(1/n-1)^{1/2}\Sigma_i|I_{hkl,j} - \langle Ihkl, j\rangle|/\Sigma_{hkl}\Sigma_i I_{hkI,j}$, where n_h denotes multiplicity and j the j-th reflection hkl. [d]$CC_{1/2}$ is as described previously [69]. [e]$R_{cryst} = \sum_{hkl}\|F_{obs(hkl)}| - |F_{calc(hkl)}\|/\sum_{hkl}|F_{obs(hkl)}|$, where $F_{obs(hkl)}$ and $F_{calc(hkl)}$ are the observed and calculated structure factors for reflection (hkl), respectively. [f]R_{free} was calculated as R_{cryst} but using only 5% of reflections randomly selected and omitted from refinement. [g]*MolProbity* score provides a single number that represents the central *MolProbity* protein quality statistics; it is a log-weighted combination of Clashscore, Ramachandran not favored, and bad side-chain rotamers, giving one number that reflects the crystallographic resolution at which those values would be expected.

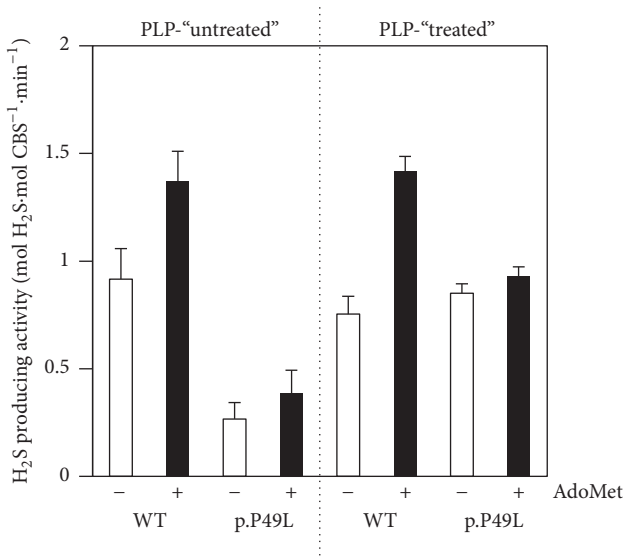

Figure 1: Hydrogen sulfide production by WT and p.P49L CBS. H_2S producing activity of CBS purified in the absence (PLP-"untreated") or presence (PLP-"treated") of PLP (20 μM). T = 37°C. Buffer: 50 mM KPi, 300 mM KCl, 10% glycerol, 100 μM EDTA, pH 7.0. Reaction mixture contained 50 μM PLP, 0.4–2.0 mM homocysteine, 260 U/ml catalase, and 10 mM cysteine. Assays were carried out in the absence (−) or presence (+) of 500 μM AdoMet.

3. Results

3.1. Hydrogen Sulfide Synthesis by CBS p.P49L. H_2S synthesis by the CBS p.P49L variant using homocysteine and cysteine as substrates was analyzed in comparison with the WT enzyme by amperometric and colorimetric (lead acetate) methods. Two sets of enzyme preparations, purified either in the absence or in the presence of the PLP cofactor, were evaluated in assays run in the presence of PLP. As shown in Figure 1, the p.P49L CBS variant isolated in the absence of PLP (PLP-"untreated") displays a basal activity more than 3-fold lower than that of the WT enzyme. Despite the markedly impaired enzymatic activity of "untreated" CBS p.P49L, activity stimulation by AdoMet is similar between WT and p.P49L (respectively, 1.5- and 1.4-fold). Conversely, the p.P49L CBS variant purified in the presence of PLP (PLP-"treated") displays a basal activity similar to the WT enzyme, despite presenting impaired activity stimulation by AdoMet (1.9-fold for WT to be compared with 1.1-fold for p.P49L). The AdoMet activation factor (≤2-fold) observed for the WT enzyme was slightly lower than usually reported (2–5-fold). This could be related to a fraction of the enzyme lacking the C-terminal domain, which was also observed for the CBS p.P49L variant (see Supplementary Figure S1 in the Supplementary Material available online at https://doi.org/10.1155/2017/8940321).

3.2. Structure of CBS p.P49L Variant. In an attempt to understand the structural impact of the proline-to-leucine substitution at position 49 of human CBS, we have determined the X-ray structure of a truncated form of the p.P49L variant (PDB entry 5MMS), lacking the C-terminal 143 residues (henceforth designated as $CBS\Delta_{409–551}$ p.P49L), similarly to the reported structure of truncated WT CBS (PDB entry 1JBQ) [65]. Crystals belong to the triclinic space group $P1$ with cell dimensions a = 86.2, b = 86.8, and c = 97.8 Å, α = 102.6°, β = 103.1°, and γ = 111.2°. *XDS* as implemented in *autoPROC* clearly identifies two different lattices in the diffraction pattern rotated by 121.4° relative to each other. This diminishes the quality of the overall statistics since in some directions an almost perfect superposition of reflections makes the integration difficult (data collection and refinement statistics are depicted in Table 1).

There are six molecules in the asymmetric unit corresponding to a Matthews coefficient [66] of 2.31 $Å^3 \cdot Da^{-1}$ and a solvent content of approximately 47%. The structure was refined to 2.80 Å resolution with R_{cryst} of 18.2% and R_{free} of 22.1%. The final model comprises the residues from R45 to E400 (in chain D), 6 hemes, 6 PLP molecules, 3 sodium ions, and 185 water molecules. The hemes are axially bridged by C52 and H65 and the PLP moieties covalently linked to the polypeptide chain through K119. The maps are generally of good quality except for two disordered loops (T193 to S199 and Q295 to T300), for which only in chain D there were complete electron densities. This contrasts with the published structure of the truncated human CBS WT (PDB entry 1JBQ), where the T193-S199 loop could not be modeled. The variant dimeric structure, shown in Figure 2(a), displays an essentially identical overall fold with respect to the WT enzyme (r.m.s.d. of 0.4 Å for 344 aligned C_α carbon atoms between chain D of $CBS\Delta_{409–551}$ p.P49L and chain A of 1JBQ) and highly conserved features in the PLP active site and the N-terminally located heme moiety (Figure 2(b)).

3.3. Spectral Properties of Ferrous p.P49L CBS. In the absence of clear structural clues for pathogenicity of the p.P49L mutation, we sought to evaluate by UV-visible absorption spectroscopy the impact of this residue substitution on the protein redox spectra, largely dominated by the heme absorption. In WT CBS, heme reduction leads to notable changes in the protein absorption spectrum, with a shift of the Soret band from 428 nm to 449 nm (Figure 3(a)). Upon incubation of the enzyme with AdoMet prior to reduction, the spectrum of the reduced enzyme is affected by a decrease in the 449 nm band intensity and the appearance of a feature centered at ~424 nm (Figure 3(a), red solid line). Regardless of AdoMet, in the oxidized state, p.P49L CBS exhibits no differences in the absorption spectrum as compared to the WT protein (Figure 3, dashed lines). In contrast, major differences can be noted by comparing the spectra of the two proteins in the reduced state, with the mutant displaying markedly more pronounced appearance of the 424 nm spectral feature and decrease of the 449 nm band (Figure 3(b), blue solid line), both further elicited in the AdoMet-bound protein (Figure 3(b), red solid line).

3.4. Enhanced Affinity of p.P49L CBS for CO. Prompted by the observed spectral differences between reduced p.P49L and WT CBS, we analyzed the affinity of the mutated protein

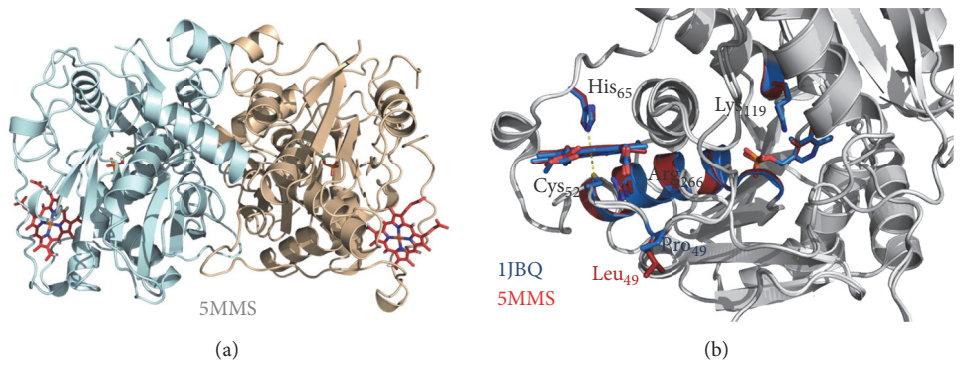

Figure 2: Structure of CBS p.P49L. X-ray crystallographic structure of CBSΔ$_{409–551}$ p.P49L solved at 2.80 Å resolution (PDB entry 5MMS). (a) Cartoon representation of the protein dimer, each monomer being represented in a different color. Pyridoxal 5′-phosphate (PLP) and heme moieties shown in stick representation. (b) Structure superposition of CBSΔ$_{409–551}$ p.P49L (PDB entry 5MMS) and truncated WT CBS (PDB entry 1JBQ), both colored in grey except for most relevant regions and residues, where CBSΔ$_{409–551}$ p.P49L is colored in red and CBSΔ$_{409–551}$ WT in blue; zoom in on the PLP and heme moieties, highlighting the proline-to-leucine substitution, as well as the R266 residue and α-helix 8 proposed to mediate communication between the heme and the PLP active site. Figure generated with PyMOL 1.8.2 (The PyMOL Molecular Graphics System, Version 1.8 Schrödinger, LLC).

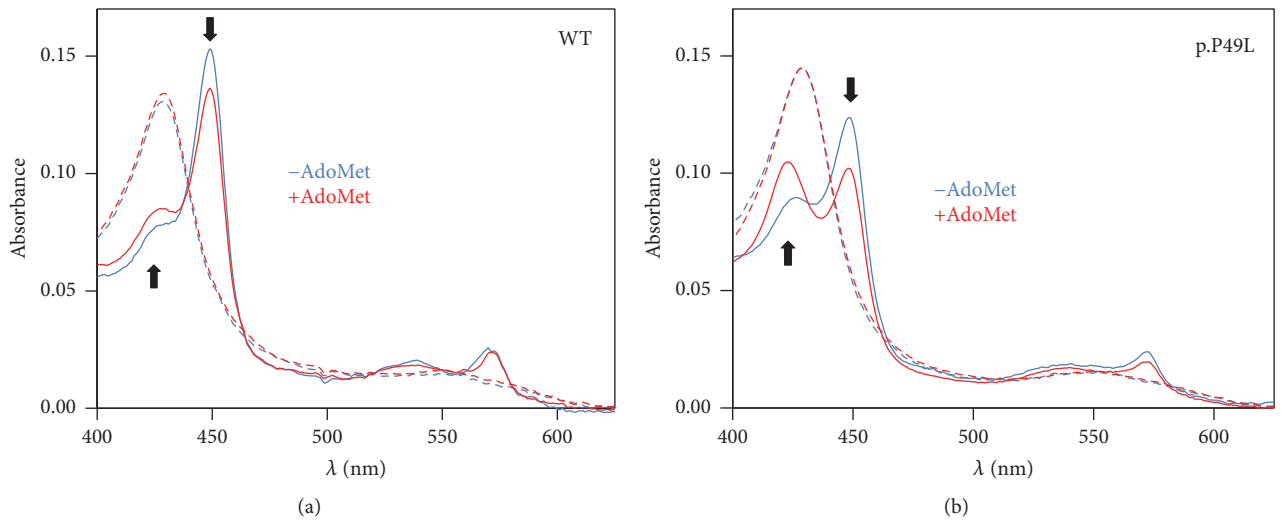

Figure 3: Absorption spectra of WT and p.P49L CBS. Absorption spectra of WT (a) and p.P49L (b) CBS (1.4–1.6 μM in heme) recorded at 20°C, in degassed buffer A (50 mM KPi, 300 mM KCl, 10% glycerol, 100 μM EDTA, pH 7.0), containing glucose oxidase (4 units·ml^{-1}), catalase (13 μg·ml^{-1}), superoxide dismutase (12 units·ml^{-1}), and glucose (3 mM). Spectra were collected in the oxidized state (dashed lines) and upon protein reduction (solid lines) by addition of 90 μM sodium dithionite, in the absence (blue lines) and presence (red lines) of AdoMet (500 μM). Arrows highlight direction of the spectral changes caused by AdoMet in the reduced proteins.

for the physiologically relevant CO ligand by performing anaerobic CO titrations. Similarly to the WT protein, conversion of ferrous CBS p.P49L to the CO adduct resulted in the appearance of a band centered at 422 nm (Figures 4(a) and 4(b)). Global fit analysis of the spectral data set acquired along the titration revealed a much higher CO affinity (>50-fold) of p.P49L CBS (Figure 4(c), full circles) as compared to the WT enzyme (Figure 4(c), dotted line). Notably, as previously reported by Vicente et al. [20] for WT CBS (Figure 4(c), dashed line) and consistent with the effect of AdoMet on the spectrum of reduced p.P49L CBS (Figure 3(b)), preincubation of the protein variant with AdoMet further enhances the CO affinity (Figure 4(c), hollow squares). CO titrations allowed us to estimate the following K_d values: $K_{dCO,1}$ = 0.06 ± 0.03 μM and $K_{dCO,2}$ = 21 ± 5 μM (with 60% and 40% relative amplitude, respectively) for AdoMet-free p.P49L CBS and $K_{dCO,1}$ ≤ 0.03 μM and $K_{dCO,2}$ = 1.5 ± 0.6 μM (with 70% and 30% relative amplitude, respectively) for the AdoMet-bound enzyme. It should be noted that the CO affinity of the AdoMet-bound p.P49L variant is so high that

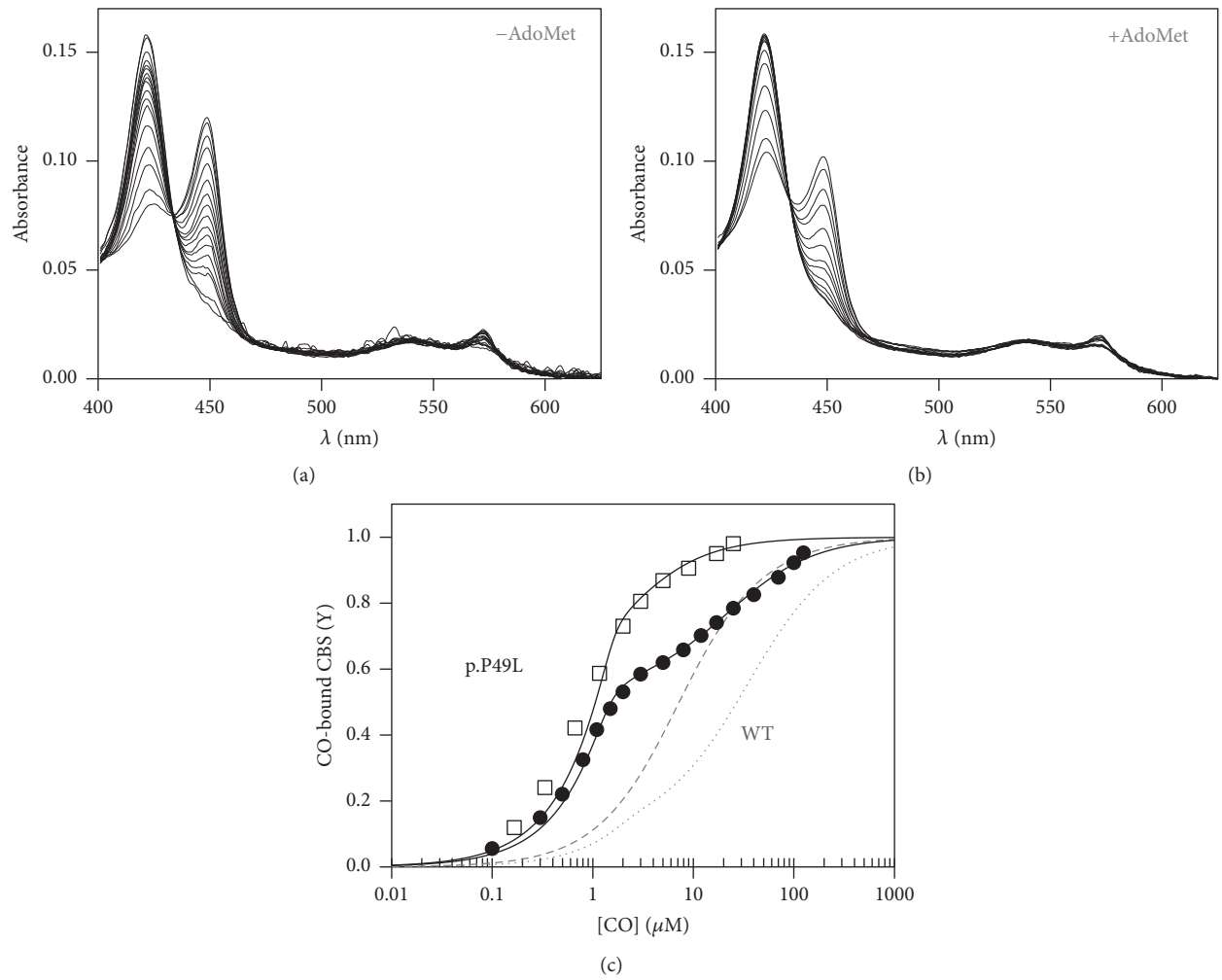

Figure 4: Enhanced CO affinity of p.P49L CBS. Absorption spectra collected upon anaerobic titration of reduced CBS p.P49L (1.4–1.6 μM in heme) with CO, in the absence (a) or presence (b) of AdoMet. T = 20°C. (c) Titration profiles obtained by global fit of the spectral data acquired in the absence (full circles) or presence (hollow squares) of 500 μM AdoMet. Data were best fitted according to (1), yielding $K_{dCO,1}$ = 0.05 μM (60%) and $K_{dCO,2}$ = 22.0 μM (40%) for AdoMet-free CBS p.P49L and $K_{dCO,1} \leq 0.03$ μM (70%) and $K_{dCO,2}$ = 2.1 μM (30%) for the AdoMet-bound enzyme. Gray lines represent titration curves for WT CBS in the absence (dotted line) and presence (dashed line) of 500 μM AdoMet.

the $K_{dCO,1}$ value actually represents an upper limit. A possible direct interference of CO with AdoMet was ruled out by performing a control experiment where an AdoMet solution was equilibrated with CO gas (or N_2 as control), yielding no spectral changes (*not shown*).

3.5. Kinetics of CO Binding and Dissociation from p.P49L CBS. The markedly higher CO affinity of p.P49L CBS as compared to the WT enzyme led us to investigate by time-resolved absorption spectroscopy the kinetics of CO binding to and dissociation from ferrous p.P49L CBS (Figure 5). Upon stopped-flow mixing reduced CBS p.P49L with 1 mM CO, the observed spectral changes were identical in shape to those shown for the CO titrations in Figure 4, that is, the predominant 449 nm Soret band and the 424 nm spectral feature both shifted to 422 nm, with similar optical transitions for the AdoMet-free and AdoMet-bound CBS p.P49L (inset to Figure 5(a)). Global fit analysis of the kinetic data revealed that both AdoMet-free and AdoMet-bound p.P49L react with CO according to multiphasic time courses (Figure 5(a)), as previously shown for WT CBS [19, 20, 51, 67]. Interestingly, despite the markedly increased CO affinity of p.P49L with respect to the WT protein, under identical experimental conditions CO binding to the either of the two proteins in the absence of AdoMet proceeds at comparable rates ($t_{1/2}$ = 26.2 ± 9.6 s for CBS p.P49L, Figure 5(a), to be compared with $t_{1/2}$ = 34.5 ± 10.5 s of WT, not shown). In the presence of AdoMet, where the spectral changes (Figure 3) and the enhanced CO affinity (Figure 4) of CBS p.P49L point to significant effects on the heme properties, a marked increase in CO association rates is observed, with $t_{1/2}$ decreasing to 5.4 ± 3.1 s (Figure 5(a)), to be compared with $t_{1/2}$ = 17.0 ± 2.7 s for WT CBS (not shown).

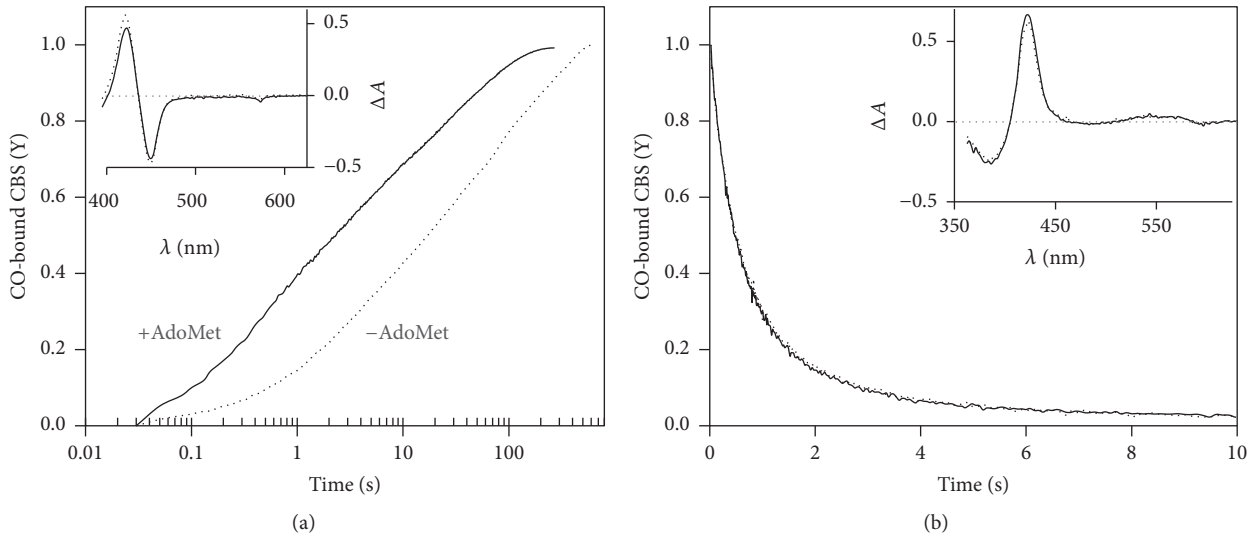

Figure 5: Kinetics of CO binding to ferrous CBS p.P49L. (a) Reaction time courses measured in the absence (dotted line) or presence of AdoMet (500 μM before mixing; solid line). Spectral data collected after stopped-flow mixing 1 mM CO with reduced CBS p.P49L (1.5 μM in heme) at 25°C, in 50 mM potassium phosphate, 300 mM KCl, 10% glycerol, pH 7.0, containing 2 mM glucose, 4 units·ml^{-1} glucose oxidase, 13 μg·ml^{-1} catalase, and 6 units·ml^{-1} superoxide dismutase. Fitted rate constants (% reaction amplitude): $k_1 = 0.48\,s^{-1}$ (25%), $k_2 = 0.05\,s^{-1}$ (30%), and $k_3 = 0.006\,s^{-1}$ (45%) for AdoMet-free CBS p.P49L ($t_{1/2} = 19.5$ s) and $k_1 = 2.55\,s^{-1}$ (35%), $k_2 = 0.26\,s^{-1}$ (30%), and $k_3 = 0.022\,s^{-1}$ (35%) for the AdoMet-bound enzyme ($t_{1/2} = 2.3$ s). *Inset*, optical transitions obtained by global fit analysis of the spectral data acquired in the absence (dotted line) or presence of AdoMet (solid line). (b) Time courses of CO displacement from ferrous CBS p.P49L by 900 μM NO•, acquired in the absence (dotted line) or presence of AdoMet (solid line; 500 μM before mixing). Traces were best fitted with the following rate constants (% reaction amplitude): $k_1 = 1.93\,s^{-1}$ (75%) and $k_2 = 0.035\,s^{-1}$ (25%) for AdoMet-free CBS p.P49L; $k_1 = 1.96\,s^{-1}$ (75%) and $k_2 = 0.038\,s^{-1}$ (25%) for the AdoMet-bound enzyme. *Inset*, optical transitions obtained by global fit analysis of the spectral data acquired in the absence (dotted line) or presence of AdoMet (solid line).

The kinetics of CO dissociation from CBS p.P49L was evaluated by anaerobically mixing in the stopped-flow apparatus the CO-bound ferrous protein with authentic NO• (900 μM after mixing) and monitoring the conversion of the 422 nm hexacoordinate CO-bound adduct spectrum into that of the pentacoordinate NO•-bound adduct with a broad absorption band centered at 395 nm (inset to Figure 5(b)). Global fit analysis of the kinetic data revealed that under identical experimental conditions CO is displaced by NO• in CBS p.P49L at comparable rates ($k_1 = 2.0 \pm 0.1\,s^{-1}$ and $k_2 = 0.37 \pm 0.05\,s^{-1}$, with 75% and 25% relative amplitude, respectively) to the WT enzyme ($k_1 = 2.0 \pm 0.1\,s^{-1}$ and $k_2 = 0.33 \pm 0.03\,s^{-1}$, with 75% and 25% relative amplitude, respectively; *data not shown*), showing no effect of AdoMet (Figure 5(b)).

4. Discussion

Classical homocystinuria is an inborn error of metabolism associated with deficiency in cystathionine β-synthase (CBS), a key enzyme in the transsulfuration pathway of methionine metabolism. By catalyzing the conversion of homocysteine and serine into cystathionine, the enzyme prevents an excessive increase in homocysteine levels, a pathological condition associated with oxidative stress and clinical complications in the vascular, neurological, and skeletal systems. CBS also has a relevant role in human physiology by being a major source of H_2S, a key endogenous signaling molecule whose dysregulation is at the basis of several human pathologies, from cardiovascular and neurodegenerative diseases to cancer. Thus far, despite decades of research on classical homocystinuria, a full understanding of the molecular events at the basis of the pathogenicity of several CBS mutations remains elusive, although protein misfolding, dysfunctional regulation by AdoMet, and impaired enzymatic activity have been put forward for some mutations [15, 28, 33–39].

This prompted us to investigate in the present study a reportedly mild pathogenic mutation associated with classical homocystinuria, a proline-to-leucine substitution at residue 49 in human CBS [44–46]. The recombinant CBS p.P49L variant was expressed in *E. coli*, purified, and characterized both structurally and functionally. In line with previous reports focused on the canonical cystathionine synthase activity, this variant displayed a H_2S synthesizing activity remarkably sensitive to PLP supplementation along the purification procedure [36, 37, 39, 40]. The functional rescue of p.P49L H_2S synthesis by PLP is indicative of a decreased affinity of this variant for the cofactor, a frequently observed consequence of missense mutations potentially associated with protein misfolding. The functional recovery of p.P49L observed upon PLP supplementation during protein purification was however not fully matched in terms of activity stimulation by AdoMet, as the H_2S-synthesizing activity of

p.P49L showed poor responsiveness to AdoMet (Figure 1) as compared to its cystathionine synthase activity [36, 37, 39, 40]. This is not surprising since for other CBS variants it has been shown that the extent of the stimulatory effect of AdoMet can differ between the canonical cystathionine synthase and the H_2S-synthesizing activities [28].

Further attempting to understand the molecular basis of pathogenicity of this mutation, the crystallographic structure of a truncated form of the CBS p.P49L variant ($CBS\Delta_{409-551}$ p.P49L) was obtained at 2.8 Å resolution and compared with that of the truncated WT enzyme (PDB 1JBQ) [65]. Within the obtained resolutions, the structures display highly conserved features (Figure 2), particularly inspecting the PLP binding pocket with the cofactor covalently bound to K119, the heme ligands C52 and H65, α-helix 8 (responsible for the heme-PLP communication), the R266 residue forming a salt-bridge with C52, and the flexible loop where the mutated P49 residue is located. Therefore, at first glance, the structural data do not seem to provide a clue for the pathogenicity of the mutation.

The effect of the mutation on the spectroscopic and ligand-binding properties of the heme moiety was also investigated. The first hint for a perturbation in the CBS p.P49L heme microenvironment arose from inspection of the dithionite-reduced spectrum of this protein variant (Figure 3). Indeed, in the spectrum of reduced CBS p.P49L, the dominating 449 nm band assigned to the hexacoordinate ferrous heme with C52 and H65 as axial ligands shows a significant intensity decrease as compared to the WT enzyme and the appearance of a band at 424 nm (Figure 3(b)). The latter spectral feature has been assigned to a ligand exchange process in CBS leading to formation of an enzymatic species (called C-424), in which the cysteine thiolate ligand is replaced by a neutral species [14, 15], negatively impacting the enzymatic activity. In WT CBS, this ligand exchange process occurs very slowly (>48 h at 37°C, [14]) in the presence of excess reductant. Similarly to p.P49L, other CBS variants have been previously reported to display an increased propensity to form the C-424 species, particularly CBS variants with mutated residues in α-helix 8 [28]. Furthermore, as observed for the WT CBS (Figure 3(a)), incubating the p.P49L variant with AdoMet prior to reduction further enhances the conversion of the "normal" 449 nm into the ligand-exchanged C-424 species in the reduced protein (Figure 3(b)). Interestingly, among the several CBS variants studied by Yadav and coworkers [28], p.T257V shows the most similar spectra to CBS p.P49L and, like this variant, it displays WT-like (and PLP-dependent) H_2S-generating activity and impaired activation by AdoMet [28]. Altogether, the spectral data herein reported point to changes at the heme moiety of CBS p.P49L that were further explored by evaluating the CO binding properties of the protein variant. CBS has been shown to be inhibited in vitro by exogenous ligands like CO and NO• [16–20], with different lines of evidence pointing to a physiological relevance of this regulatory mechanism in vivo [21–27] (see below).

By performing CO titrations under anaerobic conditions, we observed spectral changes (Figure 4) consistent with the formation of the hexacoordinate ferrous-CO adduct, with the C52 thiolate or the yet unknown "X" ligand of the C-424 species being replaced by CO, and the heme retaining the H65 endogenous ligand. Notably, the CO affinity, herein measured for the first time in a CBS variant, is markedly increased (≥50-fold) in CBS p.P49L with respect to the WT enzyme (Figure 4(c), [16, 20, 51]). As previously described for WT CBS, the CO titrations followed a biphasic profile, which has been previously attributed to heterogeneity in the heme microenvironment [16] or anticooperativity between hemes within a CBS dimer [51]. The remarkably higher CO affinity of CBS p.P49L is essentially due to the extremely low $K_{dCO,1}$ ($0.06 \pm 0.03\,\mu$M), close to the detection limit of the experimental setup. Notably, and as previously observed for the WT enzyme [20], incubation of CBS p.P49L with AdoMet induced a further increase in CO affinity (Figure 4(c)) and, therefore, only an upper limit value for $K_{dCO,1}$ ($\leq 0.03\,\mu$M) could be estimated. In the WT enzyme, the increased CO affinity observed in the presence of AdoMet is fully matched with an enhanced propensity for CO inhibition of the protein H_2S producing activity [20]. Based on the remarkable increase in CO affinity herein documented for CBS p.P49L, this protein variant is expected to be more prone to inhibition at low physiological CO levels. This may represent a more general mechanism of pathogenesis in classical homocystinuria, if other pathogenic CBS mutations will be demonstrated to lead to enhanced CO affinity, as shown for CBS p.P49L in the present study.

Although direct evidence for ferrous CBS formation in vivo is still missing in the literature, several reports have attested the physiological role of CBS inhibition by CO (reviewed in [26, 27]), which requires the heme to be in the ferrous state. Regarding regulation of cerebral microcirculation by hypoxia, decreased oxygen levels impair CO production by heme oxygenase HO-2 and the release of CBS inhibition by CO promotes H_2S synthesis that in turn mediates vasodilation of precapillary arterioles [23]. Stress-inducible levels of CO in mice liver cause metabolomic changes consistent with CBS inhibition, decrease in hepatic H_2S, and concomitant stimulation of HCO_3^--dependent bile output in wild type, but not in heterozygous CBS knockout mice [22]. Another proposed mechanism concerns the CO-mediated regulation of glucose utilization, where CBS inhibition by CO drives the demethylation of phosphofructokinase/fructose bisphosphatase type-3 (PFKFB3), diverting glucose from the glycolytic towards the NADPH-generating pentose phosphate pathway, with implications in chemoresistance and oxidative stress resistance in cancer cells [24]. Moreover, Kabil et al. [25] have recently shown that, under endoplasmic reticulum stress conditions, CBS inhibition by CO, combined with CSE induction, flips the CSE substrate preference from cystathionine to cysteine, transiently stimulating H_2S production. These multiple lines of evidence provide compelling though still indirect evidence for the formation of ferrous CBS in vivo. In line with these observations, an NADPH-dependent diflavin enzyme, methionine synthase reductase, has been shown to reduce the CBS heme in vitro in the presence of CO or nitrite, generating, respectively, the ferrous-CO or ferrous-NO CBS adducts [18, 67, 68]. In light of this evidence, the high affinity of CBS

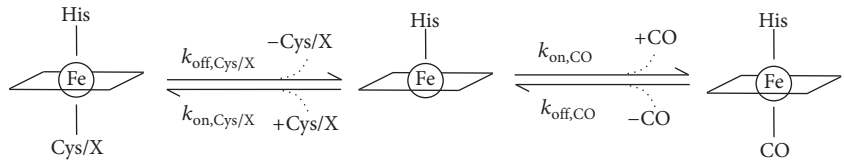

Scheme 1

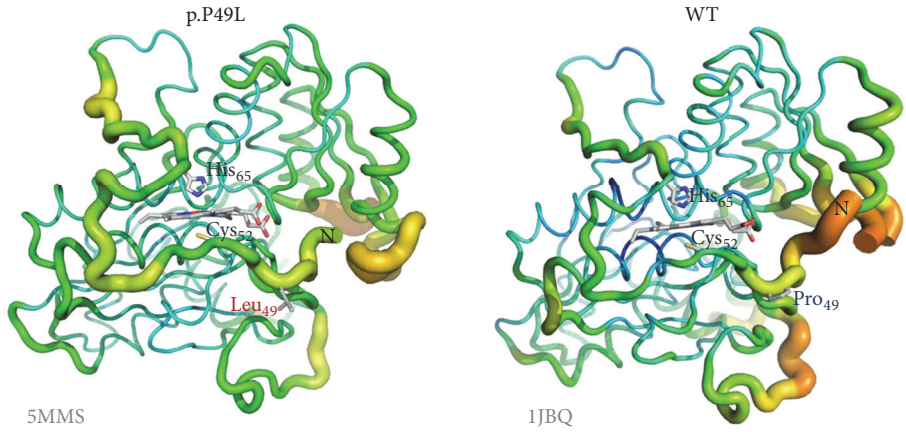

Figure 6: Increased flexibility of the heme binding loop in p.P49L CBS. Representation of *B* factor variation along the structure of CBS p.P49L (PDB entry 5MMS) and WT (PDB entry 1JBQ) monomer, displaying in first plane the regions encompassing the proline-to-leucine mutation (sticks) and the heme ligands C52 and H65. Flexibility can be visualized both by the thickness of the structural element and the respective color: highest flexibility represented in red (hot) thick elements; lowest flexibility in thin blue (cold) elements (color scale: red > orange > yellow > green > blue). Figure generated with PyMOL 1.8.2 (The PyMOL Molecular Graphics System, Version 1.8 Schrödinger, LLC).

p.P49L for CO is fully compatible with the formation of the ferrous-CO adduct at physiological CO concentrations.

To gain mechanistic insight into this high CO affinity, we studied by stopped-flow absorption spectroscopy the kinetics of CO association/dissociation to/from the reduced heme of this protein variant (Figure 5). Similarly to the WT [19, 20, 51], CO binding to reduced CBS p.P49L followed a multiphasic time-course (Figure 5(a)). Taking into account the markedly increased CO affinity of this protein variant, surprisingly the reaction proceeded only slightly faster ($t_{1/2}$ = 26.2 ± 9.6 s) than for the WT enzyme ($t_{1/2}$ = 34.5 ± 10.5 s) under identical experimental conditions. Despite this minor difference, in the presence of AdoMet the fold increase in the CO association rate was overall higher in the p.P49L variant (~4.5-fold) than in the WT enzyme (~2-fold) under identical experimental conditions. Furthermore, by analyzing the kinetics of CO replacement by NO• in this protein variant, we observed essentially identical kinetic traces for the AdoMet-free and AdoMet-bound CBS p.P49L (Figure 5(b)) and for the WT enzyme under the same experimental conditions (*not shown*).

The kinetics of CO association and dissociation therefore do not provide a clear cut explanation for the markedly higher CO affinity of CBS p.P49L, which requires further inspection. In Scheme 1 are represented the reaction steps for conversion of the hexacoordinate ferrous CBS, with the heme Fe ligated to H65 and either C52 or the unknown "X" ligand in the C-424 species, into the ferrous-CO adduct. It has been previously postulated for the WT enzyme that CO association to the ferrous CBS heme is rate-limited by dissociation of C52 [19, 20, 51]. Since we observed similar CO association kinetics for WT and p.P49L, where a fraction of the mutant enzyme is likely to be in the ligand-exchanged C-424 state, the CO association appears to be limited by the off-rate of the endogenous ligand regardless of its nature, C52 or "X" ($k_{off,Cys/X\,(p.P49L)} \approx k_{off,Cys/X\,(WT)}$ in Scheme 1). Taking into account the fact that the kinetics of CO dissociation were almost identical for WT and p.P49L CBS, regardless of AdoMet being present ($k_{off,CO\,(p.P49L)} \approx k_{off,CO\,(WT)}$ in Scheme 1), the dramatic increase in CO affinity of the p.P49L variant compared to the WT should be related to a slower rebinding of the endogenous ligand, C52 or "X" ($k_{on,Cys/X\,(p.P49L)} \ll k_{on,Cys/X\,(WT)}$ in Scheme 1), and/or a faster combination of CO with the transiently generated pentacoordinate species ($k_{on,CO\,(p.P49L)} \gg k_{on,CO\,(WT)}$ in Scheme 1).

Regardless of these mechanistic details, the perturbed spectrum of the reduced protein and its remarkably higher affinity for CO point to possibly subtle structural changes in the CBS p.P49L variant affecting heme reactivity. To this end, we further compared the structures of the variant and WT enzymes in terms of local flexibility evaluated based on the B factor (Figure 6). This analysis interestingly reveals that the differences in flexibility are mostly located in specific regions of the protein. The α-helix 8, where some mutations have been shown to affect the heme spectral properties and the H_2S-generating activity similarly to p.P49L, displays comparable rigidity between CBS p.P49L and the WT enzyme. We thus looked in greater detail at the heme binding region (Figure 6)

and found in CBS p.P49L an increased flexibility of the loop surrounding the C52 ligand, which expands to the regions between the C52 and H65 ligands and even after the latter residue. The p.P49L structure therefore displays a higher flexibility in the region harboring both heme ligands, which provides a possible structural basis for the proposed slower rebinding of the endogenous C52/X ligands upon CO dissociation, thereby accounting for the increased affinity of CBS p.P49L for CO.

5. Conclusions

Cystathionine β-synthase (CBS) is a key enzyme in the transsulfuration pathway that prevents oxidative stress conditions, both controlling homocysteine levels and promoting the expression of antioxidant enzymes through the synthesis of H_2S. Being implicated in metabolic, oncologic, and neurodegenerative diseases, CBS is currently recognized as a promising drug target. Mutations in the *CBS* gene can lead to classical homocystinuria, a human disease associated with oxidative stress that affects the vascular, neurological, and skeletal systems. Protein misfolding, enhanced propensity to aggregation, decreased cofactor affinity, and dysfunctional regulation by the allosteric activator AdoMet, together with impaired enzymatic activity, have been proposed to account for the pathogenicity of several CBS mutations. As a novel finding, herein we reported that a clinically relevant variant of CBS (p.P49L) has markedly increased affinity for CO, a known inhibitor of CBS. On this basis, this variant is expected to be much more prone than WT CBS to be inactivated by CO at the physiological levels occurring in vivo, thereby contributing to pathogenicity. The enhanced affinity for inhibitory gaseous ligands documented here may represent a new pathogenic mechanism at the basis of CBS-related diseases, like classical homocystinuria.

Abbreviations

AdoMet:	S-Adenosyl-L-methionine
CBS:	Cystathionine β-synthase
$CBS\Delta_{409-551}$:	Truncated cystathionine β-synthase lacking the C-terminal 143 residues
CBS p.P49L:	Cystathionine β-synthase variant harboring a proline-to-leucine substitution at residue 49
CO:	Carbon monoxide
CSE:	Cystathionine γ-lyase
EDTA:	Ethylenediaminetetraacetic acid
H_2S:	Hydrogen sulfide
KPi:	Potassium phosphate
MME:	Monomethyl ether
MST:	Mercaptopyruvate sulfurtransferase
NO•:	Nitric oxide
PEG:	Polyethylene glycol
PLP:	Pyridoxal 5′-phosphate
r.m.s.d.:	Root mean square deviation
SDS-PAGE:	Sodium dodecyl sulfate polyacrylamide gel electrophoresis
WT:	Wild type.

Competing Interests

The authors declare that there is no conflict of interests regarding the publication of this paper.

Acknowledgments

This work was partially supported by Fundação para a Ciência e Tecnologia (FCT, PTDC/SAU-MIC/111447/2009 project grant to João B. Vicente, SFRH/BPD/79224/2011 fellowship to José A. Brito, and PD/BD/113990/2015 fellowship to Paulo E. Santo), by Ministero dell'Istruzione, dell'Università e della Ricerca of Italy (PNR-CNR Aging Program 2012–2014 and PRIN 20158EB2CM_003 to Alessandro Giuffrè) and by a bilateral grant awarded by Consiglio Nazionale delle Ricerche of Italy and FCT to Alessandro Giuffrè and João B. Vicente. João B. Vicente was the recipient of a short term fellowship from the Federation of European Biochemical Societies. iNOVA4Health Research Unit (LISBOA-01-0145-FEDER-007344), which is cofunded by Fundação para a Ciência e Tecnologia/Ministério da Ciência e do Ensino Superior, through national funds, and by FEDER under the PT2020 Partnership Agreement, is acknowledged. ESRF support for the ID30A-3 data collection is also acknowledged.

References

[1] O. Kabil and R. Banerjee, "Enzymology of H_2S biogenesis, decay and signaling," *Antioxidants & Redox Signaling*, vol. 20, no. 5, pp. 770–782, 2014.

[2] H. Kimura, "Signaling molecules: hydrogen sulfide and polysulfide," *Antioxidants & Redox Signaling*, vol. 22, no. 5, pp. 362–376, 2015.

[3] B. D. Paul and S. H. Snyder, "H_2S: a novel gasotransmitter that signals by sulfhydration," *Trends in Biochemical Sciences*, vol. 40, no. 11, pp. 687–700, 2015.

[4] K. R. Olson and K. D. Straub, "The role of hydrogen sulfide in evolution and the evolution of hydrogen sulfide in metabolism and signaling," *Physiology*, vol. 31, no. 1, pp. 60–72, 2016.

[5] T. Chiku, D. Padovani, W. Zhu, S. Singh, V. Vitvitsky, and R. Banerjee, "H_2S biogenesis by human cystathionine γ-lyase leads to the novel sulfur metabolites lanthionine and homolanthionine and is responsive to the grade of hyperhomocysteinemia," *The Journal of Biological Chemistry*, vol. 284, no. 17, pp. 11601–11612, 2009.

[6] S. Singh, D. Padovani, R. A. Leslie, T. Chiku, and R. Banerjee, "Relative contributions of cystathionine β-synthase and γ-cystathionase to H_2S biogenesis via alternative trans-sulfuration reactions," *The Journal of Biological Chemistry*, vol. 284, no. 33, pp. 22457–22466, 2009.

[7] J. L. Wallace and R. Wang, "Hydrogen sulfide-based therapeutics: exploiting a unique but ubiquitous gasotransmitter," *Nature Reviews Drug Discovery*, vol. 14, no. 5, pp. 329–345, 2015.

[8] M. R. Hellmich, C. Coletta, C. Chao, and C. Szabo, "The therapeutic potential of cystathionine β-synthetase/hydrogen sulfide inhibition in cancer," *Antioxidants & Redox Signaling*, vol. 22, no. 5, pp. 424–448, 2015.

[9] M. R. Hellmich and C. Szabo, "Hydrogen sulfide and cancer," in *Chemistry, Biochemistry and Pharmacology of Hydrogen Sulfide*, vol. 230 of *Handbook of Experimental Pharmacology*, pp. 233–241, Springer, Berlin, Germany, 2015.

[10] A. Davoli, V. Greco, A. Spalloni et al., "Evidence of hydrogen sulfide involvement in amyotrophic lateral sclerosis," *Annals of Neurology*, vol. 77, no. 4, pp. 697–709, 2015.

[11] J. Ereño-Orbea, T. Majtan, I. Oyenarte, J. P. Kraus, and L. A. Martínez-Cruza, "Structural basis of regulation and oligomerization of human cystathionine β-synthase, the central enzyme of transsulfuration," *Proceedings of the National Academy of Sciences of the United States of America*, vol. 110, no. 40, pp. E3790–E3799, 2013.

[12] J. Ereno-Orbea, T. Majtan, I. Oyenarte, J. P. Kraus, and L. A. Martinez-Cruz, "Structural insight into the molecular mechanism of allosteric activation of human cystathionine β-synthase by S-adenosylmethionine," *Proceedings of the National Academy of Sciences of the United States of America*, vol. 111, no. 37, pp. E3845–E3852, 2014.

[13] T. J. McCorvie, J. Kopec, S.-J. Hyung et al., "Inter-domain communication of human cystathionine β-synthase: structural basis of S-adenosyl-L-methionine activation," *The Journal of Biological Chemistry*, vol. 289, no. 52, pp. 36018–36030, 2014.

[14] M. M. Cherney, S. Pazicni, N. Frank, K. A. Marvin, J. P. Kraus, and J. N. Burstyn, "Ferrous human cystathionine β-synthase loses activity during enzyme assay due to a ligand switch process," *Biochemistry*, vol. 46, no. 45, pp. 13199–13210, 2007.

[15] S. Singh, P. Madzelan, J. Stasser et al., "Modulation of the heme electronic structure and cystathionine β-synthase activity by second coordination sphere ligands: the role of heme ligand switching in redox regulation," *Journal of Inorganic Biochemistry*, vol. 103, no. 5, pp. 689–697, 2009.

[16] S. Taoka, M. West, and R. Banerjee, "Characterization of the heme and pyridoxal phosphate cofactors of human cystathionine β-synthase reveals nonequivalent active sites," *Biochemistry*, vol. 38, no. 9, pp. 2738–2744, 1999.

[17] S. Taoka and R. Banerjee, "Characterization of NO binding to human cystathionine β-synthase: possible implications of the effects of CO and NO binding to the human enzyme," *Journal of Inorganic Biochemistry*, vol. 87, no. 4, pp. 245–251, 2001.

[18] C. Gherasim, P. K. Yadav, O. Kabil, W.-N. Niu, and R. Banerjee, "Nitrite reductase activity and inhibition of H_2S biogenesis by human cystathionine β-synthase," *PLoS ONE*, vol. 9, no. 1, Article ID e85544, 2014.

[19] J. B. Vicente, H. G. Colaço, M. I. Mendes, P. Sarti, P. Leandro, and A. Giuffrè, "NO^* binds human cystathionine beta-synthase quickly and tightly," *The Journal of Biological Chemistry*, vol. 289, pp. 8579–8587, 2014.

[20] J. B. Vicente, H. G. Colaço, P. Sarti, P. Leandro, and A. Giuffrè, "S-Adenosyl-L-methionine modulates CO and NO^* binding to the human H_2S-generating enzyme cystathionine beta-synthase," *The Journal of Biological Chemistry*, vol. 291, pp. 572–581, 2016.

[21] G. A. Prathapasinghe, Y. L. Siow, Z. Xu, and O. Karmin, "Inhibition of cystathionine-β-synthase activity during renal ischemia-reperfusion: role of pH and nitric oxide," *American Journal of Physiology—Renal Physiology*, vol. 295, no. 4, pp. F912–F922, 2008.

[22] T. Shintani, T. Iwabuchi, T. Soga et al., "Cystathionine β-synthase as a carbon monoxide-sensitive regulator of bile excretion," *Hepatology*, vol. 49, no. 1, pp. 141–150, 2009.

[23] T. Morikawa, M. Kajimura, T. Nakamura et al., "Hypoxic regulation of the cerebral microcirculation is mediated by a carbon monoxide-sensitive hydrogen sulfide pathway," *Proceedings of the National Academy of Sciences of the United States of America*, vol. 109, no. 4, pp. 1293–1298, 2012.

[24] T. Yamamoto, N. Takano, K. Ishiwata et al., "Reduced methylation of PFKFB3 in cancer cells shunts glucose towards the pentose phosphate pathway," *Nature Communications*, vol. 5, article 3480, 2014.

[25] O. Kabil, V. Yadav, and R. Banerjee, "Heme-dependent metabolite switching regulates H_2S synthesis in response to Endoplasmic Reticulum (ER) stress," *The Journal of Biological Chemistry*, vol. 291, no. 32, pp. 16418–16423, 2016.

[26] Y. Kabe, T. Yamamoto, M. Kajimura et al., "Cystathionine β-synthase and PGRMC1 as CO sensors," *Free Radical Biology and Medicine*, vol. 99, pp. 333–344, 2016.

[27] M. Suematsu, T. Nakamura, Y. Tokumoto, T. Yamamoto, M. Kajimura, and Y. Kabe, "CO-CBS-H_2S axis: from vascular mediator to cancer regulator," *Microcirculation*, vol. 23, no. 3, pp. 183–190, 2016.

[28] P. K. Yadav, P. Xie, and R. Banerjee, "Allosteric communication between the pyridoxal 5′-phosphate (PLP) and heme sites in the H_2S generator human cystathionine β-synthase," *The Journal of Biological Chemistry*, vol. 287, no. 45, pp. 37611–37620, 2012.

[29] A. T. Smith, Y. Su, D. J. Stevens, T. Majtan, J. P. Kraus, and J. N. Burstyn, "Effect of the disease-causing R266K mutation on the heme and PLP environments of human cystathionine β-synthase," *Biochemistry*, vol. 51, no. 32, pp. 6360–6370, 2012.

[30] J. B. Vicente, F. Malagrinò, M. Arese, E. Forte, P. Sarti, and A. Giuffrè, "Bioenergetic relevance of hydrogen sulfide and the interplay between gasotransmitters at human cystathionine β-synthase," *Biochimica et Biophysica Acta—Bioenergetics*, vol. 1857, no. 8, pp. 1127–1138, 2016.

[31] S. H. Mudd, F. Skovby, and H. L. Levy, "The natural history of homocystinuria due to cystathionine beta-synthase deficiency," *The American Journal of Human Genetics*, vol. 37, no. 1, pp. 1–31, 1985.

[32] M. Schiff and H. J. Blom, "Treatment of inherited homocystinurias," *Neuropediatrics*, vol. 43, no. 6, pp. 295–304, 2012.

[33] M. Janošík, J. Oliveriusová, B. Janosíková et al., "Impaired heme binding and aggregation of mutant cystathionine β-synthase subunits in homocystinuria," *American Journal of Human Genetics*, vol. 68, no. 6, pp. 1506–1513, 2001.

[34] L. R. Singh, X. Chen, V. Kožich, and W. D. Kruger, "Chemical chaperone rescue of mutant human cystathionine β-synthase," *Molecular Genetics and Metabolism*, vol. 91, no. 4, pp. 335–342, 2007.

[35] V. Kožich, J. Sokolová, V. Klatovská et al., "Cystathionine β-synthase mutations: effect of mutation topology on folding and activity," *Human Mutation*, vol. 31, no. 7, pp. 809–819, 2010.

[36] T. Majtan, L. Liu, J. F. Carpenter, and J. P. Kraus, "Rescue of cystathionine β-synthase (CBS) mutants with chemical chaperones: purification and characterization of eight CBS mutant enzymes," *The Journal of Biological Chemistry*, vol. 285, no. 21, pp. 15866–15873, 2010.

[37] M. Cozar, R. Urreizti, L. Vilarinho et al., "Identification and functional analyses of CBS alleles in Spanish and Argentinian homocystinuric patients," *Human Mutation*, vol. 32, no. 7, pp. 835–842, 2011.

[38] J. Kopecká, J. Krijt, K. Raková, and V. Kožich, "Restoring assembly and activity of cystathionine β-synthase mutants by ligands and chemical chaperones," *Journal of Inherited Metabolic Disease*, vol. 34, no. 1, pp. 39–48, 2011.

[39] A. Hnízda, V. Jurga, K. Raková, and V. Kožich, "Cystathionine beta-synthase mutants exhibit changes in protein unfolding: conformational analysis of misfolded variants in crude cell

extracts," *Journal of Inherited Metabolic Disease*, vol. 35, no. 3, pp. 469–477, 2012.

[40] M. I. S. Mendes, H. G. Colaço, D. E. C. Smith et al., "Reduced response of Cystathionine Beta-Synthase (CBS) to S-Adenosylmethionine (SAM): identification and functional analysis of CBS gene mutations in Homocystinuria patients," *Journal of Inherited Metabolic Disease*, vol. 37, no. 2, pp. 245–254, 2014.

[41] M. I. S. Mendes, D. E. C. Smith, J. B. Vicente et al., "Small aminothiol compounds improve the function of Arg to Cys variant proteins: effect on the human cystathionine β-synthase p.R336C," *Human Molecular Genetics*, vol. 24, no. 25, pp. 7339–7348, 2015.

[42] P. Melenovská, J. Kopecká, J. Krijt et al., "Chaperone therapy for homocystinuria: the rescue of CBS mutations by heme arginate," *Journal of Inherited Metabolic Disease*, vol. 38, no. 2, pp. 287–294, 2015.

[43] E. M. Bublil, T. Majtan, I. Park et al., "Enzyme replacement with PEGylated cystathionine β-synthase ameliorates homocystinuria in murine model," *The Journal of Clinical Investigation*, vol. 126, no. 6, pp. 2372–2384, 2016.

[44] R. De Franchis, M. P. Sperandeo, G. Sebastio, and G. Andria, "Clinical aspects of cystathionine β-synthase deficiency: how wide is the spectrum?" *European Journal of Pediatrics*, vol. 157, no. 2, pp. S67–S70, 1998.

[45] M. Gaustadnes, B. Wilcken, J. Oliveriusova et al., "The molecular basis of cystathionine β-synthase deficiency in Australian patients: genotype-phenotype correlations and response to treatment," *Human Mutation*, vol. 20, no. 2, pp. 117–126, 2002.

[46] L. Evangelisti, L. Lucarini, M. Attanasio et al., "Vascular and connective tissue features in 5 Italian patients with homocystinuria," *International Journal of Cardiology*, vol. 134, no. 2, pp. 251–254, 2009.

[47] M. M. Bradford, "A rapid and sensitive method for the quantitation of microgram quantities of protein utilizing the principle of protein-dye binding," *Analytical Biochemistry*, vol. 72, no. 1-2, pp. 248–254, 1976.

[48] S. Carballal, P. Madzelan, C. F. Zinola et al., "Dioxygen reactivity and heme redox potential of truncated human cystathionine β-synthase," *Biochemistry*, vol. 47, no. 10, pp. 3194–3201, 2008.

[49] E. Forte, V. B. Borisov, M. Falabella et al., "The terminal oxidase cytochrome *bd* promotes sulfide-resistant bacterial respiration and growth," *Scientific Reports*, vol. 6, Article ID 23788, 2016.

[50] M. Dixon, "The acceptor specificity of flavins and flavoproteins. I. Techniques for anaerobic spectrophotometry," *BBA—Bioenergetics*, vol. 226, no. 2, pp. 241–258, 1971.

[51] M. Puranik, C. L. Weeks, D. Lahaye et al., "Dynamics of carbon monoxide binding to cystathionine β-synthase," *Journal of Biological Chemistry*, vol. 281, no. 19, pp. 13433–13438, 2006.

[52] E. R. Henry and J. Hofrichter, "Singular value decomposition—application to analysis of experimental-data," *Methods in Enzymology*, vol. 210, pp. 129–192, 1992.

[53] M.-F. Incardona, G. P. Bourenkov, K. Levik, R. A. Pieritz, A. N. Popov, and O. Svensson, "EDNA: a framework for plugin-based applications applied to X-ray experiment online data analysis," *Journal of Synchrotron Radiation*, vol. 16, no. 6, pp. 872–879, 2009.

[54] W. Kabsch, "XDS," *Acta Crystallographica Section D: Biological Crystallography*, vol. 66, no. 2, pp. 125–132, 2010.

[55] P. R. Evans, "An introduction to data reduction: Space-group determination, scaling and intensity statistics," *Acta Crystallographica Section D: Biological Crystallography*, vol. 67, no. 4, pp. 282–292, 2011.

[56] P. R. Evans and G. N. Murshudov, "How good are my data and what is the resolution?" *Acta Crystallographica Section D: Biological Crystallography*, vol. 69, no. 7, pp. 1204–1214, 2013.

[57] C. Vonrhein, C. Flensburg, P. Keller et al., "Data processing and analysis with the autoPROC toolbox," *Acta Crystallographica Section D: Biological Crystallography*, vol. 67, no. 4, pp. 293–302, 2011.

[58] A. J. McCoy, R. W. Grosse-Kunstleve, P. D. Adams, M. D. Winn, L. C. Storoni, and R. J. Read, "Phaser crystallographic software," *Journal of Applied Crystallography*, vol. 40, no. 4, pp. 658–674, 2007.

[59] P. D. Adams, P. V. Afonine, G. Bunkóczi et al., "PHENIX: a comprehensive Python-based system for macromolecular structure solution," *Acta Crystallographica Section D: Biological Crystallography*, vol. 66, no. 2, pp. 213–221, 2010.

[60] T. C. Terwilliger, R. W. Grosse-Kunstleve, P. V. Afonine et al., "Iterative model building, structure refinement and density modification with the PHENIX AutoBuild wizard," *Acta Crystallographica Section D: Biological Crystallography*, vol. 64, no. 1, pp. 61–69, 2007.

[61] E. Blanc, P. Roversi, C. Vonrhein, C. Flensburg, S. M. Lea, and G. Bricogne, "Refinement of severely incomplete structures with maximum likelihood in BUSTER-TNT," *Acta Crystallographica Section D: Biological Crystallography*, vol. 60, no. 12, pp. 2210–2221, 2004.

[62] P. Emsley, B. Lohkamp, W. G. Scott, and K. Cowtan, "Features and development of Coot," *Acta Crystallographica Section D: Biological Crystallography*, vol. 66, no. 4, pp. 486–501, 2010.

[63] S. C. Lovell, I. W. Davis, W. B. Arendall III et al., "Structure validation by Cα geometry: φ,ψ and Cβ deviation," *Proteins: Structure, Function and Genetics*, vol. 50, no. 3, pp. 437–450, 2003.

[64] I. W. Davis, A. Leaver-Fay, V. B. Chen et al., "MolProbity: all-atom contacts and structure validation for proteins and nucleic acids," *Nucleic Acids Research*, vol. 35, no. 2, pp. W375–W383, 2007.

[65] M. Meier, M. Janosik, V. Kery, J. P. Kraus, and P. Burkhard, "Structure of human cystathionine β-synthase: a unique pyridoxal 5$\prime$-phosphate-dependent heme protein," *EMBO Journal*, vol. 20, no. 15, pp. 3910–3916, 2001.

[66] B. W. Matthews, "Solvent content of protein crystals," *Journal of Molecular Biology*, vol. 33, no. 2, pp. 491–497, 1968.

[67] S. Carballal, E. Cuevasanta, I. Marmisolle et al., "Kinetics of reversible reductive carbonylation of heme in human cystathionine β-synthase," *Biochemistry*, vol. 52, no. 26, pp. 4553–4562, 2013.

[68] O. Kabil, C. L. Weeks, S. Carballal et al., "Reversible heme-dependent regulation of human cystathionine β-synthase by a flavoprotein oxidoreductase," *Biochemistry*, vol. 50, no. 39, pp. 8261–8263, 2011.

[69] P. A. Karplus and K. Diederichs, "Linking crystallographic model and data quality," *Science*, vol. 336, no. 6084, pp. 1030–1033, 2012.

Hindawi
Oxidative Medicine and Cellular Longevity
Volume 2017, Article ID 7908072, 18 pages
https://doi.org/10.1155/2017/7908072

Research Article

Alleviation of Oxidative Damage and Involvement of Nrf2-ARE Pathway in Mesodopaminergic System and Hippocampus of Status Epilepticus Rats Pretreated by Intranasal Pentoxifylline

Yunxiao Kang,[1] Wensheng Yan,[1,2] Hui Fang,[1] Guoliang Zhang,[3] Yakun Du,[4] Lei Wang,[3] Huixian Cui,[3] and Geming Shi[1]

[1]*Department of Neurobiology, Hebei Medical University, Shijiazhuang, Hebei 050017, China*
[2]*Department of Human Anatomy, Shijiazhuang Medical College, Shijiazhuang, Hebei 050599, China*
[3]*Department of Human Anatomy, Hebei Medical University, Shijiazhuang, Hebei 050017, China*
[4]*Department of Neurology, Children's Hospital of Hebei Province, Shijiazhuang, Hebei 050017, China*

Correspondence should be addressed to Geming Shi; shigeming@163.com

Received 3 December 2016; Revised 6 February 2017; Accepted 21 February 2017; Published 12 March 2017

Academic Editor: Luciano Saso

The current studies were aimed at evaluating the efficacy of intranasal pentoxifylline (Ptx) pretreatment in protecting mesodopaminergic system and hippocampus from oxidative damage of lithium-pilocarpine induced status epilepticus (SE) and the involvement of nuclear factor erythroid 2-related factor 2- (Nrf2-) antioxidant response elements pathway. Pentoxifylline was administered to rats intranasally or intraperitoneally 30 minutes before inducing SE. Our results showed the impaired visuospatial memory, the defected mesodopaminergic system, and the oxidative damage and the transient activation of Nrf2 in SE rats. The transient activation of Nrf2 in SE rats was enhanced by Ptx pretreatment, which was followed by the upregulation of heme oxygenase-1 and NAD(P)H:quinone oxidoreductase-1. Ptx pretreatment to SE rats significantly suppressed the epileptic seizures, decreased the levels of lipid peroxide and malondialdehyde, and elevated the ratio of reduced glutathione/oxidized glutathione. Compared with intraperitoneal injection, intranasal Ptx delivery completely restored the visuospatial memory and the activity of mesodopaminergic system in SE rats. Intranasal administration of Ptx may hopefully become a noninvasive, painless, and easily administered option for epileptic patients.

1. Introduction

Epilepsy is a life-threatening medical emergency that warrants immediate treatment to prevent seizure activity and associated neuronal damage [1]. Status epilepticus (SE) is one of the most severe conditions of epilepsy [2]. Patients with SE are at risk of neurologic complications. Early intervention is frequently needed to shorten seizure duration [3]. The sooner seizures are treated, the more likely they will be controlled [4]. However, intramuscular or intravenous injection cannot be implemented immediately outside of hospital settings, thus delaying or missing the best treatment time and threatening the human life. The intranasal route to administer drugs is quick and effective in targeting the brain [4, 5] and potentially provides a direct delivery of the drug to the central nervous system [6, 7] bypassing the blood-brain barrier and exerting therapeutic effects at terminating epileptic seizures. Intranasal drug administration is noninvasive, painless, and easily administered for epileptic patients [4] in the home treatment of prolonged seizures and in the treatment of prehospital seizures by emergency medical technicians [8].

The first-line drugs to stop seizures are benzodiazepines [9], which manipulate γ-aminobutyric acid receptors and make neurons resistant to excitation. In addition to controlling neuronal hyperactivity and excitotoxicity, one important factor that should be dealt with is oxidative stress in epileptic seizures [10–12]. Oxidative stress means an imbalance between oxidation and antioxidation in vivo, which leads to excessive oxygen free radical and reduced antioxidative capacity [13–15]. Excessive oxygen free radical generated

in SE dramatically impairs the structure and function of neurons [16–18]. Nuclear factor erythroid 2-related factor 2 (Nrf2), as a transcription factor, controls the basal and inducible expression of an array of antioxidant and detoxification enzymes to degrade oxygen free radical [13, 19, 20]. Disruption of Nrf2-antioxidant response elements (ARE) pathway results in an increased susceptibility to oxidative insults and other toxicants [21]. Activation of Nrf2-ARE pathway protects neurons against oxidative damage and excitotoxic damage [13, 22–24].

Pentoxifylline (Ptx), a potent antioxidant and modulator of a variety of transmitters, was initially introduced for the treatment of respiratory and peripheral circulatory disorders. Currently, a beneficial effect of Ptx is found on preventing epileptic seizures [25, 26]. The frequency and severity of epileptic seizures are ameliorated and oxidative damage is attenuated in Ptx-treated SE rats [25, 26]. Clinical and experimental studies have suggested the implication of dopaminergic system in seizures [27], such as a decreased DA content in hippocampus (Hip) and striatum of SE rats [26, 28], as well as the reduced dopamine transporter (DAT) in substantia nigra (SN) and midbrain of epilepsy patients [29, 30]. Therefore, in the present study, the efficacy of intranasal Ptx delivery in epileptic seizures was investigated by analyzing the alteration of mesodopaminergic system and hippocampus in SE rats induced by lithium-pilocarpine (Li-Pc), based on the severe implication of mesodopaminergic system and Hip in SE [26, 29]. Meanwhile, oxidative stress parameters and Nrf2-ARE pathway were examined to evaluate whether Nrf2 was involved in the effects of Ptx treatment on mesodopaminergic system and hippocampus of SE rats. For comparison purposes, the same observations were performed in SE rats that experienced intraperitoneal Ptx treatment.

2. Materials and Methods

2.1. Animals and Housing. Three-month-old male Sprague Dawley rats were supplied by the Experimental Animal Center of Hebei Medical University and were housed under controlled conditions with 12-hour light-dark diurnal cycle at 22 ± 2°C, with humidity at 50–60% and with free access to food and water. The experimental procedures followed the rules in the "Guidelines for the Care and Use of Mammals in Neuroscience and Behavioral Research" and were approved by the Committee of Ethics on Animal Experiments at Hebei Medical University.

2.2. Ptx Treatment and Induction of SE. Ptx was administered to rats either via nostril instillation or by intraperitoneal injection. For intranasal experiment, experimental rats were assigned to the following groups: CON-in (n = 25), LICI-in (n = 25), PTX-in (n = 25), SE-in (n = 35), and PTX.in-SE (n = 35). The rats in PTX-in and PTX.in-SE were intranasally given Ptx. Intranasal Ptx delivery was performed as described [31]. Briefly, fully conscious rats were held and laid upside down. The solution of Ptx (prepared in saline) was introduced by the pressure with a micropipette into one nasal cavity, without introducing the pipette tip directly into the nasal cavity, and the rats were immobilized in this position for 15 s by gently pulling the tail to prevent sneezing. The rats were discarded if sneezing happened. The same procedure was repeated in the other nostril. For intraperitoneal injection experiment, rats were divided into five groups consisting of CON-ip (n = 25), LICI-ip (n = 25), PTX-ip (n = 25), SE-ip (n = 35), and PTX.ip-SE (n = 35). The rats in PTX-ip and PTX.ip-SE received intraperitoneal Ptx injection. SE was induced in SE-in, SE-ip, PTX.in-SE, and PTX.ip-SE rats by administering an aqueous solution of lithium chloride (Li, 127 mg/kg, BDH Laboratory Supplies) intraperitoneally, followed (20 hrs later) by injecting pilocarpine hydrochloride (Pc, 20 mg/kg, Sigma) subcutaneously. Ptx was administered intranasally or intraperitoneally at the dose of 60 mg/kg (30 minutes before Pc injection) to rats corresponding to PTX.in-SE and PTX.ip-SE, respectively. The rats in CON-in, LICI-in, and PTX-in as well as CON-ip, LICI-ip, and PTX-ip received saline, lithium chloride, and Ptx (60 mg/kg, Sigma) correspondingly. After Pc injections, the rats were observed for the signs of seizure activity. Based on Racine's scale [32], the rats that showed consecutive seizures with a score of 3 or above fell in SE [25, 32]. The latency and incidence of seizures as well as mortality within 24 hrs were recorded. The rats were sacrificed 24 hrs (for oxidative parameters and Nrf2-ARE pathway) or 7 days (for Morris water maze test and parameters of mesodopaminergic system as well as oxidative parameters and Nrf2-ARE pathway) following Pc treatment. For the rats that were treated similarly in the groups CON-in (and ip), LICL-in (and ip), or SE-in (and ip), since the parameters were not substantially different (ANOVA), the data collected from them in the two experiments were clustered (cl) for analysis as CON-cl, LICL-cl, or SE-cl correspondingly, except for the data collected by Western blot.

2.3. Morris Water Maze Test. The rats in each group were tested for visuospatial memory 24 hrs after the Pc injection using Morris water maze test as described previously [24]. The water maze included a circular water tank (180 cm in diameter, 80 cm high) that was partially filled with water (23± 1°C). The water was made opaque by adding milk to prevent visualization of the platform. The pool was divided virtually into four equal quadrants. A colorless escape platform (10 cm in diameter) was hidden 1 cm below the surface of the water in a fixed location. The maze was located in a quiet room, surrounded by visual cues outside of the maze, which was used by the rats for spatial orientation. The experiments were conducted two sessions per day for 5 consecutive days, each session including four trials, with an intertrial interval of 60 s and an intersession interval of 2 hrs. In each trial, the animals were gently placed in the middle of the circular edge in a randomly selected quadrant, with the nose pointing toward the wall. If animals failed to find the escape platform within 120 s by themselves, they were placed on the platform for 10 s by the experimenter and their escape latency was accepted as 120 s. After climbing onto the platform, the animal remained there for 30 s before the commencement of the next trial. On the sixth day, a probe trial without the platform was assessed, and the time spent in the target quadrant where the platform had been located was recorded.

Table 1: Validation parameters of the LC-MS/MS method.

Analyte	r	LLOQ (ng/g)	Recovery (%)	Intraprecision (RSD%)	Interprecision (RSD%)
DA	0.9969	2.0	94.6 ± 8.7	10.3	12.4
DOPAC	0.9982	72.0	93.4 ± 6.6	8.9	7.5
HVA	0.9977	50.0	95.3 ± 7.4	7.7	11.3

DA: dopamine; DOPAC: 3,4-dihydroxyphenylacetic acid; HVA: homovanillic acid.

2.4. Sample Preparation. For biochemical, real-time quantitative PCR (qPCR) and Western blot analyses, the rats in each group were sacrificed by decapitation. The brains were removed quickly. The tissue block containing substantia nigra and ventral tegmental area (SN-VTA; between 3.00 mm and 4.08 mm) or caudate putamen (CPu; between 8.64 mm and 10.08 mm) and Hip (between 5.40 mm and 6.08 mm) relatively rostral to the interaural axis was dissected on ice-cold plate using a scalpel for ophthalmic surgery and a stereomicroscopy. The tissue blocks of rats in each group were processed for Western blot or liquid chromatography coupled with tandem mass spectrometry (LC-MS/MS) assay and the tissue blocks of others were chosen for lipid peroxide (LPO), malondialdehyde (MDA), reduced glutathione (GSH), and oxidized glutathione (GSSG) assay by spectrophotometry or prepared for qPCR analysis based on the study purposes.

2.5. Biochemical Analysis. For LPO, MDA, GSH, and GSSG assay, SN-VTA or Hip tissue block was weighed and homogenized with 10 times (w/v) ice-cold 0.1 M phosphate buffer, PH 7.4. The homogenates were used to assess LPO, MDA, GSH, and GSSG spectrophotometrically using detection kits following the manufacturer's instruction (Nanjing Jiancheng Bioengineering Institute, China).

For dopamine (DA) and metabolites assay, CPu or Hip tissue block was weighed and homogenized in 80% acetonitrile containing 0.1% formic acid (5 μL/mg). The homogenates were centrifuged at 14,000 rpm for 10 min at 4°C. The supernatants were collected and stored at −80°C. DA, 3,4-dihydroxyphenylacetic acid (DOPAC), and homovanillic acid (HVA) were determined by LC-MS/MS. The LC separation was performed on Agilent 1200 LC system (Agilent, Santa Clara, USA) using a Synergi Fusion-RP C18 column (50 mm × 3.0 mm, 4 μm) provided by Phenomenex. MS/MS detection was carried out using a 3200 QTRAP™ LC-MS/MS System (Applied Biosystems, Foster City, CA, USA). The multiple-reaction monitoring mode was used for the quantification. The principal validation parameters of the LC-MS/MS were set up as shown in Table 1, based on the previous study [33].

2.6. qPCR. 2 μg of total RNA from the SN-VTA or Hip tissue block was subjected to reverse transcription using random primer to obtain the first-strand cDNA template. qPCR was performed with 0.8 μL cDNA (diluted 1 : 10), specific primers 2 μL, and 2 × GoTaq® Green Master Mix (Promega, USA) with a final volume of 20 μL. PCR was performed as follows: an initial cycle at 95°C for 10 min, followed by 40 cycles at 95°C for 15 s, 58°C for 20 s, and 72°C for 27 s. Then PCR products were analyzed by melting curve to confirm the specificity of amplification. Expression of tyrosine hydroxylase (TH), dopamine transporter (DAT), Nrf2, heme oxygenase-1 (HO-1) and NAD(P)H:quinone oxidoreductase-1 (NQO-1) genes was detected. The relative quantification was calculated using the $2^{-\Delta\Delta ct}$ method. GAPDH was used as reference gene in all calculations. The sets of primers were as follows: TH (5′-GCTTCTCTGACCAGGTGTATCG-3′ and 5′-GCAATCTCTTCCGCTGTGTAT-3′), DAT (5′-ACTCTGTGAGGCATCTGTGTG-3′ and 5′-TGTAACTGGAGAAGGCAATCAG-3′), Nrf2 (5′-GACCTAAAGCACAGCCAACACAT-3′ and 5′-CTCAATCGGCTTGAATGTTTGTC-3′), HO-1 (5′-TGTCCCAGGATTTGTCCGAG-3′ and 5′-ACTGGGTTCTGCTTGTTTCGCT-3), NQO-1 (5′-GGGGACATGAACGTCATTCTCT-3′ and 5′-AGTGGTGACTCCTCCCAGACAG-3′), and GAPDH (5′-TGAACGGGAAGCTCACTG-3′ and 5′-GCTTCACCACCTTCTTGATG-3′).

2.7. Western Blot Analysis. For detection of TH and DAT protein levels, SN-VTA, CPu, or Hip tissue block was homogenized in Radioimmunoprecipitation Assay (RIPA) buffer containing 1% Triton X-100, 0.1% SDS, 0.5% sodium deoxycholate, and protease inhibitors (phenylmethanesulfonyl fluoride 100 μg/mL, aprotinin 30 μg/mL, and sodium orthovanadate 1 mM) and then sonicated for 4 × 10 s. After centrifugation at 12,000 ×g for 20 min at 4°C, the supernatant was collected and centrifuged again as above. The final resulting supernatant was stored at −80°C until use. Samples from SN-VTA, CPu, or Hip were diluted in 2x sample buffer (50 mM Tris, pH 6.8, 2% SDS, 10% glycerol, 0.1% bromophenol blue, and 5% β-mercaptoethanol) and heated for 5 min at 95°C before SDS-PAGE on a 10% gel and subsequently transferred to a PVDF membrane. The membrane was incubated for 2 h with 5% nonfat dry milk in Tris-buffered saline (TBS) containing 0.05% Tween-20 (TBST) (20 mM Tris–Cl, 137 mM NaCl, 0.1% Tween 20, pH 7.6) at room temperature. The membrane was rinsed in three changes of TBST and then incubated overnight with mouse anti-TH monoclonal antibody (1 : 10,000, Sigma) or rabbit anti-DAT polyclonal antibody (1 : 4000, Millipore) at 4°C. After three washes, the membrane was incubated for 1 h in IRDye® 800-conjugated goat anti-mouse second antibody (1 : 3000, Rockland) or goat anti-rabbit second antibody (1 : 3000, Rockland) at room temperature. The relative density of bands was analyzed on an Odyssey infrared scanner (LI-COR Biosciences). Following stripping, each PVDF membrane was subsequently immunoblotted with mouse anti-β-actin monoclonal antibody (1 : 6000, Santa Cruz Biotechnology). The labeling densities for TH or DAT were compared with those of β-actin, which were the endogenous control.

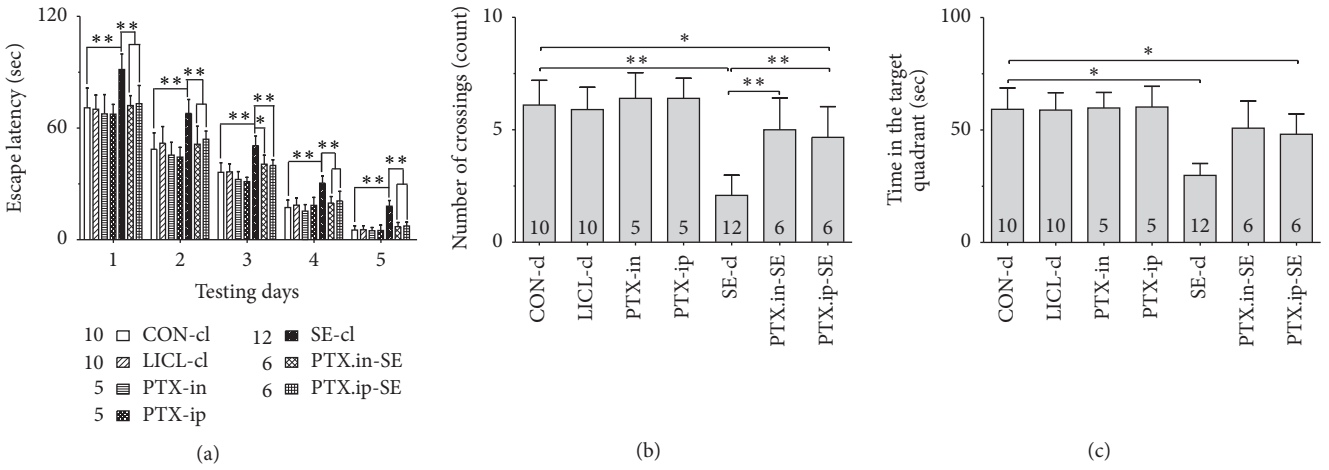

Figure 1: Effects of intranasal and intraperitoneal Ptx pretreatment on the visuospatial memory of SE rats induced by Li-Pc. (a) The escape latency to reach the platform. (b) The number of crossings. (c) The time spent in the target quadrant. The results were expressed as the means ± SD. $^{*}P < 0.05$; $^{**}P < 0.01$.

For detection of Nrf2, HO-1, or NQO-1 protein levels, SN-VTA or Hip tissue block was homogenized in ice-cold lysis buffer (10 mmol/L HEPES, pH 7.9, 10 mmol/L KCl, 0.1 mmol/L EDTA, 1 mmol/L DTT, and 0.1 mmol/L EGTA) for 15 min. After adding NP-40, the homogenate was centrifuged at 10,000 rpm at 4°C for 3 min and the supernatant was collected as cytoplasmic protein for HO-1 and NQO-1. The pellets were homogenized in ice-cold lysis buffer (20 mmol/L HEPES, pH 7.9, 400 mmol/L NaCl, 1 mmol/L EDTA, and 0.1 mmol/L EGTA) for 15 min. Then the pellets were centrifuged at 12,000 rpm at 4°C for 10 min, and the supernatant was collected. Phenylmethanesulfonyl fluoride was added to the supernatant with the final concentration of 1 mmol/L as the nuclear protein for Nrf2. Samples from SN-VTA or Hip (50 μg) were separated by SDS/PAGE and transferred onto PVDF membranes. Membranes were blocked with 5% skimmed milk for 1 h at room temperature and then were probed with polyclonal rabbit anti-Nrf2 antibody (1 : 500, Abcam), polyclonal rabbit anti-HO-1 antibody (1 : 200, Abcam), or polyclonal rabbit anti-NQO-1 antibody (1 : 200, Abcam) overnight at 4°C. After washing three times with phosphate buffered saline with 1% Tween 20, IRDye 800-conjugated goat anti-rabbit second antibody (1 : 3000, Rockland) incubated with membranes for 1 h at room temperature. The relative density of bands was analyzed on an Odyssey infrared scanner (LI-COR Biosciences). The densitometry values were normalized with respect to the values of anti-histone 3 for Nrf2 or anti-β-actin for HO-1 and NQO-1 immunoreactivity.

2.8. Statistical Analysis. Measurement data were described with mean ± SD. Levene's test was applied to test homogeneity of variance. If both normal distribution ($P > 0.1$) and homogeneity of variance ($P > 0.1$) were found, then parametric test was performed by one-way analysis of variance (one-way ANOVA) followed by a Student-Newman-Keuls (SNK) post hoc test for multiple comparisons. Otherwise, nonparametric statistics were done by Kruskal-Wallis test followed by Mann–Whitney U test for post hoc analysis between groups. A difference was considered statistically significant at a P value of less than 0.05.

3. Results

3.1. Antiepileptic Effects of Ptx Pretreatment. The effects of intranasal Ptx pretreatment on epileptic activities were analyzed. All the rats in SE-cl developed into epileptic seizures and then into SE after the injection of Pc. 10% of them died over a period of 24 hrs. Ptx pretreatment significantly extended the latency to first seizure and decreased epileptic seizures. 17.14% of rats in PTX.in-SE and 20% of rats in PTX.ip-SE developed into seizures. No rats in PTX.in-SE and PTX.ip-SE developed into SE and died (Table 2). Intranasal Ptx administration lessened epileptic activities as intraperitoneal injection of Ptx did and had antiepileptic effects.

3.2. Visuospatial Memory. Behavioral parameters in water maze test were analyzed to reveal the effects of intranasal Ptx pretreatment on visuospatial memory of SE rats. Group differences in the escape latency (Figure 1(a), 1 d: $\chi^2 = 23.338$ and $P < 0.01$; 2 d: $\chi^2 = 26.167$ and $P < 0.01$; 3 d: $F(6, 47) = 17.824$ and $P < 0.01$; 4 d: $\chi^2 = 30.381$ and $P < 0.01$; 5 d: $\chi^2 = 32.735$ and $P < 0.01$), the number of crossings (Figure 1(b), $\chi^2 = 33.250$ and $P < 0.01$), and the time in the target quadrant (Figure 1(c), $\chi^2 = 32.996$ and $P < 0.01$) were found among the CON-cl, LICL-cl, PTX-in, PTX-ip, SE-cl, PTX.in-SE, and PTX.ip-SE rats. The post hoc test showed that the rats in SE-cl exhibited the longer escape latency to reach the platform ($P < 0.01$), the reduced number of crossings ($P < 0.01$), and the less time in the target quadrant ($P < 0.05$), compared with rats in CON-cl. Intranasal or intraperitoneal Ptx pretreatment to SE rats shortened the escape latency to reach the platform ($P < 0.05$) and increased the number of crossings and the time spent in the target quadrant

Table 2: Effects of pentoxifylline pretreatment on status epilepticus rats.

Group	n	Seizures (%)	Latency to first seizure (min)	SE (%)	Mortality (%) within 24 h
CON-cl	50	0 (0)	—	—	0
LICL-cl	50	0 (0)	—	—	0
PTX-in	25	0 (0)	—	—	0
PTX-ip	25	0 (0)	—	—	0
SE-cl	70	100	13.87 ± 4.73	100	10
PTX.in-SE	35	17.14*	37.78 ± 6.25*	0	0
PTX.ip-SE	35	20*	28.08 ± 7.10*	0	0

* $P < 0.01$ versus SE group.

($P < 0.01$). There were no differences in the behavioral parameters of rats between PTX.in-SE and PTX.ip-SE. The behavioral parameters of rats in PTX.in-SE were completely restored to CON-cl rats, compared with rats in PTX.ip-SE. Intranasal Ptx pretreatment ameliorated the poor visuospatial memory of SE rats.

3.3. Mesodopaminergic System. To reveal whether intranasal Ptx pretreatment ameliorated the mesodopaminergic activity in SE rats, the markers of mesodopaminergic system were analyzed.

3.3.1. DA and Its Metabolites. Group differences among CON-cl, LICL-cl, PTX-in, PTX-ip, SE-cl, PTX.in-SE, and PTX.ip-SE rats were observed in DA (CPu: $\chi^2 = 37.676$ and $P < 0.01$; Hip: $F(6, 47) = 78.847$ and $P < 0.01$), DOPAC (CPu: $F(6, 47) = 45.800$ and $P < 0.01$; Hip: $F(6, 47) = 146.455$ and $P < 0.01$), and HVA content (CPu: $F(6, 47) = 73.834$ and $P < 0.01$; Hip: $F(6, 47) = 55.916$ and $P < 0.01$) (Table 3). The post hoc test revealed the decreased DA, DOPAC, and HVA in CPu and Hip of rats in SE-cl, compared with rats in CON-cl ($P < 0.01$). Intranasal or intraperitoneal Ptx pretreatment to SE rats increased DA and its metabolites in CPu and Hip ($P < 0.01$). No differences in DA and its metabolites were shown in CPu and Hip of rats between PTX.in-SE and PTX.ip-SE. Intranasal Ptx pretreatment completely restored DA and its metabolites of SE rats to the levels of CON-cl rats, compared with rats in PTX.ip-SE.

3.3.2. TH and DAT mRNAs. Group differences in TH mRNA (Figure 2(a), $F(6, 47) = 62.738$ and $P < 0.01$) and DAT mRNA (Figure 3(a), $\chi^2 = 37.814$ and $P < 0.01$) were detected in SN-VTA of rats among CON-cl, LICL-cl, PTX-in, PTX-ip, SE-cl, PTX.in-SE, and PTX.ip-SE. The post hoc test found that the levels of TH and DAT mRNAs were lower in SE-cl rats than in CON-cl rats ($P < 0.01$). Intranasal or intraperitoneal Ptx pretreatment to SE rats significantly increased TH and DAT mRNAs in SN-VTA ($P < 0.01$). No differences in TH and DAT mRNAs were shown in SN-VTA between PTX.in-SE rats and PTX.ip-SE rats. Intranasal Ptx pretreatment completely restored TH and DAT mRNAs of SE rats to the levels of CON-cl rats, compared with rats in PTX.ip-SE.

3.3.3. TH and DAT Proteins. Western blot was used to reveal the protein levels of TH and DAT extracted from SN-VTA, CPu, and Hip. TH and DAT were located at approximately 60 and 80 kDa, respectively. The group differences among CON-in, LICL-in, PTX-in, SE-in, and PTX.in-SE rats were found in the expression of TH (Figures 2(b) and 2(d), SN-VTA: $F(4, 22) = 144.914$ and $P < 0.01$; Figure 2(e), CPu: $F(4, 22) = 50.721$ and $P < 0.01$; Figure 2(f), Hip: $F(4, 22) = 18.219$ and $P < 0.01$) and DAT (Figures 3(b) and 3(d), SN-VTA: $\chi^2 = 14.314$ and $P < 0.01$; Figure 3(e), CPu: $\chi^2 = 16.289$ and $P < 0.01$; Figure 3(f), Hip: $\chi^2 = 17.015$ and $P < 0.01$), as well as in that of TH (Figures 2(c), 2(g)–2(i); SN-VTA, CPu, and Hip: $P < 0.01$) and DAT (Figures 3(c), 3(g)–3(i); SN-VTA, CPu, and Hip: $P < 0.01$) among CON-ip, LICL-ip, PTX-ip, SE-ip, and PTX.ip-SE rats. The post hoc test revealed the decreased TH and DAT in SE-in rats and in SE-ip rats, compared with corresponding control rats ($P < 0.01$). Intranasal delivery, as well as intraperitoneal injection, of Ptx to SE rats elevated the levels of TH and DAT in SN-VTA, CPu, and Hip ($P < 0.01$). There were no differences in the levels of TH and DAT between PTX.in-SE rats and PTX.ip-SE rats. Intranasal Ptx pretreatment to SE rats completely restored TH and DAT proteins in SN-VTA, CPu, and Hip, compared with rats in PTX.ip-SE.

3.4. LPO, MDA, GSH, and GSSG. To assess whether the amelioratory effects of intranasal Ptx pretreatment to SE rats was associated with the oxidative stress, LPO, MDA, and the ratio of GSH/GSSG in SN-VTA and Hip were analyzed. There were group differences in LPO (Figure 4(a), SN-VTA (24 hrs): $\chi^2 = 32.447$ and $P < 0.01$; SN-VTA (7 days): $\chi^2 = 33.837$ and $P < 0.01$; Figure 4(b), Hip (24 hrs): $\chi^2 = 31.413$ and $P < 0.01$; Hip (7 days): $\chi^2 = 36.309$ and $P < 0.01$), MDA (Figure 4(c), SN-VTA (24 hrs): $\chi^2 = 33.813$ and $P < 0.01$; SN-VTA (7 days): $\chi^2 = 35.623$ and $P < 0.01$; Figure 4(d), Hip (24 hrs): $\chi^2 = 36.381$ and $P < 0.01$; Hip (7 days): $\chi^2 = 26.853$ and $P < 0.01$), and the ratio of GSH/GSSG (Figure 4(e), SN-VTA (24 hrs): $\chi^2 = 38.609$ and $P < 0.01$; SN-VTA (7 days): $\chi^2 = 30.277$ and $P < 0.01$; Figure 4(f), Hip (24 hrs): $F(6, 47) = 42.160$ and $P < 0.01$; Hip (7 days): $F(6, 47) = 13.550$ and $P < 0.01$) among the CON-cl, LICL-cl, PTX-in, PTX-ip, SE-cl, PTX.in-SE, and PTX.ip-SE rats. The post hoc test detected the increased LPO and MDA contents as well as the decreased ratio of GSH/GSSG in SN-VTA and Hip of SE-cl rats, compared with CON-cl rats ($P < 0.01$). The reduced levels of LPO and MDA and the elevated ratio of GSH/GSSG

Table 3: Effects of pentoxifylline pretreatment on DA and its metabolites of status epilepticus rats.

	CON-cl	LICL-cl	PTX-in	PTX-ip	SE-cl	PTX.in-SE	PTX.ip-SE
CPu							
DA (ng/g)	223.4 ± 11.9 (5.3)	210.8 ± 13.6 (6.4)	233.2 ± 15.0 (6.4)	234.6 ± 10.0 (4.3)	121.0 ± 11.0** (9.1)	202.9 ± 20.4$^{\#}$ (10.1)	209.5 ± 21.5$^{\#}$ (10.3)
DOPAC (ng/g)	3437.5 ± 196.2 (5.7)	3264.2 ± 94.9 (2.9)	3716.2 ± 221.2 (6.0)	3634.9 ± 251.4 (6.9)	2355.7 ± 182.9** (7.8)	3231.0 ± 302.5$^{\#}$ (9.4)	3271.0 ± 224.1$^{\#}$ (6.9)
HVA (ng/g)	879.2 ± 50.0 (5.7)	852.4 ± 60.1 (7.1)	889.1 ± 75.0 (8.4)	901.1 ± 33.9 (3.8)	462.1 ± 47.1** (10.2)	791.0 ± 88.7$^{\#}$ (11.2)	842.7 ± 54.7$^{\#}$ (6.5)
Hip							
DA (ng/g)	10.7 ± 0.6 (5.9)	10.2 ± 0.8 (7.4)	11.2 ± 0.9 (8.4)	11.4 ± 1.2 (10.5)	5.1 ± 0.6** (12.1)	9.7 ± 0.8$^{\#}$ (8.5)	9.4 ± 0.6$^{*\#}$ (6.5)
DOPAC (ng/g)	365.7 ± 29.1 (8.0)	352.0 ± 20.5 (5.8)	383.7 ± 38.7 (10.0)	380.8 ± 23.4 (6.1)	116.5 ± 14.9** (12.8)	340.8 ± 25.4$^{\#}$ (7.5)	325.5 ± 29.7$^{\#}$ (9.1)
HVA (ng/g)	106.5 ± 7.3 (6.8)	98.3 ± 5.8 (5.9)	111.9 ± 8.8 (7.9)	107.6 ± 7.4 (6.8)	64.8 ± 6.0** (9.3)	100.2 ± 5.1$^{\#}$ (5.1)	96.4 ± 6.9$^{\#}$ (7.2)

CPu: caudate putamen; Hip: hippocampus; DA: dopamine; DOPAC: 3,4-dihydroxyphenylacetic acid; HVA: homovanillic acid. The value in brackets is the coefficient of variation.
$^{*}P < 0.05$ and $^{**}P < 0.01$ versus CON-cl; $^{\#}P < 0.01$ versus SE-cl.

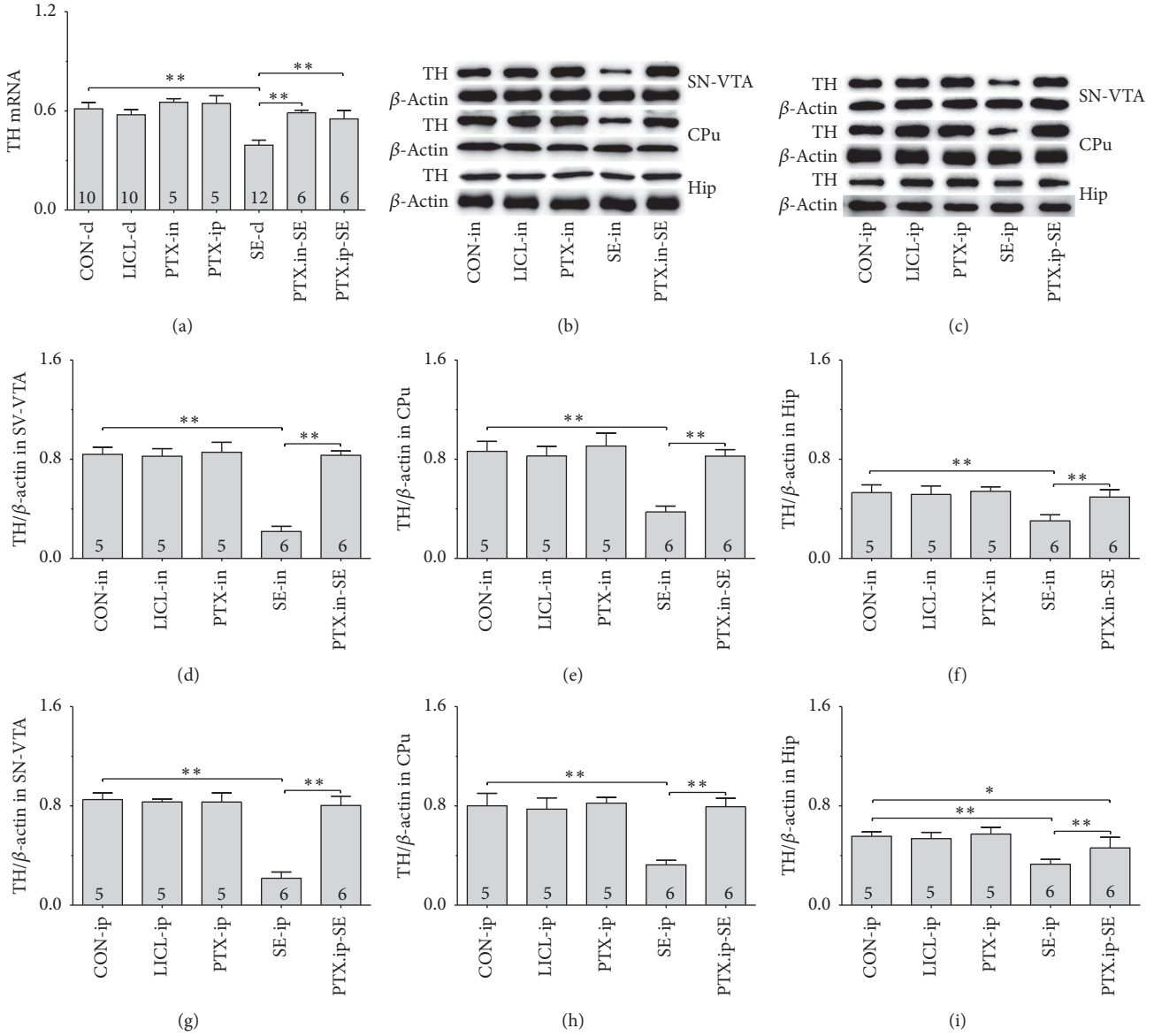

Figure 2: Effects of intranasal and intraperitoneal Ptx pretreatment on TH at mRNA and protein level of SE rats induced by Li-Pc. (a) TH mRNAs were detected in SN-VTA by qPCR. (b–i) TH protein was detected in SN-VTA, CPu, and Hip by Western blot. The results were expressed as the means ± SD. $^{*}P < 0.05$; $^{**}P < 0.01$.

in SN-VTA and Hip were detected in rats of PTX.in-SE as well as PTX.ip-SE, compared with the rats in SE-cl ($P < 0.01$). Intranasal Ptx pretreatment to SE rats mitigated the oxidative damage in SN-VTA and Hip.

3.5. Nrf2-ARE. To evaluate whether the Nrf2-ARE pathway was involved in the alleviation of the oxidative damage in SN-VTA and Hip of intranasal Ptx-pretreated SE rats, Nrf2, HO-1, and NQO-1 were examined at mRNA and protein levels.

3.5.1. Nrf2, HO-1 and NQO-1 mRNAs. Group differences among the CON-cl, LICL-cl, PTX-in, PTX-ip, SE-cl, PTX.in-SE, and PTX.ip-SE rats were found in the levels of Nrf2, HO-1, and NQO-1 mRNAs in SN-VTA (Figure 5(a), Nrf2 (24 hrs): $\chi^2 = 36.650$ and $P < 0.01$; Nrf2 (7 days): $\chi^2 = 34.573$ and $P < 0.01$; Figure 6(a), HO-1 (24 hrs): $\chi^2 = 37.430$ and $P < 0.01$; HO-1 (7 days): $F(6, 47) = 28.400$ and $P < 0.01$; Figure 7(a), NQO-1 (24 hrs): $F(6, 47) = 27.723$ and $P < 0.01$; NQO-1 (7 days): $\chi^2 = 35.171$ and $P < 0.01$), and Hip (Figure 8(a), Nrf2 (24 hrs): $\chi^2 = 35.997$ and $P < 0.01$; Nrf2 (7 days): $F(6, 47) = 37.925$ and $P < 0.01$; Figure 9(a), HO-1 (24 hrs): $\chi^2 = 39.571$ and $P < 0.01$; HO-1 (7 days): $\chi^2 = 36.662$ and $P < 0.01$; Figure 10(a), NQO-1 (24 hrs): $F(6, 47) = 15.841$ and $P < 0.01$; NQO-1 (7 days): $\chi^2 = 40.301$ and $P < 0.01$). The post hoc test revealed the elevation of Nrf2, HO-1, and NQO-1 mRNAs in SN-VTA and in Hip of SE-cl rats 24 hrs following Pc injection ($P < 0.01$) and the significant reduction of them 7 days after Pc administration ($P < 0.01$), compared with CON-cl rats.

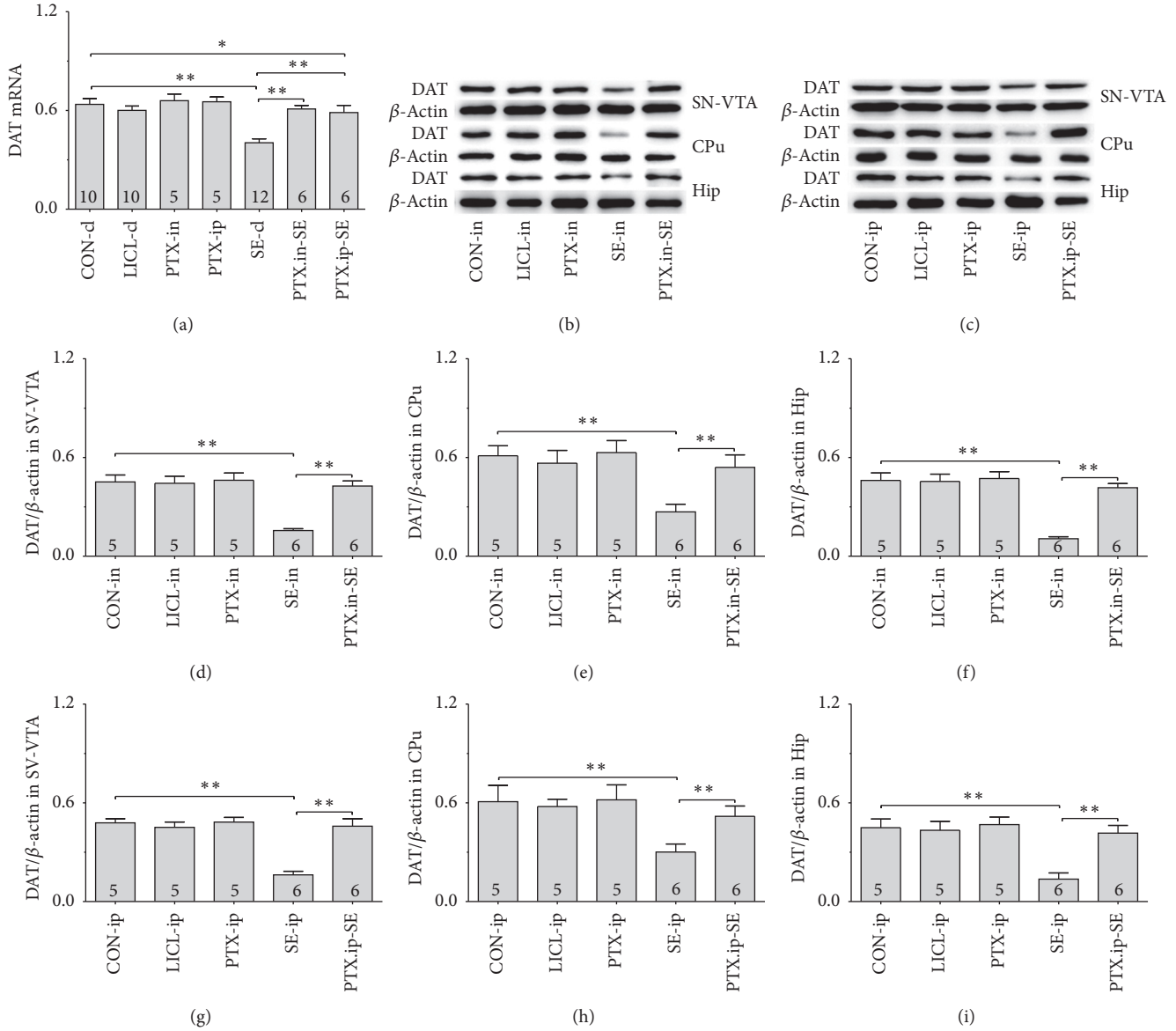

Figure 3: Effects of intranasal and intraperitoneal Ptx pretreatment on DAT at mRNA and protein level of SE rats induced by Li-Pc. (a) DAT mRNA was detected in SN-VTA by qPCR. (b–i) DAT protein was detected in SN-VTA, CPu, and Hip by Western blot. The results were expressed as the means ± SD. $^{*}P < 0.05$; $^{**}P < 0.01$.

In SN-VTA, the increased Nrf2, HO-1, and NQO-1 mRNAs were detected in PTX.in-SE and PTX.ip-SE rats ($P < 0.05$), compared with SE-cl rats, except NQO-1 mRNA in PTX.ip-SE rats 24 hrs following Pc injection ($P = 0.234$). In Hip, the elevated Nrf2, HO-1, and NQO-1 mRNAs were observed only in PTX.in-SE and PTX.ip-SE rats 7 days following Pc injection, compared with SE-cl rats ($P < 0.05$).

3.5.2. Nrf2, HO-1, and NQO-1 Proteins. The protein levels of Nrf2, HO-1, and NQO-1 extracted from SN-VTA and Hip were detected by Western blot. Nrf2, HO-1, and NQO-1 were located at approximately 110, 32, and 31 kDa, respectively. The group differences among CON-in, LICL-in, PTX-in, SE-in, and PTX.in-SE rats were found in the expression of Nrf2, HO-1, and NQO-1 in SN-VTA (Figures 5(b) and 5(c), Nrf2 (24 hrs): $F(4, 22) = 15.882$ and $P < 0.01$; Nrf2 (7 days): $F(4, 22) = 84.169$ and $P < 0.01$; Figures 6(b) and 6(c), HO-1 (24 hrs): $\chi^2 = 21.011$ and $P < 0.01$; HO-1 (7 days): $F(4, 22) = 71.535$ and $P < 0.01$; Figures 7(b) and 7(c), NQO-1 (24 hrs): $\chi^2 = 21.705$ and $P < 0.01$; NQO-1 (7 days): $\chi^2 = 17.290$ and $P < 0.01$), and Hip (Figures 8(b) and 8(c), Nrf2 (24 hrs): $\chi^2 = 20.481$ and $P < 0.01$; Nrf2 (7 days): $F(4, 22) = 27.035$ and $P < 0.01$. Figures 9(b) and 9(c), HO-1 (24 hrs): $\chi^2 = 19.504$ and $P < 0.01$; HO-1 (7 days): $F(4, 22) = 78.424$ and $P < 0.01$; Figures 10(b) and 10(c), NQO-1 (24 hrs): $\chi^2 = 17.695$ and $P < 0.01$; NQO-1 (7 days): $F(4, 22) = 67.737$ and $P < 0.01$), as well as in the levels of Nrf2 (Figures 5(b) and 5(d), SN-VTA; Figures 8(b) and

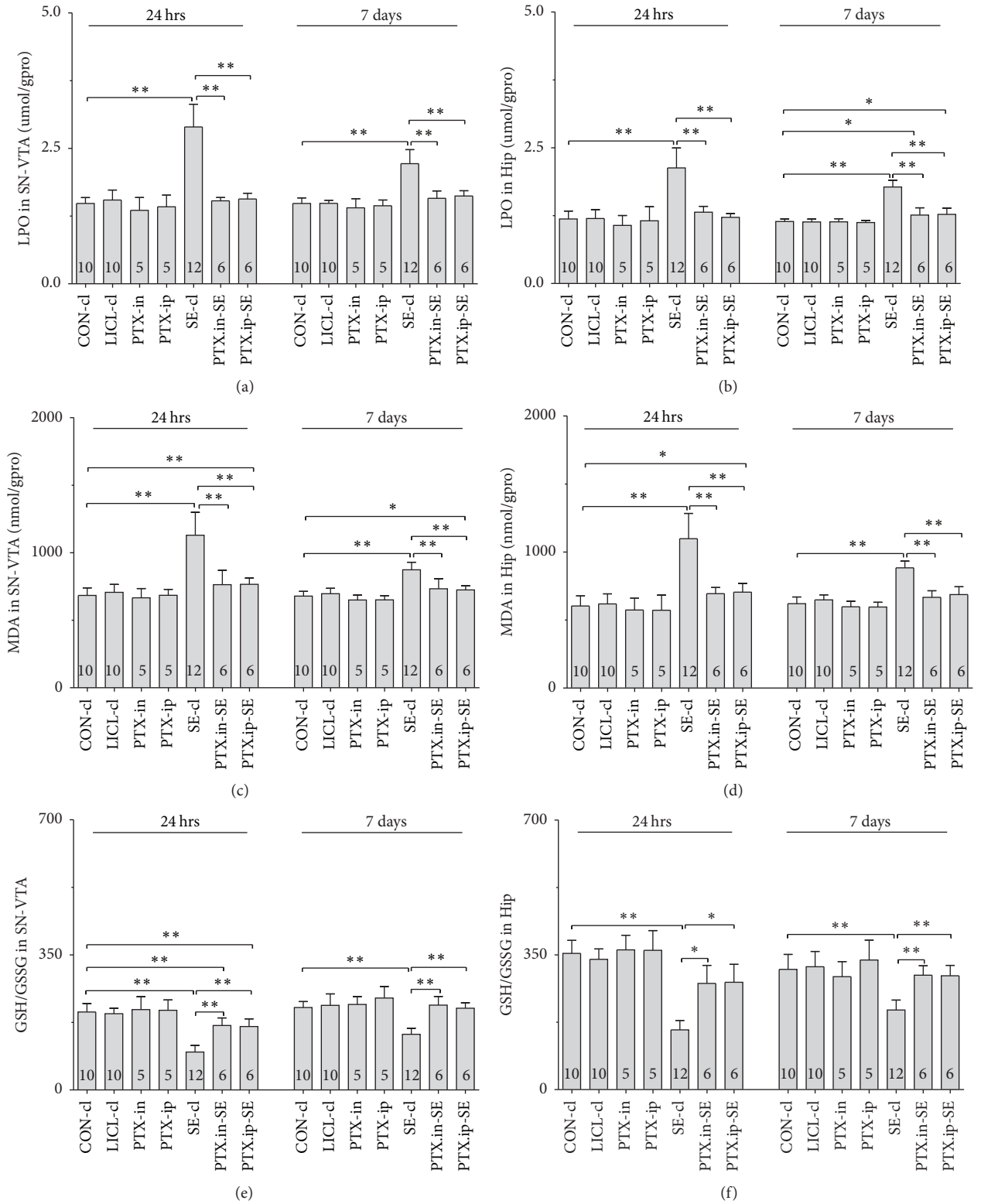

Figure 4: Effects of intranasal and intraperitoneal Ptx pretreatment on oxidative damage in SN-VTA and Hip of SE rats induced by Li-Pc 24 hrs and 7 days after Pc injection. (a) LPO in SN-VTA. (b) LPO in Hip. (c) MDA in SN-VTA. (d) MDA in Hip. (e) GSH/GSSG in SN-VTA. (f) GSH/GSSG in Hip. The results were expressed as the means ± SD. $^{*}P < 0.05$; $^{**}P < 0.01$.

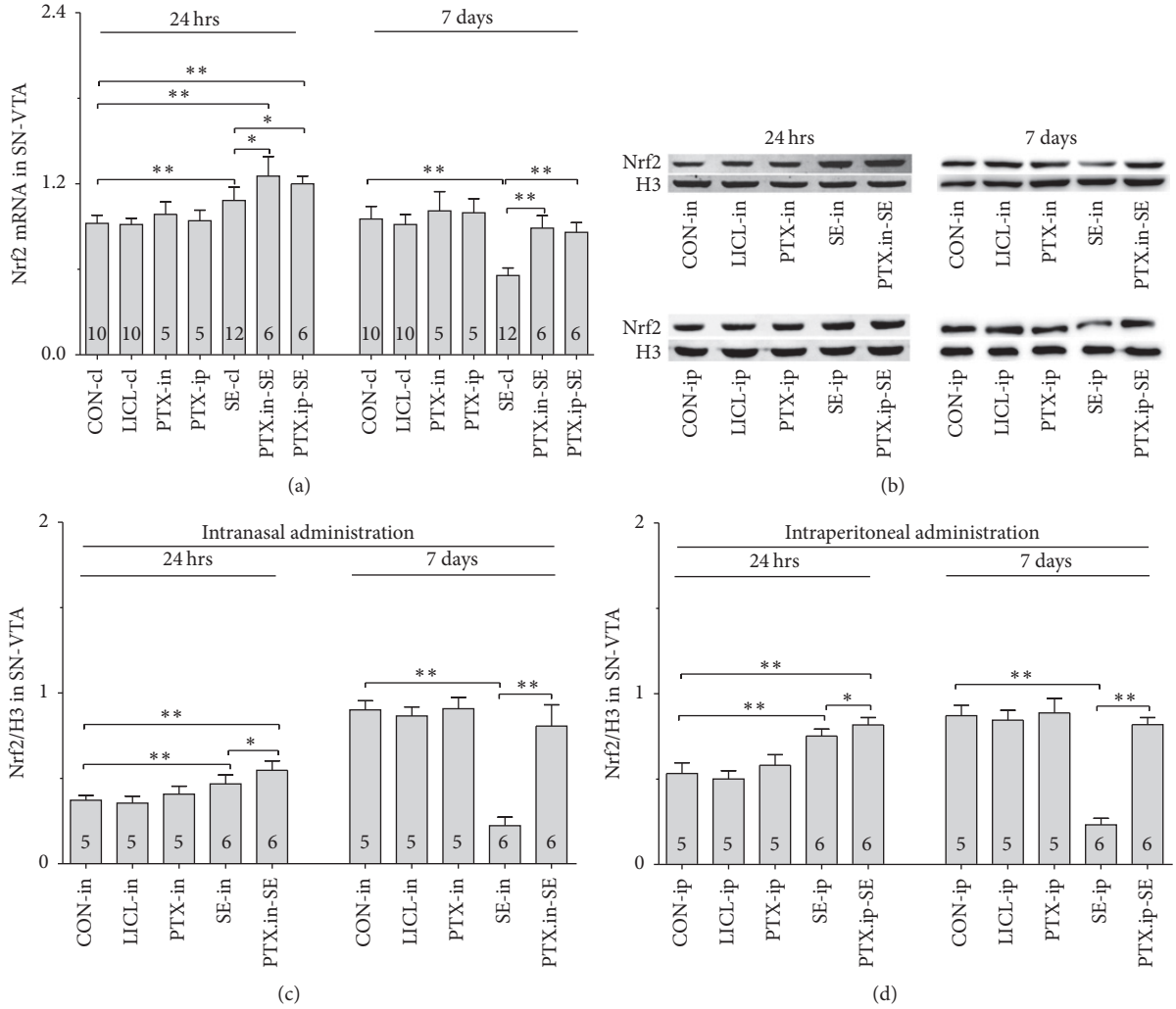

Figure 5: Effects of intranasal and intraperitoneal Ptx pretreatment on Nrf2 in SN-VTA of SE rats induced by Li-Pc 24 hrs and 7 days after Pc injection. (a) Nrf2 mRNA was detected by qPCR. (b–d) Nrf2 protein was measured by Western blot. The results were expressed as the means ± SD. $^{*}P < 0.05$; $^{**}P < 0.01$.

8(d), Hip; $P < 0.01$), HO-1 (Figures 6(b) and 6(d), SN-VTA; Figures 9(b) and 9(d), Hip; $P < 0.01$), and NQO-1 (Figures 7(b) and 7(d), SN-VTA; Figures 10(b) and 10(d), Hip; $P < 0.01$) among CON-ip, LICL-ip, PTX-ip, SE-ip, and PTX.ip-SE rats. The post hoc test showed that the expression of Nrf2, HO-1, and NQO-1 significantly increased in SN-VTA and in Hip of SE-in and SE-ip rats 24 hrs following Pc injection ($P < 0.05$) and then significantly decreased 7 days after Pc administration ($P < 0.01$), compared with corresponding control rats, respectively. In SN-VTA, Ptx pretreatment either by intranasal or intraperitoneal administration to SE rats elevated the levels of Nrf2, HO-1, and NQO-1 ($P < 0.05$). In Hip, except Nrf2 in PTX.in-SE ($P < 0.05$), the increased levels of Nrf2, HO-1, and NQO-1 were not found in PTX.in-SE and in PTX.ip-SE rats 24 hrs following Pc treatment, compared with SE rats. Seven days following Pc administration, the levels of Nrf2, HO-1, and NQO-1 of Hip were higher in Ptx-pretreated rats than in SE rats ($P < 0.05$). Nrf2, HO-1, and NQO-1 were involved in the attenuation of oxidative damage by intranasal Ptx pretreatment to SE rats.

4. Discussion

The present studies revealed that the epileptic seizures, the impaired visuospatial memory, and the defected mesodopaminergic system in SE rats induced by Li-Pc were effectively ameliorated by pretreatment of Ptx via intranasal delivery, as well as via intraperitoneal injection. Ptx pretreatment decreased the levels of LPO and MDA, increased the ratio of GSH/GSSG, and enhanced the transient activation of Nrf2 in SE rats. The enhanced transient activation of Nrf2 was followed by the upregulated HO-1 and NQO-1 in Ptx-pretreated SE rats. Compared with intraperitoneal injection, the poor visuospatial memory and the reduced levels of DA and its metabolites as well as TH and DAT were completely restored to normal levels

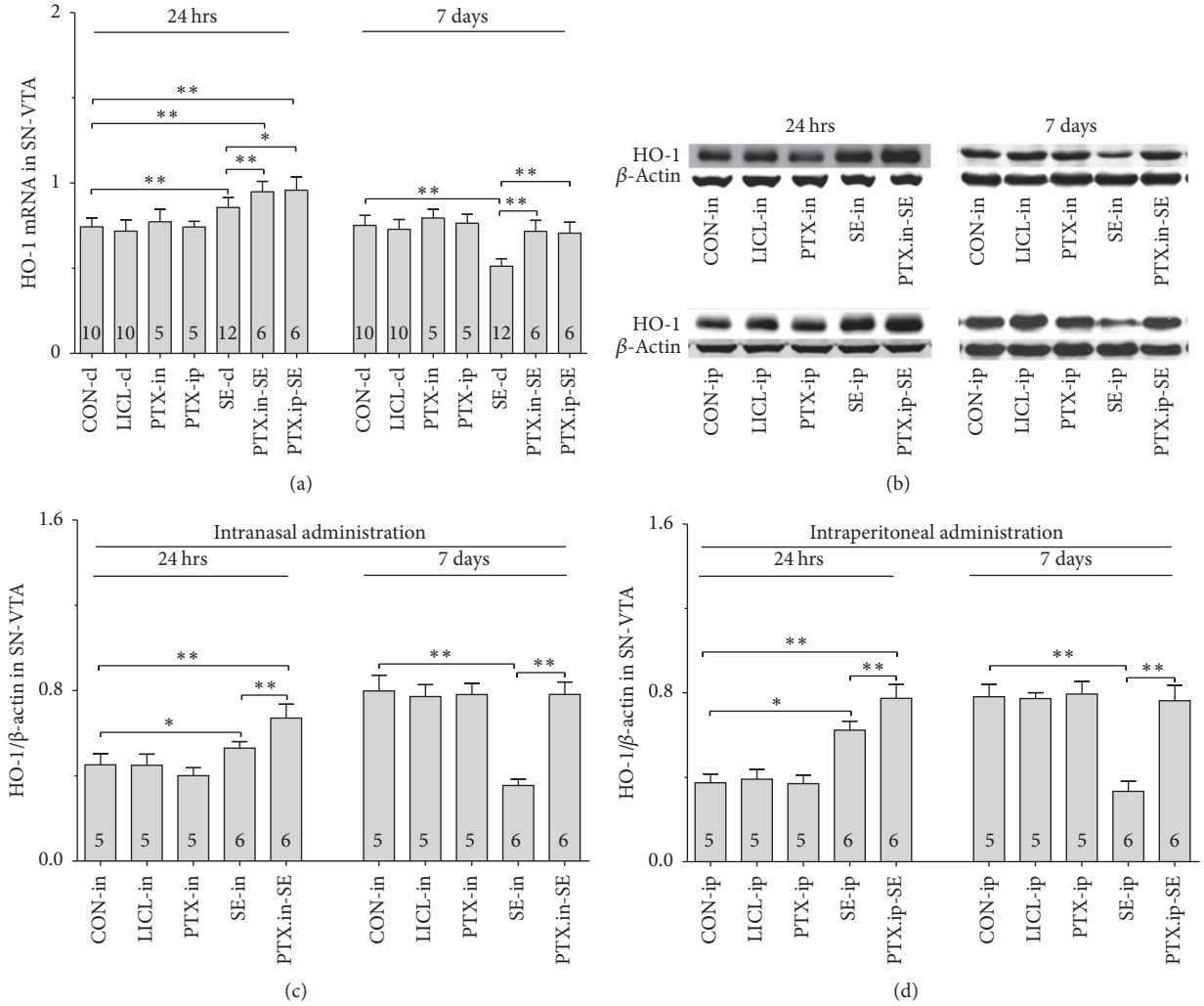

Figure 6: Effects of intranasal and intraperitoneal Ptx pretreatment on HO-1 in SN-VTA of SE rats induced by Li-Pc 24 hrs and 7 days after Pc injection. (a) HO-1 mRNA was detected by qPCR. (b–d) HO-1 protein was measured by Western blot. The results were expressed as the means ± SD. $^{*}P < 0.05$; $^{**}P < 0.01$.

by intranasal pretreatment of Ptx to SE rats. The results above demonstrated the amelioration of epileptic seizures, the alleviation of oxidative damage, and the involvement of Nrf2-ARE pathway in SE rats pretreated by intranasal Ptx.

Lithium-pilocarpine is used to induce SE to reproduce the most features of human SE [25, 26]. The SE rodent model induced by Li-Pc is one of the suitable experimental models in analyzing the pathophysiology of SE [25, 26, 34, 35]. Pilocarpine alone at higher doses not only results in a greater likelihood of induction of SE but also increases mortality rate [36, 37]; however, lithium chloride preadministered within 24 hrs effectively potentiates the epileptogenic action of Pc and simultaneously reduces the mortality of animals [38, 39]. The previous study found that, 30 minutes prior to induction of SE, intraperitoneal injection of Ptx at the dose of 60 mg/kg ameliorated the epileptic seizures best among the dose of 0, 20, 40, and 60 mg/kg [26]. Thus, 20 mg/kg Pc and 60 mg/kg Ptx were used in the present studies. Consistent with the previous studies [25, 26], it was found that all the rats treated by Li-Pc alone exhibited SE, the impaired visuospatial memory, the defected mesodopaminergic system, and the oxidative damage. Intranasal Ptx pretreatment to SE rats significantly delayed the epileptic seizures, ameliorated the deficits in visuospatial memory, restored the mesodopaminergic function, and attenuated the oxidative stress, which indicated that Ptx pretreatment to SE rats had neuroprotective effects.

Oxidative stress is one of the major factors detrimental to neurons in seizures [16, 40]. Epileptic seizures decrease the antioxidant capability and increase oxidative damage [16, 40, 41]. Redox status is a sensitive index of intracellular oxidative stress. GSH/GSSG is a biomarker of redox status in biological systems. We analyzed the ratio of GSH/GSSG by measuring GSH and GSSG in SN-VTA and Hip. GSH, the reduced form of glutathione, was significantly decreased and GSSG, the oxidized form of glutathione, was increased in SN-VTA and Hip of SE rats. GSH and GSSG are redox couples. Glutathione peroxidase catalyzes the reduction of two peroxide molecules using GSH to produce GSSG and water [42]. The diminution

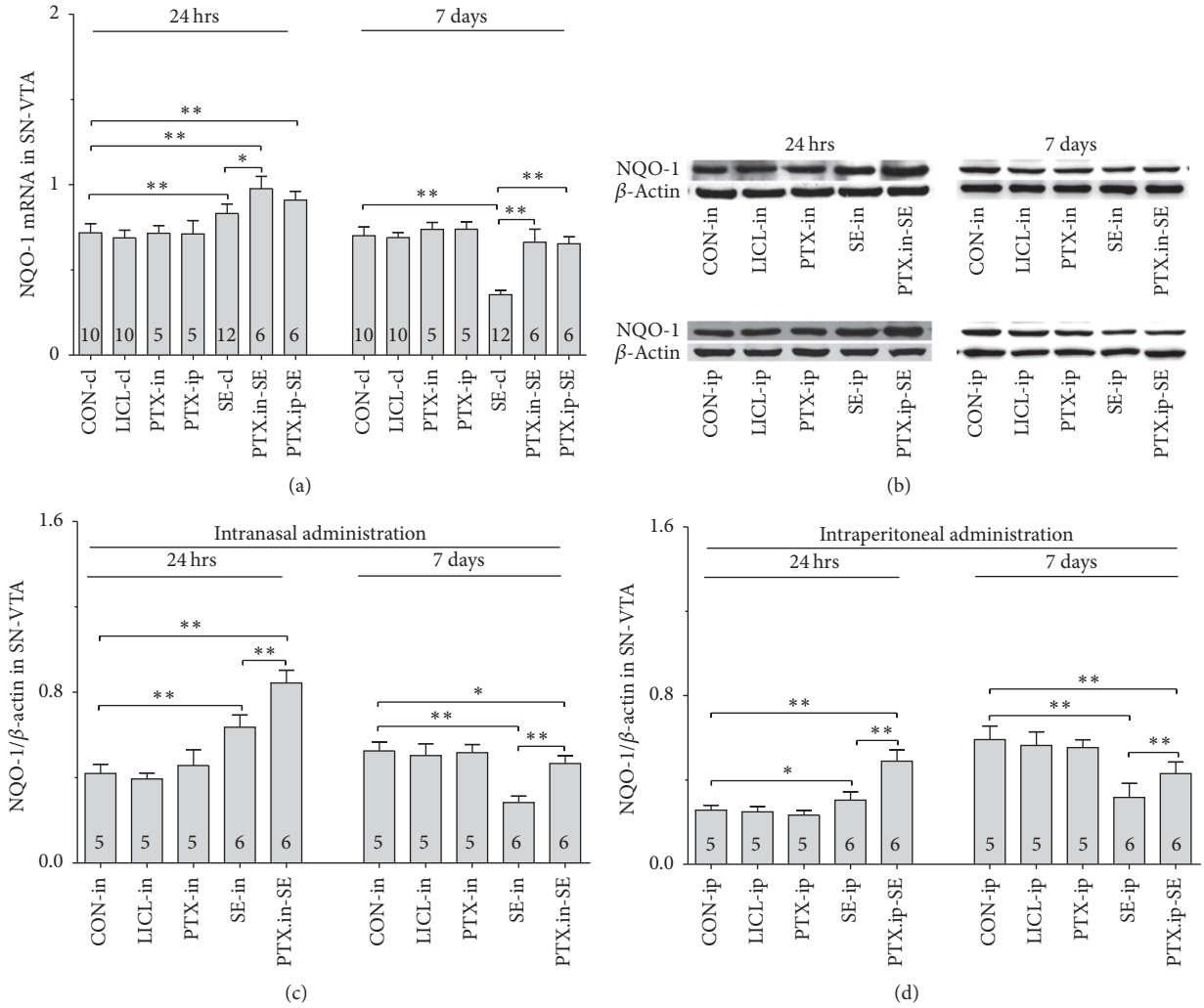

Figure 7: Effects of intranasal and intraperitoneal Ptx pretreatment on NQO-1 in SN-VTA of SE rats induced by Li-Pc 24 hrs and 7 days after Pc injection. (a–c) NQO-1 mRNA was detected by qPCR. (b–d) NQO-1 protein was measured by Western blot. The results were expressed as the means ± SD. $^{*}P < 0.05$; $^{**}P < 0.01$.

of GSH and elevation of GSSG as well as the decreased ratio of GSH/GSSG demonstrated the changes of redox status in SN-VTA and Hip of SE rats. Furthermore, two important lipid peroxidation markers, LPO and MDA, were detected in our studies. LPO and MDA are the products of the peroxidation of lipoproteins and phospholipids of biological membranes [43]. The present studies detected the high levels of LPO and MDA in SN-VTA and Hip of SE rats, which suggested that there was oxidative damage to cells in these brain regions of SE rats. Oxidative damage to cells in both Hip and SN-VTA might underlie the poor visuospatial memory of SE rats. Compared with SE rats, the reduced LPO and MDA as well as the increased ratio of GSH/GSSG suggested the higher antioxidative ability in SN-VTA and in Hip of PTX.in-SE rats. Increased antioxidative ability might be related to Nrf2-ARE pathway, one of important antioxidative defense systems in suppressing oxidative damage to neurons [44–47].

Nrf2 is a transcription factor and constitutes the main oxidative stress response in cells [13, 48]. Under the physiology condition, Nrf2 is located in the cytoplasm. When Nrf2 is activated, it is translocated into the nucleus and combined with the ARE to induce a series of cytoprotective enzymes such as HO-1 [49, 50] and NQO-1 [51, 52] to enhance the antioxidant capacity of cells and protect cells from the oxidative injury [53, 54]. In the present studies, the elevation of Nrf2, HO-1, and NQO-1 at mRNA and protein levels found in SE rats 24 hrs but not 7 days following Li-Pc injection indicated that epileptic seizures could transiently activate Nrf2-ARE pathway [55]. The transient activation of Nrf2-ARE pathway might be a response to the oxidative stress caused by SE [55], but SE-induced Nrf2 activation was not enough to protect neurons from oxidative damage, which underlay the defects in mesodopaminergic system, as well as the elevated LPO and MDA in SN-VTA and Hip of SE rats in the present studies. However, Nrf2-ARE pathway provides a potential target in controlling epileptic seizures [24, 55].

The relevance of Nrf2 in mesolimbic dopaminergic system has not been fully studied; however, it is known that

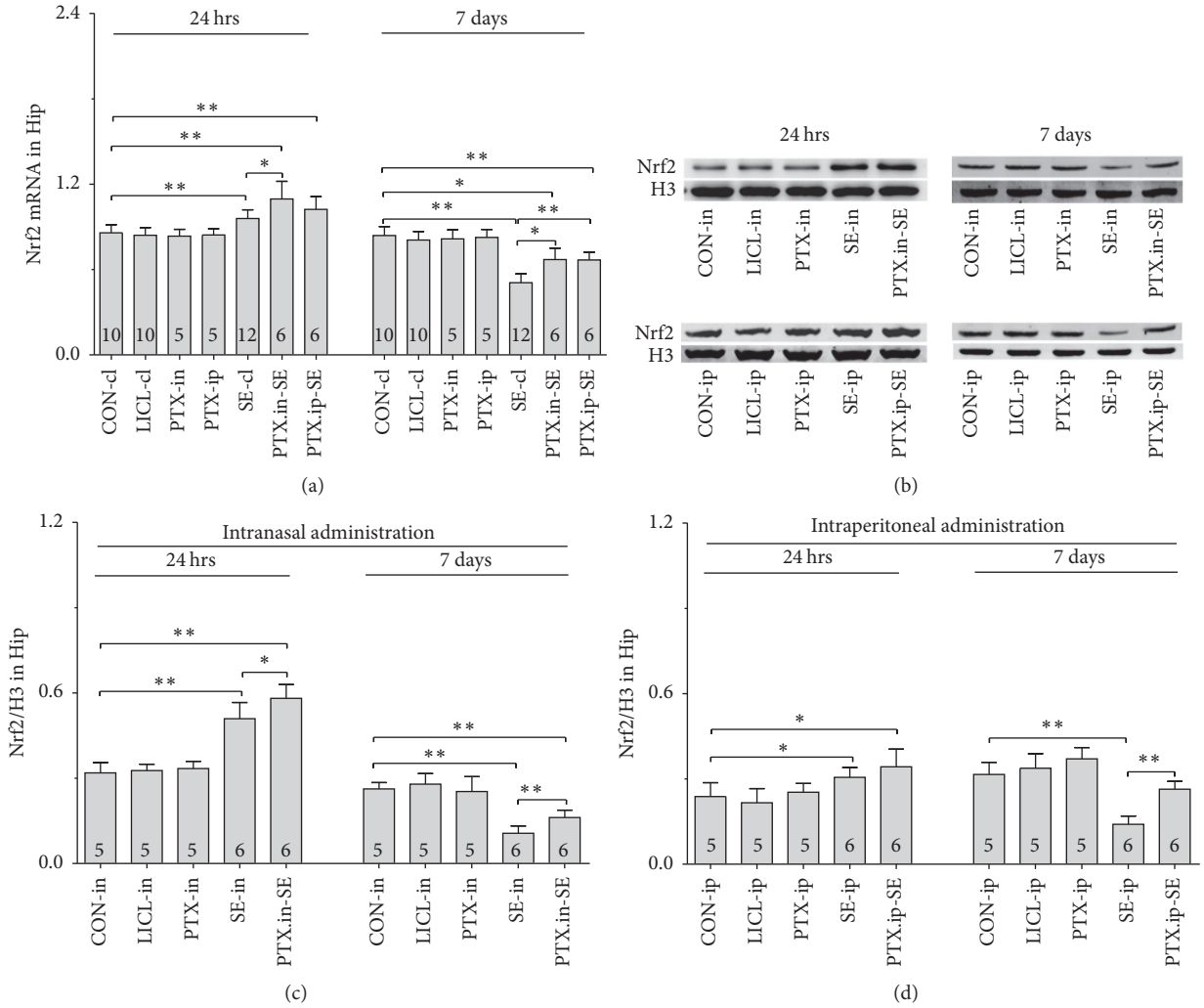

Figure 8: Effects of intranasal and intraperitoneal Ptx pretreatment on Nrf2 in Hip of SE rats induced by Li-Pc 24 hrs and 7 days after Pc injection. (a) Nrf2 mRNA was detected by qPCR. (b–d) Nrf2 protein was measured by Western blot. The results were expressed as the means ± SD. $^{*}P < 0.05$; $^{**}P < 0.01$.

Nrf2 plays more important role in maintaining normal nigral dopaminergic activity and protects the nigral dopaminergic neurons from neurodegeneration by reducing oxidative stress in Parkinson's disease [56–58]. Activation of Nrf2-ARE pathway reduces MPTP-induced neurotoxicity and the death of nigral dopaminergic neurons to a certain extent [46, 57]. Nigral dopaminergic neurons are more susceptible to MPTP-induced damage in Nrf2−/− mice than Nrf2+/+ mice [56–58]. Compared with SE rats, the significant elevation of Nrf2, HO-1, and NQO-1 in SN-VTA and Nrf2 in Hip of intranasal Ptx-pretreated SE rats 24 hrs following Pc injection indicated the region-specific involvement of Nrf2-ARE pathway. The following reasons might account for the discrepancy between SN-VTA and Hip. The first might be the fact that Nrf2 differed between various neuronal subpopulations and regulated different gene products in the nigral neurons versus hippocampal neurons [59]. The second reason might be related to DA. The neurotransmitter DA itself can be a source of oxidative stress. Prior to SE, dopaminergic neurons themselves experience the oxidative stimulus due to autooxidation of DA [60, 61].

Pentoxifylline, as a nonspecific phosphodiesterase inhibitor, might exert its pharmacological effects during the acute phase of SE by decreasing inflammatory cytokine production [62, 63]. Moreover, based on our observations on rats treated by Ptx alone, Ptx did not work as Nrf2 activator, which was consistent with the results published by Ahmed and El-Awdan [64]. Administration of Ptx to rats did not alter Nrf2 expression [64]. Evidences demonstrate that the protective role of Nrf2-ARE pathway is mediated by HO-1 and NQO-1 [24]. Compared with control rats or SE rats 24 hrs following Pc, we found that intranasal Ptx pretreatment to SE rats significantly increased the levels of Nrf2, followed by upregulation of HO-1 and NQO-1 at mRNA and protein levels in Ptx-pretreated SE rats, which suggested that intranasal administration of Ptx might increase the antioxidative capability of cells by enhancing the SE-induced transient activation of Nrf2. Due to the fact that

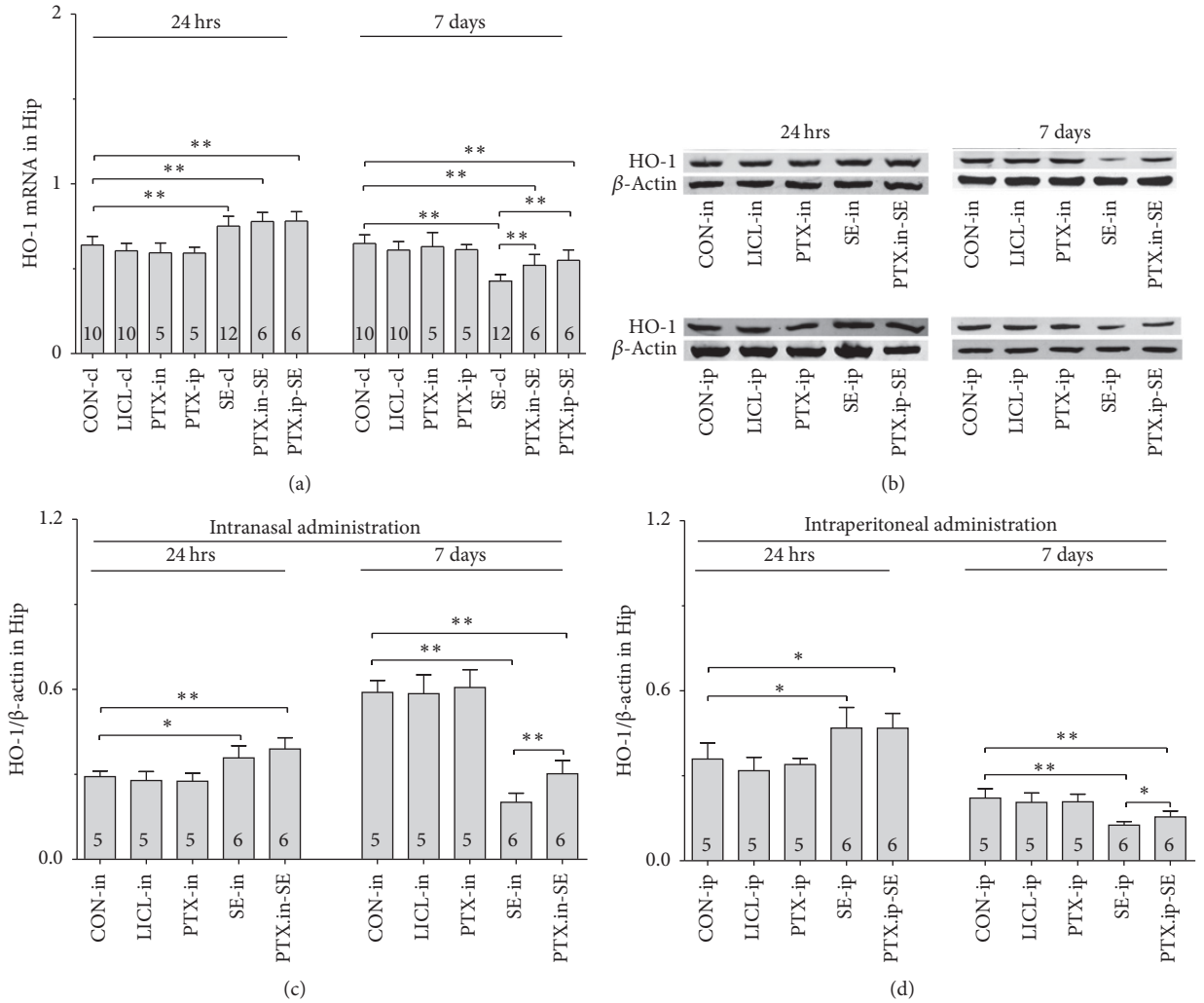

Figure 9: Effects of intranasal and intraperitoneal Ptx pretreatment on HO-1 in Hip of SE rats induced by Li-Pc 24 hrs and 7 days after Pc injection. (a) HO-1 mRNA was detected by qPCR. (b–d) HO-1 protein was measured by Western blot. The results were expressed as the means ± SD. $^{*}P < 0.05$; $^{**}P < 0.01$.

the half-life of Nrf2 is very short [65] and at 24 hrs from SE it could be degraded, the time points we choose were 24 hrs and 7 days after administration of Pc as they encompassed both the acute and latent epileptic conditions [66]. How Nrf2 was enhanced in SE rats by Ptx pretreatment might not be determined 24 hrs following Pc injection. Earlier time points in Nrf2 induction of Ptx-pretreated SE rats following Pc injection are necessary to actually unravel if Ptx is cooperating with SE to induce Nrf2 in the future studies.

The large surface area of the nasal mucosa and the abundant blood supply of the nasal cavity make intranasal administration a viable option for delivery of diverse therapeutic compounds [67, 68]. The unique anatomical connection between the nasal cavity and the brain provides direct nose-to-brain delivery of drugs to target the brain through pathways along the olfactory and trigeminal nerves innervating the nasal cavity [5, 7]. The restoration of impaired visuospatial memory and mesodopaminergic activity in PTX.in-SE rats indicated that intranasal administration of Ptx effectively targets the brain. Compared with PTX.ip-SE rats, the parameters in visuospatial memory and mesodopaminergic system observed in PTX.in-SE rats were completely recovered to the level of control rats 7 days after Pc injection; however, the partial parameters in visuospatial memory and mesodopaminergic system were still lower in PTX.ip-SE rats than in controls. Intranasal administration of Ptx seemed more efficient in controlling SE than intraperitoneal injection. In addition to nose-to-blood-to-brain route (an extensive nasal absorption of the Ptx to the bloodstream), direct nose-to-brain route might be involved in targeting a substantial fraction of Ptx to the brain. Furthermore, Ptx administered intranasally might be reaching the brain expectedly much earlier than through intraperitoneal administration prior to coming insults. Whether a direct transport of Ptx was occurring from nose to the brain, Ptx concentration levels in different cerebral regions and the corresponding rostral-to-caudal biodistribution patterns should be determined following both routes of administration in the future studies.

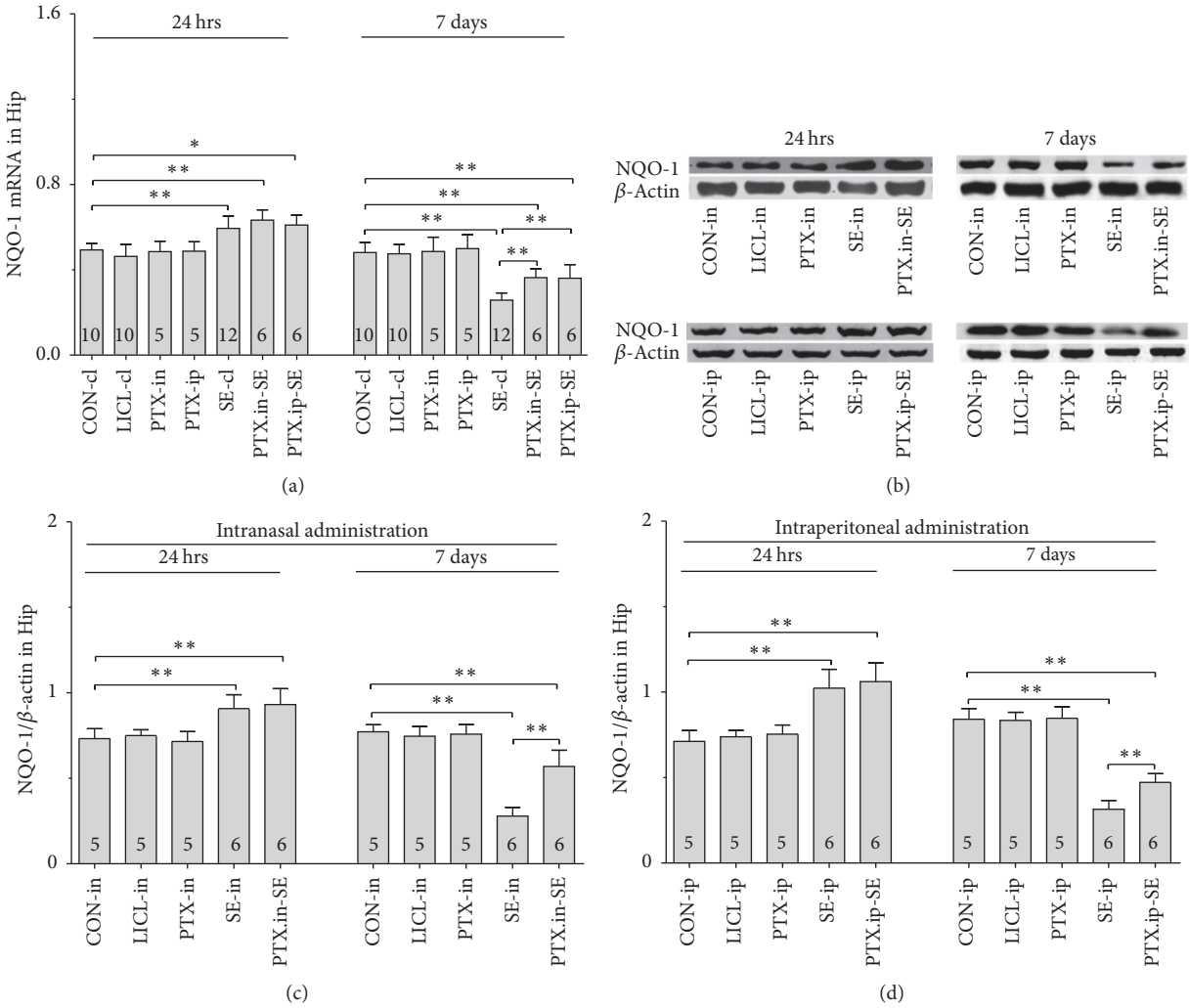

Figure 10: Effects of intranasal and intraperitoneal Ptx pretreatment on NQO-1 in Hip of SE rats induced by Li-Pc 24 hrs and 7 days after Pc injection. (a–c) NQO-1 mRNA was detected by qPCR. (b–d) NQO-1 protein was measured by Western blot. The results were expressed as the means ± SD. $^{*}P < 0.05$; $^{**}P < 0.01$.

In conclusion, intranasal delivery of Ptx to rats significantly suppressed the epileptic seizures induced by Li-Pc, ameliorated the deficits in visuospatial memory and in mesodopaminergic system, and enhanced the transient activation of Nrf2 in SE rats. Intranasal administration of Ptx could effectively protect cells from oxidative damage in SE and may hopefully become a noninvasive, painless, and easily administered option for epileptic patients.

Conflicts of Interest

The authors declare that there are no conflicts of interest.

Authors' Contributions

Yunxiao Kang and Wensheng Yan contributed equally to this work.

Acknowledgments

This work was supported by the Science and Technology Department of Hebei Province of China (Grant no. 12277728) and by Hebei Medical University (Grant no. kyfz022).

References

[1] F. Al-Mufti and J. Claassen, "Neurocritical care: status epilepticus review," *Critical Care Clinics*, vol. 30, no. 4, pp. 751–764, 2014.

[2] M. Ahmad, "Protective effects of curcumin against lithium-pilocarpine induced status epilepticus, cognitive dysfunction and oxidative stress in young rats," *Saudi Journal of Biological Sciences*, vol. 20, no. 2, pp. 155–162, 2013.

[3] R. Kälviäinen, "Intranasal therapies for acute seizures," *Epilepsy and Behavior*, vol. 49, pp. 303–306, 2015.

[4] M. Zelcer and R. D. Goldman, "Intranasal midazolam for seizure cessation in the community setting," *Canadian Family Physician*, vol. 62, no. 7, pp. 559–561, 2016.

[5] J. J. Lochhead and R. G. Thorne, "Intranasal delivery of biologics to the central nervous system," *Advanced Drug Delivery Reviews*, vol. 64, no. 7, pp. 614–628, 2012.

[6] A. Serralheiro, G. Alves, A. Fortuna, and A. Falcão, "Intranasal administration of carbamazepine to mice: a direct delivery pathway for brain targeting," *European Journal of Pharmaceutical Sciences*, vol. 60, pp. 32–39, 2014.

[7] A. Serralheiro, G. Alves, A. Fortuna, and A. Falcão, "Direct nose-to-brain delivery of lamotrigine following intranasal administration to mice," *International Journal of Pharmaceutics*, vol. 490, no. 1-2, pp. 39–46, 2015.

[8] M. Anderson, P. Tambe, H. Sammons, H. Mulla, R. Cole, and I. Choonara, "Pharmacokinetics of buccal and intranasal lorazepam in healthy adult volunteers," *European Journal of Clinical Pharmacology*, vol. 68, no. 2, pp. 155–159, 2012.

[9] M. Holsti, B. L. Sill, S. D. Firth, F. M. Filloux, S. M. Joyce, and R. A. Furnival, "Prehospital intranasal midazolam for the treatment of pediatric seizures," *Pediatric Emergency Care*, vol. 23, no. 3, pp. 148–153, 2007.

[10] J. Folbergrová, P. Ješina, N. Kubová, R. Druga, and J. Otáhal, "Status epilepticus in immature rats is associated with oxidative stress and mitochondrial dysfunction," *Frontiers in Cellular Neuroscience*, vol. 10, article 136, 2016.

[11] V. Mishra, B. Shuai, M. Kodali et al., "Resveratrol treatment after status epilepticus restrains neurodegeneration and abnormal neurogenesis with suppression of oxidative stress and inflammation," *Scientific Reports*, vol. 5, Article ID 17807, 2015.

[12] J. N. Pearson, S. Rowley, L.-P. Liang, A. M. White, B. J. Day, and M. Patel, "Reactive oxygen species mediate cognitive deficits in experimental temporal lobe epilepsy," *Neurobiology of Disease*, vol. 82, pp. 289–297, 2015.

[13] L. Carmona-Aparicio, C. Pérez-Cruz, C. Zavala-Tecuapetla et al., "Overview of Nrf2 as therapeutic target in epilepsy," *International Journal of Molecular Sciences*, vol. 16, no. 8, pp. 18348–18367, 2015.

[14] K. J. Davies, M. E. Delsignore, and S. W. Lin, "Protein damage and degradation by oxygen radicals. II. Modification of amino acids," *Journal of Biological Chemistry*, vol. 262, no. 20, pp. 9902–9907, 1987.

[15] L. Packer and E. Cadenas, "Oxidants and antioxidants revisited. New concepts of oxidative stress," *Free Radical Research*, vol. 41, no. 9, pp. 951–952, 2007.

[16] R. M. Freitas, S. M. M. Vasconcelos, F. C. F. Souza, G. S. B. Viana, and M. M. F. Fonteles, "Oxidative stress in the hippocampus after pilocarpine-induced status epilepticus in Wistar rats," *FEBS Journal*, vol. 272, no. 6, pp. 1307–1312, 2005.

[17] M. Lafon-Cazal, S. Pietri, M. Culcasi, and J. Bockaert, "NMDA-dependent superoxide production and neurotoxicity," *Nature*, vol. 364, no. 6437, pp. 535–537, 1993.

[18] E. K. Michaelis, "Molecular biology of glutamate receptors in the central nervous system and their role in excitotoxicity, oxidative stress and aging," *Progress in Neurobiology*, vol. 54, no. 4, pp. 369–415, 1998.

[19] N. Basar, L. Nahar, O. A. Oridupa et al., "Utilization of the ability to induce activation of the nuclear factor (erythroid-derived 2)-like factor 2 (Nrf2) to assess potential cancer chemopreventive activity of liquorice samples," *Phytochemical Analysis*, vol. 27, no. 5, pp. 233–238, 2016.

[20] D. M. Miller, I. N. Singh, J. A. Wang, and E. D. Hall, "Nrf2-ARE activator carnosic acid decreases mitochondrial dysfunction, oxidative damage and neuronal cytoskeletal degradation following traumatic brain injury in mice," *Experimental Neurology*, vol. 264, pp. 103–110, 2015.

[21] M.-K. Kwak, K. Itoh, M. Yamamoto, and T. W. Kensler, "Enhanced expression of the transcription factor Nrf2 by cancer chemopreventive agents: role of antioxidant response element-like sequences in the nrf2 promoter," *Molecular and Cellular Biology*, vol. 22, no. 9, pp. 2883–2892, 2002.

[22] A. S. Ahmad, H. Zhuang, and S. Doré, "Heme oxygenase-1 protects brain from acute excitotoxicity," *Neuroscience*, vol. 141, no. 4, pp. 1703–1708, 2006.

[23] G. Chen, Q. Fang, J. Zhang, D. Zhou, and Z. Wang, "Role of the Nrf2-ARE pathway in early brain injury after experimental subarachnoid hemorrhage," *Journal of Neuroscience Research*, vol. 89, no. 4, pp. 515–523, 2011.

[24] W. Wang, Y. Wu, G. Zhang et al., "Activation of Nrf2-ARE signal pathway protects the brain from damage induced by epileptic seizure," *Brain Research*, vol. 1544, pp. 54–61, 2014.

[25] M. Ahmad, G. M. Abu-Taweel, A. E. Aboshaiqah, and J. S. Ajarem, "The effects of quinacrine, proglumide, and pentoxifylline on seizure activity, cognitive deficit, and oxidative stress in rat lithium-pilocarpine model of status epilepticus," *Oxidative Medicine and Cellular Longevity*, vol. 2014, Article ID 630509, 11 pages, 2014.

[26] M. Tariq, M. Ahmad, K. A. Moutaery, and S. A. Deeb, "Pentoxifylline ameliorates lithium-pilocarpine induced status epilepticus in young rats," *Epilepsy and Behavior*, vol. 12, no. 3, pp. 354–365, 2008.

[27] Y. Bozzi and E. Borrelli, "The role of dopamine signaling in epileptogenesis," *Frontiers in Cellular Neuroscience*, vol. 7, article no. 157, 2013.

[28] R. M. De Freitas, F. C. F. De Sousa, S. M. M. Vasconcelos, G. S. B. Viana, and M. M. D. F. Fonteles, "Acute alterations of neurotransmitters levels in striatum of young rat after pilocarpine-induced status epilepticus," *Arquivos de Neuro-Psiquiatria*, vol. 61, no. 2B, pp. 430–433, 2003.

[29] C. Ciumas, T.-B. R. Wahlin, A. Jucaite, P. Lindstrom, C. Halldin, and I. Savic, "Reduced dopamine transporter binding in patients with juvenile myoclonic epilepsy," *Neurology*, vol. 71, no. 11, pp. 788–794, 2008.

[30] I. Odano, A. Varrone, I. Savic et al., "Quantitative PET analyses of regional [11C]PE2I binding to the dopamine transporter—application to juvenile myoclonic epilepsy," *NeuroImage*, vol. 59, no. 4, pp. 3582–3593, 2012.

[31] A. I. Rojo, C. Montero, M. Salazar et al., "Persistent penetration of MPTP through the nasal route induces Parkinson's disease in mice," *European Journal of Neuroscience*, vol. 24, no. 7, pp. 1874–1884, 2006.

[32] R. J. Racine, "Modification of seizure activity by electrical stimulation: II. Motor seizure," *Electroencephalography and Clinical Neurophysiology*, vol. 32, no. 3, pp. 281–294, 1972.

[33] R. R. González, R. F. Fernández, J. L. M. Vidal, A. G. Frenich, and M. L. G. Pérez, "Development and validation of an ultra-high performance liquid chromatography-tandem mass-spectrometry (UHPLC-MS/MS) method for the simultaneous determination of neurotransmitters in rat brain samples," *Journal of Neuroscience Methods*, vol. 198, no. 2, pp. 187–194, 2011.

[34] G. Curia, D. Longo, G. Biagini, R. S. G. Jones, and M. Avoli, "The pilocarpine model of temporal lobe epilepsy," *Journal of Neuroscience Methods*, vol. 172, no. 2, pp. 143–157, 2008.

[35] C. Dubé, S. Boyet, C. Marescaux, and A. Nehlig, "Relationship between neuronal loss and interictal glucose metabolism during

the chronic phase of the lithium-pilocarpine model of epilepsy in the immature and adult rat," *Experimental Neurology*, vol. 167, no. 2, pp. 227–241, 2001.

[36] D. B. Clifford, J. W. Olney, A. Maniotis, R. C. Collins, and C. F. Zorumski, "The functional anatomy and pathology of lithium-pilocarpine and high-dose pilocarpine seizures," *Neuroscience*, vol. 23, no. 3, pp. 953–968, 1987.

[37] L. Zhao, T. Nagao, G. C. Desjardins, P. Gloor, and M. Avoli, "Quantitative evaluation of neuronal loss in the dorsal hippocampus in rats with long-term pilocarpine seizures," *Epilepsy Research*, vol. 17, no. 3, pp. 237–247, 1994.

[38] R. Druga, H. Kubová, L. Suchomelová, and R. Haugvicová, "Lithium/pilocarpine status epilepticus-induced neuropathology of piriform cortex and adjoining structures in rats is age-dependent," *Physiological Research*, vol. 52, no. 2, pp. 251–264, 2003.

[39] H. Kubová, P. Mareš, L. Suchomelová, G. Brožek, R. Druga, and A. Pitkänen, "Status epilepticus in immature rats leads to behavioural and cognitive impairment and epileptogenesis," *European Journal of Neuroscience*, vol. 19, no. 12, pp. 3255–3265, 2004.

[40] B. Martinc, I. Grabnar, and T. Vovk, "Antioxidants as a preventive treatment for epileptic process: a review of the current status," *Current Neuropharmacology*, vol. 12, no. 6, pp. 527–550, 2014.

[41] T. C. Diniz, J. C. Silva, S. R. G. de Lima-Saraiva et al., "The role of flavonoids on oxidative stress in epilepsy," *Oxidative Medicine and Cellular Longevity*, vol. 2015, Article ID 171756, 9 pages, 2015.

[42] N. Cardenas-Rodriguez, B. Huerta-Gertrudis, L. Rivera-Espinosa et al., "Role of oxidative stress in refractory epilepsy: evidence in patients and experimental models," *International Journal of Molecular Sciences*, vol. 14, no. 1, pp. 1455–1476, 2013.

[43] H. F. Poon, V. Calabrese, G. Scapagnini, and D. A. Butterfield, "Free radicals and brain aging," *Clinics in Geriatric Medicine*, vol. 20, no. 2, pp. 329–359, 2004.

[44] N. G. Innamorato, A. Jazwa, A. I. Rojo et al., "Different susceptibility to the parkinson's toxin MPTP in mice lacking the redox master regulator Nrf2 or its target gene heme oxygenase-1," *PLoS ONE*, vol. 5, no. 7, Article ID e11838, 2010.

[45] H. Kumar, S. Koppula, I.-S. Kim, S. V. More, B.-W. Kim, and D.-K. Choi, "Nuclear factor erythroid 2 - related factor 2 signaling in Parkinson disease: a promising multi therapeutic target against oxidative stress, neuroinflammation and cell death," *CNS and Neurological Disorders—Drug Targets*, vol. 11, no. 8, pp. 1015–1029, 2012.

[46] Y.-H. Tsou, C.-T. Shih, C.-H. Ching et al., "Treadmill exercise activates Nrf2 antioxidant system to protect the nigrostriatal dopaminergic neurons from MPP+ toxicity," *Experimental Neurology*, vol. 263, pp. 50–62, 2015.

[47] G. Zhang, S. Li, Y. Kang et al., "Enhancement of dopaminergic activity and region-specific activation of Nrf2-ARE pathway by intranasal supplements of testosterone propionate in aged male rats," *Hormones and Behavior*, vol. 80, pp. 103–116, 2016.

[48] H. Zhang, K. J. A. Davies, and H. J. Forman, "Oxidative stress response and Nrf2 signaling in aging," *Free Radical Biology and Medicine*, vol. 88, pp. 314–336, 2015.

[49] T. Ishii, K. Itoh, S. Takahashi et al., "Transcription factor Nrf2 coordinately regulates a group of oxidative stress-inducible genes in macrophages," *Journal of Biological Chemistry*, vol. 275, no. 21, pp. 16023–16029, 2000.

[50] F. A. D. T. G. Wagener, H. E. Van Beurden, J. W. Von den Hoff, G. J. Adema, and C. G. Figdor, "The heme-heme oxygenase system: a molecular switch in wound healing," *Blood*, vol. 102, no. 2, pp. 521–528, 2003.

[51] K. Iskander, J. Li, S. Han, B. Zheng, and A. K. Jaiswal, "NQO1 and NQO2 regulation of humoral immunity and autoimmunity," *Journal of Biological Chemistry*, vol. 281, no. 41, pp. 30917–30924, 2006.

[52] A. K. Jaiswal, "Regulation of genes encoding NAD(P)H: quinone oxidoreductases," *Free Radical Biology and Medicine*, vol. 29, no. 3-4, pp. 254–262, 2000.

[53] Z. Dong, H. Shang, Y. Q. Chen, L. Pan, M. Bhatia, and J. Sun, "Sulforaphane protects pancreatic acinar cell injury by modulating Nrf2-mediated oxidative stress and NLRP3 inflammatory pathway," *Oxidative Medicine and Cellular Longevity*, vol. 2016, Article ID 7864150, 12 pages, 2016.

[54] K. Takayama, H. Kaneko, K. Kataoka et al., "Nuclear factor (Erythroid-Derived)-related factor 2-associated retinal pigment epithelial cell protection under blue light-induced oxidative stress," *Oxidative Medicine and Cellular Longevity*, vol. 2016, Article ID 8694641, 9 pages, 2016.

[55] W. Wang, W.-P. Wang, G.-L. Zhang et al., "Activation of Nrf2-ARE signal pathway in hippocampus of amygdala kindling rats," *Neuroscience Letters*, vol. 543, pp. 58–63, 2013.

[56] P.-C. Chen, M. R. Vargas, A. K. Pani et al., "Nrf2-mediated neuroprotection in the MPTP mouse model of Parkinson's disease: critical role for the astrocyte," *Proceedings of the National Academy of Sciences of the United States of America*, vol. 106, no. 8, pp. 2933–2938, 2009.

[57] A. Jazwa, A. I. Rojo, N. G. Innamorato, M. Hesse, J. Fernández-Ruiz, and A. Cuadrado, "Pharmacological targeting of the transcription factor NRf2 at the basal ganglia provides disease modifying therapy for experimental parkinsonism," *Antioxidants and Redox Signaling*, vol. 14, no. 12, pp. 2347–2360, 2011.

[58] A. I. Rojo, N. G. Innamorato, A. M. Martín-Moreno, M. L. De Ceballos, M. Yamamoto, and A. Cuadrado, "Nrf2 regulates microglial dynamics and neuroinflammation in experimental Parkinson's disease," *GLIA*, vol. 58, no. 5, pp. 588–598, 2010.

[59] A. D. Kraft, D. A. Johnson, and J. A. Johnson, "Nuclear factor E2-related factor 2-dependent antioxidant response element activation by tert-butylhydroquinone and sulforaphane occurring preferentially in astrocytes conditions neurons against oxidative insult," *Journal of Neuroscience*, vol. 24, no. 5, pp. 1101–1112, 2004.

[60] B. Fornstedt, E. Pileblad, and A. Carlsson, "In vivo autoxidation of dopamine in guinea pig striatum increases with age," *Journal of Neurochemistry*, vol. 55, no. 2, pp. 655–659, 1990.

[61] A. Slivka and G. Cohen, "Hydroxyl radical attack on dopamine," *Journal of Biological Chemistry*, vol. 260, no. 29, pp. 15466–15472, 1985.

[62] S. Kwiecień, T. Brzozowski, P. C. Konturek et al., "Gastroprotection by pentoxyfilline against stress-induced gastric damage. Role of lipid peroxidation, antioxidizing enzymes and proinflammatory cytokines," *Journal of Physiology and Pharmacology*, vol. 55, no. 2, pp. 337–355, 2004.

[63] L. J. Marques, L. Zheng, N. Poulakis, J. Guzman, and U. Costabel, "Pentoxifylline inhibits TNF-α production from human alveolar macrophages," *American Journal of Respiratory and Critical Care Medicine*, vol. 159, no. 2, pp. 508–511, 1999.

[64] M. A. E. Ahmed and S. A. El-Awdan, "Lipoic acid and pentoxifylline mitigate nandrolone decanoate-induced neurobehavioral perturbations in rats via re-balance of brain neurotransmitters, up-regulation of Nrf2/HO-1 pathway, and down-regulation of TNFR1 expression," *Hormones and Behavior*, vol. 73, pp. 186–199, 2015.

[65] A. Kobayashi, M.-I. Kang, H. Okawa et al., "Oxidative stress sensor Keap1 functions as an adaptor for Cul3-based E3 ligase to regulate proteasomal degradation of Nrf2," *Molecular and Cellular Biology*, vol. 24, no. 16, pp. 7130–7139, 2004.

[66] S. Waldbaum, L.-P. Liang, and M. Patel, "Persistent impairment of mitochondrial and tissue redox status during lithium-pilocarpine-induced epileptogenesis," *Journal of Neurochemistry*, vol. 115, no. 5, pp. 1172–1182, 2010.

[67] A. A. Hussain, "Intranasal drug delivery," *Advanced Drug Delivery Reviews*, vol. 29, no. 1-2, pp. 39–49, 1998.

[68] A. Pires, A. Fortuna, G. Alves, and A. Falcão, "Intranasal drug delivery: how, why and what for?" *Journal of Pharmacy and Pharmaceutical Sciences*, vol. 12, no. 3, pp. 288–311, 2009.

Hindawi
Oxidative Medicine and Cellular Longevity
Volume 2017, Article ID 4353462, 13 pages
https://doi.org/10.1155/2017/4353462

Research Article

Pentaerythritol Tetranitrate In Vivo Treatment Improves Oxidative Stress and Vascular Dysfunction by Suppression of Endothelin-1 Signaling in Monocrotaline-Induced Pulmonary Hypertension

Sebastian Steven,[1,2] Matthias Oelze,[1] Moritz Brandt,[1,2] Elisabeth Ullmann,[1] Swenja Kröller-Schön,[1] Tjebo Heeren,[1] Lan P. Tran,[1] Steffen Daub,[1] Mobin Dib,[1] Dirk Stalleicken,[3] Philip Wenzel,[1,2] Thomas Münzel,[1] and Andreas Daiber[1]

[1]*Center for Cardiology, Department of Cardiology, Mainz, Germany*
[2]*Center of Thrombosis and Hemostasis, University Medical Center Mainz, Mainz, Germany*
[3]*Freelancer Consultant, 76199 Karlsruhe, Germany*

Correspondence should be addressed to Andreas Daiber; daiber@uni-mainz.de

Received 21 November 2016; Accepted 19 January 2017; Published 28 February 2017

Academic Editor: Neven Zarkovic

Objective. Oxidative stress and endothelial dysfunction contribute to pulmonary arterial hypertension (PAH). The role of the nitrovasodilator pentaerythritol tetranitrate (PETN) on endothelial function and oxidative stress in PAH has not yet been defined. *Methods and Results*. PAH was induced by monocrotaline (MCT, i.v.) in Wistar rats. Low (30 mg/kg; MCT30), middle (40 mg/kg; MCT40), or high (60 mg/kg; MCT60) dose of MCT for 14, 28, and 42 d was used. MCT induced endothelial dysfunction, pulmonary vascular wall thickening, and fibrosis, as well as protein tyrosine nitration. Pulmonary arterial pressure and heart/body and lung/body weight ratio were increased in MCT40 rats (28 d) and reduced by oral PETN (10 mg/kg, 24 d) therapy. Oxidative stress in the vascular wall, in the heart, and in whole blood as well as vascular endothelin-1 signaling was increased in MCT40-treated rats and normalized by PETN therapy, likely by upregulation of heme oxygenase-1 (HO-1). PETN therapy improved endothelium-dependent relaxation in pulmonary arteries and inhibited endothelin-1-induced oxidative burst in whole blood and the expression of adhesion molecule (ICAM-1) in endothelial cells. *Conclusion*. MCT-induced PAH impairs endothelial function (aorta and pulmonary arteries) and increases oxidative stress whereas PETN markedly attenuates these adverse effects. Thus, PETN therapy improves pulmonary hypertension beyond its known cardiac preload reducing ability.

1. Introduction

In humans, pulmonary arterial hypertension (PAH) is defined by a mean pulmonary arterial pressure of ≥25 mmHg at rest. It is a complex, multifactorial disease that involves endothelial dysfunction, oxidative stress, and remodeling of pulmonary vessels [1]. Concerning the pathophysiology of PAH the imbalance of the endothelial-derived vasoactive molecules nitric oxide (NO), prostacyclin (PGI_2), superoxide ($O_2^{\bullet-}$), and endothelin-1 (ET-1) plays a critical role [2–4]. Decreased bioavailability of NO, caused by increased formation of ROS, will result in an uncontrolled proliferation of smooth muscle cells (SMC), increased vascular tone, and therefore increased vascular resistance [5, 6]. Importantly, oxidative stress can stimulate both, the expressions of the ET-1 gene in endothelial cells and in SMC [7, 8]. Likewise, ET-1 signaling can trigger the production of reactive oxygen species (ROS) and inhibition of ET-1 receptor (A and B) by bosentan reduces oxidative stress in pulmonary hypertension [9].

In rodent models of PAH several enzymatic sources being responsible for increased ROS production have been

identified such as the NADPH oxidase (Nox), xanthine oxidase (XO), an uncoupled endothelial NO synthase (eNOS), and mitochondria [10–14]. In patients suffering from PAH, increased oxidative stress and XO activity have been demonstrated [15]. 3-nitrotyrosine (3-NT) levels, a foot print for in vivo formation of the NO and superoxide ($O_2^{\bullet-}$) reaction product peroxynitrite ($ONOO^-$), have been shown to be increased in lung biopsy samples of patients suffering from PAH [16]. These data clearly indicate that lungs of PAH patients are exposed to chronic oxidative stress likely leading to reduced NO bioavailability [15, 16].

Organic nitrates, given acutely, are potent NO dependent vasodilators used for the treatment of chronic stable angina and unstable angina, myocardial infarction, congestive heart failure, and arterial hypertension [17]. Although organic nitrates are theoretically beneficial in PAH, because of their properties as a vasodilator, they have been used with limited clinical results because of the lack of pulmonary selectivity [18]. Therefore, inhaled NO and nitroglycerin (NTG) were tested for the treatment of PAH [19–21]. In experimental MCT-induced PAH, the organic nitrate and K^+-channel opener, nicorandil, showed beneficial effects: right ventricular systolic pressure (RVSP) was decreased, accompanied by higher expression of eNOS and less endothelial damage [22].

Pentaerythritol tetranitrate (PETN; IUPAC 2,2-Bis[(nitrooxy)methyl]propane-1,3-diyl dinitrate, Figure 3(a)) is an organic nitrate with fewer side effects on the vasculature than other nitrates like NTG, isosorbide-5-mononitrate (ISMN), or isosorbide dinitrate (ISDN) [17, 23, 24]. In humans PETN causes side effects like headache, hypotension, or tachycardia. However, the therapeutic range is broad since LD_{50}/24 h in rats is >900 mg/kg [25, 26]. Due to its limited solubility in water (43 mg/L at 25°C) oral treatment is preferably performed by diet [27]. In contrast to ISMN or NTG, PETN improved vascular function in animal models of diabetes and hypertension [27, 28]. The beneficial effects and favorable side effects profile of PETN have been attributed to the induction of the antioxidant enzymes heme oxygenase-1 (HO-1), ecSOD, and ferritin [28–32].

Since PAH is improved by HO-1 induction [33, 34], PETN is a potential candidate drug for treatment of this severe disease, currently investigated within the CAESAR clinical trial ("ClinicAl Efficacy Study of Pentalong® for PulmonAry Hypertension in HeaRt Failure"; EudraCT Number: 2009-015059-26). We therefore focused on the influence of the organic nitrate PETN on pulmonary arterial pressure, vascular function, and oxidative stress in MCT-induced PAH.

2. Methods

For isometric tension studies, NTG was obtained from a Nitrolingual infusion solution (1 mg/mL) from G. Pohl-Boskamp (Hohenlockstedt, Germany). The Bradford reagent was obtained from BioRad (Munich, Germany). PETN (20%)/lactose (80%) mixture was a kind gift of Actavis Deutschland GmbH (now PUREN Pharma GmbH & Co. KG, Munich, Germany). There is no measurable degradation of PETN when stored dry and solid but in this state PETN is pressure-sensitive and highly explosive. For this reason PETN is stored and shipped as a lactose mixture (usually >80 w/w% lactose). The solubility of PETN in DMSO is excellent: stock solutions of >100 mM are easy to prepare and can be stored for months at −20°C without serious loss of PETN. In aqueous solutions PETN is slowly hydrolyzed over days. All other chemicals were obtained from Fluka, Sigma-Aldrich, or Merck.

2.1. Animals and In Vivo Treatment. 90 male Wistar rats (8 weeks, 250 g) were used for the experiments. All animals were treated in accordance with the Guide for the Care and Use of Laboratory Animals as adopted by the US National Institutes of Health. Approval was granted by the Ethics Committee of the University Hospital Mainz and the Landesuntersuchungsamt (#23 177-07/G 10-1-039). Monocrotaline (MCT) injection was used as a model for pulmonary arterial hypertension. For characterization of the model, isometric tension studies were performed 2, 4, and 6 weeks after single i.v. injection of 30, 40, and 60 mg/kg body weight MCT into the *vena dorsalis penis*. In regard to effectiveness of PAH induction and mortality of the animals, the 40 mg/kg MCT dose for 4 weeks was chosen for experiments with the organic nitrate and PETN (10 mg/kg/day, p.o.) therapy by diet (Ssniff Spezialdiäten, Soest, Germany) was started 3 days after MCT injection. The control and MCT group received standard diet without PETN. After 3.5 weeks of PETN treatment, rats were killed by exsanguination in isoflurane anaesthesia, and the blood, aorta, pulmonary artery, and heart were collected.

2.2. Isometric Tension Recordings. Perivascular fat was removed from every aorta and pulmonary arteries. Concentration-relaxation curves in response to increasing concentrations acetylcholine (ACh) were performed as described [35].

2.3. Histological Staining of Lung Tissue. Trichrome staining (according to Oelze et al.) was performed with paraffin-embedded samples of lung tissue upon deparaffination as described [36]. Afterwards the nuclei were prestained with haematoxylin (according to Meloan and Puchtler) [37]. Then samples were stained for 5 minutes with Mallory red containing 100% acetic acid, fuchsine acid, and Orange G (Merck, Darmstadt, Germany), then for 15 minutes in 1% molybdatophosphoric acid hydrate (VWR, Darmstadt, Germany), and then for 5 minutes in acid light green. Finally tissue samples were dehydrated in glacial acetic acid and 100% ethanol and coverslipped in Entellan®.

2.4. Determination of Heart to Body (h/b) and Lung to Body (l/b) Weight Ratio. Heart to body and lung to body weight ratio were determined by weighing animals prior to sacrifice. After organ removal weight of heart and lung was measured. Every individual body weight was set into relation to heart and lung weight of the animal.

2.5. Small Animal Echocardiography. Anaesthesia of rats was induced in a chamber (2–4% isoflurane mixed with 0.2 L/min

100% O_2) and maintained with a face mask (1-2% isoflurane with 0.2 L/min 100% O_2). Animals were kept on a heated table mounted on a rail system (Visual Sonics, Toronto, Canada). Ultrasound was performed with the Vevo 770 System and a 25 MHz transducer (VisualSonics). Heart rate was monitored; body temperature was monitored using a rectal probe and maintained at 37°C. Two-dimensional images of the pulmonary valve were obtained from the parasternal short-axis view at the level of the aortic valve and pulsed-wave Doppler recordings of the blood flow at the tips of the cusps of the pulmonary valve were obtained with the beam oriented parallel to the flow. The sweep speed for the Doppler flow recordings was 400–800 mm/s. Pulmonary arterial acceleration time (PAT) was measured and systolic pulmonary arterial pressure (sPAP) was calculated as described [38].

2.6. Dot Blot and Western Blot Analysis. 3-nitrotyrosine positive proteins were assessed by dot blot analysis [28]. For detection of 3-NT, a primary mouse monoclonal nitrotyrosine antibody (Millipore, Billerica, USA) was used at a dilution of 1 : 1000. Detection and quantification were performed by ECL with peroxidase conjugated secondary antibodies against mouse (1 : 10000, Vector Lab., Burlingame, CA). Densitometric quantification of antibody-specific dots was performed with a ChemiLux Imager (CsX-1400M, Intas, Göttingen, Germany) and Gel-Pro Analyzer software (Media Cybernetics, Bethesda, MD).

Isolated aortic and pulmonary tissue from rat was frozen in liquid nitrogen and homogenized in buffer (Tris-HCl 20 mM, saccharose 250 mM, ethylene glycol-bis(β-aminoethyl ether)-N,N,N′,N′-tetraacetic acid (EGTA) 3 mM, ethylene diamine tetraacetic acid (EDTA) 20 mM, protease inhibitor cocktail (Roche complete, 1 tablet in 100 mL), and Triton-X-100 1 v/v%). Proteins were separated by SDS-Page and blotted onto nitrocellulose membranes [23]. After blocking, immunoblotting was performed with the following antibodies: monoclonal mouse β-actin (42 kDa) as a control for loading and transfer and polyclonal mouse NADPH oxidase 2 (Nox2, 1 : 500, BD Bioscience, USA). Detection and quantification were performed by ECL with peroxidase conjugated anti-mouse (1 : 10,000, Vector Lab., Burlingame, CA). Densitometric quantification as described above.

2.7. Detection of Oxidative Stress in Cardiac Membrane Fractions, Pulmonary Arteries, Aortic Vessels, and Serum and Blood Samples. Reactive oxygen species formation was measured by oxidative burst of leukocytes in whole blood (stimulated with the phorbol ester PDBu, 10 μM) or NADPH oxidase activity in the heart by ECL (100 μM L-012 and 5 μM lucigenin plus 200 μM NADPH, respectively) [39]. For ROS formation in pulmonary vessels, isolated pulmonary artery rings were OCT-embedded (Tissue Tek, USA) and upon staining with dihydroethidium (DHE, 1 μM) oxidative fluorescence microtopography was determined as reported [40]. Xanthine oxidase activity was measured in serum, which was diluted 1 : 1 with cytochrome c (100 μM) in PBS containing either hypoxanthine (1 mM) or allopurinol (1 mM) [41]. The superoxide-driven reduction of cytochrome c was measured by the absorption of ferrous cytochrome c at 550 nm as the difference between hypoxanthine and allopurinol containing buffer. Superoxide formation rates were calculated using ε_{550} = 19,500 mM^{-1} cm^{-1} for reduced cytochrome c. Total serum antioxidant capacity was measured by the reduction of the stabilized 2,2-diphenyl-1-picrylhydrazyl radical ($DPPH^{\bullet}$) (50 μM) by serum antioxidants tracing the absorption at 517 nm [27].

2.8. Reverse Transcription Real-Time PCR (qRT-PCR). mRNA expression was analyzed with quantitative real-time RT-PCR as previously described [42]. Briefly, total RNA from rat lung was isolated (RNeasy Fibrous Tissue Mini Kit; Qiagen, Hilden, Germany), and 50 ng of total RNA was used for real-time RT-PCR analysis with the QuantiTectTM Probe RT-PCR kit (Qiagen). TaqMan® Gene Expression assays for heme oxygenase (HO-1), vascular adhesion molecule-1 (VCAM-1), endothelin-1 (ET-1), endothelin-1 a receptor, endothelin-1 b receptor, endothelin converting enzyme-1 (ECE-1), intercellular adhesion molecule-1 (ICAM-1), and TATA box binding protein (TBP) were purchased as probe-and-primer sets (Applied Biosystems, Foster City, CA). The comparative Ct method was used for relative mRNA quantification. Gene expression was normalized to the endogenous control (TBP mRNA), and the amount of target gene mRNA expression in each sample was expressed relative to that of control.

2.9. Chemiluminescence-Based Detection of Oxidative Burst of Leukocytes in Whole Blood. Human samples were obtained and handled in accordance with the Declaration of Helsinki and our institutional ethical guidelines. Whole blood was obtained from at least four different healthy volunteers by vein puncture. Oxidative burst mainly reflects NADPH oxidase (Nox) and myeloperoxidase activity and was therefore used as a read-out for the degree of activation of white blood cells in whole blood. Briefly, blood was incubated with PETN, stimulated with the ET-1 analog BQ-3020 (0.05 μM, 0.5 μM, and 5 μM), and ROS formation was assessed in PBS containing Ca^{2+}/Mg^{2+} (1 mM) by L-012 (100 μM) enhanced chemiluminescence (ECL).

2.10. ICAM-1 Expression in Cultured Endothelial Cells. The human endothelial cell line EA.hy 926 was a gift from C.-J. S. Edgell (University of North Carolina at Chapel Hill, USA). EA.hy 926 cells were grown at 10% CO_2 in Dulbecco's modified Eagle's medium (DMEM, Sigma) with 10% fetal calf serum, 2 mM l-glutamine, 1 mM sodium pyruvate, 100 IU/mL penicillin, and 100 μg/mL streptomycin. Semiconfluent cells (6-well plates) were used for further experiments. Cultured endothelial cells (Ea.hy) were incubated with 5 μM BQ3020 (endothelin-1 analog), 100 μM PETN, or solvent (DMSO). After 24 hours cells were lyzed in GIT-buffer (guanidinium isocyanate, sodium-citrate, and N-lauroylsarcosine) and mRNA was isolated by phenol extraction.

2.11. Statistical Analysis. Results are expressed as mean ± SEM. Two-way ANOVA (with Bonferroni's correction for

comparison of multiple means) was used for comparisons of vasodilator potency and efficacy and kinetic traces of whole blood oxidative burst. *T*-test was used for comparison of MCT-induced changes in endothelial function (expressed as changes in efficacy (maximal relaxation)) between two groups. One-way ANOVA (with Bonferroni's or Dunn's correction for comparison of multiple means) was used for comparisons of heart/body and lung/body weight, echocardiography, blood, cardiac, aortic, and whole blood ROS formation, and protein and mRNA expression. p values < 0.05 were considered as statistically significant.

3. Results

3.1. MCT Induces PAH, Pulmonary Fibrosis, and Nitro-Oxidative Stress. Four weeks following MCT40 treatment, PAP of rats was significantly increased up to 53.96 ± 5.28 mmHg versus 26.63 ± 2.26 mmHg in controls ($p < 0.05$). PAH caused vascular wall thickening in small and medium sized vessels as well as fibrosis (Figure 1(a)). MCT40 and MCT60 treatment significantly increased staining of 3-NT positive proteins in the lungs, while MCT30 showed no difference to control (Figure 1(b)). The total antioxidant capacity in serum was significantly decreased by MCT40 (Figure 1(c)).

3.2. Effects of MCT-Induced PAH on Vascular Function of Aorta and Pulmonary Arteries. MCT treatment impaired endothelium-dependent relaxation of the aorta to ACh dose-dependently, with a significant difference in the MCT60 group compared to controls (Figure 2(a)). Also endothelial function of pulmonary arteries was significantly impaired in response to middle and high dose of MCT (Figure 2(b)). To further characterize the MCT-induced pulmonary hypertension model, vascular function in response to the highest MCT60 dose was tested in a time-dependent fashion (2 and 4 weeks, longer treatment (for 6 weeks) resulted in significant (>50%) mortality of the animals). Endothelium-dependent vasodilation in aorta (Figure 2(c)) and pulmonary arteries (Figure 2(d)) was examined 2 and 4 weeks after MCT administration. Vascular function was impaired significantly in response to 4 weeks of treatment for aorta and all treatment durations for pulmonary arteries. The dose of MCT40 (40 mg/kg for 4 weeks) was used for all other experiments.

3.3. Effects of PETN on Pulmonary Arterial Pressure and Cardiac and Lung/Pulmonary Artery Hypertrophy in PAH. Heart to body (h/b) and lung to body (l/b) weight ratio of MCT40 treated rats were increased as a sign for cardiac hypertrophy due to high cardiac afterload and pulmonary hypertension (Figures 3(b) and 3(c)). Additionally, pulmonary arteries were dilated (Figure 3(d)). The organic nitrate PETN significantly improved these morphological changes. PETN treatment prevented a further significant increase in PAP in the MCT40 group (Figure 3(e)).

3.4. Effects of PETN on Vascular Function of Pulmonary Arteries and Nitro-Oxidative Stress in PAH. PETN did not significantly improve PAH induced endothelial dysfunction of the aorta (Figure 4(a)) while ameliorating endothelial function of pulmonary vessels in the PAH group (MCT40) (Figure 4(b)). DHE fluorescence increased throughout the wall (endothelium, media, and adventitia) of pulmonary arteries in the setting of PAH and was normalized by PETN (Figure 4(c)). The content of 3-NT positive proteins in lung tissue, determined by dot blot analysis, was significantly increased in the PAH group and reduced by PETN (Figure 4(d)).

3.5. Effects of PETN Therapy on Systemic Oxidative Stress in PAH. Cardiac NADPH oxidase (Nox) activity, which was markedly increased in PAH, was completely normalized by PETN treatment (Figure 5(a)), which was supported by Nox2 protein expression showing a similar pattern (Figure 5(f)). The oxidative burst measured in whole blood (as a readout for phagocytic NADPH oxidase activity) was increased in MCT40 rats and normalized in the PETN group (Figure 5(b)). Furthermore, activity of xanthine oxidase (XO) was increased by MCT treatment and completely normalized by PETN therapy (Figure 5(c)). mRNA levels of the antioxidant enzyme HO-1 in lung tissue were significantly increased in pulmonary hypertension and the administration of PETN led to an additional increase in HO-1 expression (Figure 5(d)). It might be speculated that prevention of the nitro-oxidative stress by PETN therapy also ameliorated the inflammatory phenotype in the MCT40 animals as demonstrated by assessment of VCAM-1 mRNA expression (Figure 5(e)).

3.6. Effects of PETN Therapy on Endothelin-1 Signaling in PAH. In MCT-treated groups the pulmonary mRNA expression levels of ET-1, endothelin converting enzyme (ECE-1), ET_A (ET-1a), and ET_B (ET-1b) receptor were significantly increased compared to healthy control rats. Treatment of pulmonary hypertension with PETN led to a normalization of ET-1, ECE-1, ET-1a, and ET-1b mRNA expression levels (Figures 6(a)–6(d)). Incubation of human whole blood with the ET-1 analog BQ-3020 induced a concentration-dependent increase of oxidative burst (Figure 6(e)), whereas PETN incubation significantly reduced the oxidative burst in BQ-3020/zymosan A-stimulated blood (Figure 6(f)). Furthermore, longer incubations (24 hours) with the ET-1 analog BQ-3020 induced adhesion molecule (ICAM-1) mRNA expression in cultured endothelial cells (EA.hy), which was ameliorated by PETN coincubation (Figure 6(g)).

4. Discussion

The results of the present study demonstrate that the organic nitrate PETN reduces oxidative stress and improves endothelial function of pulmonary arteries in monocrotaline-induced PAH. We identified modulation of heme oxygenase-1 expression and endothelin-1 signaling to be responsible for the beneficial effects of PETN in PAH. Recent treatment guidelines recommend treatment of PAH with macitentan (endothelin-1 receptor blocker), sildenafil (PDE5-inhibitor), iloprost (prostacyclin analog), or newly introduced riociguat

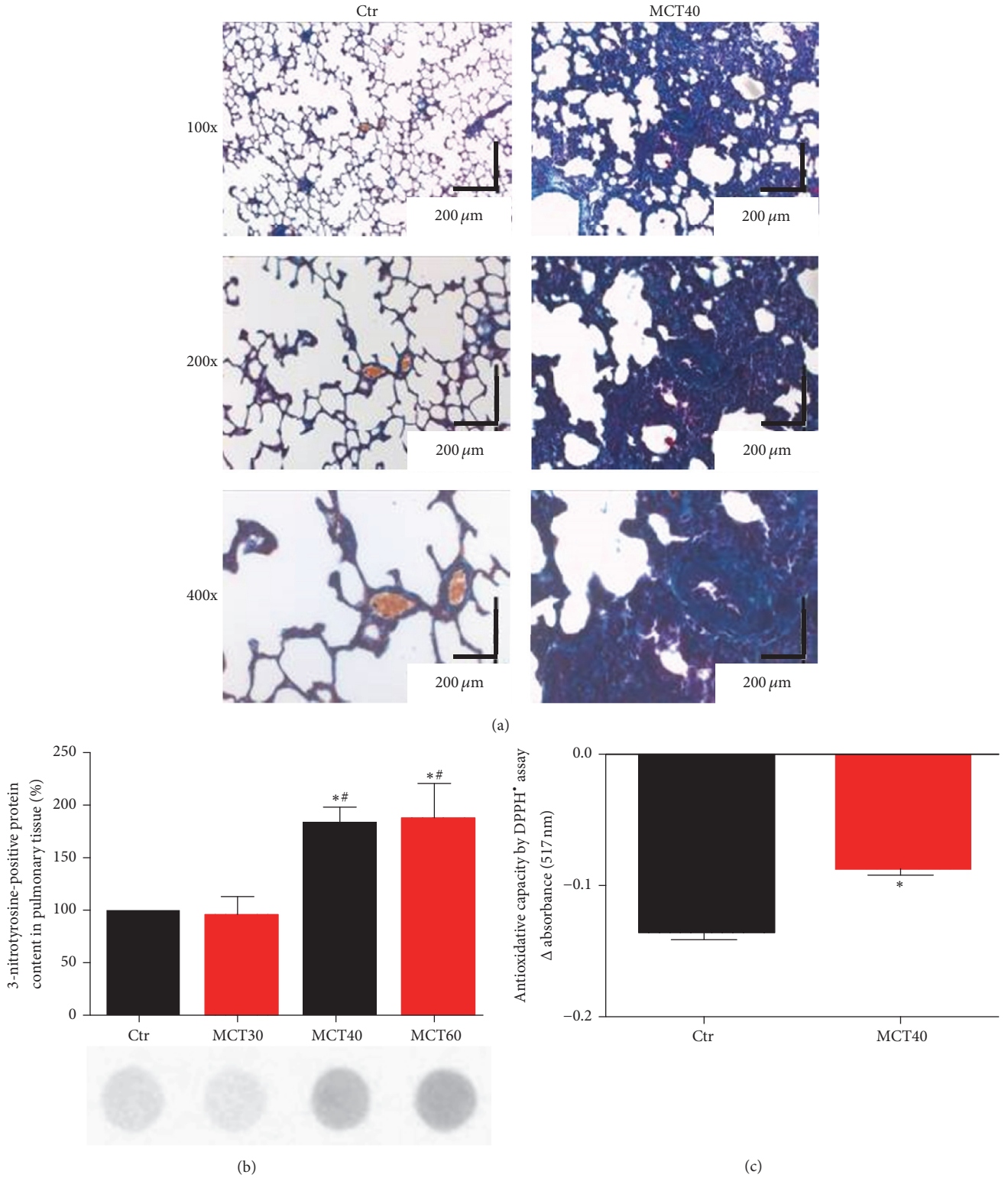

Figure 1: Characterization of morphological changes and protein nitration in lung tissue and serum antioxidant capacity of monocrotaline-treated rats. (a) Trichrome staining of paraffinated lung tissue (magnification of 100x, 200x, and 400x). (b) Levels of 3-NT positive proteins in lung tissue were assessed by dot blot analysis and specific antibodies. Representative blots are shown below the densitometric quantification. (c) Antioxidant capacity was determined by DPPH• assay (ΔE 517 nm). The data are mean ± SEM from 3–8 (a, b) and 3–6 (c) animals/group. $^{*}p < 0.05$ versus control and $^{\#}p < 0.05$ versus MCT30.

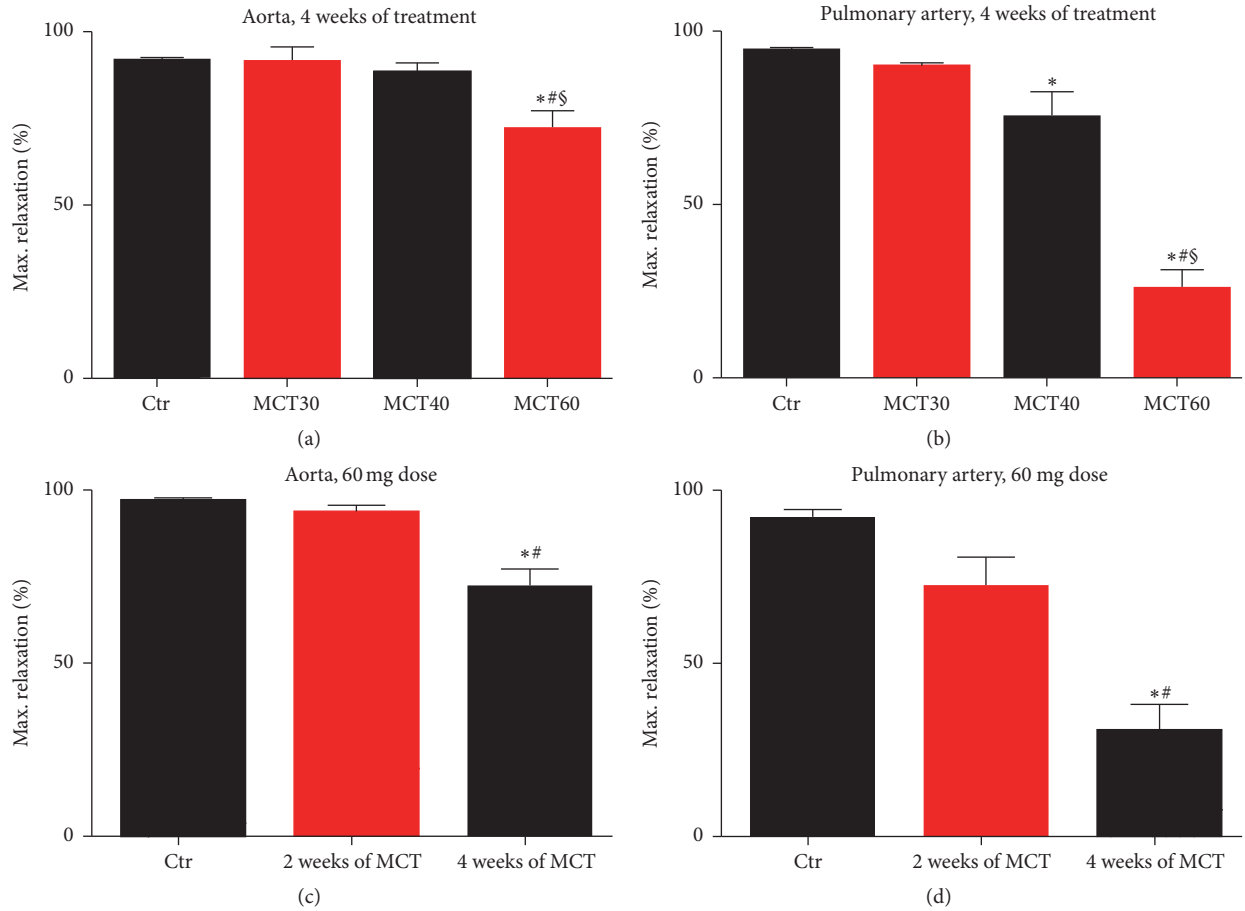

Figure 2: Characterization of vascular function in the model of monocrotaline-induced pulmonary hypertension. Endothelium-dependent (ACh) maximum relaxation was determined by isometric tension studies in aortic ring segments (a, c) and pulmonary ring segments (b, d) from rats treated with different doses of MCT and different time protocols for the induction of pulmonary hypertension. A total number of 4–22 (a, b) and 6–14 (c) and 6 (d) aortic and pulmonary artery ring segments from at least 3 male rats were used. $^{*}p < 0.05$ versus control (a–d); $^{\#}p < 0.05$ versus MCT30 (a, b) or 2 weeks (c, d); $^{\S}p < 0.05$ versus MCT40 (a, b).

(sGC stimulator) [43]. All compounds improve PAH mainly via dilation of the pulmonary vessels and therefore reduction of pulmonary vascular resistance (PVR). A vasodilating drug with additional anti-inflammatory and antioxidant properties could be a useful tool to improve therapy of PAH. Additionally, PETN was shown to reduce ET-1 plasma levels in human, which might be another approach for protective effects in PAH [44].

MCT is a toxic alkaloid from *Crotalaria spectabilis* and was used for induction of PAH. In the MCT PAH-model vascular wall thickening and pulmonary inflammation involving neutrophil infiltration lead to high afterload of the right ventricle, which consequently results in cardiac hypertrophy [45]. Antioxidant capacity in serum of MCT-treated animals was reduced and 3-nitrotyrosine-positive protein content in pulmonary vessels was increased dependent on the MCT dose used. Accordingly, endothelium-dependent relaxation not only in pulmonary arteries but also in aorta was impaired in a MCT-dose dependent fashion. Investigations on the effect of the natural phenol and antioxidant resveratrol on MCT-induced pulmonary hypertension revealed the important role of oxidative stress in PAH [10]. In pulmonary hypertensive rats, resveratrol attenuated right ventricular blood pressure, pulmonary artery remodeling (SMC proliferation), and pulmonary inflammation (reduced leukocyte infiltration). The latter study as well as other preclinical and clinical investigations on pulmonary hypertension underlines the role of oxidative stress in the pathogenesis of PAH [15, 16, 46–48].

As we demonstrated before, the organic nitrate PETN is different to other nitrates like nitroglycerin (NTG) or isosorbide dinitrate (ISDN) [17, 49, 50]. Acute treatment with organic nitrates such as NTG has potent vasodilator and antiischemic effects in patients with acute coronary syndromes, congestive heart failure, and arterial hypertension. However, long-term treatment is associated with nitrate tolerance and endothelial dysfunction, which reduces the therapeutic efficacy of these drugs. PETN seems to be different and human studies in healthy volunteers and patients with coronary artery disease showed preserved vasodilatatory potency and

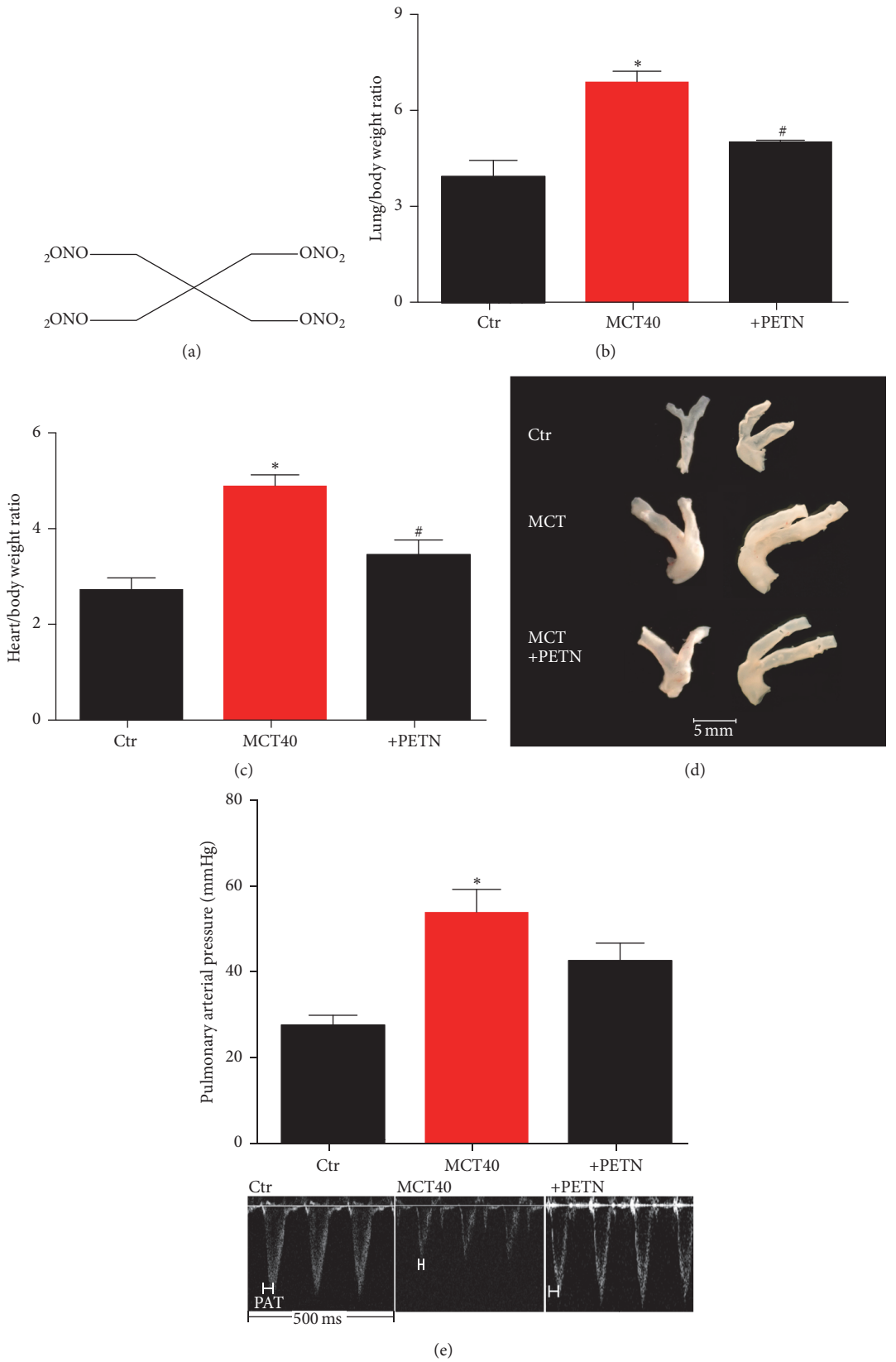

Figure 3: Effects of PETN therapy on heart/body and lung/body weight ratio, pulmonary artery dilation, and pulmonary arterial pressure in monocrotaline-treated rats (MCT40, 4 weeks). (a) Chemical structure of PETN. (b) Lung/body and (c) heart/body weight ratio were determined. (d) Pulmonary artery dilation was qualitatively envisaged by photographic images. (e) Echocardiography was used to measure pulmonary arterial pressure. The data are mean ± SEM of 4 (b, c) and 3-4 (d, e) animals per group $^{*}p < 0.05$ versus control and $^{\#}p < 0.05$ versus MCT.

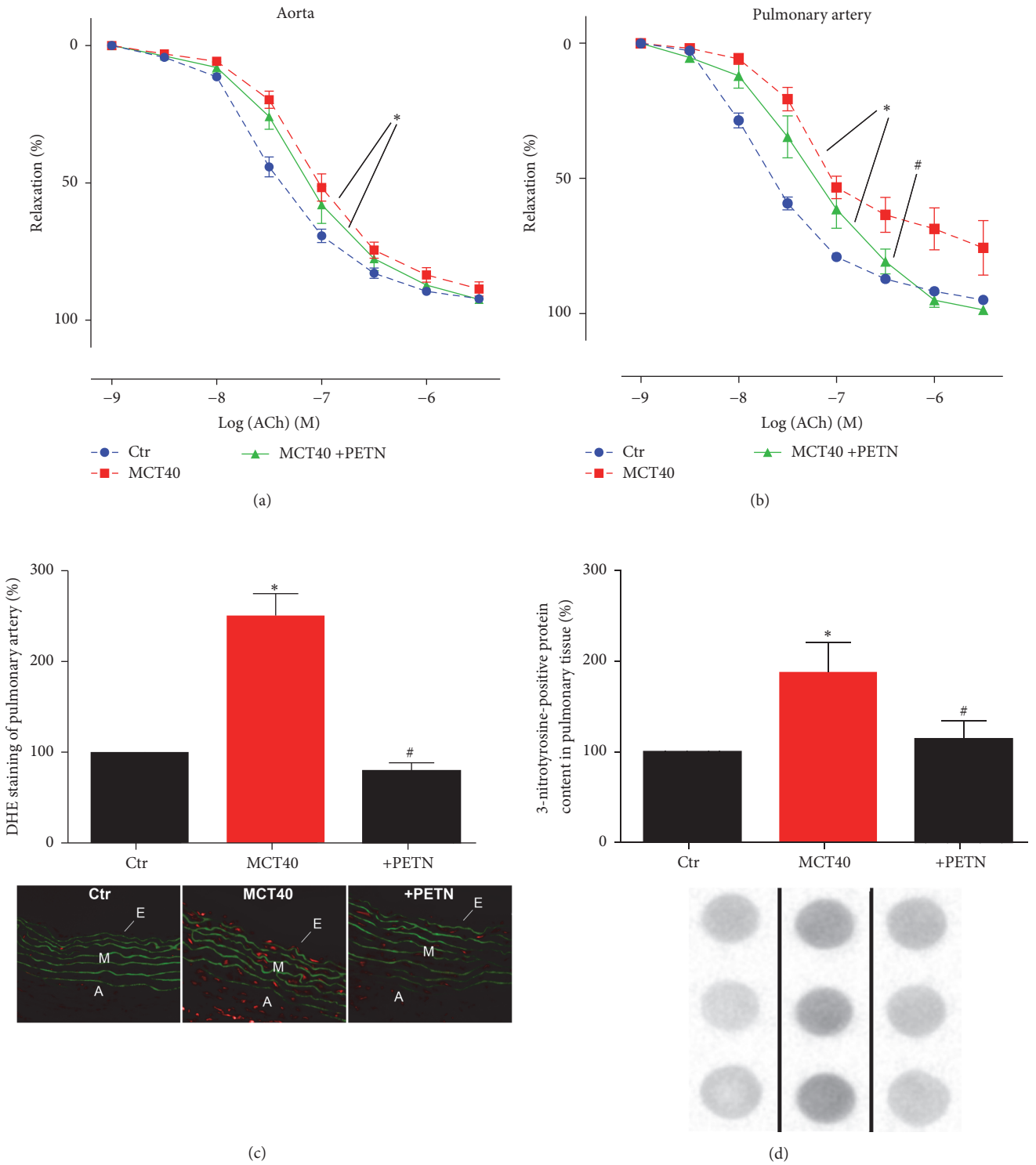

Figure 4: Effects of PETN therapy on endothelial function, oxidative stress, and protein tyrosine nitration of aorta and pulmonary artery in monocrotaline-treated rats (MCT40 4 weeks). (a, b) Endothelium-dependent (ACh) relaxation was determined by isometric tension studies in rat aortic ring segments and pulmonary ring segments. (c) DHE (1 μM) oxidative fluorescence microtopography was used to assess vascular oxidative stress. (d) Levels of 3-NT positive proteins in lung tissue were assessed by dot blot analysis and specific antibodies. Representative blots are shown below the densitometric quantification. A total number of 6–22 aortic (a) and 6–17 pulmonary tissue (b–d) ring segments from male rats were used. $^{*}p < 0.05$ versus control and $^{\#}p < 0.05$ versus MCT40.

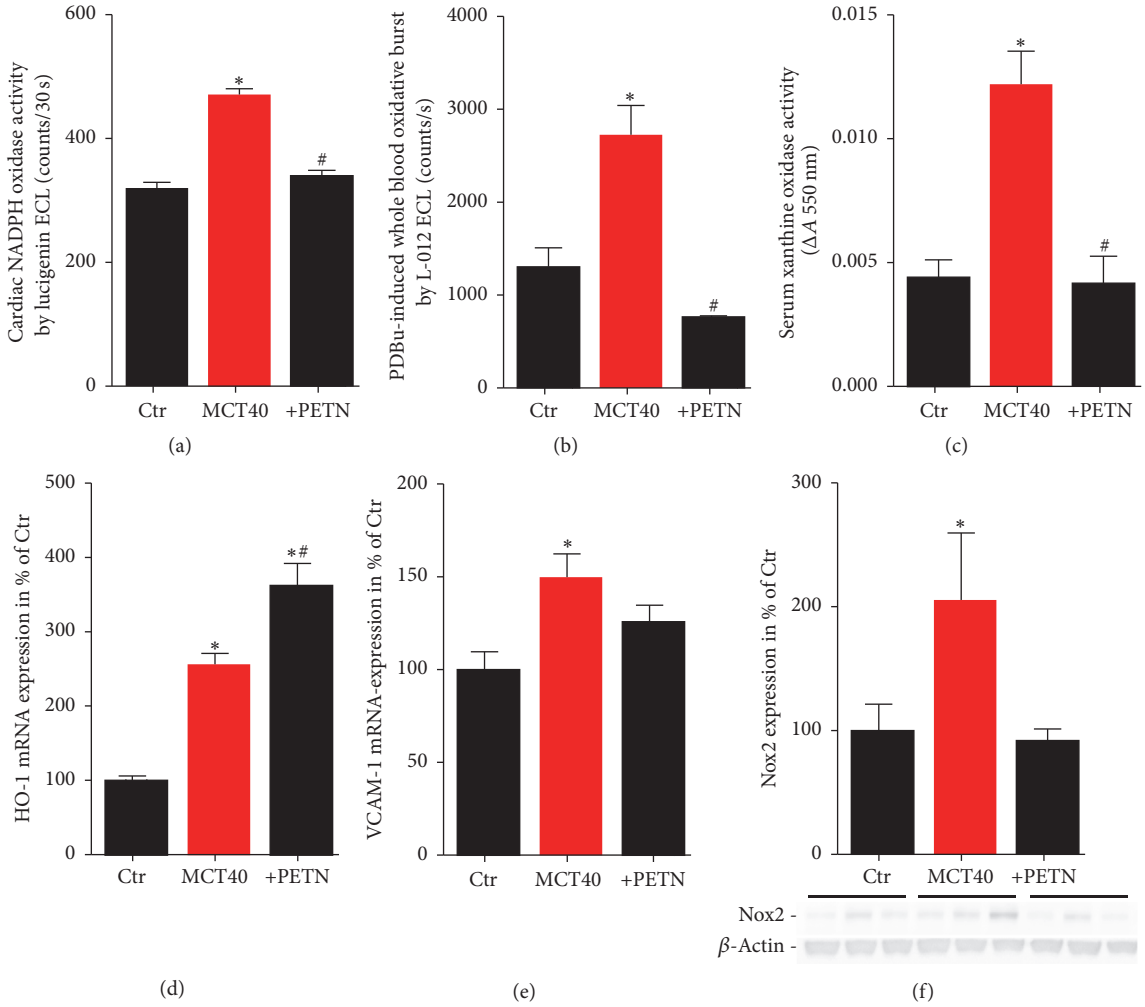

Figure 5: Effects of PETN therapy on prooxidative protein activity (Nox, XO), oxidative burst in whole blood, and antioxidant HO-1 mRNA expression in pulmonary hypertension (MCT40, 4 weeks). (a) Cardiac NADPH oxidase (Nox) activity was measured by the chemiluminescence probe lucigenin (5 μM) in the presence of NADPH (200 μM). (b) Leukocyte-derived oxidative burst in whole blood was examined by the chemiluminescence probe L-012 (100 μM) upon stimulation with PDBu (10 μM). (c) Xanthine oxidase (XO) activity was assessed by a photometric assay using cytochrome c (change in absorbance: ΔA 550 nm). qRT-PCR was used to determine mRNA expression levels of the antioxidant enzyme (d) heme oxygenase-1 (HO-1) and (e) vascular adhesion molecule-1 (VCAM-1) in lung tissue. (f) NADPH oxidase 2 (Nox2) protein expression was determined by Western blot analysis. The data are mean ± SEM from 3–6 animals/group. $^{*}p < 0.05$ versus control; $^{\#}p < 0.05$ versus MCT40.

no induction of oxidative stress or endothelial dysfunction [51–53]. Also animal studies revealed a prevention of endothelial dysfunction as well as progression of vascular lesions in established atherosclerosis by PETN [54], which might be mediated by upregulation of the antioxidant defense protein HO-1 [55]. Recently we demonstrated that HO-1 is a regulator of vascular function in arterial hypertension via modulation of inflammatory monocytes [56] and we showed HO-1 expression to be induced by PETN in a rat model for type 1 diabetes and arterial hypertension [27, 28]. HO-1 induction seems to be a potent mechanism to reduce oxidative stress and tissue inflammation, not only in arterial, but also in pulmonary hypertension. Shimzu et al. showed attenuation of pulmonary hypertension and reduced pulmonary inflammation by HO-1 induction using hemin [33]. HO-1 catalyzes the degradation of heme into biliverdin (which is converted to the antioxidant bilirubin), the gaseous transmitter carbon monoxide (CO), and free iron, the latter leading to upregulation of ferritin and reduced free iron levels in the long run. Therefore, HO-1 induction is considered as an essential physiological stress response pathway conferring antiatherosclerotic and beneficial effects on endothelial function [27, 28, 57]. Here we found an additive increase in HO-1 mRNA expression by PETN in lung tissue of PAH rats providing an attractive explanation for the beneficial effects of PETN therapy on vascular and pulmonary oxidative stress parameters and subsequent improvement of endothelial function in pulmonary arteries, PAP, and morphological changes (heart/body, lung/body ratio) observed in MCT-treated animals.

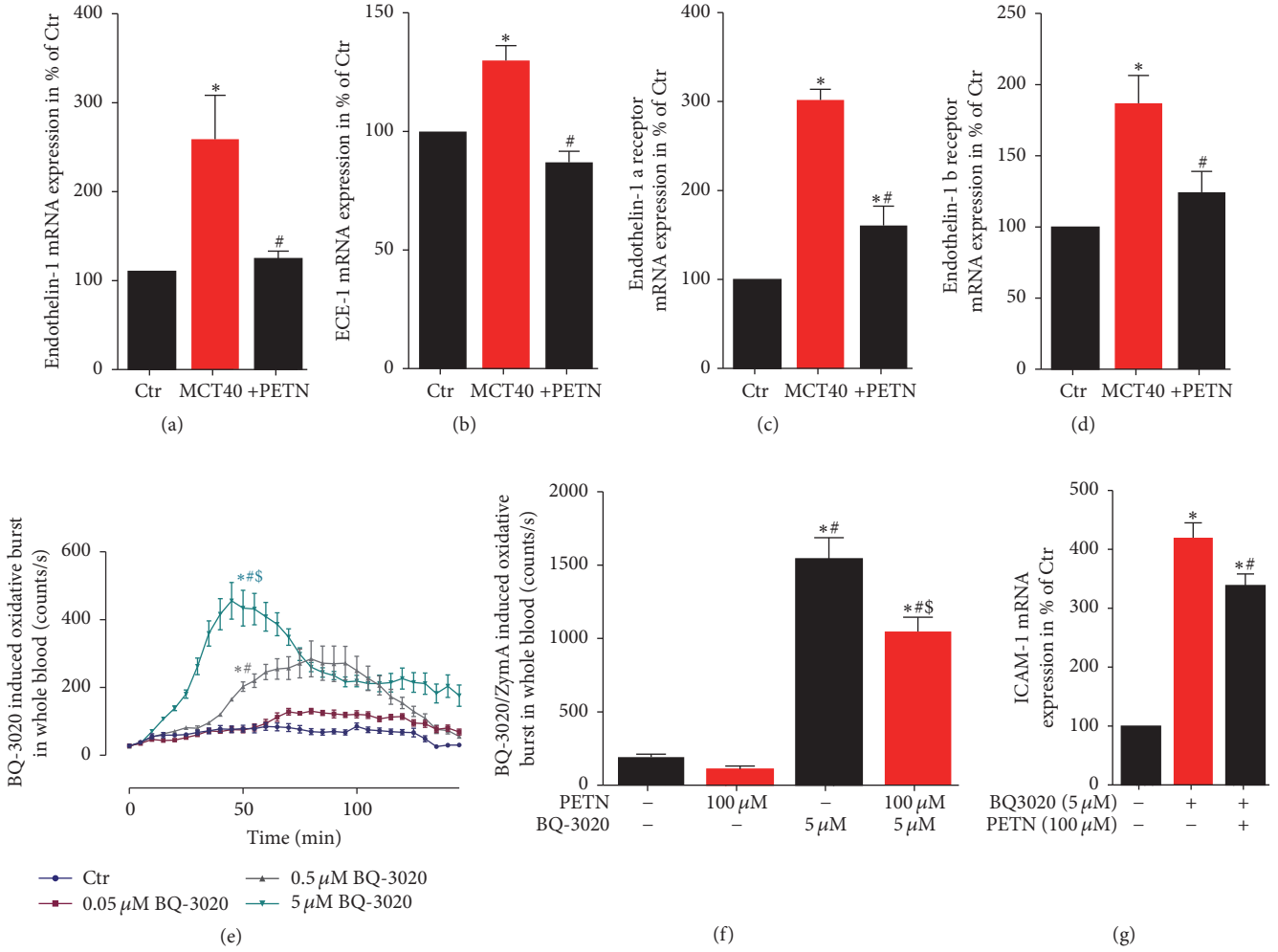

FIGURE 6: Effects of PETN therapy on endothelin-1 signaling (ET-1, ECE-1, and ET-1a/b receptor) and oxidative burst in whole blood. qRT-PCR was used to determine mRNA expression levels of (a) endothelin-1, (b) endothelin-1 converting enzyme-1, (c) endothelin-1 a receptor, and (d) endothelin-1 b receptor in lung tissue. (e) Leukocyte-derived oxidative burst in whole blood was examined by the chemiluminescence probe L-012 (100 μM) upon stimulation with the endothelin-1 agonist BQ-3020 (0.05–5 μM). (f) Effect of PETN (100 μM) on BQ-3020 (5 μM)/zymosan A (0.5 μg/mL) stimulated whole blood oxidative burst. (g) qRT-PCR was used to determine mRNA expression levels of ICAM-1 in EA.hy cells upon stimulation with BQ-3020 and PETN. The data are mean ± SEM from 6 animals/group (a–d) and 16 (e-f) or 3–7 (g) independent experiments. $^{*}p < 0.05$ versus control; $^{\#}p < 0.05$ versus MCT40.

Chen et al. demonstrated increased iNOS expression in MCT-induced PAH and ROS levels are known to be elevated in PAH [46, 58]. This can be explained by monocyte/macrophage extravasation in pulmonary tissue and increased iNOS expression by these cells. Since Nox-derived ROS are known to participate in the pathogenesis of pulmonary hypertension, increased 3-NT positive proteins indicate vascular inflammation and Nox activation. On the other hand, elevated ROS levels react with eNOS-derived NO to $ONOO^{-}$, which reduces NO bioavailability and thereby contributes to endothelial dysfunction. In turn, reduced NO bioavailability explains not only the observed endothelial dysfunction, but also smooth muscle cell (SMC) proliferation and fibrosis in small and medium sized pulmonary vessels as previously reported [6]. We assessed nitro-oxidative stress levels in lung tissue by 3-NT positive protein content reflecting peroxynitrite ($ONOO^{-}$) formation and DHE fluorescence microtopography in pulmonary arteries. Both nitro-oxidative stress parameters were clearly increased in MCT-treated animals and normalized by PETN therapy.

Endothelin-1 is known to play an essential role in the pathogenesis of PAH [3] and blockade of the ET-1 receptor with macitentan or bosentan is an established treatment option for PAH underlining the relevance of ET-1 signaling in PAH. Furthermore, it has been shown that oxidative stress leads to increased endothelial synthesis of endothelin-1 [8]. In this study, PETN therapy downregulated ET-1, ECE-1, and ET-1a/b receptor mRNA expression in MCT-induced pulmonary hypertension. Furthermore, PETN suppressed ET-1 (BQ-3020) dependent oxidative burst in whole blood and normalized ICAM-1 mRNA expression in cultured

endothelial cells (Ea.hy). It might be speculated that the beneficial effects of PETN on ET-1 signaling are mediated by suppression of oxidative stress, a potent trigger of ET-1 signaling.

5. Conclusions

PETN improves to a minor extent vascular remodeling and endothelial function and more potently suppresses oxidative stress as well as pathological changes in heart/body and lung/body weight ratio in an experimental model of PAH by induction of HO-1 but also by interference with ET-1 signaling. The MCT model clearly demonstrates some limitations as a model of clinical PAH, especially since morphological changes develop quite fast and are not easily prevented by therapeutical interventions. Most importantly, clinical data are needed to proof our experimental findings. The ongoing CAESAR clinical trial ("ClinicAl Efficacy Study of Pentalong for PulmonAry Hypertension in HeaRt Failure") will answer the question, whether PETN represents a new option for the treatment of patients with PAH.

Abbreviations

3-NT: 3-nitrotyrosine
ACh: Acetylcholine
DHE: Dihydroethidium
ecSOD: Extracellular superoxide dismutase
eNOS: Endothelial nitric oxide-synthase
ET-1: Endothelin-1
ET-1a: Endothelin-1 receptor type a
ET-1b: Endothelin-1 receptor type b
h/b ratio: Heart to body weight ratio
HO-1: Heme oxygenase-1
i.v.: Intravenously
ICAM-1: Intercellular adhesion molecule 1
ISDN: Isosorbide dinitrate
MCT: Monocrotaline
MCT30: 30 mg monocrotaline
MCT40: 40 mg monocrotaline
MCT60: 60 mg monocrotaline
NO: Nitric oxide
Nox: NADPH oxidase
NTG: Nitroglycerin
$O_2^{\bullet-}$: Superoxide
PAH: Pulmonary arterial hypertension
PAP: Pulmonary arterial pressure
PETN: Pentaerythritol tetranitrate
PGI_2: Prostacyclin
PVR: Pulmonary vascular resistance
ROS: Reactive oxygen species
RVSP: Right ventricular pressure
s.c.: Subcutaneously
SMC: Smooth muscle cell
VCAM-1: Vascular adhesion molecule-1
XO: Xanthine oxidase.

Disclosure

The work contains parts of the thesis of Elisabeth Ullmann.

Competing Interests

Andreas Daiber and Thomas Münzel received research grant support from Actavis Deutschland GmbH (now PUREN Pharma GmbH & Co. KG), Munich, Germany. Dirk Stalleicken was the former medical director of Actavis DACH (Germany, Austria, Switzerland) GmbH, Munich, Germany. All other authors have no competing financial interests.

Authors' Contributions

Sebastian Steven and Matthias Oelze contributed equally to this study and should therefore both be considered as first authors.

Acknowledgments

The authors are indebted to Angelica Karpi, Jörg Schreiner, and Jessica Rudolph for expert technical assistance. The present work was supported by a vascular biology research grant from Actavis Deutschland GmbH, Munich, Germany (Andreas Daiber and Thomas Münzel). Sebastian Steven and Moritz Brandt hold Virchow-Fellowships from the Center of Thrombosis and Hemostasis (Mainz, Germany) funded by the Federal Ministry of Education and Research (BMBF 01EO1003 to Sebastian Steven, Moritz Brandt, Philip Wenzel, Thomas Münzel, and Andreas Daiber). Elisabeth Ullmann and Lan P. Tran were supported by a medical doctor thesis stipend from the Center for Translational Vascular Biology (CTVB) and the Robert Müller Foundation (Mainz, Germany).

References

[1] M. M. Hoeper, H. J. Bogaard, R. Condliffe et al., "Definitions and diagnosis of pulmonary hypertension," *Journal of the American College of Cardiology*, vol. 62, no. 25, pp. D42–D50, 2013.

[2] D. M. Tabima, S. Frizzell, and M. T. Gladwin, "Reactive oxygen and nitrogen species in pulmonary hypertension," *Free Radical Biology and Medicine*, vol. 52, no. 9, pp. 1970–1986, 2012.

[3] A. Giaid, M. Yanagisawa, D. Langleben et al., "Expression of endothelin-1 in the lungs of patients with pulmonary hypertension," *New England Journal of Medicine*, vol. 328, no. 24, pp. 1732–1739, 1993.

[4] D. J. Stewart, R. D. Levy, P. Cernacek, and D. Langleben, "Increased plasma endothelin-1 in pulmonary hypertension: marker or mediator of disease?" *Annals of Internal Medicine*, vol. 114, no. 6, pp. 464–469, 1991.

[5] S. Adnot, B. Raffestin, S. Eddahibi, P. Braquet, and P.-E. Chabrier, "Loss of endothelium-dependent relaxant activity in the pulmonary circulation of rats exposed to chronic hypoxia," *Journal of Clinical Investigation*, vol. 87, no. 1, pp. 155–162, 1991.

[6] M. Humbert, N. W. Morrell, S. L. Archer et al., "Cellular and molecular pathobiology of pulmonary arterial hypertension," *Journal of the American College of Cardiology*, vol. 43, no. 12, supplement, pp. 13S–24S, 2004.

[7] J. Kähler, A. Ewert, J. Weckmüller et al., "Oxidative stress increases endothelin-1 synthesis in human coronary artery

smooth muscle cells," *Journal of Cardiovascular Pharmacology*, vol. 38, no. 1, pp. 49–57, 2001.

[8] J. Kähler, S. Mendel, J. Weckmüller et al., "Oxidative stress increases synthesis of big endothelin-1 by activation of the endothelin-1 promoter," *Journal of Molecular and Cellular Cardiology*, vol. 32, no. 8, pp. 1429–1437, 2000.

[9] O. Rafikova, R. Rafikov, S. Kumar et al., "Bosentan inhibits oxidative and nitrosative stress and rescues occlusive pulmonaryhypertension," *Free Radical Biology and Medicine*, vol. 56, pp. 28–43, 2013.

[10] A. Csiszar, N. Labinskyy, S. Olson et al., "Resveratrol prevents monocrotaline-induced pulmonary hypertension in rats," *Hypertension*, vol. 54, no. 3, pp. 668–675, 2009.

[11] R. P. Jankov, C. Kantores, J. Pan, and J. Belik, "Contribution of xanthine oxidase-derived superoxide to chronic hypoxic pulmonary hypertension in neonatal rats," *American Journal of Physiology - Lung Cellular and Molecular Physiology*, vol. 294, no. 2, pp. L233–L245, 2008.

[12] M. Dubois, E. Delannoy, L. Duluc et al., "Biopterin metabolism and eNOS expression during hypoxic pulmonary hypertension in mice," *PLoS ONE*, vol. 8, no. 11, Article ID e82594, 2013.

[13] J. P. Khoo, L. Zhao, N. J. Alp et al., "Pivotal role for endothelial tetrahydrobiopterin in pulmonary hypertension," *Circulation*, vol. 111, no. 16, pp. 2126–2133, 2005.

[14] L. A. Brennan, R. H. Steinhorn, S. Wedgwood et al., "Increased superoxide generation is associated with pulmonary hypertension in fetal lambs: a role for NADPH oxidase," *Circulation Research*, vol. 92, no. 6, pp. 683–691, 2003.

[15] S. Spiekermann, K. Schenk, and M. M. Hoeper, "Increased xanthine oxidase activity in idiopathic pulmonary arterial hypertension," *European Respiratory Journal*, vol. 34, no. 1, p. 276, 2009.

[16] R. Bowers, C. Cool, R. C. Murphy et al., "Oxidative stress in severe pulmonary hypertension," *American Journal of Respiratory and Critical Care Medicine*, vol. 169, no. 6, pp. 764–769, 2004.

[17] T. Münzel, A. Daiber, and T. Gori, "Nitrate therapy: new aspects concerning molecular action and tolerance," *Circulation*, vol. 123, no. 19, pp. 2132–2144, 2011.

[18] M. Packer, J. L. Halperin, K. M. Brooks, E. B. Rothlauf, and W. H. Lee, "Nitroglycerin therapy in the management of pulmonary hypertensive disorders," *The American Journal of Medicine*, vol. 86, no. 6, pp. 67–75, 1984.

[19] P. Krieg, T. Wahlers, W. Giess et al., "Inhaled nitric oxide and inhaled prostaglandin E1: effect on left ventricular contractility when used for treatment of experimental pulmonary hypertension," *European Journal of Cardio-thoracic Surgery*, vol. 14, no. 5, pp. 494–502, 1998.

[20] N. Yurtseven, P. Karaca, M. Kaplan et al., "Effect of nitroglycetin inhalation on patients with pulmonary hypertension undergoing mitral valve replacement surgery," *Anesthesiology*, vol. 99, no. 4, pp. 855–858, 2003.

[21] J. Pepke-Zaba, T. W. Higenbottam, A. T. Dinh-Xuan, D. Stone, and J. Wallwork, "Inhaled nitric oxide as a cause of selective pulmonary vasodilatation in pulmonary hypertension," *The Lancet*, vol. 338, no. 8776, pp. 1173–1174, 1991.

[22] M. Sahara, M. Sata, T. Morita, Y. Hirata, and R. Nagai, "Nicorandil attenuates monocrotaline-induced vascular endothelial damage and pulmonary arterial hypertension," *PLoS ONE*, vol. 7, no. 3, Article ID e33367, 2012.

[23] M. Oelze, M. Knorr, S. Kröller-Schön et al., "Chronic therapy with isosorbide-5-mononitrate causes endothelial dysfunction, oxidative stress, and a marked increase in vascular endothelin-1 expression," *European Heart Journal*, vol. 34, no. 41, pp. 3206–3216, 2013.

[24] T. Gori and A. Daiber, "Non-hemodynamic effects of organic nitrates and the distinctive characteristics of pentaerithrityl tetranitrate," *American Journal of Cardiovascular Drugs*, vol. 9, no. 1, pp. 7–15, 2009.

[25] M. J. Quinn Jr., L. C. B. Crouse, C. A. McFarland, E. M. Lafiandra, and M. S. Johnson, "Reproductive and developmental effects and physical and chemical properties of pentaerythritol tetranitrate (PETN) in the rat," *Birth Defects Research Part B—Developmental and Reproductive Toxicology*, vol. 86, no. 1, pp. 65–71, 2009.

[26] J. R. Bucher, J. Huff, J. K. Haseman, S. L. Eustis, H. S. Lilja, and A. S. K. Murthy, "No evidence of toxicity or carcinogenicity of pentaerythritol tetranitrate given in the diet to F344 rats and B6C3F1 mice for up to two years," *Journal of Applied Toxicology*, vol. 10, no. 5, pp. 353–357, 1990.

[27] S. Schuhmacher, M. Oelze, F. Bollmann et al., "Vascular dysfunction in experimental diabetes is improved by pentaerithrityl tetranitrate but not isosorbide-5-mononitrate therapy," *Diabetes*, vol. 60, no. 10, pp. 2608–2616, 2011.

[28] S. Schuhmacher, P. Wenzel, E. Schulz et al., "Pentaerythritol tetranitrate improves angiotensin II-induced vascular dysfunction via induction of heme oxygenase-1," *Hypertension*, vol. 55, no. 4, pp. 897–904, 2010.

[29] M. Oppermann, V. Balz, V. Adams et al., "Pharmacological induction of vascular extracellular superoxide dismutase expression in vivo," *Journal of Cellular and Molecular Medicine*, vol. 13, no. 7, pp. 1271–1278, 2009.

[30] A. Daiber, M. Oelze, P. Wenzel, F. Bollmann, A. Pautz, and H. Kleinert, "Heme oxygenase-1 induction and organic nitrate therapy: beneficial effects on endothelial dysfunction, nitrate tolerance, and vascular oxidative stress," *International Journal of Hypertension*, vol. 2012, Article ID 842632, 13 pages, 2012.

[31] P. Wenzel, M. Oelze, M. Coldewey et al., "Heme oxygenase-1: a novel key player in the development of tolerance in response to organic nitrates," *Arteriosclerosis, Thrombosis, and Vascular Biology*, vol. 27, no. 8, pp. 1729–1735, 2007.

[32] S. Oberle, P. Schwartz, A. Abate, and H. Schröder, "The antioxidant defense protein ferritin is a novel and specific target for pentaerithrityl tetranitrate in endothelial cells," *Biochemical and Biophysical Research Communications*, vol. 261, no. 1, pp. 28–34, 1999.

[33] K. Shimzu, T. Takahashi, T. Iwasaki et al., "Hemin treatment abrogates monocrotaline-induced pulmonary hypertension," *Medicinal Chemistry*, vol. 4, no. 6, pp. 572–576, 2008.

[34] H. Christou, T. Morita, C.-M. Hsieh et al., "Prevention of hypoxia-induced pulmonary hypertension by enhancement of endogenous heme oxygenase-1 in the rat," *Circulation Research*, vol. 86, no. 12, pp. 1224–1229, 2000.

[35] T. Münzel, A. Giaid, S. Kurz, D. J. Stewart, and D. G. Harrison, "Evidence for a role of endothelin 1 and protein kinase C in nitroglycerin tolerance," *Proceedings of the National Academy of Sciences of the United States of America*, vol. 92, no. 11, pp. 5244–5248, 1995.

[36] M. Oelze, S. Kröller-Schön, S. Steven et al., "Glutathione peroxidase-1 deficiency potentiates dysregulatory modifications of endothelial nitric oxide synthase and vascular dysfunction in aging," *Hypertension*, vol. 63, no. 2, pp. 390–396, 2014.

[37] S. N. Meloan and H. Puchtler, ""Harris hematoxylin," what harris really wrote and the mechanism of hemalum stains," *Journal of Histotechnology*, vol. 10, no. 4, pp. 257–261, 1987.

[38] D. Urboniene, I. Haber, Y.-H. Fang, T. Thenappan, and S. L. Archer, "Validation of high-resolution echocardiography and magnetic resonance imaging vs. high-fidelity catheterization in experimental pulmonary hypertension," *American Journal of Physiology—Lung Cellular and Molecular Physiology*, vol. 299, no. 3, pp. L401–L412, 2010.

[39] A. Daiber, M. August, S. Baldus et al., "Measurement of NAD(P)H oxidase-derived superoxide with the luminol analogue L-012," *Free Radical Biology and Medicine*, vol. 36, no. 1, pp. 101–111, 2004.

[40] P. Wenzel, E. Schulz, M. Oelze et al., "AT1-receptor blockade by telmisartan upregulates GTP-cyclohydrolase I and protects eNOS in diabetic rats," *Free Radical Biology and Medicine*, vol. 45, no. 5, pp. 619–626, 2008.

[41] M. C. Wendt, A. Daiber, A. L. Kleschyov et al., "Differential effects of diabetes on the expression of the gp91^{phox} homologues nox1 and nox4," *Free Radical Biology and Medicine*, vol. 39, no. 3, pp. 381–391, 2005.

[42] M. Hausding, K. Jurk, S. Daub et al., "CD40L contributes to angiotensin II-induced pro-thrombotic state, vascular inflammation, oxidative stress and endothelial dysfunction," *Basic Research in Cardiology*, vol. 108, no. 6, article no. 386, 2013.

[43] S. Rosenkranz, "Pulmonary hypertension 2015: current definitions, terminology, and novel treatment options," *Clinical Research in Cardiology*, vol. 104, no. 3, pp. 197–207, 2015.

[44] H.-G. Predel, H. Knigge, U. Prinz, H. J. Kramer, D. Stalleicken, and R. E. Rost, "Exercise increases endothelin-1 plasma concentrations in patients with coronary artery disease: modulatory role of LDL cholesterol and of pentaerithrityltetranitrate," *Journal of Cardiovascular Pharmacology*, vol. 26, pp. S497–S501, 1995.

[45] J. G. Gomez-Arroyo, L. Farkas, A. A. Alhussaini et al., "The monocrotaline model of pulmonary hypertension in perspective," *American Journal of Physiology—Lung Cellular and Molecular Physiology*, vol. 302, no. 4, pp. L363–L369, 2012.

[46] M.-J. Chen, L. Y. Chiang, and Y.-L. Lai, "Reactive oxygen species and substance P in monocrotaline-induced pulmonary hypertension," *Toxicology and Applied Pharmacology*, vol. 171, no. 3, pp. 165–173, 2001.

[47] V. G. DeMarco, A. T. Whaley-Connell, J. R. Sowers, J. Habibi, and K. C. Dellsperger, "Contribution of oxidative stress to pulmonary arterial hypertension," *World Journal of Cardiology*, vol. 2, no. 10, pp. 316–324, 2010.

[48] D. Xu, H. Guo, X. Xu et al., "Exacerbated pulmonary arterial hypertension and right ventricular hypertrophy in animals with loss of function of extracellular superoxide dismutase," *Hypertension*, vol. 58, no. 2, pp. 303–309, 2011.

[49] A. Daiber and T. Münzel, "Organic nitrate therapy, nitrate tolerance, and nitrate-induced endothelial dysfunction: emphasis on redox biology and oxidative stress," *Antioxidants and Redox Signaling*, vol. 23, no. 11, pp. 899–942, 2015.

[50] T. Münzel, A. Daiber, and T. Gori, "More answers to the still unresolved question of nitrate tolerance," *European Heart Journal*, vol. 34, no. 34, pp. 2666–2673, 2013.

[51] U. Jurt, T. Gori, A. Ravandi, S. Babaei, P. Zeman, and J. D. Parker, "Differential effects of pentaerythritol tetranitrate and nitroglycerin on the development of tolerance and evidence of lipid peroxidation: A Human In Vivo Study," *Journal of the American College of Cardiology*, vol. 38, no. 3, pp. 854–859, 2001.

[52] T. Gori, A. Al-Hesayen, C. Jolliffe, and J. D. Parker, "Comparison of the effects of pentaerythritol tetranitrate and nitroglycerin on endothelium-dependent vasorelaxation in male volunteers," *American Journal of Cardiology*, vol. 91, no. 11, pp. 1392–1394, 2003.

[53] B. Schnorbus, R. Schiewe, M. A. Ostad et al., "Effects of pentaerythritol tetranitrate on endothelial function in coronary artery disease: Results of the PENTA Study," *Clinical Research in Cardiology*, vol. 99, no. 2, pp. 115–124, 2010.

[54] A. Hacker, S. Müller, W. Meyer, and G. Kojda, "The nitric oxide donor pentaerythritol tetranitrate can preserve endothelial function in established atherosclerosis," *British Journal of Pharmacology*, vol. 132, no. 8, pp. 1707–1714, 2001.

[55] S. Oberle, A. Abate, N. Grosser et al., "Endothelial protection by pentaerithrityl trinitrate: bilirubin and carbon monoxide as possible mediators," *Experimental Biology and Medicine*, vol. 228, no. 5, pp. 529–534, 2003.

[56] P. Wenzel, H. Rossmann, C. Müller et al., "Heme oxygenase-1 suppresses a pro-inflammatory phenotype in monocytes and determines endothelial function and arterial hypertension in mice and humans," *European Heart Journal*, vol. 36, no. 48, pp. 3437–3446, 2015.

[57] Y. Shen, N. C. Ward, J. M. Hodgson et al., "Dietary quercetin attenuates oxidant-induced endothelial dysfunction and atherosclerosis in apolipoprotein e knockout mice fed a high-fat diet: a critical role for heme oxygenase-1," *Free Radical Biology and Medicine*, vol. 65, pp. 908–915, 2013.

[58] J. C. Yu, Y. H. Jae, G. L. Sang et al., "Temporal changes of angiopoietins and Tie2 expression in rat lungs after monocrota-line-induced pulmonary hypertension," *Comparative Medicine*, vol. 59, no. 4, pp. 350–356, 2009.

Hindawi
Oxidative Medicine and Cellular Longevity
Volume 2017, Article ID 1379430, 11 pages
https://doi.org/10.1155/2017/1379430

Research Article

Synthetic Isoliquiritigenin Inhibits Human Tongue Squamous Carcinoma Cells through Its Antioxidant Mechanism

Cuilan Hou,[1,2,3] Wenguang Li,[1,2] Zengyou Li,[4] Jing Gao,[5] Zhenjie Chen,[1,2] Xiqiong Zhao,[1,2] Yaya Yang,[1,2] Xiaoyu Zhang,[1,2] and Yong Song[6]

[1]*School of Basic Medical Sciences, Lanzhou University, Lanzhou, Gansu Province 730000, China*
[2]*Key Lab of Preclinical Study for New Drugs of Gansu Province, Lanzhou, Gansu Province 730000, China*
[3]*Department of Physiology and Pathophysiology, Fudan University Shanghai Medical College, Shanghai 200000, China*
[4]*Jining Medical University, Jining, Shandong Province 272067, China*
[5]*Northwest Nationalities University Hospital, Lanzhou, Gansu Province 730000, China*
[6]*School of Public Health, Curtin University, Centre for Genetic Origins of Health and Disease, The University of Western Australia and Curtin University, M409, 35 Stirling Highway, Crawley, WA 6009, Australia*

Correspondence should be addressed to Xiaoyu Zhang; zhangxyu@lzu.edu.cn and Yong Song; yong.song1@curtin.edu.au

Received 17 September 2016; Revised 9 December 2016; Accepted 21 December 2016; Published 22 January 2017

Academic Editor: Luciano Saso

Isoliquiritigenin (ISL), a natural antioxidant, has antitumor activity in different types of cancer cells. However the antitumor effect of ISL on human tongue squamous carcinoma cells (TSCC) is not clear. Here we aimed to investigate the effects of synthetic isoliquiritigenin (S-ISL) on TSCC and elucidate the underlying mechanisms. S-ISL was synthesized and elucidated from its nuclear magnetic resonance spectrum and examined using high performance liquid chromatography. The effects of S-ISL on TSCC cells (Tca8113) were evaluated in relation to cell proliferation, apoptosis and adhesion, migration, and invasion using sulforhodamine B assay, fluorescence microscopy technique, flow cytometry (FCM) analysis, and Boyden chamber assay. The associated regulatory mechanisms were examined using FCM and fluorescence microscopy for intracellular reactive oxygen species (ROS) generation, Gelatin zymography assay for matrix metalloproteinase (MMP) activities, and Western blot for apoptosis regulatory proteins (Bcl-2 and Bax). Our data indicated that S-ISL inhibited Tca8113 cell proliferation, adhesion, migration, and invasion while promoting the cell apoptosis. Such effects were accompanied by downregulation of Bcl-2 and upregulation of Bax, reduction of MMP-2 and MMP-9 activities, and decreased ROS production. We conclude that S-ISL is a promising agent targeting TSCC through multiple anticancer effects, regulated by its antioxidant mechanism.

1. Introduction

Squamous cell carcinoma of the tongue (TSCC) is one of the most common malignant tumors in the oral cavity and accounted for approximately 30% of all oral cancers in the United States in 2006 [1]. Moreover, its incidence has increased over the past decades worldwide [2]. Despite advances in chemotherapy, radiotherapy, and surgical therapy, the clinical outcomes and overall survival rates of TSCC have not been significantly improved over the last decades with overall five-year survival rate of less than 50% [3]. The high morbidity and mortality of oral cancers are largely due to rapid tumor growth, frequent tumor recurrence, and metastasis. Therefore, it is important to identify and develop novel agents which could simultaneously target abnormal proliferation, apoptosis, invasion, and metastasis of tongue cancer.

Isoliquiritigenin (ISL), 2′, 4′, 4′-three hydroxychalcone (molecular structure shown in Supplementary Figure a in Supplementary Material available online at https://doi.org/10.1155/2017/1379430), mainly presents in roots of licorice and many other plants, foods, beverages, and tobaccos [4].

ISL possesses a wide variety of potent biological and pharmacological activities, including anti-inflammatory [5], antivirus [6], antioxidative [5], antiaging [7], and antidiabetic activities [8]. We previously showed that ISL could significantly reduce cardiac reactive oxygen species (ROS) level during hypoxia/reoxygenation, rendering protection against myocardial ischemic injury [9] and inhibiting the growth of prostate cancer cells [10]. ISL is reported to have anticarcinogenic effects in both in vivo and in vitro experimental models. In vivo studies revealed that ISL inhibited chemically induced colonic tumorigenesis [11], skin papilloma formation [12], and lung metastasis of murine renal carcinoma cells [13]. In vitro studies showed that ISL had antiproliferation activities in skin [14], pulmonary [13], breast [15], prostate [10], and gastric cancer cells [16]. A recent study showed that ISL induced human oral squamous cell carcinoma cell cycle G_2/M phase arrest, apoptosis, and DNA damage [17], implying that ISL is a promising chemopreventive agent against oral cancer. However the antitumor effect of ISL on TSCC is not fully characterized. In the present study, we aimed to further investigate antiproliferative, proapoptotic, and antimetastatic effects of ISL on human tongue squamous carcinoma cells and elucidate the underlying mechanisms. Since natural ISL compound preparation is expensive with poor extraction rates and particularly wastes or destroys natural resources, we selected to observe antitumor effects of chemically synthesized ISL (S-ISL) in the study, which has great advantages in future preclinical development and clinical use, for example, reducing production costs and protecting licorice natural resources.

2. Materials and Methods

2.1. The Synthesis of S-ISL. S-ISL was synthesized and elucidated from its nuclear magnetic resonance spectrum (Supplementary Figure) as previously described [18]. The mixture of ethanol (5.6 mL), 2, 4-dihydroxyacetophenone (1, 6.8 g, 44.7 mmol) and 4-hydroxybenzaldehyde (2, 5.6 g, 45.9 mmol) was added to aqueous potassium hydroxide (41.6 mL, 60% w/w). The above suspension was heated at 100°C for 1.5 h and then stored overnight at room temperature. The reaction mixture was poured onto ice (100 g) and acidified to pH 4 using cold hydrochloric acid. The precipitated yellow solid was filtered, washed with water (200 mL), and air-dried to a yellow solid (3, 7.5 g, 65%). ^{1}H NMR (400 MHz, (CD_3) CO): δ 6.37 (s, 1 H), 6.47 (d, J = 8.0 Hz, 1 H), 6.93 (d, J = 8.0 Hz, 2 H), 7.74~7.86 (m, 4 H), 8.13 (d, J = 8.0 Hz, 1 H), 9.00 (s, 1 H), 9.47 (s, 1 H), 13.65 (s, 1 H); ^{13}C NMR (100 MHz, (CD_3) CO): δ 103.85, 108.76, 114.61, 116.86, 118.37, 127.67, 131.88, 133.38, 145.24, 161.07, 165.61, 167.67, 192.93 (Supplementary Figures b and c). Finally the purity of S-ISL was analyzed by high performance liquid chromatography (HPLC) method [19] with a C_{18} column (5 μm, 4.6 × 250 mm), mixture of methanol and water (80 : 20, v : v) with rate of 1.0 mL/min, and detected at 370 nm. Each sample solution (10 μL) was injected into the analysis system (Supplementary Figure e). The purity of S-ISL acquired was more than 95% and used in the subsequent studies.

2.2. Cell Culture. For comparison of specificity and sensitivity of S-ISL in carcinoma cells, we initially screened human tongue squamous carcinoma Tca8113 cells, human liver carcinoma HepG2 cells, and rat pheochromocytoma PC12 cells obtained from Chinese Academy of Sciences (Shanghai, China). The cells were grown in complete Dulbecco's modified Eagle's medium (DMEM; Invitrogen, Gibco, Grand Island, NY, USA) and supplemented with 10% heat-inactivated fetal bovine serum at 37°C in a humidified atmosphere containing 95% air/5% CO_2. Exponentially growing cells were used for experiments. S-ISL was dissolved in dimethylsulfoxide (DMSO) to make a 10 mg/mL stock solution, which was further diluted to appropriate concentration with culture medium before each experiment.

2.3. Cell Viability Analysis Using Sulforhodamine B Assay. The effects of S-ISL on the viability of Tca8113, HepG2, and PC12 cells were determined using sulforhodamine B (SRB) assay (Sigma) [20]. Tca8113 cells (3.5×10^4 cells/mL), HepG-2 cells (7×10^4 cells/mL), and PC12 cells (7×10^4 cells/mL) were seeded in 96-well plates and were separately treated with various concentrations of S-ISL for 24 h, 48 h, and 72 h. The optical density in each well was read using microplate reader at 570 nm. The experiment was repeated at least three times.

2.4. Determination of Intracellular ROS Generation. Intracellular ROS generation was evaluated using dichlorodihydrofluorescein diacetate (DCFH-DA) assay (Sigma, St Louis, MO, USA), which is a specific probe for hydrogen peroxide to form fluorescent dichlorofluorescein [9]. All groups were added with stimulant H_2O_2 (100 μM) except the vehicle group (0.5% DMSO) prior to treatment with 10 μM DCFH-DA at 37°C for 30 min. After incubation, cells were immediately submitted to fluorescence microscopy or flow cytometry and estimated using FL-1 channel.

2.5. Cell Cycle Analysis Using Flow Cytometry. Cell cycle analysis was carried out using flow cytometry (FCM) [21]. After Tca8113 cells were treated as described above, the cells were harvested and washed twice with ice-cold phosphate-buffered saline (PBS) and fixed with precooled ethanol (70% v/v) overnight. Subsequently the cells were stained with propidium iodide in PBS added with RNase in the dark at room temperature for 30 min. The sample was read on a Coulter Epics XL flow cytometry (Beckman-Coulter Inc, Fullerton, CA, USA).

2.6. Apoptosis Detection with Double Dye Annexin V-FITC/PI and 4′, 6-Diamidino-2-Phenylindole Dihydrochloride (DAPI) Staining. The double dye Annexin V-FITC/PI was used to distinguish between living cells, early and late apoptotic cells, and necrotic cells [22]. The cells were treated in the same manner as the cell cycle analysis, except no cooled 70% ethanol was added. For FCM analysis, the cells were stained with Annexin V-FITC/PI and detected by FCM using Annexin V-FITC cell Apoptosis Detection Kit (Sigma) according to manufacturer's instructions.

For fluorescence microscope examination, Tca8113 cells treated with S-ISL as described above were washed with ice-cold PBS twice, fixed with ethanol for 30 min, and stained with DAPI (0.1 μg/mL, 2 min) at room temperature away from light. The stained cells were photographed with a fluorescence microscope (Olympus, Japan) at excitation wavelength of 480 nm and emission wavelength of 530 nm.

2.7. Western Blotting Analysis. The proteins in total cell lysates were separated on a 10% sodium dodecyl sulphate (SDS)-polyacrylamide gel electrophoresis and transferred onto polyvinylidene fluoride membrane (Millipore, Bedford, MA, USA). Membranes were blocked with 5% nonfat milk in tris-buffered saline buffer (pH 7.4) containing 0.1% Tween-20 for 1 h and subsequently incubated with primary antibodies (1 : 1000 dilution) against Bcl-2, Bax (Santa Cruz Biotechnology, Texas, USA) and GAPDH (Proteintech, Rosemont, USA) at 4°C overnight. Immunoreactive bands were detected using anti-rabbit horseradish peroxidase-conjugated secondary antibodies (1 : 3000 dilution) (Beyotime Biotechnology, Jiangsu, China) and visualized using LumiPico® ECL Reagent (Beyotime Biotechnology). The densities of immunoblotting bands were analyzed using a scanning densitometer (model GS-800; Bio-Rad, Shanghai, China) coupled with Bio-Rad personal computer analysis software.

2.8. Assays for Adhesion, Migration, and Invasion. Cell-matrix adhesion assay was carried out as described previously [23]. Briefly the 96-well plates were precoated with 0.04 μg/μL matrigel 50 μL in triplicate overnight at 4°C and then washed with wash buffer (0.1% bovine serum albumin in medium). S-ISL pretreated cells were seeded in the precoated 96-well plates and incubated at 37°C. After 2 hours, nonadherent cells were washed away and attached cells were counted (Image-plus) and photographed from six randomly selected fields under an inverted microscope (Olympus, Beijing, China). The cell migration assay in vitro was performed by using a modified Boyden chamber (Millipore, Billerica, MA, USA) inserted with polyethylene terephthalate filter membrane containing 8 μm pores in 24 well culture plates [24]. For cell migration assay, Tca8113 cells (2×10^5 cells/mL) in serum-free medium, with or without S-ISL, were seeded in triplicate in the upper chamber. Complete medium was placed in the lower wells. The culture plates were incubated at 37°C in a 5% CO_2 atmosphere. After incubation, the medium in the upper chamber was removed and washed with PBS twice. The cells remaining on the upper surface of the filter membrane were removed with cotton swabs and the cells on the opposite surface of the filter membrane were stained with 0.1% crystal violet for 5 min. The migrated cells were subjected to microscopic examination as described for the adhesion assay. For invasion assay, the whole process was the same as migration assay except that Tca8113 cells were loaded on presolidified matrigel.

2.9. Gelatin Zymography Assay. The activities of matrix metalloproteinase (MMP)-2 and MMP-9 in the conditioned medium were determined by Gelatin zymography assay [25]. Briefly, the serum-free medium was collected by centrifugation to remove cells and cell debris and subsequently loaded under nonreducing sample buffer onto SDS-polyacrylamide gel polymerized with 1% Gelatin (Sigma). Following electrophoresis, the gel was washed twice with rinsing buffer at room temperature for 1.5 h to remove SDS and then incubated in a developing buffer at 37°C overnight. Gels were stained with 0.1% Coomassie Brilliant Blue R-250 and destained in the same solution without dye. Gelatinase activity was visualized as clear bands against the blue-stained Gelatin background.

2.10. Statistical Analysis. Data were expressed as mean ± SD of multiple separate experiments. Statistical comparisons were performed using analysis of variance (ANOVA) followed by Student-Newman-Keuls' post hoc test for multiple comparisons using the computer statistical package (SPSS 21.0 for Window). Differences with $P < 0.05$ were considered statistically significant.

3. Results

3.1. Effects of S-ISL on Proliferation of Tca8113, HepG2, and PC12 Cells. The effects of S-ISL on the proliferation of Tca8113, HepG2, and PC12 cells were analyzed using SRB analysis. S-ISL markedly inhibited the proliferation of the above cells (Figure 1(a)), particularly Tca8113 cells and the IC_{50} values were 17.70 μg/mL, 10.04 μg/mL, and 9.67 μg/mL after 24 h, 48 h, and 72 h treatment, respectively. HepG2 cells displayed intermediate responses to S-ISL and the IC_{50} values were 19.07 μg/mL, 15.08 μg/mL, and 14.95 μg/mL, respectively, after the same treatment time. However, PC12 cell line was particularly resistant to S-ISL and the IC_{50} values were 38.13 μg/mL, 30.94 μg/mL, and 26.85 μg/mL, respectively. As the present study demonstrated that Tca8113 were the most sensitive cells responding to S-ISL treatment, the subsequent studies were then focused on observing the effects of S-ISL on Tca8113.

3.2. Effects of S-ISL on Intracellular ROS Generation. ROS production was measured in Tca8113 cells using DCFH-DA by fluorescence microscopy and FCM. As shown in Figure 2(a), when S-ISL was incubated with Tca8113 cells at varied concentrations from 12.5~50 μg/mL, relative to H_2O_2 treatment alone, S-ISL groups reduced the fluorescence values by 2.7%, 9.3%, and 18.6%, respectively. Likewise, H_2O_2 increased ROS production by 48.7% as compared with the vehicle group under FCM analysis (Figure 2(b)). Compared with H_2O_2 treatment alone, pretreatment with S-ISL at concentrations ranging from 12.5~50 μg/mL resulted in a decrease of intracellular ROS production and inhibition rate was 9.03%, 4.31%, and 26.22%, respectively. These results indicated that S-ISL suppressed intracellular ROS production of Tca8113 cells.

3.3. Effects of S-ISL on Cell Cycle in Tca8113 Cells. Compared to the vehicle control, S-ISL (6.25~12.5 μg/mL) induced cell

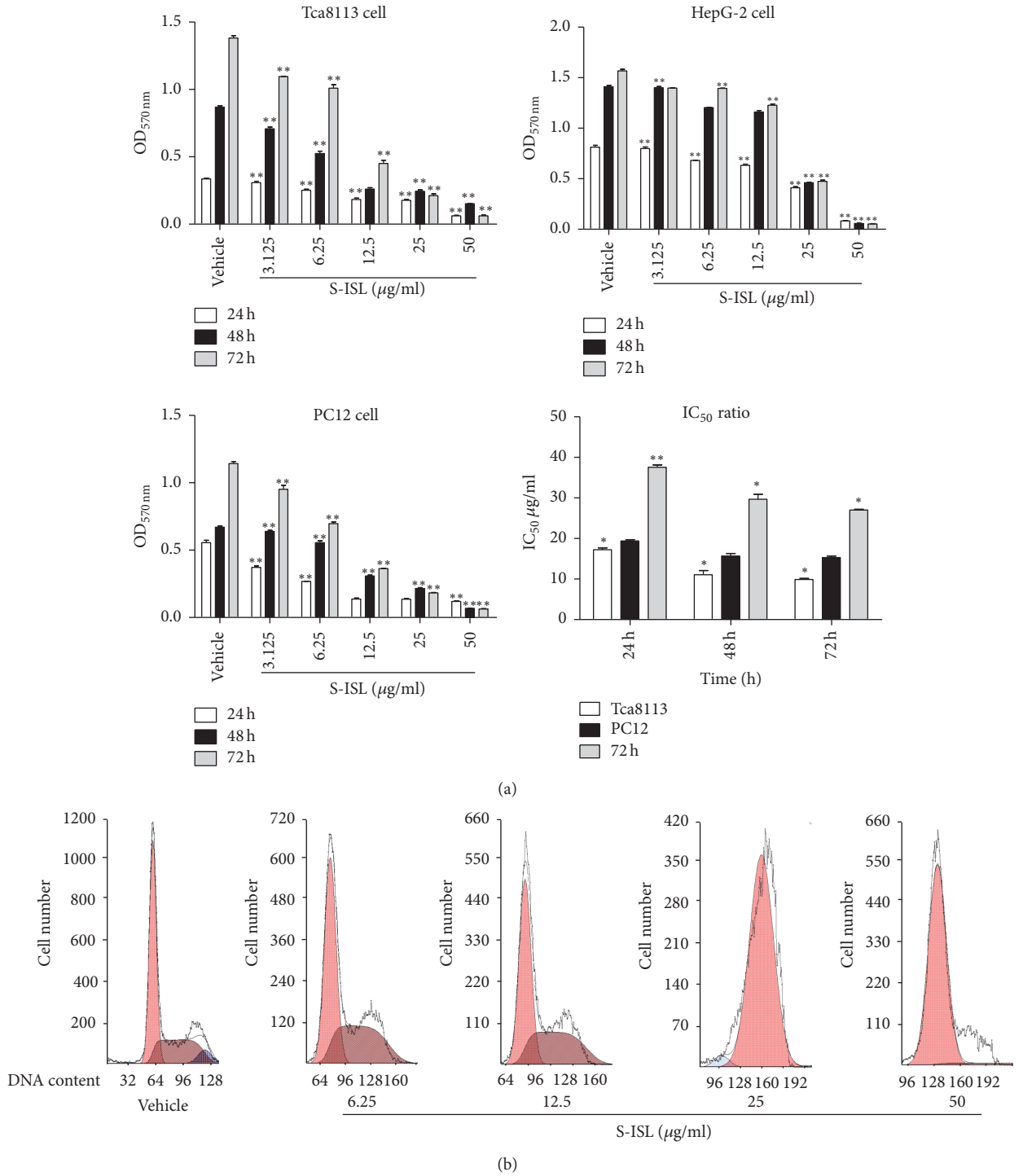

FIGURE 1: Effect of S-ISL on proliferation and cell cycle of cancer cells: The effects of S-ISL (3.125~50 μg/mL) on Tca8113, HepG2 and PC12 cells were observed for 24 h, 48 h, and 72 h using SRB assay (a) and the effects of S-ISL (6.25~50 μg/mL) on Tca8113 cell cycle were observed using FCM analysis (b). SRB results were expressed as the mean ± SD of three experiments with five replicates. S-ISL: synthetic isoliquiritigenin; SRB: sulforhodamine B; OD: optical density; IC_{50}: 50% growth inhibition concentration; FCM: flow cytometry. $^{*}P < 0.05$, $^{**}P < 0.01$ versus the vehicle group.

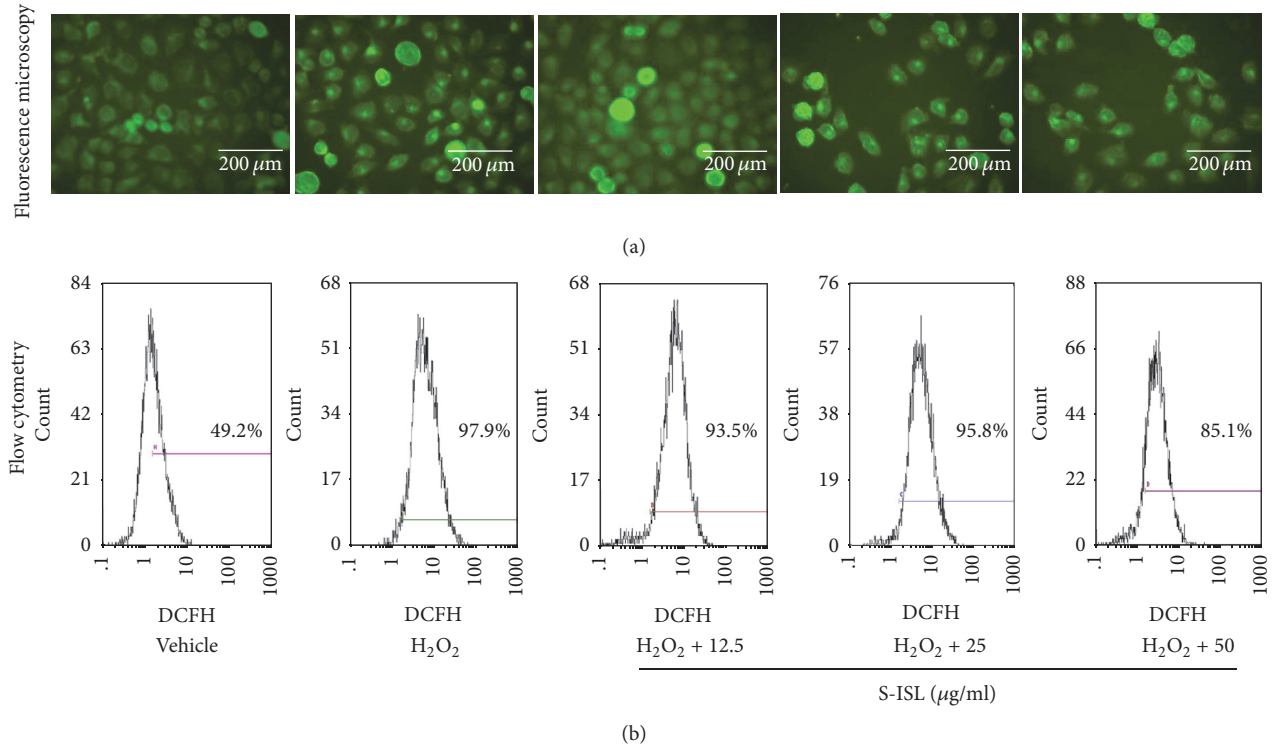

Figure 2: Effects of S-ISL on intracellular ROS levels: all groups were added with stimulant H_2O_2 (100 μM) except the vehicle group. The change of ROS levels in response to S-ISL (12.5~50 μg/mL) was examined using DCFH-DA analysis (a) and FCM analysis (b). S-ISL: synthetic isoliquiritigenin; ROS: reactive oxygen species; DCFH-DA: 2′, 7′- dichlorodihydrofluorescein diacetate; FCM: flow cytometry.

accumulation in S phase with a corresponding decrease in G_2 phase while S-ISL 25~50 μg/mL markedly induced cell accumulation in G_1 phase with a corresponding decrease in S phase (Figure 2(b)). Cell cycle studies indicated a biphasic effect of S-ISL, with a lower-concentration accumulation of the cells in the S phase and a higher-concentration in G_1 phase.

3.4. Effects of S-ISL on Apoptosis in Tca8113 Cells. As shown in Figure 2(b), a fraction of cells with hypodiploid DNA content representing apoptosis can be detected using cell cycle analysis. S-ISL (25~50 μg/mL) increased the percentage of sub-G_1 DNA content in Tca8113 cells as compared with the vehicle treated groups.

Further, apoptotic cells were identified by chromatin morphology using DAPI. After 24 h and 48 h treatment, S-ISL (6.25–50 μg/mL) induced chromatin condensation in Tca8113 cells compared to the vehicle cells (Figure 3(a)). The ratio of apoptotic cells to total cells was 0.2%, 6.2%, 10.4%, and 16.3%, respectively, after 24 h treatment of S-ISL, and the ratio for 48 h treatment was 1.6%, 12.3%, 14.6%, and 30.4%, respectively. The morphological characteristics of the vehicle cells demonstrated good spreading and flattening with no DAPI staining of nuclei (Figure 3(a)). On the other hand, Tca8113 cells pretreated with S-ISL (6.25~50 μg/mL) for 24 h and 48 h displayed cell rounding, weak spreading, shrinking, and retracting of cellular processes. S-ISL treatment resulted in brighter stained nuclei of Tca8113 cells with condensed chromatin forming crescent-shaped profiles around the periphery of the nuclei.

In addition, the apoptosis-inducing effect of S-ISL was evaluated by double staining with Annexin V-FITC/PI to distinguish between living cells, early and late apoptotic cells, and necrotic cells. As shown in Figure 3(b), when Tca8113 cells were treated without S-ISL, 97.9% of cells were in a normal condition. After the cells were incubated with S-ISL (6.25~50 μg/mL) for 24 h, 39.3%, 29.2%, 15.9%, and 4.86% of cells were in early phase of apoptosis whereas there were few cells in the late apoptotic/necrotic stage. These results indicated that S-ISL had a negative concentration-dependent effect on Tca8113 cell apoptosis induction, especially in the early phase of apoptosis.

3.5. Changes of Bax and Bcl-2 Protein Expressions in Response to S-ISL Treatment. Western blotting assay was performed to evaluate the change of apoptosis regulators (Bax and Bcl-2) in response to S-ISL treatment (Figure 4). Relative to the vehicle group, S-ISL incubation from 12.5~100 μg/mL significantly decreased Bcl-2 protein expression and increased Bax protein expression in Tca8113 cells.

3.6. Effects of S-ISL on Tca8113 Cells Adhesion, Migration, and Invasion. Cell-matrix adhesion assay showed that S-ISL treatment remarkably decreased adhesion abilities of Tca8113 cells on matrigel-coated surface. As shown in Figure 5(a), when the concentrations of S-ISL varied from 6.25 μg/mL to

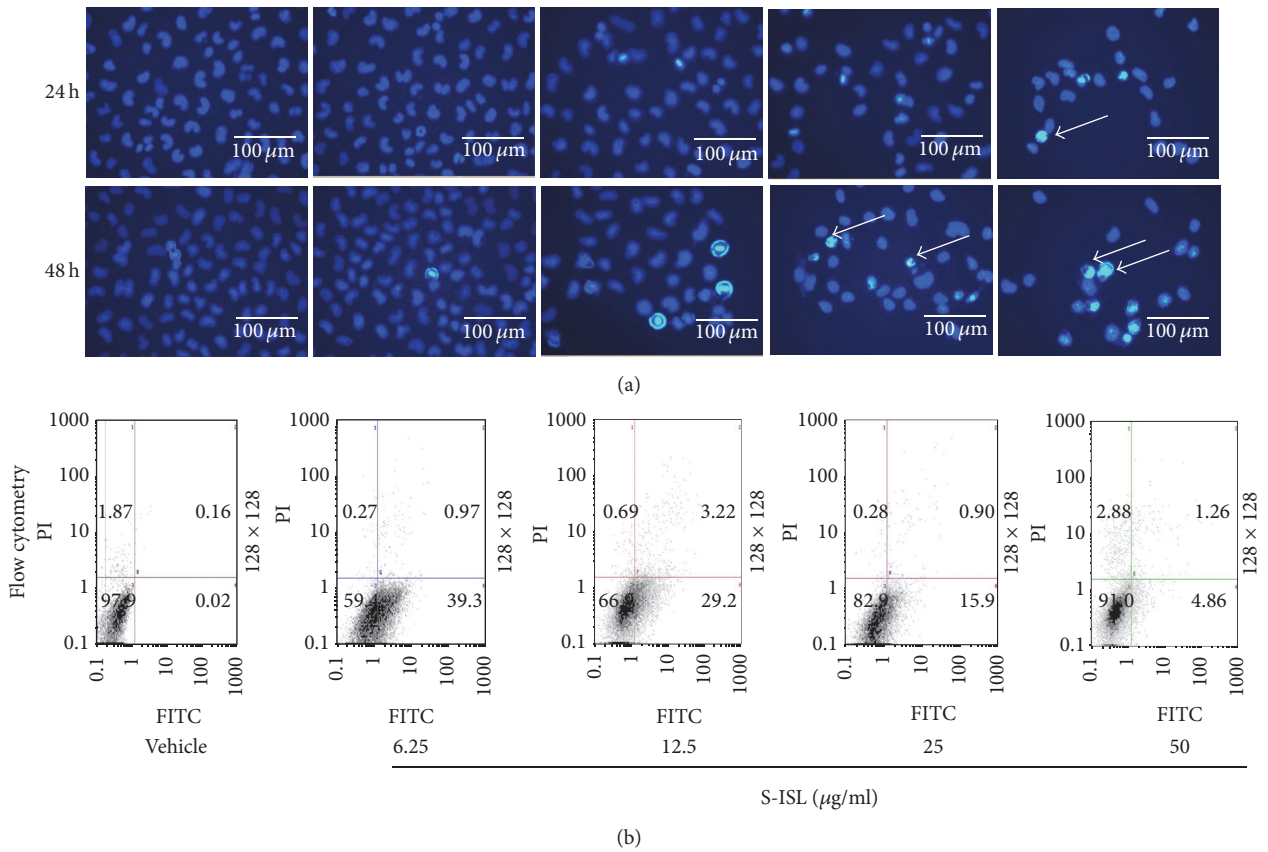

Figure 3: Effects of S-ISL on apoptosis: The effects of S-ISL (6.25~50 μg/mL) on Tca8113 cell apoptosis were examined using fluorescence microscopy technique (a) and FCM analysis (b). Apoptosis cells with powerful fluorescence bodies of nuclear fragmentation were marked by arrows. S-ISL: synthetic isoliquiritigenin; FCM: flow cytometry.

50 μg/mL, the inhibitory adhesion rates were 39.18%, 51.55%, 54.64%, and 64.95%, respectively ($P < 0.05$ compared with the control group).

Further, the effect of S-ISL on the migration of Tca8113 cells was examined using Boyden chamber assay. As shown in Figure 5(b), the number of Tca8113 cells passing through the polycarbonate membrane in S-ISL pretreated groups was significantly less than that in the vehicle group ($P < 0.05$). The inhibitory migration rates of S-ISL from 6.25 μg/mL to 50 μg/mL were 21.33%, 58.59%, 62.73%, and 79.30%, respectively.

As shown in Figure 5(c), S-ISL from 6.25 μg/mL to 50 μg/mL also significantly inhibited Tca8113 cells invasion compared to the vehicle group ($P < 0.05$) and the inhibitory rates were 28.29%, 51.05%, 51.33%, and 58.04%, respectively. These results indicated that S-ISL inhibited the adhesion, migration, and invasion abilities of Tca8113 cells in a concentration-dependent manner.

3.7. Changes of MMP-2 and MMP-9 Activities in Response to S-ISL. In order to explore the possible antimetastatic mechanism of S-ISL in Tca8113 cells, the activities of MMP-2 and MMP-9 were tested using Gelatin zymography assay. S-ISL treatment (6.25~50 μg/mL) showed a concentration-dependent reduction in MMP-2 and MMP-9 activities. The inhibitory rates of MMP-2 were 13.57%, 21.02%, 24.45%, and 38.09%, and those of MMP-9 were 13.03%, 14.01%, 17.53%, 44.76%, respectively (Figure 6). These results indicate that the inhibition of MMP-2 and MMP-9 by S-ISL might play a key role in invasion and metastasis of Tca8113 cells.

4. Discussion

Our study shows that S-ISL has multiple anticancer effects on human tongue squamous carcinoma cells, including specific and biphasic effects of inhibiting proliferation, inducing cell apoptosis and impeding adhesion, migration, and invasion. The anticancer effects are attributed to increased levels of apoptotic Bax/Bcl-2 ratio and decreased activity of MMP-2 and MMP-9, which is likely to be mediated via antioxidant mechanisms of S-ISL.

The intracellular level of ROS is generally elevated in cancer cells, affecting all characteristics of cell behaviour, including cell cycle progression and proliferation, cell survival, and apoptosis and metastasis [26]. Like its natural counterpart, our data showed that S-ISL also had the same antioxidant capacity, providing the rational basis for our ongoing investigation of its antitumor effects.

Firstly we observed the effects of S-ISL on the proliferation of human tongue squamous carcinoma line Tca8113,

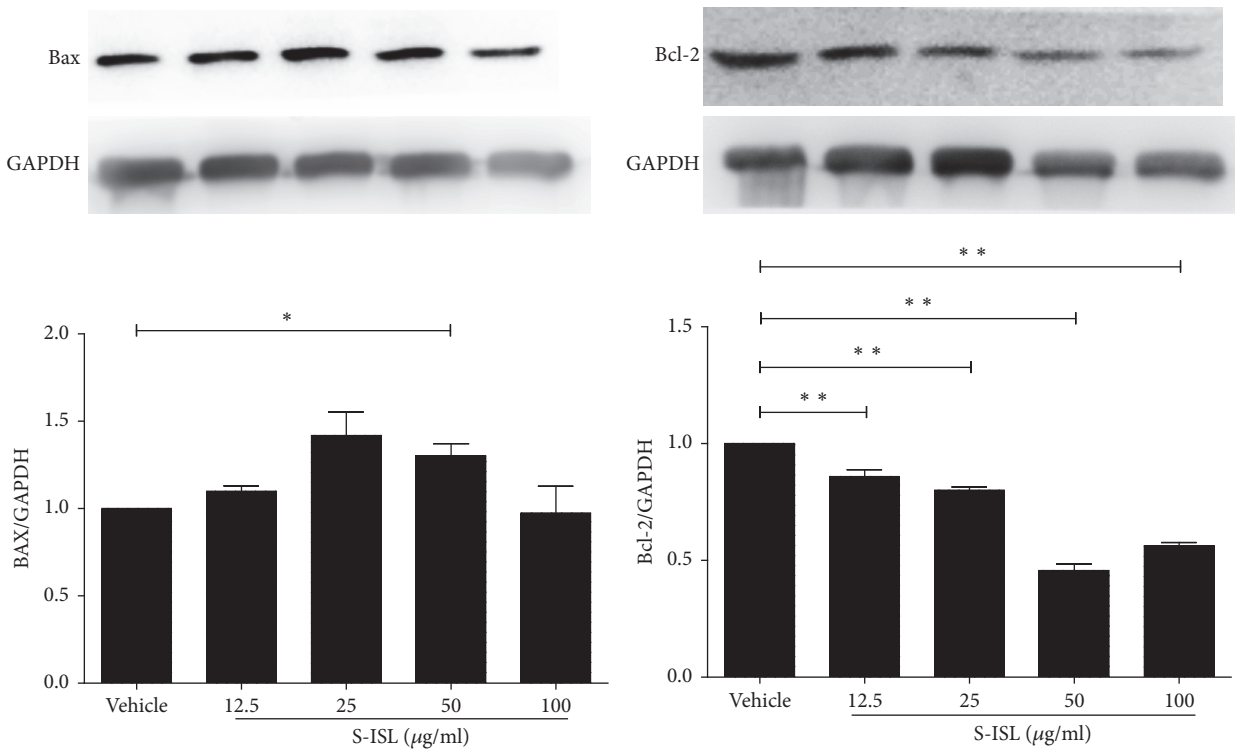

Figure 4: Bax and Bcl-2 protein expression in response to S-ISL: Western blots illustrate protein abundance of Bax and Bcl-2 using representative samples from each group above the graph. Graphs show Bax and Bcl-2 protein abundance normalized into GAPDH after S-ISL (12.5~100 μg/mL) treatment. S-ISL: synthetic isoliquiritigenin. Values are Mean (SD). $^{*}P < 0.05$, $^{**}P < 0.01$ versus the vehicle group.

in comparison with human liver carcinoma HepG2 cells and rat pheochromocytoma PC12 cells. S-ISL inhibited the growth of Tca8113, HepG2, and PC12 cells in a concentration- and time-dependent manner. Amongst these cells, Tca8113 cells exhibited the strongest response to S-ISL treatment. The inhibitory concentration of S-ISL observed was similar to the reports using the natural ISL [10, 16]. These results suggest that the effect of S-ISL against Tca8113 cells is specific and provide a first glimpse of the types of cancer cells that may benefit from such treatment. Further we revealed that the inhibitory effect of S-ISL on Tca8113 growth was due to a biphasic effect of S-ISL on Tca8113 cell cycle with a lower-concentration accumulation in the S phase and a higher-concentration in G_1 phase. Such effect is apparently different from G_2/M phase arrest induced by ISL in human lung cancer cell line A549 and human oral squamous cell carcinoma [17, 27], confirming the specific effects of S-ISL on Tca8113 cells.

Under physiological development, cell proliferation and apoptosis maintain proper balance. Compelling evidence indicates that some oncogenic mutations disrupt apoptosis, leading to tumor initiation, progression, or metastasis [28]. To test whether S-ISL could induce tumor cells apoptosis, we employed a variety of techniques including flow cytometry, DAPI staining, and double staining with Annexin V-FITC/PI to observe cell apoptosis related changes. Our data showed that S-ISL significantly increased the number of dead cells in a dose- and time-dependent manner. However, the dose dependent effects from both assays of DAPI staining and Annexin V-FITC/PI are contradictory in that the low dose of S-ISL showed strongest apoptosis-inducing effect using Annexin V-FITC/PI method while DAPI staining demonstrated a positive concentration-dependent effect of S-ISL on Tca8113 cell apoptosis induction. We argue that the apparent discrepancy is possibly attributed to different phases/aspects of apoptosis examined and different regulatory mechanisms of ISL in different concentrations. Annexin V-FITC/PI is used to detect early phase of apoptosis by probing phosphatidylserine translocated from the internal part of the plasma membrane to the external portion of the membrane. In contrast, DAPI staining is used to examine the morphological changes to quantify the apoptotic cells which are likely to happen in the late phase of apoptosis. Thus the same concentration of S-ISL may have different effects if examined in different phases of the apoptotic process. Additionally, we cannot exclude the possibility that different cell signalling pathways may be initiated to regulate the cell death under different concentrations of ISL exposure, which need further studies. In analyzing morphological characteristics, Tca8113 cells pretreated with S-ISL had typical changes including cell rounding, reduced spreading, shrinking and retracting of cellular processes, and brighter stained nuclei with condensed chromatin forming crescent-shaped profiles around the periphery of the nuclei. All of these changes indicated that S-ISL caused apoptosis of Tca8113 cells. One of the major genes that regulate apoptosis is the Bcl-2 family,

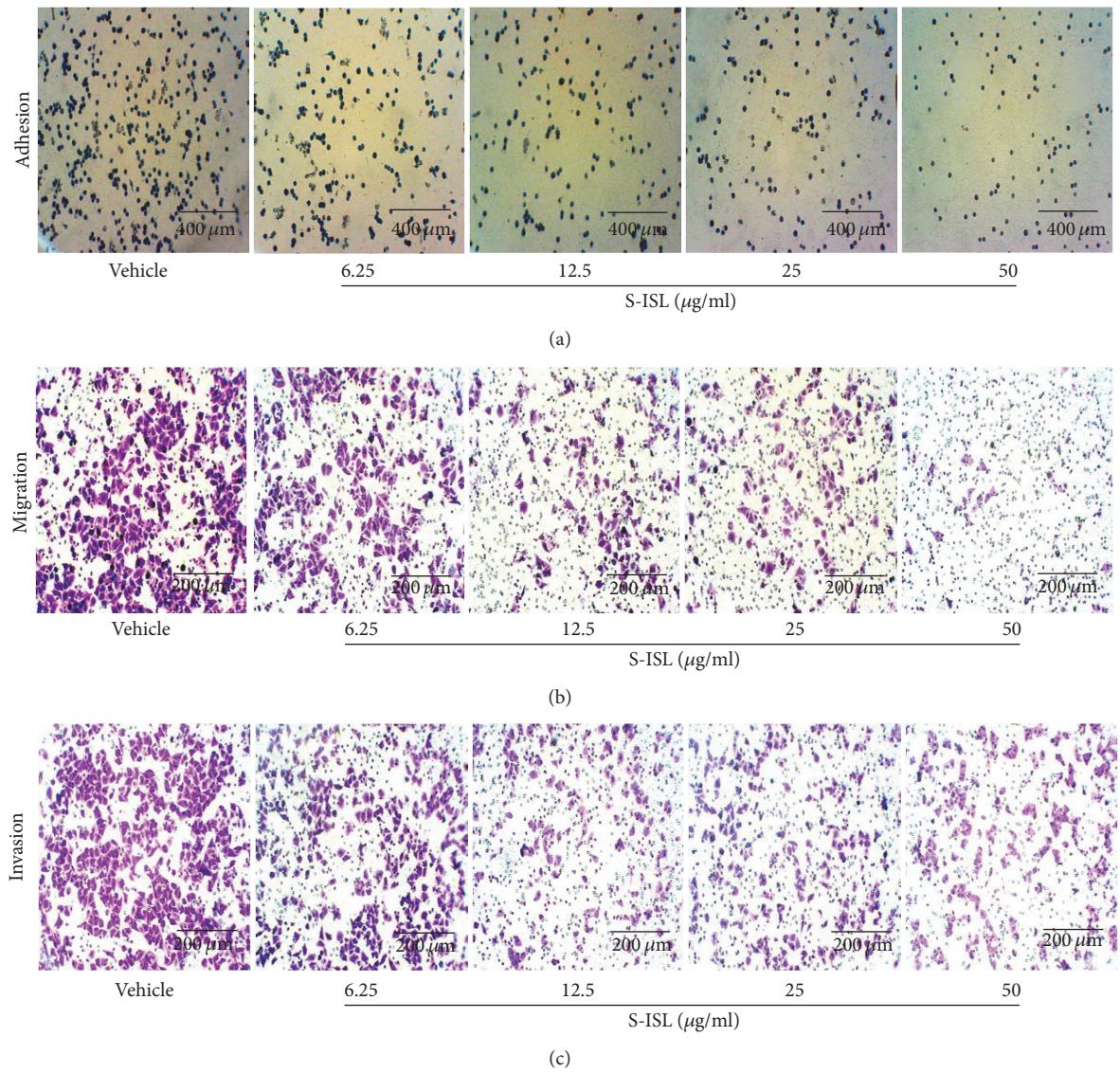

Figure 5: Effects of S-ISL on adhesion, migration, and invasion: The representative images were shown in regard to adhesion (a), migration (b), and invasion (c) of Tca8113 cells in response to S-ISL (6.25~50 μg/mL) treatment using an inverted microscope. S-ISL: synthetic isoliquiritigenin.

which plays a critical role in the mitochondrial pathway of apoptosis as either promoters (e.g., Bax) or inhibitors (e.g., Bcl-2) of the cell death process [29]. Therefore, the alteration of intracellular Bax and Bcl-2 expression ratio can affect mitochondrial content release [30] and determine susceptibility to apoptosis [31]. In agreement with the previous studies [10, 32], Tca8113 cells with S-ISL treatment had an increase of Bax and a decrease of Bcl-2 protein expression and alteration of proapoptotic Bax/antiapoptotic Bcl-2. We therefore conclude that the mechanism that S-ISL promoted apoptosis may be via changing the levels of the Bcl-2 family and the ratio of Bax and Bcl-2.

The majority of cancer related deaths are caused by metastases. Therefore, it is important to develop therapeutic interventions specifically targeting the metastatic process. The metastatic cascade includes a succession of six distinct steps: localized invasion, intravasation, translocation, extravasation, micrometastasis, and colonization [33]. The basic strategy of our interventions is aimed at disturbing cancer cells' adhesion, migration, and invasion abilities which are basic steps of metastasis. In this study, S-ISL inhibited Tca8113 cells adhesion, migration, and invasion abilities, indicating that S-ISL is a potential antimetastasis drug. MMP is regarded as a key player of tumor invasion and metastasis. The proteolytic activity of MMP is able to degrade extracellular matrix (ECM) proteins and subsequently induces or enhances tumor survival, invasion, and metastasis [34]. ROS in cancer not only regulate the expression of MMPs, but also inactivate their inhibitors TIMP (tissue inhibitor of metalloproteinase) [26]. Indeed, Tca8113 cells treated with S-ISL with antioxidant characteristic showed a concentration-dependent reduction of MMP-2 and MMP-9 activities. Thus anti-invasion and metastasis effects of S-ISL on Tca8113 are likely to be achieved via inhibiting MMP activities.

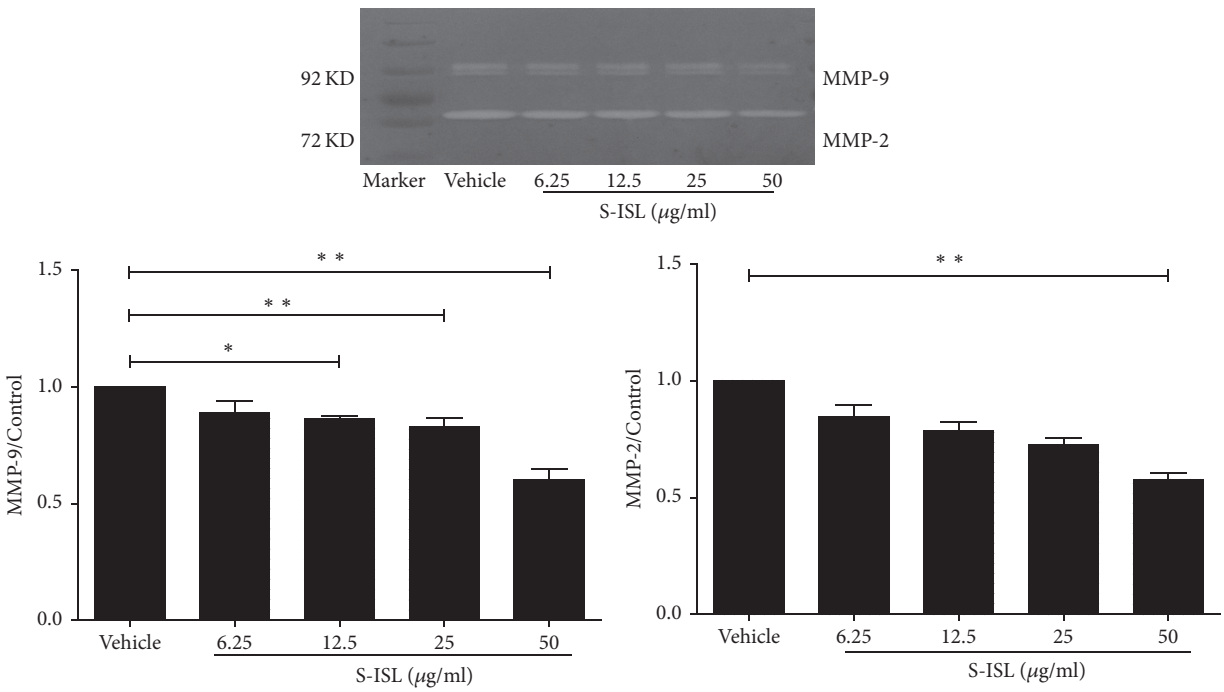

Figure 6: MMP-2 and MMP-9 activities in response to S-ISL: MMP-2 and MMP-9 proteolytic activities were measured in Tca8113 cells pretreated with S-ISL (6.25~100 μg/mL) at various concentrations for 24 h using Gelatin zymography assay. S-ISL: synthetic isoliquiritigenin; MMP: matrix metalloproteinase. Values are Mean (SD). $^{*}P < 0.05$, $^{**}P < 0.01$ versus the vehicle group.

Finally S-ISL showed a concentration-dependent manner in promotion of apoptosis, inhibiting proliferation, adhesion, migration, and invasion of Tca8113 cells, with an effective and optimal concentration from 25 to 50 μg/mL. Previously, Lee and colleagues reported that plasma ISL concentration could reach 4.16 ± 1.80 mg/mL after 30 min of administration of a 50 mg/kg intravenous dose of ISL to rats [35]. A recent study showed that intraperitoneal administration of 1 mg/kg of ISL significantly decreased tumor size and inhibited the viability of cancer cells in xenograft mouse model without apparent side effects on normal cells [36]. Therefore the concentrations of S-ISL used in this study are highly achievable in vivo, further supporting its promise in clinical application.

5. Conclusions

In summary, our data showed that S-ISL had antiproliferative, proapoptotic, and antimetastatic effects on human tongue squamous carcinoma cells through its antioxidant mechanism and potentially could be a therapeutic agent against tongue cancer.

Abbreviations

TSCC: Squamous cell carcinoma of the tongue
ISL: Isoliquiritigenin
ROS: Reactive oxygen species
S-ISL: Synthesis isoliquiritigenin
HPLC: High performance of liquid chromatography
DMEM: Dulbecco's modified Eagle's medium
DMSO: Dimethylsulfoxide
DCFH-DA: Dichlorodihydrofluorescein diacetate
SRB: Sulforhodamine B
FCM: Flow cytometry
PBS: Phosphate-buffered saline
SDS: Sodium dodecyl sulphate
MMP: Matrix metalloproteinase
ANOVA: Analysis of variance
ECM: Extracellular matrix
TIMP: Tissue inhibitor of metalloproteinase.

Competing Interests

The authors declare that there is no conflict of interests regarding the publication of this paper.

Authors' Contributions

Cuilan Hou, Wenguang Li, and Zengyou Li contributed equally to this work and should be regarded as co-first authors.

Acknowledgments

The authors thank Hongli Wang for his excellent technical assistance in S-ISL synthesis. This work was supported by the grants from the National Natural Science Foundation of China no. 21375052, Gansu Province Natural Science Foundation of China 1208RJZA231 (Xiaoyu Zhang), and

Lanzhou Science and Technology Development Project 06-1-30 (Xiaoyu Zhang).

References

[1] D. Sano and J. N. Myers, "Metastasis of squamous cell carcinoma of the oral tongue," *Cancer and Metastasis Reviews*, vol. 26, no. 3, pp. 645–662, 2007.

[2] P. A. Swango, "Cancers of the oral cavity and pharynx in the United States: an epidemiologic overview," *Journal of Public Health Dentistry*, vol. 56, no. 6, pp. 309–318, 1996.

[3] S. S. Chauhan, J. Kaur, M. Kumar et al., "Prediction of recurrence-free survival using a protein expression-based risk classifier for head and neck cancer," *Oncogenesis*, vol. 4, article e147, 2015.

[4] M. Nassiri Asl and H. Hosseinzadeh, "Review of pharmacological effects of *glycyrrhiza* sp. and its bioactive compounds," *Phytotherapy Research*, vol. 22, no. 6, pp. 709–724, 2008.

[5] T.-Y. Wu, T. O. Khor, C. L. L. Saw et al., "Anti-inflammatory/anti-oxidative stress activities and differential regulation of Nrf2-mediated genes by non-polar fractions of tea *Chrysanthemum zawadskii* and licorice *Glycyrrhiza uralensis*," *AAPS Journal*, vol. 13, no. 1, pp. 1–13, 2011.

[6] H. Traboulsi, A. Cloutier, K. Boyapelly et al., "The flavonoid isoliquiritigenin reduces lung inflammation and mouse morbidity during influenza virus infection," *Antimicrobial Agents and Chemotherapy*, vol. 59, no. 10, pp. 6317–6327, 2015.

[7] H. Cronin and Z. D. Draelos, "Top 10 botanical ingredients in 2010 anti-aging creams," *Journal of Cosmetic Dermatology*, vol. 9, no. 3, pp. 218–225, 2010.

[8] H. M. Mukhtar, S. H. Ansari, M. Ali, Z. A. Bhat, and T. Naved, "Effect of aqueous extract of *Pterocarpus marsupium* wood on alloxan-induced diabetic rats," *Pharmazie*, vol. 60, no. 6, pp. 478–479, 2005.

[9] X. Zhang, P. Zhu, X. Zhang et al., "Natural antioxidant-isoliquiritigenin ameliorates contractile dysfunction of hypoxic cardiomyocytes via AMPK signaling pathway," *Mediators of Inflammation*, vol. 2013, Article ID 390890, 10 pages, 2013.

[10] X. Zhang, E. D. Yeung, J. Wang et al., "Isoliquiritigenin, a natural anti-oxidant, selectively inhibits the proliferation of prostate cancer cells," *Clinical and Experimental Pharmacology and Physiology*, vol. 37, no. 8, pp. 841–847, 2010.

[11] M. Baba, R. Asano, I. Takigami et al., "Studies on cancer chemoprevention by traditional folk medicines XXV. Inhibitory effect of isoliquiritigenin on azoxymethane-induced murine colon aberrant crypt focus formation and carcinogenesis," *Biological and Pharmaceutical Bulletin*, vol. 25, no. 2, pp. 247–250, 2002.

[12] S. Yamamoto, E. Aizu, H. Jiang et al., "The potent anti-tumor-promoting agent isoliquiritigenin," *Carcinogenesis*, vol. 12, no. 2, pp. 317–323, 1991.

[13] S. Yamazaki, T. Morita, H. Endo et al., "Isoliquiritigenin suppresses pulmonary metastasis of mouse renal cell carcinoma," *Cancer Letters*, vol. 183, no. 1, pp. 23–30, 2002.

[14] K. Iwashita, M. Kobori, K. Yamaki, and T. Tsushida, "Flavonoids inhibit cell growth and induce apoptosis in B16 melanoma 4A5 cells," *Bioscience, Biotechnology and Biochemistry*, vol. 64, no. 9, pp. 1813–1820, 2000.

[15] M. Maggiolini, G. Statti, A. Vivacqua et al., "Estrogenic and antiproliferative activities of isoliquiritigenin in MCF7 breast cancer cells," *Journal of Steroid Biochemistry and Molecular Biology*, vol. 82, no. 4-5, pp. 315–322, 2002.

[16] J. Ma, N.-Y. Fu, D.-B. Pang, W.-Y. Wu, and A.-L. Xu, "Apoptosis induced by isoliquiritigenin in human gastric cancer MGC-803 cells," *Planta Medica*, vol. 67, no. 8, pp. 754–757, 2001.

[17] S.-M. Hsia, C.-C. Yu, Y.-H. Shih et al., "Isoliquiritigenin as a cause of DNA damage and inhibitor of ataxia-telangiectasia mutated expression leading to G2/M phase arrest and apoptosis in oral squamous cell carcinoma," *Head and Neck*, vol. 38, supplement 1, pp. E360–E371, 2016.

[18] H. Fu, Y. Zhang, X. Wang et al., "Synthesis and anti-tumor activity of novel aminomethylated derivatives of isoliquiritigenin," *Molecules*, vol. 19, no. 11, pp. 17715–17726, 2014.

[19] Y.-P. Wu, X.-S. Meng, Y.-R. Bao, and S. Wang, "Pharmacokinetic study of four flavones of *Glycyrrhiza* in rat plasma using HPLC-MS," *Journal of Ethnopharmacology*, vol. 148, no. 1, pp. 266–270, 2013.

[20] S. Huang, N. Yang, Y. Liu et al., "Grape seed proanthocyanidins inhibit angiogenesis via the downregulation of both vascular endothelial growth factor and angiopoietin signaling," *Nutrition Research*, vol. 32, no. 7, pp. 530–536, 2012.

[21] G.-S. Zhou, L.-J. Song, and B. Yang, "Isoliquiritigenin inhibits proliferation and induces apoptosis of U87 human glioma cells in vitro," *Molecular Medicine Reports*, vol. 7, no. 2, pp. 531–536, 2013.

[22] Y. Wang, J. Ma, X. Yan et al., "Isoliquiritigenin inhibits proliferation and induces apoptosis via alleviating hypoxia and reducing glycolysis in mouse melanoma B16F10 cells," *Recent Patents on Anti-Cancer Drug Discovery*, vol. 11, no. 2, pp. 215–227, 2016.

[23] Z. Wei, X. Jiang, H. Qiao et al., "STAT3 interacts with Skp2/p27/p21 pathway to regulate the motility and invasion of gastric cancer cells," *Cellular Signalling*, vol. 25, no. 4, pp. 931–938, 2013.

[24] L. Yang, M. Liu, Z. Gu, J. Chen, Y. Yan, and J. Li, "Overexpression of SASH1 related to the decreased invasion ability of human glioma U251 cells," *Tumour Biology*, vol. 33, no. 6, pp. 2255–2263, 2012.

[25] K.-L. Wang, S.-M. Hsia, C.-J. Chan et al., "Inhibitory effects of isoliquiritigenin on the migration and invasion of human breast cancer cells," *Expert Opinion on Therapeutic Targets*, vol. 17, no. 4, pp. 337–349, 2013.

[26] G.-Y. Liou and P. Storz, "Reactive oxygen species in cancer," *Free Radical Research*, vol. 44, no. 5, pp. 479–496, 2010.

[27] T. Ii, Y. Satomi, D. Katoh et al., "Induction of cell cycle arrest and $p21^{CIP1/WAF1}$ expression in human lung cancer cells by isoliquiritigenin," *Cancer Letters*, vol. 207, no. 1, pp. 27–35, 2004.

[28] S. W. Lowe and A. W. Lin, "Apoptosis in cancer," *Carcinogenesis*, vol. 21, no. 3, pp. 485–495, 2000.

[29] Y. Tsujimoto, "Role of Bcl-2 family proteins in apoptosis: apoptosomes or mitochondria?" *Genes to Cells*, vol. 3, no. 11, pp. 697–707, 1998.

[30] T. Kuwana and D. D. Newmeyer, "Bcl-2-family proteins and the role of mitochondria in apoptosis," *Current Opinion in Cell Biology*, vol. 15, no. 6, pp. 691–699, 2003.

[31] V. Kirkin, S. Joos, and M. Zörnig, "The role of Bcl-2 family members in tumorigenesis," *Biochimica et Biophysica Acta (BBA)—Molecular Cell Research*, vol. 1644, no. 2-3, pp. 229–249, 2004.

[32] F. Hirchaud, F. Hermetet, M. Ablise et al., "Isoliquiritigenin induces caspase-dependent apoptosis via downregulation of HPV16 E6 expression in cervical cancer Ca Ski cells," *Planta Medica*, vol. 79, no. 17, pp. 1628–1635, 2013.

[33] M. Iizumi, W. Liu, S. K. Pai, E. Furuta, and K. Watabe, "Drug development against metastasis-related genes and their pathways: a rationale for cancer therapy," *Biochimica et Biophysica Acta (BBA)—Reviews on Cancer*, vol. 1786, no. 2, pp. 87–104, 2008.

[34] C. Gialeli, A. D. Theocharis, and N. K. Karamanos, "Roles of matrix metalloproteinases in cancer progression and their pharmacological targeting," *The FEBS Journal*, vol. 278, no. 1, pp. 16–27, 2011.

[35] Y. K. Lee, Y.-W. Chin, J.-K. Bae, J. S. Seo, and Y. H. Choi, "Pharmacokinetics of isoliquiritigenin and its metabolites in rats: low bioavailability is primarily due to the hepatic and intestinal metabolism," *Planta Medica*, vol. 79, no. 17, pp. 1656–1665, 2013.

[36] C. H. Wu, H. Y. Chen, C. W. Wang et al., "Isoliquiritigenin induces apoptosis and autophagy and inhibits endometrial cancer growth in mice," *Oncotarget*, 2016.

Hindawi
Oxidative Medicine and Cellular Longevity
Volume 2017, Article ID 1512745, 18 pages
https://doi.org/10.1155/2017/1512745

Research Article

Oxidative Stress Triggered by Apigenin Induces Apoptosis in a Comprehensive Panel of Human Cervical Cancer-Derived Cell Lines

Raquel P. Souza,[1,2] Patrícia de S. Bonfim-Mendonça,[2] Fabrícia Gimenes,[1,2] Bianca A. Ratti,[1] Vanessa Kaplum,[3] Marcos L. Bruschi,[3] Celso V. Nakamura,[3] Sueli O. Silva,[1,3] Silvya S. Maria-Engler,[4] and Marcia E. L. Consolaro[1,2,4]

[1]*Postgraduate Program in Bioscience and Physiopathology, Universidade Estadual de Maringá (UEM), Av. Colombo 5790, 87025-210 Maringá, PR, Brazil*
[2]*Clinical Cytology and STD Laboratory, Department of Clinical Analysis and Biomedicine, Universidade Estadual de Maringá (UEM), Av. Colombo 5790, 87025-210 Maringá, PR, Brazil*
[3]*Postgraduate Program in Pharmaceutical Sciences, Laboratory of Research and Development of Drug Delivery Systems, Universidade Estadual de Maringá (UEM), Av. Colombo 5790, 87025-210 Maringá, PR, Brazil*
[4]*Postgraduate Program in Pharmaceutical Science-Clinical Analysis Area, Universidade de São Paulo (USP), Av. Lineu Prestes 580, 05508-900 São Paulo, SP, Brazil*

Correspondence should be addressed to Marcia E. L. Consolaro; melconsolaro@gmail.com

Received 30 August 2016; Revised 13 December 2016; Accepted 18 December 2016; Published 16 January 2017

Academic Editor: Luciano Saso

Recently, the cytotoxic effects of apigenin (4′,5,7-trihydroxyflavone), particularly its marked inhibition of cancer cell viability both in vitro and in vivo, have attracted the attention of the anticancer drug discovery field. Despite this, there are few studies of apigenin in cervical cancer, and these studies have mostly been conducted using HeLa cells. To evaluate the possibility of apigenin as a new therapeutic candidate for cervical cancer, we evaluated its cytotoxic effects in a comprehensive panel of human cervical cancer-derived cell lines including HeLa (human papillomavirus/HPV 18-positive), SiHa (HPV 16-positive), CaSki (HPV 16 and HPV 18-positive), and C33A (HPV-negative) cells in comparison to a nontumorigenic spontaneously immortalized human epithelial cell line (HaCaT). Our results demonstrated that apigenin had a selective cytotoxic effect and could induce apoptosis in all cervical cancer cell lines which were positively marked with Annexin V, but not in HaCaT (control cells). Additionally, apigenin was able to induce mitochondrial redox impairment, once it increased ROS levels and H_2O_2, decreased the $\Delta\psi m$, and increased LPO. Still, apigenin was able to inhibit migration and invasion of cancer cells. Thus, apigenin appears to be a promising new candidate as an anticancer drug for cervical cancer induced by different HPV genotypes.

1. Introduction

At present, cervical cancer is the fourth leading cause of cancer among women worldwide, despite the existence of highly effective prevention and screening methods [1, 2]. Persistent high-risk human papillomavirus (HR-HPV) infection is the central factor in the development of cervical cancer, and HPV 16 and HPV 18 account for approximately 70% of all cases of this cancer [1–4]. Chemoradiotherapy is a standard treatment option for patients with unresectable and locally advanced cervical cancer [5]. The 5-year survival rate of advanced cervical cancer has significantly improved due to the application of concurrent chemoradiotherapy in recent years. However, local recurrence and distant metastasis are still common posttreatment manifestations in patients with advanced cervical cancer. Once posttreatment failure occurs, prognosis becomes worse: the 1-year survival rates of patients with such failures are less than 20% [6]. Moreover, various side effects are produced that can greatly influence a patient's quality of life [7]. Despite these alarming facts, efficient methods of treatment are still lacking.

In recent decades, various natural products have been evaluated as potential anticancer drugs, both in unmodified (naturally occurring) and modified (synthetically modified) forms [8]. Almost 50% of all anticancer agents that have entered clinical use since 1940 are either natural products or their direct derivatives [9]. Flavonoids are a class of plant secondary metabolites that exhibit a variety of activities, including antibacterial, antiviral, antioxidant, and anticancer effects [10]. Flavonoids comprise approximately 6,000 compounds that are characterized and are distinguished from other aromatic compounds by having a common phenylchromanone structure (C6-C3-C6) consisting of two benzene aromatic rings (A and B rings) linked by three carbons that are usually in an oxygenated central pyrone ring (C ring) [11–13]. Based on the saturation level and opening of the central pyran ring, flavonoids can be classified into distinct subclasses including flavanols, flavanones, flavanonols, flavonols, anthocyanidins, isoflavones, and flavones [14–16]. Flavones and flavonols are structurally similar compounds, with flavonols having an extra hydroxyl substitution at the carbon 3-position. Apigenin is a flavonoid belonging to the flavone structural class and chemically known as 4′,5,7,-trihydroxyflavone (Figure 1). Apigenin is a low molecular weight flavonoid (MW 270.24) structurally forming yellow needles in pure form. It is incompatible with strong oxidizing agents [17]. Apigenin exist in propolis as well as in vegetables and fruits such as onions, oranges, and parsley [14, 18]. Apigenin possesses significant actions that suppress inflammation, viruses, oxidation, and carcinogenesis [19].

Apigenin is of particular interest as an antitumor agent since it exhibits lower intrinsic toxicity and is not mutagenic compared to other structurally related flavonoids [20–23]. Furthermore, apigenin has shown marked effects in inhibiting cancer cell growth in cell culture systems and in in vivo tumor models [14, 19] of a variety of human cancers, including colon, breast, pancreatic, oral squamous, lung, ovarian, prostate, and skin cancer as well as leukemia, by regulation of diverse signaling pathways [21, 24–30]. Apigenin has also been demonstrated to inhibit tumor cell invasion and metastasis [19, 31]. According to previous studies, apigenin inhibits insulin-like growth factor 1 (IGF-1) induced cell cycle progression and insulin receptor substrate-1 (IRS-1) tyrosine phosphorylation and upregulates insulin-like growth factor binding protein 3 (IGFBP-3) through modulation of IGF axis signaling in prostate cancer [32, 33]. IGF-1 promotes intercellular signaling through links with the IGF-1 receptor which exists in various primary cells. IGF-1 receptor signaling is associated with activation of phosphatidylinositol 3-kinase (PI3K) and mitogen-activated protein kinase (MAPK) pathways that stimulate proliferation and apoptosis of cells [34]. In addition, apigenin inhibits proliferation of lung cancer cells by inhibiting vascular endothelial growth factor (VEGF) transcriptional activation and by inhibiting the phosphorylation of AKT and P70S6K [35]. Moreover, apigenin suppresses aflatoxin B1 which is the most toxic aflatoxin involved in hepatocellular carcinoma and stimulates cell cycle arrest and reduction of CDK4 with an increase in p53 and p21, respectively, in hepatocellular carcinoma [36–38].

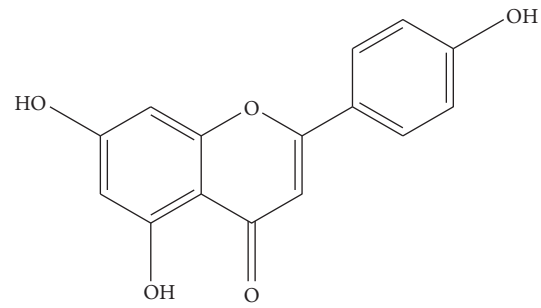

Figure 1: Chemical structure of apigenin.

Although apigenin represents a promising chemotherapeutic agent for cancer therapy, little information is available regarding the effects of apigenin against cervical cancer, and the available data were mostly obtained in the HeLa cell line [39–42]. HeLa cells were derived from a case of adenocarcinoma of the uterine cervix in 1952 and contain integrated HPV 18 [43]. Notably, previous studies did not assess the cytotoxic activity of apigenin in cell lines containing HPV 16, which is the most prevalent genotype and the main causative agent of squamous cell cervical cancer (approximately 50% of total) [1, 4, 44]. Additionally, the cytotoxic activity of apigenin has not been evaluated in cell lines derived from squamous cell cervical cancer, which is the most common type of cervical cancer worldwide (75%–85% of total) [45, 46].

In the present study, we investigated the antitumoral effects of apigenin in a comprehensive panel of human cervical cancer-derived cell lines, including HeLa (HPV 18-positive), SiHa (HPV 16-positive), CaSki (HPV 16 and 18-positive), and C33A (HPV-negative), compared to a nontumorigenic human epithelial cell line (HaCaT). The objectives of this study were to investigate effects of apigenin on HeLa, SiHa, CaSki, C33A, and HaCaT cells with respect to (i) cell cytotoxicity, migration, and invasion of those cells; (ii) cell death pathway and cellular oxidative stress. Our results demonstrated that apigenin has a selective cytotoxic effect: it induced apoptosis in all cervical cancer cell lines, but not in HaCaT cells. Additionally, apigenin induced mitochondrial redox impairment and inhibited cancer cell migration and invasion.

2. Materials and Methods

2.1. Chemicals. Apigenin (4′,5,7-trihydroxyflavone) with ≥ 98% purity was purchased from Cayman Chemical Company (Cat No. 10010275, Ann Arbor, MI, USA). Dimethyl sulfoxide (DMSO), diphenyl-1-pyrenylphosphine (DPPP), Dulbecco's modified Eagle's medium (DMEM), violet crystal, and tetramethylrhodamine ethyl ester (TMRE) were purchased from Sigma-Aldrich (St. Louis, MO, USA). Fetal bovine serum (FBS), penicillin/streptomycin, trypsin/EDTA solution, and trypan blue were purchased from Gibco (Grand Island, NY, USA). Annexin V/FITC, MTT [3-(4,5-dimethylthiazol-2-yl)-2,5-diphenyltetrazolium bromide] and propidium iodide were obtained from Invitrogen (Eugene, OR, USA). X-Gal was obtained from Life Technologies (Grand Island, NY, USA). 2′,7′-Dichlorodihydrofluorescein

diacetate (H_2DCFDA) was obtained from Molecular Probes (Eugene, OR, USA). Matrigel was purchased from Becton–Dickinson (San Jose, CA, USA). All other reagents were purchased from Synth (Diadema, SP, BR).

2.2. Cell Lines and Culture Conditions. Human cell lines derived from invasive cervical cancer, including the HeLa (integrated HPV 18), SiHa (1 to 2 copies of HPV 16 integrated per cell), and CaSki (approximately 600 copies of HPV 16 integrated per cell, as well as sequences of HPV 18) lines, as well as the spontaneously immortalized human epithelial cell line HaCaT (nontumorigenic control cells) [47, 48], were kindly donated by Dr. Luisa L. Villa (ICESP, School of Medicine, University of São Paulo/Brazil) and Dr. Silvya S. Maria-Engler (Faculty of Pharmaceutical Sciences, University of São Paulo). The C33A cell line, a human cell line derived from invasive cervical cancer, was purchased from the American Type Culture Collection (Rockville, MD; HTB-31). All cell lines were maintained in a culture flask in DMEM supplemented with 10% fetal bovine serum (FBS) and 0.5 U/mL of penicillin/streptomycin at 37°C in a 5% CO_2 atmosphere at 100% humidity. HaCaT cells were maintained under the same conditions but were cultured with high-glucose DMEM.

2.3. Treatments. Apigenin was dispersed in dimethyl sulfoxide (DMSO) at a concentration of 200 mM and stored at −20°C. After reaching subconfluence (70%–80% confluency), cells were exposed to apigenin diluted in DMEM (2.5–100 μM) [40, 41] for 24, 48, and 72 h. Cells treated with DMEM or DMSO alone (0.5% final concentration) were used as negative controls in all assays.

2.4. Cell Cytotoxicity Assays. Cell cytotoxicity was determined by both MTT and trypan blue assays. Briefly, HeLa, SiHa, CaSki, C33A, and HaCaT cells (5×10^4 cells/mL per well) were inoculated into 96-well plates upon reaching subconfluence (70%–80% confluency) and were treated with 2.5–100 μM apigenin as described above for 24, 48, or 72 h.

After the incubation, MTT (5 mg/mL) was added to each well, and the plates were incubated in the dark at 37°C for 4 h. At the end of the incubation, the medium was removed, the resulting formazan was dissolved in 150 μL DMSO, and the optical density (OD) was measured at 570 nm using a multiwell microplate reader (Bio Tek-Power Wave XS, VT, USA). The 3-(4,5-dimethyl- 2-thiazolyl)-2,5-diphenyl-2H-tetrazolium bromide (MTT) assay is based on the ability of living cells to reduce MTT to insoluble formazan crystal violet via mitochondrial dehydrogenase [49].

For the trypan blue exclusion staining [50], after the incubation period, the medium was removed, the cells were washed with phosphate-buffered saline (PBS), and 200 μL of 0.25% trypsin/EDTA solution was added to detach the cells from the plate. Cell viability was assessed by counting live versus dead cells using standard trypan blue (0.4% in PBS) on a hemocytometer under an inverted microscope (EVOS FL Cell Imaging System, Life Technologies, CA, USA). For both the MTT and trypan blue assays, the results were expressed as a percentage of the control cells, which was considered to represent 100% cell viability. The data are shown as the mean values ± standard deviation (SD) of three independent experiments conducted in triplicate.

IC_{50} (i.e., the concentration that inhibited cell growth by 50% compared to untreated controls) and IC_{90} (i.e., the concentration that inhibited cell growth by 90% compared to untreated controls) values were obtained by nonlinear regression analysis using GraphPad Prism (GraphPad Software, San Diego, CA).

Additionally, each cell line (5×10^4 cells/mL) was inoculated onto 6-well plates and cultured in 10% FBS-DMEM medium at 37°C in a humidified atmosphere with 5% CO_2. After reaching subconfluence, the cells were treated with 10% FBS-DMEM medium containing 2.5, 60, and 100 μM apigenin. Untreated cells were used as controls. The growth state and morphology of the cells were observed after 72 h under an inverted microscope (EVOS FL Cell Imaging System, Life Technologies, CA, USA).

2.5. Colony Forming Assay. To determine the long-term cytotoxicity effects of apigenin, a clonogenic assay was used [51]. All cell lines were seeded in 60 mm plates at a density of 600 cells/plate/4 mL. After 24 h, the cells were exposed to apigenin and incubated in ideal conditions for 14 days (medium was changed every 3 days). Additionally, the recovery ability of colonies was evaluated. For this purpose, we treated the plates with apigenin, which had exhibited toxic effects after 14 days of exposure in previous studies, for 1, 6, 18, 24, 48, or 72 h or 7 days. After each exposure time, supernatants were exchanged for fresh DMEM medium with 10% FBS without dye, and the cell cultures were kept for 14 days. The colonies formed from each cell line were stained with crystal violet after fixation with methanol and counted manually. The results are expressed as survival fractions, which were obtained by dividing the number of colonies that arose after treatment by the number of cells seeded and plate efficiency (PE: number of colonies formed by untreated cells/number of cells seeded) multiplied by 100.

2.6. Analysis of Senescence. Cell senescence was evaluated as described by Gary and Kindell (2005) using β-galactosidase [52]. Briefly, cell lines were incubated with apigenin (IC_{50} of each cell line) for 48 h before β-galactosidase activity determination. Then, the cells were washed twice in PBS and fixed in fixation solution containing 0.5% glutaraldehyde for 15 min. The fixation solution was removed by washing the cells twice with PBS containing $MgCl_2$, and then X-Gal staining solution was added. The cells were then incubated at 37°C in a CO_2-free environment for 4 h. Doxorubicin was used at a concentration of 5 μg/mL as a positive control. Cells with blue-stained cytoplasm were considered senescent, and the percentage of such cells was determined after counting three random fields of 100 cells each. Data are shown as the mean value ± SD of three independent experiments conducted in triplicate.

2.7. Analysis of Cell Death by Apoptosis. Apoptosis was assayed using Annexin V-FITC/propidium iodide (PI) based

on a previously described protocol with some modification [53]. Briefly, 1.0×10^4 cells/well were seeded overnight in 24-well plates. The cells were treated with apigenin (IC_{50} of each cell line) for 48 h. After treatment, the cells in the supernatant and the adherent cells were washed with PBS and binding buffer (10 mM HEPES, pH 7.5, containing 140 mM NaCl and 2.5 mM $CaCl_2$) and stained with 1 μg of FITC-conjugated Annexin-V for 15 min and 40 μg/mL of PI for 5 min. Camptothecin (20 μM) and digitonin (80 μM) were used as positive controls for apoptosis and necrosis, respectively. Cells not treated with apigenin were used as negative controls. Each sample was analyzed using an inverted flow microscope (EVOS FL Cell Imaging System, Life Technologies, CA, USA) to distinguish apoptotic (green fluorescence) and necrotic cells (red fluorescence).

2.8. Analysis of Cell Membrane Integrity. Cell membrane integrity was evaluated as described by Britta et al. (2012) with minor modifications, using PI to determine whether cell death triggered by apigenin involved the necrotic death pathway [54]. To accomplish this, cells were treated with apigenin (IC_{50} according to each cell line) for 48 h, washed with PBS, and incubated with 4 μg/mL PI for 10 min. Digitonin (80 μM) was used as a positive control, and untreated cells were used as negative controls. Fluorescence was determined at an excitation wavelength of 480 nm and an emission wavelength of 580 nm under a fluorescence microplate reader (Victor X3, PerkinElmer, Finland). Arbitrary units (relative fluorescence units, RFU) were directly based on fluorescence intensity, and the fluorescence was normalized to the number of cells [55].

2.9. Assessment of Cellular Oxidative Stress. Total reactive oxygen species (ROS), mitochondrial transmembrane potential, lipid peroxidation, and extracellular H_2O_2 levels were measured using spectrofluorometric assays with a fluorescence microplate reader (Victor X3, PerkinElmer, Finland). Arbitrary units (RFU) were based directly on fluorescence intensity, and the fluorescence was normalized to the number of cells. For all assays, cells not treated with apigenin were used as negative controls.

2.9.1. Measurement of Total Reactive Oxygen Species. Total ROS production was measured based on an increase in fluorescence caused by the conversion of nonfluorescent dye to highly fluorescent 2′,7′-dichlorodihydrofluorescein diacetate (H_2DCFDA) [56]. Cells (2.5×10^5 cells/mL) were plated in 24-well plates and incubated at 37°C in CO_2 for 24 h. Then, the cells were incubated with apigenin (IC_{50} according to cell line) for 48 h, centrifuged, washed, and resuspended in PBS (pH 7.4). Afterwards, the cells were treated with 10 μM H_2DCFDA, a permeable probe, in the dark for 30 min. H_2O_2 (200 μM) was used as a positive control. Fluorescence intensity was analyzed at an excitation wavelength of 488 nm and an emission wavelength of 530 nm.

2.9.2. Detection of Extracellular H_2O_2 Levels. We assessed the production of H_2O_2, a type of ROS, using an Amplex Red assay kit (Molecular Probes, Life Technologies) according to the manufacturer's instructions. Cells (2.5×10^5 cells/mL) were plated in 24-well plates, treated with apigenin (IC_{50} according to each cell line) and incubated for 48 h at 37°C in CO_2. Following the treatments, trypsinized cells were suspended in PBS containing Amplex Red reagent (12 μM) and horseradish peroxidase (0.05 U/ml). H_2O_2 (200 μM) was used as a positive control. Fluorescence was determined at an excitation wavelength of 563 nm and an emission wavelength of 580 nm.

2.9.3. Determination of Mitochondrial Transmembrane Potential ($\Delta\Psi m$). Changes in mitochondrial transmembrane potential ($\Delta\Psi m$) were analyzed using a TMRE (tetramethylrhodamine, ethyl ester) assay [57]. Briefly, cells (2.5×10^5 cells/mL) were seeded in 24-well plates and incubated for 48 h at 37°C in CO_2. Then, they were treated with apigenin (IC_{50} of each cell line) for 48 h at 37°C in a CO_2 incubator. Supernatants were removed from the culture dishes, and adherent cells were detached with trypsin-EDTA. The cells were collected by centrifugation, resuspended in staining solution with 25 nM TMRE, and incubated at 37°C in CO_2 for 30 min in the dark. Carbonyl cyanide m-chlorophenylhydrazone (CCCP) was used as a positive control (100 μM). Fluorescence intensity was analyzed at an excitation wavelength of 540 nm and an emission wavelength of 595 nm.

2.9.4. Lipid Peroxidation Assay. The extent of lipid peroxidation (LPO) was determined based on the amount of diphenyl-1-pyrenylphosphine (DPPP), which is essentially nonfluorescent until it is oxidized to a phosphine oxide (DPPP-O) by peroxides [58]. Cells (2.5×10^5 cells/mL) were plated in 24-well plates and incubated at 37°C in CO_2. Then, they were treated with apigenin (IC_{50} according to each cell line) for 48 h, followed by treatment with 50 μM DPPP for 15 min at room temperature. Hydrogen peroxide was used as a positive control (200 μM). Fluorescence was determined at an excitation wavelength of 355 nm and an emission wavelength of 380 nm.

2.9.5. Catalase Activity Measurement. We measured the activity of catalase, an enzyme involved in the cell antioxidant system, based on the ability of the enzyme to break down H_2O_2. Briefly, cells (5×10^5 cells/mL) were plated in 6-well plates. Then, they were treated with apigenin (IC_{50} and IC_{90} for each cell line) for 48 h at 37°C in CO_2. Following the treatments, the cells were lysed with RIPA buffer for protein extraction on ice. The lysates were added to 1 M Tris buffer containing 5 mM EDTA and 50 mM H_2O_2 (pH 8.0). The rate of H_2O_2 decomposition was monitored spectrophotometrically (UV-2550, Shimadzu, Japan) at 240 nm for 60 seconds. Catalase activity was expressed as H_2O_2 consumed/min × mg protein (ε, 33.33 $M^{-1} \times cm^{-1}$) [59].

2.10. Cell Migration and Invasion Analysis

2.10.1. Wound-Healing Migration Assay. Wound-healing assays were performed as previously described [60]. Suspensions of each cell line were seeded in 6-well plates (2.5×10^4 cells/mL) and cultured in medium containing 10% FBS.

Confluent monolayers of the cells were then mechanically scratched with a blue pipet tip (1000 μL), and cell debris was removed by washing with PBS. Then, the wounded monolayer was incubated with apigenin (IC_{30} treatment), DMSO, and culture medium (controls). Cell migration into the scratched region was recorded using an inverted microscope (EVOS FL Cell Imaging System, Life Technologies, CA, USA) at 0, 24, 48, and 72 h. Wound closure after 24, 48, and 72 h was compared to the initial measurements.

2.10.2. Invasion Assay. Transwell invasion chambers containing polycarbonate filters (8 μm, Costar Corp., Cambridge, MA) were coated on the upper surface with Matrigel (Becton-Dickinson, San Jose, CA). Cervical cancer cell lines (5×10^4 cells/mL) were suspended in serum-free DMEM and added to the upper chamber. Both the lower and upper chambers contained DMEM and apigenin (IC_{50} and IC_{90} of each cell line). Cells not treated with apigenin were used as a negative control. All cells were incubated for 48 h at 37°C in CO_2. Cells on the upper surface of the filter were completely removed by wiping them with a cotton swab. Cells that had invaded through the Matrigel and reached the lower surface of the filter were fixed in 10% formalin, stained with a toluidine blue solution, and counted under a light microscope at 20x magnification. The mean number of cells in 10 fields was calculated, and the assay was performed in triplicate [61].

2.11. Statistical Analysis. Data distributions were expressed as mean ± standard deviation (SD) of independent experiments in triplicate. Significant differences among means were identified using the GraphPad Prism® 6.0 software (CA, USA). The ANOVA test followed by Tukey–Kramer test was used to calculate the multiple comparisons, for example, cell death by apoptosis, cell membrane integrity, cellular oxidative stress, reactive oxygen species, cells migration, and invasion analysis. The Student's t-distribution was used to compare cytotoxic effects of apigenin on cervical cancer cell lines to control cells. Values of $P < 0.05$ were considered statistically significant.

3. Results

3.1. Apigenin Inhibits Cervical Cancer Cell Viability but Is Not Cytotoxic to HaCaT Cells. To study the effects of apigenin treatment on tumor cells as well as normal cells, we exposed four cervical cancer cell lines, the HeLa (integrated HPV 18), SiHa (integrated HPV 16), CaSki (integrated HPV 16 and HPV 18), and C33A (without HPV) cell lines, as well as a human immortalized keratinocyte (HaCaT) cell line (control cells), to increasing doses of apigenin over a maximum of 72 h.

As indicated in Figures 2(a)–2(c), apigenin exerted concentration-dependent cytotoxic effects on all cervical cancer cell lines tested, with an IC_{50} of 10 μM for HeLa, 68 μM for SiHa, 76 μM for CaSki, and 40 μM for C33A cells at 72 h. Apigenin showed selective action in cancer cells, as it was not able to significantly reduce HaCaT cell viability at the tested concentrations. The IC_{50} values are shown in Figure 2(b).

The dose-response graph obtained from the MTT assays and trypan blue dye exclusion tests shows a significant decrease in the percentage of cell viability of all cervical cancer cell lines compared to the HaCaT cells after apigenin exposure (Figure 2(a)). More specifically, among the cervical cancer cell lines tested, the HeLa cells showed a higher reduction of cell viability at a lower apigenin concentration (10 μM) at 48 h ($P = 0.0012$) and 72 h ($P = 0.001$) of exposure. The CaSki and SiHa cell lines showed similar decreases in cell viability, reaching significant levels at 40 μM at 48 h ($P = 0.029$ and $P = 0.017$, resp.) and at 72 h ($P = 0.012$ and $P = 0.008$, resp.). Additionally, the C33A cell line showed a significant reduction in cell viability at 40 μM ($P = 0.021$), but only after 72 h of apigenin exposure. Additionally, apigenin did not significantly reduce HaCaT cell viability at any concentration or time tested ($P = 0.321$), highlighting the selective action of apigenin towards cancer cells.

The cell growth inhibition induced by apigenin was further verified by microscopic observation. The results in Figure 2(c) show that the growth of HeLa, SiHa, CaSki, and C33A cells was effectively inhibited after exposure to 2.5–100 μM apigenin for 72 h, whereas HaCaT cell growth was unaffected. Apigenin also induced pronounced morphological changes due to cell death when the cervical cancer cell lines were exposed to 60 μM and 100 μM concentrations for 72 h. The cells exhibited retraction of cytoplasmic expansion and detachment from the plate due to cell death. Morphological changes were not observed in HaCaT cells exposed to the same concentrations of apigenin for the same length of time.

To further examine the long-term cytotoxicity of apigenin, clonogenic assays were performed. For this purpose, we exposed all cervical cancer cell lines and HaCaT cells to subtoxic doses of apigenin (IC_{30}). After 14 days of incubation, colony formation was inhibited by 100% in the HeLa, SiHa, CaSki, and C33A cells compared with untreated cells (Figure 3). In the HaCaT cells, colony formation was equivalent after 14 days of incubation with apigenin compared to the untreated cells. Based on this finding, we tested the capability of the cells to recover from damage after 1, 6, 18, 24, 48, and 72 h and 7 days of exposure to apigenin, followed by the addition of DMEM. The results presented in Figure 3 indicate that although recovery occurred after 1 h of exposure, there was a decrease in the number of colonies after this time.

These data indicate that apigenin exerts concentration-dependent cytotoxic effects on HeLa, SiHa, CaSki, and C33A cells. More importantly, apigenin showed selective action towards cancer cells, as it did not reduce HaCaT viability.

3.2. Apigenin Does Not Induce Cell Senescence. Cell senescence was studied by staining [52] with β-galactosidase, a biomarker for senescence in mammalian cells, which exhibit lysosomal-galactosidase activity at an optimal pH of 4.0. Cells that are in a state of replicative senescence express senescence-associated galactosidase activity, which is measured at pH 6.0. Senescence was not observed after apigenin exposure in any cervical cancer cell line or in the HaCaT cells, as blue SA-b-Gal staining was not observed. Therefore, we found that apigenin did not effectively induce senescence in cervical cancer cells (data not shown).

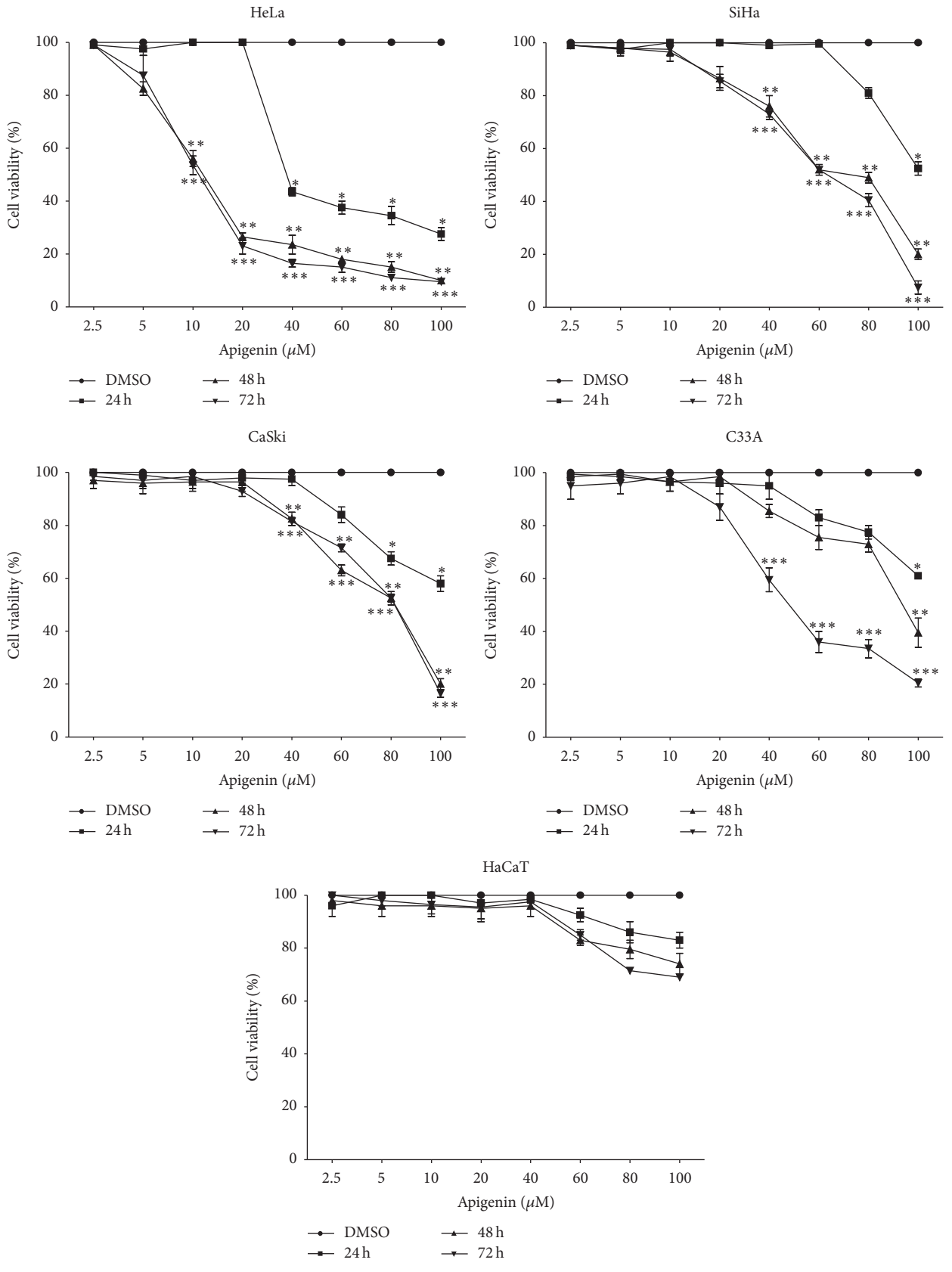

(a)

Figure 2: Continued.

	IC_{50} (μM)		
	24 h	48 h	72 h
HeLa	38	10	10
SiHa	89	72	68
CaSki	—	75	76
C33A	—	83	40
HaCaT*	—	—	—

(b)

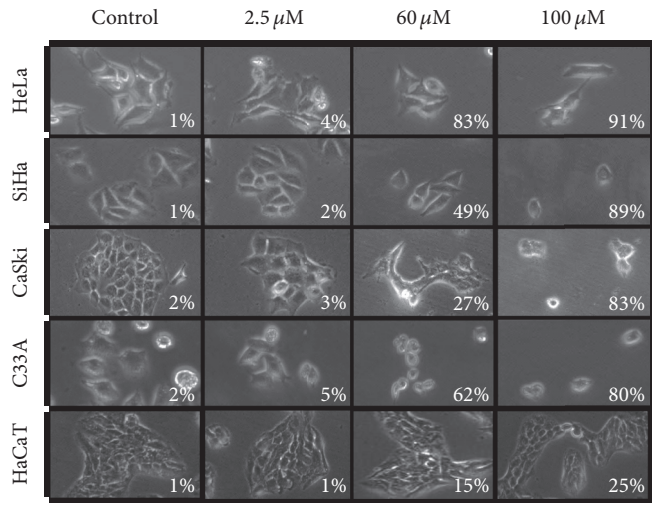

(c)

Figure 2: Cytotoxic effects of apigenin on cervical cancer cell lines (HeLa, SiHa, CaSki, and C33A cells) and a human keratinocyte cell line (HaCaT cells). (a) Dose-response curves indicating the viability of the cervical cancer cell lines and the HaCaT cells (control cells) following exposure to apigenin (2.5–100 μM) for 24, 48, and 72 h. A statistically significant difference in cell viability was observed between the HeLa, SiHa, CaSki, and C33A cells and the HaCaT cells. (*), (**), and (***) represent statistically significant ($P < 0.05$) differences (24, 48, and 72 h, resp.) between the cancer cell lines and the control cells. (b) Approximate IC_{50} values determined according to the cell viability obtained in (a). *For the HaCaT cells, the IC_{50} value was > 100 μM. Each line represents the mean ± SD of three separate experiments conducted in triplicate. (c) Differential effects on cell morphology induced by apigenin after 72 h of exposure. Cell photomicrographs were taken (20x magnification), and the percentage of cell death was determined by Trypan blue staining. Note that the HaCaT cells do not show morphological changes.

3.3. Apigenin Induces Apoptotic Death in Cervical Cancer Cells. As described above, apigenin treatment induces a significant decrease in cancer cell viability. To determine the type and extent of cell death, we analyzed whether apigenin could induce apoptosis in cervical cancer cells via an Annexin V-FITC/PI assay using fluorescence imaging. Annexin V staining detects the translocation of phosphatidylserine from the inner to the outer cell membrane during early apoptosis (green fluorescence), and PI can enter the cell during necrosis or late-stage apoptosis; it can also enter dead cells (red fluorescence) [53]. Apigenin induced apoptosis in all cervical cancer cell lines after 48 h of exposure. As shown in Figure 4(a), cellular apoptosis considerably increased in the apigenin-treated cancer cells compared to the control group. More specifically, at the IC_{50} of each cancer cell line, apigenin induced significant apoptosis, as the cells were positively marked with Annexin V (green) but not induced to undergo necrosis (unmarked PI-red). Apigenin did not induce death in HaCaT cells (unmarked by either Annexin V or PI).

In Figures 4(b)–4(f), the histograms show the mean % Annexin V-positive cells in the cell lines treated with apigenin (IC_{50} of each cancer cell line) for 48 h. Mean Annexin V-positive cell numbers of approximately 100% were found in the HeLa ($P = 0.0001$; Figure 4(b)), SiHa ($P = 0.00015$; Figure 4(c)), CaSki ($P = 0.00012$; Figure 4(d)), and C33A ($P = 0.00016$; Figure 3(e)) cells, whereas approximately 5–15% of cells were PI-positive. In Figure 4(f), the histogram shows that apigenin exposure for 48 h did not induce death in HaCaT cells; only approximately 4% of these cells were marked with Annexin V ($P = 0.2879$) and PI, similar to the negative control. These data demonstrate that apigenin can selectively induce apoptosis in cervical cancer cells.

To further confirm the mechanism of cell death triggered by apigenin, we evaluated plasma membrane integrity in cervical cancer cell lines and HaCaT cells treated with apigenin and stained with PI, which diffuses across permeable membranes and binds to nucleic acids [54]. As shown in Figure 5, all cervical cancer cell lines showed significantly lower fluorescence than the positive control (HeLa, $P = 0.011$; SiHa, $P = 0.024$; CaSki, $P = 0.001$; C33A, $P = 0.0013$) and HaCaT cells ($P = 0.0112$) after apigenin exposure (IC_{50}). These data indicate that apigenin exposure did not induce the cell membrane rupture that occurs in necrosis and late apoptosis and confirm that apoptosis is the death pathway triggered by apigenin.

3.4. Apigenin Induces Oxidative Stress in Cervical Cancer Cell Lines. We next investigated oxidative stress because of the high antioxidant potential attributed to apigenin [14, 62]. We began studying the mechanistic action of this compound by examining the production of total ROS. To accomplish this, we evaluated the effects of total ROS production after apigenin exposure in the cervical cancer cell lines and HaCaT cells using H_2DCFDA, a fluorescent probe. This probe primarily detects H_2O_2 and hydroxyl radicals and fluoresces after forming dichlorofluorescein [63]. Our results showed that apigenin significantly increased total ROS production in all cervical cancer cell lines compared with the negative control (untreated cells) (HeLa, $P = 0.013$; SiHa, $P = 0.015$; CaSki, $P = 0.0021$; C33A, $P = 0.011$). This increase in ROS

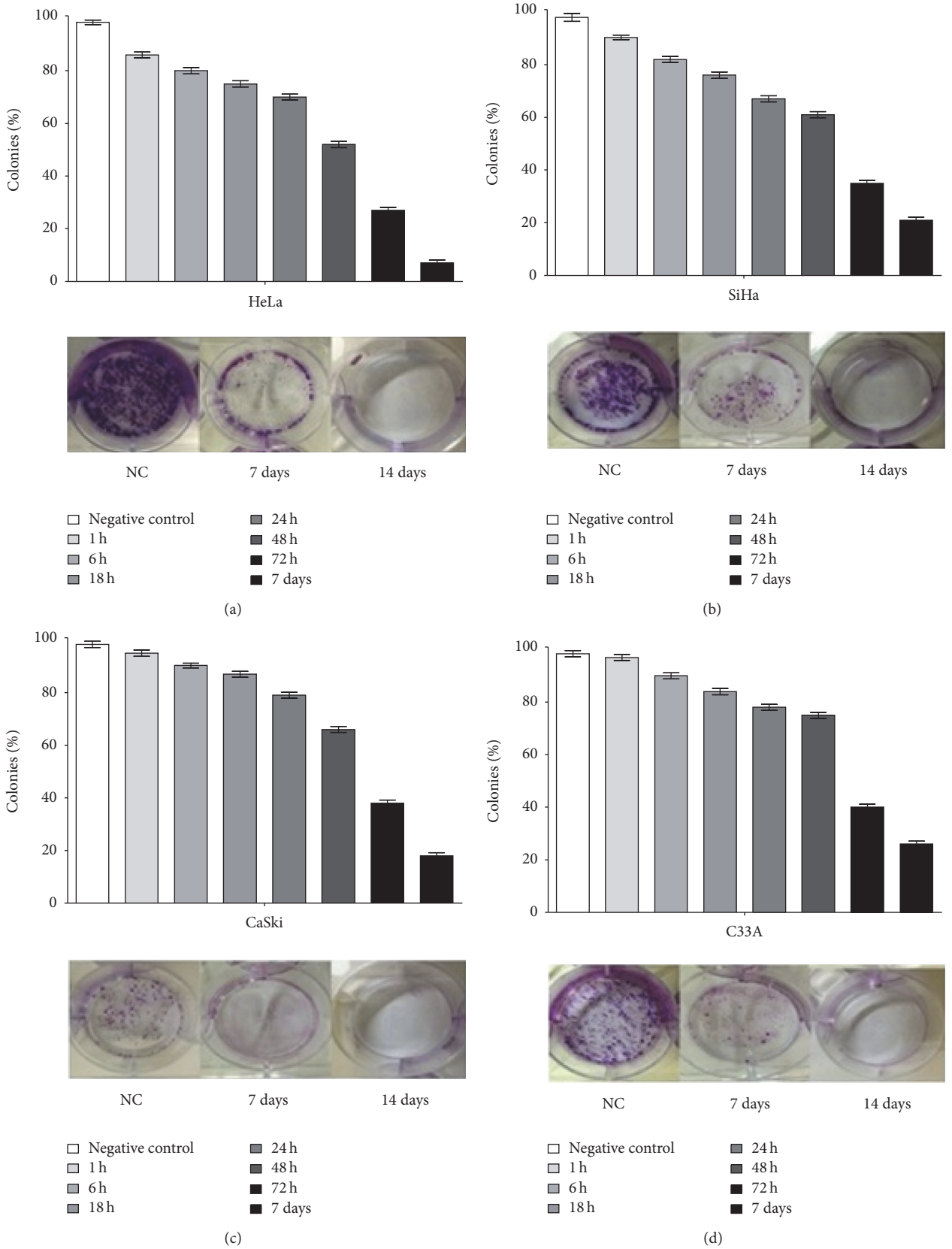

Figure 3: Continued.

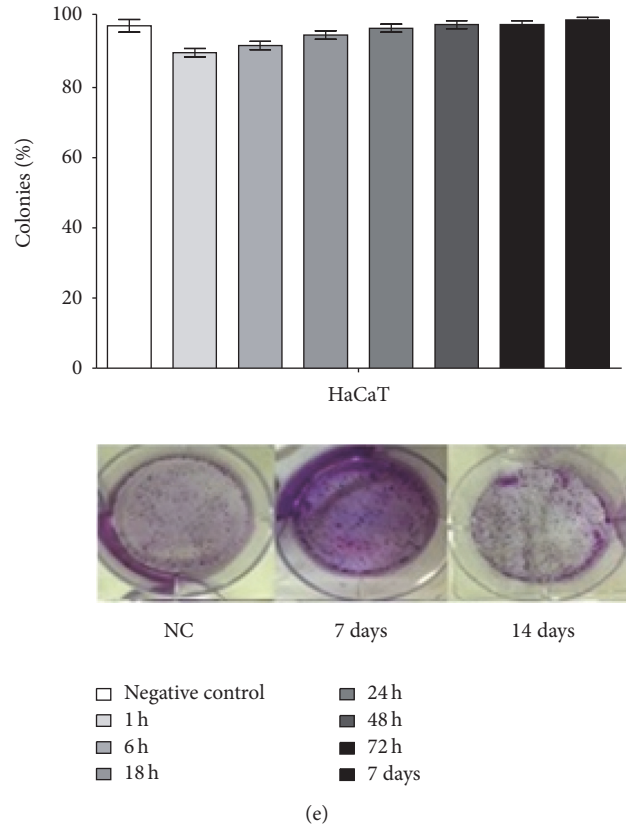

Figure 3: The effect of apigenin exposure on the clonogenicity of cervical cancer cell lines and human keratinocytes at 1, 6, 18, 24, and 48 h and 7 and 14 days followed by culture with DMEM. The graph indicates that colony recovery diminished with increasing times of exposure in cervical cancer cell lines ((a) HeLa; (b) SiHa; (c) CaSki; (d) C33A) and increased with time of exposure in HaCaT cells (e). Data are shown as the mean values ± SD of three independent experiments conducted in triplicate. Photos indicate that exposure to apigenin reduced colony formation by 7 days and prevented colony formation after 14 days in HeLa (a), SiHa (b), CaSki (c), and C33A (d) cells. In HaCaT cells (f), colony formation continued to be equivalent after 7 and 14 days of apigenin exposure.

production was similar to that induced by the positive control (cells treated only with H_2DCFDA). Moreover, total ROS production was not changed in the HaCaT cells after exposure to apigenin ($P = 0.214$); rather, the cells maintained ROS levels similar to the negative control (Figure 6(a)). Because increased ROS generation in the cytosol occurs in most apoptotic cells, these results further support that apoptosis is the cell death pathway caused by apigenin and that this is likely a result of oxidative stress.

Next, we assessed the production of H_2O_2, which is a type of ROS. Extracellular H_2O_2 levels were detected using an Amplex Red assay. Our results showed that apigenin significantly increased H_2O_2 levels in all cervical cancer cell lines compared with the negative control (untreated cells) (HeLa, $P = 0.0164$; SiHa, $P = 0.0212$; CaSki, $P = 0.0055$; C33A, $P = 0.0005$). H_2O_2 production was not changed after exposure to apigenin in HaCaT cells ($P = 0.0506$) (Figure 6(b)).

We next evaluated the effect of apigenin exposure on mitochondrial membrane potential ($\Delta\Psi m$). $\Delta\psi m$ changes are an additional indication of apoptosis; $\Delta\psi m$ contributes to the process that facilitates the exit of many apoptogenic factors to the cytosol. We used a TMRE assay, which quantifies changes in mitochondrial membrane potential in live cells, and a cell-permeable, positively charged, red-orange dye that readily accumulates in active mitochondria due to their relative negative charge. Depolarized or inactive mitochondria exhibit decreased $\Delta\psi m$ and failure to sequester TMRE [57]. Our results showed that apigenin significantly decreased the $\Delta\psi m$ in all cervical cancer cell lines compared with the negative control (untreated cells) (HeLa, $P = 0.0032$; SiHa, $P = 0.0393$; CaSki, $P = 0.0055$; C33A, $P = 0.0081$). Furthermore, $\Delta\psi m$ did not change in HaCaT cells after exposure to apigenin ($P = 0.0668$) (Figure 6(c)).

Next, we evaluated the effect of apigenin exposure on lipid peroxidation (LPO), which can be defined as a cascade of biochemical events resulting from the action of free radicals on the unsaturated lipids of cell membranes. This process primarily generates alkyl, peroxyl, and alkoxyl radicals, leading to the destruction of unsaturated lipid structure, the failure of mechanisms that exchange metabolites, and the induction of cell death by apoptosis. Therefore, LPO can be used as an indicator of cellular oxidative stress [58]. We determined the amount of diphenyl-1-pyrenylphosphine (DPPP) that is essentially nonfluorescent until it is oxidized to a phosphine oxide (DPPP-O) by peroxides. Our results showed that apigenin significantly increased LPO in all cervical cancer

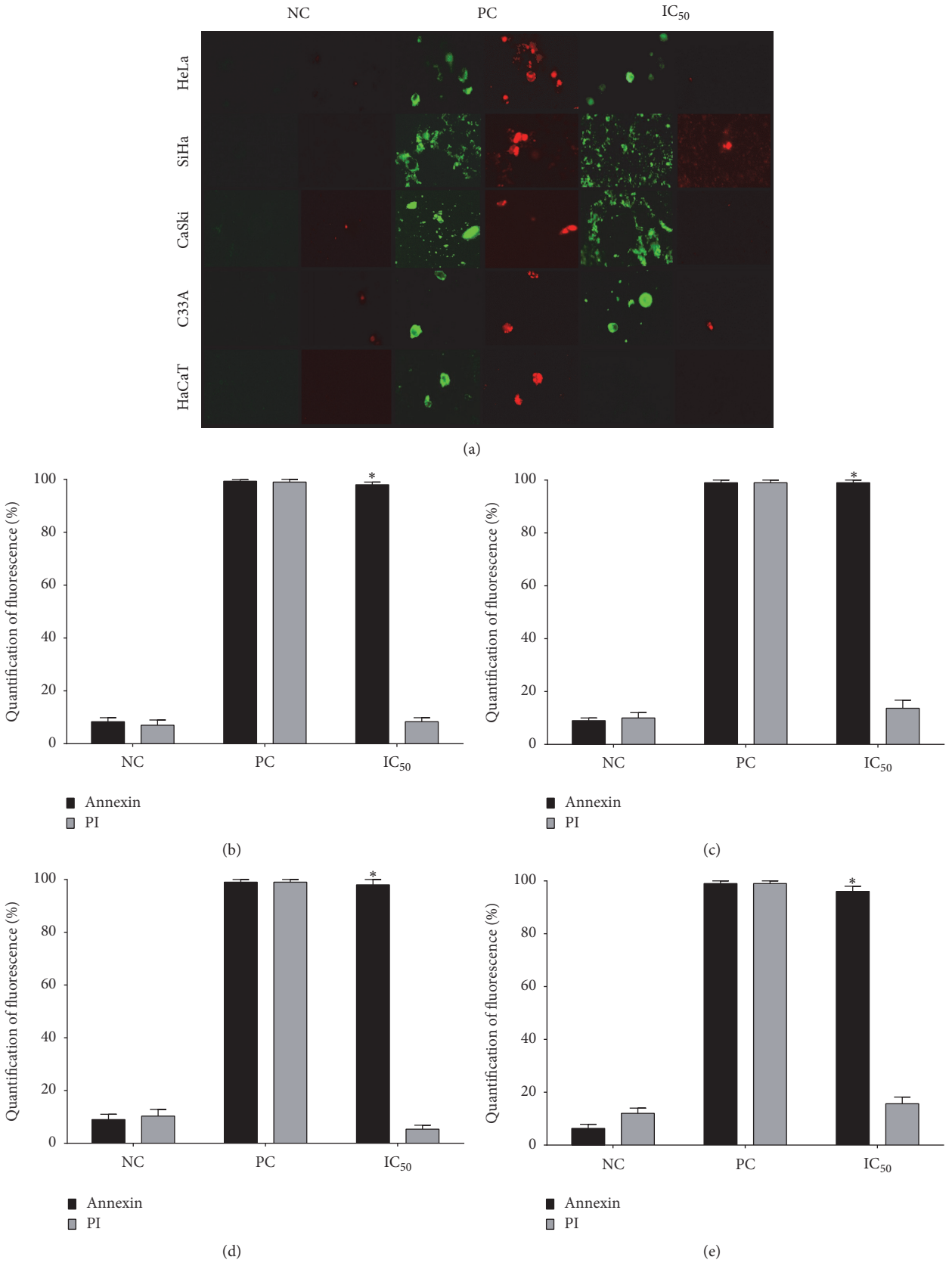

Figure 4: Continued.

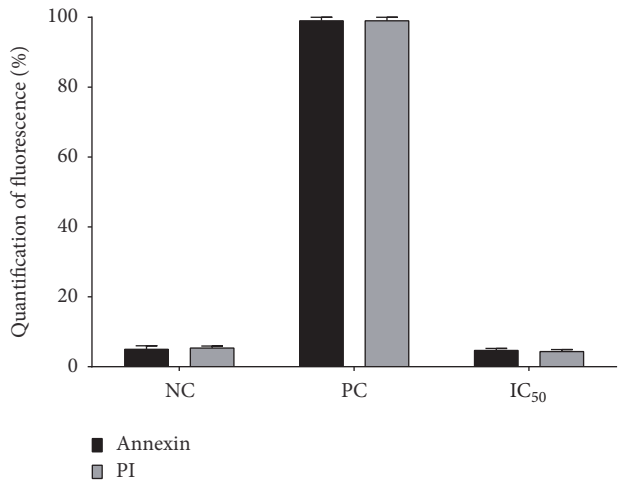

(f)

Figure 4: Assessment of death pathway associated with apigenin in cervical cancer cell lines and HaCaT cells. (a) Representative figures of cancer cell lines (HeLa, SiHa, CaSki, and C33A) and HaCaT cells exposed to apigenin (IC_{50} of each cell line) at 48 h stained with the apoptosis marker Annexin V (green fluorescence) and the necrosis marker propidium iodide (PI) (red fluorescence). (b, c, d, e, and f) Histograms show the mean % Annexin V-positive cells (HeLa, SiHa, CaSki, C33A, and HaCaT cells, resp.) treated with apigenin (IC_{50} of each cancer cell line) for 48 h. Camptothecin (20 μM) and digitonin (80 μM) were used as positive controls for apoptosis and necrosis, respectively (PC), and cells not treated with apigenin were used as negative controls (NC). Data are shown as the mean ± SD of three independent experiments conducted in triplicate. $^*P < 0.05$ versus the negative control. Magnification: 20x.

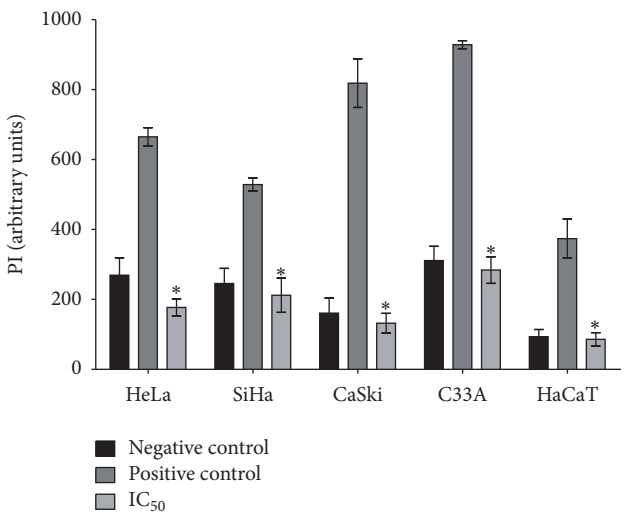

Figure 5: Effects of apigenin on cell membrane integrity in cervical cancer cell lines and HaCaT cells. HeLa, SiHa, CaSki, C33A, and HaCaT cells were exposed to apigenin (IC_{50} of each cell line), and cell membrane integrity was detected using a PI fluorescence probe. Arbitrary units (relative fluorescence units, RFU) were based directly on fluorescence intensity. Data are expressed as the mean fluorescence (in arbitrary units) ± SD of three independent experiments conducted in triplicate. $^*P < 0.05$ versus the positive control.

cell lines compared with the negative control (untreated cells) (HeLa, $P = 0.0001$; SiHa, $P = 0.001$; CaSki, $P = 0.0008$; C33A $P = 0.0022$). LPO was not changed in HaCaT cells after exposure to apigenin ($P = 0.1934$) (Figure 6(d)).

Finally, we measured the activity of catalase, an enzyme involved in the cell antioxidant system that is responsible for maintaining low levels of ROS and cell homeostasis. As shown in Figure 7, the catalase activity in HaCaT cells gradually increased after apigenin exposure (IC_{50} and IC_{90}, resp.). In HeLa, CaSki, and C33A cells, an increase in enzyme activity occurred following exposure to the IC_{50} of apigenin, whereas reduced activity was observed following exposure to the IC_{90}. In contrast, SiHa cells exhibited reduced catalase activity after exposure to the IC_{50} of apigenin, and an even greater reduction was observed following exposure to the IC_{90}.

3.5. Apigenin Inhibits Cervical Cancer Cell Migration and Invasion. The wound-healing assay revealed that apigenin (IC_{30}) effectively inhibited cell migration in all cancer cell lines studied; the greatest reduction in basal migratory ability was for HeLa cells, followed by C33A, SiHa, and CaSki cells. For the C33A and HeLa cells, apigenin significantly inhibited cell migration by up to twofold at all times tested ($P = 0.0059$ and $P = 0.029$, resp.). Additionally, apigenin inhibited CaSki and SiHa cell migration at later exposure times. For the SiHa cells, inhibition was higher than in all other cancer cell lines analyzed (up to threefold) at 72 h ($P = 0.0038$). Finally, the CaSki cells showed significant inhibition of migration (approximately twofold) only at 72 h of apigenin exposure ($P = 0.016$) (Figure 8).

Invasion ability was measured by the number of cells that migrated through a reconstituted Matrigel layer to the bottom surface of a porous membrane in a Transwell chamber assay. As shown in Figure 9, both concentrations of apigenin (IC_{50} and IC_{90} of each cell line) reduced the number of cells in

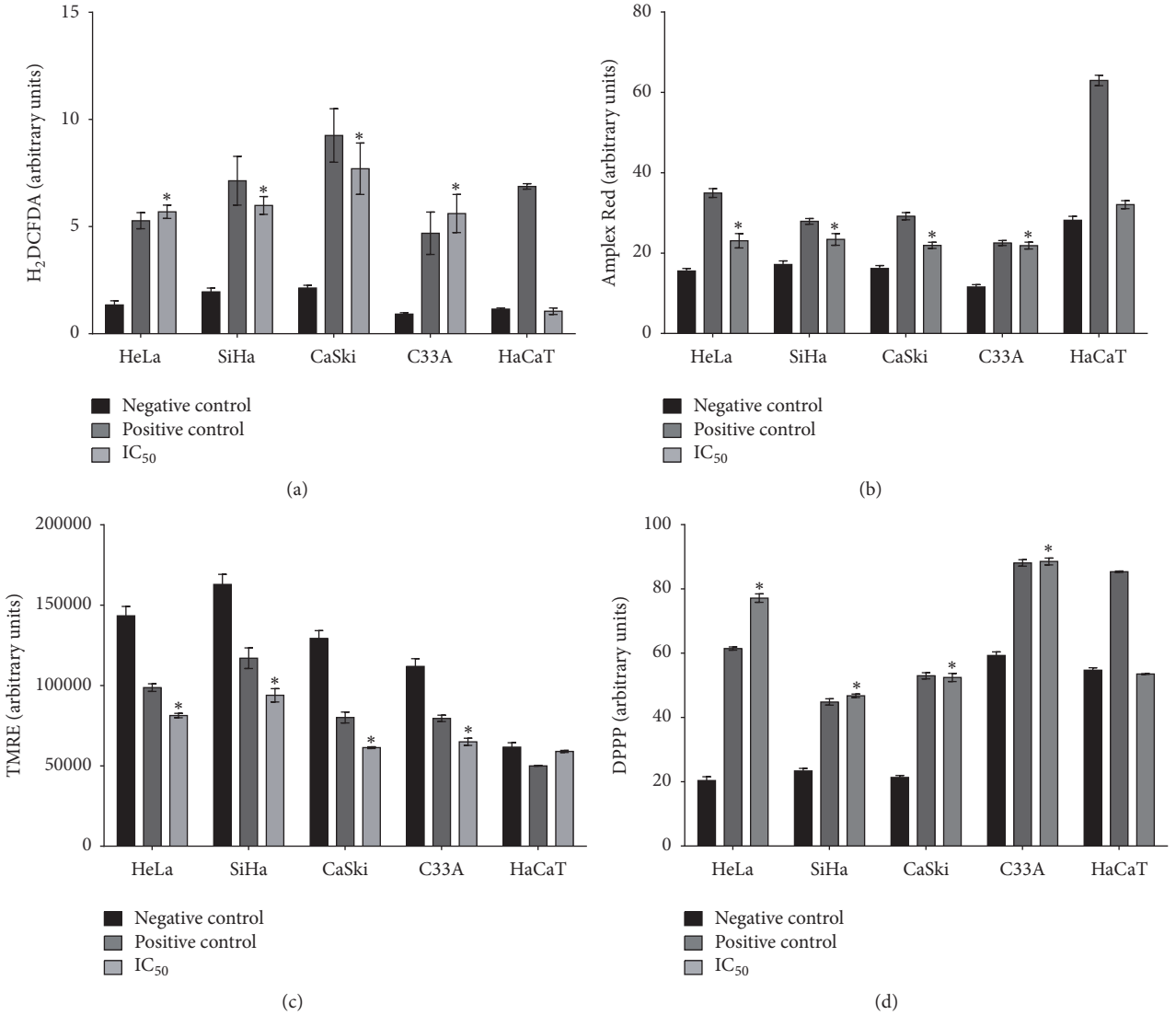

Figure 6: Effects of apigenin on cellular oxidative stress. (a) Total ROS production was evaluated during exposure of cervical cancer cell lines (HeLa, SiHa, CaSki, and C33A) and HaCaT cells to apigenin using the fluorescence probe H_2DCFDA. The positive control was treated with 10 μM H_2DCFDA in the dark. (b) Detection of extracellular H_2O_2 levels in all cell lines exposed to apigenin was conducted using an Amplex® Red assay kit. H_2O_2 was used as a positive control. (c) Mitochondrial membrane potential ($\Delta\psi m$) after exposure to apigenin measured using a TMRE fluorescence probe. Carbonyl cyanide m-chlorophenylhydrazone (CCCP) was used as a positive control. (d) Lipid peroxidation (LP) after exposure to apigenin using the fluorescence probe diphenyl-1-pyrenylphosphine (DPPP). Hydrogen peroxide was used as a positive control. Arbitrary units (relative fluorescence units, RFU) were based directly on fluorescence intensity. Data are expressed as the mean ± SD of three independent experiments conducted in triplicate. $^*P < 0.05$ versus negative control.

the bottom surface of the Transwell chamber, indicating a decrease in the invasiveness of all four cell lines. There was a further significant reduction in cell invasion observed at the IC_{50} and IC_{90} of apigenin in the HeLa ($P = 0.0018$ and $P = 0.0008$, resp.), SiHa ($P = 0.0021$ and $P = 0.0005$, resp.), CaSki ($P = 0.0025$ and $P = 0.0012$, resp.), and C33A ($P = 0.0015$ and $P = 0.0001$, resp.) cells compared to the control cells.

4. Discussion

In the present study, we evaluated the cytotoxic effects of apigenin in a comprehensive panel of human cervical cancer-derived cell lines, including HeLa (HPV 18-positive), SiHa (HPV 16-positive), CaSki (HPV 16 and 18-positive), and C33A (HPV-negative) cells, compared to a nontumorigenic spontaneously immortalized human epithelial cell line (HaCaT). The results demonstrated that apigenin exposure had a selective time- and dose-dependent cytotoxic effect in all cervical cancer cell lines, but not in HaCaT cells. Apigenin induced cancer cell death via apoptosis, which was triggered by mitochondrial redox impairment. Additionally, apigenin inhibited cancer cell migration and invasion.

Only three previous studies have evaluated the activity of apigenin specifically on cervical cancer cells; all showed

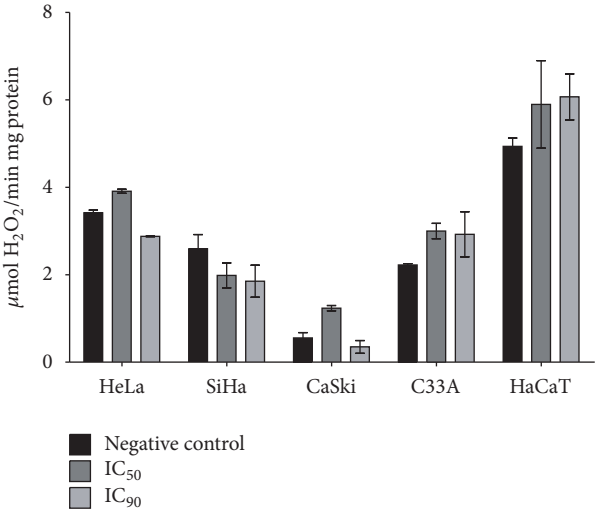

Figure 7: Effects of apigenin on catalase activity after exposure to apigenin (IC_{50} and IC_{90} of each cell line) for 48 h based on H_2O_2 consumed. Catalase activity was expressed as H_2O_2 consumed/min × mg protein (ε, 33.33 $M^{-1} \times cm^{-1}$).

a cytotoxic effect on HeLa cells [39–41]. Our results are in agreement with these reports and highlight additional important information, particularly that apigenin has a significant time- and dose-dependent cytotoxic effect on non-HeLa human cervical cancer-derived cell lines, including SiHa, CaSki, and C33A cells. Apigenin exerted cytotoxic effects on HeLa cells (IC_{50} of 10 μM), SiHa cells (IC_{50} of 68 μM), CaSki cells (IC_{50} of 76 μM), and C33A cells (IC_{50} of 40 μM) at 72 h. Among these cell lines, the HeLa cells showed the greatest reduction in cell viability at the lowest apigenin concentration (10 μM) after 48 h and 72 h of exposure. The CaSki and SiHa cells showed similar decreases in cell viability, reaching significant levels at 40 μM apigenin at 48 h and 72 h. The C33A cells showed a significant reduction in cell viability at 40 μM apigenin, but only after 72 h of exposure. Thus, apigenin showed cytotoxic effects at the lowest exposure concentration and time in cancer cell lines immortalized by HPV (HeLa followed by SiHa and CaSki cells), indicating its potential for the treatment of cervical cancers caused by HPV 16 and HPV 18, which account for approximately 70% of cases [1–4].

Regarding the cytotoxic effect of apigenin on HeLa cells, our study showed lower IC_{50} values than others, with reported IC_{50} values of 40 μM at 30 h [39] and 37 μM at 24 h [41]. We have knowledge of only one study that investigated the cytotoxic activity of apigenin on SiHa and C33A cells [64] that used the same concentrations and times used here (0–100 μM at 72 h). The results from that study are similar to ours: apigenin was cytotoxic for both SiHa and C33A cells with IC_{50} values of 50.14 μM and 45.10 μM, respectively. Likewise, only one study evaluated CaSki cell cytotoxicity after apigenin exposure. In the referenced study, 20 μM apigenin was applied for 24 h, and unlike our results, a cytotoxic effect of apigenin on CaSki cells was not detected [65].

In contrast to its cytotoxic effects on cancer cells, we showed that apigenin did not significantly reduce HaCaT cell viability at any concentration or time tested. These data highlight the selective effect of apigenin towards cancer cells, similar to studies of other human cancer types that reported its low intrinsic toxicity and differential effects in normal versus cancer cells [21–23]. We also evaluated the cytotoxic effect of apigenin using microscopy and found that apigenin induced pronounced morphological changes in all cervical cancer cell lines tested; in all cases, retraction of cytoplasmic expansion and detachment from the plate due to cell death occurred. Finally, we examined the long-term cytotoxicity of apigenin using a clonogenic assay. We found that subtoxic doses of apigenin resulted in 100% inhibition of colony formation in HeLa, SiHa, CaSki, and C33A cells compared with untreated cells. In contrast, HaCaT cells maintained colony formation after apigenin exposure. Based on these findings, we tested the capability of the cells to recover from damage after 1, 6, 18, 24, 48, and 72 h and 7 days of exposure to apigenin. The results indicated that although recovery occurred after 1 h of exposure, there was a decrease in the number of colonies after that time. Overall, these results show that apigenin decreased colony formation at subtoxic doses and had a strong and selective cytotoxic effect on cervical cancer cells immortalized by HPV 16, HPV 18, and HPV 16 and 18 together, as well as on cells not induced by HPV.

To determine the cell death pathway that results from apigenin exposure, we studied senescence with blue SA-b-Gal staining. Cellular senescence is believed to represent a natural cellular process to suppress tumor formation [66]. Our results did not show that apigenin caused cell death by inducing senescence. Next, we evaluated cell death by apoptosis and necrosis by staining with fluorescent Annexin V (detects early apoptosis) and PI (detects necrosis or late apoptosis). We found that apigenin induced death by apoptosis in all cervical cancer cell lines after 48 h exposure. To further support these results, we evaluated membrane integrity by staining with fluorescent PI, which diffuses through permeable membranes and binds to nucleic acids in necrotic cells. Our data indicate that apigenin exposure did not induce the cell membrane rupture that occurs in necrosis and late apoptosis. Together, these data indicate that apigenin exposure induces cancer cell death via apoptosis, in agreement with previous studies of different cancer cell lines, including HeLa cells [40, 41, 66].

To develop effective chemopreventive and chemotherapeutic approaches for target organ carcinogenesis, a promising strategy is to take advantage of the biochemical differences that exist between cancer cells and their normal counterparts. In this respect, agents capable of inducing selective apoptosis of cancer cells are receiving considerable attention as novel cancer-prevention options [67, 68]. The intrinsic pathway of apoptosis is related to oxidative stress, a condition in which there is an imbalance between ROS production and detoxification [69]. ROS play a role in regulating the intrinsic pathway of apoptosis and are associated with reduced mitochondrial membrane potential [70–73]. We investigated whether apigenin exposure induces oxidative stress in cervical cancer cells using assays to detect total ROS and H_2O_2 production, changes in mitochondrial

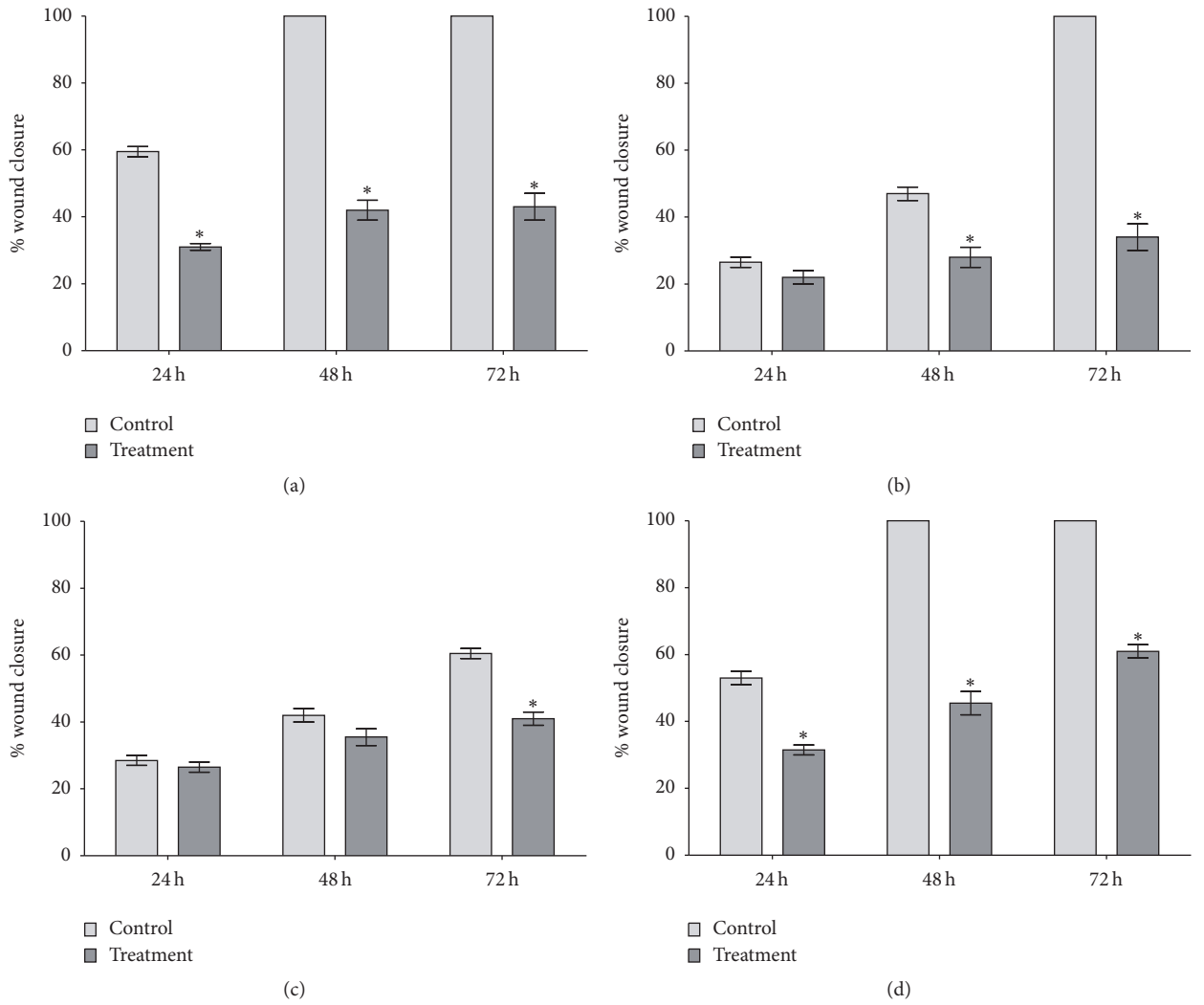

Figure 8: Cell migration analysis using a wound-healing assay. HeLa (a), SiHa (b), CaSki (c), and C33A (d) cells were tested in 6-well plates (2.5×10^4 cells/well) after scratching in the absence (negative control) and presence of apigenin. The results were calculated by comparing wound closure after 24, 48, and 72 h with the measurements taken at the initial time, and data are shown as the mean ± SD of three independent experiments conducted in triplicate. $^*P < 0.05$ versus the negative control.

membrane potential ($\Delta\Psi m$), lipid peroxidation (LPO) levels, and catalase activity. We detected significantly increased production of total ROS and extracellular H_2O_2, increased LPO levels, and significantly decreased $\Delta\psi m$ and catalase activity in HeLa, SiHa, CaSki, and C33A cells, but not in HaCaT cells. Collectively, our data provide evidence that apigenin induces oxidative stress, which leads to cervical cancer cell death via the intrinsic pathway of apoptosis. Our results are in accordance with previous studies reporting that apigenin can induce the following: (1) increased ROS production in various cancers, including skin [25], colon [66], and lung [74] cancer, as well as in HeLa cells [75, 76]; (2) apoptosis mediated by increased ROS production in human colorectal cancer cells [66]; (3) increased H_2O_2 production in the K562 human myelogenous leukemia cell line [77]; and (4) mitochondrial membrane potential collapse in choriocarcinoma cells [78]. In relation to catalase activity, mechanistic studies of compounds that induce apoptotic cell death via ROS have demonstrated the importance of catalase activity inhibition on the accumulation of ROS and consequently cell death by apoptosis [79]. Our evidence that catalase activity was reduced in cancer cell lines after apigenin exposure is compatible with the mechanism of action of apoptosis induction. Likewise, our evidence of increased LPO levels is in accordance with the theory that LPO is a toxic free radical produced by ROS and an indicator of cellular oxidative stress [80].

Still, our results of mitochondrial stress and apoptotic death after exposure to apigenin are in agreement with others in relation to structure activity of these flavone. The activity of apigenin was associated with hydroxyl group on its B ring in position $4'$ and its ability to react with free radicals. More specifically, apigenin and kaempferol exhibit similar B ring structure but the presence of a hydroxyl group in position 3

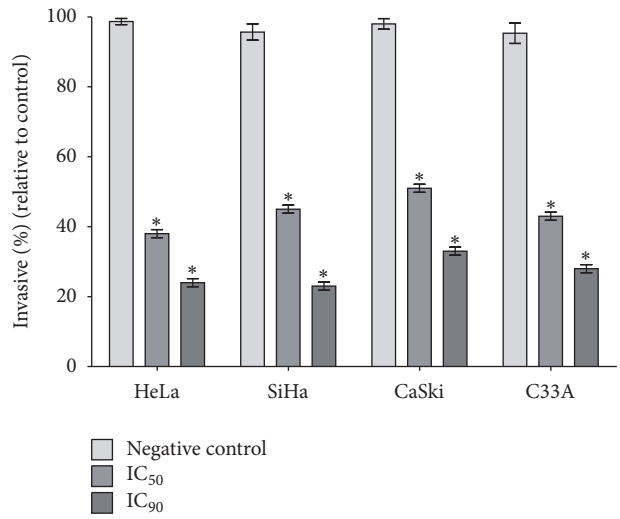

Figure 9: Effects of apigenin on cell invasion. Cervical cancer cell lines (HeLa, SiHa, CaSki, and C33A) were seeded onto Matrigel-coated filters in Boyden chambers. After 48 h of apigenin treatment (IC_{50} and IC_{90} of each cell line), the number of cells present on the bottom side of the filter was quantified and expressed as a percentage of the negative control. The values are presented as the mean ± SD of three independent experiments conducted in triplicate. $^{*}P < 0.05$ versus the negative control.

(kaempferol) decrease its cytotoxicity in HeLa cells compared to apigenin. The higher activity of apigenin compared to kaempferol in this study was at least partially dependent on its ability to react with ROS that are important to induction of apoptosis [81].

Regarding the effect of apigenin on the migration and invasion of human cervical cancer-derived cell lines, Czyz et al. (2005) showed that apigenin inhibited cell motility, which correlated with reduced invasive potential of HeLa cells after exposure to 30 and 50 μM apigenin for 24 h [40]. Noh et al. (2010) reported that 5 μM apigenin inhibited the in vitro invasion of CaSki cells [65]. Other studies of choriocarcinoma [78], colorectal cancer [76, 82] and prostate cancer [14] also showed that apigenin suppresses cell migration and invasion. Our results from the wound-healing assays and Matrigel migration and invasion assays showed that, similar to the above-mentioned studies, apigenin inhibited cancer cell migration, with the greatest reduction in basal migratory ability observed in HeLa cells, followed by C33A, SiHa, and CaSki cells, and also significantly decreased cell motility and invasion. These data suggest that apigenin exerts antitumorigenic effects not only by influencing cervical cancer cell cytotoxicity but also by affecting cell motility and thus invasion. This evidence is consistent with the large number of mechanisms that has been attributed to apigenin, including antioxidant properties and their influence on gene expression. The most common activity noted for majority of plant flavones include their role as potent antioxidants and free radical scavengers, with their biological activities related to anti-inflammatory, antimicrobial, antiviral, antimutagenic, and anticancer functions. These biological activities are considered to be related to their interactions with several enzymes and proteins, including calcium phospholipid-dependent protein kinase, DNA topoisomerases, tyrosine protein kinase, phosphorylase kinase, phosphatidylinositol 3-kinase, cytochrome 1A1 expression, and the total cellular glutathione level [83–85].

In conclusion, we found that apigenin has a selective dose-dependent cytotoxic effect and could induce apoptosis in HeLa, SiHa, CaSki, and C33A cells, but not in HaCaT cells. Additionally, apigenin induced mitochondrial redox impairment and inhibited cancer cell migration and invasion. These results show that apigenin had a strong and selective antitumoral effect on cervical cancer cells immortalized by HPV 16, HPV 18, and HPV 16 and 18 together, indicating its potential to be a powerful candidate in developing therapeutic agent for all cervical cancer types. Thus, our data support additional preclinical and clinical studies for further validation of antitumor effects of apigenin applicable to cancer cervical in the future.

Competing Interests

The authors declare that there is no conflict of interests regarding the publication of this paper.

Acknowledgments

This work was supported by grants from Coordenação de Aperfeiçoamento de Pessoal de Nível superior (CAPES), Brazilian Government (PVE A109/2013 and PROCAD 88881.068413/2014-01) and Conselho Nacional de Desenvolvimento Científico e Tecnológico (CNPq 470040/2014-9).

References

[1] International Agency for Research on Cancer (IARC), *Globocan 2012: Estimated Incidence, Mortality and Prevalence Worldwide in 2012*, International Agency for Research on Cancer, Lyon, France, 2012, http://globocan.iarc.fr/Pages/fact_sheets_cancer.aspx.

[2] W. J. Koh, B. E. Greer, N. R. Abu-Rustum et al., "Uterine sarcoma, version 1.2016: featured updates to the NCCN guidelines," *Journal of the National Comprehensive Cancer Network*, vol. 13, no. 11, pp. 1321–1331, 2015.

[3] S. K. Kjær, K. Frederiksen, C. Munk, and T. Iftner, "Long-term absolute risk of cervical intraepithelial neoplasia grade 3 or worse following human papillomavirus infection: role of persistence," *Journal of the National Cancer Institute*, vol. 102, no. 19, pp. 1478–1488, 2010.

[4] M. Schiffman, P. E. Castle, J. Jeronimo, A. C. Rodriguez, and S. Wacholder, "Human papillomavirus and cervical cancer," *Lancet*, vol. 370, no. 9590, pp. 890–907, 2007.

[5] S. Li, W. Yuan, B. Zhao et al., "Positive effect of HPV status on prognostic value of blood lymphocyte-to-monocyte ratio in advanced cervical carcinoma," *Cancer Cell International*, vol. 16, article no. 54, 2016.

[6] D. Lorusso, F. Petrelli, A. Coinu, F. Raspagliesi, and S. Barni, "A systematic review comparing cisplatin and carboplatin plus paclitaxel-based chemotherapy for recurrent or metastatic cervical cancer," *Gynecologic Oncology*, vol. 133, no. 1, pp. 117–123, 2014.

[7] J. Khalil, S. Bellefqih, N. Sahli et al., "Impact of cervical cancer on quality of life: beyond the short term (results from a single institution)," *Gynecologic Oncology Research and Practice*, vol. 2, article 7, 2015.

[8] G. M. Cragg and D. J. Newman, "Natural products: a continuing source of novel drug leads," *Biochimica et Biophysica Acta - General Subjects*, vol. 1830, no. 6, pp. 3670–3695, 2013.

[9] D. J. Newman and G. M. Cragg, "Natural products as sources of new drugs from 1981 to 2014," *Journal of Natural Products*, vol. 79, no. 3, pp. 629–661, 2016.

[10] S. Kumar and A. K. Pandey, "Chemistry and biological activities of flavonoids: an overview," *The Scientific World Journal*, vol. 2013, Article ID 162750, 16 pages, 2013.

[11] L. H. Yao, Y. M. Jiang, J. Shi et al., "Flavonoids in food and their health benefits," *Plant Foods for Human Nutrition*, vol. 59, no. 3, pp. 113–122, 2004.

[12] D. F. Birt, S. Hendrich, and W. Wang, "Dietary agents in cancer prevention: flavonoids and isoflavonoids," *Pharmacology and Therapeutics*, vol. 90, no. 2-3, pp. 157–177, 2001.

[13] J. B. Harborne and C. A. Williams, "Advances in flavonoid research since 1992," *Phytochemistry*, vol. 55, no. 6, pp. 481–504, 2000.

[14] D. Patel, S. Shukla, and S. Gupta, "Apigenin and cancer chemoprevention: progress, potential and promise (review)," *International Journal of Oncology*, vol. 30, no. 1, pp. 233–245, 2007.

[15] W.-Y. Huang, Y.-Z. Cai, and Y. Zhang, "Natural phenolic compounds from medicinal herbs and dietary plants: potential use for cancer prevention," *Nutrition and Cancer*, vol. 62, no. 1, pp. 1–20, 2010.

[16] L. Lepiniec, I. Debeaujon, J.-M. Routaboul et al., "Genetics and biochemistry of seed flavonoids," *Annual Review of Plant Biology*, vol. 57, pp. 405–430, 2006.

[17] S. Budavari, *The Merck Index*, Merck & Co, Whitehouse Station, NJ, USA, 13th edition, 1997.

[18] Y.-M. Sun, H.-L. Wu, J.-Y. Wang, Z. Liu, M. Zhai, and R.-Q. Yu, "Simultaneous determination of eight flavonoids in propolis using chemometrics-assisted high performance liquid chromatography-diode array detection," *Journal of Chromatography B: Analytical Technologies in the Biomedical and Life Sciences*, vol. 962, pp. 59–67, 2014.

[19] Y. Zhu, J. Wu, S. Li et al., "Apigenin inhibits migration and invasion via modulation of epithelial mesenchymal transition in prostate cancer," *Molecular Medicine Reports*, vol. 11, no. 2, pp. 1004–1008, 2015.

[20] H. Czeczot, B. Tudek, J. Kusztelak et al., "Isolation and studies of the mutagenic activity in the Ames test of flavonoids naturally occurring in medical herbs," *Mutation Research/Genetic Toxicology*, vol. 240, no. 3, pp. 209–216, 1990.

[21] W. Wang, L. Heideman, C. S. Chung, J. C. Pelling, K. J. Koehler, and D. F. Birt, "Cell-cycle arrest at G2/M and growth inhibition by apigenin in human colon carcinoma cell lines," *Molecular Carcinogenesis*, vol. 28, no. 2, pp. 102–110, 2000.

[22] T. Kobayashi, T. Nakata, and T. Kuzumaki, "Effect of flavonoids on cell cycle progression in prostate cancer cells," *Cancer Letters*, vol. 176, no. 1, pp. 17–23, 2002.

[23] T.-D. Way, M.-C. Kao, and J.-K. Lin, "Apigenin induces apoptosis through proteasomal degradation of HER2/neu in HER2/neu-overexpressing breast cancer cells via the phosphatidylinositol 3-kinase/Akt-dependent pathway," *Journal of Biological Chemistry*, vol. 279, no. 6, pp. 4479–4489, 2004.

[24] S. M. Nabavi, S. Habtemariam, M. Daglia, and S. F. Nabavi, "Apigenin and breast cancers: from chemistry to medicine," *Anti-Cancer Agents in Medicinal Chemistry*, vol. 15, no. 6, pp. 728–735, 2015.

[25] S. Das, J. Das, A. Samadder, N. Boujedaini, and A. R. Khuda-Bukhsh, "Apigenin-induced apoptosis in A375 and A549 cells through selective action and dysfunction of mitochondria," *Experimental Biology and Medicine*, vol. 237, no. 12, pp. 1433–1448, 2012.

[26] R. G. P. T. Jayasooriya, S.-H. Kang, C.-H. Kang et al., "Apigenin decreases cell viability and telomerase activity in human leukemia cell lines," *Food and Chemical Toxicology*, vol. 50, no. 8, pp. 2605–2611, 2012.

[27] D. Maggioni, W. Garavello, R. Rigolio, L. Pignataro, R. Gaini, and G. Nicolini, "Apigenin impairs oral squamous cell carcinoma growth in vitro inducing cell cycle arrest and apoptosis," *International Journal of Oncology*, vol. 43, no. 5, pp. 1675–1682, 2013.

[28] X. Tong and J. C. Pelling, "Targeting the PI3k/Akt/mTOR axis by apigenin for cancer prevention," *Anti-Cancer Agents in Medicinal Chemistry*, vol. 13, no. 7, pp. 971–978, 2013.

[29] D.-G. Wu, P. Yu, J.-W. Li et al., "Apigenin potentiates the growth inhibitory effects by IKK-β-mediated NF-κB activation in pancreatic cancer cells," *Toxicology Letters*, vol. 224, no. 1, pp. 157–164, 2014.

[30] S. M. Ju, J. G. Kang, J. S. Bae, H. O. Pae, Y. S. Lyu, and B. H. Jeon, "The flavonoid apigenin ameliorates cisplatin-induced nephrotoxicity through reduction of p53 activation and promotion of PI3K/Akt pathway in human renal proximal tubular epithelial cells," *Evidence-based Complementary and Alternative Medicine*, vol. 2015, Article ID 186436, 9 pages, 2015.

[31] F. Lindenmeyer, H. Li, S. Menashi, C. Soria, and H. Lu, "Apigenin acts on the tumor cell invasion process and regulates protease production," *Nutrition and Cancer*, vol. 39, no. 1, pp. 139–147, 2001.

[32] S. Shukla, A. Mishra, P. Fu, G. T. MacLennan, M. I. Resnick, and S. Gupta, "Up-regulation of insulin-like growth factor binding protein-3 by apigenin leads to growth inhibition and apoptosis of 22Rv1 xenograft in athymic nude mice," *FASEB Journal*, vol. 19, no. 14, pp. 2042–2044, 2005.

[33] S. Shukla, G. T. MacLennan, P. Fu, and S. Gupta, "Apigenin attenuates insulin-like growth factor-I signaling in an autochthonous mouse prostate cancer model," *Pharmaceutical Research*, vol. 29, no. 6, pp. 1506–1517, 2012.

[34] J.-S. Kim, E. S. Kim, D. Liu et al., "Activation of insulin-like growth factor 1 receptor in patients with non-small cell lung cancer," *Oncotarget*, vol. 6, no. 18, pp. 16746–16756, 2015.

[35] L.-Z. Liu, J. Fang, Q. Zhou, X. Hu, X. Shi, and B.-H. Jiang, "Apigenin inhibits expression of vascular endothelial growth factor and angiogenesis in human lung cancer cells: implication of chemoprevention of lung cancer," *Molecular Pharmacology*, vol. 68, no. 3, pp. 635–643, 2005.

[36] M. K. Buening, J. G. Fortner, R. L. Chang, M.-T. Huang, A. W. Wood, and A. H. Conney, "Activation and inhibition of benzo(a)pyrene and aflatoxin b1 metabolism in human liver microsomes by naturally occurring flavonoids," *Cancer Research*, vol. 41, no. 1, pp. 67–72, 1981.

[37] B. Y. Su, H. L. Jung, Y. C. Hae et al., "Inhibitory effects of luteolin isolated from Ixeris sonchifolia hance on the proliferation of HepG2 human hepatocellular carcinoma cells," *Archives of Pharmacal Research*, vol. 26, no. 2, pp. 151–156, 2003.

[38] P. V. S. Jeyabal, M. B. Syed, M. Venkataraman, J. K. Sambandham, and D. Sakthisekaran, "Apigenin inhibits oxidative stress-induced macromolecular damage in N-nitrosodiethylamine (NDEA)-induced hepatocellular carcinogenesis in Wistar albino rats," *Molecular Carcinogenesis*, vol. 44, no. 1, pp. 11–20, 2005.

[39] F. Llorens, F. A. Miró, A. Casañas et al., "Unbalanced activation of ERK1/2 and MEK1/2 in apigenin-induced HeLa cell death," *Experimental Cell Research*, vol. 299, no. 1, pp. 15–26, 2004.

[40] J. Czyz, Z. Madeja, U. Irmer, W. Korohoda, and D. F. Hülser, "Flavonoid apigenin inhibits motility and invasiveness of carcinoma cells *in vitro*," *International Journal of Cancer*, vol. 114, no. 1, pp. 12–18, 2005.

[41] P.-W. Zheng, L.-C. Chiang, and C.-C. Lin, "Apigenin induced apoptosis through p53-dependent pathway in human cervical carcinoma cells," *Life Sciences*, vol. 76, no. 12, pp. 1367–1379, 2005.

[42] J. Liu, X.-C. Cao, Q. Xiao, and M.-F. Quan, "Apigenin inhibits HeLa sphere-forming cells through inactivation of casein kinase 2α," *Molecular Medicine Reports*, vol. 11, no. 1, pp. 665–669, 2015.

[43] M. Macville, E. Schröck, H. Padilla-Nash et al., "Comprehensive and definitive molecular cytogenetic characterization of HeLa cells by spectral karyotyping," *Cancer Research*, vol. 59, no. 1, pp. 141–150, 1999.

[44] T. C. Wright Jr., L. S. Massad, C. J. Dunton, M. Spitzer, E. J. Wilkinson, and D. Solomon, "2006 consensus guidelines for the management of women with abnormal cervical cancer screening tests," *American Journal of Obstetrics and Gynecology*, vol. 197, no. 4, pp. 346–355, 2007.

[45] H. O. Smith, M. F. Tiffany, C. R. Qualls, and C. R. Key, "The rising incidence of adenocarcinoma relative to squamous cell carcinoma of the uterine cervix in the United States—a 24-year population-based study," *Gynecologic Oncology*, vol. 78, no. 2, pp. 97–105, 2000.

[46] A. Paloma Vizcaino, V. Moreno, F. Xavier Bosch, N. Muñoz, X. M. Barros-Dios, and D. Maxwell Parkin, "International trends in the incidence of cervical cancer: I. adenocarcinoma and adenosquamous cell carcinomas," *International Journal of Cancer*, vol. 75, no. 4, pp. 536–545, 1998.

[47] G. Hernandez-Flores, P. C. Ortiz-Lazareno, J. M. Lerma-Diaz et al., "Pentoxifylline sensitizes human cervical tumor cells to cisplatin-induced apoptosis by suppressing NF-kappa B and decreased cell senescence," *BMC Cancer*, vol. 11, article no. 483, 2011.

[48] A. Beckenkamp, J. B. Willig, D. B. Santana et al., "Differential expression and enzymatic activity of DPPIV/CD26 affects migration ability of cervical carcinoma cells," *PLoS ONE*, vol. 10, no. 7, Article ID e0134305, 2015.

[49] X. Shi, D. Liu, J. Zhang et al., "Extraction and purification of total flavonoids from pine needles of Cedrus deodara contribute to anti-tumor in vitro," *BMC Complementary and Alternative Medicine*, vol. 16, article no. 245, 2016.

[50] K. S. Louis and A. C. Siegel, "Cell viability analysis using trypan blue: manual and automated methods," *Methods in Molecular Biology*, vol. 740, pp. 7–12, 2011.

[51] N. A. P. Franken, H. M. Rodermond, J. Stap, J. Haveman, and C. van Bree, "Clonogenic assay of cells in vitro," *Nature Protocols*, vol. 1, no. 5, pp. 2315–2319, 2006.

[52] R. K. Gary and S. M. Kindell, "Quantitative assay of senescence-associated β-galactosidase activity in mammalian cell extracts," *Analytical Biochemistry*, vol. 343, no. 2, pp. 329–334, 2005.

[53] B. Iqbal, A. Ghildiyal, Sahabjada et al., "Antiproliferative and apoptotic effect of curcumin and TRAIL (TNF related apoptosis inducing ligand) in chronic myeloid leukaemic cells," *Journal of Clinical and Diagnostic Research*, vol. 10, no. 4, pp. XC01–XC05, 2016.

[54] E. A. Britta, A. P. Barbosa Silva, T. Ueda-Nakamura et al., "Benzaldehyde thiosemicarbazone derived from limonene complexed with copper induced mitochondrial dysfunction in Leishmania amazonensis," *PLoS ONE*, vol. 7, no. 8, Article ID e41440, 2012.

[55] C. Urani, P. Melchioretto, M. Bruschi, M. Fabbri, M. G. Sacco, and L. Gribaldo, "Impact of cadmium on intracellular zinc levels in HepG2 cells: quantitative evaluations and molecular effects," *BioMed Research International*, vol. 2015, Article ID 949514, 10 pages, 2015.

[56] A. K. Shukla, S. Patra, and V. K. Dubey, "Iridoid glucosides from Nyctanthes arbortristis result in increased reactive oxygen species and cellular redox homeostasis imbalance in Leishmania parasite," *European Journal of Medicinal Chemistry*, vol. 54, pp. 49–58, 2012.

[57] J. Xu, Z. Hao, X. Gou et al., "Imaging of reactive oxygen species burst from mitochondria using laser scanning confocal microscopy," *Microscopy Research and Technique*, vol. 76, no. 6, pp. 612–617, 2013.

[58] M. Morita, Y. Naito, T. Yoshikawa, and E. Niki, "Plasma lipid oxidation induced by peroxynitrite, hypochlorite, lipoxygenase and peroxyl radicals and its inhibition by antioxidants as assessed by diphenyl-1-pyrenylphosphine," *Redox Biology*, vol. 8, pp. 127–135, 2016.

[59] G. Valdameri, M. Trombetta-Lima, P. R. Worfel et al., "Involvement of catalase in the apoptotic mechanism induced by apigenin in HepG2 human hepatoma cells," *Chemico-Biological Interactions*, vol. 193, no. 2, pp. 180–189, 2011.

[60] C.-C. Liang, A. Y. Park, and J.-L. Guan, "In vitro scratch assay: a convenient and inexpensive method for analysis of cell migration in vitro," *Nature Protocols*, vol. 2, no. 2, pp. 329–333, 2007.

[61] K. Tomin, R. H. Goldfarb, and P. Albertsson, "In vitro assessment of human natural killer cell migration and invasion," *Methods in Molecular Biology*, vol. 1441, pp. 65–74, 2016.

[62] E. Middleton Jr., C. Kandaswami, and T. C. Theoharides, "The effects of plant flavonoids on mammalian cells: implications for inflammation, heart disease, and cancer," *Pharmacological Reviews*, vol. 52, no. 4, pp. 673–751, 2000.

[63] F. P. Garcia, D. Lazarin-Bidóia, T. Ueda-Nakamura, S. D. O. Silva, and C. V. Nakamura, "Eupomatenoid-5 isolated from leaves of piper regnellii induces apoptosis in leishmania amazonensis," *Evidence-Based Complementary and Alternative Medicine*, vol. 2013, Article ID 940531, 11 pages, 2013.

[64] M. D. C. Avelino-Flores, M. D. C. Cruz-López, F. E. Jiménez-Montejo, and J. Reyes-Leyva, "Cytotoxic activity of the methanolic extract of turnera diffusa willd on breast cancer cells," *Journal of Medicinal Food*, vol. 18, no. 3, pp. 299–305, 2015.

[65] H.-J. Noh, E.-G. Sung, J.-Y. Kim, T.-J. Lee, and I.-H. Song, "Suppression of phorbol-12-myristate-13-acetate-induced tumor cell invasion by apigenin via the inhibition of p38 mitogen-activated protein kinase-dependent matrix metalloproteinase-9 expression," *Oncology Reports*, vol. 24, no. 1, pp. 277–283, 2010.

[66] K. Banerjee and M. Mandal, "Oxidative stress triggered by naturally occurring flavone apigenin results in senescence and chemotherapeutic effect in human colorectal cancer cells," *Redox Biology*, vol. 5, pp. 153–162, 2015.

[67] S. Gupta, F. Afaq, and H. Mukhtar, "Selective growth-inhibitory, cell-cycle deregulatory and apoptotic response of apigenin in normal versus human prostate carcinoma cells," *Biochemical and Biophysical Research Communications*, vol. 287, no. 4, pp. 914–920, 2001.

[68] A. Chakrabarti, H. Patel, J. Price et al., "Carbon nanotubes in cancer therapy including Boron Neutron Capture Therapy (BNCT)," *Life Sciences*, vol. 16, pp. 403–418, 2012.

[69] S. Di Meo, T. T. Reed, P. Venditti, and V. M. Victor, "Role of ROS and RNS sources in physiological and pathological conditions," *Oxidative Medicine and Cellular Longevity*, vol. 2016, Article ID 1245049, 44 pages, 2016.

[70] H. Sies, "Strategies of antioxidant defense," *European Journal of Biochemistry*, vol. 215, no. 2, pp. 213–219, 1993.

[71] H.-L. Li, D.-D. Chen, X.-H. Li et al., "Changes of NF-kB, p53, Bcl-2 and caspase in apoptosis induced by JTE-522 in human gastric adenocarcinoma cell line AGS cells: role of reactive oxygen species," *World Journal of Gastroenterology*, vol. 8, no. 3, pp. 431–435, 2002.

[72] D. A. Ribeiro, D. M. F. Salvadori, and M. E. A. Marques, "Abnormal expression of bcl-2 and bax in rat tongue mucosa during the development of squamous cell carcinoma induced by 4-nitroquinoline 1-oxide," *International Journal of Experimental Pathology*, vol. 86, no. 6, pp. 375–381, 2005.

[73] G. Pani, O. R. Koch, and T. Galeotti, "The p53-p66shc-Manganese Superoxide Dismutase (MnSOD) network: a mitochondrial intrigue to generate reactive oxygen species," *International Journal of Biochemistry and Cell Biology*, vol. 41, no. 5, pp. 1002–1005, 2009.

[74] H.-F. Lu, Y.-J. Chie, M.-S. Yang et al., "Apigenin induces apoptosis in human lung cancer H460 cells through caspase- and mitochondria-dependent pathways," *Human and Experimental Toxicology*, vol. 30, no. 8, pp. 1053–1061, 2011.

[75] R.-M. Laberge, J. Karwatsky, M. C. Lincoln, M. L. Leimanis, and E. Georges, "Modulation of GSH levels in ABCC1 expressing tumor cells triggers apoptosis through oxidative stress," *Biochemical Pharmacology*, vol. 73, no. 11, pp. 1727–1737, 2007.

[76] Y. Xu, Y. Xin, Y. Diao et al., "Synergistic effects of apigenin and paclitaxel on apoptosis of cancer cells," *PLoS ONE*, vol. 6, no. 12, Article ID e29169, 2011.

[77] K. Horváthová, L. Novotný, D. Tóthová, and A. Vachálková, "Determination of free radical scavenging activity of quercetin, rutin, luteolin and apigenin in H_2O_2-treated human ML cells K562," *Neoplasma*, vol. 51, no. 5, pp. 395–399, 2004.

[78] W. Lim, S. Park, F. W. Bazer, and G. Song, "Apigenin reduces survival of choriocarcinoma cells by inducing apoptosis via the PI3K/AKT and ERK1/2 MAPK pathways," *Journal of Cellular Physiology*, vol. 231, no. 12, pp. 2690–2699, 2016.

[79] M. Nishikawa, K. Hyoudou, Y. Kobayashi, Y. Umeyama, Y. Takakura, and M. Hashida, "Inhibition of metastatic tumor growth by targeted delivery of antioxidant enzymes," *Journal of Controlled Release*, vol. 109, no. 1–3, pp. 101–107, 2005.

[80] G. C. Jagetia and T. K. Reddy, "Modulation of radiation-induced alteration in the antioxidant status of mice by naringin," *Life Sciences*, vol. 77, no. 7, pp. 780–794, 2005.

[81] E. Szliszka, Z. P. Czuba, M. Domino, B. Mazur, G. Zydowicz, and W. Krol, "Ethanolic extract of propolis (EEP) enhances the apoptosis-inducing potential of TRAIL in cancer cells," *Molecules*, vol. 14, no. 2, pp. 738–754, 2009.

[82] L. Chunhua, L. Donglan, F. Xiuqiong et al., "Apigenin up-regulates transgelin and inhibits invasion and migration of colorectal cancer through decreased phosphorylation of AKT," *Journal of Nutritional Biochemistry*, vol. 24, no. 10, pp. 1766–1775, 2013.

[83] G. Agati, E. Azzarello, S. Pollastri, and M. Tattini, "Flavonoids as antioxidants in plants: location and functional significance," *Plant Science*, vol. 196, pp. 67–76, 2012.

[84] Z.-P. Xiao, Z.-Y. Peng, M.-J. Peng, W.-B. Yan, Y.-Z. Ouyang, and H.-L. Zhu, "Flavonoids health benefits and their molecular mechanism," *Mini-Reviews in Medicinal Chemistry*, vol. 11, no. 2, pp. 169–177, 2011.

[85] C. S. Buer, N. Imin, and M. A. Djordjevic, "Flavonoids: new roles for old molecules," *Journal of Integrative Plant Biology*, vol. 52, no. 1, pp. 98–111, 2010.